Endothelial Dysfunction in Cardiovascular Disease

Mieke van den Heuvel

Design cover: C.S.A.M. van Spronsen
Layout cover: K.W. Bakker
Layout and printing thesis: Gildeprint
ISBN: 978-94-6233-917-0

Endothelial Dysfunction in Cardiovascular Disease

Endotheel dysfunctie in cardiovasculaire ziektes

Proefschrift

ter verkrijging van de graad van doctor aan de
Erasmus Universiteit Rotterdam
op gezag van de rector magnificus
Prof.dr. H.A.P. Pols
en volgens besluit van het College voor Promoties

De openbare verdediging zal plaatsvinden op
dinsdag 15 mei 2018 om 13.30 uur

door

Mieke van den Heuvel
geboren te Oss

Erasmus University Rotterdam

Erasmus

Promotiecommissie

Promotoren:	Prof.dr. D.J.G.M. Duncker
	Prof.dr. A.H.J. Danser
Overige leden:	Prof.dr. E.T. van Bavel
	Prof.dr. R.A. de Boer
	Prof.dr. F. Zijlstra

De onderzoeken van dit proefschrift werden uitgevoerd in het Erasmus Medisch Centrum te Rotterdam binnen de divisie Experimentele Cardiologie en Poliklinische Cardiologie van de afdeling Cardiologie en binnen de sector Farmacologie en Metabole ziektes van de afdeling Interne Geneeskunde. De financiële ondersteuning door de Erasmus Universiteit wordt dankbaar erkend.

Een deel van de onderzoeken werd mede mogelijk gemaakt door financiële ondersteuning van het Netherlands Heart Institute te Utrecht, waarvoor dankbare erkenning.

Publicatie van dit proefschrift werd mede mogelijk gemaakt door financiële ondersteuning door de Nederlandse Hartstichting, waarvoor dankbare erkenning.

Table of contents

General introduction

1

General introduction

The topic of **this thesis** is focused on alterations in endothelial function in different stages of cardiovascular disease with special attention to the microcirculation. Due to its enormous surface, the microcirculation is regarded as the largest organ in the body. Moreover, evidence is accumulating that the microcirculation plays a major role in coronary artery disease (CAD), a common and potentially life-threatening disease. Not only is (micro)vascular endothelial dysfunction involved in the development of CAD, it also has been reported as an adverse side-effect of the treatment of CAD with percutaneous coronary interventions (PCI), as **this thesis** will address. Diabetes Mellitus (DM), a disease of epidemic proportions nowadays, is an independent and strong predictor of CAD.[1] (Micro)vascular endothelial dysfunction is one of the most important contributors to the cardiovascular complications of DM, with an important role for the activated renin-angiotensin-aldosterone system (RAAS), as **this thesis** will demonstrate. A better understanding of (micro)vascular endothelial dysfunction will aid in better understanding the pathogenesis of cardiovascular disease and thereby provide novel treatment targets ultimately resulting in further improvement of treatment, or even prevention of cardiovascular disease.
In this general introduction, topics important for **this thesis** will be briefly explained. **This thesis** is subdivided into three parts with **part I** focusing on endothelial dysfunction in the development of CAD; **part II** focusing on endothelial dysfunction after PCI; and **part III** focusing on endothelial dysfunction in relation to DM and the RAAS. For a more detailed introduction into each of these three research parts, the reader is referred to **chapters 3**, **9** and **14**, respectively. Finally, **this thesis** is the result of translational research combining both clinical and preclinical studies.

Coronary artery disease

Cardiovascular disease is still one of the leading causes of morbidity and mortality in the industrialized world. In the Netherlands, in the year 2015 alone, 20.757 women and 18.543 men died of cardiovascular disease; this translates to the death of, on average, 57 women and 51 men per day. Within cardiovascular disease, CAD plays an important role (29% as a cause of death in men and 18% in women).[2] CAD is caused by atherosclerosis with endothelial dysfunction as an important initiator and contributor to the disease process.[3] When atherosclerosis proceeds, together with thrombosis, it can result in occlusive CAD, causing severe morbidity and mortality.

Atherosclerosis

Atherosclerosis is the principal cause of CAD and is considered to be a generalized inflammatory disease occurring in large and medium-sized arteries. Inflammation and highly specific cellular and molecular responses result in the accumulation of plasma lipids within the artery wall causing atherosclerotic lesions.[4] These lesions may be present throughout a person's lifetime.

The earliest type of lesion, the fatty streak, is already common in children.[5] These early lesions can progress over time, destabilize at a certain moment to result in a clinical manifestation of the disease: i.e. occlusive CAD resulting in a myocardial infarction. The initial changes that precede the formation of atherosclerotic lesions take place in the endothelium, the barrier between the blood and the vascular wall. The vascular wall of arteries is composed of three layers: the intima consisting of a single layer of endothelial cells, the media consisting predominantly of vascular smooth muscle cells, and the adventitia made of connective tissue, containing nerves as well as nutrient capillaries that supply the vessel.

Endothelium

The endothelium participates in numerous physiological processes including the regulation of vascular tone by the release of vasoactive molecules.[6] Vasodilation refers to arterial widening and vasoconstriction to arterial narrowing, both resulting from relaxation or constriction of smooth muscle cells within the vascular wall. The vasomotor response may be intrinsic, due to local processes, or extrinsic due to systemic processes. In this way, organ perfusion can be regulated, coupling perfusion to tissue metabolism.[7]

Changes in the vasomotor properties of the endothelium may represent the earliest manifestation of endothelial dysfunction, characterised for example by exaggerated vasoconstriction. Endothelial dysfunction has been implicated in the pathological process of atherosclerosis: early in the process of atherogenesis; later in the control of dynamic plaque burden, and eventually in the clinical manifestation of CAD. Even PCI strategies, developed to resolve obstructive CAD, have been associated with endothelial dysfunction (see **chapter 9**).

By secreting relaxing and contracting factors, the endothelium itself can induce vasodilation or vasoconstriction in response to shear stress and to a variety of endogenous vasoactive substances that are produced systemically or generated locally by vascular tissue or circulating blood cells. The major endothelium-derived relaxing factor is nitric monoxide (NO), which reduces intracellular calcium within the vascular smooth muscle cells resulting in vasodilation.[8] The endothelium also secretes endothelium derived hyperpolarizing factors (EDHFs),[9] and the potent vasoconstrictor endothelin-1 (ET-1).[10] Furchgott ***et al*** have demonstrated that the endothelium plays an obligatory role in the relaxation of arteries induced by acetylcholine in humans or by bradykinin in swine. They identified NO as the released factor and cyclic guanoside monophosphate (cGMP) as its key second messenger. Since then, methods have been developed to assess endothelium dependent vasomotor function.[11-13] The measurement of endothelial dysfunction has been used as a potential predictor of cardiovascular disease [3]. Indeed, prospective studies have demonstrated that endothelial dysfunction is highly predictive of future cardiovascular disease.[14]

Coronary interventions

PCI with stents is an important treatment option for obstructive CAD. The choice ranges from conventional bare metal stents (BMS), to first and second generation drug-eluting stents (DES) that are widely used in clinical practice.[15] DES are nowadays the preferred treatment for local occlusive CAD, because DES locally release high concentrations of immunosuppressive, cytostatic, or cytotoxic drugs at the coronary injury site in order to prevent vascular smooth muscle cell proliferation and therefore limiting in-stent restenosis, as seen with BMS.[16] The DES that have been approved include, in chronological order, the first generation DES like sirolimus-eluting stent, paclitaxel-eluting stent (PES), and tacrolimus-eluting stent; and second generation DES like zotarolimus-eluting stent and everolimus-eluting stent. For third generation DES, the structural backbone has been optimised with use of the same drugs as for second generation DES. DES drugs can profoundly inhibit the development of neointimal formation after stenting. Indeed, DES treatment resulted in a reduction of restenosis rates and showed significant long-term reduction in the number of target lesion revascularisation procedures as compared to BMS.[17-21] However, DES have also been associated with increased risk of stent thrombosis, the most feared complication of coronary stenting due to its high mortality rates.[22-25] As an underlying mechanism of thrombosis, impaired re-endothelialisation and delayed vascular healing have been identified.[26,27]

Subsequently PCI technology has been further developed and now goes in the direction already indicated in 1990 by prof. W.J. van der Giessen: "The next generation of coronary stents will have to be a combination of a biodegradable device with either drug eluting properties or a device seeded with normal or by DNA-technology transformed endothelial cells. The next years will learn which approach, will be the most effective."[28] Recently, as a fourth generation of DES, the bioresorbable vascular scaffold (BVS) with drug-eluting properties has been introduced with the aim to provide temporary vessel scaffolding and to be subsequently resorbed over time with restoration of vasomotion. This could be the solution to the permanent presence of a metallic cage of conventional DES and BMS. Clinical trials have demonstrated efficacy for the treatment of CAD with some restoration of vasomotion.[29-32] However, paradoxical vasoconstriction has also been observed, indicating persisting impairment of endothelial function.[29,30] In addition, higher rates of scaffold thrombosis have been reported compared to second generation DES with related morbidity and mortality.[33-35] Therefore, the problem of endothelial dysfunction after PCI still remains, requiring further study (see **part II of this thesis**). Interventional therapy will never be the ideal treatment on its own, since it only targets the consequences of CAD, i.e. the coronary obstruction, but not the atherosclerotic disease process itself. Therefore, knowledge of early disease development is of the utmost importance.

Animal models

Experimental disease models have been instrumental in enhancing our understanding of the pathogenesis of atherosclerosis development.[36,37] However, atherosclerosis is a disease influenced by a multitude of environmental factors. The different animal models which have been used differ in disease initiation and disease manifestation and represent only a part of the heterogeneous clinical situation. Prof. W.J. van der Giessen stated in his thesis: "No single animal model will give definite answers but each one provides new insights or contributes to the study of a particular problem concerning the cause, the pathogenesis or the consequences".[28] Small animal models, like mice and rats, have the advantage of low costs, availability, and easy usability. Due to genetic modification and cross-breeding, specific strains can be generated and used to unravel mechanisms involved in the cardiovascular disease process. When size becomes more important, small animal models need to be complemented by large animal models. Indeed, for the study of CAD and related diagnostic and therapeutic interventions, an animal model that closely resembles the human situation with lesions at similar anatomical locations is necessary, e.g. a porcine model with CAD (see **chapter 3**).

Coronary circulation

The coronary vasculature has traditionally been divided into large conduit arteries, which are prone to atherosclerosis development, and the microcirculation, which represents the major locus of resistance to flow. Direct measurements of microvascular pressures in beating hearts have demonstrated that during basal conditions, up to 40% of total coronary resistance resides in small arteries between 100 and 400 µm in diameter. During vasodilation, these vessels contribute to an even greater fraction of total coronary resistance,[38] making these small arteries important participants of the coronary circulation. These arteries are capable of active vasomotion by a myriad of vasodilator and vasoconstrictor signals exerted by neurohormonal influences, the endothelium, and metabolic signals form the myocardium. In this way, these vasomotor influences allow the myocardium to match the coronary blood supply with oxygen and nutrients, while maintaining a consistently high level of oxygen extraction.[39]

As described above, the endothelium is an important regulator of vasomotion and has been studied in **part I of this thesis** during different development stages of CAD: in both animal models and in patients. However, in small animals and in humans, the coronary circulation is more difficult to study. Since CAD is a representation of generalised cardiovascular disease, the study of endothelial function of the peripheral circulation can be relevant for CAD, and is translatable to the coronary circulation.[40]

In vitro vascular function assessment

In **this thesis** (micro)vascular endothelial function was studied *in vitro* in isolated arterial segments (see **chapters 5, 6, 7, 9, 10, 11, 13** and **16**). For these *in vitro* studies, organ chambers and wire myographs were used. Organ chambers are suitable for segments of conduit arteries up to 1-4 mm in diameter. Mulvany and Halpern have developed a technique to study the vascular response of isolated segments of small resistance arteries (100-300 µm in diameter), called the Mulvany wire myograph.[41] For both types of set-ups, arteries are quickly removed from freshly obtained organs and placed in cooled, oxygenated Krebs' buffer solution, which has physiological similarities to plasma. An arterial segment is then mounted on hooks or wires and set to the appropriate diameter via coupling of the hooks / wires to an isometric force transducer on one side and to a micro-meter on the other side. This will allow for precise measurement of the separation of the hooks / wires and the increasing passive force when stretching the vessel. A mounted segment is stabilised at 37°C before undergoing a passive normalisation procedure, which determines a passive length-tension curve up to 90% of the circumference that would occur at a predetermined transmural pressure. Having set the segment to a normalised passive stretch, the active force developed by a constrictor stimulus is measured as the increase in pressure against which the vessel will contract. Different concentrations of vasoactive stimuli with or without specific blockers can now be applied and the changes in force / pressure can be measured and presented as a percentage of vasodilation or vasoconstriction in concentration-response curves. Endothelial vasodilators are for example NO, EDHF, bradykinin, acetylcholine and prostaglandins generated by cyclooxygenase 1 or 2 (COX-2). Examples of vasoconstrictors are ET-1, angiotensin II (Ang II), phenylephrine and endothelium derived contractile factors (EDCF). All above mentioned substances have been used to cause *in vitro* vasomotor responses in the experiments of **this thesis** (see **chapters 5, 6, 7, 10, 11, 13, 16**). With multiple set-ups and many vessel segments per artery, vascular function can be studied in parallel and in great detail, which *in vivo* would be hampered by the potential systemic side effects of these vasoactive substances and by the interaction with each other caused by the long half-life of some substances.

Diabetes mellitus

The prevalence of DM, as well as its precursor the metabolic syndrome, is increasing worldwide and is reaching epidemic proportions.[42,43] Cardiovascular disease, including CAD, accounts for most of the morbidity and mortality in patients with DM.[44] CAD in DM patients is described as being diffuse and typically rapid in progression.[45] Revascularisation procedures in DM patients are usually associated with worse outcomes than those performed in patients without DM.[46] This is related to multiple factors including the numerous metabolic disturbances which affect these high-risk patients and ultimately determine their tendency towards an increased pro-atherothrombotic status.[47] While the most common metabolic abnormality associated with DM is hyperglycemia, there are also abnormalities in fat metabolism resulting in hyperlipidemia,

increased inflammation and oxidative stress, decreased vascular availability of NO, and an activated RAAS leading to endothelial dysfunction and subsequently to both macrovascular and microvascular injury.[44,48-51] This results in the extensive generalised cardiovascular disease of DM with typical end organ damage in kidneys, eyes and coronary circulation.

Renin-angiotensin-aldosterone system

The RAAS is an important physiological regulator of blood pressure, fluid and electrolyte homeostasis, as well as cardiovascular regulation and remodeling. It controls the circulating volume and electrolyte balances through coordinated effects on the heart, blood vessels and kidneys via a cascade of hormones. The kidneys can regulate, in reaction to reduced renal blood flow, the synthesis of renin via conversion of its precursor prorenin. Remarkably, both renin and prorenin are released into the circulation. Plasma renin then carries out the conversion of angiotensinogen, released by the liver, to angiotensin I. Angiotensin I is subsequently converted to Ang II by the enzyme angiotensin-converting enzyme (ACE), mainly located in the endothelium of the lungs, although many other tissues can also form Ang II. Ang II is the primary effector hormone of the RAAS, acting as a strong vasoconstrictor, that can work either systemically or locally.[52] Ang II stimulates the secretion of aldosterone from the adrenals and has its effects on fluid and electrolyte balance in the kidney, closing the feedback loop. If the systemic RAAS is overactive, blood pressure will be too high with subsequent adverse events. In addition, also 'local' overactive RAAS has been linked to specific tissue damage.[53] Inhibition of the RAAS, with ACE-inhibitors, Ang II type 1 receptor blockers and mineralocorticoid receptor antagonists, not only improves blood pressure control but also ameliorates endothelial function and cardiovascular outcomes in patients with DM.[54-56] These downstream blockers of the RAAS result in an increase of plasma renin via a feedback loop.[57] Previously, this was regarded as irrelevant, as long as the downstream RAAS was being blocked. However, the discovery of the (pro)renin receptor has shed a different light on the matter,[58] suggesting that elevated plasma renin levels could result in the increased tissue uptake of renin, possibly inducing deleterious effects. This discovery has resulted in the development of more upstream RAAS inhibition with a direct renin inhibitor, which has become possible since 2007 with the clinical approval of aliskiren.[59] Renin is the first and rate-limiting step of the RAAS, and therefore a logical therapeutic target. However, its clinical benefit for cardiovascular disease still needs to be proven.

It is clear that an overactive RAAS, either systemic or local, is a major contributor to cardiovascular complications, especially in the context of DM.[50,51] The exact mechanisms of RAAS induced cardiovascular pathology in DM are still incompletely understood, but in specific tissues a discordant RAAS has been postulated as an explanation for disease, as exemplified in **part III of this thesis**.

Aim and outline of the thesis

The general aim of this thesis is to study the role of endothelium-dependent (micro)vascular alterations in cardiovascular disease, specifically in (I) CAD development, (II) after PCI and (III) in relation to DM and RAAS over-activation. We investigated the specific research questions in both patients and experimental animal models. **This thesis** is divided in three parts.

Part I Endothelial dysfunction in the development of coronary artery disease

In **chapter 2**, a patient study regarding the role of generalised microvascular endothelial dysfunction in CAD development is presented. In this study, we used a validated method of peripheral microvascular endothelial function assessment, as a possible surrogate of the coronary microcirculation. Our objective was to assess the predictive value of peripheral microvascular endothelial dysfunction as an initial test to detect the presence or absence of obstructive CAD. For more in detail study of the pathological process especially in early CAD, experimental studies with animals are necessary. In the remaining chapters of **part I**, large animal models have been used for the different stages of the CAD process, ranging from generalised early atherosclerosis to specific coronary microvascular endothelial dysfunction. In **chapter 3**, a short review regarding animal models of CAD is given, focusing on the possibilities of invasive coronary imaging modalities in these models. In this review the diabetic, atherosclerotic pig model is being introduced. This model has been subsequently used in **chapter 4** for a dietary intervention study. This study characterizes and compares the pathogenic effects of different diets in DM pigs. In this study we focused on aortic atherosclerosis development. This model of early macrovascular disease was subsequently used to study CAD in more detail. In **chapter 5**, the diabetic atherosclerotic pig model has been used to examine coronary function early in the process of CAD development. This study specifically focuses on *in vitro* coronary endothelial function via NO and ET-1 systems, with separate evaluation of coronary conduit and small arterial function. To study these alterations over time, the diabetic atherosclerotic pigs were also studied at a later time point (see **chapter 6**). This study showed the possibilities of invasive coronary imaging techniques to assess more advanced CAD within this model and also assessed *in vitro* coronary macrovascular endothelial function. In **chapter 7**, *in vitro* coronary microvascular endothelial function, was studied in detail, in this model of more advanced CAD, again focusing on NO and ET-1 systems. Finally, in **chapter 8**, a study of the same diabetic atherosclerotic pigs with more advanced CAD, showed the effects of generalized microvascular dysfunction on specific end-organs including the kidney.

Part II Endothelial dysfunction after percutaneous coronary interventions

In **chapter 9**, a review regarding endothelial dysfunction after coronary interventions, in particular after DES implantation is given. In this overview, we described different methods,

including patient examinations and animal models, of both *in vivo* and *in vitro* measurements of endothelial function after PCI, focusing on different aspects of endothelial dysfunction. Again, the porcine model is introduced as the most suitable model because of its similarities to human coronary anatomy. In **chapter 10**, the healthy porcine model is used to study the early endothelial response within the stent after different DES and BMS implantations, as well as the response of the microcirculation distal to the stent. In **chapter 11**, coronary endothelial function after different DES and BMS is being further examined with the focus on the NO- and EDHF-mediated mechanisms of coronary macro- and microvascular function distal to the stent. However, the healthy porcine heart is not a disease model, possibly hampering the translation to the patient situation with CAD. Therefore, the atherosclerotic, diabetic pig model with more advanced CAD was used to study a novel type of coronary intervention, the BVS (see **chapter 12**). Finally, coronary endothelial function of both the coronary macro- and microcirculation distal to BVS implantation was studied within this model in **chapter 13**.

Part III Endothelial dysfunction related to diabetes mellitus and the renin-angiotensin-aldosterone system

In this part, the problem of increased cardiovascular disease development in DM is studied in more detail with focus on an overactive RAAS. In particular the role of prorenin is studied, since diabetic patients have greatly elevated prorenin levels.[60] In addition, these elevated prorenin levels are an early predictor of microvascular complications in DM.[61,62] In **chapter 14**, we discussed the concept of a discordant tissue RAAS as a mediator of endothelial dysfunction leading to the cardiovascular complications of DM. In particular, the concept of the prorenin-(pro)renin receptor interaction, inducing inflammation and fibrosis resulting in cardiovascular disease, is being postulated, stating that interference in this axis might be a next logical step in the search for new therapeutic regimes to reduce DM-related cardiovascular morbidity and mortality. To examine this concept, we performed a patient study and a study in a rat model of cardiovascular disease (see **part III**). In **chapter 15**, we described which RAAS component best reflects renal RAAS activity in DM and therefore could indicate a discordant tissue RAAS in DM. In this study, we measured RAAS markers as well as markers of kidney function in urinary and plasma samples of diabetic and non-diabetic patients, with or without hypertension.

To study the prorenin- (pro)renin receptor interaction in more detail, a small animal model with cardiovascular disease was used: the diabetic hypertensive transgenic (mRen2)27 rat model. These diabetic rats express the mouse renin gene; have hypertension and elevated prorenin levels. This is therefore an ideal model of DM and an overactive RAAS to study cardiovascular dysfunction. In **chapter 16** we evaluated endothelial dysfunction in diabetic, transgenic rats treated with a specific RAAS blocker: the renin inhibitor aliskiren, or aliskiren plus the putative (pro)renin receptor antagonist 'handle region peptide' (HRP). For this purpose, we studied detailed vascular function in both conduit and small arteries *in vitro*. In **chapter 17** and in

chapter 18 the effects of RAAS blockade combined with (pro)renin receptor antagonism on damage to specific end organs, the kidneys and the eyes, were evaluated within the same rat model.

Finally, in **chapter 19** all studies of these three parts are summarised and in **chapter 20** a discussion of the studies and the clinical perspectives are given.

References

1. Haffner SM, Lehto S, Ronnemaa T, Pyorala K, Laakso M. Mortality from coronary heart disease in subjects with type 2 diabetes and in nondiabetic subjects with and without prior myocardial infarction. N Engl J Med 1998;339:229-34.
2. Buddeke, van Dis, Visseren, Vaartjes, Bots. Hart- en vaatziekten in Nederland 2016, cijfers over prevalentie, ziekte en sterfte. Den Haag: Nederlandse Hartstichting 2016.
3. Verma S, Anderson TJ. Fundamentals of endothelial function for the clinical cardiologist. Circulation 2002;105:546-9.
4. Crea F, Libby P. Acute Coronary Syndromes: The Way Forward From Mechanisms to Precision Treatment. Circulation 2017;136:1155-66.
5. Stary HC, Chandler AB, Glagov S, et al. A definition of initial, fatty streak, and intermediate lesions of atherosclerosis. A report from the Committee on Vascular Lesions of the Council on Arteriosclerosis, American Heart Association. Circulation 1994;89:2462-78.
6. Ross R. The pathogenesis of atherosclerosis: a perspective for the 1990s. Nature 1993;362:801-9.
7. Duncker DJ, Koller A, Merkus D, Canty JM, Jr. Regulation of coronary blood flow in health and ischemic heart disease. Prog Cardiovasc Dis 2015;57:409-22.
8. Vanhoutte PM. Endothelium and control of vascular function. State of the Art lecture. Hypertension 1989;13:658-67.
9. Feletou M, Vanhoutte PM. Endothelium-derived hyperpolarizing factor: where are we now? Arterioscler Thromb Vasc Biol 2006;26:1215-25.
10. Yanagisawa M, Kurihara H, Kimura S, et al. A novel potent vasoconstrictor peptide produced by vascular endothelial cells. Nature 1988;332:411-5.
11. Furchgott RF, Zawadzki JV. The obligatory role of endothelial cells in the relaxation of arterial smooth muscle by acetylcholine. Nature 1980;288:373-6.
12. Palmer RM, Ferrige AG, Moncada S. Nitric oxide release accounts for the biological activity of endothelium-derived relaxing factor. Nature 1987;327:524-6.
13. Rapoport RM, Draznin MB, Murad F. Endothelium-dependent relaxation in rat aorta may be mediated through cyclic GMP-dependent protein phosphorylation. Nature 1983;306:174-6.
14. Schachinger V, Britten MB, Zeiher AM. Prognostic impact of coronary vasodilator dysfunction on adverse long-term outcome of coronary heart disease. Circulation 2000;101:1899-906.
15. Garg S, Serruys PW. Coronary stents: current status. J Am Coll Cardiol 2010;56:S1-42.
16. Serruys PW, Kutryk MJ, Ong AT. Coronary-artery stents. N Engl J Med 2006;354:483-95.
17. Stone GW, Midei M, Newman W, et al. Randomized comparison of everolimus-eluting and paclitaxel-eluting stents: two-year clinical follow-up from the Clinical Evaluation of the Xience V Everolimus Eluting Coronary Stent System in the Treatment of Patients with de novo Native Coronary Artery Lesions (SPIRIT) III trial. Circulation 2009;119:680-6.
18. Onuma Y, Kukreja N, Piazza N, et al. The everolimus-eluting stent in real-world patients: 6-month follow-up of the X-SEARCH (Xience V Stent Evaluated at Rotterdam Cardiac Hospital) registry. J Am Coll Cardiol 2009;54:269-76.
19. James SK, Stenestrand U, Lindback J, et al. Long-term safety and efficacy of drug-eluting versus bare-metal stents in Sweden. N Engl J Med 2009;360:1933-45.
20. Ong AT, Serruys PW, Aoki J, et al. The unrestricted use of paclitaxel- versus sirolimus-eluting stents for coronary artery disease in an unselected population: one-year results of the Taxus-Stent Evaluated at Rotterdam Cardiology Hospital (T-SEARCH) registry. J Am Coll Cardiol 2005;45:1135-41.
21. Frobert O, Lagerqvist B, Carlsson J, Lindback J, Stenestrand U, James SK. Differences in restenosis rate with different drug-eluting stents in patients with and without diabetes mellitus: a report from the SCAAR (Swedish Angiography and Angioplasty Registry). J Am Coll Cardiol 2009;53:1660-7.
22. McFadden EP, Stabile E, Regar E, et al. Late thrombosis in drug-eluting coronary stents after discontinuation of antiplatelet therapy. Lancet 2004;364:1519-21.

23. Luscher TF, Steffel J, Eberli FR, et al. Drug-eluting stent and coronary thrombosis: biological mechanisms and clinical implications. Circulation 2007;115:1051-8.
24. Mauri L, Hsieh WH, Massaro JM, Ho KK, D'Agostino R, Cutlip DE. Stent thrombosis in randomized clinical trials of drug-eluting stents. N Engl J Med 2007;356:1020-9.
25. Stettler C, Wandel S, Allemann S, et al. Outcomes associated with drug-eluting and bare-metal stents: a collaborative network meta-analysis. Lancet 2007;370:937-48.
26. Joner M, Finn AV, Farb A, et al. Pathology of drug-eluting stents in humans: delayed healing and late thrombotic risk. J Am Coll Cardiol 2006;48:193-202.
27. Finn AV, Joner M, Nakazawa G, et al. Pathological correlates of late drug-eluting stent thrombosis: strut coverage as a marker of endothelialization. Circulation 2007;115:2435-41.
28. van der Giessen WJ. Experimental coronary artery occlusion and reperfusion. 1990.
29. Serruys PW, Onuma Y, Garcia-Garcia HM, et al. Dynamics of vessel wall changes following the implantation of the absorb everolimus-eluting bioresorbable vascular scaffold: a multi-imaging modality study at 6, 12, 24 and 36 months. EuroIntervention 2014;9:1271-84.
30. Brugaletta S, Heo JH, Garcia-Garcia HM, et al. Endothelial-dependent vasomotion in a coronary segment treated by ABSORB everolimus-eluting bioresorbable vascular scaffold system is related to plaque composition at the time of bioresorption of the polymer: indirect finding of vascular reparative therapy? Eur Heart J 2012;33:1325-33.
31. Dudek D, Rzeszutko L, Onuma Y, et al. Vasomotor Response to Nitroglycerine Over 5 Years Follow-Up After Everolimus-Eluting Bioresorbable Scaffold Implantation. JACC Cardiovasc Interv 2017;10:786-95.
32. Serruys PW, Ormiston J, van Geuns RJ, et al. A Polylactide Bioresorbable Scaffold Eluting Everolimus for Treatment of Coronary Stenosis: 5-Year Follow-Up. J Am Coll Cardiol 2016;67:766-76.
33. Capodanno D, Gori T, Nef H, et al. Percutaneous coronary intervention with everolimus-eluting bioresorbable vascular scaffolds in routine clinical practice: early and midterm outcomes from the European multicentre GHOST-EU registry. EuroIntervention 2015;10:1144-53.
34. Wykrzykowska JJ, Kraak RP, Hofma SH, et al. Bioresorbable Scaffolds versus Metallic Stents in Routine PCI. N Engl J Med 2017;376:2319-28.
35. Ali ZA, Serruys PW, Kimura T, et al. 2-year outcomes with the Absorb bioresorbable scaffold for treatment of coronary artery disease: a systematic review and meta-analysis of seven randomised trials with an individual patient data substudy. Lancet 2017;390:760-72.
36. Badimon L. Atherosclerosis and thrombosis: lessons from animal models. Thromb Haemost 2001;86:356-65.
37. Gerrity RG, Natarajan R, Nadler JL, Kimsey T. Diabetes-induced accelerated atherosclerosis in swine. Diabetes 2001;50:1654-65.
38. Chilian WM, Eastham CL, Marcus ML. Microvascular distribution of coronary vascular resistance in beating left ventricle. Am J Physiol 1986;251:H779-88.
39. Duncker DJ, Bache RJ. Regulation of coronary blood flow during exercise. Physiol Rev 2008;88:1009-86.
40. Celermajer DS. Reliable endothelial function testing: at our fingertips? Circulation 2008;117:2428-30.
41. Mulvany MJ, Halpern W. Contractile properties of small arterial resistance vessels in spontaneously hypertensive and normotensive rats. Circ Res 1977;41:19-26.
42. Stratton IM, Adler AI, Neil HA, et al. Association of glycaemia with macrovascular and microvascular complications of type 2 diabetes (UKPDS 35): prospective observational study. BMJ 2000;321:405-12.
43. Kones R, Rumana U. Cardiometabolic diseases of civilization: history and maturation of an evolving global threat. An update and call to action. Ann Med 2017;49:260-74.
44. Grundy SM, Benjamin IJ, Burke GL, et al. Diabetes and cardiovascular disease: a statement for healthcare professionals from the American Heart Association. Circulation 1999;100:1134-46.
45. Waller BF, Palumbo PJ, Lie JT, Roberts WC. Status of the coronary arteries at necropsy in diabetes mellitus with onset after age 30 years. Analysis of 229 diabetic patients with and without clinical evidence of coronary heart disease and comparison to 183 control subjects. Am J Med 1980;69:498-506.

46. Stein B, Weintraub WS, Gebhart SP, et al. Influence of diabetes mellitus on early and late outcome after percutaneous transluminal coronary angioplasty. Circulation 1995;91:979-89.
47. Ferreiro JL, Ueno M, Capodanno D, et al. Pharmacodynamic effects of concomitant versus staggered clopidogrel and omeprazole intake: results of a prospective randomized crossover study. Circ Cardiovasc Interv 2010;3:436-41.
48. de Jager J, Dekker JM, Kooy A, et al. Endothelial dysfunction and low-grade inflammation explain much of the excess cardiovascular mortality in individuals with type 2 diabetes: the Hoorn Study. Arterioscler Thromb Vasc Biol 2006;26:1086-93.
49. Ladeia AM, Ladeia-Frota C, Pinho L, Stefanelli E, Adan L. Endothelial dysfunction is correlated with microalbuminuria in children with short-duration type 1 diabetes. Diabetes Care 2005;28:2048-50.
50. Gilbert RE, Krum H, Wilkinson-Berka J, Kelly DJ. The renin-angiotensin system and the long-term complications of diabetes: pathophysiological and therapeutic considerations. Diabet Med 2003;20:607-21.
51. Hollenberg NK. Aldosterone in the development and progression of renal injury. Kidney Int 2004;66:1-9.
52. van Thiel BS, van der Pluijm I, te Riet L, Essers J, Danser AH. The renin-angiotensin system and its involvement in vascular disease. Eur J Pharmacol 2015;763:3-14.
53. Danser AH. Local renin-angiotensin systems: the unanswered questions. Int J Biochem Cell Biol 2003;35:759-68.
54. Lewis EJ, Hunsicker LG, Clarke WR, et al. Renoprotective effect of the angiotensin-receptor antagonist irbesartan in patients with nephropathy due to type 2 diabetes. N Engl J Med 2001;345:851-60.
55. Heart Outcomes Prevention Evaluation Study I, Yusuf S, Sleight P, et al. Effects of an angiotensin-converting-enzyme inhibitor, ramipril, on cardiovascular events in high-risk patients. N Engl J Med 2000;342:145-53.
56. Zuanetti G, Latini R, Maggioni AP, Franzosi M, Santoro L, Tognoni G. Effect of the ACE inhibitor lisinopril on mortality in diabetic patients with acute myocardial infarction: data from the GISSI-3 study. Circulation 1997;96:4239-45.
57. Castrop H, Hocherl K, Kurtz A, Schweda F, Todorov V, Wagner C. Physiology of kidney renin. Physiol Rev 2010;90:607-73.
58. Nguyen G, Delarue F, Burckle C, Bouzhir L, Giller T, Sraer JD. Pivotal role of the renin/prorenin receptor in angiotensin II production and cellular responses to renin. J Clin Invest 2002;109:1417-27.
59. Danser AH. Renin academy in focus. J Renin Angiotensin Aldosterone Syst 2007;8:212.
60. Hollenberg NK, Fisher ND, Nussberger J, Moukarbel GV, Barkoudah E, Danser AH. Renal responses to three types of renin-angiotensin system blockers in patients with diabetes mellitus on a high-salt diet: a need for higher doses in diabetic patients? J Hypertens 2011;29:2454-61.
61. Deinum J, Ronn B, Mathiesen E, Derkx FH, Hop WC, Schalekamp MA. Increase in serum prorenin precedes onset of microalbuminuria in patients with insulin-dependent diabetes mellitus. Diabetologia 1999;42:1006-10.
62. Luetscher JA, Kraemer FB, Wilson DM, Schwartz HC, Bryer-Ash M. Increased plasma inactive renin in diabetes mellitus. A marker of microvascular complications. N Engl J Med 1985;312:1412-7.

Part I

Endothelial dysfunction in the develoment of coronary artery disease

Peripheral arterial tonometry cannot detect patients at low risk of coronary artery disease

van den Heuvel M., Sorop O., Musters P.J., van Domburg R.T., Galema T.W., Duncker D.J., van der Giessen W.J. and Nieman K.

Neth Heart J. 2015 Sep;23(10):468-74

2

Peripheral arterial tonometry cannot detect patients at low risk of coronary artery disease

Mieke van den Heuvel, Oana Sorop, Paul J. Musters, Ron T. van Domburg, Tjebbe W. Galema, Dirk J. Duncker, Wim J. van der Giessen, Koen Nieman

Published online: 29 May 2015

Abstract
Background Endothelial dysfunction precedes coronary artery disease (CAD) and can be measured by peripheral arterial tonometry (PAT). We examined the applicability of PAT to detect a low risk of CAD in a chest pain clinic.
Methods In 93 patients, PAT was performed resulting in reactive hyperaemia (RHI) and augmentation (AIx) indices. Patients were risk classified according to HeartScore, Diamond and Forrester pretest probability (DF), exercise testing (X-ECG), and computed tomography calcium scoring (CCS) and angiography (CTA). Correlations, risk group differences and prediction of revascularisation within 1 year were calculated.
Results RHI correlated with HeartScore ($r=-0.21$, $p=0.05$), AIx with DF ($r=0.26$, $p=0.01$). However, both were not significantly different between normal and ischaemic X-ECG groups. In addition RHI and AIx were similar between low risk as compared with intermediate-to-high risk, based on risk algorithms (RHI: 1.98 (0.67) vs 1.94 (0.78); AIx: 0.0 (21) vs 5.0 (25); $p=$NS), or CCS and CTA (RHI: 1.99 (0.58) vs 1.89 (0.82); AIx: −2.0 (24) vs 4.0 (25); $p=$NS). Finally, RHI and AIx failed to predict revascularisation (RHI: OR 1.42, CI 0.65–3.1; AIx: OR 1.02, CI 0.98–1.05).
Conclusions PAT cannot detect a low risk of CAD, possibly because RHI and AIx versus X-ECG, CCS and CTA represent independent processes.

Keywords Coronary artery disease · Peripheral vascular function · Noninvasive testing

Willem J. van der Giessen died on 6 June 2011

M. van den Heuvel (✉)
Department of Experimental Cardiology, Ee2355, Erasmus Medical Center,
Dr. Molewaterplein 50–60,
3015 GE Rotterdam, The Netherlands
e-mail: m.vandenheuvel.1@erasmusmc.nl

P.J. Musters · O. Sorop · M. van den Heuvel · R.T. van Domburg · T.W. Galema · D.J. Duncker · W.J. van der Giessen · K. Nieman
Department of Cardiology, Erasmus Medical Center Rotterdam,
's-Gravendijkwal 230,
3015 CE Rotterdam, The Netherlands

K. Nieman
Department of Radiology, Erasmus Medical Center Rotterdam,
Utrecht, The Netherlands

W.J. van der Giessen · O. Sorop · M. van den Heuvel
ICIN Netherlands Heart Institute,
Utrecht, The Netherlands

Introduction

Chest pain is a common symptom that may be caused by obstructive coronary artery disease (CAD) and requires risk stratification to assess the probability of CAD [1]. Risk algorithms have been developed based on combinations of risk factors [2, 3]. However, these models tend to overestimate the prevalence of CAD [4], and are based on population calculations rather than a direct assessment of the atherosclerotic process within an individual. Diagnostic testing with exercise electrocardiography (X-ECG) is considered to be highly discriminative [5], however is often inconclusive. Alternative tests using pharmacological stress are usually not immediately available. Computed tomography (CT) is expanding in the workup [1], using coronary calcium scoring (CCS) [6] and computed tomographic angiography (CTA) [7]. However, there are associated disadvantages such as costs, radiation exposure and administration

of contrast agent [8]. Therefore, a better discrimination of patients at low risk of clinically relevant CAD will facilitate more efficient use of subsequent diagnostics.

Endothelial dysfunction precedes and contributes to the atherosclerotic disease process. Peripheral arterial tonometry (PAT) has emerged as an easy, noninvasive test to study endothelial function at the fingertip [9, 10]. From one single PAT measurement both the reactive hyperaemia index (RHI), indicating endothelium-dependent vasodilation [11], and the augmentation index (AIx), indicating arterial stiffness [12], can be derived. RHI and AIx have shown to be altered in the presence of CAD [12–15], and can be used in CAD risk stratification [16]. However, although PAT appears promising in research settings, validation in the clinical setting beside conventional measures has only been limited [11]. Therefore, the objective of this cross-sectional study was to assess the applicability of PAT to detect low risk of clinically relevant CAD in unselected patients visiting a rapid-access outpatient chest pain clinic.

Methods

Study population

From September 2009 to February 2010, 93 consecutive patients with new onset stable chest pain without evidence of ongoing ischaemia and no prior history of CAD gave written consent to undergo finger plethysmography to measure PAT at the same time as their chest pain evaluation, after study approval by the Medical Ethics Committee. The sample size was comparable with previous PAT validation studies [11, 12, 16], and sufficiently large to observe discriminating tendencies [17]. There were no exclusion criteria. All patients were scheduled to undergo conventional diagnostics. Based on cut-off values of these diagnostics, patients at low risk of clinically relevant CAD were identified. This was verified by evaluating revascularised patients by percutaneous coronary intervention (PCI) or coronary artery bypass grafting (CABG) for up to 1 year.

Risk profiling

Cardiovascular risk factors were summarised using the HeartScore risk algorithm [3] to assess the risk of 10-year mortality of CAD and the Diamond and Forrester model (DF) [2, 4] to assess the pretest probability of CAD.

Exercise electrocardiography

X-ECG was performed by standardised protocol [5]. A non-diagnostic result was defined as discontinuation without evidence of myocardial ischaemia before reaching 85% of the target heart rate. Results were described as being non-ischaemic, inconclusive or ischaemic. Only non-ischaemic and ischaemic groups were taken into comparative anal.

Cardiac computed tomography

A non-enhanced CT scan was performed to assess the amount of coronary calcium, followed by a contrast-enhanced scan to assess plaque burden and presence of stenotic CAD. Image acquisition was conducted using a 128-slice dual-source CT (Siemens Flash, Forchheim, Germany). Coronary arteries were quantitatively evaluated per coronary segment for presence of atherosclerotic plaque and >50% stenosis [7]. CCS and total number of plaques and stenoses per patient were included in the analysis.

Peripheral arterial tonometry

The PAT response was measured with the EndoPAT 2000 device (Itamar Medical Ltd., Caesarea, Israel), according to a standardised protocol allowing simultaneous determination of both RHI and AIx. An index of pulse wave amplitude at rest and during reactive hyperaemia resulted in RHI, a measure of endothelium-dependent vasodilation [9–11, 13, 16]. Augmentation of the central pulse pressure allowed determination of AIx, representing endothelium-dependent arterial stiffness [12, 18].

Statistical analysis

Summary data are presented as numbers (proportion) or expressed as mean ± standard deviation or median (interquartile range). In case of non-normal distribution, data were logarithmically transformed before analysis. Correlations between RHI, AIx and conventional diagnostics were analysed using Pearson's correlation coefficient. Differences between two groups were assessed by *t*-testing. The predictive value of RHI and AIx for revascularisation was analysed using logistic regression and described as odds ratio (OR) with corresponding 95% confidence interval (CI). Two-tailed $p < 0.05$ was considered significant.

Results

Conventional diagnostic characteristics

Overall, patients were middle aged with equal distribution between genders (Table 1). None had a history of CAD, but cardiovascular risk factors were abundant and three quarters used cardiovascular medication. In all, conventional diagnostics besides PAT were performed to examine clinically relevant CAD (Table 2). This allowed us to examine corre-

Table 1 Patient characteristics

Demographics	
Age (years)	56 ± 11
Women	40 (43 %)
Risk factors	
Nicotine abuse	23 (25 %)
Hypertension	56 (60 %)
Diabetes mellitus	20 (22 %)
Dyslipidaemia	56 (60 %)
Body mass index (kg/m^2)	28 ± 5
Family history of cardiovascular disease	44 (47 %)
History of vascular disease	9 (10 %)
Cardiovascular medication use	70 (75 %)
Revascularisation	
PCI	10 (11 %)
CABG	2 (2 %)

PCI percutaneous coronary intervention, *CABG* coronary artery bypass grafting.

Table 2 Diagnostic characteristics

Risk scores	
HeartScore low-intermediate risk < 5 %	50 (55 %)
HeartScore high risk ≥ 5 %	41 (45 %)
Median HeartScore	4 (6)
DF low pretest probability < 30 %	24 (26 %)
DF intermediate pretest probability 30–70 %	38 (41 %)
DF high pretest probability > 70 %	31 (33 %)
Median DF pretest probability	55 (51)
X-ECG	
X-ECG	85 (91 %)
Inconclusive	32 (38 %)
Non-ischaemic	44 (52 %)
Ischaemic	9 (11 %)
CT	
CCS	92 (99 %)
Median CCS	6.1 (94)
CTA	91 (98 %)
Median plaques	6.0 (14)
Median stenosis	0 (1)
PAT	
RHI	90 (97 %)
Median RHI	1.95 (0.76)
AIx	92 (99 %)
Median Aix	3.0 (23)

DF Diamond and Forrester model, *X-ECG* exercise electrocardiography, *CT* computed tomography, *CCS* coronary calcium scoring, *CTA* computed tomography angiography, *PAT* peripheral arterial tonometry, *RHI* reactive hyperaemia index, *AIx* augmentation index.

lations between PAT and conventional diagnostics, as well as sub-group analysis for these outcomes and prediction of revascularisation within 1 year.

Digital pulse arterial tonometry testing

With regard to risk algorithms, RHI correlated weakly with HeartScore ($r = -0.21$, $p = 0.05$, Fig. 1a), whereas AIx did not ($r = 0.15$, $p =$ NS, Fig. 1b). Surprisingly, RHI did not correlate with DF ($r = 0.05$, $p =$ NS, Fig. 1c), whereas AIx did modestly ($r = 0.26$, $p < 0.05$, Fig. 1d). With regard to CT parameters, no significant correlations between RHI and CCS ($r = -0.09$, $p =$ NS), plaque ($r = -0.09$, $p =$ NS, Fig. 1e) or stenosis ($r = -0.08$, $p =$ NS) were found. Also no significant associations between AIx and CCS ($r = 0.06$, $p =$ NS), plaque ($r = 0.11$, $p =$ NS, Fig. 1f) or stenosis ($r = 0.03$, $p =$ NS) were observed.

To analyse low risk of clinically relevant CAD more specifically, patients were divided into low or intermediate-to-high risk groups based on the outcomes of risk scores, X-ECG and CT. According to the risk algorithms, patients at low risk ($n = 18$; defined as low risk of both DF and HeartScore outcomes) showed similar RHI and AIx values as compared with intermediate-to-high risk ($n = 72$; defined as intermediate-to-high risk of DF or HeartScore outcome), respectively (RHI: 1.98 (0.67) vs 1.94 (0.78); AIx: 0.00 (21) vs 5.0 (25); all $p =$ NS; Fig. 2a, b). According to X-ECG results, low risk ($n = 43$; defined as a negative X-ECG outcome) also did not significantly differ from high risk ($n = 7$; defined as a positive outcome), respectively (RHI: 1.97 (0.72) vs 1.58 (0.61); AIx: −0.50 (19) vs 8.0 (29); all $p =$ NS). According to CT outcomes, low risk ($n = 20$; defined as absence of calcium, plaque and stenosis) resembled intermediate-to-high risk ($n = 68$; defined as presence of calcium, plaque or stenosis) (RHI: 1.99 (0.58) vs 1.89 (0.82); AIx: −2.0 (24) vs 4.0 (25); all $p =$ NS; Fig. 2c, d).

Finally, both RHI and AIx could not predict revascularisation within 1 year (RHI: OR 1.42, CI 0.65–3.1; AIx: OR 1.02, CI 0.98–1.05). Although RHI was lower in the revascularised group, this was not significantly different (revascularisation + ($n = 11$) vs revascularisation − ($n = 79$): 1.94 (1.06) vs 1.96 (0.70), $p =$ NS; Fig. 3a). Also AIx showed a tendency towards an altered response in the revascularised group, however again not statistically significant (revascularisation + ($n = 11$) vs revascularisation − ($n = 81$): 4.0 (27) vs 2.0 (23), $p =$ NS; Fig. 3b). This is in contrast to conventional diagnostics: the revascularised group ($n = 7$) showed significantly more ischaemic X-ECG outcomes than the non-revascularised group ($n = 46$) (0.71 ± 0.18 vs 0.09 ± 0.04; $p < 0.01$); CCS showed a modest prediction (OR 1.01, CI 1.00–1.03), whereas CTA-assessed plaque (OR 1.11, CI 1.05–1.17) and stenosis (OR 2.8, CI 1.60–4.8) showed strong predictions of revascularisation.

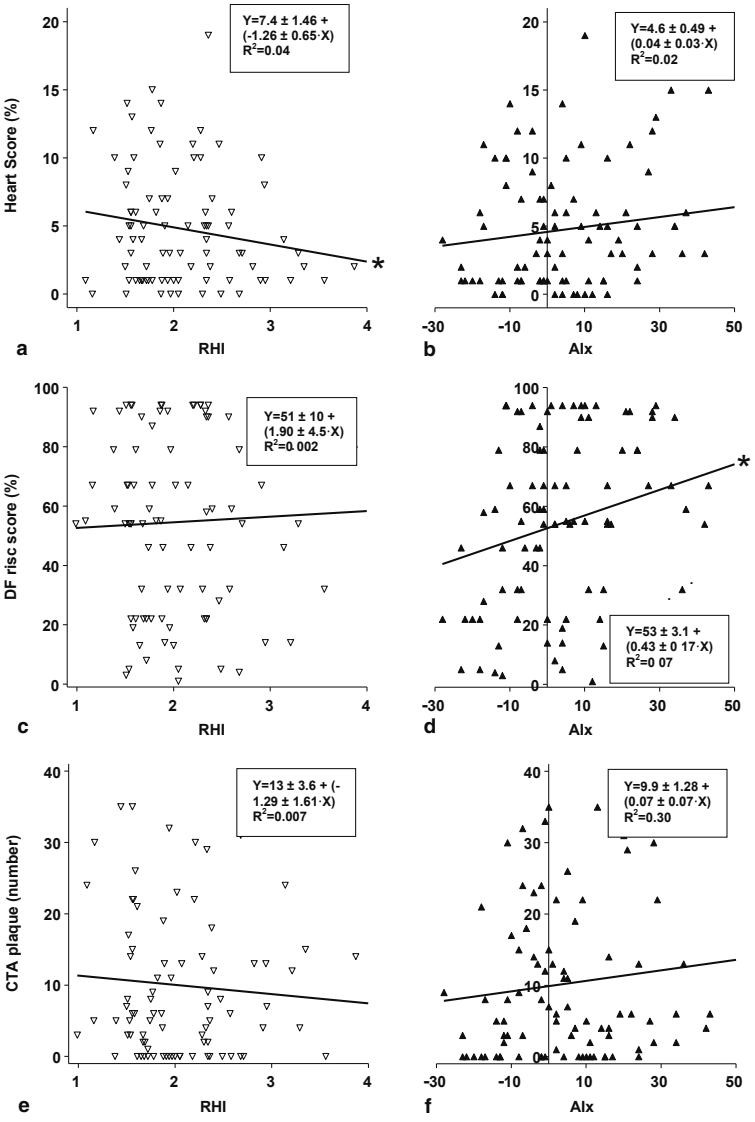

Fig. 1 Correlation graphs of reactive hyperaemia index (RHI) (panels a, c, e) and augmentation index (AIx) (panels b, d, f) with HeartScore (panels a, b), Diamond and Forrester pretest probability (DF) (panels c, d) and total amount of plaque assessed by computed tomographic angiography (CTA) (panels e, f). Regression equation and R^2 correlation coefficient are depicted per panel. Significant associations were observed between RHI and HeartScore as well as between AIx and DF, $*P \leq 0.05$

Discussion

The present study examined the applicability of PAT-derived RHI and AIx to identify patients at low risk of clinically relevant CAD. The most important findings were (i) that although RHI and AIx correlated weakly with CAD risk estimates, (ii) both RHI and AIx were not related with X-ECG or CT-imaged parameters. (iii) Most importantly, low risk based on conventional diagnostics showed non-discriminative RHI and AIx outcomes. (iv) Finally, both RHI and AIx failed to predict revascularisation within 1 year.

Clinical applicability of PAT

(i) We confirmed the modest relation of RHI with traditional risk factors, as reported previously [13]. AIx showed a weak

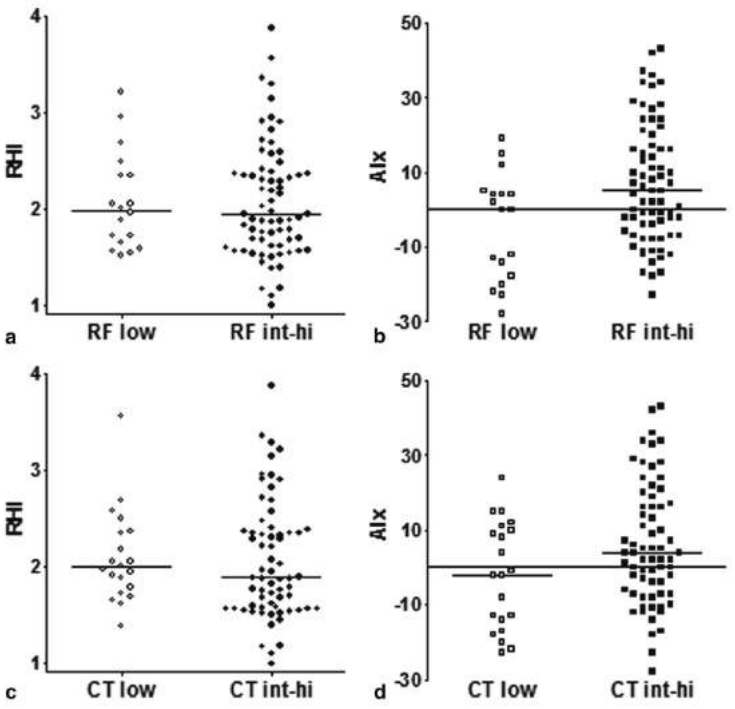

Fig. 2 Differences of reactive hyperaemia index (RHI) (panels a, c) and augmentation index (AIx) (panels b, d) between patients at low and intermediate-to-high risk of clinically relevant CAD based on the combined outcome of risk scores (a, b), and CCS and CTA assessed plaque and stenosis (c, d). Horizontal bars depict the median value. No significant differences between the groups were observed. *RF* risk factors, *X-ECG* exercise ECG, *CT* computed tomography, *low* low risk, *int-hi* intermediate-to-high risk

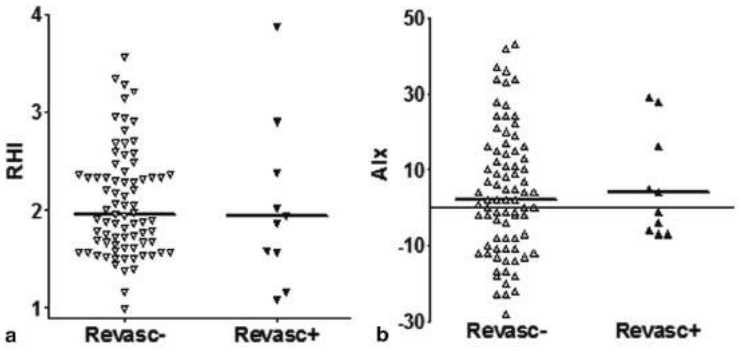

Fig. 3 Differences of reactive hyperaemia index (RHI) (panel a) and augmentation index (AIx) (panel b) between patients with and without revascularisation up to 1 year after PAT measurement. Horizontal bars depict the median value. No significant differences between the groups were observed. *Revasc* − no revascularisation; *Revasc* + revascularisation

correlation with the pretest probability of CAD. Patvardhan et al. [12] reported a strong association between AIx and age, most likely the basis for this correlation. (ii) No significant differences in either RHI or AIx were observed based on X-ECG outcome. This is remarkable since X-ECG is considered to be highly discriminative in patients at risk of obstructive CAD [5], and also RHI has shown to be able to discriminate between presence or absence of CAD [11]. Indeed, ischaemic X-ECG outcomes were more frequently present in revascularised patients of the present study whereas RHI was non-discriminative, making an independent relation likely. In addition, RHI and AIx did not significantly correlate with CCS, in contrast to a prior study of selected patients [19]. Han et al. [20] also showed no association between coronary endothelial dysfunction and calcification, reflecting that both can represent separate disease stages. In addition, brachial AIx was not independently associated with CCS [21], supporting our results. Indeed,

other vascular function tests have previously indicated that endothelial dysfunction may represent an independent response in the progression of CAD, whereas a relation with the development of atherosclerosis exists [22–26]. RHI and AIx were not significantly associated with CTA-imaged plaque or stenosis. This is contrary to previous studies with imaged CAD describing specific subgroups with proven CAD [11, 12], diabetes [14], or women [15] although the presence of CAD was not verified with CTA in any of them. (iii) Also, RHI and AIx were not able to differentiate low risk of clinically relevant CAD, in contrast to results in selected populations [11, 12, 16], complicating comparison with our unselected population. (iv) Finally, RHI and AIx failed to predict revascularisation within 1 year, contrary to Rubinshtein, who showed that RHI independently predicted revascularisation [27]. Also radial AIx predicted revascularisation [28], although for digital AIx no such studies exist to our knowledge. However, again selected patients were evaluated with adverse events occurring at long-term follow-up, which is difficult to compare with our 1-year evaluation. Indeed, patient selection may strongly influence outcome because specific risk factors have additional effects on the measurement itself besides on the CAD process, as highlighted by the study of Gargiulo [14].

Conclusions

In spite of the pathophysiological basis of endothelial dysfunction in CAD and the promising results with PAT in selected populations under controlled conditions, we found no evidence to support PAT as a diagnostic tool to detect low risk of clinically relevant CAD in an unselected outpatient population.

Acknowledgements The article is dedicated to Professor Dr. W.J. van der Giessen who sadly passed away on 6 June 2011.

Funding The present study was funded by the Erasmus Medical Center as a pilot study.

Conflict of interests None reported.

References

1. Montalescot G, Sechtem U, Achenbach S, et al. 2013 ESC guidelines on the management of stable coronary artery disease: the Task Force on the management of stable coronary artery disease of the European Society of Cardiology. Eur Heart J. 2013;34:2949–3003.
2. Diamond GA. A clinically relevant classification of chest discomfort. J Am Coll Cardiol. 1983;1:574–5.
3. Thomsen T. HeartScore: a new web-based approach to European cardiovascular disease risk management. Eur J Cardiovasc Prev Rehabil. 2005;12:424–6.
4. Genders TS, Steyerberg EW, Alkadhi H, et al. A clinical prediction rule for the diagnosis of coronary artery disease: validation, updating, and extension. Eur Heart J. 2011;32:1316–30.
5. Gibbons RJ, Balady GJ, Beasley JW, et al. ACC/AHA guidelines for exercise testing: executive summary. A report of the American College of Cardiology/American Heart Association Task Force on Practice Guidelines (Committee on Exercise Testing). Circulation. 1997;96:345–54.
6. Dedic A, Rossi A, Ten Kate GJ, et al. First-line evaluation of coronary artery disease with coronary calcium scanning or exercise electrocardiography. Int J Cardiol. 2013;163:190–5.
7. Nieman K, Galema T, Weustink A, et al. Computed tomography versus exercise electrocardiography in patients with stable chest complaints: real-world experiences from a fast-track chest pain clinic. Heart. 2009;95:1669–75.
8. Smith-Bindman R, Lipson J, Marcus R, et al. Radiation dose associated with common computed tomography examinations and the associated lifetime attributable risk of cancer. Arch Intern Med. 2009;169:2078–86.
9. Lekakis J, Abraham P, Balbarini A, et al. Methods for evaluating endothelial function: a position statement from the European Society of Cardiology Working Group on Peripheral Circulation. Eur J Cardiovasc Prev Rehabil. 2011;18:775–89.
10. Flammer AJ, Anderson T, Celermajer DS, et al. The assessment of endothelial function: from research into clinical practice. Circulation. 2012;126:753–67.
11. Kuvin JT, Mammen A, Mooney P, et al. Assessment of peripheral vascular endothelial function in the ambulatory setting. Vasc Med. 2007;12:13–6.
12. Patvardhan E, Heffernan KS, Ruan J, et al. Augmentation index derived from peripheral arterial tonometry correlates with cardiovascular risk factors. Cardiol Res Pract. 2011;2011:253758.
13. Hamburg NM, Keyes MJ, Larson MG, et al. Cross-sectional relations of digital vascular function to cardiovascular risk factors in the Framingham Heart Study. Circulation. 2008;117:2467–74.
14. Gargiulo P, Marciano C, Savarese G, et al. Endothelial dysfunction in type 2 diabetic patients with normal coronary arteries A digital reactive hyperemia study. Int J Cardiol. 2013;165:67–71.
15. Matsuzawa Y, Sugiyama S, Sugamura K, et al. Digital assessment of endothelial function and ischemic heart disease in women. J Am Coll Cardiol. 2010;55:1688–96.
16. Heffernan KS, Karas RH, Patvardhan EA, et al. Peripheral arterial tonometry for risk stratification in men with coronary artery disease. Clin Cardiol. 2010;33:94–8.
17. Sauder KA, West SG, McCrea CE, et al. Test-retest reliability of peripheral arterial tonometry in the metabolic syndrome. Diab Vasc Dis Res. 2014;11:201–7.
18. Laurent S, Cockcroft J, Van Bortel L, et al. Expert consensus document on arterial stiffness: methodological issues and clinical applications. Eur Heart J. 2006;27:2588–605.
19. Li J, Flammer AJ, Nelson RE, et al. Normal vascular function as a prerequisite for the absence of coronary calcification in patients free of cardiovascular disease and diabetes. Circ J. 2012;76:2705–10.
20. Han SH, Gerber TC, Suwaidi JA, et al. Relationship between coronary endothelial function and coronary calcification in early atherosclerosis. Atherosclerosis. 2010;209:197–200.
21. Park JS, Choi UJ, Lim HS, et al. The relationship between coronary artery calcification as assessed by multi-detector computed tomography and arterial stiffness. Clin Exp Hypertens. 2011;33:501–5.

22. Jambrik Z, Venneri L, Varga A, et al. Peripheral vascular endothelial function testing for the diagnosis of coronary artery disease. Am Heart J. 2004;148:684–9.
23. Frick M, Suessenbacher A, Alber HF, et al. Prognostic value of brachial artery endothelial function and wall thickness. J Am Coll Cardiol. 2005;46:1006–10.
24. Venneri L, Poggianti E, Jambrik Z, et al. The elusive prognostic value of systemic endothelial function in patients with chest pain syndrome. Int J Cardiol. 2007;119:109–11.
25. Nishimura RA, Lerman A, Chesebro JH, et al. Epicardial vasomotor responses to acetylcholine are not predicted by coronary atherosclerosis as assessed by intracoronary ultrasound. J Am Coll Cardiol. 1995;26:41–9.
26. Asselbergs FW, Monnink SH, Jessurun GA, et al. Assessing the prognostic value of coronary endothelial function in patients referred for a first coronary angiogram. Am J Cardiol. 2004;94:1063–7.
27. Rubinshtein R, Kuvin JT, Soffler M, et al. Assessment of endothelial function by non-invasive peripheral arterial tonometry predicts late cardiovascular adverse events. Eur Heart J. 2010;31:1142–8.
28. Weber T, Auer J, O'Rourke MF, et al. Increased arterial wave reflections predict severe cardiovascular events in patients undergoing percutaneous coronary interventions. Eur Heart J. 2005;26:2657–63.

Invasive coronary imaging in animal models of atherosclerosis

van Ditzhuijzen N.S.*, van den Heuvel M.*, Sorop O., van Duin R.W., Krabbendam-Peters I., van Haeren R., Ligthart J.M., Witberg K.T., Duncker D.J., Regar E., van Beusekom H.M. and van der Giessen W.J.
*Shared first authorship

Neth Heart J. 2011 Oct;19(10):442-6

3

Invasive coronary imaging in animal models of atherosclerosis

Nienke S. van Ditzhuijzen, Mieke van den Heuvel, Oana Sorop, Richard W.B. van Duin, Ilona Krabbendam-Peters, Rorry van Haeren, Jurgen M.R. Ligthart, Karen T. Witberg, Dirk J. Duncker, Evelyn Regar, Heleen M.M. van Beusekom, Wim J. van der Giessen

Published online: 9 September 2011

Experimental disease models have enhanced our understanding of the pathogenesis of atherosclerosis development. For example, insight has been gained into the role of the endothelium, lipids, platelets and inflammation, as well as into potential diagnostic and therapeutic interventions. Moreover, transgenic and knock-out technologies have become a widespread approach and this is a growing field to assess the role of individual genes in vascular biology and pathology. However, atherosclerosis is most of all a multifactorial disease, influenced by a multitude of environmental factors. Therefore, it is important to also study non-transgenic animal models that closely resemble the human situation with atherosclerotic lesions at anatomical locations that mimic the clinical manifestation of the disease, e.g. coronary artery disease (CAD). Although no model completely mimics human atherosclerosis, much can be learned from existing models in the study of this disease, also with respect to the development of new interventions. Here, we describe the most relevant animal models of atherosclerosis, while focusing on CAD development and the use of coronary diagnostic and therapeutic interventions. In addition, we show examples of features of a large animal model of CAD including pictures of invasive coronary imaging.

Nienke S. van Ditzhuijzen and Mieke van den Heuvel contributed equally to the manuscript

N. S. van Ditzhuijzen · M. van den Heuvel · O. Sorop · R. W. B. van Duin · I. Krabbendam–Peters · R. van Haeren · J. M. R. Ligthart · K. T. Witberg · D. J. Duncker (✉) · E. Regar · H. M. M. van Beusekom · W. J. van der Giessen
Department of Cardiology, Thoraxcenter,
Cardiovascular Research School (COEUR),
Erasmus University Medical Center,
Dr. Molewaterplein 50-60,
3015 GE Rotterdam, the Netherlands
e-mail: d.duncker@erasmusmc.nl

M. van den Heuvel
Department of Internal Medicine,
Erasmus University Medical Center,
Rotterdam, the Netherlands

N. S. van Ditzhuijzen · M. van den Heuvel · O. Sorop · W. J. van der Giessen
Interuniversity Cardiology Institute of the Netherlands (ICIN-KNAW),
Catharijnesingel 52,
3511 GC Utrecht, the Netherlands

Small versus large animal models

Small animal models, primarily small rodents and rabbits, have been used extensively in atherosclerosis research. Some of the reasons include low costs, availability, and easy usability (Table 1). However, mice do not spontaneously develop atherosclerosis without genetic manipulation since they have a lipid profile that is different from humans. Yet, due to genetic modification and cross-breeding specific strains can be generated and used to unravel molecular mechanisms involved in the atherosclerosis process [1]. However transgenic mouse models do not typically develop advanced lesions, including plaque rupture and thrombosis [2], which is typical in patients presenting with symptomatic disease. When size becomes more important, small animal models need to be complemented by larger animal models in which vessel characteristics are more similar to human arteries. The rabbit model on a high cholesterol diet has been widely used in the study of experimental atherosclerosis (Table 1). Combined with arterial wall injury, lesions at least partly resembling human plaque will develop in the aorta or iliac arteries of this model [3]. However, when coronary atherosclerosis is the object of study, pigs seem to be the most representative model (Table 1). Pigs have a highly similar anatomy and

Table 1 Animal models of atherosclerosis

Animal model	Advantages	Limitations
Mouse	1 Rapid development of atherosclerotic plaque	1 Limited resemblance to humans
	2 Short reproductive cycle+large litters	2 Limited complex atherosclerotic lesion formation
	3 Well-known genome+genome manipulation possible	3 Very high levels of blood lipids+different lipid profile
	4 Cheap	
Rat	1 Useful as restenosis model	1 No development of atherosclerotic lesions
	2 Cheap	
Rabbit	1 Fibroatheroma lesions	1 Need for high plasma cholesterol levels to develop atherosclerosis
	2 Useful as restenosis model	2 No plaque rupture model
	3 Affordable	3 Model for neointima formation+re-endothelialisation rather than atherosclerosis
		4 Coronary evaluation difficult
Pig	1 Atherosclerotic lesions similar to human disease	1 Expensive
	2 Blood lipids in human range	2 Difficult to handle due to size
	3 Invasive coronary imaging possible	3 Limited genomic tools
	4 Useful as restenosis model post-intervention	
	5 Useful for detailed coronary endothelial function studies	
Monkey	1 Atherosclerotic lesions similar to human disease	1 Ethical concerns
	2 Influence of behavioural factors, e.g. psychosocial stress	2 Very expensive
	3 Influence of hormonal status	3 Difficult to handle

physiology of the coronary system as compared to humans [4]. In addition, with use of toxin-mediated pancreatic damage and a high fat diet, human diabetes mellitus (DM)-like metabolic alterations will develop [5], followed by coronary lesions resembling the human condition closely with even some characteristics of vulnerable plaque [6, 7]. Historically monkeys have also been considered to be a good model of human atherosclerosis (Table 1); in particular the effects of hormones and the role of behaviour can be studied with this model [8, 9]. However, nowadays monkeys are not widely used due to obvious species-specific ethical concerns and costs [2].

In the validation process of coronary interventional devices and therapies for diagnosis and treatment of human CAD, both healthy rabbit [10] and pig models [11] have been used extensively, although the rat model has also been used occasionally [12] (Table 1). In these models, arterial overstretch injury with stenting will result in a restenosis process with re-endothelialisation, inflammation and neointima formation. However, these are healthy animal models in which the vascular healing response occurs faster than in diseased humans [10, 11]. Therefore, the USA Food and Drug Administration has proposed a guidance that new coronary diagnostic and therapeutic interventional devices need to be tested in more clinically relevant animal models of disease (6255companion.doc, 2008). Since the porcine model is

Table 2 Plasma characteristics

Plasma markers	Diabetic pigs	Non-diabetic pigs	Two-way ANOVA
Glucose (mmol/l)			$P<0.01$[a]
9 months	15±2.9*	4.1±0.27	
12 months	13±2.3*	4.5±0.47	
15 months	18±4.5*	5.1±0.42	
Triglycerides (mmol/l)			$P=0.02$[a]
9 months	1.15±0.26	0.64±0.27	
12 months	0.95±0.25	0.44±0.08	
15 months	1.26±0.50	0.64±0.19	
Cholesterol (mmol/l)			$P=0.86$
9 months	20±2.0	20±2.6	
12 months	18±1.8	19±2.0	
15 months	17±1.7	18±2.7	
LDL cholesterol (mmol/l)			$P=0.75$
9 months	17±1.9	16±2.2	
12 months	15±1.6	15±1.9	
15 months	14±1.7	15±2.5	
HDL cholesterol (mmol/l)			$P=0.13$
9 months	5.2±0.22	5.8±0.21	
12 months	5.7±0.31	5.7±0.31	
15 months	5.1±0.40	5.7±0.35	

Values are mean±SEM,
* $P<0.05$ diabetic vs. non-diabetic pigs at corresponding time points, [a] diabetic vs. non-diabetic pigs over time

LDL low density lipoprotein, *HDL* high density lipoprotein

the only model in which CAD can be truly studied and catheters and coronary interventional devices can be applied to the vascular bed they are designed for, this model might be considered the most suitable [13]. New types of invasive coronary imaging techniques have already been applied in the pig model, e.g. optical coherence tomography (OCT) in healthy porcine coronaries [14] and intravascular ultrasound (IVUS) in diseased porcine coronaries [7].

Present animal model

In light of the considerations outlined above, the present study was undertaken to investigate coronary atherosclerosis development over time with the use of a diseased porcine model. The study was performed in accordance with the Guide for the Care and Use of Laboratory Animals (NIH Publication No. 85-23, revised 1996), and with approval of the Erasmus MC Animal Care committee. For this purpose, diabetes was induced in a subgroup of male crossbred (Yorkshire x Landrace) pigs by single dose injection of streptozotocin (140 mg/kg) to give a subtotal destruction of pancreatic beta-cells, as described previously [5]. After 2 weeks of stable DM induction, a high fat atherogenic diet was introduced to all pigs. The pigs (diabetic: n=8; non-diabetic: n=7) were adjusted to this diet and followed up to study atherosclerosis development over time up to 15 months. Similar growth patterns were achieved in all pigs via adjustment of individual caloric intake. Moreover, blood glucose levels were monitored in diabetic pigs and insulin therapy was

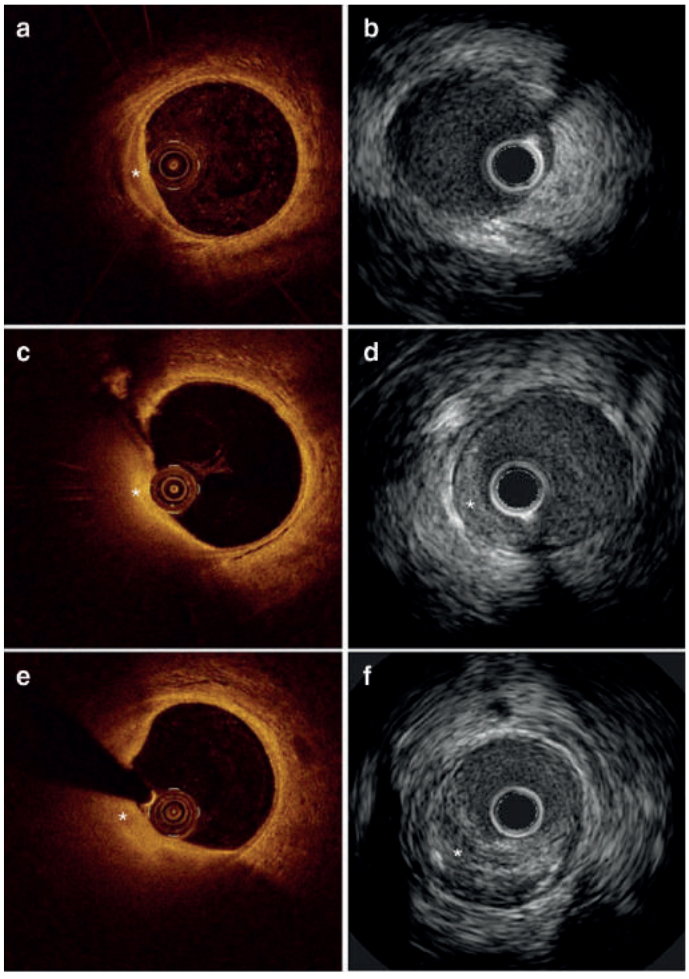

Fig. 1 Typical example of the development of an atherosclerotic plaque over time on OCT and IVUS in a diabetic pig; **a** OCT of intimal hyperplasia at 9 months (*); **b** IVUS of the same cross section as shown in **a** fails to clearly detect the early lesion; **c+d** OCT and IVUS of the growing plaque at 12 months (*); **e+f** OCT and IVUS of the same growing plaque at 15 months (*)

started only when plasma ketones appeared, to prevent severe DM-related complications. Anaesthetised pigs were imaged at 9, 12 and 15 months of study duration by two invasive coronary imaging modalities. Moreover, arterial blood samples were taken at these time points. A subgroup of pigs (n=5) was sacrificed at 12 months, the remaining animals (n=10) at 15 months to obtain coronary tissue for histology. Afterwards, plasma concentrations of glucose, total cholesterol, and low and high density lipoprotein (LDL and HDL) cholesterol were measured at the clinical chemical laboratory of the Erasmus MC using standard protocols.

Imaging modalities

Two invasive coronary imaging modalities were used in the present study: OCT and gray-scale IVUS. OCT, using an infrared light source, has an imaging depth of approximately 1.5 mm into tissue, an axial resolution of 10–15 μm and a lateral resolution of 25–40 μm. This image resolution of OCT offers the potential to assess coronary atherosclerosis in detail [15, 16]. Evaluation of atherosclerosis by OCT was performed in vivo in all pigs at 9, 12 and 15 months using the C7 XR Fourier-Domain OCT system (St. Jude Medical, Westford, MA, USA). Cross-sectional images were acquired at 100 frames per second with an automatic pullback speed of 20 mm/s.

The limited penetration depth of OCT is a shortcoming for the assessment of the total vessel wall, particularly in case of a diseased vessel. Therefore, in case of a plaque thickness >1.5 mm, evaluation of the plaque was done by gray-scale IVUS using an automated pullback speed of 0.5 mm/s (Atlantis SR Pro, Boston Scientific Corp., Natick, MA, USA). During pullback acquisition, images were obtained at a rate of 30 frames/s. This technique, using sound instead of light, has an axial resolution of 80–200 μm and a lateral resolution of 200–400 μm. The penetration depth is 4–8 mm, which permits visualisation of the total vessel wall and therefore precise assessment of the extent of atherosclerosis within a segment of a coronary artery [17].

Preliminary results

In diabetic pigs, plasma glucose levels were elevated at every measured time point as compared with the non-diabetic pigs (Table 2, P<0.05). Moreover in this group of pigs, plasma triglycerides were increased over time (Table 2, P<0.05) as well. Since both groups were fed an atherogenic diet, both showed elevated total cholesterol, LDL and HDL levels, which were not different over time (Table 2). In summary, diabetic pigs showed human-like DM characteristics of hyperglycaemia and triglyceridaemia, whereas all pigs showed evidence of hypercholesterolaemia.

These metabolic alterations were accompanied by coronary atherosclerosis development. Indeed, at 9 months small early lesions could be detected in the coronary arteries of most pigs, specifically seen with OCT imaging (Fig. 1a). With IVUS this early stage of atherosclerosis was not visible (Fig. 1b). Over time (12 and 15 months), these lesions showed progression, both in size and in quantity as exemplified with OCT and IVUS (Fig. 1c - f). Histology at 12 months confirmed the formation of more complex coronary atherosclerosis at this time point, consisting of lipid accumulation and calcification also seen on IVUS (Fig. 2a - c). All pigs

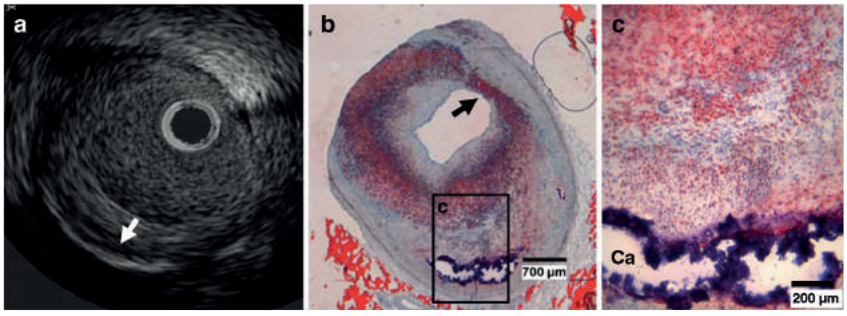

Fig. 2 Typical example of IVUS (**a**) and histology (**b**, **c**) of a coronary atherosclerotic plaque in a diabetic pig. **a** IVUS of the same plaque as seen in **b** and **c** with deep calcium (*white arrow*). **b** and **c** show an overview and detail of the plaque with circumferential lipid accumulation (*stained red*) and deep calcification (Ca, remaining rim *stained blue*). The coronary plaque even shows the presence of a thin fibrous cap (*black arrow*) overlying the superficial lipid-rich tissue, showing a likeness to a thin cap fibrous atheroma [18]. Oil-red-O stain, bar in **b** is 700 μm, bar in **c** is 200 μm

were sacrificed at 15 months because of the attained body weight and related handling difficulties (diabetic vs. non-diabetic: 97±3 vs. 96±1 kg).

Conclusion

Different animal models are useful to study different aspects in the process of atherosclerosis development (Table 1). However, for the study of CAD and related diagnostic and therapeutic interventions, a porcine disease model seems most suitable. In the presence of several metabolic alterations, lesions develop within 9 to 12 months, closely resembling human coronary atherosclerotic plaques upon examination by histology.

In addition, examples from this model show that OCT and gray-scale IVUS appear to be highly complementary imaging modalities for the evaluation of the development of coronary atherosclerotic plaque over time. The present preliminary results indicate that these modalities can be used for plaque characterisation in vivo, making this large diseased animal model ideal for studying new coronary diagnostic and therapeutic interventions.

Acknowledgement The article is dedicated to Professor Dr. W.J. van der Giessen who sadly passed away in June 2011.

References

1. Bentzon JF, Falk E. Atherosclerotic lesions in mouse and man: is it the same disease? Curr Opin Lipidol. 2010;21 (5):434–40.
2. Badimon L. Atherosclerosis and thrombosis: lessons from animal models. Thromb Haemost. 2001;86(1):356–65.
3. Aikawa M, Sugiyama S, Hill CC, et al. Lipid lowering reduces oxidative stress and endothelial cell activation in rabbit atheroma. Circulation. 2002;106(11):1390–6.
4. Duncker DJ, Bache RJ. Regulation of coronary blood flow during exercise. Physiol Rev. 2008;88(3):1009–86.
5. Koopmans SJ, Mroz Z, Dekker R, et al. Association of insulin resistance with hyperglycemia in streptozotocin-diabetic pigs: effects of metformin at isoenergetic feeding in a type 2-like diabetic pig model. Metabolism. 2006;55(7):960–71.
6. Gerrity RG, Natarajan R, Nadler JL, et al. Diabetes-induced accelerated atherosclerosis in swine. Diabetes. 2001;50 (7):1654–65.
7. Chatzizisis YS, Jonas M, Coskun AU, et al. Prediction of the localization of high-risk coronary atherosclerotic plaques on the basis of low endothelial shear stress: an intravascular ultrasound and histopathology natural history study. Circulation. 2008;117 (8):993–1002.
8. Clarkson TB, Mehaffey MH. Coronary heart disease of females: lessons learned from nonhuman primates. Am J Primatol. 2009;71 (9):785–93.
9. Shively CA, Musselman DL, Willard SL. Stress, depression, and coronary artery disease: modeling comorbidity in female primates. Neurosci Biobehav Rev. 2009;33(2):133–44.
10. Nakazawa G, Finn AV, Ladich E, et al. Drug-eluting stent safety: findings from preclinical studies. Expert Rev Cardiovasc Ther. 2008;6(10):1379–91.
11. van den Heuvel M, Sorop O, Batenburg WW, et al. Specific coronary drug-eluting stents interfere with distal microvascular function after single stent implantation in pigs. JACC Cardiovasc Interv. 2010;3(7):723–30.
12. Langeveld B, Roks AJ, Tio RA, et al. Rat abdominal aorta stenting: a new and reliable small animal model for in-stent restenosis. J Vasc Res. 2004;41(5):377–86.
13. Granada JF, Kaluza GL, Wilensky RL, et al. Porcine models of coronary atherosclerosis and vulnerable plaque for imaging and interventional research. EuroIntervention. 2009 May;5(1):140–8.
14. Tearney GJ, Jang IK, Kang DH, et al. Porcine coronary imaging in vivo by optical coherence tomography. Acta Cardiol. 2000;55 (4):233–7.
15. Yabushita H, Bouma BE, Houser SL, et al. Characterization of human atherosclerosis by optical coherence tomography. Circulation. 2002;106(13):1640–5.
16. Regar E, van Soest G, Bruining N, et al. Optical coherence tomography in patients with acute coronary syndrome. EuroIntervention. 2010;6(Suppl G):G154–60.
17. Mintz GS, Nissen SE, Anderson WD, et al. American College of Cardiology Clinical Expert Consensus Document on Standards for Acquisition, Measurement and Reporting of Intravascular Ultrasound Studies (IVUS). A report of the American College of Cardiology Task Force on Clinical Expert Consensus Documents. J Am Coll Cardiol. 2001;37(5):1478–92.
18. Virmani R, Burke AP, Farb A, et al. Pathology of the vulnerable plaque. J Am Coll Cardiol. 2006;47(8 Suppl):C13–8.

Dietary saturated fat/cholesterol, but not unsaturated fat or starch, induces C-reactive protein associated early atherosclerosis and ectopic fat deposition in diabetic pigs

Koopmans S.J., Dekker R., Ackermans M.T., Sauerwein H.P., Serlie M.J., van Beusekom H.M., van den Heuvel M. and van der Giessen W.J.

Cardiovasc Diabetol. 2011 Jul 14;10:64

4

Dietary saturated fat/cholesterol, but not unsaturated fat or starch, induces C-reactive protein associated early atherosclerosis and ectopic fat deposition in diabetic pigs

Sietse J. Koopmans[1,2]*, Ruud Dekker[1], Mariette T. Ackermans[3], Hans P. Sauerwein[4], Mireille J. Serlie[4], Heleen M.M. van Beusekom[5], Mieke van den Heuvel[5], Wim J. van der Giessen[5,6]

Abstract

Background: Diabetes is thought to accelerate cardiovascular disease depending on the type of diet. This study in diabetic subjects was performed to investigate the metabolic, inflammatory and cardiovascular effects of nutritional components typically present in a Western, Mediterranean or high glycaemic diet.

Methods: Streptozotocin-diabetic pigs (~45 kg) were fed for 10 weeks supplemental (40% of dietary energy) saturated fat/cholesterol (SFC), unsaturated fat (UF) or starch (S) in an eucaloric dietary intervention study.

Results: Fasting plasma total, LDL and HDL cholesterol concentrations were 3-5 fold higher ($p < 0.01$) in SFC compared to UF and S pigs. Fasting plasma NEFA concentrations (mmol/L) were highest ($p < 0.05$) in SFC (1.09 ± 0.17), intermediate in UF (0.80 ± 0.14) and lowest in S pigs (0.58 ± 0.14) whereas plasma glucose (~13 mmol/L), triglyceride (~0.5 mmol/L) and insulin (~24 pmol/L) concentrations were comparable among SFC, UF and S pigs. The postprandial response area under the curves (AUC, 0-4 h) for glucose but not for insulin and triglyceride responses were intermediate in SFC (617 ± 144) and lowest ($p < 0.05$) in UF (378 ± 157) compared to S pigs (925 ± 139). Fasting hepatic glucose production, hepatic and peripheral insulin sensitivity and blood pressure were not different among pigs. C-reactive protein (CRP) concentrations (mg/L) were highest ($p < 0.05$) in SFC (25 ± 4), intermediate in S (21 ± 3) and lowest in UF pigs (14 ± 2). Liver weights, liver and muscle triglyceride concentrations, and the surface area of aorta fatty streaks were highest ($p < 0.01$) in SFC pigs. A positive correlation between postprandial plasma CRP and aorta fatty streaks was observed in SFC pigs ($R^2 = 0.95$). Retroperitoneal fat depot weight (g) was intermediate in SFC (260 ± 72), lowest in S (135 ± 51) and highest ($p < 0.05$) in UF (571 ± 95) pigs.

Conclusion: Dietary saturated fat/cholesterol induces inflammation, atherosclerosis and ectopic fat deposition whereas an equally high dietary unsaturated fat load does not induce these abnormalities and shows beneficial effects on postprandial glycaemia in diabetic pigs.

Keywords: Diabetes, Insulin, Diet, Unsaturated fat, Saturated fat, Cholesterol, Inflammation, C-reactive protein, Atherosclerosis, Pigs

* Correspondence: sietsejan.koopmans@wur.nl
[1]BioMedical Research of Wageningen University and Research Center, Lelystad, The Netherlands
Full list of author information is available at the end of the article

Background

The impact of an excess in dietary fats and carbohydrates on metabolic control, inflammation and cardiovascular disease has been studied and discussed in normal and (pre)diabetic subjects in both human [1-4] and animal studies [5-7]. In general, excessive dietary saturated fats and cholesterol increase the risk for the development of obesity, diabetes and cardiovascular diseases [6,8-10] while dietary unsaturated fats are considered less harmful and do not impose an increased risk for the development of diabetes and cardiovascular diseases [1,2,6]. Dietary carbohydrates, in the form of starches, have a high glycaemic load and thereby worsen postprandial glucose, stimulate insulin secretion and de novo lipogenesis [11-14].

Most studies on the longer term (months) effects of dietary components have been carried out in normal or glucose intolerant individuals but limited information is available in diabetic subjects on metabolic control, inflammation, cardiovascular abnormalities and body composition [2,12,13,15].

Longer term studies in diabetic humans are difficult to perform because adherence to the prescribed diets has proven to be extremely difficult [16] and because dietary effects on the pathophysiology of diabetes are usually small with respect to metabolic control, insulin sensitivity, inflammation and cardiovascular diseases [17,18]. In addition, longer term studies are usually necessary to disclose any dietary effects on the pathophysiology of diabetes because part of the dietary effects are caused by changes in body composition. This can partly be overcome by studying animal models which are representative for the human situation, are highly homogenous and are kept under strictly standardized experimental conditions.

We have developed a pig model for diabetes mellitus type 2 in humans which is characterized by insulin resistance, hyperglycaemia as well as elevated plasma triglyceride and NEFA concentrations. The diabetic pigs are non-ketotic, anabolic and do not require insulin therapy [19]. Pigs are like humans omnivores and as such, the functionality of the gastrointestinal tract is comparable between pigs and man and therefore the pig is an useful animal model for the study of dietary components [20,21]. This makes the pig particular useful when the effect of diets is studied on diabetes accelerated dyslipidaemia and atherosclerosis [22-24]. Furthermore, coronary arteries of diabetic pigs have been shown to express low grade inflammation [25], a condition also described in humans with type 2 diabetes mellitus [13,26,27].

The aim of this dietary intervention study was to characterize and compare the medium/long-term (10 weeks) pathogenic effects of eucaloric diets 1) both high in supplemental fat, but differing in fat composition as reflected by mainly saturated fats and cholesterol (SFC) versus mainly unsaturated fats (UF) and 2) differing in supplemental fat (SFC or UF) versus supplemental carbohydrate (starch, S), on pre- and postprandial hyperglycaemia, lipidaemia and insulinaemia, on insulin sensitivity, blood pressure, circulating pro-inflammatory markers, retroperitoneal fat weight and on muscle, liver and aorta lipid deposits in diabetic pigs.

Methods

The performed research is in compliance with the ARRIVE guidelines on animal research [28]. Experimental protocols describing the management, surgical procedures, and animal care were reviewed and approved by the ASG-Lelystad Animal Care and Use Committee (Lelystad, The Netherlands).

Animals, housing, diets and surgery

Domestic (Landrace × Yorkshire, D-line) pigs (barrows with an initial age and body weight of ~11 weeks and ~30 kg, respectively) were obtained (Bastiaanse, Espel, The Netherlands) and kept in specially designed metabolic pens (1.15 × 1.35 m) and adapted to the light/dark cycle (lights on at 05:00 h and off at 19:00 h) and a feeding schedule. Pigs were weighed weekly and the meal size was adjusted to the individual pig's weight. The pigs were fed 2.5-fold maintenance requirements for gross energy (GE) as established in a normal pig. This corresponded with a feeding level of 1045 kJ GE kg^{-1} $BW^{0.75}$ (metabolic weight of the pigs) per day and is sufficient to ensure moderate growth in normal pigs [29].

The pigs were fed a commercial pig diet (5% crude fat, 16% crude protein, 41% starch and sugars, 20% non-starch polysaccharides, 6% ash and 12% water; Startbrok; Agrifirm, Meppel, The Netherlands) twice daily (at 06:00 and 16:00 h). Water was always available ad libitum. After 1 week, pigs were provided with a permanent blood vessel catheter in the jugular vein, as previously described by us [29,30]. One week after surgery, 21 pigs were treated with streptozotocin (140 mg/kg) as described previously [19]. Two weeks thereafter, 3 pigs showed fasting plasma glucose concentrations <10 mmol/L and were excluded from the study. The remaining 18 pigs were balanced over the 3 diet groups, based on fasting hyperglycaemia. Composition of the saturated fat/cholesterol, unsaturated fat and starch enriched diets is shown in Table 1. The experimental meals were fed twice daily (at 1045 kJ GE kg^{-1} $BW^{0.75}$ per day) for a duration of 10 weeks. In practical terms this means that the pigs on the starch-enriched diet were fed 1.31-fold the amount (on weight basis, but equal in caloric content) compared to the pigs on the fat-enriched diets in order to match the energy intake of pigs among diets.

Table 1 Composition of the experimental diets

Food ingredients	Saturated fat diet plus cholesterol	Unsaturated fat diet	Starch diet
Milk protein (caseinate)	23.2	23.2	17.7
Fructose	9.2	9.2	7.1
Maltodextrin DE 19	30.8	30.8	23.6
Native pea starch	0.0	0.0	41.4
Total sugar and starch	40.0	40.0	72.1
Soy bean oil	0.0	0.0	2.7
Lecithin	0.0	1.5	0.0
Canola oil (rape oil/Lear)	0.0	2.7	0.0
Trisun 80, high oleic sunflower oil	0.0	23.0	0.0
Beef tallow	27.2	0.0	0.0
Total fat	27.2	27.2	2.7
Fiber: Fibrim 2000	9.4	9.4	7.3
Premix[1]	0.20	0.20	0.15
Cholesterol[2]	1.0	0.0	0.0
Total (%)	100.0	100.0	100.0
Gross Energy (GE; MJ/kg)	23.4	23.4	17.9

The per-cent of each ingredient contributing to the total amount of diet (= 100%) is listed. Energy intake was matched among dietary groups and therefore pigs receiving the Starch diet were fed 1.32 times the amount of the high fat diet groups. Therefore the diets were homogenous except for starch or fat.

[1] This vitamin and trace mineral premix contained per kg diet: vit. A (retinol) - 1750 IU; vit. D_3 (cholecalciferol) - 200 IU; vit. E (tocopherol) - 11 IU; vit. K_1 (phylloquinone) - 0.5 mg; vit. B_1 (thiamin) - 1.0 mg; vit. B_2 (riboflavin) - 4 mg; d-pantothenic acid - 9 mg; niacin (vit. B_3, nicotinic acid) - 12.5 mg (available); biotin (vit. H) - 50 µg; vit. B_{12} (cyanocobalamin) - 15 µg; folic acid (folacin) - 0.3 mg; vit. B_6 (pyridoxin) - 1.5 mg; choline - 400 mg; Fe - 80 mg; Zn - 54 mg; Mn - 30 mg; Co - 0.15 mg; I - 0.14 mg; Se - 0.25 mg; antioxidants (E310,320,321) - 50 mg; with maize starch as carrier.

[2] Cholesterol has no energetic value and therefore 1 kg cholesterol was supplemented per 100 kg diet.

Supplemental saturated fat plus cholesterol (SFC), unsaturated fat (UF), or starch (S) content was 40% of total dietary energy. SFC was derived from beef tallow (i.e. ~55% saturated, ~35% mono-unsaturated, and ~10% poly-unsaturated fatty acids) plus 1% cholesterol, UF was derived from sunflower and rape oil (i.e. ~65% poly-unsaturated, ~25% mono-unsaturated, and 10% saturated fatty acids) and S was derived from pea starch, representing components of a Western, Mediterranean or high glycaemic diet, respectively.

Timeline

The timeline of the study is represented schematically in Figure 1. In short, the 3 diets were fed to the pigs (n = 6 per diet group) for 10 weeks comprising the following techniques and measurements: 1) daily food intake, 2) weekly body weight, 3) quantitative collection of urine (for determination of 24-h urinary glucose excretion) on Mondays, Wednesdays and Fridays during the dietary treatment, 4) at week 7, the pigs were provided with permanent catheters in the jugular vein and carotid artery, 5) at week 8, a meal tolerance test was performed and intra-arterial blood pressure was recorded, 6) at week 9, a hyperinsulinaemic euglycaemic clamp study using 6,6-$^2H_2$-glucose infusion was performed and 7) at week 10, pigs were killed by intravenous injection of barbiturate (administered via the jugular catheter) for tissue collection.

Meal tolerance test and blood pressure

During the one-week recovery period after surgery, the pigs were habituated to the blood sampling and experimental procedures. The carotid artery catheter was used for blood sampling and registration of blood pressure. During the blood sampling procedure, the catheters were flushed with physiological saline and sealed off with physiological saline containing 5 IU heparin per mL. From experience we know that this sampling procedure does not affect plasma NEFA concentrations.

Blood was sampled repeatedly before, during and after the morning meal (-15, 0, 30, 60, 120, 240, 360, and 480 minutes from the start of feeding). Per sampling time point, approximately 5 ml blood was sampled. The responses of insulin, glucose and triglycerides were assessed. In addition, the pre-and post-prandial levels of C-reactive protein (CRP), haptoglobin, IL-6 and TNF-α were determined on samples taken 15 minutes before and 180 minutes after the start of feeding. Subsequent to the meal tolerance test, the blood pressure and heart rate were determined five hours post-prandially on a Digital Electromanometer, Type 330 (Hugo Sachs Elektronik KG, March-Hugstetten, Germany).

Hyperinsulinaemic euglycaemic clamp and 6,6-$^2H_2$-glucose infusion

The jugular vein catheter was used for the infusion of fluids and the carotid artery catheter was used for blood

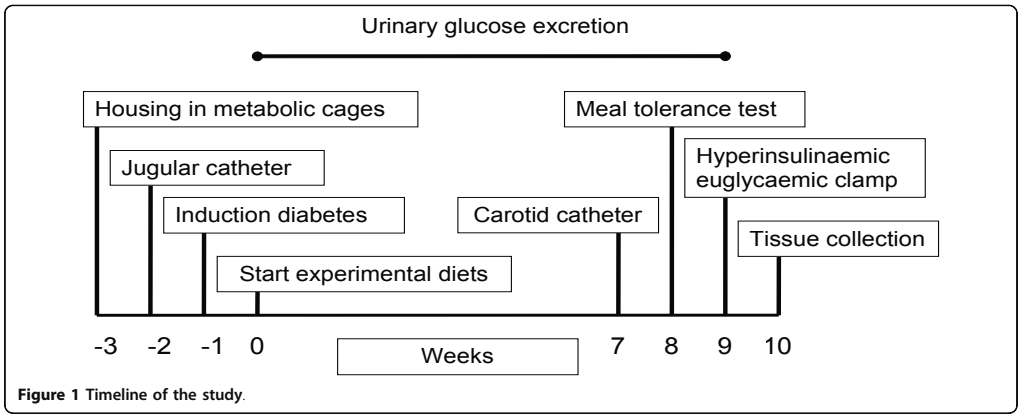

Figure 1 Timeline of the study.

sampling during the hyperinsulinaemic clamp study. Preceding the insulin clamp, overnight fasting blood samples were collected for determining the concentrations of fructosamine, glucagon, cortisol, NEFA, total cholesterol, LDL and HDL cholesterol and background glucose enrichment.

After baseline samples, a prime (4.8 mg/kg)-continuous (0.08 $mg.kg^{-1}.min^{-1}$) infusion of 6,6-$^2H_2$-glucose was administered for 150 min. After an equilibration time, blood samples were taken at 110, 120, 130, 140 and 150 min for determination of glucose, 6,6-$^2H_2$-glucose enrichment (to estimate fasting hepatic glucose production) and insulin. Subsequently, insulin was infused (prime (34 mU/kg)-continuous (2 $mU.kg^{-1}.min^{-1}$)) for 6 hours. A variable infusion of a 33% D-glucose solution was started to maintain plasma glucose at euglycaemia (~5 mmol/L). Steady state calculations were carried out during the last 40 minutes of the clamp (t = 320, 330, 340, 350 and 360 min) and the coefficients of variation for the insulin and glucose concentrations, and for the infusion rate of glucose were determined. During the last 3 hours of the insulin clamp, a prime (4.8 mg/kg)-continuous (0.08 $mg.kg^{-1}.min^{-1}$) infusion of 6,6-$^2H_2$-glucose was superimposed to estimate 1) insulin stimulated whole body glucose uptake (rate of disappearance = Rd) and 2) insulin-inhibited hepatic glucose production, as described before [19]. For this purpose blood samples were taken at t 320, 330, 340, 350 and 360 min of the clamp.

Infusates: Insulin (Actrapid MC, porcine monocomponent, Novo, Copenhagen, Denmark), 6,6-$^2H_2$-glucose (Cambridge Isotope Laboratories, Inc, MA, USA) and D-glucose (Merck, Darmstadt, Germany) were prepared as sterile solutions and passed through a 0.22 µm Millipore filter into sterile containers before use. Insulin was diluted in a saline solution containing pig plasma (final plasma concentration was 3%) in order to avoid sticking of insulin to the plastic containers and tubings. 6,6-$^2H_2$-glucose was dissolved in a saline solution and D-glucose was dissolved in aqua dest.

Plasma, urine and tissue collection and analyses

Blood samples collected in heparinised (150 USP. U. Lithium Heparin, 10 mL Venoject, Terumo, Leuven, Belgium) or EDTA (ethylenediaminetetraacetic acid, (0.47 mol/L EDTA, 10 mL Venoject, Terumo, Leuven, Belgium) tubes were immediately chilled at 0°C on water with ice, and centrifuged at 4°C for 10 minutes at 3000 rpm. Plasma aliquots were stored at -80°C for later analyses. Urine was quantitatively collected per 24 hours in buckets containing 0.5 grams Halamid-d (sodium-p-toluenesulfonchloramide, Akzo Nobel Chemicals, Amersfoort, The Netherlands) to prevent microbial breakdown of glucose. Urine samples were stored at -20°C for later glucose analyses. Muscle (m. iliopsoasis) and liver were snap-frozen in liquid nitrogen and stored at -80°C. Abdominal aorta was fixed in a 4% paraformaldehyde solution.

Plasma samples for determination of 6,6-$^2H_2$-glucose enrichment were analyzed as described previously [19]. In short, glucose was extracted from plasma, derivatised, and injected into a gas chromatograph/mass spectrometer system (HP 6890 series GC system and 5973 Mass Selective Detector, Palo Alto, CA, USA). Separation was achieved on a J&W scientific DB 17 capillary column (30 m × 0.25 mm × 0.25 µm; Agilent Technologies Nederland BV, Amstelveen, The Netherlands). Isotopic enrichment was calculated as tracer-to- tracee ratio after subtracting the isotopic enrichment of a background plasma sample. An aliquot of the 6,6-$^2H_2$-glucose infusate was analyzed for the isotope concentration to calculate the actual infusion rate for each infusion experiment.

Plasma glucose was analyzed with the Glucose liquiUV mono kit (Human, Wiesbaden, Germany), plasma non-esterified fatty acids were analyzed with the WAKO kit (Neuss, Germany) and plasma triglycerides with a kit from Human (Wiesbaden, Germany). Total, LDL and HDL cholesterol concentrations in plasma were determined with liquicolor kits (Human, Wiesbaden, Germany) and VLDL cholesterol was calculated as total cholesterol minus LDL and HDL cholesterol. Plasma insulin concentration was measured using a Delfia assay (test kit by Perkin Elmer Life Sciences Trust by Wallac Oy, Turku, Finland). This specific pig insulin assay was validated using pig insulin standards, as indicated before [30]. Plasma glucagon was measured with a kit from Euro-Diagnostica (Arnhem, The Netherlands), plasma cortisol with the Count-A-Count Cortisol kit (DPC, Los Angeles, USA) and fructosamine by a kit from Spinreact (Sant Esteve De Bas, Spain). Plasma C-reactive protein (CRP), interleukin-6 (IL-6) and tumor necrosis factor alpha (TNF-α) were analyzed with kits (CRP-hs, Human, Wiesbaden, Germany; Haptoglobin, Instruchemie, Delfzijl, The Netherlands; SW Interleukin 6, IBL, Hamburg, Germany and SW TNF-alpha Elisa Kit, Biosource Int, Camarillo, USA), respectively.

Ketones (acetoacetic acid) were determined in fresh urine by a reagent strip test (Ketostix, Bayer Diagnostics, Mijdrecht, The Netherlands).

Triglyceride concentrations in muscle and liver samples were determined with the same kit as used for the plasma samples, after saponification with an alkalin alcohol solution as previously described [31].

Aortic fatty streaks, as a marker of early atherosclerosis [22,24], (AHA class 2 lesion [32]), were quantified with use of Sudan IV fat stain in sections of the abdominal aorta ranging from the bifurcation of the renal arteries to the bifurcation of the iliac arteries. The stained aortas were then photographed and analyzed with a microscopy image analysis system (Clemex technologies Inc., Quebec, Canada) as ratio of stained area to total area.

Statistical analyses

Results are expressed as means ± SEM and the criterion of statistical significance was set at $p < 0.05$. The data were subjected to the analysis of variance procedure (ANOVA) (for repeated measurements when applicable) followed by the unpaired or paired student's t-test of Genstat 5 [33] for determination of differences between or within the three dietary groups, respectively.

Results

Body composition

Final body weights were comparable among SFC, UF and S pigs indicating that average food intake and urinary glucose excretion were in balance during the course of the study per diet group (Table 2). However, liver weights and triglyceride concentrations were higher ($p < 0.01$) in SFC pigs compared to UF and S pigs. Triglyceride concentration in muscle was highest ($p < 0.01$) in SFC pigs, intermediate in UF and lowest in S pigs. Retroperitoneal fat depot weight was intermediate in SFC (260 ± 72 g), lowest in S (135 ± 51 g) and highest ($p < 0.05$) in UF (571 ± 95) pigs.

Metabolic control

At the end of the dietary intervention, fasting plasma insulin, glucagon, glucose, fructosamine and triglyceride concentrations were similar among all diabetic pigs (Tables 3 and 4). Fasting plasma total cholesterol, HDL, LDL and VLDL concentrations were higher ($p < 0.01$) in SFC pigs compared to UF and S pigs. The ratio of HDL/LDL cholesterol was unchanged but the ratio of HDL/total cholesterol was reduced ($p < 0.05$) in SFC and UF pigs compared to S pigs (Table 4). Fasting plasma NEFA concentrations were highest ($p < 0.05$) in SFC pigs, intermediate in UF pigs and lowest S pigs (Table 4). Fasting hepatic glucose production, insulin-inhibited hepatic glucose production and insulin-stimulated whole body glucose uptake were similar among diabetic pigs (Table 3). Coefficients of variation of clamp plasma glucose, plasma insulin and glucose infusion rate in SFC versus UF versus S pigs were 5 ± 2 versus 7 ± 3 versus 3 ± 1%, 11 ± 5 versus 7 ± 2 versus 8 ± 3% and 2 ± 1 versus 3 ± 1 versus 2 ± 1%, respectively. The postprandial response area under the curves (0-4 h or 0-8 h) for glucose but not for insulin and triglyceride responses were intermediate in SFC (617 ± 144 or 471 ± 122), lowest ($p < 0.05$) in UF (378 ± 157 or 292 ± 133) and highest in S pigs (925 ± 139 or 724 ± 92 (Figures 2 and 3).

Inflammation

The fasting plasma concentrations of cortisol, haptoglobin, IL-6 and TNF-a were not statistically different between the diet groups (Table 4). By contrast, both fasting and postprandial plasma C-reactive protein (CRP) concentrations and meal-induced CRP responses (Δ) were higher ($p < 0.05$) in SFC pigs compared to UF pigs but not always higher compared to S pigs, i.e. fasting plasma CRP concentration was similar in SFC and S pigs (Figure 4).

Atherosclerosis and blood pressure

The surface area of aorta fatty streaks was higher ($p < 0.001$) in SFC pigs compared to UF and S pigs (Table 2). Visualization of the fatty streaks in the abdominal aortas of the three groups of pigs is presented in Figure 5. In SFC pigs, a positive correlation between surface area of aorta fatty streaks and postprandial plasma CRP concentration was observed ($R^2 = 0.95$, $p < 0.001$) (Figure 6). Mean arterial, systolic and diastolic blood pressures were

Table 2 Food intake, urinary glucose excretion, final body weights and tissue data of diabetic pigs fed saturated fat/cholesterol or unsaturated fat or starch enriched diets

	Saturated fat plus cholesterol diet	Unsaturated fat diet	Starch diet
Factual average food intake (MJ/day)	23.9 ± 1.3	25.0 ± 2.0	27.7 ± 0.9
Average urinary glucose excretion (MJ/day)	8.5 ± 1.0^{A}	9.1 ± 1.1^{A}	15.8 ± 2.1^{B}
Final body weight (kg)	41 ± 3	45 ± 5	48 ± 7
Liver weight (kg)	1.47 ± 0.08^{A}	1.12 ± 0.03^{B}	1.11 ± 0.03^{B}
Liver triglyceride concentration (g/kg)	49 ± 11^{A}	27 ± 1^{B}	21 ± 3^{B}
Muscle triglyceride concentration (g/kg)	21 ± 4^{A}	13 ± 3^{AB}	8 ± 1^{B}
Retroperitoneal fat weight (g)	260 ± 72^{AB}	571 ± 95^{A}	135 ± 51^{B}
Surface area aorta fatty steaks (%)	17.9 ± 4.4^{A}	0.03 ± 0.02^{B}	0.14 ± 0.07^{B}

$^{A, B}$, data with different superscripts in the same row differ at $p < 0.05$.

not statistically different between the diet groups (Table 5).

Discussion

Main findings

Pigs on dietary SFC showed a more atherogenic plasma profile with higher plasma NEFA concentrations, higher liver weights and liver triglyceride concentrations, and increased aorta fatty streak area compared to pigs on dietary UF and S. The postprandial glucose, but not insulin and triglyceride responses were intermediate in SFC pigs, lowest in UF pigs and highest in S pigs, whereas hepatic and whole body insulin sensitivities for glucose metabolism were not significantly affected by the diets. This indicates that the postprandial glucose intolerance of S pigs compared to SFC and UF pigs is caused by an increased systemic influx of dietary glucose after starch digestion and not by insulin resistance. The mechanisms behind the relative postprandial glucose intolerance in SFC pigs compared to UF pigs are unknown. However, several non-significant factors may contribute to the difference in postprandial glucose tolerance. Fasting and insulin-inhibited hepatic glucose production during the clamp were elevated by 16% (p = NS) and 50% (p = NS) and early (30 min) postprandial insulin secretion was 2-fold reduced (p = NS) in SFC pigs compared to UF pigs. For the latter, it has been suggested that the degree of saturation of fatty acids may have a negative influence on insulin release by beta-cells in vitro [34]. Taken together, these factors may add-up and act in concert to both impair non-insulin-dependent and insulin-dependent glucose tolerance in SFC pigs compared to UF pigs.

With respect to body composition, SFC pigs showed increased muscle, liver and aorta fat deposits and a reduced amount of retroperitoneal fat. The latter non-ectopic depot of adipose tissue was largest in UF pigs, indicating that body composition is most favourably affected by the UF diet compared to the SFC diet in this non-obese diabetic pig model. The UF diet is mainly stored in adipose tissue and to a lesser extent in organs and the vascular system. By contrast, the S pigs showed the lowest muscle and liver fat deposits and a low amount of retroperitoneal fat. This indicates that energy storage in the form of fat is low from dietary S, both in adipose and non-adipose tissue. The baseline markers of systemic inflammation tended to be higher in SFC pigs, but only baseline and postprandial CRP concentrations reached levels of statistical significance. A strong correlation was observed between postprandial plasma CRP and aorta fatty streak area ($R^2 = 0.95$, $p < 0.001$), suggesting that postprandial CRP is a biomarker for atherosclerosis in this diabetic pig model. This is one of the few pieces of

Table 3 Fasting hepatic glucose production, insulin-stimulated whole body glucose uptake, insulin-inhibited hepatic glucose production and plasma concentrations of metabolites and insulin in diabetic pigs fed saturated fat/cholesterol or unsaturated fat or starch enriched diets

	Saturated fat plus cholesterol diet	Unsaturated fat diet	Starch diet
Fasting plasma fructosamine (μmol/L)	449 ± 25	494 ± 62	558 ± 103
Fasting plasma glucose (mmol/L)	12.4 ± 0.4	14.4 ± 0.7	12.7 ± 1.6
Fasting plasma insulin (pmol/L)	23 ± 7	26 ± 7	22 ± 4
Fasting hepatic glucose production ($mg.kg^{-1}.min^{-1}$)	7.4 ± 0.8	6.4 ± 0.5	8.2 ± 2.0
Clamp plasma glucose (steady state, mmol/L)	5.7 ± 0.2	5.4 ± 0.2	5.4 ± 0.2
Clamp plasma insulin (steady state, pmol/L)	320 ± 27	409 ± 33	327 ± 33
Insulin-stimulated whole body glucose uptake ($mg.kg^{-1}.min^{-1}$)	10.0 ± 2.3	9.5 ± 2.1	10.8 ± 2.8
Insulin-inhibited hepatic glucose production ($mg.kg^{-1}.min^{-1}$)	1.8 ± 0.2	1.2 ± 0.3	1.8 ± 0.1

Table 4 Fasting plasma concentrations of lipid metabolites, hormones and inflammatory markers in diabetic pigs fed saturated fat/cholesterol or unsaturated fat or starch enriched diets

	Saturated fat plus cholesterol diet	Unsaturated fat diet	Starch diet
NEFA (mmol/L)	1.09 ± 0.17^{A}	0.80 ± 0.14^{AB}	0.58 ± 0.14^{B}
Triglycerides (mmol/L)	0.58 ± 0.17	0.51 ± 0.05	0.43 ± 0.11
Total cholesterol (mmol/L)	9.9 ± 1.2^{A}	2.0 ± 0.1 ^{B}	1.7 ± 0.2 ^{B}
HDL cholesterol (mmol/L)	2.1 ± 0.2^{A}	0.4 ± 0.0 ^{B}	0.5 ± 0.0 ^{B}
LDL cholesterol (mmol/L)	3.3 ± 0.3^{A}	1.3 ± 0.1 ^{B}	1.1 ± 0.1 ^{B}
VLDL cholesterol (mmol/L)	4.5 ± 0.8^{A}	0.2 ± 0.1 ^{B}	0.1 ± 0.0 ^{B}
Ratio HDL/LDL cholesterol	0.64 ± 0.08	0.35 ± 0.05	0.46 ± 0.03
Ratio HDL/total cholesterol	0.21 ± 0.01^{A}	0.23 ± 0.02^{A}	0.29 ± 0.01 ^{B}
Glucagon (pmol/L)	131 ± 25	114 ± 35	83 ± 10
Cortisol (nmol/L)	334 ± 44	284 ± 69	262 ± 50
Haptoglobin (pg/mL)	251 ± 132	394 ± 100	236 ± 52
IL-6 (pg/mL)	2224 ± 1102	818 ± 664	459 ± 270
TNF-α (pg/mL)	610 ± 289	394 ± 248	384 ± 135

$^{A, B}$, data with different superscripts in the same row differ at $p < 0.05$.

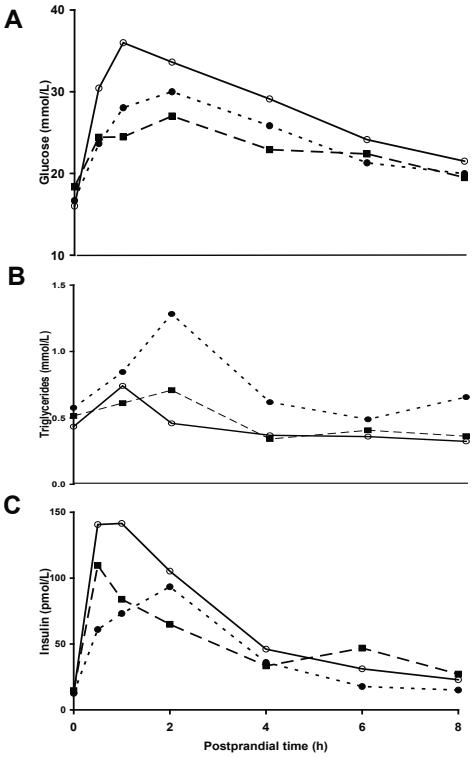

Figure 2 Postprandial curves (0-8 h) of plasma glucose (A), triglycerides (B) and insulin (C) are shown for diabetic pigs which were fed diets supplemented with starch (open circles), unsaturated fats (black squares) or saturated fats with cholesterol (black circles).

evidence that the inflammatory marker CRP is secondary to the atheromatous process itself.

Taken together, these main findings indicate that dietary saturated fat/cholesterol induces CRP associated early atherosclerosis and ectopic fat deposition whereas eucaloric unsaturated fat or starch do not induce these abnormalities and unsaturated fat shows beneficial effects on postprandial glycaemia in diabetic pigs.

Insulin resistance

After a 10-week intervention study, dietary composition had no significant effect on insulin sensitivity in diabetic pigs. This is in line with a 2-week intervention study in type 2 diabetic patients [35]. In non-diabetic rodents however, it is widely accepted that long-term feeding of dietary saturated fats induces insulin resistance whereas unsaturated fats increase insulin sensitivity [6]. This discrepancy may be caused by the fact that insulin resistance is already a prominent feature of diabetic humans [27] and pigs [19] and any modest dietary effect on insulin sensitivity does not come to expression in insulin resistant individuals. For example, both liver [6] and skeletal muscle [36] triglyceride concentrations have been shown to affect insulin sensitivity but in the present study, the diet-induced 2-fold variation in liver and skeletal muscle triglyceride concentrations is insufficient to further modulate insulin resistance in diabetic pigs.

Inflammation

Fasting plasma concentrations of the acute phase protein CRP were higher in diabetic pigs which were fed the SFC diet compared to the UF diet but not to the S diet. This underlines the anti-inflammatory effect of dietary UF [37,38]. The pro-inflammatory effect of a diet rich in saturated fats and cholesterol has been shown before in

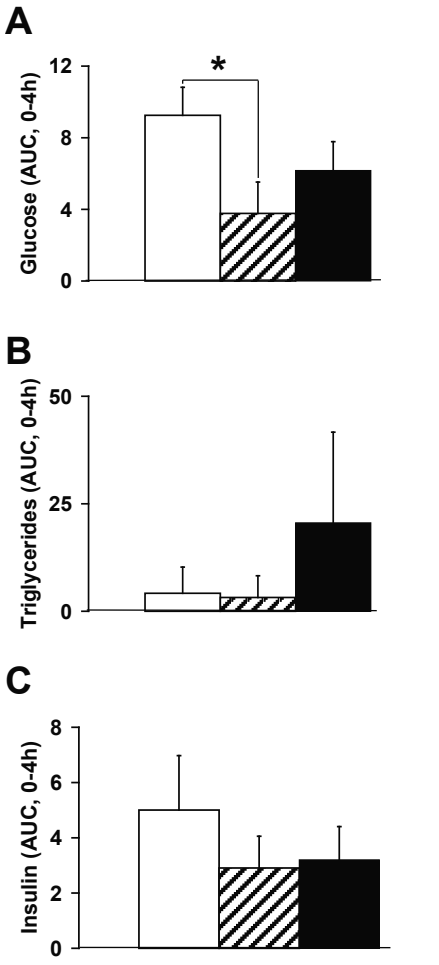

Figure 3 The postprandial response areas under the curve (Δ0-4 h) are depicted for plasma glucose (A), triglycerides (B) and insulin (C) for supplemental starch (open bars), unsaturated fats (striped bars) or saturated fats with cholesterol (black bars). Means ± SEM. *p < 0.05.

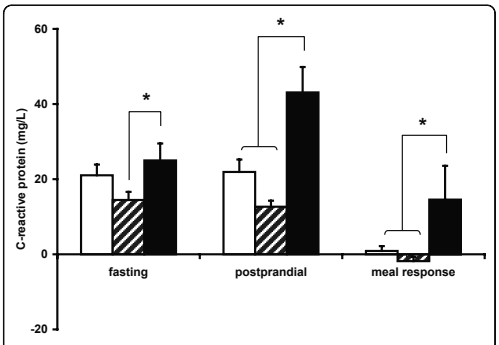

Figure 4 Overnight fasting and postprandial (3 h) plasma C-reactive protein (CRP) concentrations and the meal response over fasting (Δ) are depicted for diabetic pigs which were fed diets supplemented with starch (open bars), unsaturated fats (striped bars) or saturated fats with cholesterol (black bars). Means ± SEM. *p < 0.05.

non-diabetic humans [8,10] and in non-diabetic pigs [39,40]. In our study, postprandial plasma CRP, but not haptoglobin, IL-6 or TNF-α, positively correlated with the severity of beginning atherosclerosis. It seems therefore that postprandial CRP concentrations, which were increased 2-fold compared to fasting concentrations, react strongly to vascular damage and/or atherosclerosis [41]. Indeed, CRP has been proposed as a putative clinical biomarker for atherosclerosis [42,43] serving a possible protective role in the atherogenic process [44]. In diabetic pigs which were fed a diet rich in UF, no increase in postprandial CRP was observed. This corresponds with the absence of atherosclerosis in these diabetic pigs. The beneficial mechanism of action of UF, but not SFC, may be related to the affinity to bind to the nuclear peroxisome proliferator-activated receptor (PPAR), the same pathway which is activated by the anti-diabetic drug thiazolidinedione (TZD) [27,45-47]. Therefore, dietary UF can be regarded as a therapeutic agent to prevent some of the abnormalities of type 2 diabetes.

Diabetic pig model

Fasting plasma insulin (~25 pmol/L), glucose (~13 mmol/L) and triglyceride (~0.5 mmol/L) concentrations and a positive energy balance (body weight gain of ~1.5 kg/week) without the occurrence of ketosis indicated a mild form of diabetes in the pigs. In a previous paper we argued that the present insulin resistant pig model resembled type 2 diabetes [19]. In addition to these observations, we now showed that, after streptozotocin treatment, the residual beta-cells of the pancreas were able to increase insulin secretion ~5-7 fold upon a meal-challenge. This indicates that a substantial endogenous insulin secretion capacity is still present in this diabetic pig model.

Conclusion

When comparing dietary SFC, UF and S, dietary SFC induces CRP-associated early atherosclerosis and ectopic fat deposition whereas isoenergetic UF shows beneficial effects on postprandial glycaemia, inflammation and body composition in diabetic pigs.

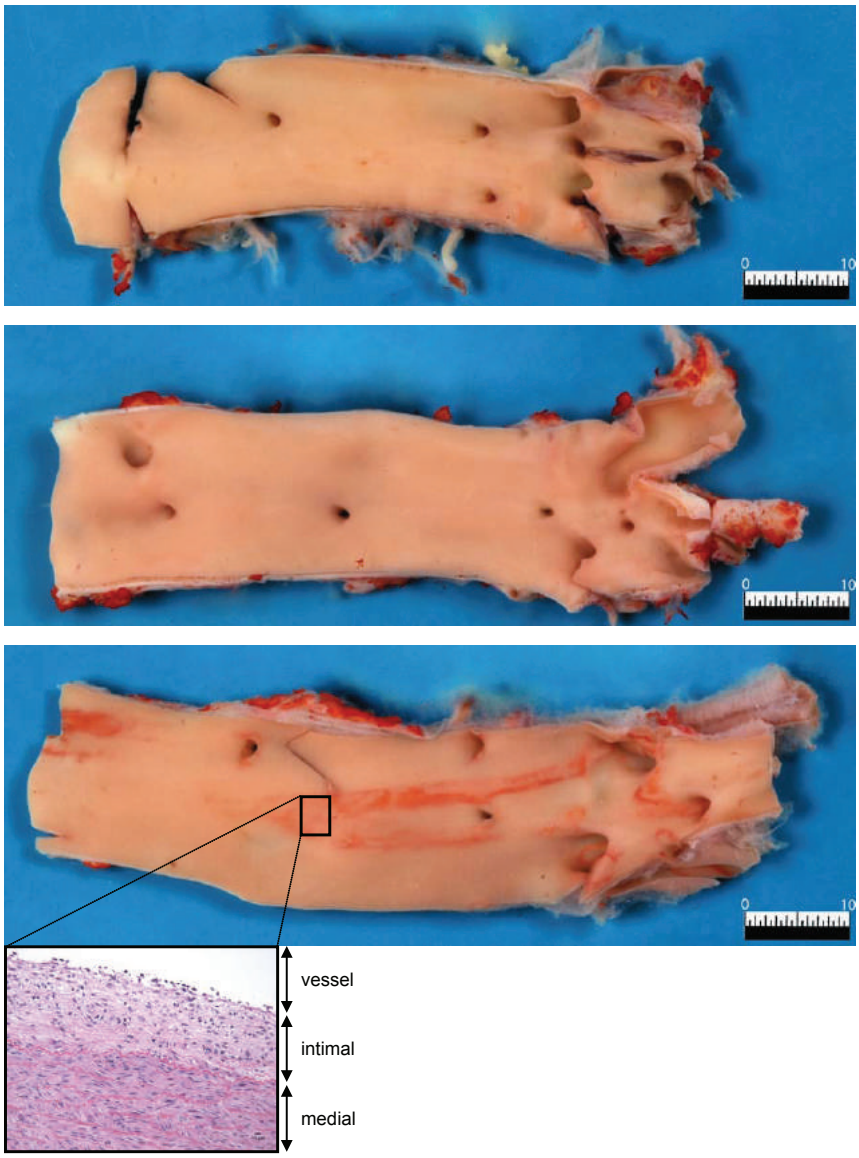

Figure 5 Images of typical examples of abdominal aorta Sudan IV fat staining of diabetic pigs, which were fed diets supplemented with starch (top picture), unsaturated fats (middle), or saturated fats with cholesterol (bottom). Red intra-luminal staining indicates presence of fatty streaks. Insert in bottom picture shows histological detail (hematoxylin-eosin staining) of fatty streak (4 × magnification). The intimal area of this part of the vessel wall consists of multiple cellular layers with empty little spaces where fat was deposited.

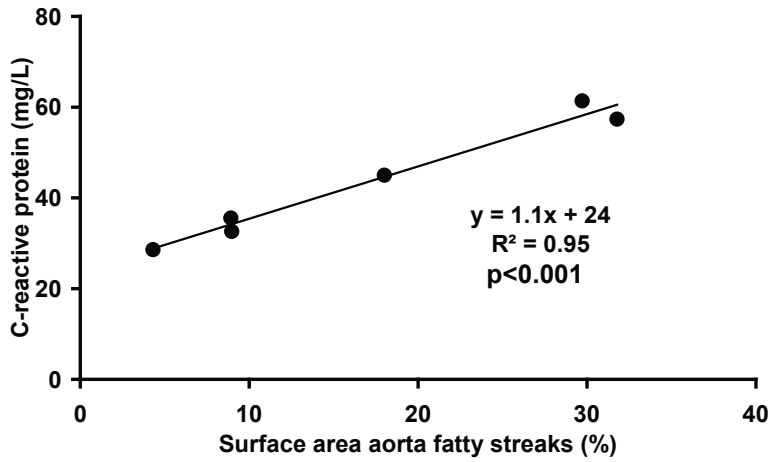

Figure 6 Correlation between plasma C-reactive protein (CRP) concentrations and the surface area of abdominal aorta fatty streaks (%) in diabetic pigs which were fed a diet supplemented with saturated fats and cholesterol. (R^2 = 0.95, p < 0.001).

Table 5 Blood pressure and heart rate in diabetic pigs fed saturated fat/cholesterol or unsaturated fat or starch enriched diets

	Saturated fat plus cholesterol diet	Unsaturated fat diet	Starch diet
Mean arterial pressure (mmHg)	113 ± 14	96 ± 5	96 ± 4
Systolic pressure (mmHg)	139 ± 18	117 ± 5	116 ± 5
Diastolic pressure (mmHg)	97 ± 13	78 ± 5	78 ± 4
Heart rate (beats per minute)	109 ± 10	92 ± 21	109 ± 22

Abbreviations
AUC: area under the curve; CRP: C-reactive protein; ME: metabolizable energy; NEFA: non-esterified fatty acids; PPAR: peroxisome proliferator-activated receptor; PUFA: polyunsaturated fatty acids; S: starch; SFC: saturated fat with cholesterol; STZ: streptozotocin; TZD: thiazolidinedione; UF: unsaturated fat.

Acknowledgements and Funding
This study is dedicated to our beloved friend and colleague WJG, deceased. This study was supported by the Ministry of Agriculture, Nature and Food Quality of The Netherlands. We thank Z. Mroz for the excellent surgical assistance.

Author details
[1]BioMedical Research of Wageningen University and Research Center, Lelystad, The Netherlands. [2]Department of Animal Sciences, Adaptation Physiology Group of Wageningen University, Wageningen, The Netherlands. [3]Clinical Chemistry, Laboratory of Endocrinology, Academic Medical Center, Amsterdam, The Netherlands. [4]Endocrinology & Metabolism, Academic Medical Center, Amsterdam, The Netherlands. [5]Experimental Cardiology, Erasmus Medical Center, Rotterdam, The Netherlands. [6]ICIN-KNAW, Utrecht, The Netherlands.

Authors' contributions
SJK was the principal investigator, involved in designing the study and writing the manuscript. RD coordinated the study and performed statistical analyses. MTA, HS and MJS were involved in developing the clamp technique in pigs and performing the stable isotope measurements and writing parts of the manuscript. HMMB, MH and WJG were involved in the cardiovascular measurements and writing parts of the manuscript. All authors participated in writing the final version of the manuscript.

Competing interests
The authors declare that they have no competing interests.

Received: 18 April 2011 Accepted: 14 July 2011 Published: 14 July 2011

References
1. Din JN, Newby DE, Flapan AD: **Omega 3 fatty acids and cardiovascular disease-fishing for a natural treatment.** *Br Med J* 2004, **328**:30-35.
2. Esposito K, Marfella R, Ciotola M, Di Palo C, Giugliano F, Giugliano G, D'Armiento M, D'Andrea F, Giugliano D: **Effect of a Mediterranean-style diet on endothelial dysfunction and markers of vascular inflammation in the metabolic syndrome.** *J Am Med Assoc* 2004, **292**:1440-1446.
3. Esposito K, Giugliano D: **Diet and inflammation: a link to metabolic and cardiovascular diseases.** *Eur Heart J* 2006, **27**:15-20.
4. Rallidis LS, Paschos G, Liakos GK, Velissaridou AH, Anastasiadis G, Zampelas A: **Dietary α-linolenic acid decreases C-reactive protein, serum amyloid A and interleukin-6 in dyslipidaemic patients.** *Atherosclerosis* 2003, **167**:237-242.
5. Jönsson T, Ahrén B, Pacini G, Sundler F, Wierup N, Steen S, Sjöberg T, Ugander M, Göransson L, Lindeberg S: **A Paleolithic diet confers higher insulin sensitivity, lower C-reactive protein and lower blood pressure than a cereal-based diet in domestic pigs.** *BMC Nutrition & Metabolism* 2006, **3**:39.

6. Buettner R, Parhofer KG, Woenckhaus M, Wrede CE, Kunz-Schughart LA, Schölmerich J, Bollheimer LC: **Defining high-fat-diet rat models: metabolic and molecular effects of different fat types.** *J Mol Endo* 2006, **36**:485-501.
7. Sinitskaya N, Gourmelen S, Schuster-Klein C, Guardiola-lemaitre B, Pévet P, Challet E: **Increasing the fat-to-carbohydrate ratio in a high-fat diet prevents the development of obesity but not a prediabetic state in rats.** *Clinical Science* 2007, **113**:417-425.
8. King DE, Egan BM, Geesey ME: **Relation of dietary fat and fiber to elevation of C-reactive protein.** *Am J Cardiol* 2003, **92**:1335-1339.
9. Storlien LH, Baur LA, Kriketos AD, Pan DA, Cooney GJ, Jenkins AB, Calvert GD, Campbell LV: **Dietary fats and insulin action.** *Diabetologia* 1996, **39**:621-631.
10. Tannock LR, O'Brien KD, Knopp RH, Retzlaff B, Fish B, Wener MH, Kahn SE, Chait A: **Cholesterol feeding increases C-reactive protein and serum amyloid A levels in lean insulin-sensitive subjects.** *Circulation* 2005, **111**:3058-3062.
11. Due A, Toubro S, Stender S, Skov AR, Astrup A: **The effect of diets high in protein or carbohydrate on inflammatory markers in overweight subjects.** *Diabetes Obesity Metabolism* 2005, **7**:223-229.
12. Garg A, Grundy SM, Koffler M: **Effect of high carbohydrate intake on hyperglycemia, islet function, and plasma lipoproteins in NIDDM.** *Diabetes Care* 1992, **15**:1572-1579.
13. Nappo F, Esposito K, Cioffi M, Giugliano G, Molinari AM, Paolisso G, Marfella R, Giugliano D: **Postprandial endothelial activation in healthy subjects and in type 2 diabetic patients: role of fat and carbohydrate meals.** *J Am Coll Cardiol* 2002, **39**:1145-1150.
14. Wolever TMS: *The Glycaemic Index A Physiological Classification of Dietary Carbohydrate* Oxfordshire, UK: CABI; 2006.
15. Jönsson T, Granfeldt Y, Ahrén B, Branell U-C, Pålsson G, Hansson A, Söderström M, Lindeberg S: **Beneficial effects of a Paleolithic diet on cardiovascular risk factors in type 2 diabetes: a randomized cross-over pilot study.** *Cardiovasc Diabetol* 2009, **8**:35.
16. Sabaté E: *Adherence to long-term therapies: evidence for action* Geneva, Switzerland: World Health Organization; 2003.
17. Afman L, Müller M: **Nutrigenomics: from molecular nutrition to prevention of disease.** *J Am Diet Assoc* 2006, **106**:569-576.
18. Müller M, Kersten S: **Nutrigenomics: goals and strategies.** *Nature Reviews Genetics* 2003, **4**:315-322.
19. Koopmans SJ, Mroz Z, Dekker R, Corbijn H, Ackermans M, Sauerwein H: **Association of insulin resistance with hyperglycemia in streptozotocin-diabetic pigs. Effects of metformin at isoenergetic feeding in a type 2-like diabetic pig model.** *Metabolism* 2006, **55**:960-971.
20. Miller ER, Ullrey DE: **The pig as a model for human nutrition.** *Ann Rev Nutr* 1987, **7**:361-382.
21. Moughan PJ, Cranwell PD, Darragh AJ, Rowan AM: **The domestic pig as a model animal for studying digestion in humans.** *Sixth International Symposium on digestive physiology in pigs II* 1994, 389-396.
22. Dixon JL, Stoops JD, Parker JL, Laughlin MH, Weisman GA, Sturek M: **Dyslipidemia and vascular dysfunction in diabetic pigs fed an atherogenic diet.** *Arterioscler Thromb Vasc Biol* 1999, **19**:2981-2992.
23. Fricker J: **The pig: a new model of diabetic atherosclerosis.** *DDT* 2001, **6**:921-922.
24. Gerrity RG, Natarajan R, Nadler JL, Kimsey T: **Diabetes-induced accelerated atherosclerosis in swine.** *Diabetes* 2001, **50**:1654-1665.
25. Zhang L, Zalewski A, Liu Y, Mazurek T, Cowan S, Martin JL, Hofmann SM, Vlassara H, Shi Y: **Diabetes-induced oxidative stress and low-grade inflammation in porcine coronary arteries.** *Circulation* 2003, **108**:472-478.
26. Festa A, D'Agostino R, Howard G, Tracy RP, Haffner SM: **Chronic subclinical inflammation as part of the insulin resistance syndrome.** *Circulation* 2000, **102**:42-47.
27. Bays H, Mandarino L, DeFronzo RA: **Role of the adipocyte, free fatty acids, and ectopic fat in pathogenesis of type 2 diabetes mellitus: peroxisomal proliferator-activated receptor agonists provide a rational therapeutic approach.** *J Clin Endo Metab* 2004, **89**:463-478.
28. Kilkenny C, Browne WJ, Cuthill IC, Emerson M, Altman DG: **Improving bioscience research reporting: the ARRIVE guidelines for reporting animal research.** *PLoS Biol* 2010, **8(6)**:e1000412..
29. Koopmans SJ, Van der Meulen J, Dekker R, Corbijn H, Mroz Z: **Diurnal variation in insulin-stimulated systemic glucose and amino acid utilization in pigs fed with identical meals at 12-hour intervals.** *Horm Metab Res* 2006, **38**:607-613.
30. Koopmans SJ, Mroz Z, Dekker R, Corbijn H, Wijdenes J, Van der Crabben S, Ackermans M, Sauerwein HP: **Insulin-stimulated net utilization of plasma glucose and amino acids in growing pigs.** In *Progress in research on energy and protein metabolism* Edited by: Souffrant WB, and Metges CC 2003, **109**:197-200.
31. Eggstein M, Kreuz FH: **Eine neue bestimmung der Neutralfette im Blutserum und Gewebe.** *Klin Wochenschr* 1966, **44**:262-267.
32. Stary HC, Chandler AB, Glagov S, Guyton JR, Insull W Jr, Rosenfeld ME, Schaffer SA, Schwartz CJ, Wagner WD, Wissler RW: **A definition of initial, fatty streak, and intermediate lesions of atherosclerosis.** *Circulation* 1994, **89**:2462-78.
33. Payne RW, Lane PW, Ainsley AE: *Genstat 5 Reference Manual* Oxford, UK: Oxford University Press; 1987.
34. Opara EC, Garfinkel M, Hubbard VS, Burch WM, Akwari OE: **Effect of fatty acids on insulin release: role of chain length and degree of unsaturation.** *Am J Physiol* 1994, **266**:E635-E639.
35. Allick G, Bisschop PH, Ackermans MT, Endert E, Meijer AJ, Kuipers F, Sauerwein HP, Romijn JA: **A low-carbohydrate/high-fat diet improves glucoregulation in type 2 diabetes mellitus by reducing postabsorptive glycogenolysis.** *J Clin Endocrinol Metab* 2004, **89**:6193-6197.
36. Pan DA, Lillioja S, Kriketos AD, Milner MR, Baur LA, Bogardus C, Jenkins AB, Storlien LH: **Skeletal muscle triglyceride levels are inversely related to insulin action.** *Diabetes* 1997, **46**:983-988.
37. Ciubotaru I, Lee YS, Wander RC: **Dietary fish oil decreases C-reactive protein, interleukin-6, and triacylglycerol to HDL-cholesterol ratio in postmenopausal women on HRT.** *J Nutr Biochem* 2003, **14**:513-521.
38. Phinney SD: **Fatty acids, inflammation, and the metabolic syndrome.** *Am J Clin Nutr* 2005, **82**:1178-1184.
39. Turk JR, Carroll JA, Laughlin MH, Thomas TR, Casati J, Bowles DK, Sturek M: **C-reactive protein correlates with macrophage accumulation in coronary arteries of hypercholesterolemic pigs.** *J Appl Physiol* 2003, **95**:1301-1304.
40. Verhamme P, Quarck R, Hao H, Knaapen M, Dymarkowski S, Bernar H, Van Cleemput J, Janssens S, Vermylen J, Gabbiani G, Kockx M, Holvoet P: **Dietary cholesterol withdrawal reduces vascular inflammation and induces coronary plaque stabilization in miniature pigs.** *Cardiovasc Res* 2002, **56**:135-144.
41. Pepys MB, Hirschfield GM, Tennent GA, Gallimore R, Kahan MC, Bellotti V, Hawkins PN, Myers RM, Smith MD, Polara A, Cobb AJA, Ley SV, Aquilina A, Robinson CV, Sharif I, Gray GA, Sabin CA, Jenvey MC, Kolstoe SE, Thompson D, Wood SP: **Targeting C-reactive protein for the treatment of cardiovascular disease.** *Nature* 2006, **440**:1217-1221.
42. Bisoendial RJ, Kastelein JJP, Stroes ESG: **C-reactive protein and atherogenesis: From fatty streak to clinical event.** *Atherosclerosis* 2007, **195**:e10-e18.
43. Koenig W, Khuseyinova N: **Biomarkers of atherosclerotic plaque instability and rupture.** *Arterioscler Thromb Vasc Biol* 2007, **27**:15-26.
44. Li SH, Szmitko PE, Weisel RD, Wang CH, Fedak PWM, Li RK, Mickle DAG, Verma S: **C-reactive protein upregulates complement-inhibitory factors in endothelial cells.** *Circulation* 2004, **109**:833-6.
45. Duplus E, Glorian M, Forest C: **Fatty acid regulation of gene transcription.** *J Biol Chem* 2000, **275**:30749-30752.
46. Ferre P: **The biology of peroxisome proliferator-activated receptors: relationship with lipid metabolism and insulin sensitivity.** *Diabetes* 2004, **53**:S43-50.
47. Ishibashi M, Egashira K, Hiasa K, Inoue S, Ni W, Zhao Q, Usui M, Kitamoto S, Ichiki T, Takeshita A: **Antiinflammatory and antiarteriosclerotic effects of pioglitazone.** *Hypertension* 2002, **40**:687-693.

Coronary microvascular dysfunction in a porcine model of early atherosclerosis and diabetes

van den Heuvel M.*, Sorop O.*, Koopmans S.J., Dekker R., de Vries R., van Beusekom H.M., Eringa E.C., Duncker D.J., Danser A.H. and van der Giessen W.J.
*Shared first authorship

Cardiovasc Diabetol. 2011 Jul 14;10:64

5

Coronary microvascular dysfunction in a porcine model of early atherosclerosis and diabetes

Mieke van den Heuvel[1,2,6]*, Oana Sorop[1,6]*, Sietse-Jan Koopmans[3,4], Ruud Dekker[3], René de Vries[2], Heleen M.M. van Beusekom[1], Etto C. Eringa[5], Dirk J. Duncker[1], A.H. Jan Danser[2], Willem J. van der Giessen[1,6†]

Departments of [1] Cardiology and [2] Internal Medicine, Division of Pharmacology, Vascular and Metabolic Diseases; Cardiovascular Research School COEUR, Erasmus University Medical Center, Rotterdam; [3] BioMedical Research of Wageningen University and Research Center, Lelystad; [4] Department of Animal Sciences, Adaptation Physiology Group of Wageningen University, Wageningen; [5] Laboratory for Physiology, Institute for Cardiovascular Research, Vrije Universiteit University Medical Center, Amsterdam; [6] Interuniversity Cardiology Institute of the Netherlands (ICIN-KNAW), Utrecht, The Netherlands

Submitted 28 March 2011; accepted in final form 28 September 2011

van den Heuvel M, Sorop O, Koopmans SJ, Dekker R, de Vries R, van Beusekom HM, Eringa EC, Duncker DJ, Danser AH, van der Giessen WJ. Coronary microvascular dysfunction in a porcine model of early atherosclerosis and diabetes. *Am J Physiol Heart Circ Physiol* 302: H85–H94, 2012. First published October 7, 2011; doi:10.1152/ajpheart.00311.2011.

Detailed evaluation of coronary function early in diabetes mellitus (DM)-associated coronary artery disease (CAD) development is difficult in patients. Therefore, we investigated coronaryconduit and small artery function in a preatherosclerotic DM porcine model with type 2 characteristics. Streptozotocin-induced DM pigs on a saturated fat/cholesterol (SFC) diet (SFC + DM) were compared with control pigs on SFC and standard (control) diets. SFC + DM pigs showed DM-associated metabolic alterations and early atherosclerosis development in the aorta. Endothelium-dependent vasodilation to bradykinin (BK), with or without blockade of nitric oxide (NO) synthase, endothelium-independent vasodilation to an exogenous NO-donor (*S*-nitroso-*N*-acetylpenicillamine), and vasocon-striction to endothelin (ET)-1 with blockade of receptor subtypes, were assessed in vitro. Small coronary arteries, but not conduit vessels, showed functional alterations including impaired BK-induced vasodilatation due to loss of NO ($P < 0.01$ vs. SFC and control) and reduced vasoconstriction to ET-1 ($P < 0.01$ vs. SFC and control), due to a decreased ET_A receptor dominance. Other vasomotor responses were unaltered. In conclusion, this model demonstrates specific coronary microvascular alterations with regard to NO and ET-1 systems in the process of early atherosclerosis in DM. In particular, the altered ET-1 system correlated with hyperglycemia in atherogenic conditions, emphasizing the importance of this system in DM-associated CAD development.

coronary circulation; diabetes mellitus; endothelial function; endothelin-1

DIABETES MELLITUS (DM) IS widespread in industrialized countries, and the incidence of type 2 is rapidly increasing worldwide. DM is an independent and strong predictor of coronary artery disease (CAD) (26), characterized by atherosclerosis of the conduit arteries (16, 23) and dysfunction of the microcirculation (51). Endothelial dysfunction is an important determinant of altered vascular reactivity and plays a major role in the genesis of DM-induced macro- and microvascular complications (51). Impaired coronary vasodilation, which is present well before the development of angiographically visible atherosclerosis in DM patients, is known to be at least partially due to impairment of the nitric oxide (NO) system (45). On the other hand, it is less clear whether and how the vasoconstricting endothelin (ET)-1 system is affected. Evidence of an altered ET-1 system in DM patients is predominantly coming from studies in the peripheral circulation in advanced stages of disease (30), and details on coronary alterations in relation to ET-1 in DM subjects are scarce (48, 62), in particular in early CAD development. Moreover, the pathological significance of the ET-1 system is still not completely established and is complicated by interactions with other vasoregulatory systems such as the NO system (57). Given that the regulation of endothelial function may vary in different vascular beds, additional research on alterations in NO and ET-1 systems in the coronary circulation during early CAD development is needed (20).

Knowledge of early coronary endothelial dysfunction is highly relevant, as it is an independent predictor of cardiovascular events (46), and its reversal might even result in the prevention of events. Such detailed evaluation is difficult to achieve in humans, since the precise onset of DM and CAD is usually unknown. Therefore, suitable animal models focusing on early disease development are necessary. Because of the highly similar anatomy and physiology of the cardiovascular system, porcine models with toxin-mediated pancreatic damage in combination with an atherogenic diet have been previously used to study DM and cardiovascular complications (16, 17, 23, 37, 41, 42, 63). However, most of these models have focused on advanced CAD with clear presence of atherosclerotic plaque.

In light of these considerations, the present study was undertaken to study coronary function early in the process of atherosclerosis development in a DM type 2-like porcine model (35) with focus on endothelial function via NO and ET-1 systems. For this purpose, we examined vasomotion in vitro of both coronary conduit and coronary small arteries of DM pigs after 10 wk on a saturated fat/cholesterol diet (SFC + DM) compared with control pigs on the same SFC diet (SFC) and to controls on a standard low fat diet (control). Because a previous study (34) indicated that there were minimal effects of

* M. van den Heuvel and O. Sorop contributed equally to this work.
† Deceased 6 June 2011.
Address for reprint requests and other correspondence: D. J. Duncker, Dept. of Experimental Cardiology, Ee2351A; Erasmus Univ. Medical Center, Dr. Molewaterplein 50-60, 3015 GE Rotterdam, The Netherlands (e-mail: d.duncker@erasmusmc.nl).

DM combined with unsaturated fat or starch diets on plasma cholesterol and central atherosclerosis development after 10 wk, a group of DM pigs on the standard diet was omitted.

MATERIALS AND METHODS

All experiments were performed in accordance with the American Physiological Society's *Guiding Principles in the Care and Use of Vertebrate Animals in Research and Training* and with approval of the Local Animal Ethics Committee of Lelystad, The Netherlands.

Animal Experiments

Before the start of the study period of 10 wk, 16 male crossbred pigs (Yorkshire × Landrace) were housed in three groups. Initially, the first group (control group, $n = 5$) was fed a standard diet for growing pigs, and the second and third groups (SFC, $n = 5$; and SFC + DM, $n = 6$) were fed a diet complemented with 25% of saturated fats and 1% of cholesterol (SFC diet). All pigs started the prestudy phase at ~30 kg of body wt and were fed ad libitum with free access to water. At ~70 kg of body wt, the pigs were individually housed in metabolism cages and fed two meals a day, during which the pigs had ad libitum access to food for 1 h. The food in the study period consisted of control diet in the case of the control pigs and of SFC diet in the case of the SFC and the SFC + DM pigs. Details of the composition of the study diets are given in Table 1.

In the first study week, pigs were anesthetized with intramuscular 2 mg/kg azaperone (Stressnil; Janssen, Tilburg, The Netherlands), followed by intravenous 15 mg/kg thiopental (Nesdonal; Rhone Merieux, Lyon, France). A permanent blood vessel catheter (Secalon Seldy, 16-G polyurethane; Becton Dickinson, Franklin Lakes, NJ) was inserted in the ear vein and fixed firmly to the ear. DM was induced in pigs of the SFC + DM group by slow titrated injection of streptozotocin (STZ; 80 mg/kg; Pharmacia and Upjohn, Kalamazoo, MI) in the ear vein to produce subtotal destruction of pancreatic β-cells, as described previously (34, 35). The following STZ injections (respectively on *days 3*, *5*, and *8* after the first dose) depended on the level of urinary glucose excretion (total STZ dose per pig ranged from 110 to 150 mg/kg), as we know from experience that urinary glucose excretion of ~400 g/day corresponded with a fasting plasma glucose concentration of 15–20 mmol/l. In the week of DM induction, the SFC + DM pigs had free access to food all day to avoid hypoglycemia. After 1 wk of DM settlement, the SFC + DM pigs were also placed on the twice daily feeding regime, as outlined above, until the end of the study.

Table 1. *Composition of the experimental diets: each ingredient contributing to the total amount of diet is listed*

Raw Material	Control Diet	SFC Diet
Soy beans, extracted	–	164.5
Potato protein	50.0	50.0
Animal fat (lard)	–	250.0
Barley	396.2	–
Wheat	500.0	–
Wheat glutenmeal	8.7	106.0
Sucrose	–	200.0
Fructose	–	200.0
Soy oil	17.3	–
Limestone	13.0	9.6
Monocalcium phosphate	6.9	10.8
Sodium chloride	4.0	4.7
Mineral/vitamin-premix	2.0	2.0
L-lysine hydrochloride	1.9	2.4
Cholesterol (extra)	–	10.0
Total, g/kg	1,000.0	1,010.0
Gross energy, MJ/kg	17.3	23.5

Ingredients are in g/kg. SFC, saturated fat/cholesterol.

In the seventh week of the study period, all pigs were sedated with 2 mg/kg of intramuscular azaperone (Stressnil), and anesthetized with 15 mg/kg of intravenous thiopental (Nesdonal). Pigs were intubated and anesthesia was maintained by inhalation of 3% sevoflurane combined with 40% oxygen and room air. All pigs were equipped with two permanent polyethylene blood vessel catheters (Tygon; Norton, Akron, OH), which were placed in the external jugular vein and in the carotid artery for blood sampling procedures and hemodynamic measurements during the study. The catheters were fixed firmly at the site of insertion, tunneled subcutaneously to the back of the pig and exteriorized between the shoulder blades. The catheters were filled and sealed off with saline containing heparin and penicillin (Procpen, Cuijk, The Netherlands) and kept in a backpack and glued to the skin. In the first week after surgery, pigs were habituated to stress-free blood sampling. In the eighth week of the study period, fasting blood samples for determination of glucose, fructosamine, insulin, β-hydroxybutyrate, nonesterified fatty acids, triglycerides, total cholesterol, very-low-density lipoprotein, low-density lipoprotein, high-density lipoprotein, tumor necrosis factor-α, and markers of liver function (aspartate aminotransferase) and kidney function (creatinine) were collected and analyzed. Moreover, at this time point a meal tolerance test was performed to assess DM metabolic characteristics. Blood was sampled repeatedly before, during, and up to 8 h after a morning meal. Per sampling time point, small amounts of blood (5 ml) were collected to monitor the responses of glucose, insulin, and triglycerides to the meal. Subsequently, blood pressure and heart rate were determined 5 h postprandially via the carotid artery using a digital electro-manometer (Type 330; Hugo Sachs Elektronik, March-Hugstetten, Germany). At the end of the study (after 10 wk), blood samples were collected for determination of plasma concentrations of ET-1. Then, all pigs were killed stress free by intravenous injection of an overdose of pentobarbital via the jugular vein catheter. Hearts were immediately excised and placed in cold, oxygenated Krebs bicarbonate buffer solution of the following composition (10^{-3} mol/l): 118 NaCl, 4.7 KCl, 2.5 $CaCl_2$, 1.2 $MgSO_4$, 1.2 KH_2PO_4, 25 $NaHCO_3$, and 8.3 glucose, pH 7.4. Coronary conduit and small arteries were isolated from the territory of the left anterior descending coronary artery for in vitro functional studies (5, 6). Furthermore, specimens of left anterior descending coronary artery and related coronary small arteries, liver, pancreas, and abdominal aorta were fixed for histology.

Vascular Function

Segments of conduit arteries (~4 mm length) were suspended in large organ baths containing Krebs bicarbonate solution aerated with 95% O_2-5% CO_2 (43). In this way, the buffer solution has a chemical composition with highest resemblance to that naturally occurring in blood and the oxygen content of the solution is high enough to compensate for lack of oxygen carriers in the in vitro setup (Radnoti tissue-organ bath principles; ADinstruments). Segments of small arteries (~2 mm length) were mounted in wire myographs (J. P. Trading, Aarhus, Denmark) and both conduit and small arteries were maintained at 37°C (5, 6). Both vessel types were subjected to the same protocol with vascular responses reflected in changes in isometric force as recorded with a Harvard isometric transducer. Following a 30-min stabilization period, the internal diameter was set to a tension equivalent to 0.9 times the estimated diameter at 100 mmHg of effective transmural pressure (27). After this normalization procedure, segments were exposed to depolarization by 10^{-1} mol/l potassium chloride (KCl; Sigma-Aldrich, Zwijndrecht, The Netherlands) to determine maximal contractile responses. Upon washout, in a first set of segments, endothelium-dependent vasodilator to bradykinin (BK; 10^{-10} to 10^{-6} mol/l; Sigma-Aldrich) was recorded upon preconstriction with the thromboxane-A_2 analog U46619 (10^{-7} mol/l). To quantify contributions of non-NO vasodilator substances to BK-induced dilation, the concentration-response curve (CRC) to BK

(10^{-10} to 10^{-6} mol/l) was constructed upon 30 min of preincubation with 10^{-4} mol/l of the NO-synthase inhibitor *N*-nitro-L-arginine methyl ester HCl (L-NAME; Sigma-Aldrich) in a second set of experiments. CRCs to ET-1 (10^{-10} to 10^{-7} mol/l; Sigma-Aldrich) were constructed from a third set of segments. In this set, endothelium-independent but NO-mediated vasodilation to the exogenous NO-donor *S*-nitroso-*N*-acetylpenicillamine (SNAP; 10^{-7} and 10^{-6} mol/l; Sigma-Aldrich) was also examined. To investigate the specific contributions of ET_A and ET_B receptors to the ET-1 response, CRCs to ET-1 (10^{-10} to 10^{-7} mol/l) were constructed after 30 min of preincubation with 10^{-6} mol/l ET_A receptor antagonist BQ123 (Sigma-Aldrich) or 10^{-8} mol/l ET_B receptor antagonist BQ788 (Sigma-Aldrich), as described previously (59).

Baseline diameters of the coronary small arteries of the functional experiments could not be accurately assessed because segments were isolated under nonpressurized conditions. However, using the measured optimal tension and point of passive stretch according to the Laplace formula obtained during the normalization procedure, the passive baseline inner-diameters were calculated (2, 27). To examine whether the small arteries had undergone changes in their passive tension characteristics, the values of the relaxed steady-state diameters at each wall tension of the normalization procedure (n = 24–29 vessels/group) were fitted by an exponential equation according to Halpern et al. (27).

Protein expression of ET_A and ET_B receptors was examined by Western blotting. Lysates of segments of coronary small arteries were loaded on gel and blotted. ET_A and ET_B expression was determined using specific primary antibodies (1:1000; sc-21193 and sc-21199; Santa Cruz Biotechnology, Heidelberg, Germany) and corrected for β-actin expression (1:100,000; A5441 Sigma-Aldrich).

Histology

Fresh sections of coronary conduit and small arteries, pancreas, liver, and abdominal aorta were fixed in 4% buffered formaldehyde for further histological analysis. Sections of paraffin-embedded coronary arteries were stained with resorcin fuchsin stain and hematoxylin eosin stain to assess the presence of intimal hyperplasia and vascular cell nuclei, respectively. In sections of pancreatic tissue, insulin content was assessed using a primary antibody against insulin (Sigma-Aldrich). Staining was visualized using a horseradish peroxidase-labeled secondary antibody and diaminobenzidine as a chromogen (DakoPatts, Amsterdam, The Netherlands). Insulin stained areas were measured using Clemex Vision PE (Clemex Technologies, Longueuil, Quebec, Canada) and are presented as a percentage of total analyzed area. Sections of liver tissue were stained with hematoxylin eosin stain. Lobular steatosis was scored (0 = fat accumulation in 0–5% of the hepatocytes per lobule; 1 = 5–33%; 2 = 33–66%; and 3 = >66%; Ref. 14). In the formaldehyde-fixed abdominal aorta, the amount of fatty streaks as a marker of early atherosclerosis development (AHA type II lesion; Ref. 60) was quantified as percentage of total area after Sudan IV fat staining (Sigma-Aldrich; Ref. 17).

Data Analysis

Comparison of normally distributed model characteristics was performed by one-way ANOVA. For skewed data, median values with interquartile ranges were calculated and the Kruskal Wallis test was used. Vasodilator responses were expressed as percentage of preconstriction to U46619 (BK) or ET-1 (SNAP). Vasoconstrictor responses to U46619, L-NAME and ET-1 were normalized to 10^{-1} mol/l KCl. Statistical analysis of CRCs was performed using two-way ANOVA for repeated measures, followed by Bonferroni's post hoc correction. For each CRC reaching a plateau, the concentration necessary to produce 50% of its maximal response was determined using logistic function (5, 6). The maximal response (E_{max}) of a vasoactive substance was assessed when appropriate. Associations between univariate data were evaluated by either Pearson or Spearman rank correlation. StatView 5.0 (SAS Institute) and SPSS 17.0 (IBM) were used for the analyses. Data are given as means ± SE or as median with interquartile ranges. Two-tailed $P < 0.05$ was considered statistically significant.

RESULTS

Model Characteristics

Gross energy intake was highest in SFC pigs, intermediate in control pigs, and lowest in SFC + DM pigs (54 ± 3.9 vs. 48 ± 1.7 vs. 44 ± 4.9 MJ/day; $P < 0.05$) without differences in hemodynamic parameters (Table 2). Although SFC + DM pigs had the lowest intake, they had a positive energy balance

Table 2. *Model characteristics*

	Control (n = 5)	SFC (n = 5)	SFC + DM (n = 6)
Anatomical parameters			
Body weight, kg	123 ± 4	131 ± 5	103 ± 8*
Corrected liver weight, %	1.37 ± 0.04	1.90 ± 0.08	2.4 ± 0.19*
Hemodynamic parameters			
Heart rate, beats/min	100 ± 4	103 ± 7	98 ± 12
Systolic blood pressure, mmHg	134 ± 5	145 ± 9	128 ± 7
Diastolic blood pressure, mmHg	88 ± 4	92 ± 7	84 ± 8
Plasma parameters			
Glucose, mmol/l	4.7 (4.6–4.8)	6.0 (5.5–6.0)	14 (10–23)*
Fructosamine, μmol/l	97 (77–100)	72 (64–78)	390 (154–588)*
Insulin, ng/ml	0.12 (0.08–0.26)	0.22 (0.13–0.32)	0.14 (0.06–0.25)
β-Hydroxybutyrate, μmol/l	<25	<25	165 ± 77*
NEFA, mmol/l	0.13 (0.12–0.18)	0.17 (0.16–0.23)	0.55 (0.21–0.58)*
Triglycerides, mmol/l	0.23 (0.18–0.25)	0.22 (0.18–0.23)	0.32 (0.16–0.47)
Total cholesterol, mmol/l	2.1 ± 0.05	9.9 ± 2.4	14 ± 2.7*
VLDL, mmol/l	0.08 ± 0.02	4.2 ± 1.59	6.9 ± 1.83*
HDL-to-LDL ratio	0.76 ± 0.07	0.23 ± 0.03	0.27 ± 0.05*
TNFα, pg/ml	46 (38–57)	49 (16–86)	82 (49–102)
Tissue parameters			
Pancreatic insulin staining, %	1.65 (1.38–2.12)	2.7 (1.88–2.8)	0.16 (0.13–0.26)*
Liver steatosis (grade)	0.00 ± 0.00	0.60 ± 0.25	1.33 ± 0.21*
Aortic fatty streak staining, %	0.04 (0.01–0.11)	0.66 (0.20–3.2)	11 (2.9–22)*

Values are means− SE or median with interquartile ranges. NEFA, nonesterified fatty acids. *$P < 0.05$ SFC + diabetes mellitus (DM) vs. SFC or control.

during the whole study period with no signs of urinary ketone body excretion. Therefore, the SFC + DM pigs did not show severe body wasting or signs of dehydration and did not require insulin therapy. In line with the lower levels of food intake, bodyweight at death was lowest in the SFC + DM group ($P < 0.05$). In contrast, relative liver weight of these pigs was significantly higher, with pronounced steatosis on histology ($P < 0.01$). Moreover, the abdominal aorta of SFC + DM pigs showed augmented fat staining ($P < 0.02$). The percentage of fatty streaks was increased >10-fold compared with SFC pigs, while control pigs demonstrated little fat staining. These fatty streaks consisted of several intimal cell layers with fat deposits (data not shown). In contrast, intimal hyperplasia was not observed in either coronary conduit or small arteries in any of the groups (Fig. 1). In summary, SFC + DM pigs showed a positive energy balance without insulin therapy, pronounced liver steatosis, and early atherosclerosis development only in the central aorta.

Plasma analysis showed significantly increased fasting glucose and fructosamine levels in SFC + DM pigs ($P < 0.01$), indicative of elevated glucose levels over the preceding week (Table 2). In contrast, fasting insulin concentrations were not altered. Therefore, a DM state was created with no absolute insulin deficiency. However, the ketone body β-hydroxybutyrate (which was below detection limit in control and SFC pigs) was significantly increased in SFC + DM pigs ($P < 0.02$), indicating a functional shortage of insulin in these animals. Indeed, immunohistochemistry confirmed a reduction in pancreatic insulin producing β-cells ($P < 0.01$). Also, nonesterified fatty acids levels were elevated in SFC + DM pigs ($P < 0.04$), again indicative of reduced insulin functionality. Although triglyceride levels tended to be highest in SFC + DM pigs, statistical significance was not reached. SFC + DM pigs also showed the most profound changes in lipid profile, characterized by significantly elevated total cholesterol and very low density lipoprotein levels and a reduced low-density lipoprotein-to-high-density lipoprotein ratio (all $P < 0.02$). Furthermore, these pigs showed a trend towards an increased inflammatory response with tumor necrosis factor-α ($P = 0.07$). In addition, the meal tolerance test showed sustained elevated postprandial plasma glucose levels in SFC + DM pigs together with a markedly reduced postprandial insulin response and a tendency toward an elevated triglyceride response as shown in Fig. 2. Taken together, SFC + DM pigs showed a markedly increased set point for plasma glucose, postprandial hypoinsulinemia with evidence of reduced insulin functionality, and dyslipidemia. No signs of liver or renal toxicity were observed between control, SFC and SFC + DM pigs (aspartate aminotransferase: 19 ± 1.6 vs. 19 ± 1.5 vs. 18 ± 2.0 U/l, P = NS; creatinine: 117 ± 5.0 vs. 124 ± 8.5 vs. 101 ± 6.4 10^{-6} mol/l, P = NS). Therefore, DM was safely induced, as previously described (28).

Coronary Vasomotor Function

Conduit arteries. SFC + DM and SFC groups showed similar baseline contractile responses to KCl and preconstriction to U46619 (both, P = NS). Segments from both groups dilated similarly to BK in a concentration-dependent manner (pEC_{50} SFC + DM vs. SFC: 7.9 ± 0.2 vs. 7.5 ± 0.3). Relaxations amounted up to 50% of the preconstriction level

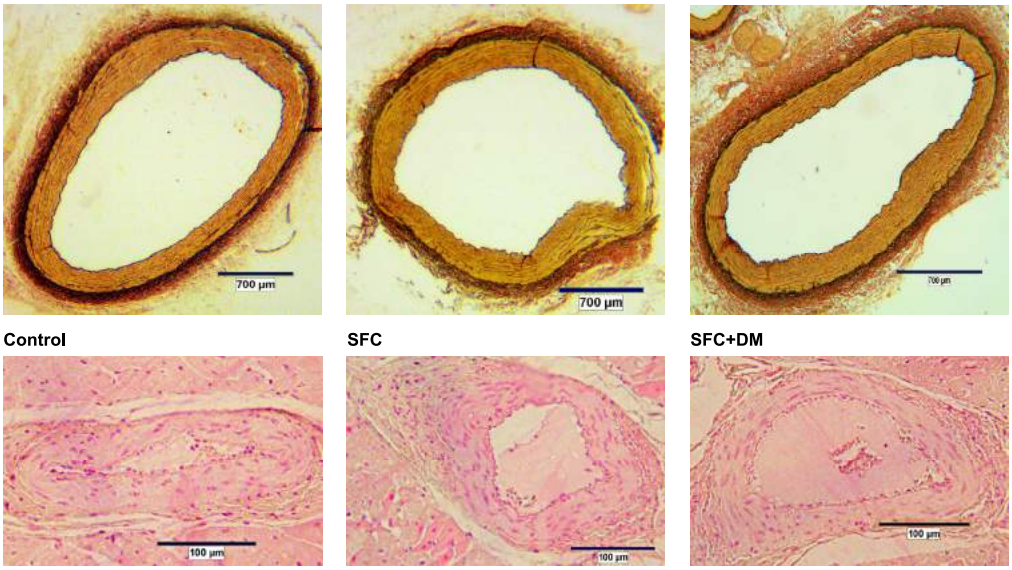

Fig. 1. Representative histological sections of coronary arteries of control (n = 5), saturated fat/cholesterol (SFC; n = 5), and SFC-diabetes mellitus (SFC + DM; n = 6) groups: conduit arteries (resorcin fuchsin stain; *top*; bar = 700 µm) and small arteries (hematoxylin eosin stain; *bottom*; bar = 100 µm).

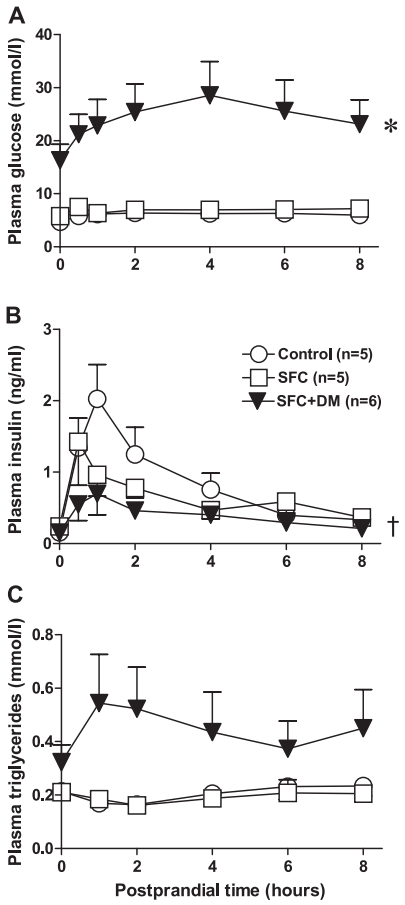

Fig. 2. Meal tolerance test: fasting levels and postprandial responses of plasma glucose (*A*), insulin (*B*), and triglycerides (*C*). Area under the curve (AUC) of the glucose response of SFC + DM pigs ($n = 6$) was significantly higher compared with both SFC ($n = 5$) and control ($n = 5$) pigs (*A*: $^{*}P < 0.01$). In contrast, the AUC of the insulin response was least in these animals compared with control pigs (*B*: $^{\dagger}P < 0.05$). AUCs of the triglyceride response of the 3 groups were not significantly different.

(Fig. 3*A*). Pretreatment with L-NAME almost completely abolished dilation to BK in both groups ($P < 0.01$, CRC L-NAME vs. no L-NAME), so that the effect of L-NAME was not different between both groups (Fig. 3*B*). ET-1 produced vasoconstriction in a concentration-dependent manner up to 125% of the response to KCl (pEC_{50} SFC + DM vs. SFC: 7.7 ± 0.2 vs. 7.5 ± 0.1) that was similar in both groups (Fig. 3*C*). Finally, the exogenous NO-donor SNAP induced identical vasodilator responses in both groups (Fig. 3*D*). These data are highly similar to those previously observed in control pigs (5).

Small arteries. The passive baseline inner-diameters of the coronary small arteries were similar (SFC + DM vs. SFC vs. control: 364 ± 19 vs. 333 ± 26 vs. 337 ± 19 μm; P = NS). Moreover, the small arteries showed similar baseline contractile responses to KCl and preconstriction to U46619, indicating equal vasoconstrictor potential between the groups (KCl SFC + DM vs. SFC vs. control: 3.6 ± 0.4 vs. 2.8 ± 0.5 vs. 2.8 ± 0.3 g; U46619: 2.5 ± 0.4 vs. 1.9 ± 0.3 vs. 2.4 ± 0.4 g; both, P = NS). Small arteries dilated to BK in a concentration-dependent manner in all groups. Relaxations amounted up to 90% of the preconstriction level but differed significantly between the groups (Fig. 4*A*). SFC + DM pigs showed a right-ward shift of the BK CRC (pEC_{50} SFC + DM vs. SFC vs. control: 8.0 ± 0.3 vs. 8.6 ± 0.2 vs. 8.5 ± 0.3; $P < 0.01$ CRC SFC + DM vs. SFC and control) without altering its maximal effect. After preincubation with L-NAME, the BK CRC of all groups was shifted to the right ($P < 0.01$, CRC L-NAME vs. no L-NAME), and the three curves were no longer significantly different. These findings indicate that the non-NO component of BK-induced vasodilation was identical in all three groups (Fig. 4*B*) and that the diminished response to BK in the absence of L-NAME was due to decreased NO production rather than a decrease in non-NO vasodilating substances, such as prostaglandins and endothelium-derived hyperpolarizing factors. The effect of L-NAME in the small arteries was more modest than in the conduit arteries, indicating a smaller NO component and a more pronounced non-NO component of the BK response, in agreement with previous results (5, 6). ET-1 induced vasoconstriction in a concentration-dependent manner (Fig. 4*C*). However, only SFC + DM pigs showed a clear downward shift of the ET-1 CRC ($P < 0.01$, SFC + DM vs. SFC vs. control), with a greatly diminished maximal response to the highest concentration of ET-1 (E_{max}: SFC + DM vs. SFC vs. control: 53 ± 16 vs. 136 ± 19 vs. 109 ± 8; $P < 0.05$). The exogenous NO-donor SNAP induced similar vasodilator responses in all groups, indicating intact vascular smooth muscle cell function (Fig. 4*D*).

ET receptor subtypes. In both SFC and control groups, ET_A receptor blockade, but not ET_B receptor blockade, attenuated the vasoconstrictor responses to ET-1 ($P < 0.05$ CRC ET_A vs. ET-1 and ET_B), indicating a predominant role for ET_A receptors in response to exogenous ET-1 (Fig. 5). However, for the SFC + DM pigs only a trend for ET_A receptor contribution could be noted ($P = 0.07$ CRC ET_A vs. ET-1), indicating a loss of ET_A dominance. Systemic ET-1 plasma levels were not different between the groups [SFC + DM vs. SFC vs. control: 1.26 (1.08–1.35) vs. 1.10 (0.96–1.28) vs. 1.07 (0.93–1.29) pg/ml; P = NS].

ET receptor expression. To examine whether altered expression of ET_A and ET_B receptors contributes to the reduced ET-1 responsiveness of small coronary arteries of the SFC + DM pigs, expression of ET_A and ET_B receptor protein in small arteries of the three groups were compared. No differences in ET_A expression were noted between the groups ($P = 0.26$; Fig. 6*A*). Similarly, no alterations in ET_B expression were observed ($P = 0.62$; Fig. 6*B*).

Arterial stiffness. The relaxed wall tension-strain relations of small arterial segments revealed no significant differences in optimal circumference among the three groups. However, the stiffness coefficient β was significantly higher in SFC + DM pigs compared with control pigs (SFC + DM vs. SFC vs. control: 8.1 ± 0.4 vs. 7.1 ± 0.4 vs. 6.6 ± 0.4; $P < 0.01$ SFC +

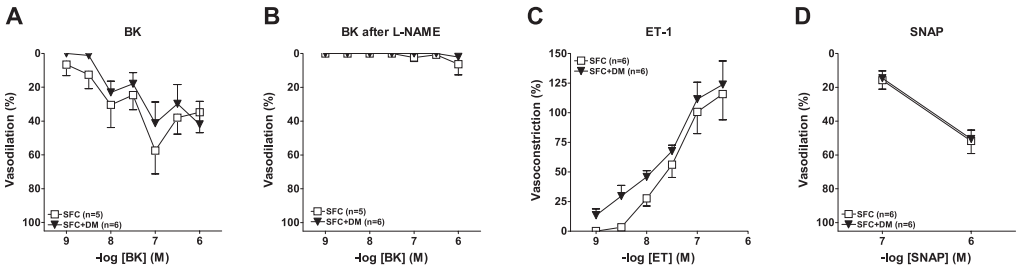

Fig. 3. Coronary conduit function of SFC and SFC + DM groups: endothelium-dependent vasodilation to bradykinin (BK; *A*) and to BK after preincubation with *N*-nitro-L-arginine methyl ester HCl (L-NAME; *B*), vasoconstriction to endothelin (ET-1; *C*), and endothelium-independent vasodilation to *S*-nitroso-*N*-acetylpenicillamine (SNAP; *D*). There were no significant differences between SFC and SFC + DM groups.

DM vs. control), suggesting an increase in stiffness in the SFC + DM pigs.

Correlation of vascular responses to metabolic alterations. The small sample size in the present study does not allow firm conclusions regarding correlations between vascular responses in vitro and metabolic abnormalities in vivo and should therefore be considered to be hypothesis generating only. Nevertheless, it is of interest to note that the maximal ET-1 response of coronary small artery function (ET-1 E_{max}) correlated well with the overall BK responsiveness (BK pEC_{50}; $r = 0.53$; $P < 0.05$), i.e., a reduced ET-1 response was associated with a reduced BK response. Moreover, ET-1 E_{max} correlated with the model characteristic of hyperglycemia: e.g., fructosamine ($r = -0.49$; $P < 0.05$), in contrast to BK pEC_{50} ($r = -0.19$; $P =$ NS).

DISCUSSION

The principal findings of this study of coronary function early in the process of diabetic atherosclerosis development are as follows: *1*) BK-induced endothelium-dependent vasodilatation was impaired in small coronary arteries of SFC + DM pigs, which was attributable to a loss of NO-mediated vasodilation. *2*) Although plasma ET-1 levels were not significantly changed, coronary small vessels of these pigs showed reduced ET-1-induced vasoconstriction, due to a decreased ET_A receptor dominance. *3*) Moreover, these vessels showed signs of structural changes reflected in an increased stiffness coefficient. *4*) In contrast to these observations in small arteries, the coronary conduit arteries of SFC + DM pigs did not show any alterations in vascular function at this stage of the disease.

Coronary endothelial dysfunction plays a key role in the pathogenesis of DM-associated cardiovascular events (46, 51). However, the affected vascular processes are not well understood and difficult to study in humans, hence requiring relevant animal models. Although small animal models are highly relevant to unravel disease mechanisms, their ability to fully mimic human disease is limited (64). Furthermore, while isolated vessels from other vascular beds, such as aorta, basilar and mesenteric arteries (12, 55, 56), or total heart perfusion (8, 61), have been studied in rodents, separate evaluation of coronary conduit vs. small artery function is difficult in small animals. Since human and porcine coronary anatomy and physiology are highly similar (19), a pig model to study CAD development with focus on vascular function appears to be highly relevant.

Coronary vascular alterations have been studied extensively in high-fat-fed prediabetic large animal models, including both dogs (33, 36, 58) and pigs (9, 10, 44), the results of which could be of value for patients with the metabolic syndrome (32). Also, atherosclerotic DM porcine models have been developed and successfully employed (16, 17, 23, 37, 41, 63). However, limited data on coronary endothelial function are available from these DM models and usually only in the presence of advanced CAD. Dixon et al. (17) studied DM minipigs, fed a high-fat, high-cholesterol diet, as early as 12 wk after DM induction and noted an increased percentage of

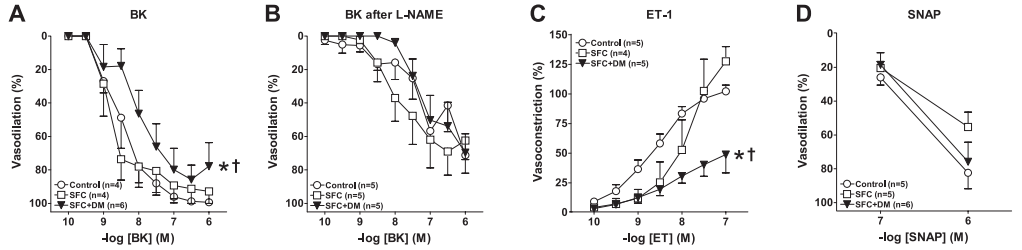

Fig. 4. Coronary small artery function of control, SFC, and SFC + DM groups: endothelium-dependent vasodilation to BK (*A*), and to BK after preincubation with L-NAME (*B*), vasoconstriction to ET-1 (*C*), and endothelium-independent vasodilation to SNAP (*D*). $*^{\dagger}P < 0.01$, SFC + DM vs. SFC and control.

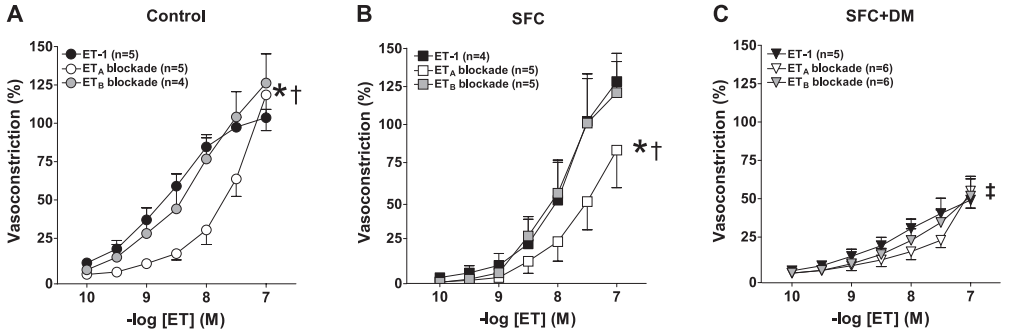

Fig. 5. Coronary small artery function: ET-1 responses after specific ET-1 receptor blockade (A = control; B = SFC; C = SFC + DM). ET_A receptor blockade resulted in impaired ET-1 induced vasoconstriction. $*^{\dagger}P < 0.01$ ET_A vs. ET-1 and ET_B; $^{\ddagger}P < 0.10$ ET_A vs. ET-1. ET_B receptor blockade had no significant effect on the ET-1 response in all groups.

contractile oscillations of coronary conduit arteries with unaffected endothelium-dependent vasodilation. Unfortunately, potential alterations in coronary microvascular function were not studied. Mokelke et al. (42) examined a specific aspect of coronary dysfunction at 20 wk of study duration in a diabetic, dyslipidemic swine model. Differential regulation of potassium currents in both coronary conduit and microvessels was studied, but the development of overall coronary endothelial dysfunction was not assessed. Therefore, information regarding the exact nature of endothelial alterations early in DM-associated coronary atherosclerosis is still incomplete and therefore new, well-characterized DM models continue to be of interest.

Using a recently developed DM type 2-like pig model (34, 35), we created conditions of hyperglycemia, hypoinsulinemia with reduced insulin functionality and dyslipidemia without requiring insulin replacement therapy and without signs of STZ-induced liver or kidney toxicity. These metabolic conditions mimic the human presentation of DM (11), in particular of advanced stage DM type 2 with hypoinsulinemia, dyslipidemia, and secondary pathology including liver steatosis and central atherosclerosis formation. We acknowledge that the model characteristics do not fully meet human DM type 2 or type 1 criteria. However, increased CAD risk caused by micro- and macrovascular complications is seen in both types of human DM. Therefore, classification may be less important than understanding the vascular alterations that mediate this complication (7). In the present DM model, we separately studied in vitro coronary function of both conduit and small sized arteries. The coronary arteries showed no signs of atherosclerosis yet. In addition, endothelium-dependent vasodilation of these arteries was unaltered and we observed no contractile oscillations during preconstruction, which contrasts with the results of Dixon et al. (17). However, we studied vascular function in normal sized pigs after 10 wk instead of 12 wk of study duration. The coronary small arteries showed changes towards increased vascular stiffness, comparable to human hypertensive DM type 2 pathology (54). Of notice, our results indicate that this process already starts before the onset of hypertension (25). Moreover, in these small arteries we confirmed the presence of endothelial dysfunction due to impaired NO-mediated vasodilation, in accordance with observations in the coronary microcirculation of DM patients (47), as well as in the coronary microcirculation (1) and the peripheral circulation (12, 49) of other large animal models of DM. This impaired endothelium-mediated, NO-dependent coronary microvascular dilation might be caused by reduced NO production, although we did not observe differences in total endothelial NO synthase expression in the small coronary arteries of the three groups (unpublished data). Alternatively, endothelial NO synthase uncoupling or NO scavenging, for example, by oxygen-derived free radicals, may have reduced NO bioavailability, as observed shortly after DM induction (1) or after long-term high-fat feeding (36) in dogs.

Interestingly, our results also demonstrate unaltered ET-1 plasma levels together with a reduction in coronary microvascular vasoconstriction to exogenous ET-1. ET-1 plasma levels have been reported to be either unchanged or elevated in DM patients, depending on disease duration and complications (30). The unaltered response to U46619 indicates that a general abnormality in vasoconstriction was not responsible for the reduced ET-1 response that we observed. In addition, evidence for a reduced responsiveness to ET-1 has been shown previously in the peripheral circulation of DM type 2 patients (15, 21, 38, 53, 54). However, such information specifically focusing on the coronary circulation of DM patients is not available. Only altered coronary responses to ET-1 have been reported after ischemia reperfusion in the specific setting of coronary intervention in DM type 2 patients with advanced CAD (22, 48, 62). In agreement with the present findings of control and SFC pigs, unaltered vasoconstriction to ET-1 was found between control and prediabetic dogs on a high-fat diet (33). In addition, unpublished data of our group show unaltered ET-1 responses in small coronary arteries of diabetic pigs fed an unsaturated fat rich diet for 10 wk. Therefore, specifically the combination of DM and an atherogenic diet appears to alter ET-1 responsiveness. In contrast, other DM animal models have reported enhanced ET-1 vascular responsiveness (31, 55, 56), also in the coronary circulation (8, 61). These differences between DM models are not readily explained but may involve differences in vascular beds (55, 56), genetically modified strains (8, 55, 56), and different temporal stages of DM-induction with subsequent other metabolic alterations (31, 61).

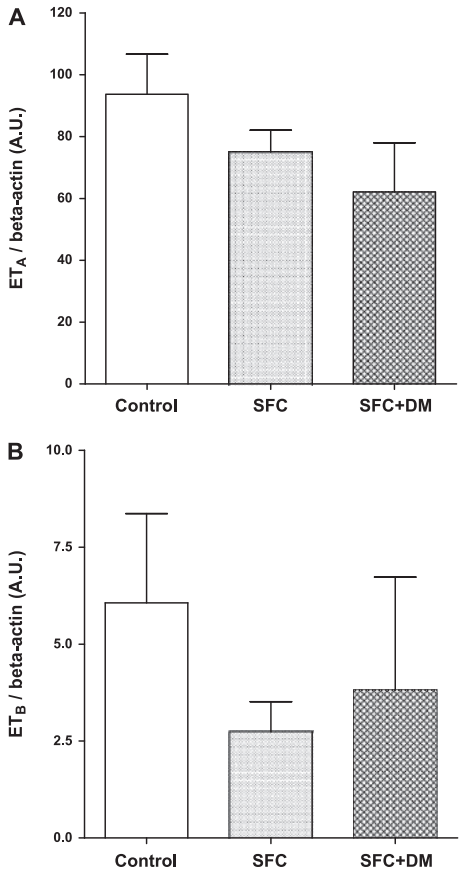

Fig. 6. ET-1 receptor protein expression in segments of coronary small arteries of control (n = 5), SFC (n = 5), and SFC + DM (n = 6) groups. No differences in ET_A (*A*) or ET_B (*B*) receptor expression were observed between the groups (P = NS). A.U., arbitrary units.

In the present model, ET-1 reactivity strongly correlated with hyperglycemia in atherogenic conditions, suggesting a mutual interaction between metabolic and vascular aspects. However, future studies are required to investigate these correlations in more detail.

The hyperglycemic state is thought to affect endothelial function via several biochemical pathways (3), unified by Brownlee (13) and Giacco and Brownlee (24). According to this mechanism the production of reactive oxygen species generated by mitochondrial uncoupling causes increased polyol pathway flux, increased intracellular formation of advanced glycation end-products (AGEs), increased expression of the receptor for AGEs and its activating ligands, activation of protein kinase C, and overactivity of the hexosamine pathway (3). High glucose levels also cause the formation of extracellular AGEs, which may affect endothelial function directly or via receptor-mediated mechanisms. In general, AGEs result in altered cellular signaling, promotion of gene expression, release of proinflammatory molecules and again the generation of oxidative stress (4). The results of the present study show evidence of chronic hyperglycemia, inflammation, and coronary endothelium-dependent microvascular dysfunction making the contribution of both reactive oxygen species and AGEs likely. Indeed, AGE-associated oxidative stress has been shown to reduce the bioavailability of endothelium-derived NO in several ways (4), which could result in blunted NO-mediated dilation. In addition, both AGEs (52) and oxidative stress (18) result in increased ET-1 expression, which via increased interstitial ET-1 concentrations and subsequent receptor desensitization could explain the reduced ET-1-mediated microvascular constriction of the present study.

In healthy humans and pigs, ET-1 contributes to basal coronary vascular tone mainly via the ET_A receptor (40, 50). In contrast, in our model of early DM-related atherosclerosis development, ET_A-receptor-mediated vasoconstriction was markedly reduced, indicating a switch in ET-1 receptor subtype contribution. Since both ET_A and ET_B receptor expressions were not significantly different between the three groups of pigs, specific ET_A receptor desensitization possibly played a role. However, the signaling cascade of ET-1 via the ET_A receptor involves several steps, culminating in an increase in intracellular calcium concentrations (29). Hence specific post-receptor signaling mechanisms associated with altered vasoconstrictor responses may be involved. Clinical studies (15, 21, 39) have reported unaltered, enhanced, and decreased ET_A receptor mediated responses in the peripheral circulation, which might be explained by differences in disease duration of the populations studied. Also, in animal models differences in receptor expression have been reported. High-fat-fed prediabetic dogs showed a decrease in ET_A receptor transcription of both coronary conduit and small arteries, although ET-1 responsiveness was still unaltered (33). An advanced atherosclerotic DM pig model demonstrated a switch in ET-1 receptor contribution with reduced ET_A dominance in vascular smooth muscle cells of coronary conduit arteries (37). Moreover, although a DM type 2 mouse model showed increased ET-1 induced coronary vasoconstriction, ET-1 receptor subtype contribution was altered with ET_A reactivity depending on intravascular NO availability (8). Also in the present model, coronary small artery alterations in NO and ET-1 systems were associated. Therefore, altered ET-1 responsiveness is likely to be accompanied by altered ET-1 receptor subtype contributions, either by receptor desensitization or at postreceptor level, and reflects the balance between both NO and ET-1 systems within a specific vascular bed.

In conclusion, in the present model of early atherosclerosis and DM, the loss of NO-mediated coronary microvascular dilation may be counteracted by the blunted ET-1 constriction, which may facilitate hyperemia. Indeed, according to the hemodynamic hypothesis of DM microangiopathy (38), an initial increase in microvascular blood flow followed by microvascular stiffness and disturbed autoregulation could finally result in decreased microvascular perfusion and exaggerated DM associated CAD development. Future studies with this DM model are warranted to prove this concept in vitro and to assess its relevance to the coronary vascular bed in vivo.

DISCLOSURES

No conflicts of interest, financial or otherwise, are declared by the author(s).

AUTHOR CONTRIBUTIONS

M.v.d.H., O.S., S.J.K., R.D. and R.d.V. analyzed data; M.v.d.H., O.S., S.J.K., H.M.M.v.B., E.C.E., D.J.D., A.H.J.D., and W.J.v.d.G. interpreted results of experiments; M.v.d.H. and O.S. prepared figures; M.v.d.H. drafted manuscript; M.v.d.H., O.S., S.J.K., E.C.E., D.J.D., A.H.J.D., and W.J.v.d.G. edited and revised manuscript; M.v.d.H., O.S., S.J.K., R.D. and R.d.V. performed experiments; O.S., S.J.K., A.H.J.D., W.J.v.d.G. conception and design of research; D.J.D., A.H.J.D., and W.J.v.d.G. approved final version of manuscript.

REFERENCES

1. **Ammar RF Jr, Gutterman DD, Brooks LA, Dellsperger KC.** Free radicals mediate endothelial dysfunction of coronary arterioles in diabetes. *Cardiovasc Res* 47: 595–601, 2000.
2. **Angus JA, Wright CE.** Techniques to study the pharmacodynamics of isolated large and small blood vessels. *J Pharmacol Toxicol Methods* 44: 395–407, 2000.
3. **Bakker W, Eringa EC, Sipkema P, van Hinsbergh VW.** Endothelial dysfunction and diabetes: roles of hyperglycemia, impaired insulin signaling and obesity. *Cell Tissue Res* 335: 165–189, 2009.
4. **Barlovic DP, Soro-Paavonen A, Jandeleit-Dahm K.** A RAGE biology, atherosclerosis and diabetes. *Clin Sci (Lond)* 121: 43–55, 2011.
5. **Batenburg WW, de Vries R, Saxena PR, Danser AHJ.** L-S-nitrosothiols: endothelium-derived hyperpolarizing factors in porcine coronary arteries? *J Hypertens* 22: 1927–1936, 2004.
6. **Batenburg WW, Popp R, Fleming I, de Vries R, Garrelds IM, Saxena PR, Danser AHJ.** Bradykinin-induced relaxation of coronary microarteries: S-nitrosothiols as EDHF? *Br J Pharmacol* 142: 125–135, 2004.
7. **Bellinger DA, Merricks EP, Nichols TC.** Swine models of type 2 diabetes mellitus: insulin resistance, glucose tolerance, and cardiovascular complications. *ILAR J* 47: 243–258, 2006.
8. **Bender SB, Klabunde RE.** Altered role of smooth muscle endothelin receptors in coronary endothelin-1 and α_1-adrenoceptor-mediated vasoconstriction in type 2 diabetes. *Am J Physiol Heart Circ Physiol* 293: H2281–H2288, 2007.
9. **Borbouse L, Dick GM, Asano S, Bender SB, Dincer UD, Payne GA, Neeb ZP, Bratz IN, Sturek M, Tune JD.** Impaired function of coronary BK(Ca) channels in metabolic syndrome. *Am J Physiol Heart Circ Physiol* 297: H1629–H1637, 2009.
10. **Borbouse L, Dick GM, Payne GA, Berwick ZC, Neeb ZP, Alloosh M, Bratz IN, Sturek M, Tune JD.** Metabolic syndrome reduces the contribution of K^+ channels to ischemic coronary vasodilation. *Am J Physiol Heart Circ Physiol* 298: H1182–H1189, 2010.
11. **Boullion RD, Mokelke EA, Wamhoff BR, Otis CR, Wenzel J, Dixon JL, Sturek M.** Porcine model of diabetic dyslipidemia: insulin and feed algorithms for mimicking diabetes mellitus in humans. *Comp Med* 53: 42–52, 2003.
12. **Brondum E, Nilsson H, Aalkjaer C.** Functional abnormalities in isolated arteries from Goto-Kakizaki and streptozotocin-treated diabetic rat models. *Horm Metab Res* 37, *Suppl* 1: 56–60, 2005.
13. **Brownlee M.** Biochemistry and molecular cell biology of diabetic complications. *Nature* 414: 813–820, 2001.
14. **Brunt EM, Neuschwander-Tetri BA, Oliver D, Wehmeier KR, Bacon BR.** Nonalcoholic steatohepatitis: histologic features and clinical correlations with 30 blinded biopsy specimens. *Hum Pathol* 35: 1070–1082, 2004.
15. **Cardillo C, Campia U, Bryant MB, Panza JA.** Increased activity of endogenous endothelin in patients with type II diabetes mellitus. *Circulation* 106: 1783–1787, 2002.
16. **Chatzizisis YS, Jonas M, Coskun AU, Beigel R, Stone BV, Maynard C, Gerrity RG, Daley W, Rogers C, Edelman ER, Feldman CL, Stone PH.** Prediction of the localization of high-risk coronary atherosclerotic plaques on the basis of low endothelial shear stress: an intravascular ultrasound and histopathology natural history study. *Circulation* 117: 993–1002, 2008.
17. **Dixon JL, Stoops JD, Parker JL, Laughlin MH, Weisman GA, Sturek M.** Dyslipidemia and vascular dysfunction in diabetic pigs fed an atherogenic diet. *Arterioscler Thromb Vasc Biol* 19: 2981–2992, 1999.
18. **Donato AJ, Gano LB, Eskurza I, Silver AE, Gates PE, Jablonski K, Seals DR.** Vascular endothelial dysfunction with aging: endothelin-1 and endothelial nitric oxide synthase. *Am J Physiol Heart Circ Physiol* 297: H425–H432, 2009.
19. **Duncker DJ, Bache RJ.** Regulation of coronary blood flow during exercise. *Physiol Rev* 88: 1009–1086, 2008.
20. **Ergul A.** Endothelin-1 and diabetic complications: Focus on the vasculature. *Pharmacol Res* 63: 477–482, 2011.
21. **Feng J, Liu Y, Khabbaz KR, Hagberg R, Robich MP, Clements RT, Bianchi C, Sellke FW.** Decreased contractile response to endothelin-1 of peripheral microvasculature from diabetic patients. *Surgery* 149: 247–252, 2011.
22. **Feng J, Liu Y, Khabbaz KR, Hagberg R, Sodha NR, Osipov RM, Sellke FW.** Endothelin-1-induced contractile responses of human coronary arterioles via endothelin-A receptors and PKC-alpha signaling pathways. *Surgery* 147: 798–804, 2010.
23. **Gerrity RG, Natarajan R, Nadler JL, Kimsey T.** Diabetes-induced accelerated atherosclerosis in swine. *Diabetes* 50: 1654–1665, 2001.
24. **Giacco F, Brownlee M.** Oxidative stress and diabetic complications. *Circ Res* 107: 1058–1070, 2010.
25. **Grey E, Bratteli C, Glasser SP, Alinder C, Finkelstein SM, Lindgren BR, Cohn JN.** Reduced small artery but not large artery elasticity is an independent risk marker for cardiovascular events. *Am J Hypertens* 16: 265–269, 2003.
26. **Haffner SM, Lehto S, Ronnemaa T, Pyorala K, Laakso M.** Mortality from coronary heart disease in subjects with type 2 diabetes and in nondiabetic subjects with and without prior myocardial infarction. *N Engl J Med* 339: 229–234, 1998.
27. **Halpern W, Mulvany MJ, Warshaw DM.** Mechanical properties of smooth muscle cells in the walls of arterial resistance vessels. *J Physiol* 275: 85–101, 1978.
28. **Hara H, Lin YJ, Zhu X, Tai HC, Ezzelarab M, Balamurugan AN, Bottino R, Houser SL, Cooper DK.** Safe induction of diabetes by high-dose streptozotocin in pigs. *Pancreas* 36: 31–38, 2008.
29. **Haynes WG, Webb DJ.** Endothelin as a regulator of cardiovascular function in health and disease. *J Hypertens* 16: 1081–1098, 1998.
30. **Hopfner RL, Gopalakrishnan V.** Endothelin: emerging role in diabetic vascular complications. *Diabetologia* 42: 1383–1394, 1999.
31. **Hopfner RL, McNeill JR, Gopalakrishnan V.** Plasma endothelin levels and vascular responses at different temporal stages of streptozotocin diabetes. *Eur J Pharmacol* 374: 221–227, 1999.
32. **Knudson JD, Dincer UD, Bratz IN, Sturek M, Dick GM, Tune JD.** Mechanisms of coronary dysfunction in obesity and insulin resistance. *Microcirculation* 14: 317–338, 2007.
33. **Knudson JD, Rogers PA, Dincer UD, Bratz IN, Araiza AG, Dick GM, Tune JD.** Coronary vasomotor reactivity to endothelin-1 in the prediabetic metabolic syndrome. *Microcirculation* 13: 209–218, 2006.
34. **Koopmans SJ, Dekker R, Ackermans MT, Sauerwein HP, Serlie MJ, van Beusekom HM, van den Heuvel M, van der Giessen WJ.** Dietary saturated fat/cholesterol, but not unsaturated fat or starch, induces C-reactive protein associated early atherosclerosis and ectopic fat deposition in diabetic pigs. *Cardiovasc Diabetol* 10: 64, 2011.
35. **Koopmans SJ, Mroz Z, Dekker R, Corbijn H, Ackermans M, Sauerwein H.** Association of insulin resistance with hyperglycemia in streptozotocin-diabetic pigs: effects of metformin at isoenergetic feeding in a type 2-like diabetic pig model. *Metabolism* 55: 960–971, 2006.
36. **Kume T, Kawamoto T, Okura H, Neishi Y, Hashimoto K, Hayashida A, Watanabe N, Kanda Y, Mochizuki S, Goto M, Yoshida K.** Evaluation of coronary endothelial function by catheter-type NO sensor in high-fat-diet-induced obese dogs. *Circ J* 73: 562–567, 2009.
37. **Lee DL, Wamhoff BR, Katwa LC, Reddy HK, Voelker DJ, Dixon JL, Sturek M.** Increased endothelin-induced Ca2+ signaling, tyrosine phosphorylation, and coronary artery disease in diabetic dyslipidemic Swine are prevented by atorvastatin. *J Pharmacol Exp Ther* 306: 132–140, 2003.
38. **McAuley DF, McGurk C, Nugent AG, Hanratty C, Hayes JR, Johnston GD.** Vasoconstriction to endothelin-1 is blunted in noninsulin-dependent diabetes: a dose-response study. *J Cardiovasc Pharmacol* 36: 203–208, 2000.
39. **McAuley DF, Nugent AG, McGurk C, Maguire S, Hayes JR, Johnston GD.** Vasoconstriction to endogenous endothelin-1 is impaired in patients with type II diabetes mellitus. *Clin Sci (Lond)* 99: 175–179, 2000.
40. **Merkus D, Houweling B, Mirza A, Boomsma F, van den Meiracker AH, Duncker DJ.** Contribution of endothelin and its receptors to the regulation of vascular tone during exercise is different in the systemic, coronary and pulmonary circulation. *Cardiovasc Res* 59: 745–754, 2003.

41. **Mohler ER III, Sarov-Blat L, Shi Y, Hamamdzic D, Zalewski A, Macphee C, Llano R, Pelchovitz D, Mainigi SK, Osman H, Hallman T, Steplewski K, Gertz Z, Lu MM, Wilensky RL.** Site-specific atherogenic gene expression correlates with subsequent variable lesion development in coronary and peripheral vasculature. *Arterioscler Thromb Vasc Biol* 28: 850–855, 2008.
42. **Mokelke EA, Dietz NJ, Eckman DM, Nelson MT, Sturek M.** Diabetic dyslipidemia and exercise affect coronary tone and differential regulation of conduit and microvessel K^+ current. *Am J Physiol Heart Circ Physiol* 288: H1233–H1241, 2005.
43. **Mulvany MJ, Halpern W.** Contractile properties of small arterial resistance vessels in spontaneously hypertensive and normotensive rats. *Circ Res* 41: 19–26, 1977.
44. **Neeb ZP, Edwards JM, Alloosh M, Long X, Mokelke EA, Sturek M.** Metabolic syndrome and coronary artery disease in Ossabaw compared with Yucatan swine. *Comp Med* 60: 300–315, 2010.
45. **Nitenberg A, Paycha F, Ledoux S, Sachs R, Attali JR, Valensi P.** Coronary artery responses to physiological stimuli are improved by deferoxamine but not by L-arginine in non-insulin-dependent diabetic patients with angiographically normal coronary arteries and no other risk factors. *Circulation* 97: 736–743, 1998.
46. **Nitenberg A, Valensi P, Sachs R, Cosson E, Attali JR, Antony I.** Prognostic value of epicardial coronary artery constriction to the cold pressor test in type 2 diabetic patients with angiographically normal coronary arteries and no other major coronary risk factors. *Diabetes Care* 27: 208–215, 2004.
47. **Nitenberg A, Valensi P, Sachs R, Dali M, Aptecar E, Attali JR.** Impairment of coronary vascular reserve and ACh-induced coronary vasodilation in diabetic patients with angiographically normal coronary arteries and normal left ventricular systolic function. *Diabetes* 42: 1017–1025, 1993.
48. **Papadogeorgos NO, Bengtsson M, Kalani M.** Selective endothelin A-receptor blockade attenuates coronary microvascular dysfunction after coronary stenting in patients with type 2 diabetes. *Vasc Health Risk Manag* 5: 893–899, 2009.
49. **Park Y, Capobianco S, Gao X, Falck JR, Dellsperger KC, Zhang C.** Role of EDHF in type 2 diabetes-induced endothelial dysfunction. *Am J Physiol Heart Circ Physiol* 295: H1982–H1988, 2008.
50. **Pernow J, Kaijser L, Lundberg JM, Ahlborg G.** Comparable potent coronary constrictor effects of endothelin-1 and big endothelin-1 in humans. *Circulation* 94: 2077–2082, 1996.
51. **Prior JO, Quinones MJ, Hernandez-Pampaloni M, Facta AD, Schindler TH, Sayre JW, Hsueh WA, Schelbert HR.** Coronary circulatory dysfunction in insulin resistance, impaired glucose tolerance, and type 2 diabetes mellitus. *Circulation* 111: 2291–2298, 2005.
52. **Quehenberger P, Bierhaus A, Fasching P, Muellner C, Klevesath M, Hong M, Stier G, Sattler M, Schleicher E, Speiser W, Nawroth PP.** Endothelin 1 transcription is controlled by nuclear factor-kappaB in AGE-stimulated cultured endothelial cells. *Diabetes* 49: 1561–1570, 2000.
53. **Rizzoni D, Porteri E, Guelfi D, Muiesan ML, Piccoli A, Valentini U, Cimino A, Girelli A, Salvetti M, De Ciuceis C, Tiberio GA, Giulini SM, Sleiman I, Monteduro C, Rosei EA.** Endothelial dysfunction in small resistance arteries of patients with non-insulin-dependent diabetes mellitus. *J Hypertens* 19: 913–919, 2001.
54. **Rizzoni D, Porteri E, Guelfi D, Muiesan ML, Valentini U, Cimino A, Girelli A, Rodella L, Bianchi R, Sleiman I, Rosei EA.** Structural alterations in subcutaneous small arteries of normotensive and hypertensive patients with non-insulin-dependent diabetes mellitus. *Circulation* 103: 1238–1244, 2001.
55. **Sachidanandam K, Elgebaly MM, Harris AK, Hutchinson JR, Mezzetti EM, Portik-Dobos V, Ergul A.** Effect of chronic and selective endothelin receptor antagonism on microvascular function in type 2 diabetes. *Am J Physiol Heart Circ Physiol* 294: H2743–H2749, 2008.
56. **Sachidanandam K, Harris A, Hutchinson J, Ergul A.** Microvascular versus macrovascular dysfunction in type 2 diabetes: differences in contractile responses to endothelin-1. *Exp Biol Med (Maywood)* 231: 1016–1021, 2006.
57. **Schmitz-Spanke S, Schipke JD.** Potential role of endothelin-1 and endothelin antagonists in cardiovascular diseases. *Basic Res Cardiol* 95: 290–298, 2000.
58. **Setty S, Sun W, Tune JD.** Coronary blood flow regulation in the prediabetic metabolic syndrome. *Basic Res Cardiol* 98: 416–423, 2003.
59. **Sorop O, Merkus D, de Beer VJ, Houweling B, Pistea A, McFalls EO, Boomsma F, van Beusekom HM, van der Giessen WJ, VanBavel E, Duncker DJ.** Functional and structural adaptations of coronary microvessels distal to a chronic coronary artery stenosis. *Circ Res* 102: 795–803, 2008.
60. **Stary HC, Chandler AB, Glagov S, Guyton JR, Insull W Jr, Rosenfeld ME, Schaffer SA, Schwartz CJ, Wagner WD, Wissler RW.** A definition of initial, fatty streak, and intermediate lesions of atherosclerosis A report from the Committee on Vascular Lesions of the Council on Arteriosclerosis, American Heart Association. *Circulation* 89: 2462–2478, 1994.
61. **Verma S, Arikawa E, Lee S, Dumont AS, Yao L, McNeill JH.** Exaggerated coronary reactivity to endothelin-1 in diabetes: reversal with bosentan. *Can J Physiol Pharmacol* 80: 980–986, 2002.
62. **Verma S, Maitland A, Weisel RD, Fedak PW, Li SH, Mickle DA, Li RK, Ko L, Rao V.** Increased endothelin-1 production in diabetic patients after cardioplegic arrest and reperfusion impairs coronary vascular reactivity: reversal by means of endothelin antagonism. *J Thorac Cardiovasc Surg* 123: 1114–1119, 2002.
63. **Wang YX, Fitch R, Li W, Werner M, Halks-Miller M, Lillis B, Vergona R, Post J, Sullivan ME, Verhallen PF.** Reduction of cardiac functional reserve and elevation of aortic stiffness in hyperlipidemic Yucatan minipigs with systemic and coronary atherosclerosis. *Vascul Pharmacol* 39: 69–76, 2002.
64. **Wu KK, Huan Y.** Diabetic atherosclerosis mouse models. *Atherosclerosis* 191: 241–249, 2007.

Serial coronary imaging of early atherosclerosis development in fast-food-fed diabetic and nondiabetic swine

van Ditzhuijzen N.S., van den Heuvel M., Sorop O., Rossi O., Veldhof T., Bruining N., Roest S., Ligthart J.M.R., Witberg K.T., Dijkshoorn M.L., Nieman K., Mulder M.T., Zijlstra F., Duncker D.J., van Beusekom H.M.M. and Regar E.

JACC Basic to Translational Science. 2016 Oct;449-6

6

Serial coronary imaging of early atherosclerosis development in fast-food-fed diabetic and nondiabetic swine

Nienke S. van Ditzhuijzen, MSc[a], Mieke van den Heuvel, MD[a], Oana Sorop, PhD[a], Alexia Rossi, MD, PhD[b], Timothy Veldhof, MSc[a], Nico Bruining, PhD[a], Stefan Roest, BSc[a], Jurgen M.R. Ligthart, RT[a], Karen Th. Witberg, CCRN[a], Marcel L. Dijkshoorn, BSc[a], Koen Nieman, MD, PhD[a], Monique T. Mulder, PhD[c], Felix Zijlstra, MD, PhD[a], Dirk J. Duncker, MD, PhD[a], Heleen M.M. van Beusekom, PhD[a], Evelyn Regar, MD, PhD[a]

From the [a] Department of Cardiology, Thoraxcenter, Cardiovascular Research School COEUR, Erasmus University Medical Center, Rotterdam, the Netherlands; [b] Department of Radiology, Erasmus University Medical Center, Rotterdam, the Netherlands; [c] the Department of Internal Medicine, Erasmus University Medical Center, Rotterdam, the Netherlands. Dr. Dijkshoorn is a consultant for Siemens Healthcare. Dr. Regar has received research support from St. Jude Medical through her institution. All other authors have reported that they have no relationships relevant to the contents of this paper to disclose.

Manuscript received April 4, 2016; revised manuscript received August 5, 2016, accepted August 22, 2016.

VISUAL ABSTRACT

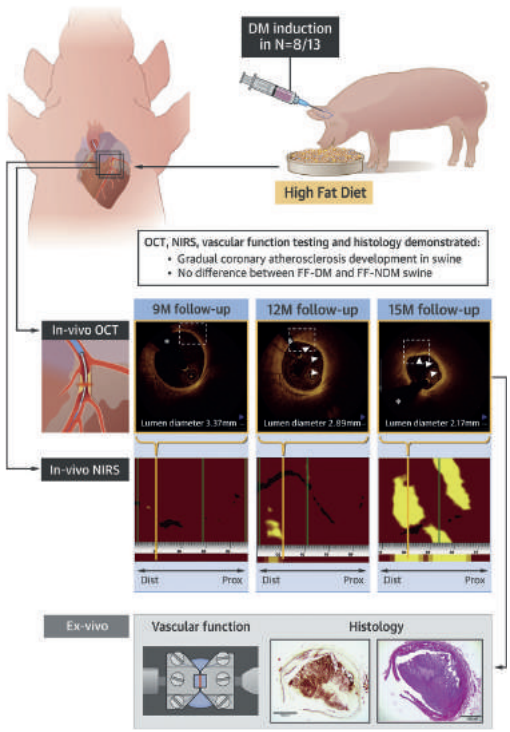

van Ditzhuijzen, N.S. et al. J Am Coll Cardiol Basic Trans Science. 2016;1(6):449-60.

HIGHLIGHTS

In swine with and without diabetes mellitus fed a fast-food diet:

- **OCT, NIRS, CCTA, vascular function testing, and histology can be consecutively and longitudinally performed to assess gradual coronary atherosclerosis development**
- **OCT and NIRS enabled detailed assessment of early coronary atherosclerosis development, whereas CCTA was not able to detect discrete early atherosclerotic changes.**
- **OCT, NIRS, vascular function testing, and histology demonstrated no differences in early atherosclerosis development.**

SUMMARY

Patients with diabetes mellitus (DM) are at increased risk for atherosclerosis-related events compared to non-DM (NDM) patients. With an expected worldwide epidemic of DM, early detection of anatomic and functional coronary atherosclerotic changes is gaining attention. To improve our understanding of early atherosclerosis development, we studied a swine model that gradually developed coronary atherosclerosis. Interestingly, optical coherence tomography, near-infrared spectroscopy (NIRS), vascular function, and histology demonstrated no differences between development of early atherosclerosis in fast-food-fed (FF) DM swine and that in FF-NDM swine. Coronary computed tomography angiography did not detect early atherosclerosis, but optical coherence tomography and near-infrared spectroscopy demonstrated coronary atherosclerosis development in FF-DM and FF-NDM swine. (J Am Coll Cardiol Basic Trans Science 2016;1:449–60)

Patients with diabetes mellitus (DM) have a 2- to 6-fold increased risk of encountering atherosclerosis-related events compared to their non-DM (NDM) counterparts (1). With a worldwide DM epidemic expected, early detection of anatomical and functional atherosclerotic changes in the coronary vasculature is gaining attention. However, patients typically present to the clinician with advanced atherosclerotic disease, thus complicating the study of early atherosclerosis development.

Animal models may provide a solution. Several small animal models, such as a rodent model, have been used to unravel disease mechanisms of coronary artery disease, but their ability to mimic human coronary artery disease is limited (2). The swine coronary artery model can be especially suitable for evaluation of human-like coronary artery disease development. First, the anatomy and physiology of swine hearts are similar to those of human hearts. Second, swine can be rendered diabetic by injection of streptozotocin. Third, patient-like spontaneous coronary atherosclerosis development can be mimicked by additionally feeding the swine a high-cholesterol, high-sugar diet (3); and fourth, in vivo longitudinal invasive and noninvasive imaging can be performed using imaging techniques such as optical coherence tomography (OCT), near-infrared spectroscopy (NIRS), and coronary computed tomography angiography (CCTA) (4). Ex vivo coronary endothelial function can be tested to compare functional with morphological coronary changes, and histology can be performed to assess the magnitude of coronary and aortic atherosclerosis at different time points (4,5).

Because there is little understanding about whether DM affects atherosclerosis development at the onset of coronary artery disease, the aim of our observational study was to assess whether DM affects early atherosclerosis development as assessed by OCT, NIRS, and CCTA in swine fed a high-cholesterol, high sugar ("fast-food") diet.

METHODS

This experimental study was approved by the Erasmus Medical Center Animal Ethics committee and performed in accordance with the Guide for Care and Use of Laboratory Animals (6).

See the Supplemental Appendix for a detailed description of all anaesthesia procedures. Thirteen male crossbred (Yorkshire × Landrace) swine ~11 weeks of age, with an average weight of ~30 kg were included. DM was induced in 8 randomly selected anesthetized swine by streptozotocin (single-dose intravenous injection, 140 mg/kg) (4). All swine were given a fast-food-fed (FF) diet containing 10% sucrose, 15% fructose, 25% (swine) lard, 1% cholesterol, and 0.7% sodium cholate (bile salts). Follow-up

FIGURE 1 **Study Flow Chart and Matching of Invasive Imaging**

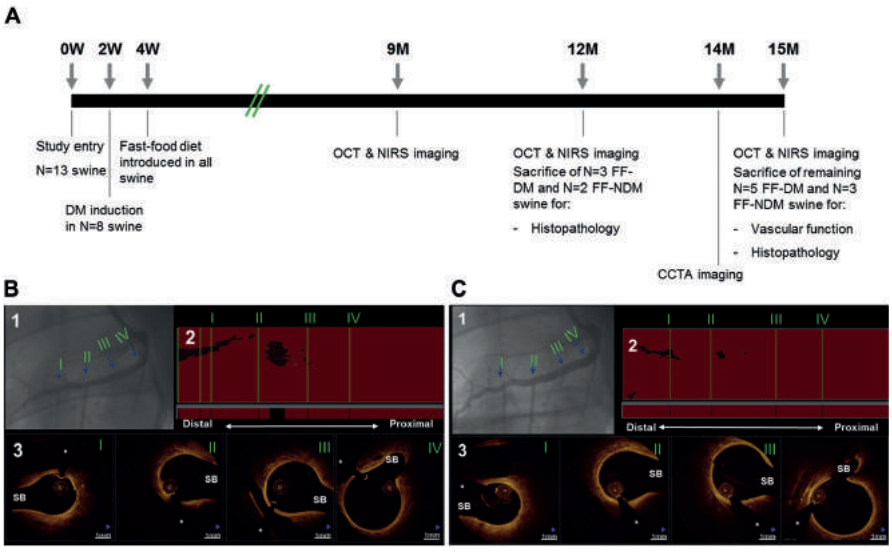

Study flow chart **(A)** and matching of invasive imaging **(B and C)**. The coronary angiograms **(B1 and C1)** were used to match the OCT **(B3 and C3)** and NIRS pullbacks **(B2 and C2)** within and at the various time points. Large side branches on the coronary angiogram **(I to IV)** were indicated on the NIRS chemogram **(B2 and C2, green lines, I to IV)** and matched to the OCT cross-sections **(B3 and C3, I to IV)**. *Guidewire. FF-DM = fast-food-fed swine with diabetes mellitus; FF- NDM = fast-food-fed swine without diabetes mellitus; M = month; NIRS = near-infrared spectroscopy; OCT = optical coherence tomography; SB = side branch; W = weeks.

duration was 12 months (n = 8 FF-DM swine; n = 5 FF-NDM swine) or 15 months (n = 5 FF-DM swine; n = 3 FF-NDM swine), during which similar growth patterns were achieved by adjusting individual caloric intake. See **Figure 1A** for the study flow chart.

Arterial access was obtained by introducing a 9-F sheath into the carotid artery to monitor blood pressure and obtain fasting blood samples to assess plasma insulin, glucose, triglyceride, total cholesterol (TC), low-density lipoprotein (LDL), and high-density lipoprotein (HDL) cholesterol levels and lipoprotein profiles. As control, fasting blood samples were taken from 5 weight-, age-, and sex-matched crossbred swine fed standard chow. In FF-DM swine, blood glucose and ketone levels were monitored weekly by 24-h urine samples, and insulin was administered when needed to prevent ketoacidosis. To obtain lipoprotein profiles, we used density gradient ultracentrifugation and measured cholesterol and triglyceride concentrations spectrophotometrically in the fractions in FF-DM (n = 7), FF-NDM (n = 3), and 1 age-, weight-, and sex-matched control swine (please see Supplemental Appendix for detailed methodology).

To evaluate insulin sensitivity, we calculated the quantitative insulin sensitivity check index, (QUICKI), as $[1/[(\log(I_o) + \log(G_o)]$, in which I_o is the fasting plasma insulin level in μU/ml, and G_o is the fasting blood glucose level in mg/dl, at 9, 12, and 15 months.

IN VIVO OCT, NIRS, AND CCTA. Serial OCT (C7XR FD system; St. Jude Medical, St. Paul, Minnesota) and NIRS (InfraReDx; Nipro, Osaka, Japan) were performed to assess the coronary arteries at 9, 12, and 15 months. The region of interest was defined as the region in which both the OCT and NIRS were available at all 2 time points (9 and 12 months) or all 3 time points (9, 12, and 15 months) and divided

FIGURE 2 **Early Atherosclerosis Development in FF-DM and FF-NDM Swine**

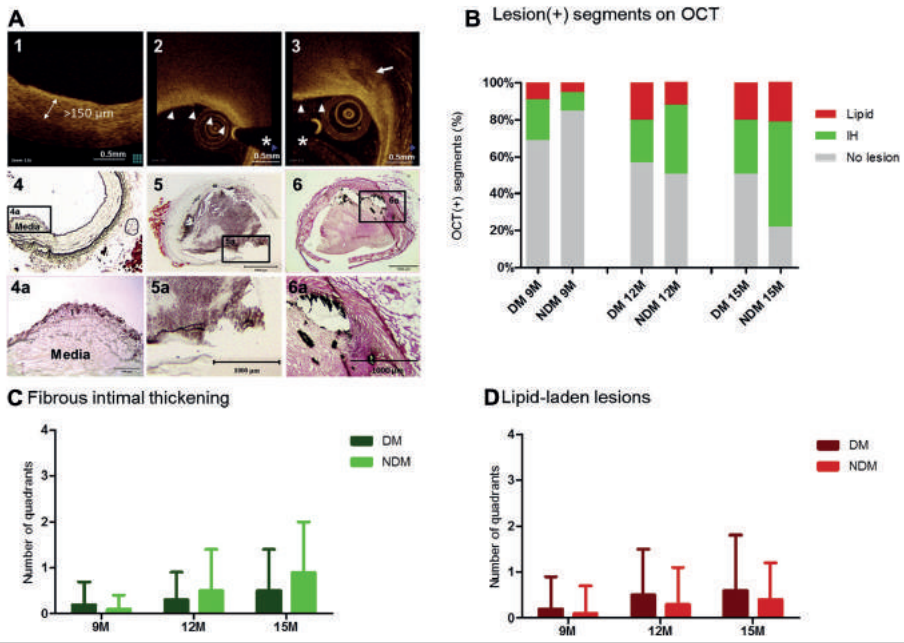

Several lesion types were assessed by OCT **(A1 to A3)** and matched with histology (oil-red-O stain **[A4 and A5]** and von Kossa stain **[A6]**). Intimal hyperplasia was defined as a fibrous lesion >150-μm thickness on OCT **(A1)**, a lipid-laden lesion **(A2 and A5)** as diffusely delineated signal-poor region **(A2, arrowheads)** and a mixed lesion **(A3 and A6)** as a lesion containing both lipid **(A3, arrowheads)** and calcium, which was defined as a sharply delineated signal-poor region **([A3] arrow)**. In histology, red stain denotes lipid **(A5)**, and closed bars denote calcium **(A6)** deposits. **(B)** The prevalence and burden **(C and D)** of disease increased from 9 to 15 months, without any significant differences between FF-DM and FF-NDM. *Guidewire artifact. Abbreviations as in Figure 1.

into 5-mm subsegments. On the NIRS chemogram, side branches were marked during image acquisition based on the location of the catheter in the coronary angiogram. Afterwards, NIRS and angiographically determined side branches were matched to side branches visible in the OCT pullback (**Figures 1B and 1C**).

See Supplemental Appendix for the OCT acquisition methods. Mean lumen area and diameter and minimum lumen diameter were documented for every frame within the region of interest using Curad vessel analysis software (Curad, Maastricht, the Netherlands).

OCT TISSUE CLASSIFICATION. The incidence of lesion-positive subsegments was noted, with lesions classified as fibrous intimal thickening (FIT), lipid-laden (LL), calcified, or mixed (**Figure 2A**), as published previously (7,8) (see Supplemental Appendix for lesion definitions). According to the lesion, lesion burden was calculated as the average number of lesion-positive quadrants (see the Supplemental Appendix for lesion definitions).

For NIRS, the catheter was withdrawn automatically with 0.5 mm/s pullback speed. Within the region of interest, NIRS documented the probability that lipid core plaque (LCP) was present. The data are displayed in a 2-dimensional arterial map, the chemogram. A summary of the results for each 2 mm of artery is computed (block chemogram) and mapped to a color scale with 4 discrete

colors. The colors correspond to the probability that LCP is present, with red indicating low probability and yellow high probability (red = $p \leq 0.57$; orange = 0.57; $\leq p < 0.84$; tan = $0.84 \leq p < 0.98$; yellow = $p \geq 0.98$) (9). In the current analysis, yellow, tan, or orange blocks were considered NIRS-positive.

See the Supplemental Appendix for description of the CCTA acquisition methods. CCTA was performed using the electrocardiography (ECG)-gated spiral scan mode. Data sets with optimal image quality were reconstructed mainly in the mid- to end-diastolic phase, with a slice thickness of 0.75 mm at an increment of 0.4 mm. Coronary lesions were classified as high-density or low-density as described previously (10). High-density was recognized as >220 HU, low density as <220 HU.

EX VIVO ASSESSMENT. Sacrifice was scheduled after imaging at 12 months (n = 3 FF-DM, n = 2 FF-NDM) or 15 months (n = 5 FF-DM, n = 3 FF-NDM). The hearts were removed, and the coronary tree was dissected free and placed in cold, oxygenated Krebs bicarbonate buffer solution or fixed in formalin.

Vascular function. To assess coronary endothelial function at 15 months, segments of coronary arteries (~4 mm in length) were suspended in organ baths. Vascular responses were measured as changes in isometric force to different concentrations of vasoactive substances, as described previously using pEC_{50} values (11-13). Endothelium-dependent relaxation to bradykinin (BK; 10^{-10} to 10^{-6} mol/l) was recorded upon pre-constriction with the thromboxane analog U46619 (10^{-6} mol/l). Similarly, endothelium-independent vasodilation to *S*-nitroso-*N*-acetylpenicillamine (SNAP; 10^{-9} to 10^{-5} mol/l) and endothelium-dependent vasoconstriction to endothelin-1 (10^{-10} to 10^{-7} mol/l) were assessed.

Histology. The remaining coronary artery segments were used for histological analysis. Two-millimeter segments taken from areas that demonstrated vascular wall changes by coronary angiography or OCT were embedded in optimal cutting temperature compound and then frozen. Tissue sections were cut and stained with hematoxylin-eosin as an overview stain, with oil-red-O (Abcam, Cambridge, United Kingdom) for lipid, and with von Kossa for calcium. The sections were matched with OCT and NIRS images by using angiographic images, pullback length, and arterial landmarks. Abdominal aortae were harvested and stained en face by oil-red-O to assess atherosclerotic burden, expressed as a percentage of stained area to total area.

STATISTICAL ANALYSIS. SPSS version 20.0 software (Chicago, Illinois) was used for statistical analysis. Normally distributed data are mean ± SD. For swine-level analysis, an independent sample Student *t* test was used, and for segment-level analysis, generalized estimating equations modeling was used. For swine-level repeated measures, repeated-measures analysis of variance and for segment-level generalized estimating equations modeling were performed using a linear response model with an autoregressive (1) structure for the within-cluster correlation matrix. A p value of <0.05 was considered statistically significant.

RESULTS

In all 13 swine plasma measurements were obtained. In **Figure 3A**, average plasma insulin, glucose, and cholesterol levels at the time of anesthesia were documented at 9, 12, and 15 months. TC, LDL, HDL, and triglyceride levels were higher in FF-DM and FF-NDM swine than in age-, weight-, and sex-matched control swine (TC: 2.14 ± 0.6 mmol/l; HDL: 0.94 ± 0.2 mmol/l; LDL: 1.22 ± 0.6 mmol/l; triglycerides: 0.20 ± 0.1 mmol/l). DM was successfully induced, as indicated by higher glucose levels in FF-DM than in FF-NDM swine ($p < 0.05$), and glucose levels remained fairly stable over time (**Figure 3B**). Mean arterial pressures were similar between FF-DM and FF-NDM swine at 15 months (89 ± 10 mm Hg, 85 ± 5 mm Hg, respectively; $p > 0.10$), and, because similar growth patterns were maintained by monitoring individual caloric intake (**Figure 3C**), mean final weights were comparable (FF-DM: 97.3 ± 7.3 kg; FF-NDM: 96.5 ± 3.3 kg; $p = 0.87$). Moreover, we created hyperglycemic levels in FF-DM swine without evidence of hypoglycemia.

Because lipoprotein profiles were comparable at 9, 12, and 15 months, all lipid profiles for FF-DM and FF-NDM swine were combined. LDL and triglycerides were higher and HDL lower in FF-DM and FF-NDM swine compared with an age-, weight-, and sex-matched control. Furthermore, the LDL peak was dramatically increased and shifted to the right in FF-DM and FF-NDM swine compared with control, indicating a lower density of LDL (Supplemental Figure 1).

QUICKI results were slightly lower in FF-DM swine (0.56 ± 0.10 at 9 months, 0.69 ± 0.14 at 12 months, and 0.53 ± 0.03 at 15 months) than in FF-NDM swine at 9 and 15 months (0.68 ± 0.11 at 9 months; 0.72 ± 0.14 at 12 months; and 0.60 ± 0.04 at 15 months; $p = 0.04$ at 9 months; $p = 0.69$ at 12 months; and $p = 0.02$ at 15 months). Compared with age-, weight-,

FIGURE 3 Plasma Measurement Results and Individual Insulin and Food Administration

A

	9M			12M			15M		
	FF-DM (n=8)	FF-NDM (n=5)	P-value *	FF-DM (n=8)	FF-NDM (n=5)	P-value *	FF-DM (n=5)	FF-NDM (n=3)	P-value*
Plasma measurements									
Glucose, mmol/L	15.31±8.08	4.38±0.66	0.01	12.96±6.43	4.7±1.44	0.01	17.64±10.15	5.37±1.22	0.09
Insulin, µ/mL	0.28±0.07	0.44±0.18	0.04	0.19±0.15	0.36±0.20	0.12	0.35±0.26	0.52±0.07	0.33
Total cholesterol, mmol/L	20.30±5.75	17.84±5.10	0.45	18.23±4.97	15.84±2.38	0.34	16.82±3.83	14.33±4.16	0.42
LDL, mmol/L	16.57±5.41	14.63±4.56	0.52	14.63±0.57	12.67±1.95	0.39	13.63±3.82	11.30±3.54	0.43
HDL, mmol/L	5.22±0.63	5.64±0.55	0.26	5.68±0.87	5.33±0.60	0.46	5.12±0.90	5.27±0.68	0.81
Triglycerides, mmol/L	1.15±0.73	0.43±0.22	0.03	0.95±0.71	0.37±0.20	0.06	1.26±1.12	0.35±0.07	0.14

B

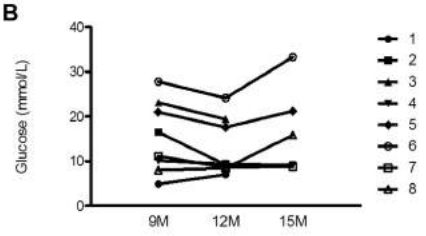

C

Animal	1	2	3	4	5	6	7	8	9	10	11	12	13
Sacrifice moment	12M	12M	12M	15M	15M	15M	15M	15M	12M	12M	15M	15M	15M
Frequency of insulin given	8	8	47	12	9	56	8	8	-	-	-	-	-
Total insulin given (U)	70	70	357	120	85	489	70	70	-	-	-	-	-
Average diet (gram/week)	661± 84	738± 83	873± 79	793± 80	786 ± 97	1295± 316	690± 99	725± 86	634± 63	589± 69	661± 73	661± 92	673± 86

Plasma measurement results **(A and B)** and individual insulin and food administration **(C)**. Data are mean ± SD. Animals 1 to 8 are FF-DM; 9 to 13 are FF-NDM. 9M = 9-month follow-up; 12M = 12-month follow-up; 15M = 15-month follow-up. *p value = comparison between FF-DM and FF-NDM swine.

and sex-matched control swine, QUICKI results were reduced in both the FF-DM and the FF-NDM swine at 9 months ($p = 0.02$) and 15 months ($p < 0.01$), suggesting that insulin resistance occurred due to experimentally induced islet dysfunction as well as the FF diet.

OCT, NIRS, AND CCTA FINDINGS. Serial 9- and 12-month OCT and NIRS were performed in 12 of 13 swine, and additional 15-month evaluations were performed in 7 of 8 swine. Due to technical difficulties, NIRS could not be performed in 1 swine at 9 months, which was excluded from analysis. Additionally, 1 swine died during imaging at 15 months due to a technical complication that caused myocardial ischemia. CCTA was performed in all 8 swine at 14 months ($n = 5$ FF-DM, $n = 3$ FF-NDM).

Mean and minimal lumen diameters decreased slightly from 9 to 15 months in all swine ($p > 0.10$), without a significant difference between FF-DM and FF-NDM swine ($p > 0.10$) (Supplemental Table 1).

OCT demonstrated focal lesions that were highly variable in presence, location, and morphology. Between FF-DM and FF-NDM, there were no differences regarding lesion type ($p = 0.42$ for FIT; $p = 0.77$ for LL) or burden ($p = 0.17$ for intimal hyperplasia; $p = 0.49$ for LL), except for 1 mixed lesion that developed in an FF-DM swine with a

FIGURE 4 **Lipid-Containing Lesion Development Observed by OCT, NIRS, and Histology**

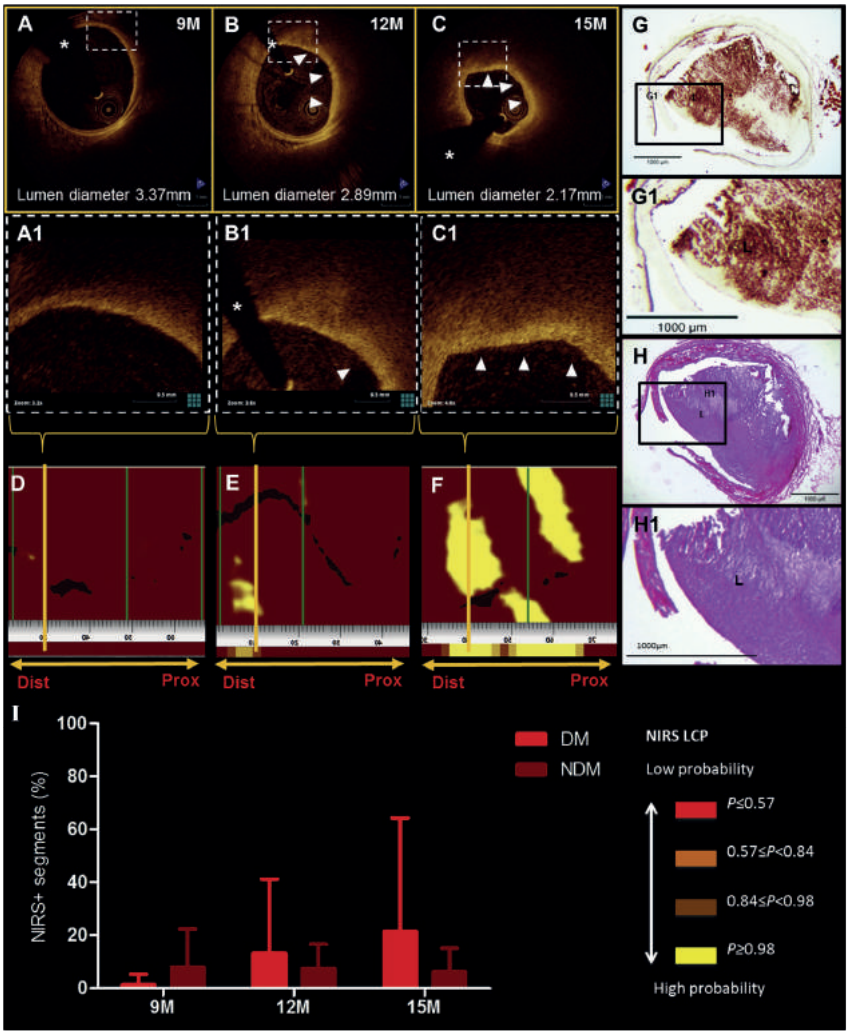

The development of an eccentric LL lesion was observed by OCT **(A to C, arrowheads)** and NIRS **(D to F, yellow)** from 9 (9M) to 12 (12M) and 15 (15M) months. The OCT cross-sections **(A to C)** correspond to the region in the NIRS chemograms **(D to F)**, shown by the **orange lines**. At 15 months, a high lipid burden was detected by OCT **(C, arrowheads)** and NIRS **(F, yellow)**. Histological analysis **(G and H)** of sequential sections stained with Oil red-O **(G)** and hematoxylin and eosin **(H)** stain confirmed the development of an eccentric atheromatous plaque with a large lipid pool **(L in G1 and H1)**. The percentage of NIRS-positive segments increased over time in both FF-DM and FF-NDM swine **(I)**. The graph shows the mean percentage of NIRS-positive segments per swine. Dist = distal; Prox = proximal; LCP = lipid core plaque; LL = lipid laden; other abbreviations as in Figure 1.

FIGURE 5 Concentration Response Curves to BK, SNAP, and ET-1

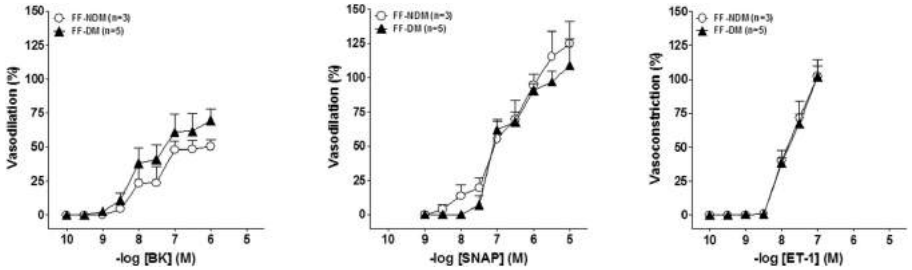

Concentration response curves to BK **(left)**, SNAP **(middle),** and ET-1 **(right)** of coronary segments of FF-DM and FF-NDM swine. No significant differences in vasodilatory or vasoconstrictor responses were noted. BK = bradykinin; ET = endothelin; SNAP = *S*-nitroso-*N*-acetylpenicillamine; other abbreviations as in Figure 1.

calcified burden that increased from 2 lesion-positive quadrants at 9 months to 3 lesion-positive quadrants at 15 months. Of the 115 segments analyzed at 9 months (n = 74 FF-DM; n = 41 FF-NDM), 17% demonstrated FIT and 8% LL. From 9 to 15 months, the prevalence of disease increased in FF-DM and FF-NDM (**Figures 2B to 2D**). At 12 months, 28% of subsegments displayed FIT and 18% LL. At 15 months, 40% demonstrated FIT and 21% LL. Similarly, lesion burden increased, indicated by the increased number of lesion-positive quadrants (**Figures 2B to 2D**). Hence, lipid burden increased, but no OCT-derived thin-cap fibroatheroma developed in any swine (mean cap thickness: 0.21 ± 0.00 mm in FF-DM; 0.18 ± 0.00 mm in FF-NDM; $p > 0.10$; minimal cap thickness: 0.07 mm in FF-DM; 0.10 mm in FF-NDM at 15 months).

Similar to the OCT results that demonstrated an increase in LL appearance (7% to 21%) and lipid burden, NIRS demonstrated an increase in the probability that LCP was present from 9 to 15 months (3% to 12% NIRS-positive subsegments) (**Figure 4**). Agreement between OCT and NIRS for the presence of lipid-containing lesions was moderate ($\kappa = 0.56$).

CCTA documented a single low-density lesion (186.0 ± 38.3 HU) in the swine that died during the intracoronary imaging procedure at 15 months (Supplemental Figure 2). In the remaining swine, CCTA was unable to detect any coronary lesion, despite the fact that OCT and NIRS showed the development of calcified lesions or lipid-containing lesions, respectively.

EX VIVO FINDINGS. Vascular function. The contractile response to the endothelium-independent vasoconstrictor (U46619) was not different between FF-DM and FF-NDM at 12 months (91 ± 47 mm vs. 98 ± 45 mm, respectively; $p > 0.10$). Coronary segments dilated to endothelium-dependent and -independent vasodilators (BK and SNAP) in a concentration-dependent manner. FF-DM swine demonstrated a reduced response to the endothelium-dependent vasodilator BK similar to that of FF-NDM swine (pEC50: FF-DM 7.6 ± 0.5 vs. FF-NDM 7.7 ± 0.3; $p > 0.10$). The response to the endothelium-independent vasodilator SNAP remained unaltered in FF-DM and FF-NDM ($p > 0.10$), and the response to the endothelium-dependent vasoconstrictor ET-1 was increased (Emax FF-DM: 102 ± 18 vs. FF-NDM: 102 ± 22; $p > 0.10$) (**Figure 5**).

Histology. Of the swine that died during the imaging procedure, histological analysis demonstrated an eccentric atherosclerotic lesion with necrotic core in the distal left circumflex coronary artery (Supplemental Figure 3). In the remaining swine, coronary atherosclerosis was heterogeneously divided between and within swine, ranging from early (**Figure 2A4**) to more advanced atherosclerosis (**Figures 2A5 and 2A6**), as was also documented by OCT (**Figure 2**).

Substantial aortic atherosclerosis developed in all swine at 12 months (72 ± 6% surface area covered by plaque in FF-DM and 58 ± 12% in FF-NDM) and at 15 months (67 ± 9% FF-DM and 46 ± 31% FF-NDM; $p > 0.10$) (Supplemental Figure 4). There was no correlation between the percentage of aortic

atherosclerosis and triglyceride (R^2: 0.12; p = 0.24), TC (R^2 0.26; p = 0.08), LDL (R^2 0.22; p = 0.11) or HDL levels (R^2: 0.25; p = 0.09). Furthermore, there was no relationship between abdominal aortic atherosclerosis and coronary atherosclerosis. The R^2 value was 0.01 (p = 0.73) for aortic atherosclerosis compared with that for any lesion observed by OCT, and R^2 was 0.10 (p = 0.34) for aortic atherosclerosis compared to that for NIRS-positive lesions.

DISCUSSION

We present a longitudinal, multimodal imaging study assessing early atherosclerosis development in FF-DM and FF-NDM swine. OCT, NIRS, vascular function, and histology demonstrated no differences in early atherosclerosis development between FF-DM and FF-NDM swine. OCT and NIRS enabled the detailed assessment of early coronary atherosclerosis, demonstrating focal lesions that were highly variable in presence, location, and morphology in all swine, whereas CCTA was not able to detect these discrete early atherosclerotic changes.

ATHEROSCLEROSIS DEVELOPMENT IN FF-DM VERSUS FF-NDM SWINE. As expected, coronary and aortic atherosclerosis progressed in all swine over time. In line with findings by Fernandez-Friera et al. (14), who demonstrated variable distribution of subclinical atherosclerosis in coronary arteries and aortae of middle-aged patients, we observed no correlation between aortic and coronary atherosclerosis within swine. Furthermore, a gene expression study demonstrated that inflammatory genes were markedly upregulated in coronary arteries compared with aorta from the same animal, potentially explaining the different atherosclerosis development in the different vascular beds (15).

Between FF-DM and FF-NDM swine, there were no significant differences in extent or morphology of atherosclerosis as assessed by intracoronary imaging, and there were no differences in endothelium-dependent and independent vasodilation. This might indicate a final common pathway in the atherosclerotic disease process, as has also recently been described in a mini-pig model, with a similar atherosclerosis development in DM and NDM swine (16). However, Duff et al. (17) was one of the first to assess experimental atherosclerosis and suggested that hyperglycemia served as a protective factor against the development of experimental atherosclerosis in rabbits. The differences between our study findings and those by Duff et al. (17) regarding the effect of hyperglycemia on the development of atherosclerosis may be explained by several factors, including species differences, duration of DM, the toxins used to induce DM, and the type and amount of diet given to the swine (18).

First, rabbits are highly responsive to cholesterol manipulation and develop lesions in a fairly short time. Lesions are generally fattier and more macrophage rich than human lesions (19). Swine, on the other hand, develop spontaneous coronary atherosclerosis similar to humans (4). Second, follow-up by Duff et al. (17) reached up to 4 months, whereas we followed the FF-DM and FF-NDM swine from 9 months to either 12 or 15 months. The protective effect of hyperglycemia might only have been apparent in the early stages of the disease. This observation of protection against atherosclerosis development is in line with observations by Niccoli et al. (20), who demonstrated that diabetic patients experience their first event at a later stage of atherosclerotic disease than nondiabetic patients. Third, Duff et al. (17) used alloxan to render the rabbits diabetic, whereas we used a single-dose injection of streptozotocin. Differences in the toxin used to induce DM might have resulted in noncomparable atherosclerosis development. Fourth, we fed our swine twice daily but monitored individual caloric intake to maintain similar growth patterns, whereas Duff et al. (17) fed their rabbits ad libitum. Monitoring individual caloric intake might have accounted for similar atherosclerosis development in FF-DM and FF-NDM swine.

Interestingly, DM was associated with accelerated atherogenesis under comparable conditions of hyperlipidemia in other swine models. Moreover, Dixon et al. (21) and Gerrity et al. (22) demonstrated enhanced lesion development in diabetic hyperlipidemic swine. The differences between our findings of a similar atherosclerosis development between FF-DM and FF-NDM swine and the findings by Dixon et al. (21) and Gerrity et al. (22) may also be explained by differences in species, duration of diabetic disease, toxins used to induce diabetes mellitus, and type and amount of diet given to the swine (18). Dixon et al. (21) used male Sinclair miniature swine and induced diabetes mellitus by using alloxan, whereas Gerrity et al. (22) used Yorkshire swine and induced diabetes by using 50 mg/kg streptozotocin each day for 3 days; we used crossbred Yorkshire × Landrace swine and induced diabetes by a single-dose injection of 140 mg/kg streptozotocin.

Furthermore, Gerrity et al. (22) fed the swine ad libitum in the beginning of the study, whereas we fed our swine twice daily and monitored individual caloric intake to achieve similar growth patterns. This might have resulted in similar atherosclerosis development in the FF-DM and FF-NDM swine in our study.

Because our swine demonstrated lipid profiles similar to those of the swine studied by Gerrity et al. (22) and Dixon et al. (21) but demonstrated different patterns of atherosclerosis development, we believe that hypercholesterolemia, with or without hyperglycemia, is not the only factor contributing to the development of atherosclerosis in these animal models.

Factors such as duration of DM and hypertension may attribute to the severity of atherosclerotic disease. Moreover, hypertension, not present in the current study, has been associated with adverse atherosclerosis-related events in DM patients (23). Future studies in atherosclerotic swine should consider using older-aged swine and include risk factors such as hypertension to accurately evaluate development of advanced coronary atherosclerosis.

COMPARISON OF IMAGING TECHNIQUES. Over time, the prevalence and extent of disease increased in FF-DM and FF-NDM swine as detected by OCT and NIRS. OCT demonstrated increasing LL appearance and lipid burden (**Figure 2**), and NIRS demonstrated an increase in the probability that LCP was present from 9 to 15 months (**Figure 4**). Interestingly, a moderate agreement was observed between OCT and NIRS for the detection of lipid. This finding is in line with a previously published study that demonstrated a moderate correlation between OCT and NIRS for detection of lipid and measurement of lipid contents (24). In contrast to OCT, which visualizes vessel structure and thus lipid morphology directly, NIRS provides calculated values of the probability of lipid in each pixel on the vessel surface (9). This difference in data acquisition may contribute to the moderate correlation between the 2 modalities.

CCTA did not detect any of the lesions documented by OCT or NIRS. Subtle differences in tissue contrast were not noted because most of the lesions were small, nonobstructive, and noncalcified, with a lesion burden of 1 to 2 lesion-positive quadrants. Moreover, the small nonobstructive coronary plaques observed in our swine appeared to be beyond the resolution of the technology (25). In previous studies, CT emerged as a noninvasive technique to exclude coronary artery disease and demonstrated good accuracy for detection of coronary artery stenosis and assessment of high-density and low-density lesions (10,26). However, CCTA is limited by the fact that the image contrast between plaque and other soft tissues (e.g., FIT) is small (27). This may affect identification and sizing of coronary plaque and most likely explains the inability of CCTA to detect the mainly noncalcified lesions in the present study.

OCT, NIRS, and CCTA acquire data differently and thus provide different types of information, which can be complementary and highly valuable for evaluating atherosclerosis development (28).

STUDY LIMITATIONS. Sample size was relatively small, especially at 15 months. To study differences in vascular function and histology over several time points, sacrifice of a small number of swine was mandatory. Furthermore, differences remain between swine and human. Although swine, like humans, develop spontaneous coronary atherosclerosis, in the present study, swine were relatively young and thus did not develop advanced atherosclerosis, as can be observed in older-aged patients who suffer from hypercholesterolemia and/or DM for a longer time period. However, the aim of our study was to assess the effect of DM on early atherosclerosis development.

CONCLUSIONS

Our swine model allowed assessment of early coronary atherosclerosis development using intracoronary OCT and NIRS. CCTA could not detect early atherosclerotic lesions, but OCT and NIRS demonstrated a similar gradual development of early atherosclerosis in FF-DM and FF-NDM swine. Moreover, OCT, NIRS, vascular function, and histology demonstrated no differences in early atherosclerosis development between FF-DM and FF-NDM swine up to 15 months.

ACKNOWLEDGMENTS Dedicated to Prof. Dr. W.J. van der Giessen, who helped to design and conduct this preclinical study, but passed away before its completion.

REPRINT REQUESTS AND CORRESPONDENCE: Dr. Evelyn Regar, Department of Cardiology, Thoraxcenter, BA-585, Erasmus University Medical Centre, "s-Gravendijkwal 230, 3015 CE Rotterdam, the Netherlands. E-mail: e.regar@erasmsumc.nl.

PERSPECTIVES

COMPETENCY IN MEDICAL KNOWLEDGE: The number of patients with DM increases every year, and these individuals have a 2- to 6-fold increased risk of encountering atherosclerosis-related events compared with non-DM patients. Early detection of anatomic and functional atherosclerotic changes seems warranted. However, patients typically present to the clinician with advanced atherosclerotic disease, thus complicating the study of early atherosclerosis development. The swine coronary artery model may offer advantages: 1) the anatomy and physiology of swine heart are similar to those of human hearts; 2) swine can be rendered diabetic by injection of streptozotocin; 3) patient-like spontaneous coronary atherosclerosis development can be mimicked by additionally feeding the swine a high-cholesterol, high-sugar diet; 4) in vivo longitudinal invasive and noninvasive imaging can be performed; 5) ex vivo coronary endothelial function can be tested; and 6) histology can be performed to assess the magnitude of coronary atherosclerosis at different time points. Moreover, the swine coronary artery model can help improve our understanding of the effect of DM on the development of coronary atherosclerosis, which may modulate medical therapeutic strategies and thereby enhance prevention of cardiovascular events in the clinical setting.

TRANSLATIONAL OUTLOOK: To enable development of new therapeutic strategies and to reduce the health care burden, we believe that it is important to increase our understanding of early coronary atherosclerosis development. However, because patients suffering coronary artery disease typically present to the clinician relatively late, with advanced stages of disease, we used a swine coronary artery model suitable for evaluation of human-like coronary artery disease development. Interestingly, our study showed that hypercholesterolemia or hyperglycemia were not the only predictors of coronary atherosclerosis development in swine. Future studies in atherosclerotic swine should consider using older-aged swine and include additional risk factors such as hypertension. Furthermore, we were able to demonstrate that a number of coronary imaging techniques, including OCT, NIRS, and CCTA, can be consecutively used for longitudinal assessment of the atherosclerotic disease process, which may offer the possibility for future studies in a reduced number of animals.

REFERENCES

1. Norhammar A, Malmberg K, Diderholm E, et al. Diabetes mellitus: the major risk factor in unstable coronary artery disease even after consideration of the extent of coronary artery disease and benefits of revascularization. J Am Coll Cardiol 2004;43:585–91.

2. Wu KK, Huan Y. Diabetic atherosclerosis mouse models. Atherosclerosis 2007;191:241–9.

3. Skold BH, Getty R, Ramsey FK. Spontaneous atherosclerosis in the arterial system of aging swine. Am J Vet Res 1966;27:257–73.

4. van Ditzhuijzen NS, van den Heuvel M, Sorop O, et al. Invasive coronary imaging in animal models of atherosclerosis. Neth Heart J 2011;19:442–6.

5. van den Heuvel M, Sorop O, Koopmans SJ, et al. Coronary microvascular dysfunction in a porcine model of early atherosclerosis and diabetes. Am J Physiol Heart Circ Physiol 2012;302:H85–94.

6. Guide for the Care and Use of Laboratory Animals. 8th edition. Washington, DC: National Academies Press, 2011.

7. Tearney GJ, Regar E, Akasaka T, et al. Consensus standards for acquisition, measurement, and reporting of intravascular optical coherence tomography studies: a report from the International Working Group for Intravascular Optical Coherence Tomography Standardization and Validation. J Am Coll Cardiol 2012;59:1058–72.

8. Prati F, Regar E, Mintz GS, et al. Expert review document on methodology, terminology, and clinical applications of optical coherence tomography: physical principles, methodology of image acquisition, and clinical application for assessment of coronary arteries and atherosclerosis. Eur Heart J 2010;31:401–15.

9. Gardner CM, Tan H, Hull EL, et al. Detection of lipid core coronary plaques in autopsy specimens with a novel catheter-based near-infrared spectroscopy system. J Am Coll Cardiol Img 2008;1:638–48.

10. Motoyama S, Kondo T, Sarai M, et al. Multislice computed tomographic characteristics of coronary lesions in acute coronary syndromes. J Am Coll Cardiol 2007;50:319–26.

11. van den Heuvel M, Sorop O, Batenburg WW, et al. Specific coronary drug-eluting stents interfere with distal microvascular function after single stent implantation in pigs. J Am Coll Cardiol Intv 2010;3:723–30.

12. Batenburg WW, de Vries R, Saxena PR, Danser AH. L-S-nitrosothiols: endothelium-derived hyperpolarizing factors in porcine coronary arteries? J Hypertens 2004;22:1927–36.

13. Batenburg WW, Popp R, Fleming I, et al. Bradykinin-induced relaxation of coronary microarteries: S-nitrosothiols as EDHF? Br J Pharmacol 2004;142:125–35.

14. Fernandez-Friera L, Penalvo JL, Fernandez-Ortiz A, et al. Prevalence, vascular distribution, and multiterritorial extent of subclinical atherosclerosis in a middle-aged cohort: the PESA (Progression of Early Subclinical Atherosclerosis) study. Circulation 2015;131:2104–13.

15. Mohler ER III, Sarov-Blat L, Shi Y, et al. Site-specific atherogenic gene expression correlates with subsequent variable lesion development in coronary and peripheral vasculature. Arterioscler Thromb Vasc Biol 2008;28:850–5.

16. Ludvigsen TP, Kirk RK, Christoffersen BO, et al. Gottingen minipig model of diet-induced atherosclerosis: influence of mild streptozotocin-induced diabetes on lesion severity and markers of inflammation evaluated in obese, obese and diabetic, and lean control animals. J Transl Med 2015;13:312.

17. Duff GL, Mc MG. The effect of alloxan diabetes on experimental cholesterol atherosclerosis in the rabbit. J Exp Med 1949;89:611–30.

18. Granada JF, Kaluza GL, Wilensky RL, Biedermann BC, Schwartz RS, Falk E. Porcine models of coronary atherosclerosis and vulnerable

plaque for imaging and interventional research. EuroIntervention 2009;5:140–8.

19. Badimon L. Atherosclerosis and thrombosis: lessons from animal models. Thromb Haemost 2001;86:356–65.

20. Niccoli G, Giubilato S, Di Vito L, et al. Severity of coronary atherosclerosis in patients with a first acute coronary event: a diabetes paradox. Eur Heart J 2013;34:729–41.

21. Dixon JL, Stoops JD, Parker JL, Laughlin MH, Weisman GA, Sturek M. Dyslipidemia and vascular dysfunction in diabetic pigs fed an atherogenic diet. Arterioscler Thromb Vasc Biol 1999;19: 2981–92.

22. Gerrity RG, Natarajan R, Nadler JL, Kimsey T. Diabetes-induced accelerated atherosclerosis in swine. Diabetes 2001;50:1654–65.

23. Raggi P, Shaw LJ, Berman DS, Callister TQ. Prognostic value of coronary artery calcium screening in subjects with and without diabetes. J Am Coll Cardiol 2004;43:1663–9.

24. Yonetsu T, Suh W, Abtahian F, et al. Comparison of near-infrared spectroscopy and optical coherence tomography for detection of lipid. Catheter Cardiovasc Interv 2014;84:710–7.

25. van der Giessen AG, Toepker MH, Donelly PM, et al. Reproducibility, accuracy, and predictors of accuracy for the detection of coronary atherosclerotic plaque composition by computed tomography: an ex vivo comparison to intravascular ultrasound. Invest Radiol 2010;45: 693–701.

26. Miller JM, Rochitte CE, Dewey M, et al. Diagnostic performance of coronary angiography by 64-row CT. N Engl J Med 2008;359: 2324–36.

27. Halliburton SS, Schoenhagen P, Nair A, et al. Contrast enhancement of coronary atherosclerotic plaque: a high-resolution, multidetector-row computed tomography study of pressure-perfused, human ex-vivo coronary arteries. Coronary artery disease 2006;17:553–60.

28. Koskinas KC, Ughi GJ, Windecker S, Tearney GJ, Raber L. Intracoronary imaging of coronary atherosclerosis: validation for diagnosis, prognosis and treatment. Eur Heart J 2016;37:524–35.

KEY WORDS **animal model, coronary artery disease, coronary computed tomography angiography, diabetes mellitus, near-infrared spectroscopy, optical coherence tomography**

APPENDIX **For an expanded methods section as well as supplemental figures and table, please see the online version of this article.**

Coronary microvascular dysfunction after long-term diabetes and hypercholesterolemia

Sorop O.*, van den Heuvel M.*, van Ditzhuijzen N.S., de Beer V.J., Heinonen I., van Duin R.W., Zhou Z., Koopmans S.J., Merkus D., van der Giessen W.J., Danser A.H. and Duncker D.J.
*Shared first authorship

Am J Physiol Heart Circ Physiol. 2016 Dec 1;311(6)

7

Coronary microvascular dysfunction after long-term diabetes and hypercholesterolemia

Oana Sorop[1,3]*, Mieke van den Heuvel[1,2]*, Nienke S. van Ditzhuijzen[1], Vincent J. de Beer[1], Ilkka Heinonen[1], Richard W.B. van Duin[1], Zhichao Zhou[1], Sietse J. Koopmans[4], Daphne Merkus[1], Wim J. van der Giessen[1,3†], A. H. Jan Danser[2], Dirk Jan Duncker[1]

[1] Division of Experimental Cardiology, Department of Cardiology, Thoraxcenter, Cardiovascular Research School COEUR, Erasmus University Medical Center, Rotterdam, The Netherlands; [2] Department of Internal Medicine, Cardiovascular Research School COEUR, Erasmus University Medical Center, Rotterdam, The Netherlands; [3] Netherlands Heart Institute, Utrecht, The Netherlands; [4] Livestock Research, Wageningen University and Research Center, Wageningen, The Netherlands

Submitted 12 June 2015; accepted in final form 1 September 2016

Sorop O, van den Heuvel M, van Ditzhuijzen NS, de Beer VJ, Heinonen I, van Duin RW, Zhou Z, Koopmans SJ, Merkus D, van der Giessen WJ, Danser AH, Duncker DJ. Coronary microvascular dysfunction after long-term diabetes and hypercholesterolemia. *Am J Physiol Heart Circ Physiol* 311: H1339–H1351, 2016. First published September 2, 2016; doi:10.1152/ajpheart.00458.2015.—Coronary microvascular dysfunction (CMD) has been proposed as an important component of diabetes mellitus (DM)- and hypercholesterolemia-associated coronary artery disease (CAD). Previously we observed that 2.5 mo of DM and high-fat diet (HFD) in swine blunted bradykinin (BK)-induced vasodilation and attenuated endothelin (ET)-1-mediated vasoconstriction. Here we studied the progression of CMD after 15 mo in the same animal model of CAD. Ten male swine were fed a HFD in the absence (HFD, $n = 5$) or presence of streptozotocin-induced DM (DM + HFD, $n = 5$). Responses of small (~300-μm-diameter) coronary arteries to BK, ET-1, and the nitric oxide (NO) donor *S*-nitroso-*N*-acetylpenicillamine were examined in vitro and compared with those of healthy (Normal) swine ($n = 12$). Blood glucose was elevated in DM + HFD (17.6 ± 4.5 mmol/l) compared with HFD (5.1 ± 0.4 mmol/l) and Normal (5.8 ± 0.6 mmol/l) swine, while cholesterol was markedly elevated in DM + HFD (16.8 ± 1.7 mmol/l) and HFD (18.1 ± 2.6 mmol/l) compared with Normal (2.1 ± 0.2 mmol/l) swine (all $P < 0.05$). Small coronary arteries showed early atherosclerotic plaques in HFD and DM + HFD swine. Surprisingly, DM + HFD and HFD swine maintained BK responsiveness compared with Normal swine due to an increase in NO availability relative to endothelium-derived hyperpolarizing factors. However, ET-1 responsiveness was greater in HFD and DM + HFD than Normal swine (both $P < 0.05$), resulting mainly from ET_B receptor-mediated vasoconstriction. Moreover, the calculated vascular stiffness coefficient was higher in DM + HFD and HFD than Normal swine (both $P < 0.05$). In conclusion, 15 mo of DM + HFD, as well as HFD alone, resulted in CMD. Although the overall vasodilation to BK was unperturbed, the relative contributions of NO and endothelium-derived hyperpolarizing factor pathways were altered. Moreover, the vasoconstrictor response to ET-1 was enhanced, involving the ET_B receptors. In conjunction with our previous study, these findings highlight the time dependence of the phenotype of CMD.

coronary microvascular dysfunction; diabetes; endothelin-1; hypercholesterolemia; swine

NEW & NOTEWORTHY

Coronary microvascular dysfunction (CMD) is an increasingly recognized feature of coronary artery disease. We found that progression of CMD in diabetic + hypercholesterolemic swine from 2.5 to 15 mo of follow-up involved a shift from impaired endothelium-dependent vasodilation to bradykinin to exaggerated vasoconstriction to endothelin, highlighting the time dependence of the phenotype of CMD.

DIABETES MELLITUS (DM) and hypercholesterolemia are widespread risk factors for ischemic heart disease, and their prevalence continues to increase worldwide (3, 4, 6, 48). A large contribution to morbidity and mortality of diabetic patients can be attributed to the accelerated development of obstructive proximal coronary artery disease (CAD) (11). However, it is also increasingly recognized that coronary microvascular dysfunction (CMD) is an early feature of DM and hypercholesterolemia that may precede macrovascular disease and constitutes a major component of DM-associated CAD (18, 19, 52, 57, 66). Although the pathogenesis of CMD is incompletely understood, DM-induced progressive endothelial dysfunction is thought to be a key player in this process. This endothelial dysfunction encompasses a shift in the secretion of endothelium-derived relaxing factors from nitric oxide (NO) to endothelium-derived hyperpolarizing factor (EDHF), as well as an imbalance between these relaxing factors and endothelium-derived constricting factors such as endothelin (ET)-1 (35, 52, 71).

In a recent study we demonstrated impaired coronary microvascular NO bioavailability and reduced ET-1 responsiveness in diabetic swine fed a high-fat diet (HFD) during 2.5 mo of follow-up (71). The present study was undertaken to characterize the progression of CMD in this model. Specifically, we tested the hypothesis that prolonged exposure to hyperglyce-

† Deceased 6 June 2011.

* O. Sorop and M. van den Heuvel, contributed equally to this work.
Address for reprint requests and other correspondence: D. J. Duncker, Division of Experimental Cardiology, Dept. of Cardiology, Thoraxcenter, Erasmus Univ. Medical Center, PO Box 2040, 3000 CA Rotterdam, The Netherlands (e-mail: d.duncker@erasmusmc.nl).

mia and hypercholesterolemia leads to further impairment of NO availability and to increased ET-1-mediated vasoconstriction. For this purpose, vascular function of small coronary arteries was studied in vitro at 15 mo of follow-up in DM + HFD swine and compared with vascular function in HFD, as well as healthy (Normal), swine.

MATERIALS AND METHODS

The study was performed in a total of 16 swine in accordance with the "Guiding Principles in the Care and Use of Laboratory Animals," as approved by the Council of the American Physiological Society, and with approval of the Animal Care Committee at Erasmus University Medical Center Rotterdam; an additional 12 swine hearts were obtained from a slaughterhouse.

Animals

Ten castrated male Yorkshire × Landrace swine (18.2 ± 0.4 kg body wt) were studied. In five animals, DM was induced by streptozotocin injection (140–180 mg/kg iv) to destroy ~80% of the pancreatic β-cell islets (36, 71). At 4 wk after DM induction, a HFD consisting of 10% sucrose, 15% fructose, 25% saturated fats, 1% cholesterol, and 0.7% sodium cholate (bile salts) was gradually introduced to DM (DM + HFD group) and non-DM (HFD group) animals (71). Swine were housed in metabolic cages and fed two meals a day, during each of which they had access to food for 1 h. Food intake was monitored for each animal separately and titrated to maintain growth at ~1.5 kg/wk. All 10 animals completed the 15-mo study duration. The diabetic status of the DM + HFD swine was regularly monitored by measurements of urinary and venous blood glucose and ketone levels.

Six weight-matched Yorkshire × Landrace normal control (Normal) swine were studied for comparison of heart rate, blood pressure, and plasma characteristics, while three of these animals were also used for vascular function experiments. In addition, 12 fresh healthy normal hearts were obtained from slaughterhouse swine of similar body weight (~100 kg at euthanization) for comparison of vascular function characteristics. Since in a separate study no differences in the small artery functional responses to bradykinin (BK), ET-1, and *S*-nitroso-*N*-acetylpenicillamine (SNAP) were observed between male (n = 8) and female (n = 9) swine of this size (Fig. 1), data from normal, control animals of both sexes were included.

Plasma Characteristics

At euthanization, animals were sedated with Zoletil (tiletamine/zolazepam, 5 mg/kg), Rompun (xylazine, 2.25 mg/kg), and atropine (2 ml im), anesthetized with pentobarbital sodium (20 mg·kg^{-1}·h^{-1} iv), and artificially ventilated. Arterial access was obtained by introduction of a 9F sheath into the carotid artery to monitor blood pressure and heart rate and to collect fasting arterial blood samples. Plasma levels of glucose, triglycerides, total cholesterol, LDL, HDL, aspartate aminotransferase, alanine aminotransferase, and creatinine were measured using standardized protocols at the clinical chemical laboratory of the Erasmus Medical Center. Arterial plasma concentrations of insulin (Mercodia, Uppsala, Sweden), ET-1, (ELISA, Enzo Life Sciences, Lausen, Switzerland), and TNFα (R & D Systems Europe, Abingdon, UK) were determined using ELISA kits.

Vascular Function In Vitro

After all blood samples had been obtained and following thoracotomy, hearts were arrested and immediately excised and placed in cold, oxygenated Krebs bicarbonate buffer solution. For the HFD and DM + HFD swine, small (~300 μm diameter) epicardial coronary arteries were isolated from the perfusion areas of the left anterior descending, left circumflex, or right coronary artery such that, in both groups, vessels from all three perfusion areas were evenly distributed. In the Normal swine, vessels were isolated from the apical part of the heart, so that vessels originating from both left and right coronary artery perfusion areas were included. The isolated segments were studied in vitro in a Mulvany wire myograph (DMT, Aarhus, Denmark), as previously described (71). Briefly, during the vascular function experiments, vessel segments (~2 mm long) were maintained at 37°C in 10^{-3} M Krebs buffer (in mM: 118 NaCl, 4.7 KCl, 2.5 $CaCl_2$, 1.2 $MgSO_4$, 1.2 KH_2PO_4, 25, $NaHCO_3$, and 8.3 glucose; pH 7.4). After a 30-min stabilization period, the normalization procedure was started; during this procedure, the internal diameter was set to a tension equivalent to 90% of the estimated diameter at 100 mmHg effective transmural pressure (27). Thereafter, the vascular segments were depolarized by 100 mM KCl (Sigma-Aldrich, Zwijndrecht, The Netherlands) to determine the maximal contractile response of the small artery segments.

Subsequently, concentration-response curves (CRCs) for various substances (all from Sigma-Aldrich) were acquired using separate, but in vivo adjacently positioned, segments. Endothelium-dependent vasodilation was studied by construction of the CRC for BK (10^{-10}–10^{-6} M) upon preconstriction by the thromboxane A_2 analog U46619 (10^{-6} M) (10). It was previously shown that prostaglandins are not involved in BK-induced responses in healthy porcine small coronary arteries (10). To assess the contribution of NO and EDHF to BK-induced vasodilation, the same BK experiment was performed in separate small artery segments upon 30 min of preincubation with the NO synthase inhibitor *N*-nitro-L-arginine methyl ester (L-NAME, 10^{-4} M), the small- and intermediate-conductance Ca^{2+}-activated K^+ (K_{Ca}) channel inhibitors apamin (10^{-7} M) and TRAM 34 (10^{-5} M), or apamin + TRAM 34. Endothelium-independent vasodilation was studied in separate small artery segments by construction of CRCs to

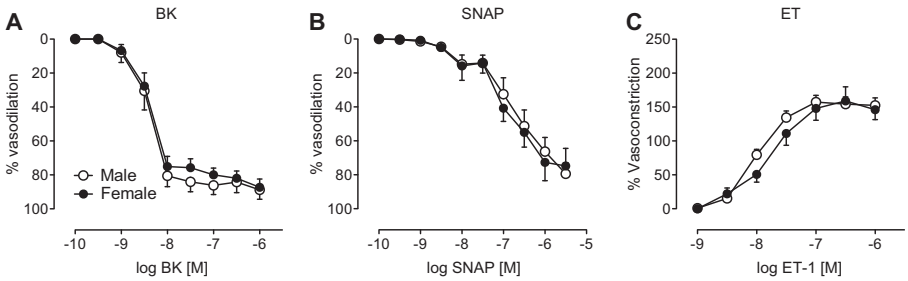

Fig. 1. Concentration-response curves for bradykinin (BK; *A*), *S*-nitroso-*N*-acetylpenicillamine (SNAP; *B*), and endothelin-1 (ET-1; *C*) in small coronary arteries isolated from male (n = 8) and female (n = 9) slaughterhouse pigs. No sex differences were observed for any of the vasoactive factors.

the exogenous NO donor SNAP (10^{-10}–3×10^{-5} M). In additional small artery segments, CRCs to ET-1 (10^{-10}–10^{-6} M) were constructed. To test the specific contributions of the ET_A and ET_B receptors to this response, the same experiment was performed upon 30 min of incubation with the ET_A receptor antagonist BQ123 (10^{-6} M), the ET_B receptor antagonist BQ788 (10^{-7} M), or BQ123 + BQ788.

To examine whether small coronary arteries had undergone changes in passive tension characteristics, the values of the relaxed steady-state diameters at each wall tension of the normalization procedure were fitted by an exponential equation according to Halpern et al. (27), and the stiffness coefficient was calculated.

Histology

After completion of the vascular function studies, each vascular segment was fixed in 4% buffered formaldehyde, embedded in paraffin, and stained with resorcin-fuchsin to assess atherosclerosis development. Atherosclerotic plaques of different complexity were described according to the American Heart Association classification (63).

Quantitative Real-Time PCR Analysis

Small arteries, dissected simultaneously with vessels isolated for the vascular function studies, were used to study the expression of endothelial NO synthase (eNOS), ET_A and ET_B receptors, and small-, intermediate-, and big-conductance K^+ channel mRNA. A Qiagen RNA kit was used to extract RNA from frozen vessel samples. cDNA was synthesized from 100 ng of total RNA with iScript reverse transcriptase (Bio-Rad Laboratories, Veenendaal, The Netherlands). Quantitative real-time PCR (MyIQ, Bio-Rad Laboratories) was performed with SYBR Green (Bio-Rad Laboratories). Target gene mRNA levels are expressed relative to the housekeeping genes glyceraldehyde-3-phosphate dehydrogenase and cyclophilin as endogenous controls (76). Primer sequences are shown in Table 1.

Microvascular NO Production

Microvascular NO production was evaluated in homogenized segments of microvessels (snap-frozen directly after excision from the hearts) of the same size and from the same animals used for the functional studies. Production of the NO metabolites NO_2^- and NO_3^- was measured using the Griess reaction colorimetric assay (Cayman Chemical, Ann Arbor, MI).

Data Analysis

Values are means ± SE. Normally distributed model characteristics were compared by one-way ANOVA followed by Scheffé's post hoc test (StatView 5.0, SAS Institute). Vasodilator responses to BK and SNAP are expressed as percentage of the preconstriction to U46619. Vasoconstrictor responses to U46619, and ET-1 were normalized to 100 mM KCl. Statistical analysis of CRCs was performed using two-way ANOVA (with the increasing agonist concentrations and antagonists as independent variables), followed by Fisher's PLSD post hoc correction. Two-tailed $P < 0.05$ was considered statistically significant.

RESULTS

Hemodynamic Parameters and Plasma Characteristics

At euthanization, body weights of DM + HFD, HFD, and Normal swine were similar: 93 ± 3, 109 ± 5, and 103 ± 19 kg, respectively. Furthermore, heart rate (114 ± 3, 111 ± 3, and 87 ± 7 beats/min for DM + HFD, HFD, and Normal, respectively, $P > 0.05$) and mean arterial pressure (103 ± 4, 105 ± 6, and 121 ± 7 mmHg for DM + HFD, HFD, and Normal, respectively, $P > 0.10$), as measured under anesthesia, were similar.

Plasma levels of glucose, insulin, lipids, and inflammation markers are summarized in Fig. 2. Plasma glucose was significantly increased in DM + HFD compared with HFD and Normal swine. Plasma insulin values tended to be increased in DM + HFD (14.5 ± 4.4 pg/ml), and particularly in HFD (18.2 ± 1.4 pg/ml), compared with Normal (10.1 ± 1.6 pg/ml) swine but failed to reach statistical significance ($P = 0.21$). However, the quantitative insulin sensitivity check index (32) QUICKI, calculated as $1/[\log(I_0) + \log(G_0)]$, where I_0 is fasting plasma insulin level (in μU/ml) and G_0 is fasting blood glucose level (in mg/dl), showed significantly lower values in DM + HFD and HFD than Normal swine, indicative of insulin resistance in both groups. The high-fat diet resulted in increased plasma total cholesterol and LDL cholesterol in DM + HFD and HFD compared with Normal swine. Plasma triglycerides were higher in both HFD groups, reaching statistical significance only in DM + HFD swine ($P < 0.05$ vs. Normal). TNFα trended toward increased levels (without reaching statistical significance, $P = 0.14$) in DM + HFD compared with HFD and Normal swine. No significant differences between the three groups were observed in plasma markers of liver and kidney function (quantitative data not shown). Plasma ET-1 levels were elevated only in DM + HFD swine (Fig. 2).

Small Coronary Artery Structure and Function

Figure 3 shows representative examples of resorcin-fuchsin-stained small coronary arteries from all three groups. Plaques with different degrees of complexity (from fatty streaks to more complex plaques) were observed in small arteries from HFD (Fig. 3, *C* and *D*) and DM + HFD (Fig. 3, *E* and *F*) swine to a similar extent, but not Normal swine (Fig. 3, *A* and *B*).

Table 1. *Primer sequences*

Primer	Sequence	
	Sense	Antisense
eNOS	CTCTCCTGTTGGCCTGACCA	CCGGTTACTCAGACCCAAGG
ET_A receptor	TTTATCCTGGCCATCCCTGA	GCTCTTCGCCCTTGTATTCAA
ET_B receptor	CCCCTTCATCTCAGCAGGATT	GCACCAGCAGCATAAGCATG
Small-conductance K^+ channels	TGGTGAAGAAGCCAGACCAC	CCGGAGCTTCTGAGCTTGAT
Intermediate-conductance K^+ channels	CCATCAACACGTTCCGCCAG	AGCTGCAGGTCACACAGGAT
Big-conductance K^+ channels	ATTGCTGAGGAGAATGCGCT	TAACAACCACCATCCCCCAG
GAPDH	TCGGAGTGAACGGATTTG	CCTGGAAGATGGTGATGG
Cyclophillin	GTCTCCTTCGAGCTGTTTGC	AATCCTTTCTCCCCAGTGCT

eNOS, endothelial nitric oxide synthase; ET_A and ET_B, endothelin receptor types A and B.

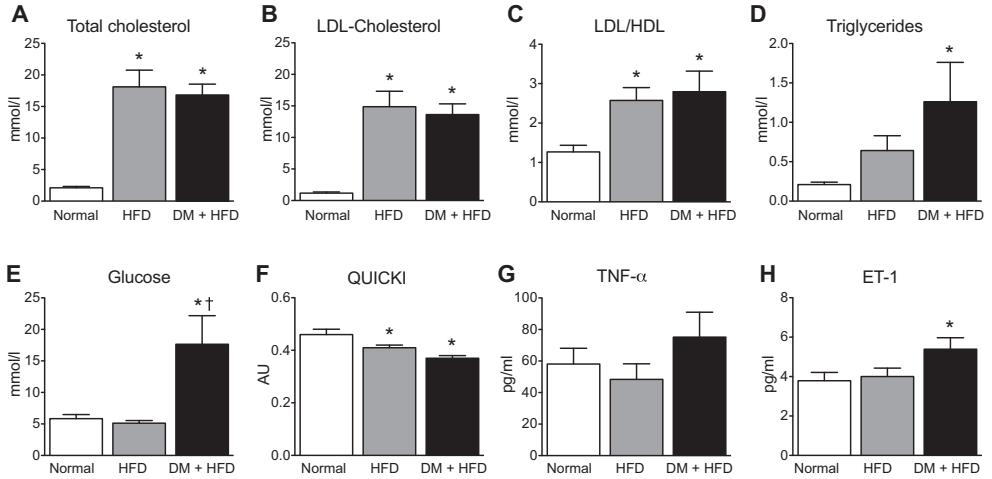

Fig. 2. *A–C*: increased levels of total cholesterol and LDL-cholesterol and increased LDL-to-HDL-cholesterol ratio in high-fat diet (HFD)-fed swine ($n = 5$) and HFD-fed swine with streptozotocin-induced diabetes mellitus (DM + HFD, $n = 5$) compared with Normal swine ($n = 6$). *D, E,* and *H*: significantly increased triglycerides, glucose, and ET-1 only in DM + HFD swine. *F*: significantly reduced QUICKI index (AU, arbitrary units) in HFD and DM + HFD compared with Normal swine, suggestive of insulin resistance. *G*: TNFα plasma levels in DM + HFD and HFD swine were not significantly different from Normal swine. *$P < 0.05$ vs. Normal. †$P < 0.05$ vs. HFD.

The constrictor responses to 10^{-6} M U46619 (used for preconstriction) were similar among the three groups (74 ± 5%, 66 ± 4%, and 67 ± 6% of the response to 100 mM KCl for DM + HFD, HFD, and Normal, respectively, $P = 0.56$), indicating equal preconstriction levels. Coronary microvascular responses to BK, SNAP, and ET-1 are summarized in Fig. 4. Surprisingly, endothelium-dependent vasodilation to BK was similar among the three groups (Fig. 4*A*). The response to the exogenous NO donor SNAP was also similar among all groups, indicating preserved vascular smooth muscle responsiveness to NO (Fig. 4*B*). In contrast, vasoconstriction to ET-1 was significantly increased in DM + HFD and HFD compared with Normal swine (Fig. 4*C*).

Mechanism of BK-induced vasodilation. The specific contributions of NO and EDHF to the endothelium-dependent BK-mediated vasodilation were studied by blockade of eNOS and of small- and intermediate-conductance K_{Ca} channels, respectively (Fig. 5). In all groups, eNOS blockade with L-NAME resulted in a significant reduction in the vasodilator response to BK (all $P < 0.05$; Fig. 5). However, while EDHF blockade blunted the vasodilation to BK in Normal swine (Fig. 5*A*), no effect was observed in the HFD or DM + HFD swine (Fig. 5, *B* and *C*). Yet combined eNOS and EDHF blockade resulted in larger reductions in vasodilator response to BK than eNOS alone in all three groups (Fig. 5), suggesting that small arteries from HFD and DM + HFD swine were able to produce EDHF, but only during inhibition of NO production.

Mechanism of ET-1-induced vasoconstriction. The specific contributions of ET_A and ET_B receptors to exogenous ET-1-induced vasoconstriction are shown in Fig. 6. ET_A receptor blockade blunted ET-1-induced vasoconstriction in all three groups (all $P < 0.05$), at a magnitude that was similar between groups ($P = 0.54$). In contrast, while ET_B receptor blockade significantly enhanced the vasoconstrictor response to ET-1 in Normal swine ($P < 0.001$; Fig. 6*A*), it had no effect in DM + HFD swine (Fig. 6*C*) and significantly blunted vasoconstriction in HFD swine ($P < 0.05$; Fig. 6*B*). Similarly, compared with ET_A receptor blockade alone, combined $ET_A + ET_B$ (ET_{AB}) receptor blockade produced further blunting of the ET-1-induced vasoconstriction in HFD swine ($P < 0.05$) and showed a trend toward further blunting in DM + HFD ($P = 0.15$ at 3×10^{-9}–10^{-7} M), but not Normal, swine.

Quantitative Real-Time PCR Analysis and Microvascular NO Production

eNOS expression was similar in DM + HFD and Normal swine and tended to be lower in HFD swine ($P = 0.13$, HFD vs. DM + HFD and Normal; Fig. 7*A*). Interestingly, consistent with eNOS expression, similar levels of the NO metabolites NO_2^- and NO_3^- in small arteries indicated similar basal NO production in the DM + HFD and Normal swine, while a significant reduction in microvascular NO production was observed in HFD compared with Normal swine (Fig. 7*B*).

Expression of small-conductance K^+ channels in DM + HFD swine was significantly decreased ($P < 0.05$; Fig. 8*A*), and a trend toward a decrease in the HFD group ($P = 0.07$) was observed compared with Normal swine. Expression of intermediate-conductance K^+ channels was significantly lower in HFD than DM + HFD swine ($P < 0.05$; Fig. 8*B*) and tended to be lower than in Normal swine ($P = 0.11$). Expression of big-conductance K^+ channels was similar between the three groups (Fig. 8*C*).

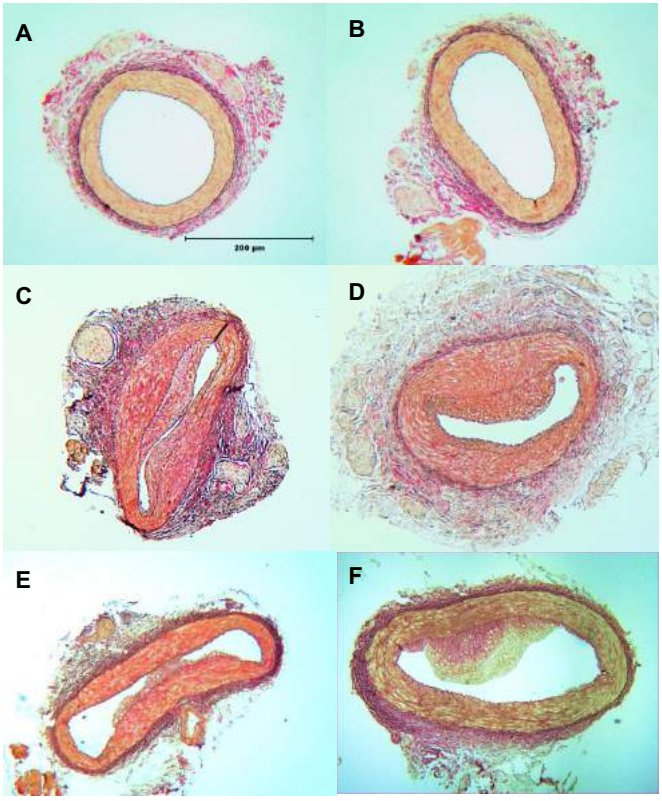

Fig. 3. Resorcin-fuchsin-stained small coronary arteries. Note plaques with different degrees of complexity in vessels from HFD (*C* and *D*) and DM + HFD (*E* and *F*), but not Normal (*A* and *B*), swine.

Expression profiles of the ET receptors indicated significantly increased mRNA expression of both ET_A (2-fold) and ET_B receptors (5-fold) in DM + HFD compared with Normal swine (Fig. 9). In contrast, only ET_B receptor mRNA expression was significantly increased (2-fold) in HFD compared with Normal swine.

Vascular Stiffness and Wall-to-Lumen Ratio

The stiffness coefficient, as calculated from the relaxed wall tension-strain relations, was significantly increased in both DM + HFD (6.45 ± 0.14, $n = 93$ vessels from 5 swine) and HFD (6.65 ± 0.15, $n = 48$ vessels from 5 swine) compared with Normal (5.48 ± 0.17, $n = 70$ vessels from 15 swine) animals (both $P < 0.05$). These findings indicate an increased stiffness in HFD and DM + HFD swine, which occurred in the absence of media hypertrophy; also, wall-to-lumen ratios measured on histological images were similar among DM + HFD, HFD, and Normal swine (0.36 ± 0.03, 0.27 ± 0.02, and 0.37 ± 0.03, respectively, $P = 0.11$).

DISCUSSION

We previously showed that 2.5 mo of exposure to DM and HFD resulted in an impaired BK-induced endothelium-dependent vasodilation due to loss of NO availability, accompanied by a reduced ET-1-mediated vasoconstriction due to decreased ET_A receptor contribution (71). The present study was undertaken to characterize the progression of CMD at a later stage of the disease (i.e., 15 mo) in the same swine model of DM and HFD (72). The main findings of the present study were as follows. *1*) Coronary microvessels from HFD and DM + HFD swine showed plaques with different degrees of complexity. *2*) The vasodilator response to BK was not further decreased but, rather, was maintained in DM + HFD and HFD swine due to the ability of the NO/EDHF-mediated mechanisms to interact in synergy. *3*) An increased ET-1 responsiveness was present in DM + HFD and HFD swine that appeared to be principally due to loss of ET_B receptor-mediated vasodilation and increased ET_B receptor-mediated constriction, in particular in HFD swine. *4*) Coronary microvessels from HFD and DM + HFD swine demonstrated increased stiffness, which occurred

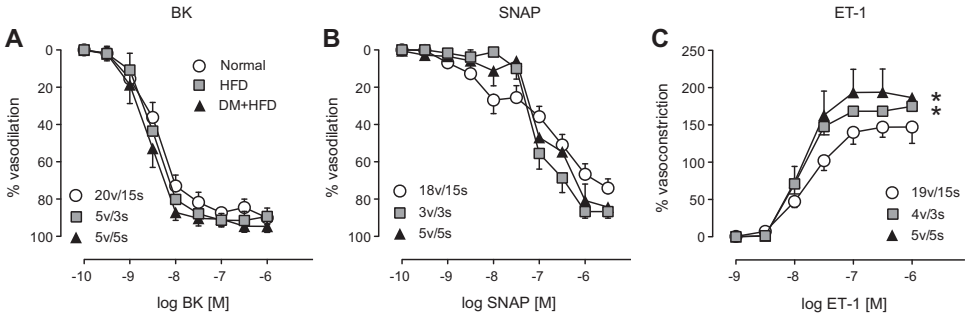

Fig. 4. *A–C*: concentration-response curves for BK, SNAP, and ET-1 in vessels (v) from Normal, HFD, and DM + HFD swine (s). No differences were seen in endothelium-dependent and -independent responses, respectively, to BK and SNAP between groups. However, HFD and DM + HFD swine showed increased responsiveness to ET-1 compared with Normal swine. *$P < 0.05$ vs. Normal.

in the absence of medial hypertrophy. The implications of these findings are discussed below.

Model Characteristics

In the present study, DM induction, through partial pancreatic β-cell destruction, combined with HFD, resulted in markedly elevated plasma glucose and cholesterol levels after 15 mo of follow-up. Previously we performed similar experiments using the same experimental model followed for only 2.5 mo of HFD with or without DM (71). The DM + HFD group demonstrated increased insulin resistance (reflected in the QUICKI index) at 2.5 mo (71) and 15 mo (present study), while increased insulin resistance was observed in the HFD group at 15 mo (present study), but not at 2.5 mo (71). Furthermore, in the HFD group, total cholesterol levels were further elevated at 15 mo compared with 2.5 mo (71). Importantly, only prolonged exposure to hypercholesterolemia + hyperglycemia resulted in hypertriglyceridemia, a form of dyslipidemia common in diabetic patients and associated with the onset of CAD (70). In our swine model, atherosclerotic plaques were observed in the large coronary arteries of DM + HFD and HFD animals after 15 mo and did not appear to produce flow-limiting obstructions (72). In the present study we also observed plaques of different complexities in small (2nd- and 3rd-order) coronary arteries of both groups. Unfortunately, our focus on functional studies (requiring freshly isolated small arteries) precluded perfusion fixation of hearts under physiological pressures, which is a prerequisite for accurate quantification of plaque burden. Consequently, we limited the description of coronary atherosclerosis to the presence of plaques of heterogeneous complexity (from small fatty streaks to more complex fibroatheromatous plaques), which appeared similar in both groups. Plaques were not observed in Normal or in HFD or DM + HFD swine studied previously at 2.5 mo (71), underscoring the importance of long-term exposure of the coronary vasculature to pathological stimuli when developing a large-animal model of coronary atherosclerosis.

Although coronary plaque formation required a longer follow-up time, functional and structural abnormalities of the small arteries were observed in DM + HFD swine as early as 2.5 mo of follow-up (71). These findings are in accordance with clinical observations that microvascular alterations precede obstructive CAD in patients without DM (61), as well as in patients with DM and increased insulin resistance (52, 59,

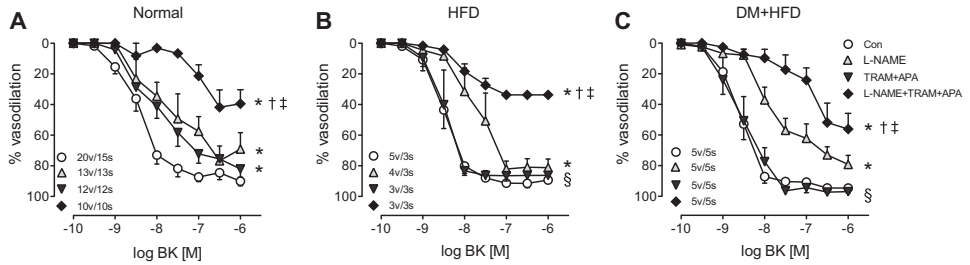

Fig. 5. Concentration-response curves for BK upon blockade of the nitric oxide (NO) system [nitro-L-arginine methyl ester (L-NAME)], endothelium-derived hyperpolarizing factor (EDHF) system [TRAM + apamin (APA)], and their combination (L-NAME + TRAM + APA). *A*: significant reduction in BK-induced vasodilation in Normal swine after individual blockade of NO- and EDHF-dependent mechanisms, the combined blockade response being the sum of the individual mechanisms. *B* and *C*: no effect of EDHF blockade in HFD or DM + HFD swine, suggesting that this system is becoming important only in conditions of reduced NO bioavailability (L-NAME), since in both groups, combined blockade resulted in a larger response than endothelial NO synthase blockade alone. *$P < 0.05$ vs. control (Con). †$P < 0.05$, L-NAME + TRAM + APA vs. L-NAME. ‡$P < 0.05$, L-NAME + TRAM + APA vs. TRAM + APA. §$P < 0.05$, TRAM + APA effect in HFD and DM + HFD vs. Normal.

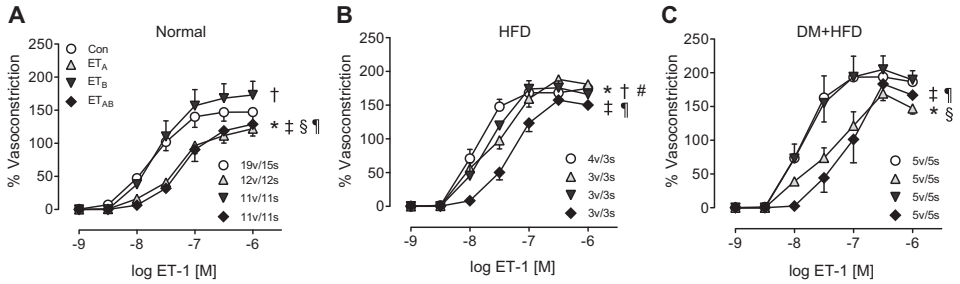

Fig. 6. Concentration-response curves for ET-1 upon blockade of the ET_A (BQ123) and ET_B (BQ788) receptors, alone or in combination (BQ123 + BQ788). *A*: in Normal swine, ET_B receptor blockade resulted in enhanced vasoconstriction, indicating involvement of ET_B receptors in ET-1-dependent vasodilation. ET_A receptor blockade resulted in blunted vasoconstriction. ET_A + ET_B (ET_{AB}) receptor blockade was not different from ET_A receptor blockade, suggesting that ET-1-mediated vasoconstriction is mainly mediated via the ET_A receptor. *B* and *C*: ET_B receptor-mediated vasodilation was abolished in HFD and DM + HFD swine. In HFD swine, individual ET_A and ET_B receptor blockade resulted in blunted vasoconstriction, their contribution to the total response being additive, since ET_{AB} receptor blockade approximated the sum of the individual blockades. In DM + HFD swine, ET_B receptor blockade had no effect on the response to ET-1; however, after ET_A receptor blockade, ET_{AB} receptor blockade tended ($P = 0.15$) to result in greater inhibition of ET-1-mediated vasoconstriction than ET_A receptor blockade alone. *$P \leq 0.05$, ET_A vs. control. †$P < 0.05$, ET_B vs. control. ‡$P < 0.05$, ET_{AB} vs. control. §$P < 0.05$, ET_A vs. ET_B. ¶$P < 0.05$, ET_{AB} vs. ET_B. #$P < 0.05$, ET_{AB} vs. ET_A.

60, 66). Furthermore, there is evidence that coronary flow reserve is impaired not only in DM patients without CAD, but also in prediabetic subjects, compared with healthy individuals, indicating the early presence of CMD (20, 55). Microvascular dysfunction is associated with factors such as oxidative stress, poor glycemic control, insulin resistance, and hypercholesterolemia (62), which were present in our DM + HFD swine model. Since endothelial dysfunction is considered a key factor in development of DM-associated coronary vascular disease (62), we investigated coronary endothelial function in more detail.

Endothelium-Dependent Vasodilation

In patients with DM, the severity of peripheral endothelial dysfunction correlates with duration of the disease (49). Although coronary microvascular endothelial dysfunction is also likely related to the duration of DM, most animal studies (Table 2) have investigated CMD at a single time point only, usually rather early in the disease (24, 45, 50, 71). One study in Zucker obese rats assessed multiple time points and showed that acetylcholine-induced coronary microvascular dilation was preserved up to 24 wk of age but was almost completely abolished in older animals as a result of increased oxidative stress (51), while another study in type 2 DM Goto-Kakizaki rats showed impaired BK-induced vasodilation from 10 to 20 wk of age (46). However, while overall coronary endothelium-dependent vasodilation may be preserved early in the disease, the signaling pathways contributing to this vasodilation may already be altered. Thus acetylcholine-mediated endothelium-dependent vasodilation in coronary arterioles of obese rats after 10 wk of HFD was maintained due to enhanced soluble guanylate cyclase activity that increased coronary vascular sensitivity to NO (30). Similarly, in aortic rings of female rats 4 wk after induction of streptozotocin-induced diabetes, the overall vasodilator response to acetylcholine was preserved, as a reduction in NO bioavailability appeared to be compensated by a downregulation of phosphodiesterase activity in combination with an increased vasodilator contribution of prostanoids (1). In contrast, 4 wk of high-fructose diet, which resulted in increased insulin resistance, did not alter the NO-dependent small coronary artery vasodilator response to acetylcholine but, rather, reduced the contribution of EDHF (45), while in the coronary arterioles of *db/db* mice with advanced type 2 DM, EDHF compensated for diminished NO-dependent vasodilation to acetylcholine (54). These findings suggest that compensatory mechanisms may vary, depending on species, DM model, and possibly the duration of exposure to risk factors.

In the human coronary circulation (Table 2), DM and CAD have been proposed to be associated with microvascular dysfunction (43, 75) and a shift in mediators of endothelium-dependent vasodilation from NO to EDHF (47) and prostacy-

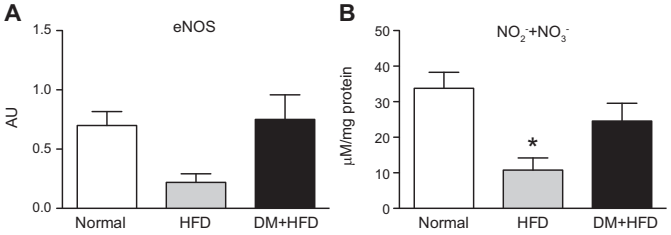

Fig. 7. *A*: expression of endothelial NO synthase (eNOS) measured by quantitative PCR in small arteries of normal ($n = 4$), HFD ($n = 3$), and DM + HFD ($n = 5$) swine. *B*: production of the NO metabolites NO_2^- and NO_3^- in small arteries isolated from Normal ($n = 6$), HFD ($n = 3$), and DM + HFD ($n = 5$) swine. Similar levels of basal NO production were measured in DM + HFD and Normal swine, while microvascular NO production was significantly reduced in HFD compared with Normal swine. *$P < 0.05$ vs. Normal.

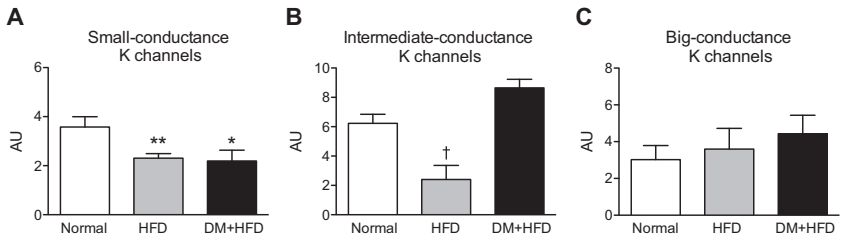

Fig. 8. Expression of small- (*A*), intermediate- (*B*) and big-conductance (*C*) K^+ channel receptors measured by quantitative PCR in small arteries of Normal (n = 6), HFD (n = 3), and DM + HFD (n = 5) swine. Expression of small-conductance K^+ channels in DM + HFD swine was significantly decreased (P = 0.03), and a trend toward a decrease was found in HFD (P = 0.07) compared with Normal swine. Expression of intermediate-conductance K^+ channels was significantly lower in HFD than DM + HFD swine (P = 0.02) and tended to be lower than in Normal swine (P = 0.1). No difference in expression of the big-conductance K^+ channels was recorded between the three groups. *$P < 0.05$, **$P = 0.07$ vs. Normal. †$P < 0.05$, DM + HFD vs. HFD.

clin (PGI2) (65), although it is unclear when this shift occurs. In the present study we did not test the contribution of cyclooxygenase to BK-induced dilation in HFD or DM + HFD swine. However, data in healthy swine indicate no effect of cyclooxygenase inhibition on BK-induced dilation (10). In our swine model, vasodilation to BK was impaired early in the disease process (after 2.5 mo), but only in DM + HFD animals, which was due to a reduction in NO bioavailability, while the contribution of EDHF was preserved (71). In contrast, after 15 mo of exposure to DM + HFD, the overall response to BK was restored to control levels. This restoration of NO-mediated dilation was consistent with the preserved basal NO production and eNOS expression in small coronary arteries of DM + HFD compared with Normal swine. It was surprising that basal NO production was significantly reduced in HFD swine, which was paralleled by a similar trend toward a reduction in eNOS expression. NO and EDHF may influence each other via intracellular and intercellular mechanisms (58), as eNOS is capable of producing both NO and superoxide, which in the presence of adequate antioxidant defense can be converted to H_2O_2, which could potentially contribute to BK-induced vasodilation by acting as an EDHF (16). In the present study we observed a reduced expression, as well as a reduced contribution, of K_{Ca} channels to the BK-induced vasodilation in HFD and DM + HFD swine, suggesting that NO remains the predominant eNOS metabolite contributing to BK-induced vasodilation and that the interaction between NO and putative EDHF(s) is altered. Furthermore, the observation that vasodilation in response to the NO donor SNAP was similar in all groups implies that NO responsiveness was maintained and, hence, guanylate cyclase and phosphodiesterase activities were unaltered. Taken together, the results from the present study show that, even after prolonged exposure to HFD and DM and despite the presence of CAD, the vasodilator response to BK is preserved and is largely mediated by NO. In addition, despite a reduction in small-conductance K^+ channel expression, EDHF was able to contribute to BK-induced vasodilation, but only when NO bioavailability was reduced.

In the present study we did not unravel the molecular mechanisms through which factors such as hyperglycemia, hypercholesterolemia, and inflammation result in endothelial dysfunction. However, it has been shown that high glucose levels can produce endothelial dysfunction by altering EDHF-dependent mechanisms (69) and can also cause the formation of extracellular advanced glycation end-products, which may result in altered cellular signaling, release of proinflammatory molecules, and oxidative stress (9). Furthermore, inflammatory cytokines released from perivascular fat in hypercholesterolemia may also contribute to increased superoxide production and eNOS uncoupling, thereby limiting basal NO bioavailability (8, 21, 37). This is in agreement with the reduced microvascular NO production and eNOS expression in the HFD swine, but not with the data obtained in the DM + HFD swine, where both eNOS expression and NO production were essentially maintained. Furthermore, inflammation and hyperglycemia have also been suggested to result in inactivation of small- and intermediate-conductance K^+ channels, leading to an impaired EDHF-mediated vasodilation (17, 41). Our results confirm such reduction

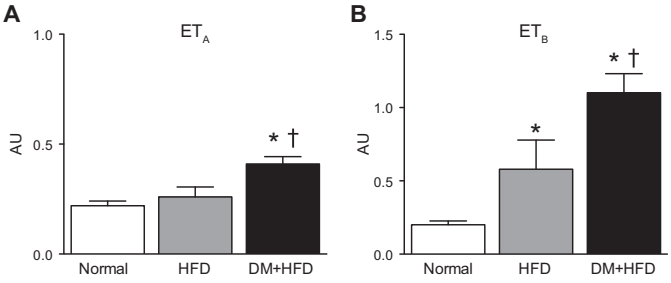

Fig. 9. Expression of ET_A (*A*) and ET_B (*B*) receptors measured by quantitative PCR in small arteries of Normal (n = 6), HFD (n = 3), and DM + HFD (n = 5) swine. Expression of ET_A and ET_B receptors was increased in DM + HFD compared with HFD and Normal swine. ET_B receptor expression was also increased in HFD compared with Normal swine. *$P < 0.05$ vs. Normal. †$P < 0.05$, DM + HFD vs. HFD.

Table 2. *Studies investigating effects of BK on coronary microvascular function in hypercholesterolemia and/or metabolic derangement*

Study	Species	Model	Tissue	FU Time	Administration	Vasorelaxation	Mechanism
Mishra et al. (46)	Rat	Goto-Kakizaki (nonobese, type 2 DM)	Isolated full heart (coronary flow)	10–12 wk, 18–20 wk	Acute administration	↓	K_{Ca} ↔, NO?
Given et al. (24)	Rat	STZ (type 1 DM)	Coronary microvasculature	12 wk	Acute administration	↔	K_{Ca} ↔, cGMP ↔
Obrosova et al. (50)	Rat	STZ (type 1 DM)	Isolated coronary arterioles	6 wk	Incubation BK	↓	Peroxynitrite ↑
Tsai et al. (69)	Pig	Glucose incubation	Isolated healthy coronary arterioles	1 h	Incubation BK	↓	EDHF ↓
Van den Heuvel et al. (71)	Pig	Type 2 DM + HFD	Isolated coronary arterioles	2.5 mo	Incubation BK	↓	NO ↓ EDHF↔
Present study	Pig	Type 2 DM + HFD	Isolated coronary arterioles	15 mo	Incubation BK	↔	NO and EDHF interact in synergy
Yoshino et al. (75)	Human	Types 1 and 2 DM + dyslipidemia	In vivo CBF	?	IC administration	↓	
Szerafin et al. (65)	Human	Types 1 and 2 DM	Isolated coronary arterioles	?	Incubation BK	↑	COX-2 ↑
Matsumoto et al. (43)	Human	DM (type not specified)	In vivo CBF (LAD)	?	IC administration	↓ CBF with ↑ oxLDL	

BK, bradykinin; FU, follow-up; DM, diabetes mellitus; STZ, streptozotocin; HFD, high-fat diet; CBF, coronary blood flow; LAD, left anterior descending coronary artery; IC, intracoronary; K_{Ca}, Ca^{2+}-activated K^+ channel; oxLDL, oxidized low-density lipoprotein; NO, nitric oxide; EDHF, endothelium-derived hyperpolarizing factor; COX-2, cyclooxygenase 2; ?, unknown.

in the expression of the small- and intermediate-conductance K^+ channels, which can also partially explain the impaired basal EDHF-mediated contribution to BK-induced vasodilation.

ET-1-Mediated Vascular Responses

Proper control of vascular tone requires an optimal balance between vasodilator and vasoconstrictor influences (19). Diabetes and insulin resistance are known to alter the production of, and the response to, endothelium-derived vasoconstrictors (62). For example, the ET-1 system is activated in diabetes, resulting in increased ET-1 plasma levels (5, 23), which correlates well with diabetic microangiopathy (2). However, conflicting data have been reported regarding ET-1 reactivity, with reduced responsiveness to exogenous ET-1 in the peripheral circulation of obese (74) and type 2 DM (15, 44, 59) patients and increased ET-1 vasoconstriction in animal models of DM (31, 67, 73). Although this discrepancy is not readily explained, the present study, in conjunction with our previous observations (71), demonstrates that disease progression might be one explanation. Thus a reduced responsiveness to ET-1 was observed in DM + HFD swine at 2.5 mo of follow-up in the absence of atherosclerotic plaques, while plasma ET-1 levels were still unchanged (71). This is in accordance with reports in DM patients without evidence of atherosclerotic disease (15, 44, 59). In addition, short-term exposure to HFD in a dog model did not alter plasma ET-1 levels and ET-1 responsiveness (34), which was also observed in obese Zucker rats at 16–18 wk of age (56), similar to our results in HFD swine at 2.5 mo (71). In contrast, in the present study, 15 mo of exposure to DM + HFD, but not HFD alone, resulted in increased plasma ET-1 levels, in accordance with observations in patients (2, 23), as well as the presence of coronary atherosclerotic plaques. At this later time point, both HFD and DM + HFD swine showed an increased responsiveness to exogenous ET-1. These results are in agreement with rat models of long-term type 1 DM showing exaggerated coronary ET-1 responsiveness combined with increased ET-1 plasma levels, although the presence of CAD was not verified (29, 31).

Comparison of ET-1 responsiveness of the coronary circulation in animal models with results obtained in patients with CAD is difficult, since no data are available regarding the response to exogenous ET-1 in the coronary circulation of patients. However, endogenous ET-1 activity has been studied in the coronary vasculature of patients by using ET-1 receptor antagonists. The limited data on coronary circulation available from clinical studies yield conflicting results (Table 3). The coronary vasoconstrictor influence of ET-1 was increased in obese compared with healthy humans, which correlated with the cholesterol levels (42). Furthermore, Kyriakides et al. reported a reduced effect of endogenous ET-1 on proximal coronary arterial compliance in patients with type 2 DM (40) and improved coronary arterial compliance by acute ET_A receptor antagonism in patients with CAD (39), while in hypertensive patients the effect was not different from that in controls (38). In the coronary microcirculation of stable CAD patients with or without DM, endogenous ET_A receptor activity exerts a vasoconstrictor influence, while endogenous ET_B receptor activity exerts a vasodilator influence (14, 26, 53). In contrast, Feng et al. reported, besides ET_A receptor-mediated vasoconstriction, absence of an ET_B receptor-mediated vasodilating response in small coronary arteries of hypertensive, diabetic patients undergoing coronary bypass grafting, possibly a more advanced-disease group (22). Therefore, increased coronary ET-1 activity seems to be present in obese, insulin-resistant individuals as well as in overt DM patients. In our swine model, we previously showed that at 2.5 mo the responsiveness to exogenous ET-1 was maintained in the HFD group and actually decreased in the DM + HFD animals due to reduced ET_A receptor-mediated constriction (71). ET_A receptor expression was not significantly altered, suggesting that ET_A

Table 3. *Studies investigating effects of ET-1 on coronary microvascular function in hypercholesterolemia and/or metabolic derangement*

Study	Species	Model	Tissue	FU Time	Administration	Vasoconstriction	Mechanism
Kamata et al. (31)	Rat	STZ-diabetic (type 1)	Isolated heart	9 mo	Heart perfusion	↑	
Verma et al. (73)	Rat	STZ-diabetic (type 1)	Isolated heart	8 wk	Heart perfusion	↑	Reversed by bosentan
Tickerhoof et al. (67)	Rat	STZ-diabetic (type 1)	Isolated coronary arterioles	6 wk	Incubation ET-1	↑	
Prakash et al. (56)	Rat	Obese Zucker (pre-DM)	Isolated coronary arterioles	16–18 wk	Incubation ET-1	↓	
Van den Heuvel et al. (71)	Pig	Type 2 DM + HFD	Isolated coronary arterioles	2.5 mo	Incubation ET-1	↓	↓ ET_A
Present study	Pig	Type 2 DM + HFD	Isolated coronary arterioles	15 mo	Incubation ET-1	↑	↑ ET_A, ↑ ET_B
Knudson et al. (34)	Dog	Metabolic syndrome	Isolated coronary arterioles	6 wk	Incubation ET-1	↔	
Feng et al. (22)	Human	Hypertension and DM (type not specified)	Isolated coronary arterioles	?	Incubation ET-1	↔	↓ ET_B
Altieri et al. (5)	Human	Type 2 DM and CAD	IC levels of circulating ET-1			↑	
Bohm et al. (14)	Human	Hypercholesterolemia and CAD	Coronary flow	?	IC infusion of BQ123 and BQ788	↑	
Halcox et al. (26)	Human	Hypercholesterolemia and CAD	Coronary microvascular vasomotion	?	IC infusion of BQ123 and BQ788	↑ ET_B	↓ ET-1 clearance and NO bioavailability
Papadogeorgos et al. (53)	Human	Type 2 DM and CAD	Coronary flow	?	IC infusion of BQ123 and bosentan	↑	
Mather et al. (42)	Human	Obesity	Myocardial perfusion (PET)	?	IC infusion of BQ123	↔	↑ Effect with increased BMI and cholesterol

DM, diabetes mellitus; STZ, streptozotocin; HFD, high fat diet; CAD, coronary artery disease; IC, intracoronary; BQ123, ET_A receptor antagonist; BQ788, ET_B receptor antagonist; BMI, body mass index; ?, unknown.

receptor signaling was reduced at this early disease state. In contrast, at 15 mo, both DM + HFD and HFD swine showed increased ET-1 responsiveness that was accompanied by increased expression of ET_B receptors in both groups and, only in DM + HFD swine, by a small increase in ET_A receptor expression. Accordingly, the enhanced ET-1 vasoconstrictor responses appeared to be principally ET_B receptor-mediated. Thus the vasodilator influence of the ET_B receptors in Normal swine was lost in DM + HFD swine and was reversed to a vasoconstrictor influence in HFD swine. Consequently, we hypothesize that the increased ET_B receptor expression occurred predominantly in coronary vascular smooth muscle cells, similar to observations in the cerebral vasculature of diabetic rats (64). Importantly, these results suggest that, with disease progression, not only is signaling of ET_A receptors restored between 2.5 and 15 mo of exposure to DM + HFD but also, at 15 mo, ET_B receptor signaling has shifted from ET_B receptor-mediated vasodilation to ET_B receptor-mediated vasoconstriction. Finally, in all three groups, ET_{AB} receptor blockade appeared to be slightly greater than the sum of the individual effects of ET_A and ET_B receptor blockade, suggesting an interaction between the two receptors. Indeed, the formation of ET_A-ET_B receptor dimers has been shown to enhance the vasoconstrictor response to ET-1 (7, 12, 28). Whether this ET-1 receptor dimerization plays a role in the in vivo responsiveness of the coronary microcirculation should be the subject of future investigations.

Vascular Stiffness

A chronic increase in vascular tone is capable of inducing inward remodeling due to extracellular matrix restructuring (7). Hence, the increased circulating levels of ET-1 in the DM + HFD swine, together with the increased responsiveness of the small coronary arteries to exogenous ET-1 in vitro, may have led to a chronic increase in coronary microvascular tone and, thus, extracellular matrix remodeling. Although we did not find evidence for microvascular inward remodeling, we did observe an increase in vascular stiffness, particularly in DM + HFD swine. These observations contrast with a study by Katz et al., who reported reduced coronary arteriolar stiffness in type 2 diabetic mice, associated with inward hypertrophic remodeling and increased elastin-to-collagen ratio in the vascular wall (33). Studying Ossabaw swine with metabolic syndrome, Trask et al. also reported a reduced microvascular coronary stiffness that was associated with inward remodeling, capillary rarefaction, augmented myogenic tone, and reduced coronary blood flow reserve (68). The divergent observations are not readily explained but could be due to differences in disease severity. Indeed, an increased stiffness of resistance, but not large, arteries due to hyperglycemia was observed in type 1 DM patients (25).

Conclusions

In summary, the present study, in conjunction with our previous study (71), demonstrates that the balance of vasodi-

lator and vasoconstrictor mechanisms contributing to CMD changes markedly during disease progression. Thus, whereas at 2.5 mo after induction of hyperglycemia and hypercholesterolemia, impaired endothelium-dependent vasodilation was accompanied by a reduced ET-1-mediated vasoconstriction (71), the present study demonstrates that at 15 mo, microvascular dysfunction was principally characterized by an increased vasoconstrictor response to ET-1, but with a normal endothelium-dependent vasodilator response to BK. In hypercholesterolemia only, the progression of microvascular dysfunction is more subtle, and no significant alterations could be observed at 2.5 mo (71). In contrast, at 15 mo in the present study, responses were characterized by a normal vasodilator response to BK and increased vasoconstriction to ET-1 that was principally due to enhanced ET_B receptor-mediated vasoconstrictor response. These findings indicate that the nature of CMD early in the disease process can be very different from, and is not necessarily predictive of, the nature of CMD during later stages of the disease process. Furthermore, these findings highlight the importance of performing longitudinal studies of microvascular function in experimental studies of DM and CAD.

GRANTS

This study was supported by European Commission FP7-Health-2010 Grant MEDIA-261409 (to D. J. Duncker and D. Merkus); the Netherlands CardioVascular Research Initiative, supported by Dutch Heart Foundation Grant CVON2014-11 RECONNECT (to D. J. Duncker and D. Merkus); and Academy of Finland Grant 251272 and funds from the Finnish Diabetes Research Foundation and the Finnish Foundation for Cardiovascular Research (to I. Heinonen).

DISCLOSURES

No conflicts of interest, financial or otherwise, are declared by the authors.

AUTHOR CONTRIBUTIONS

O.S., M.v.d.H., W.v.d.G., and D.J.D. developed the concept and designed the research; O.S., M.v.d.H., N.S.v.D., R.W.B.v.D., and Z.Z. performed the experiments; O.S. and M.v.d.H. analyzed the data; O.S., M.v.d.H., D.M., and D.J.D. interpreted the results of the experiments; O.S. and M.v.d.H. prepared the figures; O.S. and M.v.d.H. drafted the manuscript; O.S., M.v.d.H., N.S.v.D., V.J.d.B., I.H., R.W.B.v.D., Z.Z., S.J.K., D.M., A.J.D., and D.J.D. edited and revised the manuscript; O.S., M.v.d.H., N.S.v.D., V.J.d.B., I.H., R.W.B.v.D., Z.Z., S.J.K., D.M., A.J.D., and D.J.D. approved the final version of the manuscript.

REFERENCES

1. **Abboud K, Bassila JC, Ghali-Ghoul R, Sabra R.** Temporal changes in vascular reactivity in early diabetes mellitus in rats: role of changes in endothelial factors and in phosphodiesterase activity. *Am J Physiol Heart Circ Physiol* 297: H836–H845, 2009.
2. **Ak G, Buyukberber S, Sevinc A, Turk HM, Ates M, Sari R, Savli H, Cigli A.** The relation between plasma endothelin-1 levels and metabolic control, risk factors, treatment modalities, and diabetic microangiopathy in patients with type 2 diabetes mellitus. *J Diabetes Complications* 15: 150–157, 2001.
3. **Almdal T, Scharling H, Jensen JS, Vestergaard H.** Higher prevalence of risk factors for type 2 diabetes mellitus and subsequent higher incidence in men. *Eur J Intern Med* 19: 40–45, 2008.
4. **Almdal T, Scharling H, Jensen JS, Vestergaard H.** The independent effect of type 2 diabetes mellitus on ischemic heart disease, stroke, and death: a population-based study of 13,000 men and women with 20 years of follow-up. *Arch Intern Med* 164: 1422–1426, 2004.
5. **Altieri PI, Marcial JM, Banchs HL, Escobales N, Crespo M, Gonzalez W.** Coronary levels of angiotensin-II and endothelin-I in diabetic patients with and without coronary artery disease. *Bol Asoc Med PR* 107: 5–7, 2015.
6. **Ather S, Chan W, Bozkurt B, Aguilar D, Ramasubbu K, Zachariah AA, Wehrens XH, Deswal A.** Impact of noncardiac comorbidities on morbidity and mortality in a predominantly male population with heart failure and preserved versus reduced ejection fraction. *J Am Coll Cardiol* 59: 998–1005, 2012.
7. **Bakker EN, Sorop O, Spaan JA, VanBavel E.** Remodeling of resistance arteries in organoid culture is modulated by pressure and pressure pulsation and depends on vasomotion. *Am J Physiol Heart Circ Physiol* 286: H2052–H2056, 2004.
8. **Bakker W, Eringa EC, Sipkema P, van Hinsbergh VW.** Endothelial dysfunction and diabetes: roles of hyperglycemia, impaired insulin signaling and obesity. *Cell Tissue Res* 335: 165–189, 2009.
9. **Barlovic DP, Soro-Paavonen A, Jandeleit-Dahm KA.** RAGE biology, atherosclerosis and diabetes. *Clin Sci (Lond)* 121: 43–55, 2011.
10. **Batenburg WW, Popp R, Fleming I, de Vries R, Garrelds IM, Saxena PR, Danser AH.** Bradykinin-induced relaxation of coronary microarteries: *S*-nitrosothiols as EDHF? *Br J Pharmacol* 142: 125–135, 2004.
11. **Bittencourt C, Piveta VM, Oliveira CS, Crispim F, Meira D, Saddi-Rosa P, Giuffrida FM, Reis AF.** Association of classical risk factors and coronary artery disease in type 2 diabetic patients submitted to coronary angiography. *Diabet Med* 6: 46, 2014.
12. **Boesen EI.** Endothelin ET_B receptor heterodimerization: beyond the ET_A receptor. *Kidney Int* 74: 693–694, 2008.
13. **Bohm F, Ahlborg G, Johansson BL, Hansson LO, Pernow J.** Combined endothelin receptor blockade evokes enhanced vasodilatation in patients with atherosclerosis. *Arterioscler Thromb Vasc Biol* 22: 674–679, 2002.
14. **Bohm F, Jensen J, Svane B, Settergren M, Pernow J.** Intracoronary endothelin receptor blockade improves endothelial function in patients with coronary artery disease. *Can J Physiol Pharmacol* 86: 745–751, 2008.
15. **Cardillo C, Campia U, Bryant MB, Panza JA.** Increased activity of endogenous endothelin in patients with type II diabetes mellitus. *Circulation* 106: 1783–1787, 2002.
16. **Chuaiphichai S, McNeill E, Douglas G, Crabtree MJ, Bendall JK, Hale AB, Alp NJ, Channon KM.** Cell-autonomous role of endothelial GTP cyclohydrolase 1 and tetrahydrobiopterin in blood pressure regulation. *Hypertension* 64: 530–540, 2014.
17. **Cotter MA, Gibson TM, Nangle MR, Cameron NE.** Effects of interleukin-6 treatment on neurovascular function, nerve perfusion and vascular endothelium in diabetic rats. *Diabetes Obes Metab* 12: 689–699, 2010.
18. **Crea F, Camici PG, Bairey Merz CN.** Coronary microvascular dysfunction: an update. *Eur Heart J* 35: 1101–1111, 2014.
19. **Duncker DJ, Koller A, Merkus D, Canty JM Jr.** Regulation of coronary blood flow in health and ischemic heart disease. *Prog Cardiovasc Dis* 57: 409–422, 2015.
20. **Erdogan D, Yucel H, Uysal BA, Ersoy IH, Icli A, Akcay S, Arslan A, Aksoy F, Ozaydin M, Tamer MN.** Effects of prediabetes and diabetes on left ventricular and coronary microvascular functions. *Metabolism* 62: 1123–1130, 2013.
21. **Eringa EC, Bakker W, van Hinsbergh VW.** Paracrine regulation of vascular tone, inflammation and insulin sensitivity by perivascular adipose tissue. *Vascul Pharmacol* 56: 204–209, 2012.
22. **Feng J, Liu Y, Khabbaz KR, Hagberg R, Sodha NR, Osipov RM, Sellke FW.** Endothelin-1-induced contractile responses of human coronary arterioles via endothelin-A receptors and PKCα signaling pathways. *Surgery* 147: 798–804, 2010.
23. **Ferri C, Bellini C, Desideri G, Baldoncini R, Properzi G, Santucci A, De Mattia G.** Circulating endothelin-1 levels in obese patients with the metabolic syndrome. *Exp Clin Endocrinol Diabetes* 105 *Suppl* 2: 38–40, 1997.
24. **Given MB, Greenberg SS, Giles TD.** Coronary vasodilator responses to bradykinin in euglycemic and diabetic rats. *Am J Hypertens* 14: 446–454, 2001.
25. **Gordin D, Ronnback M, Forsblom C, Heikkila O, Saraheimo M, Groop PH.** Acute hyperglycaemia rapidly increases arterial stiffness in young patients with type 1 diabetes. *Diabetologia* 50: 1808–1814, 2007.
26. **Halcox JP, Nour KR, Zalos G, Quyyumi AA.** Endogenous endothelin in human coronary vascular function: differential contribution of endothelin receptor types A and B. *Hypertension* 49: 1134–1141, 2007.
27. **Halpern W, Mulvany MJ, Warshaw DM.** Mechanical properties of smooth muscle cells in the walls of arterial resistance vessels. *J Physiol* 275: 85–101, 1978.

28. **Hasselblatt M, Kamrowski-Kruck H, Jensen N, Schilling L, Kratzin H, Siren AL, Ehrenreich H.** ET_A and ET_B receptor antagonists synergistically increase extracellular endothelin-1 levels in primary rat astrocyte cultures. *Brain Res* 785: 253–261, 1998.
29. **Hopfner RL, McNeill JR, Gopalakrishnan V.** Plasma endothelin levels and vascular responses at different temporal stages of streptozotocin diabetes. *Eur J Pharmacol* 374: 221–227, 1999.
30. **Jebelovszki E, Kiraly C, Erdei N, Feher A, Pasztor ET, Rutkai I, Forster T, Edes I, Koller A, Bagi Z.** High-fat diet-induced obesity leads to increased NO sensitivity of rat coronary arterioles: role of soluble guanylate cyclase activation. *Am J Physiol Heart Circ Physiol* 294: H2558–H2564, 2008.
31. **Kamata K, Ozawa Y, Kobayashi T, Matsumoto T.** Effect of long-term streptozotocin-induced diabetes on coronary vasoconstriction in isolated perfused rat heart. *J Smooth Muscle Res* 44: 177–188, 2008.
32. **Katz A, Nambi SS, Mather K, Baron AD, Follmann DA, Sullivan G, Quon MJ.** Quantitative insulin sensitivity check index: a simple, accurate method for assessing insulin sensitivity in humans. *J Clin Endocrinol Metab* 85: 2402–2410, 2000.
33. **Katz PS, Trask AJ, Souza-Smith FM, Hutchinson KR, Galantowicz ML, Lord KC, Stewart JA Jr, Cismowski MJ, Varner KJ, Lucchesi PA.** Coronary arterioles in type 2 diabetic (*db/db*) mice undergo a distinct pattern of remodeling associated with decreased vessel stiffness. *Basic Res Cardiol* 106: 1123–1134, 2011.
34. **Knudson JD, Rogers PA, Dincer UD, Bratz IN, Araiza AG, Dick GM, Tune JD.** Coronary vasomotor reactivity to endothelin-1 in the prediabetic metabolic syndrome. *Microcirculation* 13: 209–218, 2006.
35. **Koller A, Balasko M, Bagi Z.** Endothelial regulation of coronary microcirculation in health and cardiometabolic diseases. *Intern Emerg Med* 8 *Suppl* 1: S51–S54, 2013.
36. **Koopmans SJ, Dekker R, Ackermans MT, Sauerwein HP, Serlie MJ, van Beusekom HM, van den Heuvel M, van der Giessen WJ.** Dietary saturated fat/cholesterol, but not unsaturated fat or starch, induces C-reactive protein associated early atherosclerosis and ectopic fat deposition in diabetic pigs. *Cardiovasc Diabetol* 10: 64, 2011.
37. **Kougias P, Chai H, Lin PH, Lumsden AB, Yao Q, Chen C.** Adipocyte-derived cytokine resistin causes endothelial dysfunction of porcine coronary arteries. *J Vasc Surg* 41: 691–698, 2005.
38. **Kyriakides Z, Kyrzopoulos S, Paraskevaidis I, Kolokathis F, Tsopotos I, Lyras T, Kremastinos D.** Endothelin-A receptor antagonism promotes decreased vasodilation but has no differential effect on coronary artery compliance in hypertensive patients. *J Cardiovasc Pharmacol 44* Suppl 1: S85–S88, 2004.
39. **Kyriakides ZS, Kremastinos DT, Kolokathis F, Kostopoulou A, Georgiadis M, Webb DJ.** Acute $endothelin_A$ receptor antagonism improves coronary artery compliance in coronary artery disease patients. *Clin Sci (Lond)* 103 *Suppl* 48: 179S–183S, 2002.
40. **Kyriakides ZS, Kremastinos DT, Raptis AE, Johnston N, Raptis SA, Webb DJ, Kyrzopoulos S, Sbarouni E.** Impaired effect of endothelin-1 on coronary artery stiffness in type 2 diabetes. *Int J Cardiol* 112: 207–212, 2006.
41. **Liu Y, Xie A, Singh AK, Ehsan A, Choudhary G, Dudley S, Sellke FW, Feng J.** Inactivation of endothelial small/intermediate conductance of calcium-activated potassium channels contributes to coronary arteriolar dysfunction in diabetic patients. *J Am Heart Assoc* 4: e002062, 2015.
42. **Mather KJ, Lteif AA, Veeneman E, Fain R, Giger S, Perry K, Hutchins GD.** Role of endogenous ET-1 in the regulation of myocardial blood flow in lean and obese humans. *Obesity (Silver Spring)* 18: 63–70, 2010.
43. **Matsumoto T, Takashima H, Ohira N, Tarutani Y, Yasuda Y, Yamane T, Matsuo S, Horie M.** Plasma level of oxidized low-density lipoprotein is an independent determinant of coronary macrovasomotor and microvasomotor responses induced by bradykinin. *J Am Coll Cardiol* 44: 451–457, 2004.
44. **McAuley DF, McGurk C, Nugent AG, Hanratty C, Hayes JR, Johnston GD.** Vasoconstriction to endothelin-1 is blunted in non-insulin-dependent diabetes: a dose-response study. *J Cardiovasc Pharmacol* 36: 203–208, 2000.
45. **Miller AW, Katakam PV, Ujhelyi MR.** Impaired endothelium-mediated relaxation in coronary arteries from insulin-resistant rats. *J Vasc Res* 36: 385–392, 1999.
46. **Mishra RC, Wulff H, Cole WC, Braun AP.** A pharmacologic activator of endothelial K_{Ca} channels enhances coronary flow in the hearts of type 2 diabetic rats. *J Mol Cell Cardiol* 72: 364–373, 2014.
47. **Miura H, Wachtel RE, Liu Y, Loberiza FR Jr, Saito T, Miura M, Gutterman DD.** Flow-induced dilation of human coronary arterioles: important role of Ca^{2+}-activated K^+ channels. *Circulation* 103: 1992–1998, 2001.
48. **Mokdad AH, Ford ES, Bowman BA, Dietz WH, Vinicor F, Bales VS, Marks JS.** Prevalence of obesity, diabetes, and obesity-related health risk factors, 2001. *JAMA* 289: 76–79, 2003.
49. **Naka KK, Papathanassiou K, Bechlioulis A, Kazakos N, Pappas K, Tigas S, Makriyiannis D, Tsatsoulis A, Michalis LK.** Determinants of vascular function in patients with type 2 diabetes. *Cardiovasc Diabetol* 11: 127, 2012.
50. **Obrosova IG, Drel VR, Oltman CL, Mashtalir N, Tibrewala J, Groves JT, Yorek MA.** Role of nitrosative stress in early neuropathy and vascular dysfunction in streptozotocin-diabetic rats. *Am J Physiol Endocrinol Metab* 293: E1645–E1655, 2007.
51. **Oltman CL, Richou LL, Davidson EP, Coppey LJ, Lund DD, Yorek MA.** Progression of coronary and mesenteric vascular dysfunction in Zucker obese and Zucker diabetic fatty rats. *Am J Physiol Heart Circ Physiol* 291: H1780–H1787, 2006.
52. **Paneni F, Beckman JA, Creager MA, Cosentino F.** Diabetes and vascular disease: pathophysiology, clinical consequences, and medical therapy: part I. *Eur Heart J* 34: 2436–2443, 2013.
53. **Papadogeorgos NO, Bengtsson M, Kalani M.** Selective endothelin A-receptor blockade attenuates coronary microvascular dysfunction after coronary stenting in patients with type 2 diabetes. *Vasc Health Risk Manag* 5: 893–899, 2009.
54. **Park Y, Capobianco S, Gao X, Falck JR, Dellsperger KC, Zhang C.** Role of EDHF in type 2 diabetes-induced endothelial dysfunction. *Am J Physiol Heart Circ Physiol* 295: H1982–H1988, 2008.
55. **Pitkanen OP, Nuutila P, Raitakari OT, Ronnemaa T, Koskinen PJ, Iida H, Lehtimaki TJ, Laine HK, Takala T, Viikari JS, Knuuti J.** Coronary flow reserve is reduced in young men with IDDM. *Diabetes* 47: 248–254, 1998.
56. **Prakash R, Mintz JD, Stepp DW.** Impact of obesity on coronary microvascular function in the Zucker rat. *Microcirculation* 13: 389–396, 2006.
57. **Pries AR, Badimon L, Bugiardini R, Camici PG, Dorobantu M, Duncker DJ, Escaned J, Koller A, Piek JJ, de Wit C.** Coronary vascular regulation, remodelling, and collateralization: mechanisms and clinical implications on behalf of the working group on coronary pathophysiology and microcirculation. *Eur Heart J* 35: 3134–3146, 2015.
58. **Rath G, Dessy C, Feron O.** Caveolae, caveolin and control of vascular tone: nitric oxide (NO) and endothelium derived hyperpolarizing factor (EDHF) regulation. *J Physiol Pharmacol* 60 *Suppl* 4: 105–109, 2009.
59. **Rizzoni D, Porteri E, Guelfi D, Muiesan ML, Piccoli A, Valentini U, Cimino A, Girelli A, Salvetti M, De Ciuceis C, Tiberio GA, Giulini SM, Sleiman I, Monteduro C, Rosei EA.** Endothelial dysfunction in small resistance arteries of patients with non-insulin-dependent diabetes mellitus. *J Hypertens* 19: 913–919, 2001.
60. **Rizzoni D, Porteri E, Guelfi D, Muiesan ML, Valentini U, Cimino A, Girelli A, Rodella L, Bianchi R, Sleiman I, Rosei EA.** Structural alterations in subcutaneous small arteries of normotensive and hypertensive patients with non-insulin-dependent diabetes mellitus. *Circulation* 103: 1238–1244, 2001.
61. **Sara JD, Widmer RJ, Matsuzawa Y, Lennon RJ, Lerman LO, Lerman A.** Prevalence of coronary microvascular dysfunction among patients with chest pain and nonobstructive coronary artery disease. *JACC Cardiovasc Interventions* 8: 1445–1453, 2015.
62. **Sena CM, Pereira AM, Seica R.** Endothelial dysfunction—a major mediator of diabetic vascular disease. *Biochim Biophys Acta* 1832: 2216–2231, 2013.
63. **Stary HC, Chandler AB, Glagov S, Guyton JR, Insull W Jr, Rosenfeld ME, Schaffer SA, Schwartz CJ, Wagner WD, Wissler RW.** A definition of initial, fatty streak, and intermediate lesions of atherosclerosis. A report from the Committee on Vascular Lesions of the Council on Arteriosclerosis, American Heart Association. *Circulation* 89: 2462–2478, 1994.
64. **Sundell J, Knuuti J.** Insulin and myocardial blood flow. *Cardiovasc Res* 57: 312–319, 2003.
65. **Szerafin T, Erdei N, Fulop T, Pasztor ET, Edes I, Koller A, Bagi Z.** Increased cyclooxygenase-2 expression and prostaglandin-mediated dilation in coronary arterioles of patients with diabetes mellitus. *Circ Res* 99: e12–e17, 2006.

66. **Task Force Members, Montalescot G, Sechtem U, Achenbach S, Andreotti F, Arden C, Budaj A, Bugiardini R, Crea F, Cuisset T, Di Mario C, Ferreira JR, Gersh BJ, Gitt AK, Hulot JS, Marx N, Opie LH, Pfisterer M, Prescott E, Ruschitzka F, Sabate M, Senior R, Taggart DP, van der Wall EE, Vrints CJ, ESC Committee for Practice Guidelines , Zamorano JL, Achenbach S, Baumgartner H, Bax JJ, Bueno H, Dean V, Deaton C, Erol C, Fagard R, Ferrari R, Hasdai D, Hoes AW, Kirchhof P, Knuuti J, Kolh P, Lancellotti P, Linhart A, Nihoyannopoulos P, Piepoli MF, Ponikowski P, Sirnes PA, Tamargo JL, Tendera M, Torbicki A, Wijns W, Windecker S, Document R, Knuuti J, Valgimigli M, Bueno H, Claeys MJ, Donner-Banzhoff N, Erol C, Frank H, Funck-Brentano C, Gaemperli O, Gonzalez-Juanatey JR, Hamilos M, Hasdai D, Husted S, James SK, Kervinen K, Kolh P, Kristensen SD, Lancellotti P, Maggioni AP, Piepoli MF, Pries AR, Romeo F, Ryden L, Simoons ML, Sirnes PA, Steg PG, Timmis A, Wijns W, Windecker S, Yildirir A, Zamorano JL.** 2013 ESC Guidelines on the Management of Stable Coronary Artery Disease: the Task Force on the Management of Stable Coronary Artery Disease of the European Society of Cardiology. *Eur Heart J* 34: 2949–3003, 2013.
67. **Tickerhoof MM, Farrell PA, Korzick DH.** Alterations in rat coronary vasoreactivity and vascular protein kinase C isoforms in type 1 diabetes. *Am J Physiol Heart Circ Physiol* 285: H2694–H2703, 2003.
68. **Trask AJ, Katz PS, Kelly AP, Galantowicz ML, Cismowski MJ, West TA, Neeb ZP, Berwick ZC, Goodwill AG, Alloosh M, Tune JD, Sturek M, Lucchesi PA.** Dynamic micro- and macrovascular remodeling in coronary circulation of obese Ossabaw pigs with metabolic syndrome. *J Appl Physiol (1985)* 113: 1128–1140, 2012.
69. **Tsai SH, Hein TW, Kuo L, Yang VC.** High glucose impairs EDHF-mediated dilation of coronary arterioles via reduced cytochrome P450 activity. *Microvasc Res* 82: 356–363, 2011.
70. **Tseng KH.** Standards of medical care in diabetes—2006: response to the American Diabetes Association. *Diabetes Care* 29: 2563–2564; author reply 2564–2565, 2006.
71. **van den Heuvel M, Sorop O, Koopmans SJ, Dekker R, de Vries R, van Beusekom HM, Eringa EC, Duncker DJ, Danser AH, van der Giessen WJ.** Coronary microvascular dysfunction in a porcine model of early atherosclerosis and diabetes. *Am J Physiol Heart Circ Physiol* 302: H85–H94, 2012.
72. **van Ditzhuijzen NS, van den Heuvel M, Sorop O, van Duin RW, Krabbendam-Peters I, van Haeren R, Ligthart JM, Witberg KT, Duncker DJ, Regar E, van Beusekom HM, van der Giessen WJ.** Invasive coronary imaging in animal models of atherosclerosis. *Neth Heart J* 19: 442–446, 2011.
73. **Verma S, Arikawa E, Lee S, Dumont AS, Yao L, McNeill JH.** Exaggerated coronary reactivity to endothelin-1 in diabetes: reversal with bosentan. *Can J Physiol Pharmacol* 80: 980–986, 2002.
74. **Weil BR, Westby CM, Van Guilder GP, Greiner JJ, Stauffer BL, DeSouza CA.** Enhanced endothelin-1 system activity with overweight and obesity. *Am J Physiol Heart Circ Physiol* 301: H689–H695, 2011.
75. **Yoshino T, Nakae I, Matsumoto T, Mitsunami K, Horie M.** Association between brachial-ankle pulse wave velocity and endothelium-dependent and -independent coronary vasomotor function. *Clin Exp Pharmacol Physiol* 38: 34–41, 2011.
76. **Zhou Z, Merkus D, Cheng C, Duckers HJ, Jan Danser AH, Duncker DJ.** Uridine adenosine tetraphosphate is a novel vasodilator in the coronary microcirculation which acts through purinergic P1 but not P2 receptors. *Pharmacol Res* 67: 10–17, 2013.

Early systemic microvascular damage in pigs with atherogenic diabetes mellitus coincides with renal angiopoietin dysbalance

Khairoun M., van den Heuvel M., van den Berg B.M., Sorop O., de Boer R., van Ditzhuijzen N.S., Bajema I.M., Baelde H.J., Zandbergen M., Duncker D.J., Rabelink T.J., Reinders M.E., van der Giessen W.J. and Rotmans J.I.

PLoS One. 2015 Apr 24;10(4)

8

Early systemic microvascular damage in pigs with atherogenic diabetes mellitus coincides with renal angiopoietin dysbalance

Meriem Khairoun[1], Mieke van den Heuvel[4], Bernard M. van den Berg[1,2], Oana Sorop[4], Rients de Boer[1], Nienke S. van Ditzhuijzen[4], Ingeborg M. Bajema[3], Hans J. Baelde[3], Malu Zandbergen[3], Dirk J. Duncker[4], Ton J. Rabelink[1,2], Marlies E.J. Reinders[1,2], Wim J. van der Giessen[4†], Joris I. Rotmans[1,2*]

[1] Department of Nephrology, Leiden University Medical Center, Leiden, The Netherlands; [2] Einthoven Laboratory for Experimental Vascular Research, Leiden University Medical Center, Leiden, The Netherlands; [3] Department of Pathology, Leiden University Medical Center, Leiden, The Netherlands; [4] Division of Experimental Cardiology, Department of Cardiology, Erasmus Medical Center Rotterdam, Rotterdam, The Netherlands

† Deceased.
* j.i.rotmans@lumc.nl

Abstract

Background

Diabetes mellitus (DM) is associated with a range of microvascular complications including diabetic nephropathy (DN). Microvascular abnormalities in the kidneys are common histopathologic findings in DN, which represent one manifestation of ongoing systemic microvascular damage. Recently, sidestream dark-field (SDF) imaging has emerged as a noninvasive tool that enables one to visualize the microcirculation. In this study, we investigated whether changes in the systemic microvasculature induced by DM and an atherogenic diet correlated spatiotemporally with renal damage.

Methods

Atherosclerotic lesion development was triggered in streptozotocin-induced DM pigs (140 mg/kg body weight) by administering an atherogenic diet for approximately 11 months. Fifteen months following induction of DM, microvascular morphology was visualized in control pigs (n = 7), non-diabetic pigs fed an atherogenic diet (ATH, n = 5), and DM pigs fed an atherogenic diet (DM+ATH, n = 5) using SDF imaging of oral mucosal tissue. Subsequently, kidneys were harvested from anethesized pigs and the expression levels of well-established markers for microvascular integrity, such as Angiopoietin-1 (Angpt1) and Angiopoietin-2 (Angpt2) were determined immunohistochemically, while endothelial cell (EC) abundance was determined by immunostaining for von Willebrand factor (vWF).

Results

Our study revealed an increase in the capillary tortuosity index in DM+ATH pigs (2.31±0.17) as compared to the control groups (Controls 0.89±0.08 and ATH 1.55±0.11; $p<0.05$). Kidney biopsies showed marked glomerular lesions consisting of mesangial expansion and podocyte lesions. Furthermore, we observed a disturbed Angpt2/ Angpt1balance in the cortex of the kidney, as evidenced by increased expression of Angpt2 in DM+ATH pigs as compared to Control pigs ($p<0.05$).

Conclusion

In the setting of DM, atherogenesis leads to the augmentation of mucosal capillary tortuosity, indicative of systemic microvascular damage. Concomitantly, a dysbalance in renal angiopoietins was correlated with the development of diabetic nephropathy. As such, our studies strongly suggest that defects in the systemic microvasculature mirror the accumulation of microvascular damage in the kidney.

Introduction

Diabetes mellitus (DM) is associated with macrovascular and microvascular complications that lead to retinopathy, neuropathy and nephropathy. Diabetic nephropathy is the leading cause of chronic kidney disease (CKD) worldwide [1,2]. In this disease setting, the combination of endothelial dysfunction and an imbalanced angiogenic response play an important role in the development of microvascular complications. Recently, the angiopoietins have gained much attention as critical regulators of of diverse pathological angiogenic conditions, including vascular complications associated with diabetes. The tight control of Angiopoietin-1 (Angpt1) and Angiopoietin- 2 (Angpt2) levels is critical in minimizing microvascular derangements that are the direct result of negative interference of Angpt2 with Angpt1-mediated Tie-2 signaling. This in turn disturbs the expression levels of key angiogenic factors such as von Willebrand factor (vWF) and vascular endothelial growth factor (VEGF). The ensuing loss of EC-pericyte interactions is responsible for destabilization of the capillary network and the loss of microvascular integrity. [3,4, 5, 6].

Histopathological findings in patients with diabetic nephropathy (DN) include mesangial expansion, mesangial sclerosis and vascular lesions such as hyalinosis [7]. These renal abnormalities could potentially be indicative of the systemic microvascular damage [8]. However, the detection of such pathophysiologies in DN is complex, as it is asymptomatic in early stages, while at later stages the direct demonstration of renal injury requires renal biopsy material, which is an unattractive tool for screening purposes due to the invasive nature of the procedure. Therefore, methods geared towards the non-invasive monitoring for early signs of microvascular changes is of clinical importance in patients with DM. However, at present these tools do not exist. Sidestream dark-field (SDF) imaging is a relatively new, non-invasive tool that enables one to visualize the microcirculation without the use of fluorescent dyes [9]. Recently, we used this apparatus to assess labial mucosal capillary tortuosity and density in diabetic patients compared with healthy non-diabetic controls, studies that revealed increased capillary density and tortuosity in diabetic patients [10]. These studies focused on the effects of prolonged diabetes in patients (24 ± 14 years). However, at present there is limited data regarding how disturbance of the microvasculature in early diabetes correlates with renal damage.

In light of these considerations, we sought to investigate whether an atherogenic diet in the early stages of DM could accelerate microvascular disease, and could serve as a diagnostic tool for DM-induced renal damage. Using SDF imaging, we show that an atherogenic diet during the early stages of DM leads to microvascular abnormalities, and immunohistochemically confirm that these systemic effects are associated with renal endothelial dysfunction, as evidenced by a disturbed Angpt2/Angpt1 balance and microalbuminuria.

Materials and Methods

Animal experiments

The experimental protocol was performed in compliance with the ARRIVE guidelines on animal research [11]. Protocols describing the management, surgical procedures, and animal care were reviewed and approved by the ASG-Lelystad Animal Care and Use Committee (Lelystad, The Netherlands) and by the Institutional Review Board for animal experimentation of the Erasmus University Medical Center (Rotterdam, The Netherlands). Ten neutered male domestic pigs (Landrace x Yorkshire, T-line) with an age ~11 weeks and a body weight of ~30 kg entered the study. After one week of acclimatization, DM was induced in a subgroup of 5 pigs by slow intravenous injection of streptozotocin (STZ 140 mg/kg; Enzo Life Sciences, Raamsdonkveer, The Netherlands) as described previously [12–15]. Five non-diabetic pigs received placebo treatment. Three weeks after DM induction, all of the pigs were gradually introduced to an atherogenic diet (ATH), containing 25% of saturated fats and 1% of cholesterol [16]. The 5 diabetic pigs (DM+ATH) and 5 non-diabetic pigs (ATH) were subsequently followed for up to 15 months, during which similar growth patterns were observed in both groups by adjusting individual caloric intake. In the diabetic pigs, glucose and ketone levels in plasma and urine were regularly checked in the 15-month follow-up period. Insulin therapy was started only in instances where plasma ketones were detected. Following 12 months, 24h urine samples were obtained from all pigs, while microcirculatory imaging and plasma samples were obtained from anesthetized pigs (20mg/kg ketamine + 1 mg/kg midazolam+ 1 mg atropine, i.m. and 12mg/kg thiopental, i.v.) at 14 and 15 months of follow up, respectively. At 15 months, the pigs were sacrificed by intravenous injection of an overdose of pentobarbital via the jugular vein catheter at 15 months, at which point plasma samples were obtained and the kidneys were har-vested for histological examination. Invasive imaging analyses prompted us to choose this time frame as after 12 months of follow up more complex atherosclerotic lesions were present in the coronary arteries of the studied pigs [23].

In addition, we also studied a separate control group (Controls) of 7 female domestic pigs (Landrace) at the age of 5 months with a body weight of ~78 kg, who were fed a standard diet for growing pigs.

Microcirculatory imaging and analysis of SDF measurements

SDF microscanning (MicroVision Medical Inc., Wallingford, PA, U.S.A) and analysis of images was performed as described earlier with minor modifications [10,16]. Anaesthetized pigs were imaged at 14 months of study duration. All pigs were studied during standardized conditions of general anesthesia by a trained observer.

Laboratory assessment

Serum Angpt1 and Angpt2 concentrations were measured after 12 months by enzyme-linked immunosorbent assay (ELISA) (Bioconnect, Huissen, The Netherlands and Antibodies-online, Atlanta, USA).

At 12 months, protein and creatinine levels were measured in 24h urine samples. To calculate the urinary albumin-creatinine ratio, we measured albumin excretion by ELISA (ITK diagnostics, Uithoorn, The Netherlands), and urinary creatinine concentration was measured by standard laboratory methods. Both the plasma and urinary creatinine levels were measured as previously described.

Plasma samples collected at 15 months were used to measure concentrations of glucose, total cholesterol, triglycerides and low and high-density lipoproteins (LDL and HDL) and creatinine by standardized methods at the clinical chemical laboratory of the Erasmus Medical Center (Rotterdam, The Netherlands). In the absence of an established mathematical formula to estimate creatinine clearance in pigs, we expressed creatinine levels in μmol/L/kg to adjust for body weight. Blood collection tubes were centrifuged for 10 minutes at 3000 rpm after which serum was stored in microcentrifuge tubes at -20°C until required for analysis.

Histological analysis of the kidney

Immunohistochemical analyses of snap-frozen porcine kidney cortex sections (4 μm) were air-dried and acetone fixed as previously described [17]. Monoclonal antibodies utilized were directed against mouse anti-human Angpt1 (clone 171718; R&D Systems, Abingdon, UK), mouse anti-human VEGF (sc-7269 Santa Cruz Biotechnology, Huissen, the Netherlands) and mouse anti-human plasminogen activator inhibitor-1 (clone HD-PAI-1 14.1) (American Diagnostica, Pfungstadt, Germany). Polyclonal antibodies were used directed against goat anti-mouse Angpt2 (clone F18; sc-7017; Santa Cruz Biotechnology, Huissen, the Netherlands) and rabbit anti-human vWF (Codenr A0082; Dako, Glostrum, Germany). Primary antibody binding was detected using the following isotype-matching secondary horseradish peroxidase (HRP)-labeled antibodies; goat anti-mouse IgG (Angpt1), rabbit anti-goat IgG (Angpt2), anti-mouse Envision K4007 (VEGF) or goat anti-rabbit IgG (vWF) (all purchased from Dako, Glostrum, Germany). Quantification of immunohistochemistry was performed in a blinded manner by assessing 10 consecutive high power fields (magnification, ×200) using Image J software. Glomerular and large vessels were excluded from analysis. For VEGF-A quantifica-tion, 15 consecutive glomeruli per subject were selected and the percentage of VEGF-A positive area was calculated using Image J.

Data are presented in terms of the Angpt2/Angpt1 ratio as previously described[18,19]. Immuofluorescent double stainings were performed for desmin (pericyte marker; mouse anti-pig clone DE-B-5; Millipore, Amsterdam, the Netherlands)/Angpt1 (goat anti-human; clone N-18; sc-6319; Santa Cruz Biotechnology, Huissen, the Netherlands) and vWF/Angpt2. Secondary antibodies were Alexa-488 labeled donkey anti- rabbit (vWF) and alexa-546 labelled rabbit anti-mouse (desmin), Furthermore, HRP labelled rabbit anti-goat (Angpt1) and donkey anti-goat (Angpt2) were used. Nuclei were visualized using Hoechst (Molecular Probes, Leiden, the Netherlands). Photomicrographs were made using a fluorescence microscope (DM5500B; Leica, Rijswijk, the Netherlands).

Next, we performed periodic acid-Schiff (PAS) staining on paraffin sections of renal cortex for the evaluation of histopathological changes and morphometric analysis of the glomeruli. In a blinded fashion, 25 consecutive glomeruli were selected from both superficial and deep cortex and the mesangial expansion index was scored. Subsequently, we determined the extent of increase in mesangial matrix (defined as mesangial area) by quantitating PAS-positive and nuclei-free areas in the mesangium using Image J [20,21]. Evaluation of histopathological lesions was performed by a pathologist who was blinded to the code of the sections.

Electron microscopy

Kidney tissues for electron microscopy were processed as described previously [22]. In typical cases from the ATH and DM+ATH groups, the glomerular basement membrane (GBM) width was measured.

RNA isolation and Real-Time PCR

To analyze renal Angpt1 and Angpt2 mRNA levels, RT-PCR was performed as described previously [23]. Expression was normalized against β-actin mRNA levels. RT-PCR analysis for biological replicates was performed in duplicate. The primer sequences were as follows: β-actin (forward 5'-ATCGTGCGGGACATCAAGGA-3' and reverse 5'-AGGAAGGAGGGCTGG-AAGAG-3'), Angpt1 (forward 5'-AGGAGCAAGTTTTGCGAGAG-3' and reverse 5'-CTCA-GAGCGTTTGTGTTGT-3') and Angpt2 (forward 5'-AAAGTTGCTGCAGGGAA-AGA-3' and reverse 5'-TCACAGCTCAGAGCGAAGAA-3').

Statistical analysis

All data are presented as mean ± standard error of the mean (SEM). Differences between experimental groups were analyzed using one way-analysis of variance followed by post-hoc testing with an unpaired Student's t-test. Analyses were performed with GraphPad software (GraphPad Software Inc., San Diego, CA, U.S.A.). P-values less than 0.05 (two-tailed) were considered statistically significant.

Results

Model characteristics

Initial plasma profiling of DM+ATH and ATH pigs revealed that DM significantly influenced glucose levels (17.64±4.54 mmol/L vs. 5.12±0.42 mmol/L; $p<0.05$) (Table 1) at 15 months. Total cholesterol, triglycerides, HDL and LDL were not significantly affected by the induction of DM in pigs. Two pigs were administered insulin during the study period due to elevated plasma ketone levels. The mean body weight at the time of microvascular imaging was comparable between DM+ATH (96±2.8kg) and ATH group (93±0.4kg, $p>0.05$). At the time of sacrifice, substantial coronary lesions as well as generalised atherosclerosis for example in the aorta were observed in both DM+ATH and ATH groups, as described previously [24].

Table 1. Model characteristics at 15 months of follow up.

	Controls (N = 7)	ATH (N = 5)	DM+ATH (N = 5)
Glucose (mmol/l)	4.26±0.29	5.12±0.42	17.64±4.54*#
Triglycerides (mmol/l)	0.18±0.02	0.64±0.2	1.26±0.50*
Total Cholesterol (mmol/l)	1.50±0.05	18.10±2.66*	16.82±1.72*
LDL (mmol/l)	0.76±0.29	14.87±2.45*	13.63±1.3*
HDL (mmol/l)	0.60±0.03	5.70±0.35*	5.12±0.40*

All data are mean ±SEM. ATH: pigs on atherogenic diet. DM+ATH: pigs with diabetes mellitus on atherogenic diet. Controls: healthy control pigs on a standard diet. LDL: Low density lipoprotein. HDL: High density lipoprotein.

* P<0.05 compared with Controls.
# P<0.05 compared with ATH pigs.

Early atherogenic diabetes mellitus leads to systemic microvascular damage

The microvascular morphology of the oral mucosal tissue in DM+ATH pigs was significantly disturbed as compared with the Controls (Fig 1A). Indeed, the capillary tortuosity index was sig-nificantly increased in DM+ATH pigs (2.3±0.2) as compared with ATH pigs (1.6±0.1, $p<0.01$; Fig 1B). Furthermore, capillary density was significant lower in the DM+ATH (18.6 ±1.3 capillaries/mm^2) pigs as compared with the Controls (24.9 ±0.8 capillaries/mm^2, $p<0.01$; Fig 1C).

Renal damage after induction of atherogenic DM in pigs

Plasma creatinine levels were elevated in ATH pigs (2.12±0.03 μmol/L/kg) as compared with DM+ATH pigs (1.60±0.13 μmol/L/kg, $p<0.01$) group. However, urinary albumin/creatinine ratio was not found to differ between the DM+ATH group (0.045±0.0182 mg/mmol) and ATH pigs (0.002±0.0007 mg/mmol, $p>0.05$).

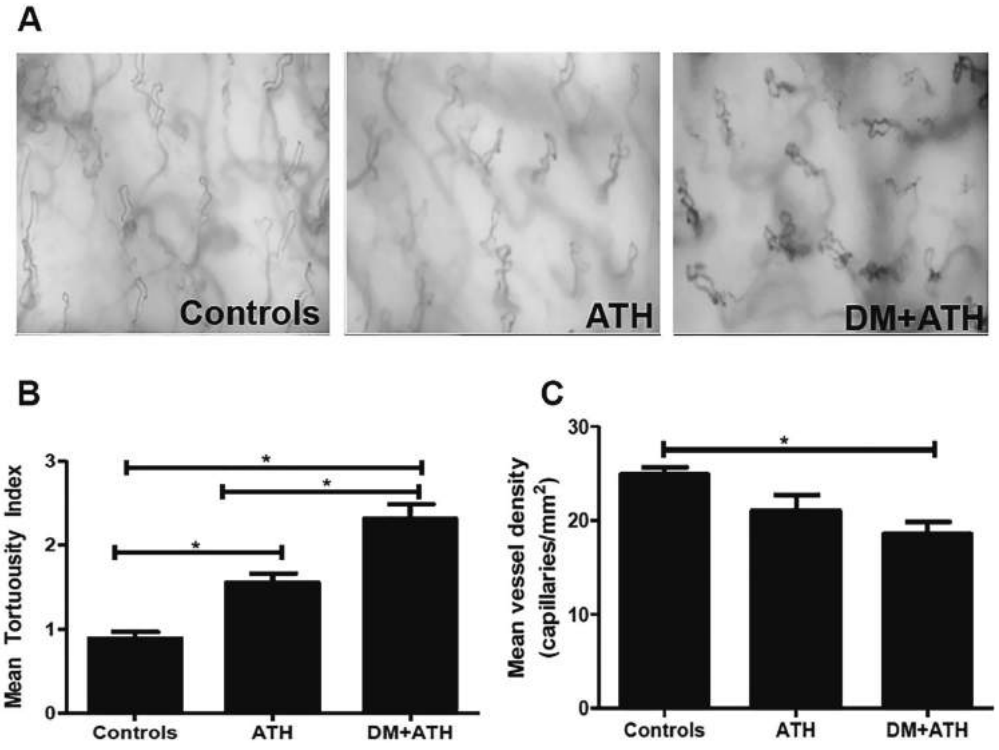

Fig 1. Early atherogenic DM leads to increased capillary tortuosity. A. Sidestream darkfield images of the oral mucosa visualizing the microvascular capillaries of a representative pig in the Controls, ATH and DM+ATH group. B. Mean tortuosity index of microvascular capillaries in the Controls (n = 7), ATH (n = 5) and DM+ATH pigs (n = 5). C. Mean vessel density (capillaries/mm^2) in Controls (n = 7), ATH (n = 5) and DM+ATH (n = 5) pigs. Data shown are mean±SEM. *P<0.05 compared to Controls or ATH pigs. Mean vessel density (capillaries/mm^2) was calculated by evaluation of number of vessels per selected microcirculatory image. Subsequently, tortuosity of capillary loops was assessed according to a validated scoring system (0: no twists to 4: four or more twists) and the average of assessed capillary tortuosity was used to calculate mean tortuosity index per patient.

PAS-stained renal sections revealed marked tubular changes with foamy cytoplasm and hyalin droplets in all DM+ATH pigs and there were glomerular lesions consisting of mesangial expansion and podocyte lesions, also with foamy cytoplasm and hyaline droplets in four DM +ATH pigs (Fig 2A). In contrast, but one ATH pig displayed similar lesions (Fig 2A). Some glomeruli were found to have dilated capillaries containing numerous red blood cells, a phenomenon that is highly reminiscent of microangiopathic injury lesions that have been described to be the result of fibrinolytic/proteolytic activation system in combination with increased PAI-1 staining [25]. In keeping with this notion, we observed both co-localization and increased PAI-1 staining in the herein described lesions (Fig 2A) .

Next, we determined the mesangial expansion index in renal cross-sections. These studies showed significantly higher scores in the ATH pigs (0.62±0.05, p = 0.03) and a trend towards increased scores in the DM+ATH (0.58±0.05,p = 0.066) compared with the Controls (0.49 ±0.03; Fig 2B). Interestingly, the width of the GBM increased from 215 nM in a Controls animal to 252 and 279 nM in cases with mild and severe DN of the DM+ATH group, respectively. Moreover, lipid deposits were observed in kidneys of mild and severe DN pigs (Fig 2C).

Diabetes and atherogenic diet induces Angpt2/Angpt1 dysbalance in pigs

Serum Angpt-1 levels in the DM+ATH pigs were increased as compared to control pigs (26035 ±1228 pg/ml versus 18061±1228 pg/ml, $p<0.01$). There were no significant differences in serum Ang-1 levels between DM+ATH and ATH pigs (19832±1166 pg/ml, $p>0.05$). Angpt-2 levels were not detectable in the circulation of the different groups.

With regard to Angpt1 staining in the kidneys, we observed positive Angpt1 staining in the glomeruli and in a capillary-like pattern between the tubuli of pigs in the Controls group (Fig 3A). We found no difference in renal Angpt1 protein expression between ATH (78020±12216 pixels/area) and DM+ATH (46763±12360 pixels/area, $p>0.05$) pigs, but Angpt1expression was significantly higher in the Controls group (91788±9777 pixels/area, $p < 0.05$; Fig 3A). The Angpt1mRNA levels in the kidney were significantly lower in the DM+ATH and ATH group compared with the Controls pigs (Fig 3D). Double staining of Angpt1 and the pericyte marker desmin revealed predominantly expression of desmin in the glomeruli and Angpt1 expression in the same pattern as described above (Fig 3B; left panel). However, no co-localization was observed, suggesting that other cells than pericytes might produce Angpt1 in the glomerulus.

Angpt2 staining was predominantly present in glomeruli and tubuli (Fig 3A) and showed a significant increase in DM+ATH (54813±3140 pixels/area) pigs compared to the Controls (22862±3354 pixels/area, $p<0.001$) and ATH (31005±5011 pixels/area, $p<0.01$) pigs (Fig 3C). Consequently, a higher Angpt2/ Angpt1ratio was observed in DM+ATH (1.63±0.43) pigs compared with Controls (0.28±0.07, $p<0.001$) and ATH (0.43±0.07, $p<0.01$) group (Fig 3C). The Angpt2 mRNA levels in the kidney did not significantly differ between groups (Fig 3D). Importantly, additional staining of vWF and Angpt2 revealed co-expression, suggesting that endothelial cells produce Angpt2 (Fig 3B; middle and right panel).

Staining of the endothelial marker vWF showed expression in the glomeruli and peritubular space, in the same pattern as Angpt1 (Fig 4A). No significant differences were observed in vWF expression between the Controls (86611±6163 pixels/area), ATH (84547±9000 pixels/area) and DM+ATH pigs (102961±13633 pixels/area) ($p>0.05$).

VEGF-A staining revealed expression in podocytes, parietal epithelial cells and tubuli (most extensively) in all groups (Fig 4B). There was no difference in VEGF-A expression between the DM+ATH (16.94±0.72), ATH (21.22±2.30) and Controls (20.70±1.24) ($p\geq 0.05$).

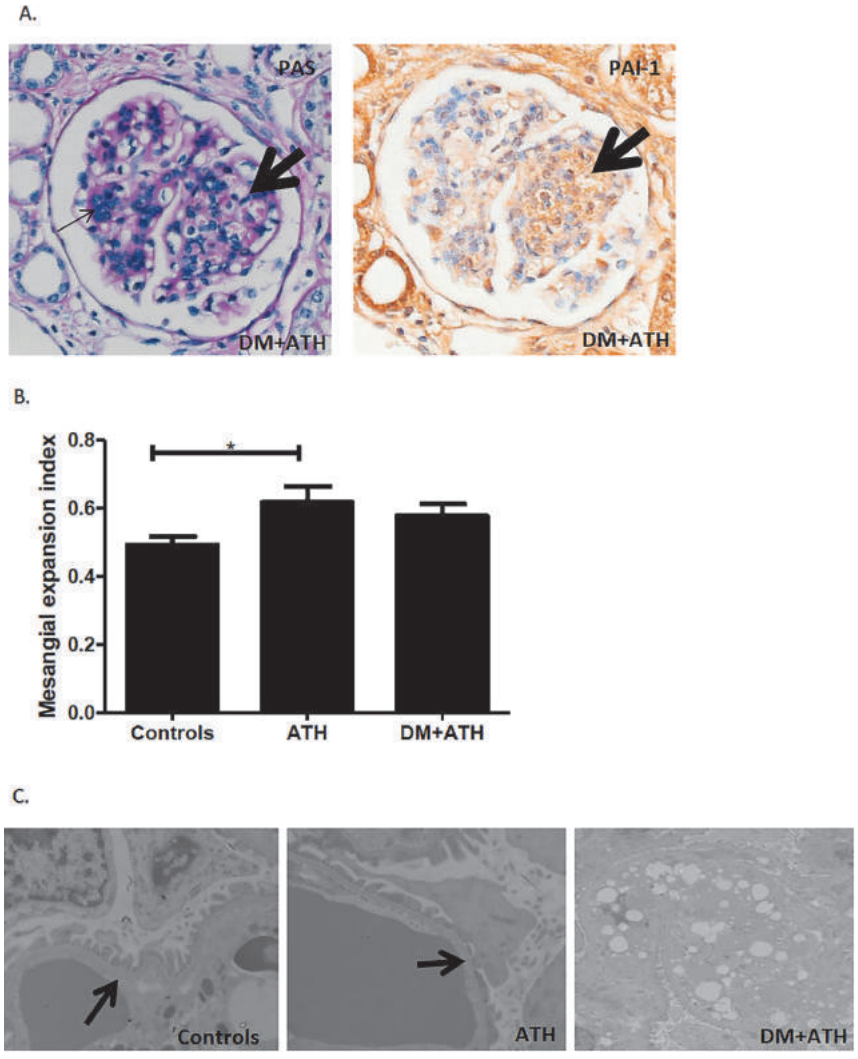

Fig 2. Early stages of atherogenic DM leads to renal damage. A: Representative illustration of PAS stained glomeruli from a DM+ATH pig, showing mesangial proliferation and matrix expansion with capillary loops lying around the mesangium as a corona, reminiscent of a beginning Kimmelstiel-Wilson nodule (left panel; thin black arrow). Dilated capillary loops with red cell fragments show intense PAI-1 staining on consecutive slides (right panel; thick black arrow). B: Mesangial expansion index in Controls (n = 7), ATH (n = 5) and DM+ATH (n = 5) pigs. C. Electron microscopy images illustrating a normal GBM architecture (left panel; thick arrow) of the Controls pig. In ATH, there is slight effacement of the podocyte pedicles (middle panel; thick arrow). In DM +ATH, marked lipid deposits were found (right panel). Data are shown as mean ± SEM. *P<0.05 compared to Controls or ATH pigs. Original magnification of A: x400 and C: x8000.

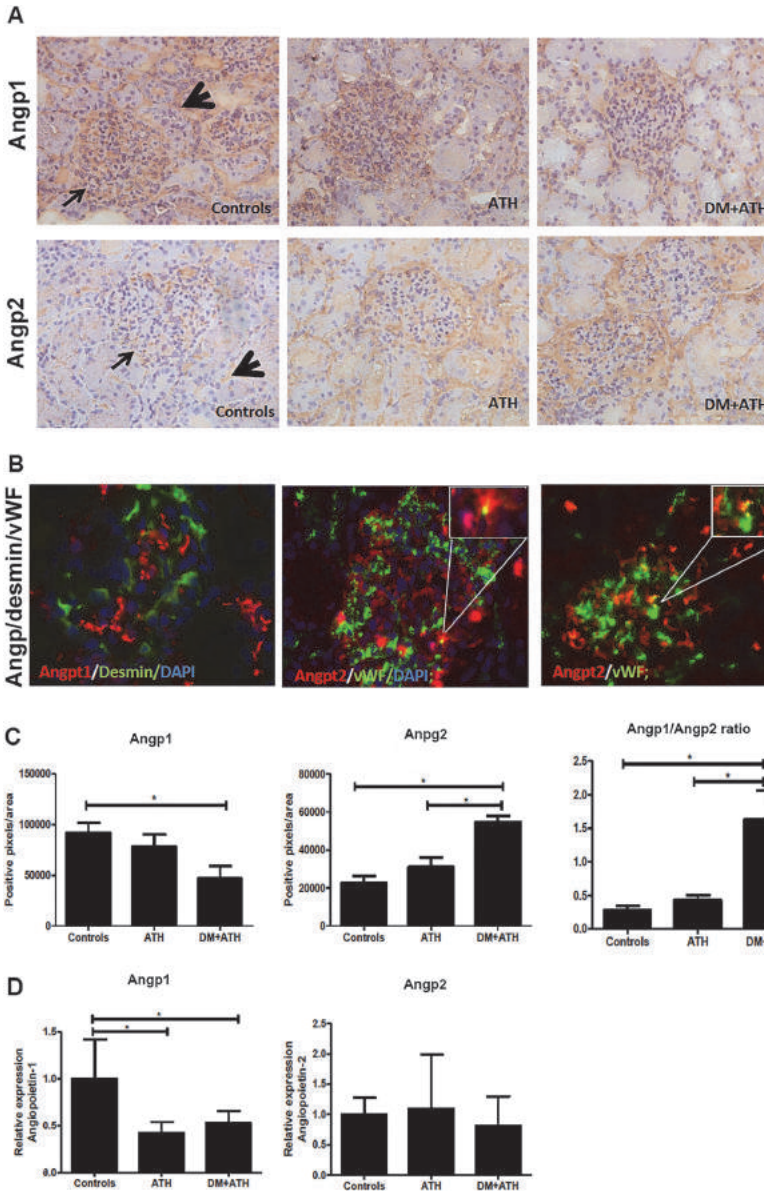

Fig 3. The Angpt2/Angpt1 balance is disturbed in atherogenic DM pigs. A. Representative illustrations of kidney sections stained with Angpt1 (upper panels; arrow: glomerulus; arrowhead: peritubular area) or Angpt2 (lower panels; arrow: glomerulus; arrowhead: tubular staining) in Controls, ATH, and DM+ATH pigs. B. Immunofluorescent double staining of representative kidney sections for desmin (green)/Angpt1 (red;left panel) and vWF (green/Angpt2 (red; middle/right panel). Insets: double positivity for vWF/Angpt2 staining in yellow. C: Quantitative analysis of renal expression of Angpt1, Angpt2 and Angpt2/Angpt1 ratio. D. Relative mRNA expression of Angpt1 and Angpt2. Data are shown as mean ± SEM. *P<0.05 compared to Controls or ATH pigs. Original magnification of A and B: x400.

Angpt2/Angpt1 dysbalance and creatinine levels are correlated with capillary tortuosity

Correlation analyses were performed between renal Angpt1, Angpt2, Angpt2/Angpt1ratio, creatinine levels and albumin/creatinine ratio and oral mucosal capillary tortuosity and density indices. No correlation was found between capillary density index and renal angiopoietin expression or urinary markers for renal function. However, a negative correlation was found between renal Angpt1expression and microvascular tortuosity index ($r = -0.60$, $p = 0.0100$; Fig 5A). Moreover, we demonstrated a positive correlation between capillary tortuosity and Angpt2 staining ($r = 0.70$, $p = 0.0017$; Fig 5B) and Angpt2/Angpt1ratio ($r = 0.80$, $p = 0.0002$; Fig 5C).

No significant correlation was found between urinary albumin/creatinine ratio, creatinine levels and capillary tortuosity index.

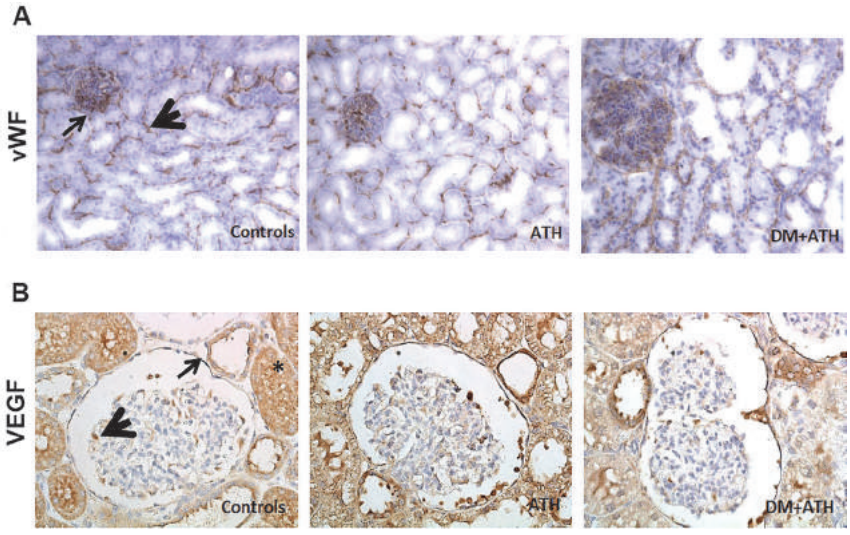

Fig 4. No difference in renal vWf and VEGF-A expression. A. Representative illustrations of kidney sections stained with endothelial marker vWF (arrow: glomerulus; arrowhead: peritubular area) in Controls, ATH, and DM+ATH pigs. B. Representative images of kidney sections stained with VEGF in Controls, ATH, and DM+ATH pigs showing expression in podocytes (arrow head), parietal epithelial cells (thin arrow) and tubuli (asterix). Original magnification of A: x 200 and B: x400.

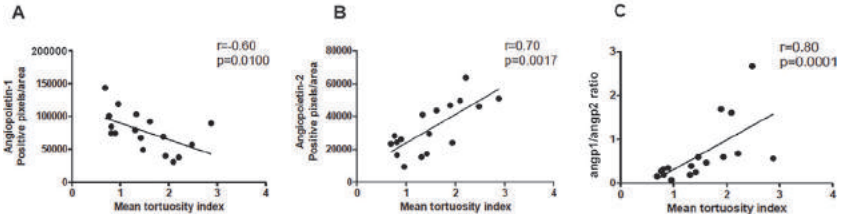

Fig 5. Correlation between capillary tortuosity and Angpt2/Angpt1balance and creatinine levels. Scatter plot showing the correlation of renal protein expression of Angpt1(A), Angpt2 (B), Angpt2/ Angpt1ratio (C).

Discussion

In the present study, we show that the combination of an atherogenic diet and recent onset of DM leads to abnormalities in the systemic microvasculature, yielding SDF-detectable increases in capillary tortuosity and increased levels of serum Angpt1. Furthermore, we discovered that glomerular lesions develop during the early stages of DN and that the tight control of the Angpt2/Angpt1balance is perturbed in the kidneys of diabetic atherogenic pigs.

Microvascular dysfunction is one of the most important causes of persistent diabetic complications. This is the result of disturbed hemodynamics and impaired endothelial function induced by metabolic alterations [26,27]. However, the early events involved in the pathogenesis of diabetic microvascular complications are not well understood, and are difficult to study in humans without the use of invasive techniques. SDF imaging allows for the easy, and rapid assessment of the presence of systemic microvascular derangements that could precede the development of diabetic macrovascular complications. In our study, we observed increased capillary tortuosity between the DM+ATH and ATH groups, already at ~15 months following DM induction. Using SDF imaging, we recently demonstrated increased capillary tortuosity in diabetes patients, and reversal of microvascular tortuosity after simultaneous pancreas-kidney transplantation [16]. Moreover, we have previously shown that increased capillary tortuosity in diabetic patients was associated with macrovascular disease [10]. In concordance with our observations, Sasongko et al demonstrated increased tortuosity in patients with diabetic retinopathy, suggesting that this may be an early sign of microvascular damage in DM [28,29]. However, these studies did not include patients with early stage DM and did not focus on the role of angiopoietins in microvascular alterations and renal injury in atherogenic DM.

In addition to increased microvascular tortuosity, we also observed increased serum levels of Angpt-1 in DM+ATH pigs compared with the control group. These data are in line with previous clinical studies in patients with moderate and severe non-proliferative diabetic retinopathy [30] and in patients with hypertension [31] that showed increased Angpt1 serum levels in these patients as well. While serum Angpt1 levels were increased in DM+ATH pigs, we found a decrease in Angpt1 protein and mRNA expression in kidneys of diabetic pigs compared to control groups. This observation suggests shedding of Angpt1 from renal vasculature into the circulation.

Interestingly, DM+ATH pigs were characterized by higher expression levels of Angpt2 protein as compared to the ATH group, resulting in a higher Angpt2/ Angpt1 ratio in the DM +ATH pigs. This is in agreement with Rizkalla and co-workers, who previously have shown

that both Angpt1 and Angpt2 protein levels are increased in the early phase of STZ-induced DM in rats [32]. However, disease progression was found to trigger a decrease in Angpt1expression while Angpt2 continued to increase, a switch that both markedly alters but also disturbs the Angpt2/Angpt1balance [32]. Although a difference in angiopoietin expression between rats and pigs cannot be excluded, these findings suggest that angiopoietins undergo time-dependent changes in expression at different stages of DM. Our identification that an increased urinary albumin/creatinine ratio is associated with a higher Angpt2/Angpt1 ratio (in DM+ATH pigs) is in keeping with recent studies that demonstrated an inability to express Angpt1 leads to extensive glomerular damage and proteinuria, indicating a protective role of Angpt1[33]. These data suggest that angiopoietins might play an important role in the pathophysiology of glomerular disease in DN.

Aside from angiopoietins, numerous other mechanisms have been proposed to be causal for microvascular complications in DM, such as VEGF. Under pathological conditions, Angpt2 acts in concert with VEGF to induce inflammatory angiogenesis. By promoting pericyte dropout, Angpt2 will lead to destabilization between ECs and pericytes. In the presence of VEGF, Angpt2 can eventually lead to an active, sprouting state of ECs, but when VEGF is absent, Angpt2 promotes vessel regression [34–36]. Our immunohistochemical assessment of VEGF protein in the different groups revealed high expression levels in podocytes and parietal—and tubular epithelial cells, which is in keeping with literature [34,37–40]. However, in contrast to previous studies, we did not observe differences between the different groups.

An additional observation we made was the marked increase in PAI-1 expression in regions of microvascular injury. PAI-1, a protease and fibrinolysis inhibitor that is poorly expressed in healthy kidneys, which is a critical player in angiogenesis and vascular remodeling [41]. Previous studies in rats and humans by the group of Fogo have shown that the expression level of PAI-1 in normal glomeruli is low and increases in pathological conditions, such as diabetic nephropathy [25,42].

Our observation that glomerular and tubular expression of PAI-1 is increased in DM+ATH pigs is noteworthy due to the fact that: 1) PAI-1 was found to be prominently expressed in Kimmelstiel-Wilson nodules, in particular those with active microvascular damage [25]; 2) unilateral ureteral obstruction [43] and glomerulonephritis [44] have also been associated with increased expression of tubular PAI-1; and 3) endogenous PAI-1 deficiency protects diabetic mice from glomerular injury [45]. Collectively, these data support for a pathogenic role for PAI-1 in diabetic renal disease.

In the current study, there was a tendency towards increased mesangial expansion in the DM+ATH pigs, and significantly more mesangial expansion in kidneys of ATH pigs. The data confirm previous reports on pig studies which revealed that consumption of high-fat diet leads to the development of renal injury, characterized by mesangial expansion and increased plasma creatinine levels [46,47]. Moreover, rodent studies demonstrated that hyperlipidemia exacerbates the development and progression of renal diseases, including DN [48,49]. Furthermore, our study also showed higher creatinine levels in the ATH group than the DM+ATH and Controls, which could be explained by the increased mesangial expansion observed in ATH pigs. The latter has been associated with obliteration of capillary lumen and decreased capillary perfusion in previous studies [50]. Furthermore, our study suggests that the combined hyperglycemia and hyperlipidemia in the DM +ATH pigs, induces a dysbalance in renal angiopoietins that results in albuminuria and endothelial damage in the kidney. The potential contribution of tubular injury to albuminuria needs to be addressed in additional studies.

Some aspects of our porcine study require further discussion. First, it would have been interesting to study an additional group of pigs with only diabetes (i.e. without ATH) to explore the early effects of only hyperglycemia on the microvasculature. However, the clinically most

relevant group of DN also reflects DM patients with some presence of atherosclerosis as well. Secondly, it could be argued that the differences in gender, age and weight between healthy control pigs (Controls) versus DM+ATH and ATH pigs may explain part of the difference in the observed capillary tortuosity between these groups. This is, however, unlikely as in a human study, age did not influence capillary tortuosity [16].

In conclusion, we present SDF imaging as a novel means of documenting capillary tortuosity, an event that is illustrative of renal injury in the setting of early DM and atherosclerosis. This technique enables one to non-invasively detect systemic microvascular damage. Furathermore, we also identified changes in the Angpt2/Angpt1 balance may represent initiating events of renal injury in early DM. We propose that the targeted intervention of angiopoietins signaling could be an effective modality in minimizing microvascular damage that could serve as an early initiator of DN.

Acknowledgments

Eric van der Veer is greatly acknowledged for carefully reading the manuscript and providing constructive comments.

Author Contributions

Conceived and designed the experiments: JR TR MK WvdG MR. Performed the experiments: MK RdB MvdH OS. Analyzed the data: MK RdB HB MZ IB. Contributed reagents/materials/analysis tools: DD BvdB NSvD. Wrote the paper: JR MK MvdH.

References

1. Cumbie BC, Hermayer KL. Current concepts in targeted therapies for the pathophysiology of diabetic microvascular complications. Vasc Health Risk Manag. 2007; 3: 823–32. PMID: 18200803
2. Tooke JE. Microvasculature in diabetes. Cardiovasc Res. 1996; 32: 764–71. PMID: 8915194
3. Feng D, Bursell SE, Clermont AC, Lipinska I, Aiello LP, Laffel L, et al. von Willebrand factor and retinal circulation in early-stage retinopathy of type 1 diabetes. Diabetes Care. 2000; 23: 1694–8. PMID: 11092294
4. Targher G, Bertolini L, Zoppini G, Zenari L, Falezza G. Increased plasma markers of inflammation and endothelial dysfunction and their association with microvascular complications in Type 1 diabetic patients without clinically manifest macroangiopathy. Diabet Med. 2005; 22: 999–1004. PMID: 16026364
5. Fiedler U, Augustin HG. Angiopoietins: a link between angiogenesis and inflammation. Trends Immunol. 2006; 27: 552–8. PMID: 17045842
6. Hammes HP, Lin J, Renner O, Shani M, Lundqvist A, Betsholtz C, et al. Pericytes and the pathogenesis of diabetic retinopathy. Diabetes. 2002; 51: 3107–12. PMID: 12351455
7. Tervaert TW, Mooyaart AL, Amann K, Cohen AH, Cook HT, Drachenberg CB, et al. Pathologic classification of diabetic nephropathy. J Am Soc Nephrol. 2010; 21: 556–63. doi: 10.1681/ASN.2010010010 PMID: 20167701
8. Edwards MS, Wilson DB, Craven TE, Stafford J, Fried LF, Wong TY, et al. Associations between retinal microvascular abnormalities and declining renal function in the elderly population: the Cardiovascular Health Study. Am J Kidney Dis. 2005; 46: 214–24. PMID: 16112039
9. Goedhart PT, Khalilzada M, Bezemer R, Merza J, Ince C. Sidestream Dark Field (SDF) imaging: a novel stroboscopic LED ring-based imaging modality for clinical assessment of the microcirculation. Opt Express. 2007; 15: 15101–14. PMID: 19550794
10. Djaberi R, Schuijf JD, de Koning EJ, Wijewickrama DC, Pereira AM, Smit JW, et al. Non-invasive assessment of microcirculation by sidestream dark field imaging as a marker of coronary artery disease in diabetes. Diab Vasc Dis Res. 2012.
11. Kilkenny C, Browne WJ, Cuthill IC, Emerson M, Altman DG. Improving bioscience research reporting: the ARRIVE guidelines for reporting animal research. Osteoarthritis Cartilage. 2012; 20: 256–60. doi: 10.1016/j.joca.2012.02.010 PMID: 22424462
12. Gerrity RG, Natarajan R, Nadler JL, Kimsey T. Diabetes-induced accelerated atherosclerosis in swine. Diabetes. 2001; 50: 1654–65. PMID: 11423488

13. van den Heuvel M, Sorop O, Koopmans SJ, Dekker R, de VR, van Beusekom HM, et al. Coronary microvascular dysfunction in a porcine model of early atherosclerosis and diabetes. Am J Physiol Heart Circ Physiol. 2012; 302: H85–H94. doi: 10.1152/ajpheart.00311.2011 PMID: 21984550

14. Koopmans SJ, Mroz Z, Dekker R, Corbijn H, Ackermans M, Sauerwein H. Association of insulin resistance with hyperglycemia in streptozotocin-diabetic pigs: effects of metformin at isoenergetic feeding in a type 2-like diabetic pig model. Metabolism. 2006; 55: 960–71. PMID: 16784971

15. Koopmans SJ, Dekker R, Ackermans MT, Sauerwein HP, Serlie MJ, van Beusekom HM, et al. Dietary saturated fat/cholesterol, but not unsaturated fat or starch, induces C-reactive protein associated early atherosclerosis and ectopic fat deposition in diabetic pigs. Cardiovasc Diabetol. 2011; 10: 64. doi: 10.1186/1475-2840-10-64 PMID: 21756316

16. Khairoun M, de Koning EJ, van den Berg BM, Lievers E, de Boer HC, Schaapherder AF, et al. Microvascular damage in type 1 diabetic patients is reversed in the first year after simultaneous pancreas-kidney transplantation. Am J Transplant. 2013; 13: 1272–81. doi: 10.1111/ajt.12182 PMID: 23433125

17. Khairoun M, van der Pol P, de Vries DK, Lievers E, Schlagwein N, de Boer HC, et al. Renal ischemia-reperfusion induces a dysbalance of angiopoietins, accompanied by proliferation of pericytes and fibrosis. Am J Physiol Renal Physiol. 2013; 305: F901–F910. doi: 10.1152/ajprenal.00542.2012 PMID: 23825073

18. David S, Kumpers P, Hellpap J, Horn R, Leitolf H, Haller H, et al. Angiopoietin 2 and cardiovascular disease in dialysis and kidney transplantation. Am J Kidney Dis. 2009; 53: 770–8. doi: 10.1053/j.ajkd.2008.11.030 PMID: 19268412

19. David S, Kumpers P, Lukasz A, Fliser D, Martens-Lobenhoffer J, Bode-Boger SM, et al. Circulating angiopoietin-2 levels increase with progress of chronic kidney disease. Nephrol Dial Transplant. 2010; 25: 2571–6. doi: 10.1093/ndt/gfq060 PMID: 20179005

20. Sugaru E, Sakai M, Horigome K, Tokunaga T, Kitoh M, Hume WE, et al. SMP-534 inhibits TGF-beta-induced ECM production in fibroblast cells and reduces mesangial matrix accumulation in experimental glomerulonephritis. Am J Physiol Renal Physiol. 2005; 289: F998–1004. PMID: 15900023

21. Sugaru E, Nakagawa T, Ono-Kishino M, Nagamine J, Tokunaga T, Kitoh M, et al. SMP-534 ameliorates progression of glomerular fibrosis and urinary albumin in diabetic db/db mice. Am J Physiol Renal Physiol. 2006; 290: F813–F820. PMID: 16278277

22. Trouw LA, Groeneveld TW, Seelen MA, Duijs JM, Bajema IM, Prins FA, et al. Anti-C1q autoantibodies deposit in glomeruli but are only pathogenic in combination with glomerular C1q-containing immune complexes. J Clin Invest. 2004; 114: 679–88. PMID: 15343386

23. van der Pol P, Schlagwein N, van Gijlswijk DJ, Berger SP, Roos A, Bajema IM, et al. Mannan-binding lectin mediates renal ischemia/reperfusion injury independent of complement activation. Am J Transplant. 2012; 12: 877–87. doi: 10.1111/j.1600-6143.2011.03887.x PMID: 22225993

24. van Ditzhuijzen NS, van den Heuvel M, Sorop O, van Duin RW, Krabbendam-Peters I, van HR, et al. Invasive coronary imaging in animal models of atherosclerosis. Neth Heart J. 2011; 19: 442–6. doi: 10.1007/s12471-011-0187-0 PMID: 21904848

25. Paueksakon P, Revelo MP, Ma LJ, Marcantoni C, Fogo AB. Microangiopathic injury and augmented PAI-1 in human diabetic nephropathy. Kidney Int. 2002; 61: 2142–8. PMID: 12028454

26. Kalani M. The importance of endothelin-1 for microvascular dysfunction in diabetes. Vasc Health Risk Manag. 2008; 4: 1061–8. PMID: 19183753

27. Kuryliszyn-Moskal A, Dubicki A, Zarzycki W, Zonnenberg A, Gorska M. Microvascular abnormalities in capillaroscopy correlate with higher serum IL-18 and sE-selectin levels in patients with type 1 diabetes complicated by microangiopathy. Folia Histochem Cytobiol. 2011; 49: 104–10. PMID: 21526496

28. Sasongko MB, Wong TY, Nguyen TT, Cheung CY, Shaw JE, Wang JJ. Retinal vascular tortuosity in persons with diabetes and diabetic retinopathy. Diabetologia. 2011; 54: 2409–16. doi: 10.1007/s00125-11-2200-y PMID: 21625945

29. Sasongko MB, Wong TY, Donaghue KC, Cheung N, Jenkins AJ, Benitez-Aguirre P, et al. Retinal arteriolar tortuosity is associated with retinopathy and early kidney dysfunction in type 1 diabetes. Am J Ophthalmol. 2012; 153: 176–83. doi: 10.1016/j.ajo.2011.06.005 PMID: 21907319

30. Patel JI, Hykin PG, Gregor ZJ, Boulton M, Cree IA. Angiopoietin concentrations in diabetic retinopathy. Br J Ophthalmol. 2005; 89: 480–3. PMID: 15774928

31. Nadar SK, Blann A, Beevers DG, Lip GY. Abnormal angiopoietins 1&2, angiopoietin receptor Tie-2 and vascular endothelial growth factor levels in hypertension: relationship to target organ damage [a substudy of the Anglo-Scandinavian Cardiac Outcomes Trial (ASCOT)]. J Intern Med. 2005; 258: 336–43. PMID: 16164572

32. Rizkalla B, Forbes JM, Cao Z, Boner G, Cooper ME. Temporal renal expression of angiogenic growth factors and their receptors in experimental diabetes: role of the renin-angiotensin system. J Hypertens. 2005; 23: 153–64. PMID: 15643138

33. Jeansson M, Gawlik A, Anderson G, Li C, Kerjaschki D, Henkelman M, et al. Angiopoietin-1 is essential in mouse vasculature during development and in response to injury. J Clin Invest. 2011; 121: 2278–89. doi: 10.1172/JCI46322 PMID: 21606590

34. Jain RK. Molecular regulation of vessel maturation. Nat Med. 2003; 9: 685–93. PMID: 12778167

35. Kim KL, Shin IS, Kim JM, Choi JH, Byun J, Jeon ES, et al. Interaction between Tie receptors modulates angiogenic activity of angiopoietin2 in endothelial progenitor cells. Cardiovasc Res. 2006; 72: 394–402. PMID: 17054925

36. Lobov IB, Brooks PC, Lang RA. Angiopoietin-2 displays VEGF-dependent modulation of capillary structure and endothelial cell survival in vivo. Proc Natl Acad Sci U S A. 2002; 99: 11205–10. PMID: 12163646

37. Baelde HJ, Eikmans M, Doran PP, Lappin DW, de HE, Bruijn JA. Gene expression profiling in glomeruli from human kidneys with diabetic nephropathy. Am J Kidney Dis. 2004; 43: 636–50. PMID: 15042541

38. Baelde HJ, Eikmans M, Lappin DW, Doran PP, Hohenadel D, Brinkkoetter PT, et al. Reduction of VEGF-A and CTGF expression in diabetic nephropathy is associated with podocyte loss. Kidney Int. 2007; 71: 637–45. PMID: 17264876

39. Cooper ME, Vranes D, Youssef S, Stacker SA, Cox AJ, Rizkalla B, et al. Increased renal expression of vascular endothelial growth factor (VEGF and its receptor VEGFR-2 in experimental diabetes. Diabetes. 1999; 48: 2229–39. PMID: 10535459

40. Hohenstein B, Hausknecht B, Boehmer K, Riess R, Brekken RA, Hugo CP. Local VEGF activity but not VEGF expression is tightly regulated during diabetic nephropathy in man. Kidney Int. 2006; 69: 1654–61. PMID: 16541023

41. Stefansson S, McMahon GA, Petitclerc E, Lawrence DA. Plasminogen activator inhibitor-1 in tumor growth, angiogenesis and vascular remodeling. Curr Pharm Des. 2003; 9: 1545–64. PMID: 12871067

42. Nakamura S, Nakamura I, Ma L, Vaughan DE, Fogo AB. Plasminogen activator inhibitor-1 expression is regulated by the angiotensin type 1 receptor in vivo. Kidney Int. 2000; 58: 251–9. PMID: 10886570

43. Ishidoya S, Ogata Y, Fukuzaki A, Kaneto H, Takeda A, Orikasa S. Plasminogen activator inhibitor-1 and tissue-type plasminogen activator are up-regulated during unilateral ureteral obstruction in adult rats. J Urol. 2002; 167: 1503–7. PMID: 11832778

44. Barnes JL, Mitchell RJ, Torres ES. Expression of plasminogen activator-inhibitor-1 (PAI-1) during cellular remodeling in proliferative glomerulonephritis in the rat. J Histochem Cytochem. 1995; 43: 895–905. PMID: 7642963

45. Lassila M, Fukami K, Jandeleit-Dahm K, Semple T, Carmeliet P, Cooper ME, et al. Plasminogen activator inhibitor-1 production is pathogenetic in experimental murine diabetic renal disease. Diabetologia. 2007; 50: 1315–26. PMID: 17415547

46. Deji N, Kume S, Araki S, Soumura M, Sugimoto T, Isshiki K, et al. Structural and functional changes in the kidneys of high-fat diet-induced obese mice. Am J Physiol Renal Physiol. 2009; 296: F118–F126. doi: 10.1152/ajprenal.00110.2008 PMID: 18971213

47. Taneja D, Thompson J, Wilson P, Brandewie K, Schaefer L, Mitchell B, et al. Reversibility of renal injury with cholesterol lowering in hyperlipidemic diabetic mice. J Lipid Res. 2010; 51: 1464–70. doi: 10.1194/jlr.M002972 PMID: 20110440

48. Thompson J, Wilson P, Brandewie K, Taneja D, Schaefer L, Mitchell B, et al. Renal accumulation of biglycan and lipid retention accelerates diabetic nephropathy. Am J Pathol. 2011; 179: 1179–87. doi: 10.1016/j.ajpath.2011.05.016 PMID: 21723246

49. Bonnet F, Cooper ME. Potential influence of lipids in diabetic nephropathy: insights from experimental data and clinical studies. Diabetes Metab. 2000; 26: 254–64. PMID: 11011217

50. Steffes MW, Osterby R, Chavers B, Mauer SM. Mesangial expansion as a central mechanism for loss of kidney function in diabetic patients. Diabetes. 1989; 38: 1077–81. PMID: 2670639

Part II

Endothelial dysfunction after percutaneous coronary interventions

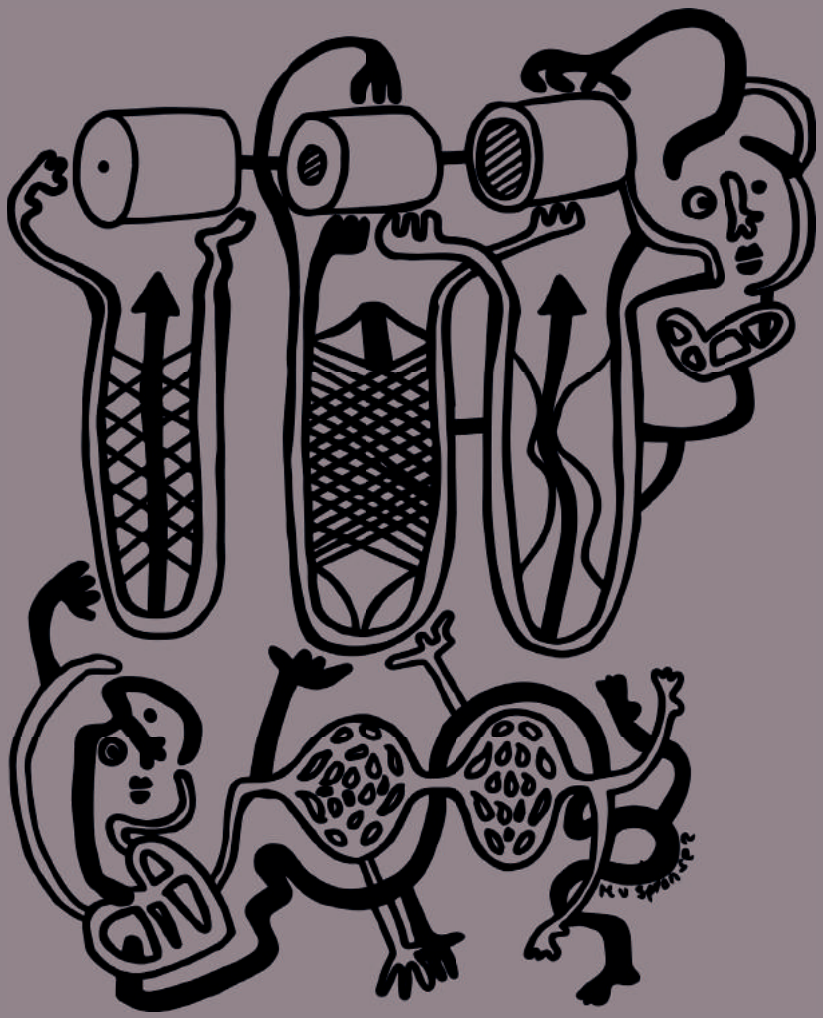

Endothelial dysfunction after drug eluting stent implantation

van den Heuvel M., Sorop O., van Beusekom H.M. and van der Giessen W.J.

Minerva Cardioangiol. 2009 Oct;57(5):629-43

9

Endothelial dysfunction after drug eluting stent implantation

Mieke van den Heuvel[1,2], Oana Sorop[1], Heleen M.M. van Beusekom[1], Wim J. van der Giessen[1,3]

[1] Department of Cardiology Cardiovascular Research Sehaal COEUR Erasmus Medical Center Rotterdam, The Netherlands; [2] Division of Pharmacology Vascular and Metabolie Diseases Department of Interna] Medicine Cardiovascular Research Sehaal COEUR Erasmus Medical Center Rotterdam, The Netherlands; [3] Interuniversity Cardiology Institute ofthe Netherlands, ICIN-KNAW Utrecht, The Netherlands

Endothelial dysfunction has been implicated in the pathological process of coronary artery disease as well as an adverse event after coronary drug eluting stent (DES) implantation. In this review, an overview will be given of the evidence to date regarding the effects of coronary DES on endothelial function obtained from both clinical and experimental studies. Stenting in general and DES seem to impair several aspects of endothelial function: provision of a permeable barrier function; modulation of adhesion, thrombosis and inflammation; and regulation of vascular tone. However, new insights show that the effects of DES can extend beyond the stent and peri-stent area: the vascular bed distal to the stent, starting with the distal conduit vessels up to the distal microvasculature, might be at risk. In addition, insight into the mechanism of DES induced endothelial dysfunction has been gained. To finalize this review, clinical complications and solutions of DES associated endothelial dysfunction will be discussed.

Key words: **Drug-eluting stents - Endothelial function - Coronary vasomotion - Stents - Thrombosis.**

The endothelium is a continuous cellular monolayer lining blood vessels throughout the body and has classically been described as a barrier between the blood and the vascular wall. It participates in numerous physiological processes including: formation of a permeable barrier for exchange and active transport of (macro)molecules; provision of an anti-thrombogenic defence and non-adherent surface for inflammatory cells; and regulation of vascular tone by release of vasoactive molecules (modified from [1]). Changes in one or more of these properties may represent the earliest manifestations of endothelial dysfunction characterised for example by: altered permeability with invasion of atherogenic substances, excessive thrombosis and inflammation and exaggerated vasoconstriction. Consequently, endothelial dysfunction has been implicated in the pathological process of atherosclerosis as evidenced early in the process of atherogenesis, but also later on in the control of dynamic plaque burden and eventually in

Corresponding author: W. J. van der Giessen, Department of Cardiology, Ee2393; Erasmus University Medical Center, 's Gravendijkwal 320, 3015 CE Rotterdam, The Netherlands. E-mail: w.j.vandergiessen@erasmusmc.nl

the clinical manifestations of coronary artery disease (CAD).[2] Paradoxically, percutaneous coronary intervention (PCI) strategies developed to resolve obstructive CAD have also been associated with endothelial dysfunction. More recently, drug eluting stents (DES) have been implicated in impairment of endothelial function. In this review, an overview will be given of the evidence obtained from both clinical and experimental studies, regarding specific aspects of endothelial dysfunction after DES implantation.

Endothelial function and coronary interventions

By secreting relaxing and contracting factors the endothelium can induce vasodilation or vasoconstriction in response to shear stress and to a variety of endogenous vasoactive substances that are either produced systemically or generated locally by vascular tissues or circulating blood cells. The major endothelium-derived relaxing factor is nitric oxide (NO), which reduces intracellular calcium within the vascular smooth muscle cells (VSMC) resulting in vasodilation.[3] The endothelium also secretes endothelial hyperpolarizing factors (EDHFs) [4] and the potent vasoconstrictor endothelin-1 (ET-1).[5] Since Furchgott *et al.* have demonstrated that the endothelium plays an obligatory role in the relaxation of arteries induced by achetylcholine (Ach),[6] and the released factor has been identified as NO [7] with its key second messenger cyclic guanoside monophosphate (cCMP);[8] methods have been developed to assess coronary endothelium-dependent vasomotor function in the catheterisation laboratory. NO-dependent vasodilator responses to locally infused Ach in coronary conduit arteries have shown paradoxical vasoconstriction in patients with cardiovascular risk factors, overt atherosclerosis and ischemic manifestations of CAD.[2, 9, 10]

In contrast, PCI modalities developed to reduce locally obstructive lesions caused by CAD, have already for a long time been associated with extensive arterial wall injury.[11] Our recent studies in swine have shown that even coronary imaging catheters used to guide PCI already cause considerable amounts of acute endothelial cell damage, however this injury tends to heal within a few days.[12] Although the endothelial barrier appears to regenerate, endothelium-dependent vascular function remains impaired long after endothelial regrowth.[13] Indeed, early clinical studies have demonstrated abnormal endothelium-dependent vasomotion of the treated coronary artery several months after balloon angioplasty.[14, 15] Coronary stenting has appeared to cause even more severe arterial injury than balloon angioplasty. Earlier work from our group in the pig model compared the effects of balloon angioplasty and stent implantation on certain aspects of long term vascular integrity: endothelial permeability and proliferation.[16] Leakage of the endothelium for large molecules such as Evans blue dye bound to albumin as well as prolonged endothelial proliferation was seen up to three months after the procedure, and was more pronounced after stenting than after angioplasty with a stent-specific pattern. In the early phase (two weeks post-stenting) the loss of the endothelial barrier was characterized by endothelial cell retraction and loose intercellular connections (Figure 1), while at three months expression of surface folds and adhesion of leukocytes was seen.[16] In addition, clinically Caramori *et al.* showed more severely depressed endothelium-dependent vascular tone at on average one-and-a-half years after stenting in patients as compared to balloon angioplasty and directional atherectomy.[17] Therefore, endothelial dysfunction as an adverse effect after PCI has already been known for a long time and is not a recently discovered phenomenon after DES implantation. However, with DES being the most commonly used PCI modality at the moment and with new types of DES intended to reduce endothelial dysfunction being developed, evaluation of adverse effects of DES on endothelial function seems useful. As the endothelium is such a versatile multifunctional vascular layer, several aspects of endothelial function can be affected.

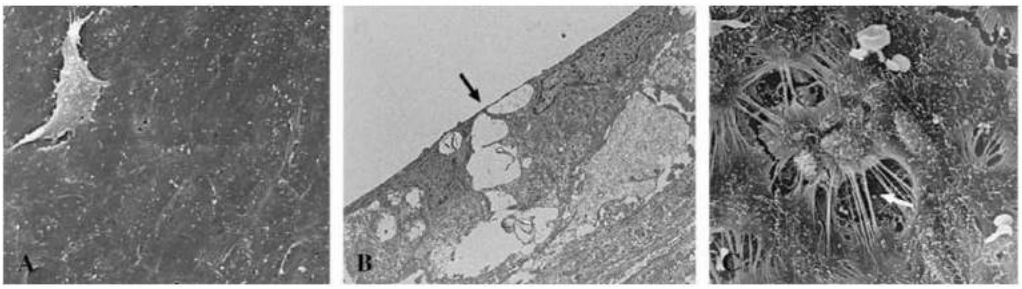

Figure 1.—Scanning electron microscopy images of the endothelium between the stent struts (A) and on top of the stent struts (B, C), two weeks after stenting with a BMS. While the endothelium between the struts has a healthy appearance (A), loose cell-cell junctions (B, arrow) and endothelial cell retraction (C, arrow) were seen, contributing to an increased permeability of the endothelial layer upon stenting; adapted with permission from van Beusekom *et al.*[16]

Therefore, below we will discuss the evidence regarding DES and endothelial dysfunction subdivided in separate endothelial functions: DES and impaired permeability barrier; DES and impaired modulation of adhesion, thrombosis and inflammation; DES and impaired vascular tone.

Coronary drug-eluting stents

Coronary DES, developed to limit in-stent restenosis as seen after stenting with bare metal stents (BMS), have now been approved for use in patients for more than six years. DES release high concentrations of immunosuppressive, cytostatic, or cytotoxic drugs locally at the coronary injury site in order to prevent VSMC proliferation.[18] The devices currently approved by the United States Food and Drug Administration are first-generation DES sirolimus-eluting stent (SES, 2003) and paclitaxel-eluting stent (PES, 2004); and second-generation DES zotarolimus-eluting stent (ZES, 2008) and everolimus-eluting stent (EES, 2008). Sirolimus, zotarolimus and everolimus belong to the limus family and inhibit VSMC proliferation by binding to FKBP12, which subsequently binds to the mammalian target of rapamycin and blocks the cell cycle in the G to S phase.[19, 20] Paclitaxel, the active drug of PES, stabilizes polymerized microtubules and inhibits microtubule disassembly, resulting in cell replication arrest in the G_0/G_1 and G_2/M phases of the cell cycle.[21, 22] In this way, DES drugs can inhibit profoundly the development of neointima formation after stenting. Indeed, DES resulted in a reduction of restenosis rates below 10% and significant long-term reduction in the number of target lesion revascularization procedures as compared to BMS in patients with CAD. However, the results vary with the different types of DES used and also depend on the studied patient population.[23-27]

Although most data converge towards a sustained reduction of restenosis rates by DES as compared to BMS, there is less agreement concerning the suggested association of DES with increased risk for late and very late stent thrombosis (LST), an undesirable event occurring between 1-12 months after DES implantation but also later on. While some studies report increased rates of LST in patients who underwent PES and SES implantation,[28-34] other randomized clinical trials showed that the incidence of LST does not differ significantly between patients receiving DES or BMS.[35, 36] Thus studies are not unequivocal. A meta-analysis performed by Stettler *et al.* showed no increase in LST with SES and only a small increase with PES.[37] Altogether, it seems clear that more clinical data with a longer follow up duration are needed to provide more consistent estimates of DES and LST safety. As an underlying mechanism of LST, DES associated impaired re-endothelialisation and delayed vascular healing [32, 38] as well as inflammation and secondary stent malapposition [39] have been put

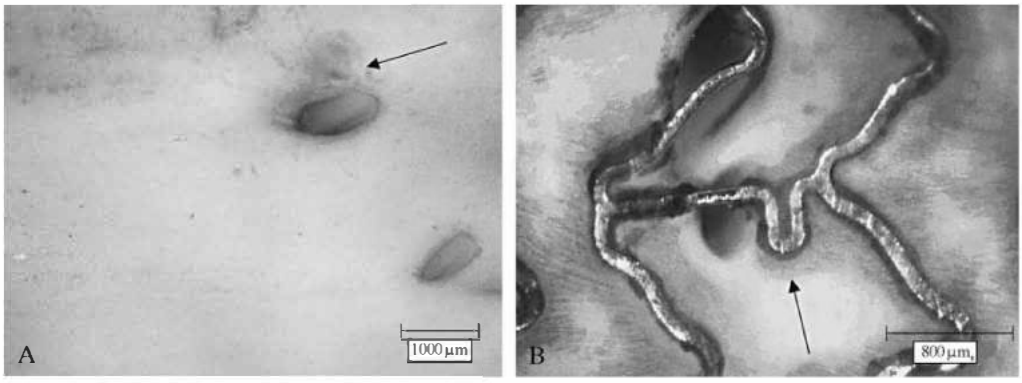

Figure 2.—Macroscopic images of the Evans blue dye exclusion test in a non-stented porcine coronary control vessel (A) and a vessel receiving a DES, five days post-implantation. While the control artery shows only occasional blue areas, mainly at branching points (A, arrow), extensive blue staining is seen near the stent struts (B, arrow) indicating endothelial leakage of Evans blue; adapted with permission from van der Giessen *et al.*[12]

forward. Indeed, DES seem to interfere with several aspects of endothelial function as described below. However, whether these specific aspects of endothelial dysfunction are due to specific DES implantation or to the general stenting procedure remains to be solved.

DES and impaired permeability barrier

DES alter the endothelial permeable barrier as evidenced by loss of cells, usually interpreted as delayed in-stent endothelial regrowth, and leaky cells as shown by an increased vascular permeability after stenting. These phenomena together may result in the observed delayed healing after DES implantation. Most of these data have been obtained from experimental studies, with the main animal models used being the porcine coronary and the rabbit iliac artery model. However, delayed vascular healing after DES implantation has also been described in clinical autopsy, angioscopy, and atherectomy studies.

With regard to endothelial leakage, unpublished data of our group suggests that following direct stenting of healthy porcine coronaries, extensive blue staining near the stent struts after the dye-exclusion test [16] is observed after five days, regardless of using BMS or DES (Figure 2B), as compared to only occasional blue areas mainly at branching points in the control non-stented artery (Figure 2A). This leakage of Evans blue dye points towards increased endothelial permeability early after stent implantation.

Regarding impaired endothelialisation and delayed vascular healing, the reports vary. In our studies of direct stenting in a healthy pig model, extensive coverage (>75%) of the stent struts by endothelium can be seen early after stent implantation (Figure 3). In this study, we showed similar high levels of endothelial coverage of the stent struts five days post stenting between BMS, SES and PES (mean±SD: 96±6% in BMS, 90±14% in SES, and 76±27% in PES).[40] Also, Frey *et al.* showed in a porcine overstretched coronary artery model that high levels of endothelial regrowth could be seen 3-14 days after implantation of BMS, SES, and a SES with extended release.[41] The extent of endothelial coverage on the stent struts was above 72% at 7 days and 85% at 14 days. In addition, Suzuki *et al.* reported similar rates of re-endothelialisation between SES and BMS at four weeks in overstretched porcine coronary arteries.[42] However, in this study more fibrin deposition was observed in SES treated arteries, which is considered to be a sign of delayed vascular healing. Our study of direct stenting in porcine coronary arteries with a DES with

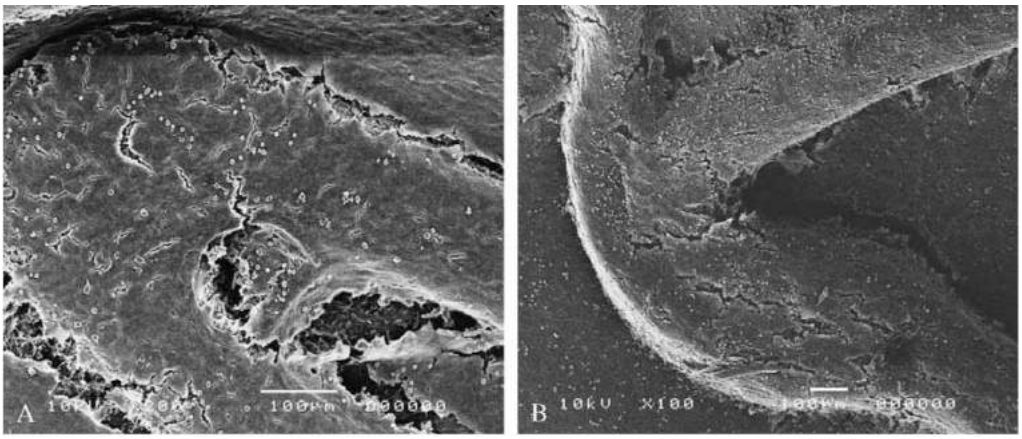

Figure 3.—Scanning electron microscopy images showing an extensive coverage of the stent struts by endothelium already five days after implantation of a BMS (A), and a DES (B) after direct stenting in healthy porcine coronary arteries; adapted with permission from van Beusekom *et al.*[40]

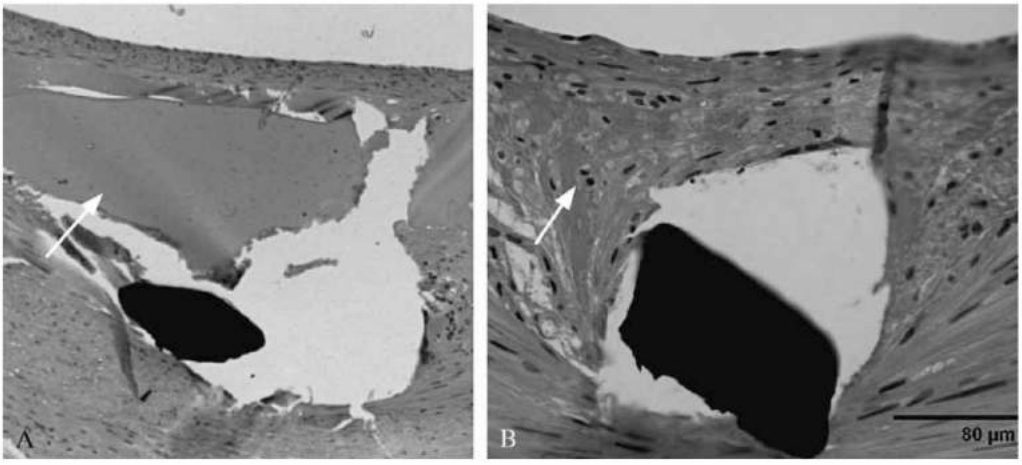

Figure 4.—Details of stent struts surrounded by fibrinoid (arrow) (HE stain). The amount of fibrinoid in Cypher (A) is considerably larger than in a SES with an intermediate dose of sirolimus (40 µg) (B), 28 days after stent implantation; reproduced with permission from van der Giessen *et al.*[43]

sirolimus released from a nonpolymeric hydroxyapatite coated stent showed that with increasing sirolimus dose, a dose dependent increase in fibrinoid deposition could be seen (Figure 4) with unaltered neointimal thickness.[43] This indicates that by reducing the dose of sirolimus, signs of delayed vascular healing could be reduced without compromising efficacy. Also in rabbit iliac arteries, Klugherz *et al.* observed a re-endothelialisation rate above 86% independent of stent type (BMS vs. polymer-only stent vs. SES), four weeks post implantation.[44]

Different results were obtained by Finn *et al.* in balloon injured rabbit iliac arteries, four weeks after implantation of overlapping DES.[45] The authors report low levels of endothelial coverage together with more local inflammation and fibrin deposition only significantly so at overlapping sites of PES as

compared to SES or BMS suggesting both delayed endothelialisation and vascular healing. The results of this study may be attributed to the extent of injury or to higher local drug concentrations after overlapping stent implantation. Data obtained more recently by the same group in endothelium-denuded iliac arteries showed that non-overlapping SES had the lowest percentage of re-endothelialisation of the stent struts at 14 days, followed by PES, ZES, EES versus BMS.[46] According to the authors, this incomplete endothelialisation could be part of a transitional healing surface. At 28 days no significant difference in endothelial coverage between the DES was seen. In addition, in a porcine model with overlapping stents, Lim *et al.* showed a lower endothelial coverage after four weeks of overlapping PES implantation as compared to overlapping BMS, SES and SES+PES combined.[47] The same overlapping DES group also showed an increased vascular inflammation score.

Altogether, an altered endothelial permeable barrier is to be expected early after stenting. However, no clear consistency could be shown in the effects of DES on in-stent re-endothelialisation, making the conclusion that DES impair endothelial recovery and that specific DES have more negative effects difficult to formulate. In contrast, DES do seem to be associated with multifactorial delayed vascular healing as evidenced by increased amounts of fibrin deposition and inflammation within the stented vascular wall. This delayed healing has also been witnessed in clinical studies.

Joner *et al.*[32] examined autopsy data from 23 patients receiving SES and PES for more than 30 days versus 25 patients with BMS. DES were associated with incomplete endothelialisation and persistent delayed healing characterized by more fibrin deposition as compared to BMS. From the same registry of human autopsies, Finn *et al.*[38] concluded that incomplete endothelial coverage of the stent struts was the best predictor of thrombosis. However, DES lesions with thrombus also showed higher amounts of vascular fibrin deposition. The drawback of small numbered autopsy studies is that the results may not be representative for the majority of surviving patients receiving DES.

Moreover, several angioscopy studies have speculated about DES impaired endothelialisation based on delayed neointimal coverage (NIC) of the stent struts after DES implantation. Awata *et al.* showed that serial angioscopic findings up to two years after SES implantation were markedly different with lower grades of NIC as compared to BMS.[48, 49] In addition, different platforms of DES were compared using angioscopy. When assessing the effects of SES and PES implantation after nine months, more heterogeneous NIC was found after PES implantation.[50] ZES showed greater NIC than SES eight months after implantation, and more competent arterial healing was suggested in ZES than SES.[51] However, clear conclusions based on these studies with regard to DES and endothelial coverage are difficult to draw, since angioscopy is a macroscopic technique not sensitive enough to discriminate between an uncovered stent-strut and a strut covered by translucent tissue of only a few cell-layers thick. In addition, one can only speculate about the cell type covering the struts.

Histology of in-stent restenosis tissue obtained by atherectomy can clarify the nature of these cellular contents. Our study comparing in-stent restenosis between DES and BMS, showed incomplete neointimal healing as late as two years after DES implantation.[52] PES showed more pronounced signs of delayed healing than SES as evidenced by a higher amount of fibrinoid. Since this was observed in atherectomy specimens, endothelialisation could not be assessed.

Overall, DES seem to cause delayed vascular healing of the stented vessel segment consisting of more factors than impaired endothelialisation alone such as neointimal organisation, specific tissue constituents such as fibrin, specific extracellular matrix build up and the presence of inflammation. However, only assessing vascular healing after DES implantation does not give a complete endothelial health status of the stented segment, since a completed vascular healing with presence of regenerated endothelium does not guarantee normal endothelial func-

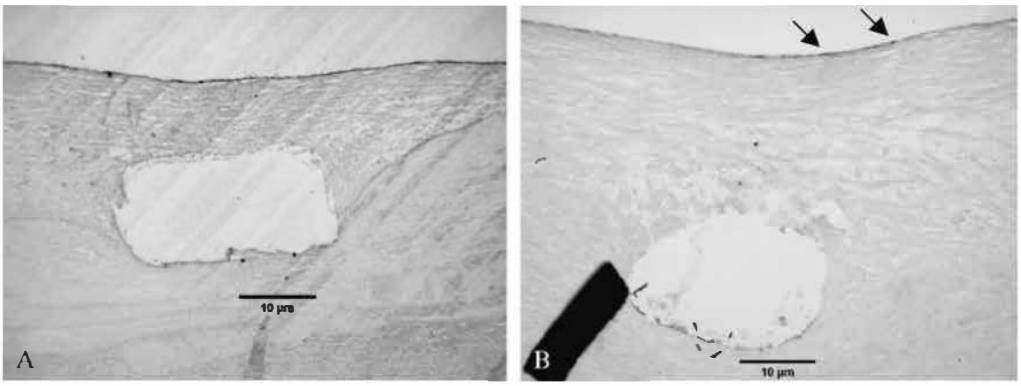

Figure 5.—In-stent immunocytochemic staining for eNOS (A) and vWF (B) in porcine coronary arteries receiving a DES for 28 days. While a continuous eNOS staining over the whole vascular circumference was seen, indicating high eNOS expression within the stent, the expression of vWF was very weak, with only scarce cells showing vWF staining (arrows); adapted with permission from van Beusekom *et al.*[40]

tion.[53] Therefore, it might be useful to assess the influence of DES on endothelial modulatory functions within the stented vessel as well.

DES and impaired modulation of adhesion, thrombosis and inflammation

The endothelium maintains vascular homeostasis by production, release and expression of modulatory molecules to balance the interactions between adhesion, coagulation, fibrinolytic and inflammatory regulatory systems. Expression of these molecules by endothelial cells has been used as specific markers to evaluate in-stent endothelial function after DES implantation, mainly *ex vivo* using immunocytochemistry or Western blot analysis on excised stented vessel material. However to date, there is no consensus regarding a specific expression marker of DES associated in-stent endothelial dysfunction. The following examples have been described:

Endothelial nitric oxide synthase (eNOS), plays a key role in vascular homeostasis by producing NO from L-arginine in vascular endothelial cells. The cofactor tetrahydrobiopterin (BH_4) has emerged as a critical determinant of eNOS activity, as in conditions of reduced BH_4 bioavailability uncoupled eNOS produces superoxide instead of NO.[54, 55] Ota *et al.* have shown in cultured human endothelial cells that ten days of treatment with 2.5nmol/l paclitaxel, sirolimus or everolimus resulted in reduced expression of eNOS, pointing towards endothelial dysfunction induced by the three drugs.[56] However, local NO production by eNOS is difficult to quantify *in vivo*. Therefore, most data come from NO-metabolite measurements in plasma or from protein assays of arterial specimens. But these metabolite data do not provide a specific measure of eNOS function within the stented segment. In contrast to previous assays, we assessed in-stent eNOS expression by immunocytochemistry (Figure 5A) in BMS, SES and PES 28 days after stent implantation.[40] Our results showed a similar high eNOS expression in SES and BMS, but a reduced eNOS expression in PES. Although these data give an indication of endothelial function within the stent and the effects of different DES on endothelial expression, our assay cannot distinguish between functional eNOS and its uncoupled form. Therefore, eNOS expression might be a valid endothelial homeostasis expression marker when accompanied by superoxide measurements.

Platelet endothelial cell adhesion molecule (PECAM-1) is a major constituent of endothe-

lial intercellular junctions; human endothelial cells express nearly 10^6 PECAM-1 molecules per cell.[57] PECAM-1 has been shown to play an important role in endothelial flow sensing and NO-production by forming complexes with eNOS.[58] When endothelial cell contact is altered, a loss of PECAM-1 immunostaining at the endothelial junctions can be seen. Reduced PECAM-1 expression translates in a reduced adhesion interaction between adjacent endothelial cells with subsequent enhanced permeability of the endothelial cell layer.[58, 59] Joner *et al.* assessed in-stent endothelial PECAM-1 expression above the stent struts in iliac arteries of rabbits receiving SES, PES, ZES, EES *versus* BMS for 14 or 28 days.[46] PECAM-1 expression after SES and PES implantation was reduced after both 14 and 28 days, suggesting an inhibition of endothelial cell proliferation and migration and/or endothelial injury. Therefore, PECAM-1 might be a valid endothelial adhesion expression marker.

Von Willebrand factor (vWF) is a large glycoprotein produced almost exclusively by the endothelium. Its primary function is to bind to other haemostatic proteins, particularly Factor VIII, and is important in clot formation and platelet adhesion to the endothelium.[60] VWF is regarded as a useful clinical marker of risk associated with atherosclerosis since systemic plasma levels of vWF are elevated in the setting of atherosclerotic cardiovascular disease in a graded manner proportionate to the risk of cardiovascular disease events. Pathophysiological evidence suggests that vWF is not only a marker but also a mediator of cardiovascular disease events. VWF is produced and released by endothelial cells in response to a variety of stimuli, e.g. to inflammatory cytokines in response to vascular injury.[61] In one of our studies in the pig model, we used the immunocytochemical detection of expressed vWF in the endothelium of coronary arteries receiving DES and BMS (Figure 5B). Our results showed only very low levels of in-stent endothelial vWF expression (less than 10% of the total stent endothelial circumference was positive for vWF), with no differences seen between BMS, SES or PES at 28 days post stenting.[40] Because endothelial expression of vWF seems to return to normal several days after arterial injury,[62] this expression marker might not be sensitive enough on its own to detect chronic endothelial dysfunction.

Thrombomodulin is an integral membrane protein expressed on the surface of endothelial cells, having an anticoagulant function by forming high affinity inhibitory binding complexes with thrombin. It has been suggested that inflammatory cytokines generated in the injured vascular wall (as after stenting) may down-regulate thrombomodulin promoting a pro-thrombotic state.[63] Joner *et al.* have measured the expression of thrombomodulin 14 and 28 days post-stenting of SES, PES, ZES, EES and BMS in denuded, overstretched arteries.[46] The authors described that overall staining for thrombomodulin was moderate in BMS although not as high as in non-stented vascular segments; while in DES irrespective of type, thrombomodulin expression was very weak if not absent at both follow-up times. This suggests that endothelial dysfunction with an increased pro-thrombotic state, as indicated by reduced thrombomodulin expression, can be induced by stenting itself and be exacerbated by DES. Therefore, thrombomodulin might be a sensitive endothelial coagulation-related expression marker.

Platelet derived growth factor (PDGF) is one of the first identified endothelial-derived, paracrine signals required for recruitment and communication with surrounding cells in the vessel wall.[64] In coronary arteries of Yucatan minipigs receiving SES or PES for one month, in-stent expression of PDGF was higher in PES than in SES. Since the stented vascular segments were almost completely re-endothelialised with no differences between the DES, this suggested a higher recruited inflammatory state by PES as compared to SES.[65] Therefore, PDGF might be a useful endothelial inflammation-related expression marker.

Thus, the markers described above are examples used to date to evaluate different modulatory aspects of in-stent endothelial function early after DES implantation in

experimental studies. On their one, they are not capable of providing a complete and specific characterization of an integrated functional endothelium. It has been shown that in circumstances of vascular injury, inflammation shifts haemostatic mechanisms in favor of thrombosis. In addition, dysfunctional anticoagulant pathways may play a role in dampening inflammatory responses.[63] Therefore, one aspect of endothelial function might influence other aspects and the task of defining a single best marker to assess complete endothelial functionality seems impossible. Thus, we propose that a combination of markers covering different endothelial modulatory functions rather than only one would give a more complete overview of endothelial function within the stent. For example, in our study comparing different DES, we evaluated both eNOS and vWF staining at 28 days after stent implantation in pigs (Figure 5). While vWF expression was similar for all DES, PES showed diminished eNOS expression.[66] In this way, both endothelial homeostasis and the thrombotic state within the stent were evaluated. An even more complete combination of endothelial expression markers could also include PECAM-1, thrombomodulin and PDGF to more fully assess endothelial permeability, cell-cell adhesion, and the thrombotic and inflammatory state. However, of notion all above described endothelial modulatory expression markers have only been used in a limited number of experimental animal studies. Whether extrapolation to the human situation is valid remains to be determined. In addition, evaluation of overall endothelial function is not possible with use of only in-stent endothelial expression markers, since modulation of vascular tone cannot be fully assessed in a motion-limited stented vessel segment.

DES and impaired vascular tone

DES effects on endothelium-dependent vascular tone can only be measured outside the motion-limiting stent. Both physiological and pharmacological stimuli have been used for the evaluation of coronary endothelial function after DES implantation in conduit arterial segments adjacent to the stent. These stimuli act as potent vasodilators in normal coronary arteries by promoting the release of NO in endothelial cells and via its key second messenger cGMP relaxation of VSMC. However when endothelial NO release of a vessel segment is impaired or insufficient, these stimuli can cause paradoxical vasoconstriction.

Hofma *et al.* was the first to report abnormal coronary conduit vasoconstrictive responses distal to the stent to the stimulus Ach after SES implantation for six months as compared to BMS.[67, 68] Constrictive responses of the same vessel segments were present, directly after implantation in both BMS and SES groups indicating that while in BMS endothelial dysfunction was restored in time, SES induced prolonged dysfunction. Togni *et al.* evaluated coronary vasodilatory function to exercise, six months after SES or BMS implantation. In this study, SES was associated with exercise-induced paradoxical vasoconstriction, while BMS did not affect the response.[69] Fuke *et al.* performed a comparison of coronary vasomotion function in the peri-stent area with intracoronary infusion of Ach both before and six months after SES implantation. They demonstrated that no coronary vasoconstriction was present before SES implantation, but Ach induced significant vasoconstriction six months after SES implantation.[70] Togni *et al.* also showed the effects of PES on endothelial vasomotion.[71] PES implantation was associated with exercise-induced coronary vasoconstriction in the peri-stent area up to one year as compared to BMS. Shin *et al.* demonstrated that both SES and PES implantation were associated with endothelial dysfunction at six to nine months post intervention, not only in the distal but also in the far distal conduit arterial segments of the treated vessel.[72] Moreover, Kim *et al.* compared vascular function of larger patient groups of SES and PES with BMS, six months after stenting.[73] Again, both SES and PES showed peri-stent endothelial dysfunction especially in the arterial segments distal to DES.

To summarize, most clinical studies found

DES-associated conduit endothelial dysfunction in the peri-stent area; however the segment distal to the stent was always most severely affected. In addition, even far distal conduit arterial segments can be affected. These data probably reflect a dose-dependent effect of specific DES on the endothelium distal to the stent. Therefore with the advent of new types of DES or DES with different pharmacokinetic drug release characteristics, we may observe other responses. Hamilos *et al.* compared coronary conduit vasomotion of a second generation biolimus A9-eluting stent (BES) with SES and found preserved endothelium-dependent vasomotion adjacent to BES.[74] According to Shin *et al.* also after ZES implantation for six to nine months endothelium-dependent vascular function distal to the stent was less altered as compared to SES.[75] Kim *et al.* compared endothelial function six months after ZES implantation with both SES and BMS.[76] Although both DES affected vasomotion in the peri-stent area, paradoxical vasoconstriction was less pronounced after ZES.

Therefore, in particular first generation DES seem to impair endothelial regulation of vascular tone in the peri-stent area as compared to BMS in the early time period after stenting. However, only these specific DES have been most extensively studied as compared to the newer generation DES. A limitation of above described clinical studies is that testing of *in vivo* endothelial function in patients is a technically difficult procedure, irrespective of the stimulus used. Thus, sample sizes are usually small and little comparative data of different DES are available. Overall, although stenting on its own has already been associated with long term vascular dysfunction,[17] there is convincing evidence that first generation DES even further impair this endothelium-dependent vascular function up to almost one year after DES implantation.

New insights in DES induced alterations in vascular tone

Recently, new insights have appeared with regard to the extent and the underlying mechanism of DES induced impairments in vascular tone. Especially the coronary vasculature distal to DES seems to be at increased risk for endothelium-dependent vasodilatory alterations. Li *et al.* confirmed abnormal coronary vasomotor function distal to SES in a porcine model one month after implantation.[77] Besides reduced endothelium-dependent dilation, increased vasoconstriction to ET-1 of distal conduit arteries was observed. Moreover, Pendyala *et al.* showed in a pig model additionally impaired endothelium-dependent vascular function of small arteries far distally from overlapping PES.[78] From our own studies of single DES implantation for five weeks in a healthy porcine model, we also report PES induced vascular alterations in endothelial function of distal small arteries.[79] Specifically the EDHF component of microvascular endothelial function seemed to be affected by PES under conditions of reduced NO bioavailability (Figure 6). Two clinical studies support the concept that DES effects can extend far in the distal flow area of the stent. Meier *et al.* reported impaired distal collateral function six months after both SES and PES implantation for *de novo* CAD.[80] In addition, according to Obata *et al.* SES implantation may also adversely affect distal endothelium-dependent microvascular function after ischemia-reperfusion two weeks after an acute myocardial infarction.[81] Altogether, these data converge towards the conclusion that DES induced alterations in the endothelial regulation of vascular tone might be a more generalized distal phenomenon than just occurring locally adjacent to the stent.

Experimental studies have provided preliminary insight into the nature of these endothelial alterations for both SES and PES. Jabs *et al.* showed that continuous infusion of sirolimus for seven days induced a marked degree of vascular dysfunction in rats.[82] According to the investigators, increased vascular superoxide production and release might contribute to the dysfunctions. In addition, Pendyala *et al.* showed that overlapping PES implantation was also associated with increased superoxide generation in the peri-stent area, probably affecting the NO-medi-

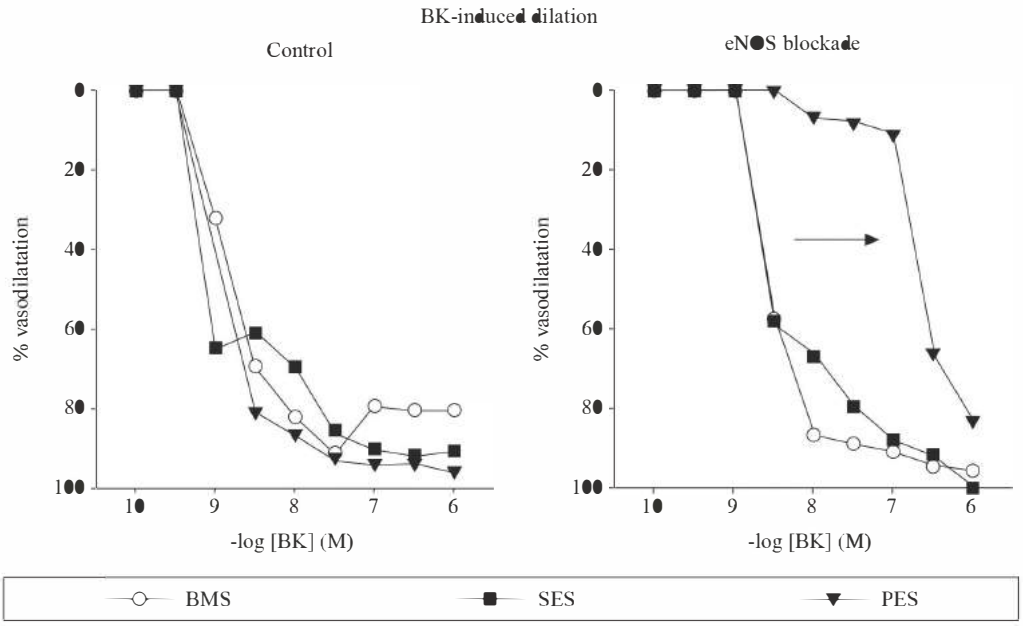

Figure 6.—Effects of five weeks of single implanted BMS, SES, and PES in the three coronary arteries of a pig on *in vitro* endothelium-depend0ent vasodilation to bradykinin (BK) (control) or to BK after eNOS blockade, in small arteries (vessel diameter ~300µm) distal to the stent. While no differences in the BK-induced response were seen under control conditions, PES resulted in impaired BK-induced dilation after eNOS blockade. This suggests that PES implantation affects the EDHF component of BK-induced vasodilation; adapted with permission from van den Heuvel *et al.*[79]

ated vasodilator response of conduit arteries of this area.[78] However, direct evidence of DES induced effects causing NO impairment is scarce, mostly because of the difficulties with the direct measurement of NO. Nevertheless, it is tempting to speculate that impaired endothelial vasomotion mirrors DES induced oxidative stress imposed on the vascular wall, impairing profoundly endothelial NO bioavailability and perhaps also EDHF availability under certain circumstances.

Conclusions

Abnormal endothelial function has been implicated both in CAD development and as an adverse effect after PCI procedures including DES implantation. The link between atherosclerosis development and endothelial dysfunction induced by DES placement may be related to a decreased local bioavailability of NO.[83, 84]

In case of DES, evidence indicates that overall endothelial dysfunction may be due to an altered permeable barrier function after stenting in general, delayed vascular healing specific to some DES, affected endothelial modulatory functions after some DES implantations, and impaired regulation of vascular tone after stenting and specific to some DES. These aspects might predispose to a procoagulant and pro-inflammatory state within the DES and paradoxical vasoconstriction outside the DES with the distal circulation receiving the highest drug concentrations at highest risk. However, it is currently unknown whether these impaired aspects of endothelial function remain present after years, long after stenting and DES implantation. Therefore, the link between enhanced DES associated endothelial dysfunction and adverse clinical events is speculative and has yet to be established. However when persistent, endothelial dysfunction of coronary conduit arteries has been associated with long-

term CAD development, disease progression and clinical event rates.[85] In addition, impaired distal endothelium-dependent vasodilation of the coronary microcirculation has been associated with exercise-induced myocardial ischemia, even in patients without hemodynamically significant obstructive coronary lesions.[86]

Finally, if DES-associated endothelial dysfunction proves to be a real harmful phenomenon, then what may provide a solution? Reduction of DES associated endothelial dysfunction may be provided by optimal medical therapy. Besides blood pressure and lipid lowering, angiotensin converting enzyme inhibitors,[87] angiotensin receptor blockers,[88] selective beta-blockers,[89] statins [90] and fibrates [91] have shown clinical beneficial effects on general endothelial function. However, whether additional aggressive therapy translates in improved endothelial outcome after DES implantation remains to be determined.

Moreover, drug choice, release kinetics, polymer-type or non-polymer coatings, and stent-type are probably the most important components of DES technology determining the type of vascular response and the time-course of healing. Newer, perhaps better DES are presently designed and tested that may eliminate these adverse effects. Our results with a new DES consisting of another limus drug, tacrolimus, together with a biodegradable polymer and its own stent-design showed promising results with regard to suppression of inflammation and early re-endothelialisation in the pig model.[92] However, clinically it failed to prevent in-stent restenosis despite of the theoretical advantages of tacrolimus, which has less inhibitory effects on endothelial cells than VSMC.[93] Therefore, modifications in dose and release of tacrolimus from this DES seem to be mandatory, highlighting the delicate balance of a DES between wanted restored endothelial function and unwanted restenosis. With the development of completely bioabsorbable DES, short-term vessel scaffolding together with inhibition of cell proliferation can be provided, without the long-term restrictions of metallic stents. Indeed, Serruys *et al.* showed promising two year results after implantation of a bioabsorbable everolimus-eluting coronary stent system with regard to prevented restenosis and restored vasomotion at both the stented site and the peri-stent area.[94] However, future experimental and clinical studies are needed to evaluate the efficacy and safety of this promising new approach.

To conclude, DES associated endothelial dysfunction is a fascinating complex phenomenon likely to be related to the fundamental mechanisms of CAD development. Together the evolution of biotechnology and stent design with increased knowledge of fundamental disease mechanisms might lead to further improvements in future DES with the prospect of even better patient outcomes.

Riassunto

La disfunzione endoteliale dopo impianto di stent medicati

La disfunzione endoteliale è implicata nei processi patologici della malattia coronarica come evento avverso dopo l'impianto di uno stent medicato (*drug eluting stents*, DES). In questa revisione viene offerto un quadro generale delle dimostrazioni scientifiche, ottenute da studi sia clinici che sperimentali, degli effetti dei DES sulle funzioni endoteliali. Gli stent in generale e i DES sembrano danneggiare diversi aspetti della funzione endoteliale tra i quali quella di fungere da barriera permeabile, modulare l'adesione, la trombosi e l'infiammazione, oltre che regolare il tono vascolare. In ogni caso, nuove ipotesi propongono che gli effetti dei DES possono essere estesi oltre l'area di impianto dello stent che l'area adiacente allo stesso: il letto vascolare distale allo stent, dai vasi distali alla microvascolatura distale, possono essere a rischio. Inoltre, sono state formulate diverse ipotesi sul meccanismo con il quale i DES inducono la disfunzione endoteliale. Concludendo, verranno discussi le complicazioni cliniche dei DES associati alla disfunzione endoteliale e le relative soluzioni.

Parole chiave: Stent medicati - Cellule endoteliali - Vasospasmo coronarico - Stent - Trombosi.

References

1. Ross R. The pathogenesis of atherosclerosis: a perspective for the 1990s. Nature 1993;362:801-9.
2. Celermajer DS. Endothelial dysfunction: does it matter? Is it reversible? J Am Coll Cardiol 1997;30:325-33.
3. Vanhoutte PM. Endothelium and control of vascular

function. State of the Art lecture. Hypertension 1989;13(6 Pt 2):658-67.
4. Feletou M, Vanhoutte PM. Endothelium-derived hyperpolarizing factor: where are we now? Arterioscler Thromb Vasc Biol 2006;26:1215-25.
5. Yanagisawa M, Kurihara H, Kimura S, Tomobe Y, Kobayashi M, Mitsui Y *et al.* A novel potent vasoconstrictor peptide produced by vascular endothelial cells. Nature 1988;332:411-5.
6. Furchgott RF, Zawadzki JV. The obligatory role of endothelial cells in the relaxation of arterial smooth muscle by acetylcholine. Nature 1980;288:373-6.
7. Palmer RM, Ferrige AG, Moncada S. Nitric oxide release accounts for the biological activity of endothelium-derived relaxing factor. Nature 1987;327:524-6.
8. Rapoport RM, Draznin MB, Murad F. Endothelium-dependent relaxation in rat aorta may be mediated through cyclic GMP-dependent protein phosphorylation. Nature 1983;306:174-6.
9. Ludmer PL, Selwyn AP, Shook TL, Wayne RR, Mudge GH, Alexander RW *et al.* Paradoxical vasoconstriction induced by acetylcholine in atherosclerotic coronary arteries. N Engl J Med 1986;315:1046-51.
10. Zeiher AM, Drexler H, Wollschlager H, Just H. Modulation of coronary vasomotor tone in humans. Progressive endothelial dysfunction with different early stages of coronary atherosclerosis. Circulation 1991;83:391-401.
11. Waller BF. Pathology of transluminal balloon angioplasty used in the treatment of coronary heart disease. Hum Pathol 1987;18:476-84.
12. Van Der Giessen WJ, Krabbendam SC, Van Beusekom HM. Endovascular Imaging Causes Significant But Temporary Endothelial Injury. 81st Annual Scientific Session of the American-Heart-Association, Nov 08-12 2008. New Orleans, LA. Lippincott Williams & Wilkins: S736-S.
13. Shimokawa H, Flavahan NA, Shepherd JT, Vanhoutte PM. Endothelium-dependent inhibition of ergonovine-induced contraction is impaired in porcine coronary arteries with regenerated endothelium. Circulation 1989;80:643-50.
14. Mc Fadden EP, Bauters C, Lablanche JM, Quandalle P, Leroy F, Bertrand ME. Response of human coronary arteries to serotonin after injury by coronary angioplasty. Circulation 1993;88(5 Pt 1):2076-85.
15. Vassanelli C, Menegatti G, Zanolla L, Molinari J, Zanotto G, Zardini P. Coronary vasoconstriction in response to acetylcholine after balloon angioplasty: possible role of endothelial dysfunction. Coron Artery Dis 1994;5:979-86.
16. van Beusekom HM, Whelan DM, Hofma SH, Krabbendam SC, van Hinsbergh VW, Verdouw PD *et al.* Long-term endothelial dysfunction is more pronounced after stenting than after balloon angioplasty in porcine coronary arteries. J Am Coll Cardiol 1998;32: 1109-17.
17. Caramori PR, Lima VC, Seidelin PH, Newton GE, Parker JD, Adelman AG. Long-term endothelial dysfunction after coronary artery stenting. J Am Coll Cardiol 1999;34: 1675-9.
18. Serruys PW, Kutryk MJ, Ong AT. Coronary-artery stents. N Engl J Med 2006;354:483-95.
19. Marx SO, Jayaraman T, Go LO, Marks AR. Rapamycin-FKBP inhibits cell cycle regulators of proliferation in vascular smooth muscle cells. Circ Res 1995;76:412-7.
20. Poon M, Marx SO, Gallo R, Badimon JJ, Taubman MB, Marks AR. Rapamycin inhibits vascular smooth muscle cell migration. J Clin Invest 1996;98:2277-83.
21. Sollott SJ, Cheng L, Pauly RR, Jenkins GM, Monticone RE, Kuzuya M *et al.* Taxol inhibits neointimal smooth muscle cell accumulation after angioplasty in the rat. J Clin Invest 1995;95:1869-76.
22. Axel DI, Kunert W, Goggelmann C, Oberhoff M, Herdeg C, Kuttner A *et al.* Paclitaxel inhibits arterial smooth muscle cell proliferation and migration *in vitro* and *in vivo* using local drug delivery. Circulation 1997;96:636-45.
23. Stone GW, Midei M, Newman W, Sanz M, Hermiller JB, Williams J *et al.* Randomized comparison of everolimus-eluting and paclitaxel-eluting stents: two-year clinical follow-up from the Clinical Evaluation of the Xience V Everolimus Eluting Coronary Stent System in the Treatment of Patients with de novo Native Coronary Artery Lesions (SPIRIT) III trial. Circulation 2009;119:680-6.
24. Onuma Y, Kukreja N, Piazza N, Eindhoven J, Girasis C, Schenkeveld L *et al.* The everolimus-eluting stent in real-world patients: 6-month follow-up of the X-SEARCH (Xience V Stent Evaluated at Rotterdam Cardiac Hospital) registry. J Am Coll Cardiol 2009;54: 269-76.
25. James SK, Stenestrand U, Lindback J, Carlsson J, Scherstén F, Nilsson T *et al.* Long-term safety and efficacy of drug-eluting versus bare-metal stents in Sweden. N Engl J Med 2009;360:1933-45.
26. Ong AT, Serruys PW, Aoki J, Hoye A, van Mieghem CA, Rodriguez-Granillo GA *et al.* The unrestricted use of paclitaxel- versus sirolimus-eluting stents for coronary artery disease in an unselected population: one-year results of the Taxus-Stent Evaluated at Rotterdam Cardiology Hospital (T-SEARCH) registry. J Am Coll Cardiol 2005;45:1135-41.
27. Frobert O, Lagerqvist B, Carlsson J, Lindback J, Stenestrand U, James SK. Differences in restenosis rate with different drug-eluting stents in patients with and without diabetes mellitus: a report from the SCAAR (Swedish Angiography and Angioplasty Registry). J Am Coll Cardiol 2009;53:1660-7.
28. McFadden EP, Stabile E, Regar E, Cheneau E, Ong AT, Kinnaird T *et al.* Late thrombosis in drug-eluting coronary stents after discontinuation of antiplatelet therapy. Lancet 2004;364:1519-21.
29. Ong AT, McFadden EP, Regar E, de Jaegere PP, van Domburg RT, Serruys PW. Late angiographic stent thrombosis (LAST) events with drug-eluting stents. J Am Coll Cardiol 2005;45:2088-92.
30. Park DW, Yun SC, Lee SW, Kim YH, Lee CW, Hong MK *et al.* Stent thrombosis, clinical events, and influence of prolonged clopidogrel use after placement of drug-eluting stent data from an observational cohort study of drug-eluting versus bare-metal stents. JACC Cardiovasc Interv 2008;1:494-503.
31. Feres F, Costa JR, Jr., Abizaid A. Very late thrombosis after drug-eluting stents. Catheter Cardiovasc Interv. 2006;68:83-8.
32. Joner M, Finn AV, Farb A, Mont EK, Kolodgie FD, Ladich E *et al.* Pathology of drug-eluting stents in humans: delayed healing and late thrombotic risk. J Am Coll Cardiol 2006;48:193-202.
33. Luscher TF, Steffel J, Eberli FR, Joner M, Nakazawa G, Tanner FC *et al.* Drug-eluting stent and coronary thrombosis: biological mechanisms and clinical implications. Circulation 2007;115:1051-8.
34. Kuchulakanti PK, Chu WW, Torguson R, Ohlmann P, Rha SW, Clavijo LC *et al.* Correlates and long-term outcomes of angiographically proven stent thrombosis with sirolimus- and paclitaxel-eluting stents. Circulation. 2006;113(8):1108-13.
35. Mauri L, Hsieh WH, Massaro JM, Ho KK, D'Agostino R, Cutlip DE. Stent thrombosis in randomized clinical trials of drug-eluting stents. N Engl J Med 2007;356:1020-9.
36. Spaulding C, Daemen J, Boersma E, Cutlip DE, Serruys

PW. A pooled analysis of data comparing sirolimus-eluting stents with bare-metal stents. N Engl J Med 2007;356:989-97.
37. Stettler C, Wandel S, Allemann S, Kastrati A, Morice MC, Schomig A *et al.* Outcomes associated with drug-eluting and bare-metal stents: a collaborative network meta-analysis. Lancet 2007;370:937-48.
38. Finn AV, Joner M, Nakazawa G, Kolodgie F, Newell J, John MC *et al.* Pathological correlates of late drug-eluting stent thrombosis: strut coverage as a marker of endothelialization. Circulation 2007;115:2435-41.
39. Cook S, Ladich E, Nakazawa G, Eshtehardi P, Neidhart M, Vogel R *et al.* Correlation of intravascular ultrasound findings with histopathological analysis of thrombus aspirates in patients with very late drug-eluting stent thrombosis. Circulation 2009;120:391-9.
40. van Beusekom HM, Sorop O, van den Heuvel M, Onuma Y, Duncker DJ, Danser AH *et al.* Early endothelialization in Paclitaxel-eluting stents is similar to other drug-eluting stents but shows transient endothelial dysfunction. Eurointervention. 2009;5 (Supplement E):65.
41. Frey D, Billinger M, Meier P, Beslac O, Grossenbacher R, Hanni B *et al.* Endothelialization of sirolimus-eluting stents with slow and extended drug release in the porcine overstretch model. J Invasive Cardiol 2008;20:631-4.
42. Suzuki T, Kopia G, Hayashi S, Bailey LR, Llanos G, Wilensky R *et al.* Stent-based delivery of sirolimus reduces neointimal formation in a porcine coronary model. Circulation 2001;104:1188-93.
43. van der Giessen WJ, Sorop O, Serruys PW, Peters-Krabbendam I, van Beusekom HM. Lowering the dose of sirolimus, released from a nonpolymeric hydroxyapatite coated coronary stent, reduces signs of delayed healing. JACC Cardiovasc Interv 2009;2:284-90.
44. Klugherz BD, Llanos G, Lieuallen W, Kopia GA, Papandreou G, Narayan P *et al.* Twenty-eight-day efficacy and phamacokinetics of the sirolimus-eluting stent. Coron Artery Dis 2002;13:183-8.
45. Finn AV, Kolodgie FD, Harnek J, Guerrero LJ, Acampado E, Tefera K *et al.* Differential response of delayed healing and persistent inflammation at sites of overlapping sirolimus- or paclitaxel-eluting stents. Circulation 2005;112:270-8.
46. Joner M, Nakazawa G, Finn AV, Quee SC, Coleman L, Acampado E *et al.* Endothelial cell recovery between comparator polymer-based drug-eluting stents. J Am Coll Cardiol 2008;52:333-42.
47. Lim SY, Jeong MH, Hong SJ, Lim do S, Moon JY, Hong YJ *et al.* Inflammation and delayed endothelization with overlapping drug-eluting stents in a porcine model of in-stent restenosis. Circ J 2008;72:463-8.
48. Kotani J, Awata M, Nanto S, Uematsu M, Oshima F, Minamiguchi H *et al.* Incomplete neointimal coverage of sirolimus-eluting stents: angioscopic findings. J Am Coll Cardiol 2006;47:2108-11.
49. Awata M, Kotani J, Uematsu M, Morozumi T, Watanabe T, Onishi T *et al.* Serial angioscopic evidence of incomplete neointimal coverage after sirolimus-eluting stent implantation: comparison with bare-metal stents. Circulation 2007;116:910-6.
50. Awata M, Nanto S, Uematsu M, Morozumi T, Watanabe T, Onishi T *et al.* Heterogeneous arterial healing in patients following paclitaxel-eluting stent implantation: comparison with sirolimus-eluting stents. JACC Cardiovasc Interv 2009;2:453-8.
51. Awata M, Nanto S, Uematsu M, Morozumi T, Watanabe T, Onishi T *et al.* Angioscopic comparison of neointimal coverage between zotarolimus- and sirolimus-eluting stents. J Am Coll Cardiol 2008;52:789-90.
52. van Beusekom HM, Saia F, Zindler JD, Lemos PA, Swager-Ten Hoor SL, van Leeuwen MA *et al.* Drug-eluting stents show delayed healing: paclitaxel more pronounced than sirolimus. Eur Heart J. 2007;28:974-9.
53. Thollon C, Bidouard JP, Cambarrat C, Delescluse I, Villeneuve N, Vanhoutte PM *et al.* Alteration of endothelium-dependent hyperpolarizations in porcine coronary arteries with regenerated endothelium. Circ Res 1999;84:371-7.
54. Tiefenbacher CP. Tetrahydrobiopterin: a critical cofactor for eNOS and a strategy in the treatment of endothelial dysfunction? Am J Physiol Heart Circ Physiol 2001;280:H2484-8.
55. Tiefenbacher CP, Bleeke T, Vahl C, Amann K, Vogt A, Kubler W. Endothelial dysfunction of coronary resistance arteries is improved by tetrahydrobiopterin in atherosclerosis. Circulation 2000;102:2172-9.
56. Ota H, Eto M, Ako J, Ogawa S, Iijima K, Akishita M *et al.* Sirolimus and everolimus induce endothelial cellular senescence via sirtuin 1 down-regulation: therapeutic implication of cilostazol after drug-eluting stent implantation. J Am Coll Cardiol 2009;53:2298-305.
57. Newman PJ. The role of PECAM-1 in vascular cell biology. Ann N Y Acad Sci 1994;714:165-74.
58. Dusserre N, L'Heureux N, Bell KS, Stevens HY, Yeh J, Otte LA *et al.* PECAM-1 interacts with nitric oxide synthase in human endothelial cells: implication for flow-induced nitric oxide synthase activation. Arterioscler Thromb Vasc Biol 2004;24:1796-802.
59. Stevens HY, Melchior B, Bell KS, Yun S, Yeh JC, Frangos JA. PECAM-1 is a critical mediator of atherosclerosis. Dis Model Mech 2008;1(2-3):175-81;discussion 9.
60. Mannucci PM. von Willebrand factor: a marker of endothelial damage? Arterioscler Thromb Vasc Biol 1998;18:1359-62.
61. Spiel AO, Gilbert JC, Jilma B. von Willebrand factor in cardiovascular disease: focus on acute coronary syndromes. Circulation 2008;117:1449-59.
62. Giddings JC, Banning AP, Ralis H, Lewis MJ. Redistribution of von Willebrand factor in porcine carotid arteries after balloon angioplasty. Arterioscler Thromb Vasc Biol 1997;17:1872-8.
63. Esmon CT. The interactions between inflammation and coagulation. Br J Haematol 2005;131:417-30.
64. Zerwes HG, Risau W. Polarized secretion of a platelet-derived growth factor-like chemotactic factor by endothelial cells *in vitro*. J Cell Biol 1987;105:2037-41.
65. Silva GV, Fernandes MR, Madonna R, Clubb F, Oliveira E, Jimenez-Quevedo P *et al.* Comparative healing response after sirolimus- and paclitaxel-eluting stent implantation in a pig model of restenosis. Catheter Cardiovasc Interv 2009;73:801-8.
66. Van Der Giessen WJ, Sorop O, Krabbendam-Peters I, Onuma Y, van Beusekom HM. Drug Eluting Stents Do Not Delay Early Endothelialization But Show Distinct Differences In Endothelial Function. 81st Annual Scientific Session of the American-Heart-Association, Nov 08-12 2008. New Orleans, LA. S650-S1.
67. Hofma SH, Van der Giessen WJ, Van Dalen B, Lemos PA, Serruys PW. Prolonged endothelial dysfunction late after stenting with sirolimus-eluting stent compared to bare metal stent. ESC Congress 2004, Aug 28-Sep 01 2004. Munich, Germany.
68. Hofma SH, van der Giessen WJ, van Dalen BM, Lemos PA, McFadden EP, Sianos G *et al.* Indication of long-term endothelial dysfunction after sirolimus-eluting stent implantation. Eur Heart J 2006;27:166-70.
69. Togni M, Windecker S, Cocchia R, Wenaweser P, Cook S, Billinger M *et al.* Sirolimus-eluting stents associated with paradoxic coronary vasoconstriction. J Am Coll Cardiol 2005;46:231-6.

70. Fuke S, Maekawa K, Kawamoto K, Saito H, Sato T, Hioka T *et al.* Impaired endothelial vasomotor function after sirolimus-eluting stent implantation. Circ J 2007;71:220-5.
71. Togni M, Raber L, Cocchia R, Wenaweser P, Cook S, Windecker S *et al.* Local vascular dysfunction after coronary paclitaxel-eluting stent implantation. Int J Cardiol 2007;120:212-20.
72. Shin DI, Kim PJ, Seung KB, Kim DB, Kim MJ, Chang K *et al.* Drug-eluting stent implantation could be associated with long-term coronary endothelial dysfunction. Int Heart J 2007;48:553-67.
73. Kim JW, Suh SY, Choi CU, Na JO, Kim EJ, Rha SW *et al.* Six-month comparison of coronary endothelial dysfunction associated with sirolimus-eluting stent versus Paclitaxel-eluting stent. JACC Cardiovasc Interv 2008;1:65-71.
74. Hamilos MI, Ostojic M, Beleslin B, Sagic D, Mangovski L, Stojkovic S *et al.* Differential effects of drug-eluting stents on local endothelium-dependent coronary vasomotion. J Am Coll Cardiol 2008;51:2123-9.
75. Shin DI, Seung KB, Kim PJ, Chang K, Choi JK, Jeon DS *et al.* Long-term coronary endothelial function after zotarolimus-eluting stent implantation. A 9 month comparison between zotarolimus-eluting and sirolimus-eluting stents. Int Heart J 2008;49:639-52.
76. Kim JW, Seo HS, Park JH, Na JO, Choi CU, Lim HE *et al.* A prospective, randomized, 6-month comparison of the coronary vasomotor response associated with a zotarolimus- versus a sirolimus-eluting stent: differential recovery of coronary endothelial dysfunction. J Am Coll Cardiol 2009;53:1653-9.
77. Li J, Jabara R, Pendyala L, Otsuka Y, Shinke T, Hou D *et al.* Abnormal vasomotor function of porcine coronary arteries distal to sirolimus-eluting stents. JACC Cardiovasc Interv 2008;1:279-85.
78. Pendyala LK, Li J, Shinke T, Geva S, Yin X, Chen JP *et al.* Endothelium-dependent vasomotor dysfunction in pig coronary arteries with Paclitaxel-eluting stents is associated with inflammation and oxidative stress. JACC Cardiovasc Interv 2009;2:253-62.
79. van den Heuvel M, Sorop O, Batenburg WW, de Vries R, Koopmans SJ, van Beusekom HMM *et al.* Drug-Eluting Stents Chronically Impair Distal Microvascular Function. 12th Annual Transcatheter Cardiovascular Therapeutics Conference, Oct 12-17 2008. Washington, CA. 281-I.
80. Meier P, Zbinden R, Togni M, Wenaweser P, Windecker S, Meier B *et al.* Coronary collateral function long after drug-eluting stent implantation. J Am Coll Cardiol 2007;49:15-20.
81. Obata JE, Kitta Y, Takano H, Kodama Y, Nakamura T, Mende A *et al.* Sirolimus-eluting stent implantation aggravates endothelial vasomotor dysfunction in the infarct-related coronary artery in patients with acute myocardial infarction. J Am Coll Cardiol 2007;50: 1305-9.
82. Jabs A, Gobel S, Wenzel P, Kleschyov AL, Hortmann M, Oelze M *et al.* Sirolimus-induced vascular dysfunction. Increased mitochondrial and nicotinamide adenosine dinucleotide phosphate oxidase-dependent superoxide production and decreased vascular nitric oxide formation. J Am Coll Cardiol 2008;51:2130-8.
83. Cooke JP, Tsao PS. Is NO an endogenous antiatherogenic molecule? Arterioscler Thromb 1994;14:653-5.
84. Blum A, Schneider DJ, Sobel BE, Dauerman HL. Endothelial dysfunction and inflammation after percutaneous coronary intervention. Am J Cardiol 2004;94:1420-3.
85. Schachinger V, Britten MB, Zeiher AM. Prognostic impact of coronary vasodilator dysfunction on adverse long-term outcome of coronary heart disease. Circulation 2000;101:1899-906.
86. Zeiher AM, Krause T, Schachinger V, Minners J, Moser E. Impaired endothelium-dependent vasodilation of coronary resistance vessels is associated with exercise-induced myocardial ischemia. Circulation 1995;91:2345-52.
87. Mancini GB, Henry GC, Macaya C, O'Neill BJ, Pucillo AL, Carere RG *et al.* Angiotensin-converting enzyme inhibition with quinapril improves endothelial vasomotor dysfunction in patients with coronary artery disease. The TREND (Trial on Reversing ENdothelial Dysfunction) Study. Circulation 1996;94:258-65.
88. Koh KK, Quon MJ, Lee Y, Han SH, Ahn JY, Chung WJ *et al.* Additive beneficial cardiovascular and metabolic effects of combination therapy with ramipril and candesartan in hypertensive patients. Eur Heart J 2007;28:1440-7.
89. Tzemos N, Lim PO, MacDonald TM. Nebivolol reverses endothelial dysfunction in essential hypertension: a randomized, double-blind, crossover study. Circulation 2001;104:511-4.
90. Wassmann S, Laufs U, Baumer AT, Muller K, Ahlbory K, Linz W *et al.* HMG-CoA reductase inhibitors improve endothelial dysfunction in normocholesterolemic hypertension via reduced production of reactive oxygen species. Hypertension 2001;37:1450-7.
91. Koh KK, Han SH, Quon MJ, Yeal Ahn J, Shin EK. Beneficial effects of fenofibrate to improve endothelial dysfunction and raise adiponectin levels in patients with primary hypertriglyceridemia. Diabetes Care 2005;28:1419-24.
92. van Beusekom H, Sorop O, Weymaere M, Duncker D, van der Giessen W. The neointimal response to stents eluting tacrolimus from a degradable coating depends on the balance between polymer degradation and drug release. EuroIntervention 2008;4:139-47.
93. Onuma Y, Serruys P, den Heijer P, Joesoef KS, Duckers H, Regar E *et al.* MAHORORBA, first-in-man study: 6-month results of a biodegradable polymer sustained release tacrolimus-eluting stent in de novo coronary stenoses. Eur Heart J 2009;30:1477-85.
94. Serruys PW, Ormiston JA, Onuma Y, Regar E, Gonzalo N, Garcia-Garcia HM *et al.* A bioabsorbable everolimus-eluting coronary stent system (ABSORB): 2-year outcomes and results from multiple imaging methods. Lancet 2009;373:897-910.

Endothelial function rather than endothelial restoration is altered in paclitaxel- as compared to bare metal-, sirolimus- and tacrolimus-eluting stents

van Beusekom H.M., Sorop O., van den Heuvel M., Onuma Y., Duncker D.J., Danser A.H. and van der Giessen W.J.

EuroIntervention. 2010 May;6(1):117-25

10

Endothelial function rather than endothelial restoration is altered in paclitaxel- as compared to bare metal-, sirolimus- and tacrolimus-eluting stents

Heleen M.M. van Beusekom[1*], PhD; Oana Sorop[1], PhD; Mieke van den Heuvel[1,2], MD, MSc; Yoshinobu Onuma[1], MD; Dirk J. Duncker[1], MD, PhD; A.H. Jan Danser[2], PhD; Willem J. van der Giessen[1,3], MD, PhD

[1] Department of Cardiology, Erasmus MC, Rotterdam, The Netherlands; [2] Division of Pharmacology, Vascular and Metabolic Diseases, Department of Internal Medicine, Erasmus MC, Rotterdam, The Netherlands; [3] Interuniversity Cardiology Institute of the Netherlands, ICIN-KNAW, Utrecht, The Netherland

KEYWORDS
Tacrolimus-, sirolimus-, paclitaxel-, drug-eluting stents, delayed healing, neointima, stent thrombosis, endothelium, microcirculation, nitric oxide

Abstract

Aims: Drug eluting stents (DES) are under scrutiny for late stent thrombosis. Impaired re-endothelialisation is proposed as an explanation but coronary and peripheral-artery models disagree. We assessed physical and functional endothelial restoration within bare (BMS), paclitaxel, sirolimus and tacrolimus eluting stents and the distal microvasculature in porcine coronary arteries.

Methods and results: Endothelium within and distal to DES and BMS was assessed for stent-strut endothelial-restoration (five days) and endothelial-function (five, 28 days, by eNOS and vWF expression) and by *in vitro* microvascular function. There were no significant differences (P=0.3) in stent strut endothelial-restoration at five days between DES (76-90%) and BMS (95%). However, the microvasculature distal to PES showed a decreased NO bioavailability at five days, which improved at 28 days. Within the stent, however, PES still showed a reduced eNOS expression at 28 days ($P \leq 0.002$).

Conclusions: DES in porcine coronary arteries show no significant early differences in re-endothelialisation as compared to BMS. However, PES did affect endothelial function both within and distal to stents. These results extend the concept of delayed healing in DES to include delayed restoration of function rather than endothelial presence as a possible explanation for late unwanted sequelae. Microvascular dysfunction does not predict in-stent delayed endothelialisation in this model.

** Corresponding author: Department of Cardiology, Ee 2355a; Erasmus MC Rotterdam, Gravendijkwal 320, 3015 CE Rotterdam, The Netherlands*
E-mail: h.vanbeusekom@erasmusmc.nl

Introduction

Sirolimus-eluting stents (SES) and paclitaxel-eluting stents (PES) have markedly reduced the rate of in-stent restenosis and late lumen loss compared to bare-metal stents (BMS), resulting in a significantly reduced need for repeat revascularisations.[1-3] Enthusiasm for this technology has been dampened by concerns about late thrombosis, an event often with serious clinical consequences.[4,5] Aside from rarely occurring delayed hypersensitivity to DES constituents, impaired re-endothelialisation has been suggested as the likely cause of late DES thrombosis based on one clinical autopsy study[6] and experimental overlapping DES implantation in denuded and injured rabbit peripheral arteries.[7,8] Although data from denudation and overlap models cannot be dismissed, they do not represent the full spectrum of the clinical arena. Indeed, there is consistent evidence pointing towards late endothelial dysfunction as the main derangement after DES. This was shown both experimentally and clinically as impaired responses to endothelial dependent vasodilators or exercise.[9-11]

Combining assessment of in-stent re-endothelialisation with endothelial-function of the newly formed neointima and distal vasculature has not been reported. This combined assessment is important as altered endothelial-function could be the result of both dysfunction as well as absence of endothelium. Discriminating between these two is, however, difficult to do in patients and a correlation between these two parameters might theoretically be a diagnostic tool for endothelium within the stent.

Predicting which animal model mimics the human situation the closest, is difficult and may well differ between drugs due to species differences in sensitivity. Even the choice for healthy, injured or atherosclerotic models will affect outcome. While in atherosclerosis general endothelial-function may be affected, there is no indication it delays endothelial-regrowth.[12,13] We therefore studied the effects of three distinctively different DES on early endothelial-regrowth (five-days follow-up) as well as early and late endothelial-function (five and 28 days follow-up) both with the stent and in the distal coronary microvasculature (i.e., not the epicardial coronary artery) in normal, non-atherosclerotic swine.

Materials and methods

Stents

Four different stent types with a length of 12-13 mm (diameter 3.0 and 3.5 mm) were studied: 1) 15 bare metal controls (BMS, Kaneka corporation, Osaka, Japan), 2) 25 tacrolimus eluting stents (TES, 0.9 μg/mm^2, Kaneka corporation, Osaka, Japan) 3) 25 sirolimus eluting stents (SES, 1.4 μg/mm^2, Cordis, Johnson & Johnson, Warren, NJ, USA) and 4) 25 Paclitaxel eluting stents (PES, 1 μg/mm^2, Boston Scientific, Natick, MA, USA).

Polymers

The TES coating consists of a fully degradable polylactide-polyglycolide polymer (PLGA), with a degradation rate ≥90 days.[14,15] SES is coated with biostable poly-ethylene-vinyl-acetate-poly-butylene-methyl-acetylate (PEVA-PBMA), PES is coated with a biostable styrene-b-isobutylene-b-styrene (SIBS).[16]

Drugs

The intracellular receptors of tacrolimus are the FK binding proteins (FKBP, including FKBP12). The tacrolimus-FKBP complex binds to the calcineurin-calmodulin complex.[17] Tacrolimus effects on endothelium includes inhibition of expression of endothelial adhesion molecules, and reduction of free radical and inflammatory cytokine release.[18,19] Sirolimus also binds to FKBP12, but the Sirolimus-FKBP complex then inhibits mTOR[20], halting cell cycle progression from G1 to S, as well as vascular cell migration. Paclitaxel inhibits depolymerisation of tubulin, thereby arresting cellular replication and inhibiting migration of vascular smooth muscle cells.[21,22]

Animals and preparation

Experiments and animal preparation were performed in farm-bred swine (Yorkshire-Landrace, 30-35 kg) as previously described.[23,24] The study was approved by the animal ethics committee of the Erasmus University, Rotterdam and complied with the "Guide for the care and use of laboratory animals" (NIH publication 85-23). In short, animals were pretreated with 300 mg acetyl salicylic acid (ASA) and a loading dose of 300 mg of clopidogrel (Plavix; Sanofi Aventis, Gouda, The Netherlands) one day prior to the procedure. After induction of anaesthesia and connection to the ventilator, antibiotic prophylaxis was administered by an intramuscular injection of streptomycin, penicillin procaine (0.1 mg/kg). An introducer sheath was placed in the carotid artery for arterial access. A dose of 250 mg ASA and 10.000 i.u. heparin was administered (i.a.).

Stent implantation and angiography

Stent implantation was performed as described before.[23,24] Under guidance of quantitative angiography (QCA, CAAS II; PIE Medical, Maastricht, The Netherlands), arterial segments of 2.5-3.2 mm in diameter were selected in each of the coronary arteries. Stents were placed with a balloon-artery (B/A) ratio of 1.1 without prior injury. Animals received one stent per coronary artery, according to a predetermined randomisation scheme for stent type. After the final angiogram, animals were allowed to recover from anaesthesia and returned to animal care facilities for postoperative recovery. During follow-up, 300 mg ASA and 75 mg clopidogrel were administered daily. Only in swine followed for 28 days, follow-up angiography was planned prior to euthanasia. This was omitted for the five day group to prevent catheter induced injury.

Tissue harvesting

Animals were euthanised by an overdose of pentobarbital. Hearts were pressure fixed in situ in preparation for histology.[24] In case of *in vitro* vasomotor tone experiments, fixation was preceded by excision of small myocardial samples from the distal perfusion area of the stent for the isolation of the vessels (Table 1).

Endpoints

Completeness of the endothelial layer by scanning electron microscopy (SEM) and endothelial function by eNOS- and vWF-expression were studied at five days. Endothelial presence, histology and endothelial eNOS- and vWF-expression were studied

Table 1. Angiographic parameters measured by QCA at implantation and follow-up. No differences were seen in vascular diameters pre- or post-implantation, balloon/artery ratio or acute gain between groups at either follow-up pointS Late loss was however increased in SES at 28 days as compared to TES and PES (*P=0.02).

	BMS	TES		SES		PES	
	5 days N=15 I; S; F	5 days N=13 I; S; F	28 days N=12 I; F	5 days N=14 I; S; F	28 days N=11 I; F	5 days N=13 I; S; F	28 days N=12 I; F
Diam. pre. (mm)	2.94±0.25	2.89±0.22	3.00±0.27	2.94±0.25	2.83±0.23	3.00±0.27	2.90±0.14
Diam. post. mm)	3.05±0.27	3.09±0.25	3.11±0.24	3.09±0.23	2.98±0.31	3.20±0.29	2.99±0.20
Acute gain	0.11±0.12	0.18±0.08	0.11±0.08	0.15±0.08	0.16±0.11	0.16±0.07	0.12±0.06
B/A ratio	1.08±0.05	1.12±0.06	1.12±0.04	1.09±0.06	1.14±0.04	1.10±0.02	1.12±0.06
Late Loss	n.d.	n.d.	0.30±0.22	n.d.	0.45±0.40*	n.d.	0.17±0.08

TES: tacrolimus-eluting stent; SES: sirolimus-eluting stent, PES: paclitaxel-eluting stent. S: indicates in which groups SEM was performed for assessment of re-endothelialisation; I: immunocytochemistry (eNOS and vWF); F: *in vitro* microvascular function experiments; n.d.: not determined

by light microscopy at 28 days. In a subset of the animals (Figure 4), distal vasomotor tone was assessed by *in vitro* functional tests at five and 28 days.

Scanning electron microscopy

After fixation with 2.5% glutaraldehyde in 0.15 mol/l cacodylate buffer, the arteries were further processed as previously described.[25] From photographs, the stent struts were traced, the endothelium marked, and the percentage endothelial coverage of the stent struts quantified using computer assisted planimetry, (Clemex vision PE; Clemex Technologies Inc., Longueuil, Canada).

Histology

The arteries were processed for plastic embedding.[23,26] Sections were collected at three levels (proximal, mid and distal) of the stented segments. The sections were stained with haematoxylin-eosin and resorcin-fuchsin (elastin stain) for quantitative and qualitative analysis.

Morphometry

Analysis of neointima and injury was performed as described before[25]. As at 5-days all stents were covered by thrombus and granulation tissue containing inflammatory cells, inflammatory scores were only determined at 28 days, on HE stained sections, and given as the ratio of inflamed over total number of struts at each level (proximal, mid and distal) and averaged per stent.

Immunocytochemistry

The complete circumference of the stented vascular segment was assessed semi-quantitatively for eNOS (sc-654; Santa Cruz Biotechnology, Inc., Santa Cruz, CA, USA) and von Willebrand Factor (vWF) (A0082; DakoCytomation, Copenhagen, Denmark). Scores were assigned as: 0=0% positive circumference, 1=0-10%, 2=10-40%, 3=40-70%, 4=70-90%, 5=90-100%.

In vitro microvascular function

Upon sacrifice, microvascular coronary arteries (~300 µm diameter) were dissected free from the myocardial tissue in the perfusion territory of the stent. Experiments were performed as previously described.[27-29]

In brief the arteries were cut into segments of ~2 mm length and mounted in a Mulvany wire myograph (DMT A/S, Aarhus, Denmark). Following 30-minutes stabilisation, the optimal internal diameter was set to a tension equivalent of 0.9 times the estimated diameter at 100 mmHg effective transmural pressure.[30] Vascular responses were measured as changes in isometric force. Segments from the same vessel were randomly assigned to a different experimental protocol, such that in each perfusion territory all measurements were performed. After stabilisation, the vessel segments were exposed to 100 mM KCl to determine the maximal contractile response to KCl. Upon wash-out of KCl, the segments were allowed to equilibrate for 30 minutes. The endothelium-dependent relaxation to bradykinin (10^{-10}-10^{-6} M) and endothelium-independent relaxation to the exogenous nitric oxide (NO) donor, S-nitroso-N-acetylpenicillamine (SNAP, 10^{-7}-10^{-6} M) was recorded upon preconstriction with the thromboxane analog U46619 (1nM). In order to test the contribution of NO-mediated mechanism to the bradykinin-induced relaxation, the concentration–response curve for bradykinin was constructed after 30 min. incubation with the eNOS inhibitor N-Nitro-L-Arginine methyl ester (L-NAME, 10^{-4} M), in a separate set of vessels. Data of six historic control vessels from two animals receiving a BMS for 28 days were used for comparison in the vascular function study.

Statistical analysis

All data are given as mean ±SD except for *in vitro* microvascular function which is given as mean ±SEM. Histology and QCA were analysed with SPSS version 16, (SPSS Inc., Chicago, IL, USA). Intergroup differences were assessed using one-way ANOVA followed by post-hoc analysis with a Bonferroni correction in case of statistical significance. $P<0.05$ was considered statistically significant. *In vitro* relaxant responses to bradykinin and SNAP are expressed as a percentage of the contraction to U46619 and were analysed using Stat View (version 5.1). Statistical significance was established by a two-way ANOVA followed by post-hoc analysis with a Bonferroni correction in case of statistical significance. $P<0.05$ was considered statistically significant. Further testing was performed using linear regression analysis (SPSS). For QCA the main model parameters consisted of follow-up time, balloon-artery

ratio and stent type. For morphometry and immunocytochemistry the model parameters also included the morphologic injury score and inflammation score. For SEM analysis the model parameters were procedural characteristics (B/A ratio, acute gain) and stent characteristics (drug, design, metal to surface ratio, strut width).

Results

Quantitative angiography showed no differences in diameters between pre- or post-implantation or stent/artery at either follow-up time (Table 1). Late loss at 28 days was not different between TES (0.3±0.2) and PES (0.2±0.1), only SES showed a significant late lumen loss (0.5±0.4 mm, p=0.02 versus PES by ANOVA), as a result of inflammation. Regression analysis did not yield a significant predictive model (ANOVA p=0.6).

Scanning electron microscopy

Data (Table 2), indicate that as early as 5-days the stent struts were covered with endothelium to a large extent. There were no significant differences in re-endothelialisation between DES and BMS (one way ANOVA p=0.3) (Figure 1), indicating that the drugs did not inhibit re-endothelialisation. Regression analysis (ANOVA p=0.02) confirmed that the drug did not predict re-endothelialisation. Only stent-artery ratio (p=0.03), stent design (p=0.02) and metal to surface ratio (p=0.02) were independent predictors of re-endothelialisation. The predictive value of the model was, however, rather low (r^2=0.4).

Table 2. Quantitative scanning electron microscopy: percentage endothelium covering the stent struts at five days. ANOVA showed no significant differences between the groups.

	% endothelial coverage ± SD
BMS (n=11)	95.5 ± 6.4
TES (n=10)	82.6 ± 13.2
SES (n=9)	89.7 ± 14.3
PES (n=11)	76.3 ± 26.7

BMS: bare-metal stent; TES: tacrolimus-eluting stent; SES: sirolimus-eluting stent; PES: paclitaxel-eluting stent

Histology

At 5-days all stents showed immature granulation tissue in varying stages of development (Figure 2). Consistent with SEM, stent struts were already endothelialised to a large extent. Lack of endothelium often coincided with presence of macrophage giant cells. Leukocytes were often found adhering to the endothelium. In general, TES showed a response similar to BMS. This granulation tissue was more mature in terms of inflammation and colonisation with smooth muscle (SMC)-like cells than in PES, while SES generally showed the most immature healing response.

At 28 days re-endothelialisation was virtually complete in all groups, and in general the neointima showed a mature and organised appearance (Figure 3). Each drug, however, had a specific appearance: PES showed apoptotic cells and mitotic figures in both neointima and media. SES showed luminal and adventitial

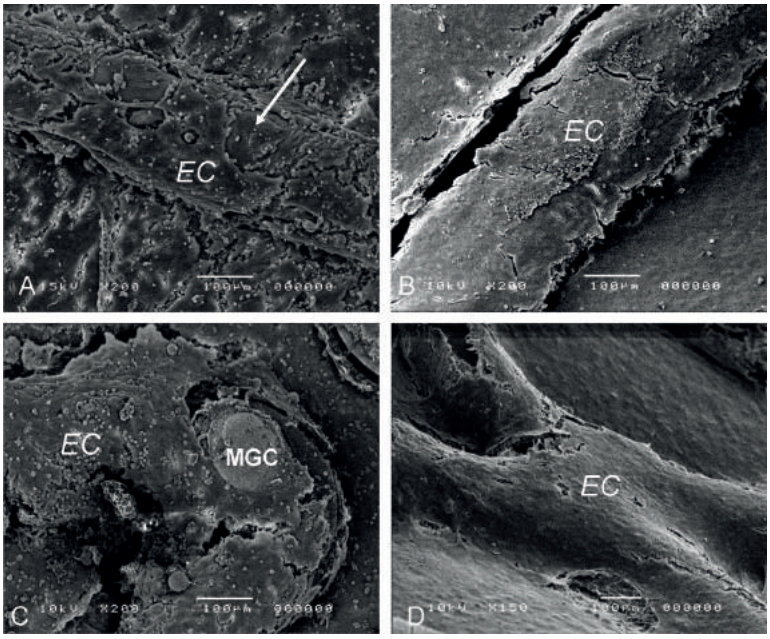

Figure 1. Scanning EM of the endothelial layer overlying stent struts in Bare (A), TES (B), SES (C) and PES (D), showing extensive endothelial (EC) coverage of the struts. Areas devoid of EC (arrow) often show presence of macrophage giant cells (MGC).

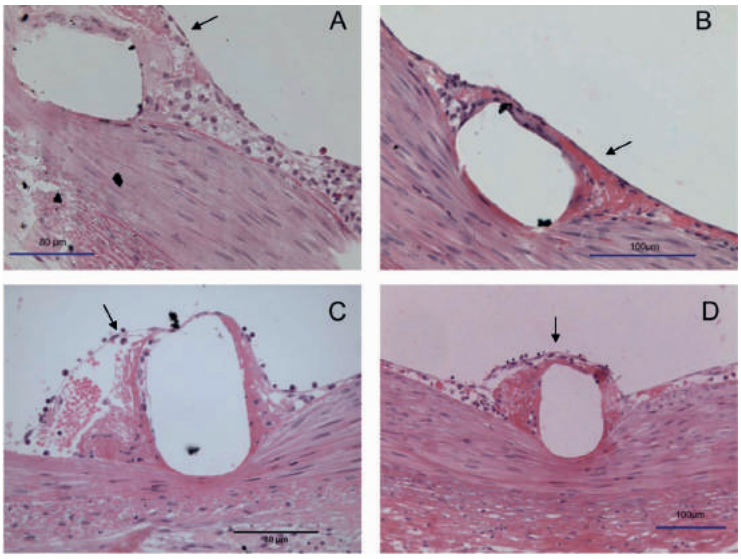

Figure 2. Light microscopy images of stent struts covered with immature granulation tissue showing scarce cellular infiltration and loose endothelium (arrows) at 5-days following implantation of BMS (A), TES (B), SES (C) and PES (D).

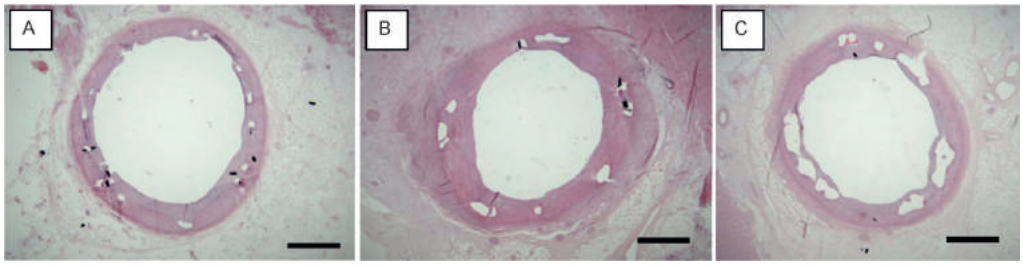

Figure 3. Three examples of coronary arteries at 28-days following stenting with TES (A), SES (B) and PES (C), showing complete coverage with an endothelialised fibrocellular neointimal thickening. HE-stain. Bar=1000 µm

eosinophilic granulocytes and abundant fibrinoid in the intima-media border zone. TES showed acidic proteins in the intima-media border zone, possibly proteoglycans.

Morphometry

Data is summarised in Table 3. At 5-days, all stents tend to show thrombus being incorporated and cleared by granulation tissue. The damage to the tissue induced by histological sectioning overlying the struts was however too great to yield reliable quantitative data and morphometry of the intima was not performed. At 28-days, SES induced a considerable inflammatory response in a number of animals which increased intimal thickening considerably. We therefore compared the results also in the SES subgroup without inflammation. This showed that neointima thickness (NIT) was not

Table 3. Morphometric analysis: thickness of neointima, media and adventitia was measured at 28 days on elastin-stained sections taken from the proximal, medial, and distal region of the stent.

	Injury score	Inflammation score	Mitotic figures (%)	NIT (µm)	NIT without inflamm. (µm)	Media (µm)	Adventitia (µm)
TES (n=12)	0.26±0.17 *	0*	0.01±0.02*	248±43	248±43	122±29	140±30
SES (n=11)	0.95±0.76	0.46±0.47	n.a.	435±216*	259±43	72±38*	327±228
PES (n=12)	0.16±0.18¶	0.04±0.11¶	0.12±0.14	258±42	267±38	118±66	159±54
ANOVA p-values	*0.005 and ¶0.001 vs SES	*0.001 and ¶0.003 vs SES	*0.03 vs. PES	*0.004 and 0.003 vs. TES, PES		*0.07 vs PES and TES	

TES: tacrolimus-eluting stent; SES: sirolimus-eluting stent; PES: paclitaxel-eluting stent; NI: neointima thickness

significantly different between the groups upon exclusion of stents with severe inflammation. Injury and inflammation score, when analysed separately as model parameters in regression analysis, were both strong predictors of NIT (p<0.0001). However, when used simultaneously they were not independent. Endothelial-function (eNOS, vWF) was not an independent predictor of NIT.

Immunocytochemistry

This data is summarised in Table 4. At 5-days all DES contained eNOS positive endothelium (Figure 4). The damage to the tissue overlying the struts was however too large to yield reliable quantitative data. At 28 days regression analysis of eNOS expression (ANOVA p=0.001, R^2=0.6) indicated that eNOS expression was significantly less in PES as compared to TES and SES (See Table 4, p<0.002). Inflammation had no effect on eNOS expression (p=0.18), only injury score was an independent negative predictor of eNOS expression (p=0.006). In all groups, the number of cells expressing vWF was very low (score ~1-1.3), showing no significant differences between groups.

Table 4. Semi-quantitative analysis of immunocytochemical staining for eNOS and vWF at 28 days. A score of 0 designates 0%, 1=<10%, 2=10-40%, 3=40-70%, 4=70-90%, 5=90-100%.

	eNOS	vWF
TES (n=8+6)	4.50±0.5¶	1.17±0.4
SES (n=8+7)	4.00±0.9‡	1.29±0.5
PES (n=8+8)	3.25±0.5	1.25±0.5

ANOVA, ¶p=0.00002 and ‡p=0.002 vs PES; TES: tacrolimus-eluting stent; SES: sirolimus-eluting stent; PES: paclitaxel-eluting stent; eNOS: endothelial nitric oxide synthase; vWF: von Willebrand factor

In vitro vasomotor tone

Data show that bradykinin induced similar levels of endothelium-dependent vasodilation in the microvasculature, independent of stent type and follow-up time. Therefore the five and 28 day data on control bradykinin responses were pooled (Figure 5A). Distal to BMS, TES and SES, eNOS-blockade resulted in a significant impairment in bradykinin-induced dilation both at five and 28 days (Figures 5B, C). In the PES area, however, at 5 days L-NAME had little effect on the dilation indicating a reduced contribution of NO to this response (Figure 5B). This lack of NO-bioavailability was not correlated to re-endothelialisation within that stented segment

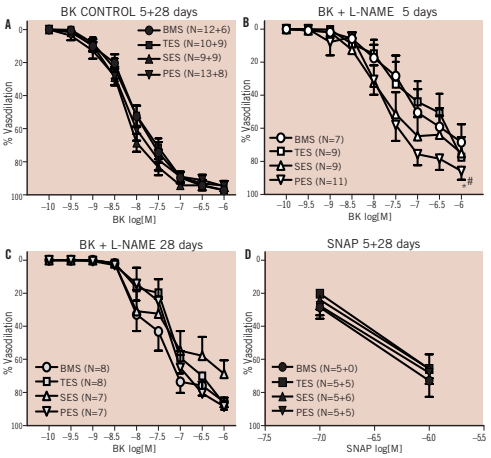

*Figure 5. Endothelial-dependent dilation to bradykinin and –independemt to SNAP in small coronary arteries distal to BMS, TES, SES and PES. No difference was seen between control curves at 5 and 28 days, therefore, data were pooled (Fig. 5A). eNOS blockade by L-NAME resulted in a significant reduction in BK-induced dilation. However, at 5 days, the effect of eNOS blockade was impaired distal to PES (Fig. 5B, * P<0.05 vs BMS, # P<0.05 vs TES) as compared to the other stents. No difference was seen between stents at 28 days (Fig. 5C). No difference was seen in SNAP responses at 5 or 28 days (5D).*

(Regression analysis, ANOVA p=0.4). The NO contribution did recover at 28 days (Figure 5C). Endothelial-independent dilation to SNAP was similar for all stents and follow-up times (Figure 5D).

Discussion

We set out to assess differences in re-endothelialisation and endothelial function after implantation of TES, SES, PES and BMS in normal swine coronary arteries. We found that DES demonstrated 76-95% in-stent endothelialisation at five days after implantation. This was not statistically different from BMS. In-stent endothelial function as assessed by eNOS expression, was already demonstrable at 5-days, and almost complete for TES and SES at 28 days after implantation. PES, however, showed a significantly reduced in-stent eNOS expression at 28 days. Consistent with this

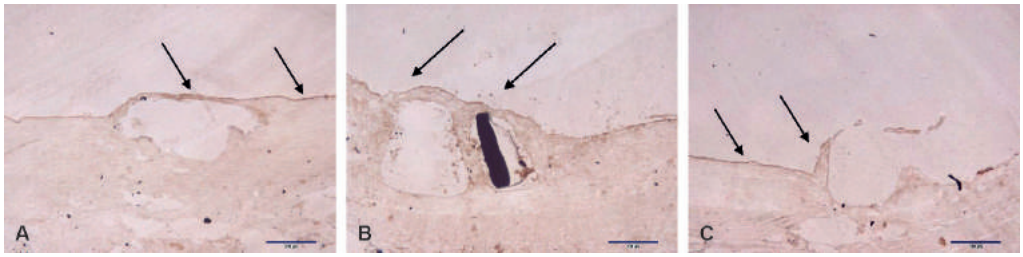

Figure 4. eNOS staining of porcine coronary arteries at 5-days following stenting with a TES-(A), SES (B), and PES (C) stent. The brown staining, both on the stent struts and between the stent struts, denotes eNOS positivity (arrows).

finding we demonstrated a transient impairment in the NO contribution to endothelial-dependent relaxation in the microcirculation distal to PES, suggesting abnormal functioning eNOS, which was not correlated to re-endothelialisation.

The current study demonstrates that the functional impairment of the endothelium can be shown even in presence of apparent structural integrity. This finding does not automatically allow to dismiss the idea that in atherosclerotic arteries there can be instances where the endothelial regrowth is incomplete following DES placement. The clinical sequelae of DES are probably resulting in individual cases from either structural or functional compromise of cellular coverage, or both acting in concert in some other cases.

Re-endothelialisation

The current view is that DES impair re-endothelialisation, supported by data from a single institution reporting one human autopsy study (coronary), and non-coronary DES implantation in rabbit iliac arteries.[6-8] Clinical angioscopy and OCT studies imaging DES also suggest delayed endothelialisation[31-34]. But because the resolution of angioscopy and OCT are insufficient to detect endothelium on stents, we regard those studies as not contributing to the evidence. Our results do not support the concept of delayed endothelialisation as we show no significant difference in re-endothelialisation between DES and BMS as early as five days. This is compatible with previous animal studies. In a study by Klugherz et al in a rabbit iliac artery model, no evidence of delayed endothelialisation was noted with 28-day SES compared with polymer-coated stents or BMS.[35] In addition, in SES and PES a similar degree of re-endothelialisation (>75%) was reported in porcine coronary models[36-38]. Thus, overall, the support for the delayed re-endothelialisation concept is equivocal.

Factors influencing endothelialisation

In order to assess the influence of stent and experimental conditions on re-endothelialisation, we performed regression analysis with stent characteristics (design, drug, strut width, metal to surface ratio) and implantation characteristics (balloon-artery ratio and acute gain) as model parameters. Design, metal to surface ratio, and balloon-artery ratio were independent predictors, while drug, strut width and acute gain were not. However, the predictive value of the model was rather low (R^2=0.4), suggesting that other factors, like the kinetics of drug elution and retention in the vascular wall should be examined in order to fully explain the data. There was no significant correlation between in-stent re-endothelialisation and distal microvascular dysfunction.

A recent study indicates that in rabbits, DES do inhibit re-endothelialisation in previously denuded and injured peripheral arteries at "early' time points (14 days).[8] A comparison with previous data from the same group indicates that endothelial regrowth at 28 days varies considerably for some (but not all) drugs and may be subject to experimental conditions.[7] In addition, a rabbit is much smaller than a swine or a human, and there are large species differences of drug stability in plasma and cellular sensitivity in culture.[39-41] Therefore, predicting which animal model mimics closest the human situation is difficult and may well differ between drugs.

Endothelial function

While a large percentage of endothelial coverage at early stages is considered important by many, it should be clear that this does not guarantee full functional integrity of the endothelium.[24] In a similar regression model as described above, in-stent eNOS expression was negatively predicted by morphologic injury score (acute implantation damage in combination with chronic irritation by the stent) while inflammation was not an independent predictor, nor any angiographic parameter, indicating that chronic vascular damage plays an important role in the functionality of the endothelial layer after stenting. The reduced in-stent eNOS expression observed in our study in PES at 28 days, when the stent is almost completely re-endothelialised, shows that presence of endothelium is not synonymous to endothelial-function. Indeed, late in-stent endothelial dysfunction may lead to increased platelet and leukocyte adhesion which could be one of the possible mechanisms responsible for the increased risk for late stent thrombosis reported in patients receiving PES.[42,43]

Microvascular vasomotor function

It has been shown clinically that DES affect vascular function immediately distal to stents[9,10,44]. Our *in vitro* data indicate that early following stent implantation, these effects extend also into the distal microvasculature. We used bradykinin, a clinically relevant agent[45] as an alternative to acetylcholine as porcine coronary arteries have limited presence of muscarinic receptors and acetylcholine therefore does not induce sufficient vasodilation[46-48]. In the small vessels distal to PES we found a significant reduction of the NO contribution to the bradykinin-induced dilation at 5-days follow-up. This was not due to a reduced smooth muscle cells sensitivity to NO, as the response to the exogenous NO donor SNAP remained unchanged. In healthy porcine coronary arteries bradykinin-induced dilation is mediated only by NO or EDHF (endothelium-derived hyperpolarising factor)[28]. Our data do indicate that EDHF fully compensated for the reduced NO production in PES. Interestingly in-stent re-endothelialisation in PES was not correlated to distal microvascular dysfunction in PES, nor any other parameter studied in regression analysis. It is unclear what is needed to predict microvascular dysfunction.

Although PES still showed a reduced in-stent eNOS expression at 28 days, no overt endothelial dysfunction was seen in the distal microvasculature at this time. Thus distal endothelial NO production appeared to recover faster than within the stent itself. Our *in vitro* observations are consistent with Togni[44] who also showed an improvement in endothelial function over time following PES implantation in patients.

Conclusion

In this study, all DES and BMS showed similar early re-endothelialisation. While PES showed a significant effect on endothelial function both within the stent as well as in the distal microvasculature, we did not find a correlation between the two phenomena. These results extend the concept of delayed healing in DES to include delayed restoration of function as a possible explanation for late unwanted sequelae. Microvascular dysfunction does not predict in-stent delayed endothelialisation in this model.

Acknowledgements

The technical assistance of I. Krabbendam-Peters, BSc; S.C. Krabbendam, BSc is gratefully acknowledged.

References

1. Morice MC, Serruys PW, Sousa JE, Fajadet J, Ban Hayashi E, Perin M, Colombo A, Schuler G, Barragan P, Guagliumi G, Molnar F, Falotico R. A randomized comparison of a sirolimus-eluting stent with a standard stent for coronary revascularization. *N Engl J Med.* 2002;346:1773-1780.

2. Moses JW, Leon MB, Popma JJ, Fitzgerald PJ, Holmes DR, O'Shaughnessy C, Caputo RP, Kereiakes DJ, Williams DO, Teirstein PS, Jaeger JL, Kuntz RE. Sirolimus-eluting stents versus standard stents in patients with stenosis in a native coronary artery. *N Engl J Med.* 2003;349:1315-1323.

3. Park SJ, Shim WH, Ho DS, Raizner AE, Park SW, Hong MK, Lee CW, Choi D, Jang Y, Lam R, Weissman NJ, Mintz GS. A paclitaxel-eluting stent for the prevention of coronary restenosis. *N Engl J Med.* 2003;348:1537-1545.

4. McFadden EP, Stabile E, Regar E, Cheneau E, Ong AT, Kinnaird T, Suddath WO, Weissman NJ, Torguson R, Kent KM, Pichard AD, Satler LF, Waksman R, Serruys PW. Late thrombosis in drug-eluting coronary stents after discontinuation of antiplatelet therapy. *Lancet.* 2004;364:1519-1521.

5. Ong AT, McFadden EP, Regar E, de Jaegere PP, van Domburg RT, Serruys PW. Late angiographic stent thrombosis (LAST) events with drug-eluting stents. *J Am Coll Cardiol.* 2005;45:2088-2092.

6. Finn AV, Joner M, Nakazawa G, Kolodgie F, Newell J, John MC, Gold HK, Virmani R. Pathological correlates of late drug-eluting stent thrombosis: strut coverage as a marker of endothelialization. *Circulation.* 2007;115:2435-2441.

7. Finn AV, Kolodgie FD, Harnek J, Guerrero LJ, Acampado E, Tefera K, Skorija K, Weber DK, Gold HK, Virmani R. Differential response of delayed healing and persistent inflammation at sites of overlapping sirolimus- or paclitaxel-eluting stents. *Circulation.* 2005;112:270-278.

8. Joner M, Nakazawa G, Finn AV, Quee SC, Coleman L, Acampado E, Wilson PS, Skorija K, Cheng Q, Xu X, Gold HK, Kolodgie FD, Virmani R. Endothelial cell recovery between comparator polymer-based drug-eluting stents. *J Am Coll Cardiol.* 2008;52:333-342.

9. Togni M, Windecker S, Cocchia R, Wenaweser P, Cook S, Billinger M, Meier B, Hess OM. Sirolimus-eluting stents associated with paradoxic coronary vasoconstriction. *J Am Coll Cardiol.* 2005;46:231-236.

10. Hofma SH, van der Giessen WJ, van Dalen BM, Lemos PA, McFadden EP, Sianos G, Ligthart JM, van Essen D, de Feyter PJ, Serruys PW. Indication of long-term endothelial dysfunction after sirolimus-eluting stent implantation. *Eur Heart J.* 2006;27:166-170.

11. Shin DI, Kim PJ, Seung KB, Kim DB, Kim MJ, Chang K, Lim SM, Jeon DS, Chung WS, Baek SH, Lee MY. Drug-eluting stent implantation could be associated with long-term coronary endothelial dysfunction. *Int Heart J.* 2007;48:553-567.

12. Walker LN, Bowyer DE. Endothelial healing in the rabbit aorta and the effect of risk factors for atherosclerosis. Hypercholesterolemia. *Arteriosclerosis* 1984;4:479-488.

13. Prescott MF, Muller KR. Endothelial regeneration in hypertensive and genetically hypercholesterolemic rats. *Arteriosclerosis* 1983;3:206-214.

14. van Beusekom H, Sorop O, Weymaere M, Duncker D, van der Giessen W. The neointimal response to stents eluting tacrolimus from a degradable coating depends on the balance between polymer degradation and drug release. *EuroIntervention.* 2008;4:139-147.

15. Tanimoto S, van der Giessen WJ, van Beusekom HMM, Sorop O, Kukreja N, Fukaya T, Nishide T, Nakano R, Maeda H, Serruys PWS. MAHOROBA: Tacrolimus eluting coronary stent. *EuroIntervention.* 2007:149-153.

16. Commandeur S, van Beusekom HM, van der Giessen WJ. Polymers, drug release, and drug-eluting stents. *J Interv Cardiol.* 2006;19:500-506.

17. Ho S, Clipstone N, Timmermann L, Northrop J, Graef I, Fiorentino D, Nourse J, Crabtree GR. The mechanism of action of cyclosporin A and FK506. *Clin Immunol Immunopathol.* 1996;80:S40-45.

18. St Peter SD, Moss AA, Mulligan DC. Effects of tacrolimus on ischemia-reperfusion injury. *Liver Transpl.* 2003;9:105-116.

19. Halloran PF. Immunosuppressive drugs for kidney transplantation. *N Engl J Med.* 2004;351:2715-2729.

20. Cowan PA, Heizer KE. Sirolimus: mammalian target of rapamycin inhibitor to prevent kidney rejection. *Nephrol Nurs J.* 2000;27:623-625.

21. Farb A, Heller PF, Shroff S, Cheng L, Kolodgie FD, Carter AJ, Scott DS, Froehlich J, Virmani R. Pathological analysis of local delivery of paclitaxel via a polymer-coated stent. *Circulation.* 2001;104:473-479.

22. Schiff PB, Horwitz SB. Taxol stabilizes microtubules in mouse fibroblast cells. *Proc Natl Acad Sci U S A.* 1980;77:1561-1565.

23. van Der Giessen WJ, Regar E, Harteveld MS, Coen VL, Bhagwandien R, Au A, Levendag PC, Ligthart J, Serruys PW, den Boer A, Verdouw PD, Boersma E, Hu T, van Beusekom HM. "Edge Effect" of (32)p radioactive stents is caused by the combination of chronic stent injury and radioactive dose falloff. *Circulation.* 2001;104:2236-2241.

24. van Beusekom HM, Whelan DM, Hofma SH, Krabbendam SC, van Hinsbergh VW, Verdouw PD, van der Giessen WJ. Long-term endothelial dysfunction is more pronounced after stenting than after balloon angioplasty in porcine coronary arteries. *J Am Coll Cardiol.* 1998;32:1109-1117.

25. Whelan DM, van der Giessen WJ, Krabbendam SC, van Vliet EA, Verdouw PD, Serruys PW, van Beusekom HM. Biocompatibility of phosphorylcholine coated stents in normal porcine coronary arteries. *Heart.* 2000;83:338-345.

26. Derkx P, Nigg AL, Bosman FT, Birkenhager-Frenkel DH, Houtsmuller AB, Pols HA, van Leeuwen JP. Immunolocalization and quantification of noncollagenous bone matrix proteins in methylmethacrylate-embedded adult human bone in combination with histomorphometry. *Bone.* 1998;22:367-373.

27. Batenburg WW, Popp R, Fleming I, de Vries R, Garrelds IM, Saxena PR, Danser AH. Bradykinin-induced relaxation of coronary microarteries: S-nitrosothiols as EDHF? *Br J Pharmacol.* 2004;142:125-135.

28. Batenburg WW, de Vries R, Saxena PR, Danser AH. L-S-nitrosothiols: endothelium-derived hyperpolarizing factors in porcine coronary arteries? *J Hypertens.* 2004;22:1927-1936.

29. Batenburg WW, Garrelds IM, Bernasconi CC, Juillerat-Jeanneret L, van Kats JP, Saxena PR, Danser AH. Angiotensin II type 2 receptor-mediated vasodilation in human coronary microarteries. *Circulation.* 2004;109:2296-2301.

30. Mulvany MJ, Halpern W. Contractile properties of small arterial resistance vessels in spontaneously hypertensive and normotensive rats. *Circ Res.* 1977;41:19-26.

31. Awata M, Kotani J, Uematsu M, Morozumi T, Watanabe T, Onishi T, Iida O, Sera F, Nanto S, Hori M, Nagata S. Serial angioscopic evidence of incomplete neointimal coverage after sirolimus-eluting stent implantation: comparison with bare-metal stents. *Circulation.* 2007;116:910-916.

32. Kotani J, Awata M, Nanto S, Uematsu M, Oshima F, Minamiguchi H, Mintz GS, Nagata S. Incomplete neointimal coverage of sirolimus-eluting stents: angioscopic findings. *J Am Coll Cardiol.* 2006;47:2108-2111.

33. Oyabu J, Ueda Y, Ogasawara N, Okada K, Hirayama A, Kodama K. Angioscopic evaluation of neointima coverage: sirolimus drug-eluting stent versus bare metal stent. *Am Heart J.* 2006;152:1168-1174.

34. Yao ZH, Matsubara T, Inada T, Suzuki Y, Suzuki T. Neointimal coverage of sirolimus-eluting stents 6 months and 12 months after implantation: evaluation by optical coherence tomography. *Chin Med J (Engl).* 2008;121:503-507.

35. Klugherz BD, Llanos G, Lieuallen W, Kopia GA, Papandreou G, Narayan P, Sasseen B, Adelman SJ, Falotico R, Wilensky RL. Twenty-eight-day efficacy and phamacokinetics of the sirolimus-eluting stent. *Coron Artery Dis.* 2002;13:183-188.

36. Suzuki T, Kopia G, Hayashi S, Bailey LR, Llanos G, Wilensky R, Klugherz BD, Papandreou G, Narayan P, Leon MB, Yeung AC, Tio F, Tsao PS, Falotico R, Carter AJ. Stent-based delivery of sirolimus reduces neointimal formation in a porcine coronary model. *Circulation.* 2001;104:1188-1193.

37. Seifert PS, Huibregtse BA, Polovick J, Poff B. Early vascular response to overlapped paclitaxel-eluting stents in swine coronary arteries. *Cardiovasc Revasc Med.* 2007;8:251-258.

38. Wilson GJ, Polovick JE, Huibregtse BA, Poff BC. Overlapping paclitaxel-eluting stents: long-term effects in a porcine coronary artery model. *Cardiovasc Res.* 2007;76:361-372.

39. Ferron GM, Jusko WJ. Species differences in sirolimus stability in humans, rabbits, and rats. *Drug Metab Dispos.* 1998;26:83-84.

40. Metcalfe S, Svvennsen R, Calne RY. FK506 and rapamycin: differential sensitivity of human, baboon, cynomolgus monkey, dog and pig lymphocytes. *Transpl Int.* 1992;5 Suppl 1:S514-515.

41. Mohacsi PJ, Tuller D, Hulliger B, Wijngaard PL. Different inhibitory effects of immunosuppressive drugs on human and rat aortic smooth muscle and endothelial cell proliferation stimulated by platelet-derived growth factor or endothelial cell growth factor. *J Heart Lung Transplant.* 1997;16:484-492.

42. Stettler C, Wandel S, Allemann S, Kastrati A, Morice MC, Schomig A, Pfisterer ME, Stone GW, Leon MB, de Lezo JS, Goy JJ, Park SJ, Sabate M, Suttorp MJ, Kelbaek H, Spaulding C, Menichelli M, Vermeersch P, Dirksen MT, Cervinka P, Petronio AS, Nordmann AJ, Diem P, Meier B, Zwahlen M, Reichenbach S, Trelle S, Windecker S, Juni P. Outcomes associated with drug-eluting and bare-metal stents: a collaborative network meta-analysis. *Lancet.* 2007;370:937-948.

43. Schomig A, Dibra A, Windecker S, Mehilli J, Suarez de Lezo J, Kaiser C, Park SJ, Goy JJ, Lee JH, Di Lorenzo E, Wu J, Juni P, Pfisterer ME, Meier B, Kastrati A. A meta-analysis of 16 randomized trials of sirolimus-eluting stents versus paclitaxel-eluting stents in patients with coronary artery disease. *J Am Coll Cardiol.* 2007;50:1373-1380.

44. Togni M, Raber L, Cocchia R, Wenaweser P, Cook S, Windecker S, Meier B, Hess OM. Local vascular dysfunction after coronary paclitaxel-eluting stent implantation. *Int J Cardiol.* 2007;120:212-220.

45. Kuga T, Egashira K, Mohri M, Tsutsui H, Harasawa Y, Urabe Y, Ando S, Shimokawa H, Takeshita A. Bradykinin-induced vasodilation is impaired at the atherosclerotic site but is preserved at the spastic site of human coronary arteries in vivo. *Circulation.* 1995;92:183-189.

46. Cowan CL, McKenzie JE. Cholinergic regulation of resting coronary blood flow in domestic swine. *Am J Physiol.* 1990;259(1 Pt 2):H109-115.

47. Furusho N, Araki H, Sakaino N, Nishi K, Miyauchi Y. Effects of perivascular nerve stimulation on the flow rate in isolated epicardial coronary arteries of pigs. *Eur J Pharmacol.* 1988;154:79-84.

48. Hata H, Egashira K, Fukai T, Ohara Y, Kasuya H, Takahashi T, Takeshita A. The role of endothelium-derived nitric oxide in acetylcholine-induced coronary vasoconstriction in closed-chest pigs. *Coron Artery Dis.* 1993;4:891-898.

Specific coronary drug-eluting stents interfere with distal microvascular function after single stent implantation in pigs

van den Heuvel M., Sorop O., Batenburg W.W., Bakker C.L., de Vries R., Koopmans S.J., van Beusekom H.M., Duncker D.J., Danser A.H. and van der Giessen W.J.

JACC Cardiovasc Interv. 2010 Jul;3(7):723-30

11

Specific coronary drug-eluting stents interfere with distal microvascular function after single stent implantation in pigs

Mieke van den Heuvel, MD, MSc*†, Oana Sorop, PHD*, Wendy W. Batenburg, PhD†, Charlotte L. Bakker, BSc*, René de Vries, BSc†, Sietse Jan Koopmans, PhD‡, Heleen M.M. van Beusekom, PhD*, Dirk J. Duncker, MD, PhD*, A.H. Jan Danser, PhD†, Willem J. van der Giessen, MD, PhD*§

Rotterdam, Lelystad, Utrecht, the Netherlands

Objectives The aim of this study was to compare the effects of single drug-eluting stents (DES) on porcine coronary function distal to the stent in vivo and in vitro.

Background The mechanism of endothelial dysfunction occurring in human coronary conduit arteries up to 9 months after DES implantation is unknown.

Methods A sirolimus-eluting stent (SES), paclitaxel-eluting stent (PES), and a bare-metal stent (BMS) were implanted in the 3 coronary arteries of 11 pigs. After 5 weeks, in vivo responses in distal coronary flow to different doses of bradykinin (BK) and nitrates were measured. In vitro, vasodilation to BK and nitrates, as well as vasoconstriction to endothelin (ET)-1 were assessed in both distal coronary conduit and small arteries. In addition, contributions of nitric oxide (NO) and endothelium-derived hyperpolarizing factors (EDHFs) and cyclic guanosine monophosphate (cGMP) responses to BK-stimulation were determined in vitro.

Results Both DES did not alter in vivo distal vasomotion. In vitro distal conduit and small arterial responses to BK were also unaltered; DES did not alter the BK-induced increase in cGMP. However, after NO synthase blockade, PES showed a reduced BK-response in distal small arteries as compared with BMS and SES ($p < 0.05$). The ET-1–induced vasoconstriction and vascular smooth muscle cell function were unaltered.

Conclusions In this study of single stenting in healthy porcine coronaries for 5 weeks, SES did not affect distal coronary vascular function, whereas PES altered distal endothelial function of small ar-teries under conditions of reduced NO bioavailability. Therefore, specifically the EDH-component of microvascular function seems affected by PES. (J Am Coll Cardiol Intv 2010;3:723–30) © 2010 by the American College of Cardiology Foundation

From the *Department of Cardiology, Thoraxcenter, and the †Department of Internal Medicine, Sector of Pharmacology and Metabolic Diseases, Cardiovascular Research School COEUR, Erasmus University Medical Center, Rotterdam, the Netherlands; ‡BioMedical Research, Wageningen University and Research Center, Lelystad, the Netherlands; and the §Interuniversity Cardiology Institute, ICIN/KNAW, Utrecht, the Netherlands.

Manuscript received July 13, 2009; revised manuscript received April 13, 2010, accepted May 1, 2010.

Percutaneous coronary intervention with stenting is an established treatment in most patients with obstructive coronary artery disease. Clinical trials have shown that the 2 first-generation drug-eluting stents (DES), the sirolimus-eluting stent (SES) and paclitaxel-eluting stent (PES), reduce restenosis and revascularization rates by at least 50% as compared with bare-metal stents (BMS) (1). Despite beneficial effects of DES on restenosis, coronary endothelial dysfunction has been observed in areas adjacent to SES (2–4) and PES (5) versus BMS, on average 6 months after implantation. This evidence clearly points toward chronic coronary endothelial dysfunction in the peri-stent area of conduit arteries after both types of DES-implantation. In addition, 9 months after single SES and PES placement, conduit arterial dysfunction was shown predominantly in distal and far distal segments of the stent (6). This observation suggests that, after single DES, especially the distal coronary flow area is at high risk for adverse effects. However, the exact nature of this distal coronary dysfunction is difficult to study in clinical settings. Experimental studies might help to investigate the underlying mechanism(s) (7).

Abbreviations and Acronyms

BK = bradykinin

BMS = bare-metal stent(s)

cGMP = cyclic guanosine monophosphate

CRC = concentration-response curve

DES = drug-eluting stent(s)

EDHF = endothelium-derived hyperpolarizing factor

ET = endothelin

L-NAME = N-nitro-L-arginine methyl ester

NO = nitric oxide

pEC50 = concentration necessary to produce 50% of the maximal response

PES = paclitaxel-eluting stent(s)

SES = sirolimus-eluting stent(s)

SNAP = S-nitroso-N-acetylpenicillamine

Overlapping PES implantation in a porcine model resulted in, besides distal conduit dysfunction, abnormal endothelium-dependent relaxation of distal small arteries (8). Currently, no data are available comparing the effects of single DES on endothelial function of the coronary microcirculation distal to the stent. In addition, it is presently unknown which specific components of endothelial function might be particularly affected. This information is important, because a functional microvascular endothelium plays a key role in the regulation of local vascular tone and myocardial perfusion by releasing vasodilating factors, including nitric oxide (NO) and endothelium derived hyperpolarizing factors (EDHFs) (9). The latter is believed to be more prominent in circumstances of impaired NO-mediated vasodilatation (10,11).

Consequently, the present study was undertaken to compare the effects of single BMS, SES, and PES on distal coronary function in healthy pigs (12) with focus on the microcirculation, in both in vivo and in vitro settings. We hypothesized that DES implantation would result in distal endothelium-dependent microvascular dysfunction, evidenced by decreased vasodilation and increased vasoconstriction. Specifically, we focussed on the NO and EDHF components of vascular function.

Methods

Coronary intervention. Eleven Yorkshire-Landrace pigs of either sex (57 ± 4 kg at implantation; 75 ± 7 kg at death) entered the study. The study was performed in accordance with the Guide for Care and Use of Laboratory Animals (National Institutes of Health Publication No. 85-23, revised 1996), after approval of the local Animal Ethics Committee.

Animal preparation and stent implantation were performed as described previously (12). In short, 1 day before surgery animals received 300-mg acetylsalicylic acid and a loading dose of 300-mg clopidogrel. Under general anesthesia, left and right coronary angiography were performed to select arterial segments of 2.5 to 3.5 mm in diameter in the left anterior descending, left circumflex, and right coronary arteries. Three types of commercially available stents were randomly implanted in selected uninjured coronary segments with a balloon/artery ratio of 1:1, such that each animal received all stents (1 stent/coronary artery) in a random fashion: a BMS (R-stent Evolution/Prodigy, 316L stainless steel stent, 15-mm length, 3.0- to 3.5-mm diameter, Orbus MT, Fort Lauderdale, Florida), a SES (Cypher: DES with 1.4-$\mu g/mm^2$ sirolimus-loading, 316L stainless steel stent, 13-mm length, 3.0- to 3.5-mm diameter, Cordis, Miami, Florida), and a PES (Taxus: DES with 1.0-$\mu g/mm^2$ paclitaxel-loading, 316L stainless steel stent, 12-mm length, 3.0- to 3.5-mm diameter, Boston Scientific, Natick, Massachusetts). After repeat angiography, the animals were allowed to recover and followed for 5 weeks. This period is believed to result in maximal neointimal thickness after BMS implantation in animals, comparable to the response at 6 to 9 months in patients (13). During follow-up, the animals received 300-mg acetylsalicylic acid and 75-mg clopidogrel daily.

In vivo coronary function assessment. After 5 weeks, changes in coronary flow velocities distal to the stent induced by different agonists were measured with a Doppler tipped guidewire (FloWire, Volcano Therapeutics, Inc., Rancho Cordova, California). Intracoronary flow velocity measurements were performed continuously, both at stable baseline hemodynamic status and during intracoronary infusion of the endothelium-dependent vasodilator bradykinin (BK) (0.05 to 1.0 $\mu g/kg/min$), the endothelium-independent vasodilating agent sodium nitroprusside (5 to 20 $\mu g/kg/min$), and at maximal vasodilation to adenosine (100 $\mu g/kg/min$) (14,15). The $alpha_1$-adrenoceptor agonist phenylephrine was co-infused to maintain mean arterial pressure at approximately 90 mm Hg, while leaving coronary microvascular tone unperturbed (15). Each agonist

concentration was maintained for 3 min, followed by a 5-min washout period to allow for restoration of baseline flow. The peak-increase in distal coronary flow velocity was calculated for each concentration as maximum minus baseline.

Tissue collection. All pigs were killed after 5 weeks of follow-up. Hearts were immediately excised and collected in cold, oxygenated Krebs bicarbonate buffer (16,17). Segments of epicardial conduit arteries (>2 mm diameter), starting approximately 0.5 cm distal to the stent and segments of epicardial small arteries (approximately 300 μm diameter) in the specific distal flow area of the stented artery, were isolated and placed in buffer for in vitro functional studies. The stented segment was placed in 4% buffered formaldehyde for histology.

In vitro coronary conduit and small arterial function assessment. Segments of conduit arteries (approximately 4 mm length) were suspended on stainless steel hooks in organ baths. Segments of small arteries (approximately 2 mm length) were mounted in a Mulvany wire myograph (DMT A/S, Aarhus, Denmark). Vascular responses were measured as changes in isometric force (16,17).

Both conduit and small arteries were subjected to the same experimental protocol. After stabilization, segments were exposed to depolarization by 0.1 mol/l potassium chloride. Upon wash-out of potassium chloride, after equilibration, in a first set of segments, endothelium-dependent relaxation to BK (10^{-10} to 10^{-6} mol/l) was recorded upon pre-constriction with the thromboxane analogue U46619 (10^{-8} to 10^{-7} mol/l). To determine NO-dependent and -independent contributions to BK-induced relaxation, in a second set of pre-constricted segments, the concentration-response curve (CRC) for BK was constructed after 30 min of pre-incubation with 10^{-4} mol/l of the NO-synthase inhibitor N-nitro-L-arginine methyl ester (L-NAME). From a third set, CRCs for endothelin (ET)-1 (10^{-10} to 10^{-7} mol/l) were constructed to study vasoconstriction, followed by endothelium-independent but NO-mediated vasodilation to S-nitroso-N-acetylpenicillamine (SNAP) (10^{-7} to 10^{-6} mol/l).

Cyclic guanosine monophosphate measurements. To study BK-induced cyclic guanosine monophosphate (cGMP) production, segments of small arteries distal to the stent of a subset of pigs (n = 5) were nonexposed (control subjects) or exposed to BK (10^{-6} mol/l) with or without pre-incubation with L-NAME (10^{-4} mol/l). The cGMP concentrations were determined by enzyme-linked immunoadsorbent assay and expressed as pmol $\times$ mg^{-1} protein (17).

Histology. Fixed stented segments were plastic embedded and stained with hematoxylin-eosin (routine stain) and resorcin-fuchsin (elastin stain) for quantitative and qualitative analysis. Neointimal thickness at the stent struts and inflammation scores directly adjacent to the struts were determined (12).

Data analysis. Differences between the stent-types of individual outcome variables (procedural, histology data, single vascular function data, and the like) were assessed with paired *t* tests with correction for multiple testing. Statistical analysis of logarithmic vascular function CRCs was performed with a nonlinear mixed-effects model fit by maximum likelihood with nested random effects (statistical program R, version 2.10.1, The R Foundation for Statistical Computing, Wien, Austria).

In vitro vascular relaxant responses to BK and SNAP were expressed as percentage of contraction to U46619 and ET-1, respectively. Constrictor responses were normalized to 0.1 mol/l potassium chloride. The concentration necessary to produce 50% of its maximal response (pEC_{50}) was determined for each CRC reaching a maximum, with logistic function (16,17). Data are given as mean ± SEM. A value of $p < 0.05$ was considered statistically significant.

Results

Procedural characteristics. Quantitative coronary angiography analysis of selected segments revealed no differences in mean coronary diameter of the 3 stent groups, both before and immediately after stenting. Also, procedural characteristics showed no differences in mechanical vessel injury at stent implantation (Table 1). Furthermore, in a subset of pigs (n = 5), quantitative coronary angiography analysis of the stented segments was performed 5 weeks after implantation. No significant differences in percentage late lumen loss were observed (BMS vs. SES, PES: 16.8 ± 3.4% vs. 17.7 ± 5.5%, 6.9 ± 1.5%; p = NS).

Effects of DES on distal coronary conduit and small arterial function. IN VIVO ASSESSMENT. During flow measurements distal to the stent, no significant changes occurred in heart

Table 1. QCA Assessment of Coronary and Procedural Characteristics at the Time of Stent Implantation

Group	Pre-Stenting (mm)	Post-Stenting (mm)	Balloon Size (mm)	Max Inflation Pressure (atm)	BA-Ratio
BMS (n = 10)	3.02 ± 0.09	3.15 ± 0.10	3.30 ± 0.09	13.4 ± 1.5	1.09 ± 0.01
SES (n = 10)	3.13 ± 0.11	3.29 ± 0.09	3.35 ± 0.10	14.4 ± 1.1	1.07 ± 0.03
PES (n = 11)	3.19 ± 0.10	3.37 ± 0.11	3.49 ± 0.11	14.9 ± 1.2	1.09 ± 0.01

Pre- and post-stenting: mean coronary lumen diameter at site of intervention before and directly after stent placement. Balloon size: mean diameter of contrast-filled balloon during maximal inflation. Max inflation pressure: maximal inflation pressure used for stent placement.

BA = balloon-to-artery; BMS = bare-metal stent(s); PES = paclitaxel-eluting stent(s); QCA = quantitative coronary angiography; SES = sirolimus-eluting stent(s).

rate (85 ± 2 beats/min) and mean arterial pressure (92 ± 3 mm Hg) at baseline or during infusion of BK, sodium nitroprusside, or adenosine. Also, no significant differences in distal vasodilatory responses to BK, sodium nitroprusside, or adenosine were reported after 5 weeks of BMS, SES, and PES implantation (Fig. 1).

IN VITRO ASSESSMENT. Contractile responses to potassium chloride and pre-constriction to U46619 were similar between stent types, both for conduit and small arteries (data not shown).

CONDUIT ARTERIES. Segments of coronary conduit arteries distal to the stent dilated to BK in a dose-dependent manner (pEC_{50} BMS vs. SES vs. PES: 8.2 ± 0.2 vs. 8.0 ± 0.3 vs. 8.0 ± 0.1). Relaxations corresponded with approximately 70% of the pre-constriction level by U46619, with no differences between the different stents (Fig. 2A). Pre-treatment with L-NAME greatly reduced dilation to BK ($p < 0.01$, L-NAME vs. no L-NAME for all stent-types). The effect of L-NAME was not different between the stents (Fig. 2B). The compound ET-1–induced vasoconstriction in a concentration-dependent manner to 100% of the response to 0.1 mol/l potassium chloride (pEC_{50} BMS vs. SES vs. PES: 7.5 ± 0.1 vs. 7.7 ± 0.1 vs. 7.5 ± 0.1). This effect was not significantly altered by either SES or PES (Fig. 2C). The exogenous NO-donor SNAP resulted in vasodilation similar for all stent types (Fig. 2D).

SMALL ARTERIES. Segments of coronary small arteries distal to the stent dilated to BK in a concentration-dependent manner (pEC_{50} BMS vs. SES vs. PES: 8.3 ± 0.2 vs. 8.2 ± 0.2 vs. 8.0 ± 0.1). Relaxations amounted up to 90% of the pre-constriction level and were influenced by stent-type (Fig. 2E), in that chronic PES implantation caused a modest rightward shift of the BK-CRC ($p < 0.01$, PES vs. SES; $p = 0.1$, PES vs. BMS) (Fig. 2E). After pre-incubation with L-NAME, the BK-CRC was clearly shifted to the right ($p < 0.01$, L-NAME vs. no L-NAME for all stent-types) (Fig. 2F). The effect of L-NAME in small arteries was more modest than in conduit arteries. This confirms that the NO-independent component of the BK response in small arteries is more pronounced than in conduit arteries (16,17). The PES implantation shifted the BK-CRC in the presence of L-NAME approximately 10 times to the right as compared with BMS and SES ($p = 0.02$, PES vs. BMS; $p = 0.02$, PES vs. SES) (Fig. 2F). Thus, small arteries distal of PES showed impaired vasodilation upon incubation with L-NAME (pEC_{50} BMS vs. SES vs. PES: 7.6 ± 0.3 vs. 7.9 ± 0.2 vs. 7.0 ± 0.3). The PES-type of stent specifically reduced the NO-independent component of the BK response. The compound ET-1–induced vasoconstriction in a concentration-dependent manner up to 150% of the response to 0.1 mol/l potassium chloride (pEC_{50} BMS vs. SES vs. PES: 7.7 ± 0.1 vs. 7.6 ± 0.1 vs. 7.6 ± 0.1), unaffected by stent-type (Fig. 2G). The exogenous NO-donor SNAP resulted in vasodilation of the small arteries similar for all stent-types, indicating intact vascular smooth muscle cell function (Fig. 2H).

Cyclic GMP measurements in distal small arteries. After BK-stimulation, distal microvascular cGMP levels were 1.95 (0.5 to 11.9) pmol × mg^{-1}, 1.01 (0.2 to 2.3) pmol × mg^{-1}, and 1.63 (0.6 to 7.7) pmol × mg^{-1} protein (geometric mean and range of BMS vs. SES vs. PES; p = NS). Pre-incubation with L-NAME reduced the microvascular cGMP content after BK-stimulation by 80.4 ± 7.7% vs. 61.8 ± 22.3% vs. 73.0 ± 6.3%, respectively (p = NS).

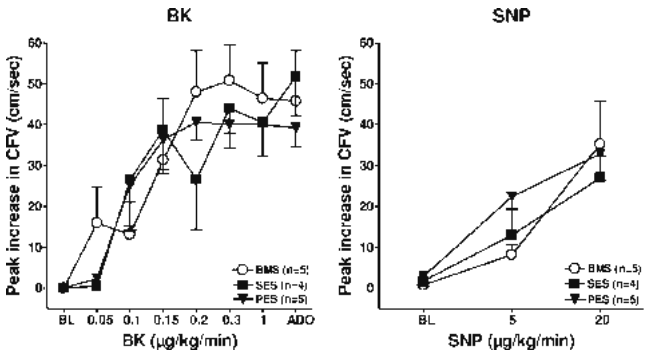

Figure 1. In Vivo Coronary Function

Effects of 5 weeks of single stents on baseline (BL), endothelium-dependent (bradykinin [BK]), adenosine (ADO) and endothelium-independent (sodium nitroprusside [SNP]) peak increases in coronary flow velocity (CFV) of the distal coronary circulation in vivo (n = 5 pigs). BMS = bare-metal stent(s); PES = paclitaxel-eluting stent(s); SES = sirolimus-eluting stent(s).

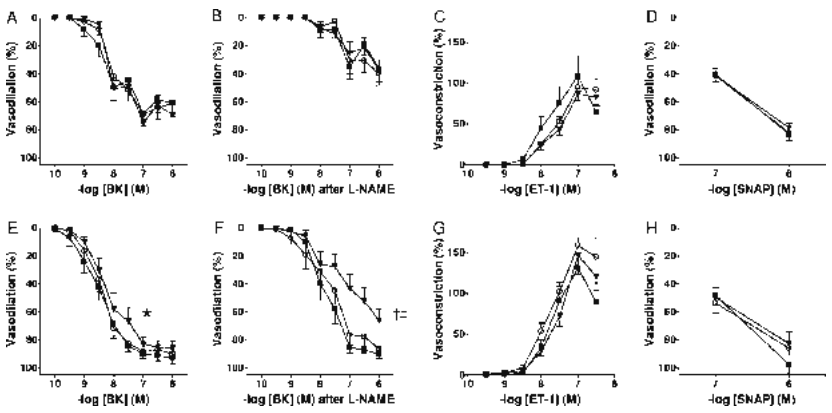

Figure 2. In Vitro Coronary Conduit Arterial Function and In Vitro Coronary Small Arterial Function

Effects of 5 weeks of single stents on distal endothelium-dependent (BK, BK after pre-incubation with N-nitro-L-arginine methyl ester [L-NAME]), endothelium-independent vasodilation (S-nitroso-N-acetylpenicillamine [SNAP]), and vasoconstriction (endothelin [ET]-1) of coronary conduit arteries and small arteries in vitro (n = 11 pigs). **Top panels:** conduit arteries; **bottom panels:** small arteries. Concentration-response curves (CRCs) to BK (**A, E**: *p < 0.01, PES vs. SES); CRCs to BK after pre-incubation with L-NAME (**B, F**: †p = 0.02, PES vs. BMS; ‡p = 0.02, PES vs. SES); CRCs to ET-1 **(C, G)**; CRCs to SNAP **(D, H)**. Abbreviations as in Figure 1.

These results agree with previously published data on BK-stimulated porcine coronary small arteries (17).

Histology of stented coronary arteries. Qualitative analysis showed that the vascular response after stenting followed patterns typical for BMS (Fig. 3A) and DES (Figs. 3B and 3C) in pigs (12). The neointima in BMS consisted of vascular smooth muscle-like cells within a collagenous matrix largely covered by endothelial cells. The neointima in DES was similar, including the presence of endothelial cells in all DES. Typically for DES, the neointima also contained fibrinoid deposition—a marker of delayed healing (18)—surrounding the stent struts (Figs. 3B and 3C). In PES, mitotic figures characteristic for paclitaxel were observed (Fig. 3C), whereas SES showed more inflammation resulting in increased neointimal formation on top of the struts (BMS vs. SES vs. PES: 313 ± 49.3 μm vs. 524 ± 82.9 μm vs. 268 ± 36.0 μm; $p < 0.01$ SES vs. PES). Neointimal thickness was not significantly different among the groups upon exclusion of stents with a high inflammation score (BMS vs. SES vs. PES: 313 ± 49.3 μm vs. 355 ± 58.2 μm vs. 235 ± 16.6 μm; p = NS).

Discussion

In the present study, we compared the effects of first-generation DES on endothelial function of the distal coronary vasculature with special focus on the microcirculation, in both in vivo and in vitro settings in healthy pigs. We hypothesized that DES implantation would result in distal endothelial dysfunction evidenced by decreased vasodilation and increased vasoconstriction. The main findings were that after 5 weeks of DES implantation, in vivo vascular function distal to DES was essentially unaffected. This was confirmed in vitro, because SES implantation did not alter BK-mediated vasodilation, whereas PES had only modest effects. However, under conditions of reduced NO bioavailability, PES-induced defects in distal microvascular function in vitro were clearly exposed. These defects were principally due to impairment of the NO-independent component of BK-induced vasodilation. Specifically, endothelial function was affected, because the vasodilation response to an exogenous NO donor was unaltered. The PES-type of stent did not alter the cGMP response upon BK stimulation in vitro, the key second messenger system of NO-dependent vasodilation, a finding in agreement with the vascular function results.

DES effects on distal coronary function. This study indicates for the first time that the effects of single DES might extend into the distal coronary microcirculation of healthy pigs. This conclusion is based on results obtained in vitro in isolated coronary small arteries. Five weeks after stenting, microvascular alterations are not primarily induced by circulating concentrations of DES drugs, because 30 days after DES placement, drug-release from the stent is minimal (1).

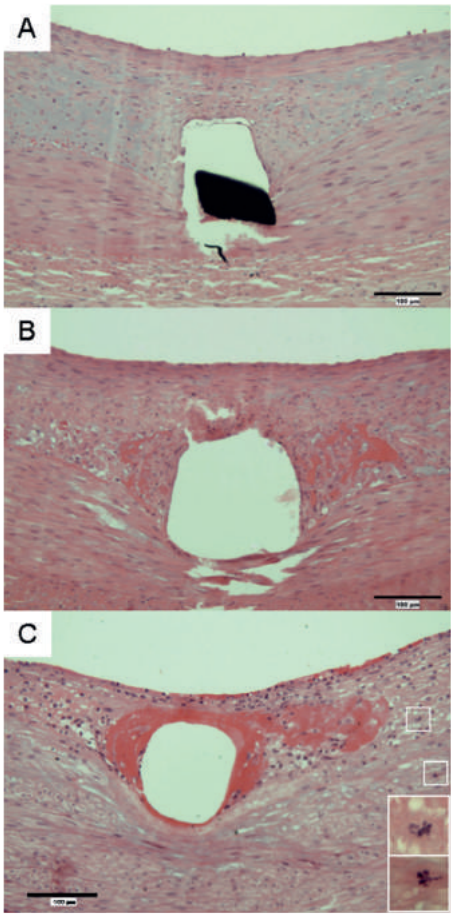

Figure 3. In Stent Histology

Representative in-stent histological sections. The BMS shows a well-healed neointima with vascular smooth muscle cells in a collagenous matrix **(A)**; SES shows less cellularity and moderate amounts of fibrinoid **(red) (B)**; PES also shows fibrinoid surrounding the stent struts as well as mitotic spindles (**C**, **magnifications**). All stents were largely covered by endothelium (hematoxylin-eosin stain; **bar** = 100 μm; **magnification inserts:** 2× original image; **white squares:** areas of magnification). Abbreviations as in Figure 1.

In addition, in-stent histology showed neointimal healing for all groups, thereby minimizing ongoing drug release in the circulation.

A recent pig study already showed abnormal endothelium-dependent relaxation of distal small arteries after 1 month of exposure to PES (8). However, in this study overlapping PES were implanted, creating a more profound local injury and inflammatory reaction contributing to the vasomotor dysfunction in the peri-stent area as compared with the present study. Furthermore, with overlapping DES implantation, additional drug concentrations will be eluted from the stents, aggravating local side effects. The authors reported a decreased NO-mediated conduit arterial response adjacent to overlapping PES, most likely due to locally enhanced oxidative stress. However, the mechanisms of the impaired small arterial responses of the distal perfusion bed were not examined. Of note, the reported abnormal endothelium-dependent relaxation of distal small arteries did not result in enhanced ET-1–induced vasoconstriction (8).

In the present study no clear differences were observed in distal microvascular functions with BK alone or with SNAP, either in vivo or in vitro. Only after NO synthase blockade in vitro, significant differences were demonstrated in microvascular responses of PES-treated coronary arteries. This suggests that PES specifically affected the NO-independent component of BK-induced microvascular endothelial vasodilation (i.e., EDHF) (17). Classically, this EDHF component can be blocked by applying inhibitors of small and intermediate conductance calcium-dependent potassium channels (apamin and charybdotoxin) (17). Preliminary data from our laboratory confirm that adding apamin and charybdotoxin on top of L-NAME fully blocked the microvascular BK-response after chronic DES-implantation (data not shown). The EDHFs are known to be of particular importance in small arteries, although their exact molecular mechanisms and pathways remain to be unravelled (16,17,19,20). In agreement with an alteration in EDHF and not in NO, the cGMP-response—the key second messenger system of NO—was unaltered by PES in vitro. The PES did not affect ET-1–induced microvascular constriction, possibly because NO and ET-1 are balanced (21).

The exact molecular mechanisms by which 5 weeks of single PES resulted in alterations of distal EDHF-mediated microvascular function cannot be derived from the present study. However, it is of interest to note that, although both DES reduce restenosis rates effectively (1), they have different mechanisms of action (18). Accumulation of extracellular reactive oxygen species is a crucial step for paclitaxel-induced cancer cell death (22). In addition, overlapping PES implantation was associated with enhanced local oxidative stress affecting NO-mediated vasodilation of, in particular, conduit arteries in the peri-stent area (8). However, reactive oxygen species increase—in particular, a rise in hydrogen peroxide—also has been reported to inhibit EDHF-synthesis by cytochrome P450 epoxygenases (17,23,24). Therefore, local vascular accumulation of paclitaxel might give rise to local oxidative stress, modifying

specific components of endothelial function, perhaps depending on the affected vessel size.

Clinical studies. The in vivo observations of the current study, made in conduit arteries immediately distal to both DES, showed unaffected vascular function. These observations contrast with clinical studies reporting coronary endothelial dysfunction up to 9 months after DES implantation (2–6). An explanation for this discrepancy could involve different study time-frames, protocols, and the use of healthy porcine vessels. First, stent healing in healthy pigs is much faster as compared with diseased patients. Although the results obtained in pigs after 5 weeks of stenting might correlate to patient results obtained 6 to 9 months after stenting, one should be cautious with extrapolation of DES-results (13). Second, in contrast to human coronary arteries, porcine coronaries respond poorly to acetylcholine as an agonist, due to limited presence of muscarinic receptors within the vascular wall. Although the acetylcholine response is a hallmark in the detection of impaired coronary endothelial function in patients, BK-induced endothelium-dependent vasodilation is clinically relevant as well (25). Finally, in the clinical setting severely diseased vessels are stented instead of the healthy, uninjured coronary arteries of the pigs of the present study. Obviously, in patients, endothelial vulnerability of conduit arteries might have existed before stenting, and this might explain why an impaired conduit endothelial response after DES implantation was already observed in humans without NO synthase blockade, whereas in healthy pigs it could only be observed in the more sensitive small arteries in the presence of L-NAME.

Study limitations. In the present study, part of the experiments were performed in an in vitro setting. Although in vitro not all the influencing factors of in vivo are present, this specifically allowed us to examine vascular responses with and without NO bioavailability in the DES-exposed coronary vessels of each animal. In the in vivo setting, such an extensive vasoactive protocol would be hampered both by the potential systemic effects of NO blockade as well as BK-induced tachyphylaxis, which needs to be taken into account when studying vasomotion with and without NO blockade.

Additionally, the present study reports the in vitro results of PES in a relatively limited number of pigs that was large enough to show clear changes like the microvascular response to BK after pre-incubation with L-NAME but might have been too low to draw conclusions on the basis of a small difference such as the microvascular response to BK.

Conclusions

We compared the functional effects of first-generation single DES on the distal coronary circulation. Particularly PES might show distal endothelium-dependent microvascular dysfunction, because the loss of local EDHF-mediated vasodilation eventually might alter the vasomotor balance and therefore local myocardial perfusion in the in vivo setting. Our results might be relevant for vulnerable coronary artery disease patients with severe microvascular endothelial dysfunction, given their already existing reduced microvascular NO-bioavailability. However, the in vitro observations of the present study warrant further studies to examine distal vascular alterations caused by PES over time in more detail as well as at longer follow-up.

Acknowledgment

The authors would like to acknowledge Magdalena Murawska, MSc, for statistical help.

Reprint requests and correspondence: Dr. Willem J. van der Giessen, Erasmus University Medical Center, Thoraxcenter, Room Ee2393, 's-Gravendijkwal 230, 3015 CE Rotterdam, the Netherlands. E-mail: w.j.vandergiessen@erasmusmc.nl.

REFERENCES

1. Serruys PW, Kutryk MJ, Ong AT. Coronary-artery stents. N Engl J Med 2006;354:483–95.
2. Fuke S, Maekawa K, Kawamoto K, et al. Impaired endothelial vasomotor function after sirolimus-eluting stent implantation. Circ J 2007;71:220–5.
3. Hofma SH, van der Giessen WJ, van Dalen BM, et al. Indication of long-term endothelial dysfunction after sirolimus-eluting stent implantation. Eur Heart J 2006;27:166–70.
4. Togni M, Windecker S, Cocchia R, et al. Sirolimus-eluting stents associated with paradoxic coronary vasoconstriction. J Am Coll Cardiol 2005;46:231–6.
5. Togni M, Raber L, Cocchia R, et al. Local vascular dysfunction after coronary paclitaxel-eluting stent implantation. Int J Cardiol 2007;120: 212–20.
6. Shin DI, Kim PJ, Seung KB, et al. Drug-eluting stent implantation could be associated with long-term coronary endothelial dysfunction. Int Heart J 2007;48:553–67.
7. van den Heuvel M, Sorop O, van Beusekom HM, van der Giessen WJ. Endothelial dysfunction after drug eluting stent implantation. Minerva Cardioangiol 2009;57:629–44.
8. Pendyala LK, Li J, Shinke T, et al. Endothelium-dependent vasomotor dysfunction in pig coronary arteries with Paclitaxel-eluting stents is associated with inflammation and oxidative stress. J Am Coll Cardiol Intv 2009;2:253–62.
9. Duncker DJ, Bache RJ. Regulation of coronary blood flow during exercise. Physiol Rev 2008;88:1009–86.
10. Nishikawa Y, Stepp DW, Chilian WM. Nitric oxide exerts feedback inhibition on EDHF-induced coronary arteriolar dilation in vivo. Am J Physiol Heart Circ Physiol 2000;279:H459–65.
11. Thollon C, Fournet-Bourguignon MP, Saboureau D, et al. Consequences of reduced production of NO on vascular reactivity of porcine coronary arteries after angioplasty: importance of EDHF. Br J Pharmacol 2002;136:1153–61.
12. van der Giessen WJ, Sorop O, Serruys PW, Peters-Krabbendam I, van Beusekom HM. Lowering the dose of sirolimus, released from a nonpolymeric hydroxyapatite coated coronary stent, reduces signs of delayed healing. J Am Coll Cardiol Intv 2009;2:284–90.
13. Virmani R, Kolodgie FD, Farb A, Lafont A. Drug eluting stents: are human and animal studies comparable? Heart 2003;89:133–8.
14. Dick GM, Katz PS, Farias M III, et al. Resistin impairs endothelium-dependent dilation to bradykinin, but not acetylcholine, in the coronary circulation. Am J Physiol Heart Circ Physiol 2006;291:H2997–3002.

15. Fallavollita JA, Malm BJ, Canty JM Jr. Hibernating myocardium retains metabolic and contractile reserve despite regional reductions in flow, function, and oxygen consumption at rest. Circ Res 2003;92: 48–55.
16. Batenburg WW, de Vries R, Saxena PR, Danser AH. L-S-nitrosothiols: endothelium-derived hyperpolarizing factors in porcine coronary arteries? J Hypertens 2004;22:1927–36.
17. Batenburg WW, Popp R, Fleming I, et al. Bradykinin-induced relaxation of coronary microarteries: S-nitrosothiols as EDHF? Br J Pharmacol 2004;142:125–35.
18. van Beusekom HM, Saia F, Zindler JD, et al. Drug-eluting stents show delayed healing: paclitaxel more pronounced than sirolimus. Eur Heart J 2007;28:974–9.
19. Batenburg WW, Garrelds IM, van Kats JP, Saxena PR, Danser AH. Mediators of bradykinin-induced vasorelaxation in human coronary microarteries. Hypertension 2004;43:488–92.
20. Kato M, Shiode N, Yamagata T, Matsuura H, Kajiyama G. Bradykinin induced dilatation of human epicardial and resistance coronary arteries in vivo: effect of inhibition of nitric oxide synthesis. Heart 1997;78: 493–8.
21. Lerman A, Sandok EK, Hildebrand FL Jr., Burnett JC Jr. Inhibition of endothelium-derived relaxing factor enhances endothelin-mediated vasoconstriction. Circulation 1992;85:1894–8.
22. Alexandre J, Batteux F, Nicco C, et al. Accumulation of hydrogen peroxide is an early and crucial step for paclitaxel-induced cancer cell death both in vitro and in vivo. Int J Cancer 2006;119:41–8.
23. Larsen BT, Gutterman DD, Sato A, et al. Hydrogen peroxide inhibits cytochrome p450 epoxygenases: interaction between two endothelium-derived hyperpolarizing factors. Circ Res 2008;102:59–67.
24. Gutterman DD, Miura H, Liu Y. Redox modulation of vascular tone: focus of potassium channel mechanisms of dilation. Arterioscler Thromb Vasc Biol 2005;25:671–8.
25. Kuga T, Egashira K, Mohri M, et al. Bradykinin-induced vasodilation is impaired at the atherosclerotic site but is preserved at the spastic site of human coronary arteries in vivo. Circulation 1995;92:183–9.

Key Words: coronary ■ drug-eluting stent ■ endothelial function ■ endothelium derived hyperpolarizing factors ■ microcirculation.

Neoatherosclerosis development following bioresorbable vascular scaffold implantation in diabetic and non-diabetic swine

van Ditzhuijzen N.S., Kurata M., van den Heuvel M., Sorop O., van Duin R.W.B., Krabbendam-Peters I., Ligthart J., Witberg K., Murawska M., Bouma B., Villiger M., Garcia-Garcia H.M., Serruys P.W., Zijlstra F., van Soest G., Duncker D.J., Regar E. and van Beusekom H.M.M.

PLoS One. 2017 Sep 12;12(9):e0183419

12

Neoatherosclerosis development following bioresorbable vascular scaffold implantation in diabetic and non-diabetic swine

Nienke S. van Ditzhuijzen[1], Mie Kurata[1], Mieke van den Heuvel[1], Oana Sorop[1], Richard W.B. van Duin[1], Ilona Krabbendam-Peters[1], Jurgen Ligthart[1], Karen Witberg[1], Magdalena Murawska[2], Brett Bouma[3], Martin Villiger[3], Hector M. Garcia-Garcia[4], Patrick W. Serruys[4], Felix Zijlstra[1], Gijs van Soest[1], Dirk-Jan Duncker[1], Evelyn Regar[1,5], Heleen M.M. van Beusekom[1]*

[1] Department of Cardiology, Thoraxcenter, Cardiovascular Research school COEUR, Erasmus University edical Center, Rotterdam, The Netherlands; [2] Department of Biostatistics, Erasmus University Medical Center, Rotterdam, The Netherlands; [3] Wellman Center for Photomedicine, Massachusetts General Hospital, Harvard Medical School, Boston, Massachusetts, United States of America; [4] Cardialysis B.V., Rotterdam, The Netherlands; [5] Dept. of Cardiovascular Surgery, University Hospital Zurich, Zurich, Switzerland

* h.vanbeusekom@erasmusmc.nl

Abstract

Background

DM remains a risk factor for poor outcome after stent-implantation, but little is known if and how DM affects the vascular response to BVS.

Aim

The aim of our study was to examine coronary responses to bioresorbable vascular scaffolds (BVS) in swine with and without diabetes mellitus fed a 'fast-food' diet (FF-DM and FF-NDM, respectively) by sequential optical coherence tomography (OCT)-imaging and histology.

Methods

Fifteen male swine were evaluated. Eight received streptozotocin-injection to induce DM. After 9 months (M), 32 single BVS were implanted in epicardial arteries with a stent to artery (S/A)-ratio of 1.1:1 under quantitative coronary angiography (QCA) and OCT guidance. Lumen, scaffold, neointimal coverage and composition were assessed by QCA, OCT and near-infrared spectroscopy (NIRS) pre- and/or post-procedure, at 3M and 6M. Additionally, polarization-sensitive (PS)-OCT was performed in 7 swine at 6M. After sacrifice at 3M and 6M, histology and polymer degradation analysis were performed.

Results

Late lumen loss was high (~60%) within the first 3M after BVS-implantation (P<0.01 FF-DM vs. FF-NDM) and stabilized between 3M and 6M (<5% change in FF-DM, ~10% in FF-NDM;

P>0.20). Neointimal coverage was highly heterogeneous in all swine (DM vs. NDM P>0.05), with focal lipid accumulation, irregular collagen distribution and neointimal calcification. Likewise, polymer mass loss was low (~2% at 3M, ~5% at 6M;P>0.20) and not associated with DM or inflammation.

Conclusion

Scaffold coverage showed signs of neo-atherosclerosis in all FF-DM and FF-NDM swine, scaffold polymer was preserved and the vascular response to BVS was not influenced by diabetes.

Introduction

Patients with diabetes mellitus (DM) are generally at risk for worse outcome after stent-implantation than patients without DM.[1] Due to the complex and multifactorial nature of the disease process, including metabolic abnormalities and vascular dysfunction, the vascular response to stent-implantation is generally impaired, complicating current stenting strategies.[2–4]

The everolimus-eluting bioresorbable vascular scaffold (BVS) may offer advantages. It elutes everolimus in the first 3 to 6 months after implantation, inhibiting excessive neointimal growth [5] and starts losing structural integrity 3 months after implantation,[5] potentially enabling vascular function restoration.[6]

Histology in healthy swine demonstrated that struts are covered at 28 days and resorbed around 3 years with minimal calcification and inflammation.[7, 8] In selected patients from the ABSORB Cohort A (BVS 1.0) and B (BVS 1.1) trials, excellent results for treatment of coronary artery lesions were observed.[9, 10] However, only 3%-20% of the study population suffered DM and no studies were performed in diabetic animals. Thus, little is known about the effect of DM on the vascular response to BVS. DM may cause inflammation, which could influence scaffold degradation by disregulated acid-base balance or body-temperature.[11]

Animal models reflecting the impact of atherosclerosis and DM can be useful, as they allow us to study vascular responses and scaffold degradation in a more complex setting.[12] Moreover, swine can be rendered diabetic and in combination with an atherogenic diet they develop atherosclerosis comparable to humans.[13] Scaffolds can be placed in coronary arteries and in-vivo sequential intracoronary imaging can be performed by optical coherence tomography (OCT), polarization-sensitive (PS)-OCT and near-infrared spectroscopy (NIRS). After sacrifice, histology and gel permeation chromatography (GPC) can be performed to assess scaffold coverage and degradation of the polymer.

We examined the mechanistic and morphological aspects of the coronary response to BVS1.1 in DM and non-DM swine fed a fast-food diet (FF-DM, FF-NDM respectively) using longitudinal intracoronary imaging and histology.

Materials and methods

Experimental design

The Erasmus MC Animal Ethics committee approved the study, performed in accordance with the Guide for Care and Use of Laboratory Animals.[14] Fifteen male [Yorkshire x Landrace] swine with an age of ~11 weeks and a body weight of ~30kg were included (see S1 File

for a detailed description). DM was induced by streptozotocin (140mg/kg iv, single dose) in 8 randomly selected male crossbred swine.[15] During streptozotocin injection, the swine were anesthetized with intramuscular azaperone (2 mg/kg, Stressnil, Janssen, Tilburg, The Netherlands), followed by intravenous thiopental (15 mg/kg, Nesdonal, Rhone Merieux, Lyon, France). The swine were housed in metabolic cages and were fed two fast-food (FF) meals a day during which they had access to food for one hour. The FF-diet is a diet containing 10% sucrose, 15% fructose, 25% (swine) lard, 1% cholesterol and 0.7% sodiumcholate (bile salts). The food intake was monitored for each animal separately and titrated to maintain growth at ~1.5 kg/week.

After 9 months, all 8 FF-DM and 5 FF-NDM received single 3.0x18.0mm Absorb BVS1.1 implants in 2, and 2 FF-NDM received single Absorb BVS1.1 implants in all 3 coronary arteries to ensure an even amount of scaffolds in FF-DM (N = 16) and FF-NDM (N = 16) (see S1 File for details about the BVS1.1). One day prior to BVS1.1-implantation the swine received 300 mg acetylsalicylic acid and a loading dose of 300 mg clopidogrel (Plavix, Sanofi). After an overnight fast, the swine were sedated using ketamine/ midazolam (20 mg/kg / 1 mg/kg i.m.) and atropine (1mg/30kg i.m.). After induction of anesthesia with thiopental (15 mg /kg i.v.; Nesdonal, Aventis), the swine were connected to a ventilator that administered a mixture of oxygen and nitrous oxide (1:2 [vol/vol]). Vascular access was obtained with an 8F vascular sheath in the carotid artery, 10.000 IU heparin was administered initially and thereafter 5000 IU of heparin was administered every hour. Anesthesia was maintained using 0.5–2.5 vol% isoflurane (Florence, Abbott Laboratories) as guided by hemodynamics and pain reflexes to ensure adequate analgesia and sedation. Antibiotic prophylaxis was administered by an intramuscular injection of 8 mL 200 mg/mL procaine-benzylpenicillin and 250 mg/mL streptomycin. After BVS-implantation, all swine were treated with clopidogrel (75mg) and acetylsalicylic acid (300mg) daily, until the end of the study. The latter also functions as analgesia during the post-operative recovery.

Sequential coronary imaging included QCA and OCT pre-, immediately, 3 and 6 months (M) post-implantation and NIRS pre-, 3M and 6M post-implantation. PS-OCT was performed in N = 3 FF-DM and N = 4 FF-NDM BVS at 6M. 3M imaging was included when pre and/or post-implantation imaging were available and 6M imaging was included when pre- and/or post—and 3M imaging were available. After the 3M imaging assessment, 3 FF-DM and 2 FF-NDM were sacrificed and after the 6M imaging assessment the remaining swine were sacrificed. After sacrifice, hearts were removed, the coronary tree dissected free and coronary arteries containing BVS randomized to histological (3M N = 5/10, 6M N = 12/22) or GPC analysis (3M N = 5/10, 6M N = 10/22) (Fig 1).

Fasting blood samples were obtained at baseline, 3M and 6M to measure glucose, total, low- and high-density lipoprotein cholesterol (TC, LDL, HDL) and triglyceride levels. Furthermore, in the FF-DM swine, glucose levels were assessed weekly by 24-hour urine samples. When glucose appeared in undiluted urine samples, venous glucose and ketone levels were checked via ear vein puncture and a handheld reader. When glucose levels were high (>20 mmol/L), in combination with ketone production, subcutaneous insulin (approx. 5–15 units once daily) was given to eliminate detectable ketone production while maintaining hyperglycemic state.

In-vivo QCA, (PS)-OCT and NIRS analysis

See S1 File for a detailed description of the imaging analyses. Coronary angiograms were obtained in two orthogonal views and QCA-analysis was performed (CAAS, version 5.9.2 Pie Medical Imaging BV). Mean (LD) and minimal lumen diameter (MLD), scaffold to artery

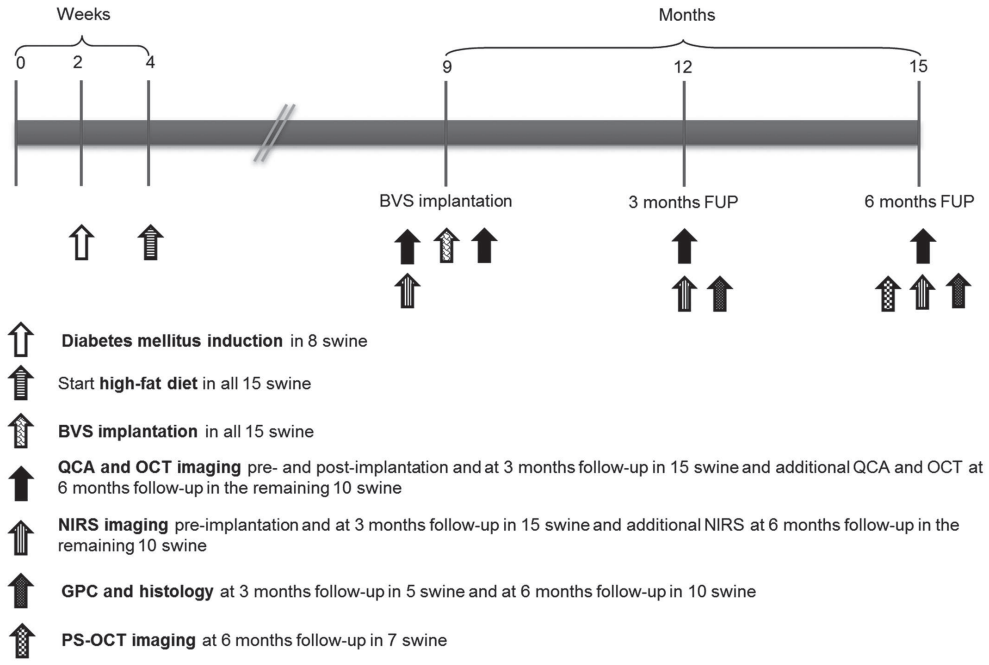

Fig 1. Study design. BVS = bioresorbable vascular scaffold, FUP = follow-up, QCA = quantitative coronary angiography, PS = Polarization Sensitive, OCT = optical coherence tomography, NIRS = near-infrared spectroscopy, GPC = gel permeation chromatography.

(S/A) ratio, acute gain and late lumen loss (LL) were documented. Longitudinal matching of OCT pullbacks (C7XR Fourier-Domain, St. Jude Medical) was performed as described previously using dedicated CURAD analysis software (CURAD BV).[16]

OCT parameters for vascular reaction, including lumen and scaffold dimensions and scaffold strut appearance, apposition, neointimal coverage and coverage morphology were assessed in 1-mm intervals using off-line OCT analysis software according to previously published methodology.[17] In pre-implantation lesions not exceeding the penetration depth of OCT, plaque burden (PB) was determined. Mean number of discernible struts were documented immediately post-implantation and at follow-up. Changes in strut appearances were categorised as preserved, open, dissolved bright, and dissolved black box.[18] Struts were scored as covered or uncovered and the morphology of the coverage—defined as [SA—LA] [16]–was described as homogeneous or heterogeneous. Heterogeneous coverage was furthermore described as lipid-laden, calcified, surrounding the struts or subluminal, or mixed (S1 Fig).[19]

PS-OCT was performed using a prototype imaging system. PS-OCT provides a measure of tissue birefringence, an optical tissue property that describes the interaction with polarized light. It grossly relates to microscopic tissue organization, and enables characterization of collagen content and smooth muscle cell (SMC) density in atherosclerotic plaques.[20]

NIRS analysis (LipiScan, InfraReDx) was used for lipid core plaque (LCP) characterization.[21] Lipid-core burden index (LCBI) was documented, indicating high probability that LCP is present. To evaluate the agreement between OCT and NIRS for detection of lipid, we compared—per scaffold—the LCBI score to the percentage of OCT cross-sections with lipid-containing morphology.

Ex-vivo degradation analysis

GPC was performed as described previously (see S1 File).[7] Degradation in our model was studied in relation to DM, time, inflammation, scaffold recoil, OCT-derived strut appearance and pre-implantation plaque burden.

Ex-vivo histological analysis

See S1 File for a detailed analysis. Proximal, middle and distal sections within each BVS were obtained. Tissue sections were stained by Hematoxylin-Eosin (HE) as an overview stain, Resorcin-Fuchsin for elastin, Alcian-Blue for proteoglycans, Oil-red-O (ORO) for lipids, Picrosirius Red (PSR) for collagen, von Kossa for calcium, and immunohistochemistry for smooth muscle cells (aSMA, clone 1A4, Dako, the Netherlands) and leukocytes (CD45, clone MCA 1447, AbD Serotec, UK). Polarization microscopy was performed to assess scaffold struts.

Histological analysis included neointimal healing and organization, collagen distribution, injury and inflammation score, lipid accumulation and presence of calcium classified as subluminal or surrounding struts (S2 Fig).

Statistical analysis

Statistical analysis (SPSS 20.0) entailed the Kolmogorov-Smirnov test for normality of the data. Normal distribution was expressed as mean ± standard deviation. Non-normally distrib-uted data were presented as median with interquartile range. Comparison of in-vivo imaging between FF-DM and FF-NDM was performed by generalized estimating equations (GEE) modeling. GEE is a statistical method that accounts for the clustered nature of >1 scaffold analyzed from one swine, which might result in unknown correlations among measurements within these scaffold clusters. A linear response model was applied with an exchangeable structure for the within-cluster correlation matrix. For repeated measures, GEE modeling was performed using a linear response model with an autoregressive (AR(1)) structure for the within-cluster correlation matrix. Comparison of ex-vivo GPC between FF-DM and FF-NDM swine was performed by independent samples t-test. To assess variable relations, the Spearman correlation coefficient was computed. All statistical tests were 2 tailed, and $P<0.05$ was considered statistically significant.

Results

Plasma measurements

Average TC, LDL and HDL were similar between FF-DM and FF-NDM (TC 18.7±5.0mmol/l and 19.0±5.8mmol/l (P = 0.86); LDL 15.1±5.1mmol/l and 15.6±5.1mmol/l (P = 0.75); HDL 5.4 ±0.8mmol/l and 5.7±0.7mmol/l (P = 0.13) in FF-DM and FF-NDM respectively). In the 8 swine that received a steptozotocin-injection, DM was successfully induced. Average plasma glucose and triglyceride levels were elevated in FF-DM compared to FF-NDM (15.0±7.8mmol/l vs. 4.5±1.0 mmol/l ($P<0.01$), 1.1±0.8mmol/l vs. 0.6±0.5mmol/l (P = 0.02), respectively). All FF-DM swine received insulin in the first 10 weeks after streptozotocin injection and 2 FF-DM

swine received insulin throughout the entire study based on detectable venous ketone body production."

In-vivo QCA, (PS)-OCT and NIRS

All 32 BVS were successfully implanted with a mean S/A-ratio of 1.1±0.1 in FF-DM and FF-NDM (P = 0.20).

QCA findings are presented in Fig 2A + 2B and S1 Table. Pre-implantation lesions were mild and similar between FF-DM and FF-NDM (P = 0.33). In all swine, mean LD decreased from post-implantation to 3M (P<0.01) and remained fairly stable from 3M to 6M (P = 0.34 and P = 0.54, respectively).

Quantitative OCT findings are presented in Fig 2C–2F and S1 Table. Pre-implantation lumen dimensions (LD, LA and MLA) were similar between FF-DM and FF-NDM (P = 0.46, P = 0.46 and P = 0.74) and pre-implantation %PB was mild (9±2% FF-DM, 10±1% FF-NDM; P = 0.58). Scaffolds were implanted according to protocol with an S/A ratio ≥1.1. Thus, LD increased in all swine from pre- to post-implantation (P>0.10). No signs of scaffold damage nor procedure-related injury were documented. No edge dissection or thrombus was observed and minor tissue prolapse was documented. Mild acute ISA was observed in 2 FF-DM BVS (mean ISA area 0.26±0.11mm^2) and 1 FF-NDM BVS (mean ISA area 0.03mm^2; P<0.01). From post-implantation to 3M, mean LD, LA and MLA decreased (~60%). At 3M, all ISA resolved, no late acquired ISA developed and all struts were covered. Restenosis, however, hampered OCT imaging at 3M in one FF-NDM. At 6M, OCT demonstrated a substantial neointima with a highly heterogeneous morphology, which was confirmed by histology (S3 Fig). From 3M to 6M, mean LD, LA, MLA, SD and SA remained fairly stable in all swine (Fig 2C–2E; S1 Table)

Changes in coverage morphology. See Table 1 for OCT findings. A heterogeneous morphology predominated in all swine at 3M, with a relatively high prevalence of calcium (25% (16%; 43%) in FF-DM and 16% (5%; 36%) in FF-NDM; P = 0.49). At 6M, the heterogeneous pattern predominated and was mainly characterized by calcium (41% (33%; 66%) in FF-DM and 59% (37%; 85%) in FF-NDM) (P = 0.82) (S1 and S2 Videos). Moreover, the accumulation of calcium increased (P<0.05), whereas the accumulation of lipid remained moderate (FF-DM P = 0.67, FF-NDM P = 0.97).

PS-OCT was only qualitatively analyzed and showed a heterogeneous neointima with spots of elevated birefringence (Fig 3E and 3K). Rapid depolarization of the signal was often observed, focally (Fig 3F2) and in areas with the appearance of lipid-rich plaque and inflammation (Fig 3F and 3L).

See S2 Table for NIRS findings. Similar to OCT, the prevalence of lipid was relatively low in FF-DM (9/15 BVS) and FF-NDM (3/11 BVS) at 3M with relatively low LCBI scores (3.00 (0.00; 22.50) in FF-DM, 0.00 (0.00; 3.00) in FF-NDM; P = 0.69). From 3M to 6M, the prevalence of lipid increased numerically, in FF-DM (6/6 BVS) and FF-NDM (5/8 BVS). Subsequently, LCBI scores slightly increased (17.50 (9.75; 26.00) in FF-DM, 6.50 (0.00; 47.25) in FF-NDM; P = 0.49).

The association of LCBI-score and percentage of OCT cross-sections with a lipid-laden or mixed appearance was modest at 3M (Spearman's rho 0.397; P = 0.05) but became stronger at 6M (Spearman's rho 0.666; P<0.01).

Changes in strut appearance. See S3 Table. The number of discernible struts per OCT cross-section was similar post-implantation (8±2 in FF-DM, 8±1 in FF-NDM) and at 3M (8±1 in FF-DM, FF-NDM) and decreased to 6M (7±1 in FF-DM, 6±2 in FF-NDM). The majority kept a preserved box appearance from 3M (79% in FF-DM, 81% in FF-NDM) to 6M (77% in

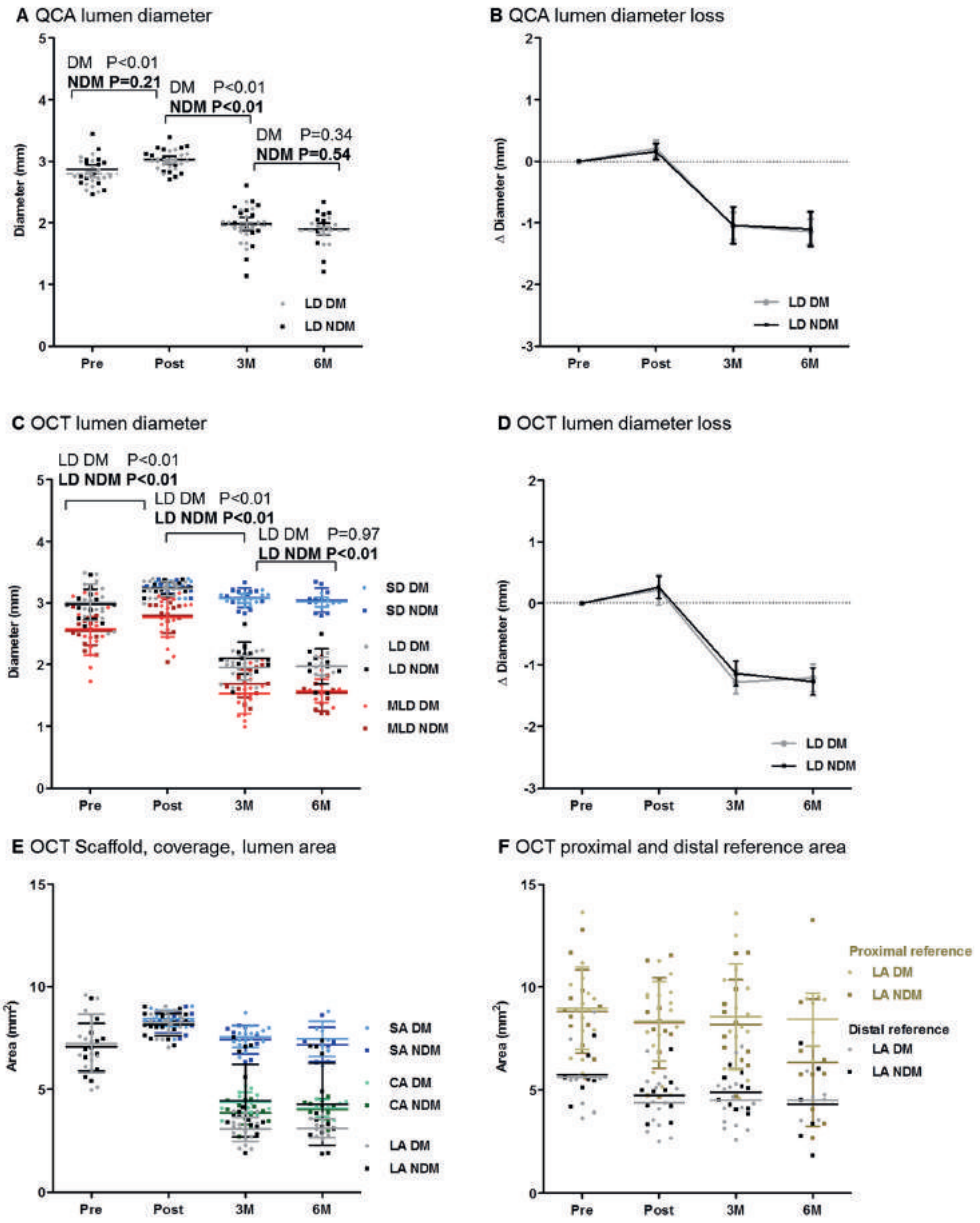

Fig 2. QCA and OCT analysis results. A+B) Mean lumen diameter (LD) slightly increased from pre-to post-implantation, decreased from post-implantation to 3M and remained stable from 3M to 6M. Grey: FF-DM, black: FF-NDM. **C-E**) Mean lumen area (LA), lumen diameter (LD) and minimal lumen diameter (MLD) increased slightly from pre- to post-implantation. Mean LA, LD and MLD and mean scaffold area (SA) and scaffold diameter (SD) decreased from post-implantation to 3M and mean LA, LD, MLD, SA, SD and coverage area (CA) remained stable from 3M to 6M. **F**) Proximal and distal reference LA slightly decrease from pre- to post-implantation and stabilized from post-implantation to 3M and 6M.

Table 1. OCT coverage analysis.

	3M			6M			P‡	
	FF-DM	FF-NDM	P*	FF-DM	FF-NDM	P*	FF-DM	FF-NDM
Coverage thickness, mm	0.42±0.08	0.39±0.11	0.50	0.39±0.06	0.41±0.11	0.59	0.05	0.38
Coverage area, mm^2	4.38±0.48	4.03±0.67	0.19	4.09±0.42	4.20±0.59	0.65	0.03	0.10
Coverage appearance								
Homogeneous, %	0 (0;6)	0 (0;4)	0.17	0 (0;0)	0 (0;4)	0.51	0.05	0.09
Heterogeneous, %	100 (94;100)	100 (96;100)	0.17	100 (100;100)	100 (96;100)	0.51	0.05	0.09
Lipid-laden, %	0 (0;12)	0 (0;14)	0.57	6 (6;11)	6 (0;15)	0.97	0.54	0.79
Calcified, %	25 (16;43)	16 (5;40)	0.49	41 (33; 66)	72 (37;87)	0.64	0.01	<0.01
Strut area, %	19 (10;31)	13 (0;34)	0.70	29 (13;63)	15 (5;47)	0.49	0.14	0.05
Subluminal, %	3 (0;7)	0 (0;4)	0.51	5 (0;6)	3 (0;29)	0.29	0.49	0.07
Strut area + subluminal, %	0 (0;0)	0 (0;0)	0.55	5 (0;8)	19 (3;29)	0.11	0.09	<0.01
Mixed, %	0 (0;7)	0 (0;9)	0.99	22 (12;48)	13 (1;40)	0.71	<0.01	0.04

Normally distributed data are presented as mean±SD, non-normally distributed data as median (interquartile range). FF-DM = fast-food fed diabetic swine, FF-NDM = fast-food fed non-diabetic swine, OCT = optical coherence tomography, 3M = 3 months follow-up, 6M = 6 months follow-up.

*P-value for the comparison between FF-DM and FF-NDM swine,

‡P-value for the difference between 3M and 6M.

FF-DM, 68% in FF-NDM). Interestingly, a substantial amount of struts appeared as dissolved black box at 3M (20% in FF-DM, 18% in FF-NDM) and 6M (22% in FF-DM, 31% in FF-NDM).[22]

Ex-vivo GPC

See Table 2. The initial Mn, Mw and PDI were 109.55 KDa, 229.68 KDa and 2.10 respectively. The initial mass was 8.53±0.08mg in FF-DM and 8.50±0.07mg in FF-NDM. Up to 6M, Mn, Mw and PDI decreased and mass loss was low: 5.5±1.9% in FF-DM and 4.3±1.4% in FF-NDM (P = 0.28).

There was no relationship between scaffold degradation and DM (P>0.10), or with OCT-derived pre-implantation %PB (P = 0.22), scaffold recoil (P = 0.59), preserved (P = 0.92), open (P = 0.45) or dissolved black box appearance (P = 0.99) at 3M, or at 6M (P = 0.29, P = 0.73 P = 0.27, P = 0.36 and P = 0.64 respectively).

Ex-vivo histology

See Table 2. All struts were covered by neointima 3M post-implantation (FF-DM 0.76 ±0.1mm, FF-NDM 0.62±0.1mm; P>0.10). Neointimal organization score was higher at 3M than 6M (P<0.01) in FF-DM and FF-NDM (P = 0.14). Injury was moderate. Injury scores were 1.30±0.42 and 1.10±0.14 (P = 0.58) at 3M and 1.10±0.13 and 1.04±0.33 (P = 0.74) at 6M in FF-DM and FF-NDM, respectively.

Collagen poor regions were observed within the neointima. They contained leukocytes, were evident at sites with extracellular lipids and often coincided with calcifications (Fig 4). Collagen poor but SMC positive tissue generally contained lipid accumulation (P>0.10 for FF-DM vs. FF-NDM) (Fig 4G–4I). Mainly intra- and extracellular lipid deposits with few cholesterol crystals were observed and advanced necrotic cores were absent.

Neointimal and peristrut calcifications were observed in FF-DM and FF-NDM **(P = 0.04)** at 3M and 6M (Fig 3, Table 2), with varying size, shape and location between animals, suggesting an inter-animal difference. From 3M to 6M, lipid-accumulation remained (Fig 5) and

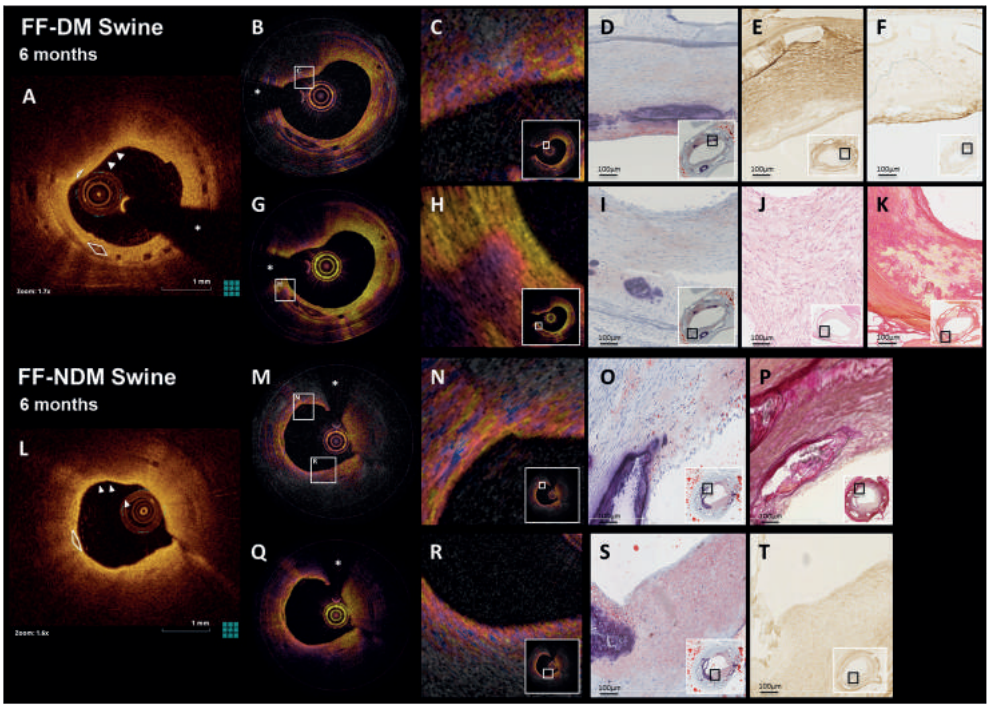

Fig 3. (PS)-OCT and corresponding histology at 6M. OCT demonstrated the development of a highly heterogeneous neointima with lipid and calcium accumulation in FF-DM and FF-NDM swine at 6 months (**A, L**), which was confirmed by histology (**D, I, O, S**; Oil-red-O). Phase retardation corresponding to tissue birefringence (**B, M**) and depolarization (**G, Q**) imaged by PS-OCT, demonstrated enhanced birefringence and depolarization (**C**) in an SMC-poor area (**E**; aSMA) with inflammation (**F**; CD45). Furthermore, PS-OCT demonstrated focal depolarization (**H**) in a collagen-poor area with loss of structure and evidence of early necrosis (**J, K**; HE, PSR). **N** shows coarse-grained high birefringence in an area with strongly circumferentially organized intimal SMCs (**P**; RF); lipid-rich, SMC-poor tissue (**T**; SMA) exhibits a more finely speckled heterogeneity, associated with a rapid loss of polarization degree (**R**). Asterisk (*) indicates guidewire artefact, arrowheads lipid, white lines calcium.

calcifications were observed more frequently subluminally (in 3/5 FF-DM BVS, 6/7 FF-NDM BVS).

At 6M, signs of myxoid degeneration with lipid accumulation were present (S4 Fig). In 3 BVS (N = 1 FF-DM, N = 2 FF-NDM) thrombus remnants were observed at 6M but not at 3M.

Furthermore, the polymeric scaffold struts demonstrated birefringence with polarized light, confirming preservation of scaffold struts in all swine.

Discussion

The present study describes the coronary artery response to BVS1.1 in FF-DM and FF-NDM swine. A remarkable neotintima burden with a highly heterogeneous appearance was observed in all swine, with lipid accumulation and calcification, indicative for the formation of

Table 2. GPC and histology results.

	3M			6M		
	FF-DM	FF-NDM	P*	FF-DM	FF-NDM	P*
GPC results						
BVS evaluated, n	3	2		5	5	
Mn, KDa	82.76±4.36	80.13±0.85	0.41	67.17±3.11	65.55±3.40	0.46
Mw, KDa	159.31±7.07	160.39±4.03	0.84	134.55±2.47	132.23±8.03	0.56
PDI	1.93±0.02	2.00±0.03	0.10	2.01±0.09	2.02±0.04	0.84
%Mass loss	2.6±0.6	2.0±6.6	0.86	5.5±1.9	4.3±1.4	0.28
Histological results						
BVS evaluated, n	3	2		5	7	
Neointimal thickness, mm	0.76±0.08	0.62±0.07	0.13	0.60±0.06	0.65±0.11	0.38
Medial thickness, mm	0.06±0.01	0.06±0.03	1.00	0.07±0.02	0.09±0.03	0.17
Adventitial thickness, mm	0.13±0.02	0.14±0.09	0.95	0.10±0.02	0.11±0.03	0.32
Scaffold area, mm^2	7.20±0.36	6.53±0.97	0.50	5.61±0.73	5.65±0.63	0.92
Injury sore	1.30±0.42	1.10±0.14	0.58	1.10±0.13	1.04±0.33	0.74
Inflammation score	0.95±0.32	0.32±0.08	0.08	0.22±0.18	0.30±0.47	0.71
Lipid accumulation, %	7.2 (5.4;17.3) 3.72.8;5.3)	15.8 (9.5;20.0) (9.0;(0.9;1.4)	0.83	19.5 (15.8;19.8)	9.4 (6.1;24.6)	0.76
Calcium						
Surrounding strut, %	88.03±8.21	94.05±8.41	0.48	72.54±11.63	74.21±19.63	0.87
Score per-strut	1.23±0.24	1.20±0.14	0.87	0.86±0.38	0.94±0.26	0.67
Subluminal, n	2	1	0.79	3	6	0.36

GPC = gel permeation chromatography, Mn = number average molecular weight, Mw = weight average molecular weight, PDI = polydispersity index [Mn/Mw]. Percentage (%) mass loss = [(Initial mass prior to scaffold implantation [T = 0] (mg)–Found mass (mg)) / Initial mass [T = 0] (mg) x 100].
*P-value for the comparison between FF-DM and FF-NDM swine. Footnotes and the remaining abbreviations are as listed in Table 1.

neoatherosclerosis. The scaffold polymer was preserved up to 6M, independent of inflammation or the presence of DM in FF-swine.

Neoatherosclerosis development following BVS-implantation

Interestingly, considerable neointima formation with complete strut coverage was observed in all swine, independent of the presence of DM. This is relevant, as uncovered struts have been associated with adverse events like stent thrombosis.[23] However, the neointima was highly heterogeneous in all swine, with substantial lipid- and calcium accumulation and lack of intimal organization at 6M, consistent with neoatherosclerosis formation. This is of note, as previously published experimental studies in healthy swine and clinical studies in selected patients demonstrated a favorable vascular response with rather homogeneous coverage following BVS-implantation.[7, 10, 24] There are three main differences between our study and the previously published experimental study by Onuma et al., namely 1: the version of the BVS; 2: the species in which the majority of the study was performed (miniswine) and 3: the presence of diabetes and hypercholesterolemia; In addition, we expect that, given the size of the animals in our study, our stents were implanted more distally.

First, in the histological evaluation of the first-generation BVS, revision 1.0, implanted in the coronary arteries of healthy Yorkshire x Landrace or Yucatan miniswine of unspecified age, minor calcifications were observed around the scaffold struts in the majority of BVS as early as 28 days post-implantation.[7] After an initial increase, the presence of calcifications decreased to 17.2% between two and four years post-implantation. In our study, implantation

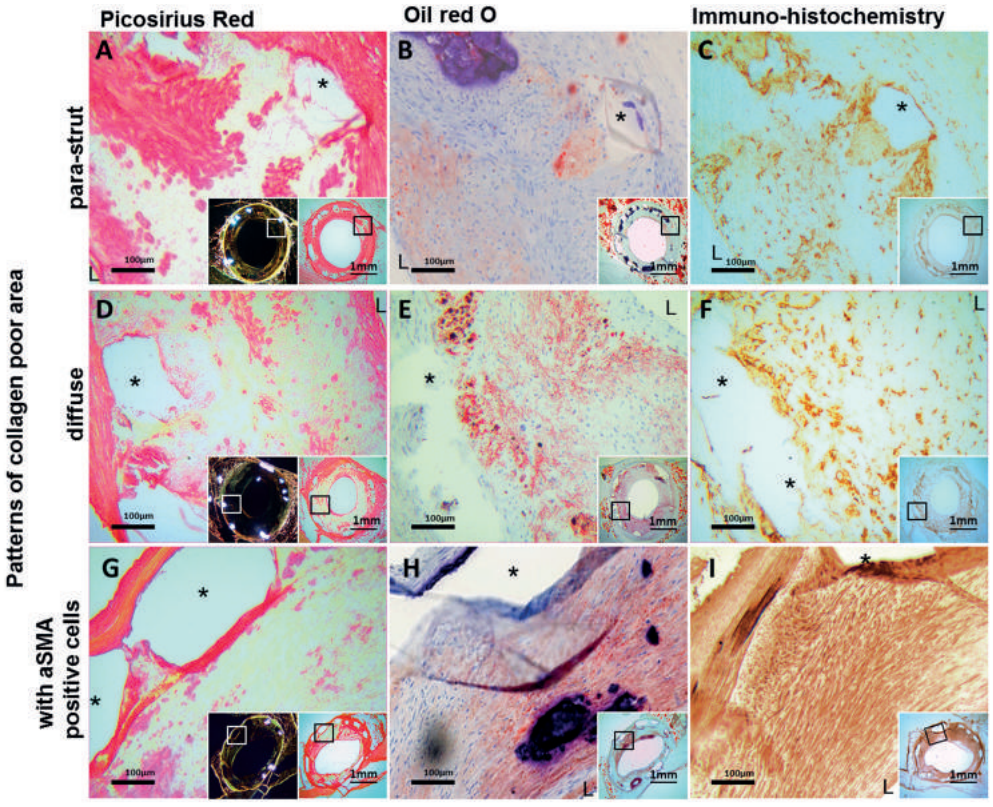

Fig 4. Irregular collagen distribution in the neointima. Collagen poor areas in peri-strut regions and neointima (**A, D**; Picrosirius Red) often demonstrated lipid accumulation (**B, E**; Oil-red-O), and leucocytes (**C, F**; CD45). Additionally, **G** (Picrosirius Red) demonstrates a patchy collagen poor lesion with lipid accumulation (**H**; Oil-red-O) and smooth muscle cells (**I**; aSMA). *: strut void, **L**: lumen.

of BVS 1.1 demonstrated calcifications around the majority of scaffold struts at 3M, which included calcifications of the luminal border at 6M in both FF-DM and FF-NDM swine. Second, the majority of swine coronary arteries studied by Onuma et al. were from Yucatan miniswine, whereas we studied the coronary arteries of Yorkshire x Landrace swine with a similar race as the 28-day Onuma data, showing calcifications as early as 28 days. Although strain differences have not been described before as cause of a different vascular response to the polymer, this cannot be excluded as a cause for the different vascular response observed between the study by Onuma et al. and our study. The final main difference between the study by Onuma et al. and our study is the presence of hypercholesterolemia in all animals, and of DM in a subgroup, where especially the former seems to drive the response for the vascular response. Hypercholesterolemia is indeed detrimental to the endothelium, diminishing the

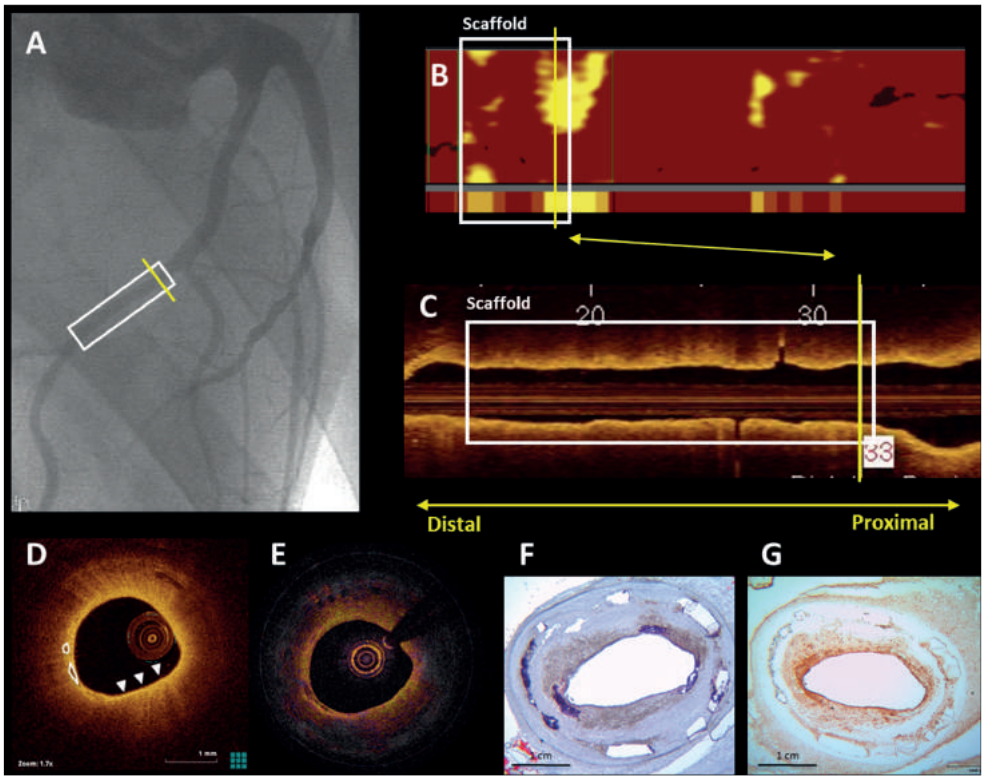

Fig 5. Corresponding QCA, OCT, NIRS and histology at 6M. QCA (**A**) demonstrates the scaffolded region (white block), with the yellow line indicating the region corresponding to the NIRS, (PS)-OCT and histology images (**B-G**). The NIRS chemogram demonstrates presence of lipid (**B**), also observed by OCT (**D**; arrowheads) that additionally demonstrates the presence of calcium (white circles). The PS-OCT phase retardation image demonstrates a finely grained pattern (**E**) consistent with lipid-rich neointima (**F**; Oil-Red-O) and active inflammation (**G**; CD45).

vascular wall barrier-function against excessive uptake of circulating lipids, resulting in neoatherosclerosis formation.[25, 26] In humans, calcification is accelerated by young age and mechanical stress and this might explain why we found such a high incidence in our swine model.[27] While it is not completely clear to what extent our observations can be extrapolated to the clinical setting, our observation of considerable neoatherosclerosis formation under diet induced dyslipidemia might point at neoatherosclerosis as an important contributor to BVS failure at long term, similar to that described for DES and BMS.[28, 29, 30] It might also be in line with individual observations of asyptomatic neoplaque rupture after BVS-implantation and recently reported cases of BVS thrombosis.[10, 17, 24, 31]

Furthermore interesting is the fact that neoatherosclerosis development was observed in all swine, independent of the presence of DM. Kereiakes et al. demonstrated that diabetic patients who were receiving insulin treatment had a worse outcome after stent-implantation compared

to those who were not receiving insulin.[32] In our study we did not observe a correlation between the amount of insulin given and the development of neoatherosclerosis. Of note, the swine receiving the most insulin, were not the swine that developed the worst neoatherosclerosis. Even in the two swine that received insulin throughout the entire study, who also received the greatest amount of food to ensure a similar growth pattern in all swine, neoatherosclerosis development was similar compared to all other FF-DM and FF-NDM swine. Factors such as duration of DM and hypertension may attribute to the severity of atherosclerotic disease and may therefore attribute to a more human-like evaluation of the coronary vascular healing response after BVS-implantation. Moreover, hypertension, not present in the current study, has been associated with adverse atherosclerosis-related events in DM patients.[33] Future studies assessing the coronary healing response after stent or scaffold-implantation in swine should consider using mature swine, and include risk factors such as hypertension to accurately evaluate the coronary vascular healing response to stent-implantation in a model that mimics human coronary atherosclerotic disease.

This study presents the first data of neoatheroasclerotic tissue organization characterized with PS-OCT. We observed enhanced tissue birefringence in areas with SMC alignment in the neointima, as well as in areas with inflammation. Macrophage recruitment in atherosclerosis has been associated with formation of cholesterol crystals [34], which are highly birefringent [35]. The contrast provided by PS-OCT, consisting of birefringence and depolarization, reflects tissue organization, which has an impact on structural plaque stability. A fuller understanding of the features highlighted by PS-OCT may complete our comprehension of neoatherogenesis and its impact on clinical sequelae.

Preserved scaffold integrity

GPC and histology demonstrated preserved scaffold integrity up to 6M after BVS1.1-implantation in all swine, which was not affected by DM or inflammation. This is expected as the scaffold starts losing structural integrity at 3–6 months, and scaffold resorption is driven by hydration, rather than inflammation. Although, theoretically, other factors associated with inflammation such as deregulated acid-base balance or body-temperature could influence scaffold degradation, this was not seen in the present study.[11]

Interestingly, OCT did demonstrate morphological changes at individual strut levels despite preserved scaffold integrity. The OCT classification of strut appearances was developed in the ABSORB Cohort A trial to characterize the optical changes of the struts during the process of bioresorption.[9] However, preclinical evaluation of BVS1.0 demonstrated full degradation of the scaffold struts by GPC, while OCT demonstrated the presence of so-called 'preserved black boxes' within the vascular wall.[7] As the OCT signal is arising from the interface of structures with different optical indices, OCT reflects changes of tissue surrounding the struts, rather than changes in strut morphology. This should be kept in mind when interpreting in-vivo clinical and preclinical OCT observations in BVS.

Methodological considerations

Sacrifice was planned for 1/3 of the swine at 3M, and thus the serial BL, 3M and 6M sample size was relatively small. The aim of our study, however, was to longitudinally examine mechanistic and morphological aspects of the coronary response to BVS1.1 in FF-DM and FF-NDM swine. To accurately assess the mechanistic aspects—e.g. scaffold resorption—at various time points, additional planned sacrifice at 3M was beneficial. Furthermore, atherosclerotic lesions that developed in FF-DM and FF-NDM swine before scaffold-implantation were relatively small. However, distribution and size of the lesions were similar in both groups, allowing for

adequate comparison of vascular responses following BVS-implantation between FF-DM and FF-NDM swine.

Conclusions

Scaffold coverage showed signs of neo-atherosclerosis in all FF-DM and FF-NDM swine, scaffold polymer was preserved and the vascular response to BVS was not influenced by diabetes.

Supporting information

S1 Fig. Qualitative OCT analysis of the scaffold coverage. In the top OCT cross-sections of a homogeneous, heterogeneous, lipid-laden, calcified and mixed appearance of the coverage are depicted and on the bottom the magnifications. The 'open' stars indicate the black boxes of the scaffold struts at follow-up. The asterix (*) indicates the guide wire artifact. The arrowheads indicate the region containing lipid and the drawn white lines indicate calcified regions.
(TIF)

S2 Fig. Schematic representation of histological regions of interest. Within the neointima, 2 specific regions were discerned: para-strut neointima, defined as in contact with the struts, and subluminal: located near the lumen.
(TIF)

S3 Fig. Restenosis at 3M. Restenosis of a BVS implanted in an FF-NDM swine at 3M. Coronary angiography post-implantation (A) and at 3M (B) demonstrates a significant lumen loss, with a percentage diameter stenosis (%DS) of 70% which persisted at 6M, (C). At 3M OCT was not performed as the lesion was considered too tight to allow passage of an OCT catheter without risk of causing ischemia and all the potential sequelae thereof. Therefore OCT was restricted to 6M follow-up, the scheduled sacrifice time point. OCT demonstrated a highly heterogeneous neointima (D), which is confirmed by histology demonstrating a large neointimal burden with calcification subluminal and surrounding the struts (E H&E + F, ORO).
D Lesion = Diameter of the lesion, Ref D Lesion = Reference diameter.
(TIF)

S4 Fig. Organized and non-organized luminal layers in the neointima. The vessels with well-organized neointimal layers (two arrows in **A**-**D**) showed dense elastic fibers (**B**) with 3 or more layers of αSMA positive cells (**C**) without lipid accumulation (**D**). The unorganized neointima showed myxoid degeneration (double arrow in **E**-**H**) with disarray and low density of αSMA positive cells (**G**). In the same area, lipid accumulation was clearly seen (**H**). αSMA: alpha smooth muscle cell actin, L: lumen, **A**-**D**: 3 months DM, **E**-**H**: 6 months non-DM, **A** and **E**: H&E, **B** and **F**: Resorcin-Fuchsin, **C** and **G**: αSMA, **E** and **H**: Oil red O, Scale bar in **A** -**H**: 100 μm, insert bar of **A** and **E**: 1000 μm.
(TIF)

S1 Table. Quantitative QCA and OCT analysis results. Normally distributed data are presented as mean ± SD, non-normally distributed data as median (interquartile range).
FF-DM = fast-food fed diabetic swine, FF-NDM = fast-food fed non-diabetic swine,
QCA = Quantitative coronary angiography, OCT = optical coherence tomography,
BVS = bioresorbable vascular scaffold, post = post-implantation, 3M = 3 months follow-up,
6M = 6 months follow-up. *P-value for the comparison between FF-DM and FF-NDM swine,
†P-value for the difference between post-procedure and 3M, ‡P-value for the difference between 3M and 6M.
(DOCX)

S2 Table. NIRS analysis results. NIRS = Near-infrared spectroscopy, LCBI = lipid core burden index. §P-value for the difference between pre-procedure and 3M. Remaining footnotes and abbreviations are as listed in Table 1.
(DOCX)

S3 Table. OCT strut appearance. Percentages are calculated as mean from the total (100%). Footnotes and abbreviations are as listed in Table 1.
(DOCX)

S1 Video. 6M OCT pullback of a BVS implanted in a FF-DM swine. OCT imaging at 6M in a FF-DM swine demonstrates a highly heterogeneous appearance of the coverage. The red line in the longitudinal view of the OCT pullback (middle panel) corresponds to the location of the OCT catheter in the 2D pullback (left panel) and 3D pullback (right panel). The asterisk (*) indicates the guidewire artefact, the green line delineates the contour of the lumen area, the stars indicate scaffold struts, the arrowheads lipid, the white circles calcium and the red circle indicates the marker of the scaffold. Word did not find any entries for your table of contents.
(MP4)

S2 Video. 6M OCT pullback of BVS in an FF-NDM swine. OCT imaging at 6M in an FF-NDM swine demonstrates a highly heterogeneous appearance of the coverage. The red line in the longitudinal view of the OCT pullback (middle panel) corresponds to the location of the OCT catheter in the 2D pullback (left panel) and 3D pullback (right panel). The green line delineates the contour of the lumen area, the stars indicate scaffold struts, the arrowheads lipid and the white circles indicate calcium.
(MP4)

S1 File. Supporting material and methods. Supporting information accompanying the manuscript titled: "Neoatherosclerosis development following bioresorbable vascular scaffold implantation in diabetic and non-diabetic swine coronary arteries".
(DOC)

Acknowledgments

We dedicate this work to Prof. Dr. W.J. van der Giessen, who helped to design and conduct this preclinical study, but passed away before its completion.

Author Contributions

Conceptualization: Nienke S. van Ditzhuijzen, Mieke van den Heuvel, Oana Sorop, Evelyn Regar.

Data curation: Nienke S. van Ditzhuijzen, Oana Sorop, Jurgen Ligthart, Karen Witberg, Gijs van Soest, Dirk-Jan Duncker, Evelyn Regar, Heleen M. M. van Beusekom.

Formal analysis: Nienke S. van Ditzhuijzen, Mie Kurata, Magdalena Murawska, Brett Bouma, Martin Villiger, Gijs van Soest, Evelyn Regar.

Funding acquisition: Dirk-Jan Duncker, Heleen M. M. van Beusekom.

Investigation: Nienke S. van Ditzhuijzen, Mie Kurata, Mieke van den Heuvel, Evelyn Regar, Heleen M. M. van Beusekom.

Methodology: Nienke S. van Ditzhuijzen, Dirk-Jan Duncker, Evelyn Regar, Heleen M. M. van Beusekom.

Project administration: Richard W. B. van Duin, Ilona Krabbendam-Peters, Heleen M. M. van Beusekom.

Supervision: Dirk-Jan Duncker, Evelyn Regar.

Writing – original draft: Nienke S. van Ditzhuijzen.

Writing – review & editing: Nienke S. van Ditzhuijzen, Mie Kurata, Mieke van den Heuvel, Oana Sorop, Richard W. B. van Duin, Ilona Krabbendam-Peters, Jurgen Ligthart, Karen Witberg, Magdalena Murawska, Brett Bouma, Martin Villiger, Hector M. Garcia-Garcia, Patrick W. Serruys, Felix Zijlstra, Gijs van Soest, Dirk-Jan Duncker, Evelyn Regar, Heleen M. M. van Beusekom.

References

1. Scheen AJ, Warzee F, Legrand VM. Drug-eluting stents: meta-analysis in diabetic patients. Eur Heart J. 2004; 25(23):2167–8; author reply 8–9. Epub 2004/12/02. https://doi.org/10.1016/j.ehj.2004.07.041 PMID: 15571834.
2. Berry C, Tardif JC, Bourassa MG. Coronary heart disease in patients with diabetes: part I: recent advances in prevention and noninvasive management. J Am Coll Cardiol. 2007; 49(6):631–42. Epub 2007/02/13. https://doi.org/10.1016/j.jacc.2006.09.046 PMID: 17291928.
3. Creager MA, Luscher TF, Cosentino F, Beckman JA. Diabetes and vascular disease: pathophysiology, clinical consequences, and medical therapy: Part I. Circulation. 2003; 108(12):1527–32. https://doi.org/10.1161/01.CIR.0000091257.27563.32 PMID: 14504252.
4. Qin SY, Zhou Y, Jiang HX, Hu BL, Tao L, Xie MZ. The association of diabetes mellitus with clinical outcomes after coronary stenting: a meta-analysis. PloS one. 2013; 8(9):e72710. Epub 2013/09/26. https://doi.org/10.1371/journal.pone.0072710 PMID: 24066025.
5. Oberhauser JP, Hossainy S, Rapoza RJ. Design principles and performance of bioresorbable polymeric vascular scaffolds. EuroIntervention. 2009; 5 Suppl F:F15–22. Epub 2009/12/15. https://doi.org/10.4244/EIJV5IFA3 PMID: 22100671.
6. Gomez-Lara J, Brugaletta S, Diletti R, Garg S, Onuma Y, Gogas BD, et al. A comparative assessment by optical coherence tomography of the performance of the first and second generation of the everolimus-eluting bioresorbable vascular scaffolds. Eur Heart J. 2011; 32(3):294–304. Epub 2010/12/03. https://doi.org/10.1093/eurheartj/ehq458 PMID: 21123276.
7. Onuma Y, Serruys PW, Perkins LE, Okamura T, Gonzalo N, Garcia-Garcia HM, et al. Intracoronary optical coherence tomography and histology at 1 month and 2, 3, and 4 years after implantation of everolimus-eluting bioresorbable vascular scaffolds in a porcine coronary artery model: an attempt to decipher the human optical coherence tomography images in the ABSORB trial. Circulation. 2010; 122(22):2288–300. Epub 2010/10/27. https://doi.org/10.1161/CIRCULATIONAHA.109.921528 PMID: 20975003.
8. Otsuka F, Pacheco E, Perkins LE, Lane JP, Wang Q, Kamberi M, et al. Long-term safety of an everolimus-eluting bioresorbable vascular scaffold and the cobalt-chromium XIENCE V stent in a porcine coronary artery model. Circulation Cardiovascular interventions. 2014; 7(3):330–42. https://doi.org/10.1161/CIRCINTERVENTIONS.113.000990 PMID: 24895447.
9. Serruys PW, Ormiston JA, Onuma Y, Regar E, Gonzalo N, Garcia-Garcia HM, et al. A bioabsorbable everolimus-eluting coronary stent system (ABSORB): 2-year outcomes and results from multiple imaging methods. Lancet. 2009; 373(9667):897–910. Epub 2009/03/17. https://doi.org/10.1016/S0140-6736(09)60325-1 PMID: 19286089.
10. Serruys PW, Onuma Y, Garcia-Garcia HM, Muramatsu T, van Geuns RJ, de Bruyne B, et al. Dynamics of vessel wall changes following the implantation of the Absorb everolimus-eluting bioresorbable vascular scaffold: a multi-imaging modality study at 6, 12, 24 and 36 months. EuroIntervention. 2013. https://doi.org/10.4244/EIJV9I11A217 PMID: 24291783.
11. Liu L, Li S, Garreau H, Vert M. Selective enzymatic degradations of poly(L-lactide) and poly(epsilon-caprolactone) blend films. Biomacromolecules. 2000; 1(3):350–9. Epub 2001/11/17. PMID: 11710123.
12. Koopmans SJ, Mroz Z, Dekker R, Corbijn H, Ackermans M, Sauerwein H. Association of insulin resistance with hyperglycemia in streptozotocin-diabetic pigs: effects of metformin at isoenergetic feeding in a type 2-like diabetic pig model. Metabolism. 2006; 55(7):960–71. Epub 2006/06/21. https://doi.org/10.1016/j.metabol.2006.03.004 PMID: 16784971.
13. Dixon JL, Stoops JD, Parker JL, Laughlin MH, Weisman GA, Sturek M. Dyslipidemia and vascular dysfunction in diabetic pigs fed an atherogenic diet. Arterioscler Thromb Vasc Biol. 1999; 19(12):2981–92. Epub 1999/12/11. PMID: 10591679.

14. Guide for the Care and Use of Laboratory Animals, 8th edition. Washington, DC: National Academies Press (US); 2011.

15. van den Heuvel M, Sorop O, Koopmans SJ, Dekker R, de Vries R, van Beusekom HM, et al. Coronary microvascular dysfunction in a porcine model of early atherosclerosis and diabetes. American journal of physiology. 2012; 302(1):H85–94. Epub 2011/10/11. https://doi.org/10.1152/ajpheart.00311.2011 PMID: 21984550.

16. van Ditzhuijzen NS, Karanasos A, Bruining N, van den Heuvel M, Sorop O, Ligthart J, et al. The impact of Fourier-Domain optical coherence tomography catheter induced motion artefacts on quantitative measurements of a PLLA-based bioresorbable scaffold. The international journal of cardiovascular imaging. 2014; 30(6):1013–26. Epub 2014/05/17. https://doi.org/10.1007/s10554-014-0447-3 PMID: 24831994.

17. Serruys PW, Onuma Y, Ormiston JA, de Bruyne B, Regar E, Dudek D, et al. Evaluation of the second generation of a bioresorbable everolimus drug-eluting vascular scaffold for treatment of de novo coronary artery stenosis: six-month clinical and imaging outcomes. Circulation. 2010; 122(22):2301–12. Epub 2010/11/26. https://doi.org/10.1161/CIRCULATIONAHA.110.970772 PMID: 21098436.

18. Ormiston JA, Serruys PW, Regar E, Dudek D, Thuesen L, Webster MW, et al. A bioabsorbable everolimus-eluting coronary stent system for patients with single de-novo coronary artery lesions (ABSORB): a prospective open-label trial. Lancet. 2008; 371(9616):899–907. Epub 2008/03/18. https://doi.org/10.1016/S0140-6736(08)60415-8 PMID: 18342684.

19. Kang SJ, Mintz GS, Akasaka T, Park DW, Lee JY, Kim WJ, et al. Optical coherence tomographic analysis of in-stent neoatherosclerosis after drug-eluting stent implantation. Circulation. 2011; 123(25):2954–63. Epub 2011/06/08. https://doi.org/10.1161/CIRCULATIONAHA.110.988436 PMID: 21646494.

20. Nadkarni SK, Pierce MC, Park BH, de Boer JF, Whittaker P, Bouma BE, et al. Measurement of collagen and smooth muscle cell content in atherosclerotic plaques using polarization-sensitive optical coherence tomography. J Am Coll Cardiol. 2007; 49(13):1474–81. Epub 2007/04/03. https://doi.org/10.1016/j.jacc.2006.11.040 PMID: 17397678.

21. Waxman S, Dixon SR, L'Allier P, Moses JW, Petersen JL, Cutlip D, et al. In vivo validation of a catheter-based near-infrared spectroscopy system for detection of lipid core coronary plaques: initial results of the SPECTACL study. JACC Cardiovasc Imaging. 2009; 2(7):858–68. Epub 2009/07/18. https://doi.org/10.1016/j.jcmg.2009.05.001 PMID: 19608137.

22. van Soest G, Regar E, Goderie TP, Gonzalo N, Koljenovic S, van Leenders GJ, et al. Pitfalls in plaque characterization by OCT: image artifacts in native coronary arteries. JACC Cardiovasc Imaging. 2011; 4(7):810–3. https://doi.org/10.1016/j.jcmg.2011.01.022 PMID: 21757174.

23. Finn AV, Joner M, Nakazawa G, Kolodgie F, Newell J, John MC, et al. Pathological correlates of late drug-eluting stent thrombosis: strut coverage as a marker of endothelialization. Circulation. 2007; 115(18):2435–41. Epub 2007/04/18. https://doi.org/10.1161/CIRCULATIONAHA.107.693739 PMID: 17438147.

24. Karanasos A, Simsek C, Gnanadesigan M, van Ditzhuijzen NS, Freire R, Dijkstra J, et al. OCT Assessment of the Long-Term Vascular Healing Response 5 Years After Everolimus-Eluting Bioresorbable Vascular Scaffold. J Am Coll Cardiol. 2014; 64(22):2343–56. Epub 2014/12/04. https://doi.org/10.1016/j.jacc.2014.09.029 PMID: 25465421.

25. Ross R. Atherosclerosis—an inflammatory disease. N Engl J Med. 1999; 340(2):115–26. Epub 1999/01/14. https://doi.org/10.1056/NEJM199901143400207 PMID: 9887164.

26. van Beusekom HM, Whelan DM, Hofma SH, Krabbendam SC, van Hinsbergh VW, Verdouw PD, et al. Long-term endothelial dysfunction is more pronounced after stenting than after balloon angioplasty in porcine coronary arteries. J Am Coll Cardiol. 1998; 32(4):1109–17. Epub 1998/10/13.. PMID: 9768740.

27. Schoen FJ, Levy RJ. Calcification of tissue heart valve substitutes: progress toward understanding and prevention. Ann Thorac Surg. 2005; 79(3):1072–80. Epub 2005/03/01. https://doi.org/10.1016/j.athoracsur.2004.06.033 PMID: 15734452.

28. van Beusekom HM, Post MJ, Whelan DM, de Smet BJ, Duncker DJ, van der Giessen WJ. Metalloproteinase inhibition by batimastat does not reduce neointimal thickening in stented atherosclerotic porcine femoral arteries. Cardiovasc Radiat Med. 2003; 4(4):186–91. Epub 2004/08/24. https://doi.org/10.1016/j.carrad.2004.02.004 PMID: 15321056.

29. Nakazawa G, Otsuka F, Nakano M, Vorpahl M, Yazdani SK, Ladich E, et al. The pathology of neoatherosclerosis in human coronary implants bare-metal and drug-eluting stents. J Am Coll Cardiol. 2011; 57(11):1314–22. Epub 2011/03/08. https://doi.org/10.1016/j.jacc.2011.01.011 PMID: 21376502.

30. van Beusekom HM, van der Giessen WJ, van Suylen R, Bos E, Bosman FT, Serruys PW. Histology after stenting of human saphenous vein bypass grafts: observations from surgically excised grafts 3 to 320 days after stent implantation. J Am Coll Cardiol. 1993; 21(1):45–54. Epub 1993/01/01. PMID: 8417075.

31. Karanasos A, Van Mieghem N, van Ditzhuijzen N, Felix C, Daemen J, Autar A, et al. Angiographic and optical coherence tomography insights into bioresorbable scaffold thrombosis: single-center experience. Circulation Cardiovascular interventions. 2015; 8(5). Epub 2015/05/15. https://doi.org/10.1161/CIRCINTERVENTIONS.114.002369 PMID: 25969547.

32. Kereiakes DJ, Ellis SG, Kimura T, Abizaid A, Zhao W, Veldhof S, et al. Efficacy and Safety of the Absorb Everolimus-Eluting Bioresorbable Scaffold for Treatment of Patients With Diabetes Mellitus: Results of the Absorb Diabetic Substudy. JACC Cardiovascular interventions. 2017; 10(1):42–9. Epub 2016/12/27. https://doi.org/10.1016/j.jcin.2016.10.019 PMID: 28017311.

33. Raggi P, Shaw LJ, Berman DS, Callister TQ. Prognostic value of coronary artery calcium screening in subjects with and without diabetes. J Am Coll Cardiol. 2004; 43(9):1663–9. Epub 2004/05/04. https://doi.org/10.1016/j.jacc.2003.09.068 PMID: 15120828.

34. Duewell P, Kono H, Rayner KJ, Sirois CM, Vladimer G, Bauernfeind FG, et al. NLRP3 inflammasomes are required for atherogenesis and activated by cholesterol crystals. Nature. 2010; 464(7293):1357–61. http://www.nature.com/nature/journal/v464/n7293/suppinfo/nature08938_S1.html. PMID: 20428172

35. Ioannou GN, Haigh WG, Thorning D, Savard C. Hepatic cholesterol crystals and crown-like structures distinguish NASH from simple steatosis. J Lipid Res. 2013; 54(5):1326–34. https://doi.org/10.1194/jlr.M034876 PMID: 23417738

The effect of bioresorbable vascular scaffold implantation on distal coronary endothelial function in dyslipidemic swine with and without diabetes

van den Heuvel M., Sorop O., van Ditzhuijzen N.S., de Vries R., van Duin R.W.B., Krabbendam-Peters I., van Loon J.E., de Maat M.P., van Beusekom H.M., van der Giessen W.J., Danser A.H.J. and Duncker D.J.

Int J Cardiol. 2018 Feb 1;252:44-51

13

The effect of bioresorbable vascular scaffold implantation on distal coronary endothelial function in dyslipidemic swine with and without diabetes

Mieke van den Heuvel[a,b,d,1], Oana Sorop[a,d,1], Nienke S. van Ditzhuijzen[a,1], René de Vries[b,1], Richard W.B. van Duin[a,1], Ilona Krabbendam-Peters[a,1], Janine E. van Loon[a,c,1], Moniek P. de Maat[c,1], Heleen M. van Beusekom[a,1], Wim J. van der Giessen[a,d,2], A.H. Jan Danser[b,1], Dirk J. Duncker[a,d,*,1]

[a] *Department of Cardiology, Thoraxcenter, Erasmus University Medical Center, Rotterdam, The Netherlands;*
[b] *Department of Internal Medicine, Sector Pharmacology and Metabolic Diseases, Erasmus University Medical Center, Rotterdam, The Netherlands;*
[c] *Department of Hematology, Erasmus University Medical Center, Rotterdam, The Netherlands;*
[d] *Netherlands Heart Institute, Utrecht, The Netherlands*

ARTICLE INFO

Article history:
Received 20 June 2017
Received in revised form 3 October 2017
Accepted 13 November 2017
Available online 20 November 2017

Keywords:
Bioresorbable vascular scaffold
Endothelial function
Diabetes

ABSTRACT

Background: We studied the effect of bioresorbable vascular scaffold (BVS) implantation on distal coronary endothelial function, in swine on a high fat diet without (HFD) or with diabetes (DM + HFD).
Methods: Five DM + HFD and five HFD swine underwent BVS implantation on top of coronary plaques, and were studied six months later. Conduit artery segments >5 mm proximal and distal to the scaffold and corresponding control segments of non-scaffolded coronary arteries, as well as segments of small arteries within the flow-territories of scaffolded and non-scaffolded arteries were harvested for in vitro vasoreactivity studies.
Results: Conduit segments proximal and distal to the BVS edges showed reduced endothelium-dependent vasodilation as compared to control vessels ($p < 0.01$), with distal segments being most prominently affected ($p < 0.01$). Endothelial dysfunction was only observed in DM + HFD swine and was principally due to a loss of NO. Endothelium-independent vasodilation and vasoconstriction were unaffected. Surprisingly, segments from the microcirculation distal to the BVS showed enhanced endothelium-dependent vasodilation ($p < 0.01$), whereas endothelium-independent vasodilation and vasoconstriction were unaltered. This enhanced vasorelaxation was only observed in DM + HFD swine, and did not appear to be either NO- or EDHF-mediated.
Conclusions: Six months of BVS implantation in DM + HFD swine causes NO-mediated endothelial dysfunction in nearby coronary segments, which is accompanied by a, possibly compensatory, increase in endothelial function of the distal microcirculation. Endothelial dysfunction extending into coronary conduit segments beyond the implantation-site, is in agreement with recent reports expressing concern for late scaffold thrombosis and of early BVS failure in diabetic patients.

Drug-eluting stents (DES) are widely used for the treatment of obstructive coronary artery disease (CAD), including in patients with dia-betes mellitus (DM) [1]. However, the use of, in particular first generation, DES has raised concern regarding long-term endothelial dysfunction adjacent to the stent including the distal microcirculation [2,3], which could be related to adverse events including late stent thrombosis [4]. Second generation DES have partially succeeded in reducing thrombosis, however paradoxical vasoconstriction adjacent to the stent has still been reported [4–6].

The everolimus-eluting bioresorbable vascular scaffold (BVS) has been introduced with the aim to provide temporary vessel scaffolding and to be subsequently resorbed over time with restoration of vasomotion. Indeed, the ABSORB trials have demonstrated efficacy for the treatment of simple CAD in selected DM and non-DM patients up to five years with some restoration of vasomotion [7–10]. Conversely, paradoxical vasoconstriction has also been observed within the scaffold and adjacent segments even at five years after implantation [7,8],

☆ This study was partly supported by a grant from Abbott Vascular (Grant No: CP001 / EMC 109-09-03).
* Corresponding author at: Division of Experimental Cardiology, Department of Cardiology, Thoraxcenter, Erasmus University Medical Center, PO Box 2040, 3000 CA Rotterdam, The Netherlands.
E-mail address: d.duncker@erasmusmc.nl (D.J. Duncker).
[1] These authors take responsibility for all aspects of the reliability and freedom from bias of the data presented and their discussed interpretation.
[2] Deceased 6 June 2011.

indicating persisting impairment of endothelial function. Of concern, higher rates of BVS thrombosis have recently been reported in unselected populations and in meta-analyses of all randomized trials up to 24 months after BVS implantation as compared to a specific second generation DES [11–13], as well as lack of superior vasomotor reactivity after 36 months [14] and still incomplete vasomotion after 5 years [9]. Therefore, endothelial dysfunction with its subsequent associated adverse events still remains an issue, also after BVS implantation. Moreover, whether BVS affects endothelial function in the distal perfusion territory of the scaffold is presently unknown. This is of importance since a healthy microcirculation plays a key role in the regulation of optimal myocardial perfusion [15], also after percutaneous coronary intervention (PCI).

A significant proportion of PCIs involves DM patients that experience a higher incidence of treatment failure, including stent thrombosis [1]. Indeed, DM has been shown to be an independent predictor of revascularisation failure six months after BVS implantation [11]. DM and endothelial dysfunction are closely related [16]. However, in the setting of DM, detailed studies of endothelial function of both coronary macro- and micro-circulation in the restoration phase of the BVS are currently lacking.

Swine are an excellent model for the evaluation of coronary scaffolds because of the anatomical similarities between porcine and human coronary arteries [17,18]. In addition, DM-induction in combination with a high fat diet (HFD) is known to generate atherosclerosis, and specific components of endothelial function can be studied to unravel underlying mechanisms [19,20]. Although the effects of BVS implantation have been studied in healthy swine, showing resemblance to the human situation including lack of vasomotion of the scaffold six months after implantation [17,18], details regarding endothelial function in the restoration phase in an atherosclerosis model with and without DM are currently lacking. Consequently, the present study was undertaken to evaluate in vitro the effect of BVS on adjacent endothelial function, as well as of the distal microcirculation, six months after implantation in dyslipidemic swine with or without DM.

1. Methods

1.1. Study device

The ABSORB™ BVS (Abbott Vascular, USA) is a balloon-expandable, fully bioresorbable scaffold that consists of a poly (L-lactide) backbone with a poly (D,L-lactide) coating in a 1:1 ratio with everolimus.

1.2. Experimental design

The protocol was approved by the local animal ethics committee and the study was performed according to the National Institutes of Health guide for the care and use of Laboratory animals. The protocol has been described in detail elsewhere [19–21]. In short, ten male crossbred (Yorkshire × Landrace) swine were fed a cholesterol-rich diet (HFD). Five animals were rendered DM (DM + HFD) by a single-dose injection of streptozotocin. After nine months of atherogenesis, quantitative coronary angiography (QCA) was performed. All anesthetized swine (isoflurane, 1–2.5% *v/v*) received randomly assigned single 3.0 × 18.0 mm BVS implants in two epicardial coronary arteries with a scaffold to artery ratio of 1.1 on top of an atherosclerotic lesion, based on the angiogram, with follow up (FU) of six months. The untreated coronary artery served as a control. After stent implantation, all swine received acetylsalicylic acid (300 mg) and clopidogrel (75 mg) once daily. Blood samples were obtained, as published previously [19,20]. Also, plasma von Willebrand factor (vWf) levels were determined as described previously [22].

At six months FU, QCA was repeated in anesthetized swine (pentobarbital sodium 20 $mg \cdot kg^{-1} \cdot h^{-1}$) and afterwards they were euthanized. The hearts were excised and placed in Krebs buffer [3,19]. Of each animal, one coronary artery treated with a BVS and one untreated artery were used. Segments of epicardial conduit arteries (>2 mm diameter) of a BVS treated artery, located >5 mm proximal or distal to the scaffold's edges, were isolated. Also, segments of the untreated artery at approximately similar locations were obtained. In addition, segments of epicardial small arteries (~300 μm diameter) in the distal flow area of the scaffold and of a similar location of the untreated control artery were dissected out for subsequent functional studies. The scaffold, including immediately adjacent ~5 mm proximal and distal vessel segments, was used in a separate study [21].

1.3. Quantitative coronary angiography

QCA analysis was performed by the Coronary Angiographic Analysis System (CAAS, version 5.9.2 Pie Medical Imaging BV, The Netherlands). After maximal vasodilation with isosorbide dinitrate (1 mg/artery i.c.), minimal and maximal lumen diameter were measured both proximal and distal to the BVS and in corresponding segments of unscaffolded reference coronary arteries.

1.4. In vitro coronary conduit and small arterial function assessment

Segments of conduit arteries (~4 mm length) were suspended in organ baths. Segments of small arteries (~2 mm length) were mounted in Mulvany wire-myographs (DMT, Denmark). Vascular responses were measured as changes in isometric force. Both conduit and small arteries were subjected to the same experimental protocol as described previously [3,19]. In short, after determination of the maximal contractile response to 0.1 mol/l potassium chloride (KCl), concentration-response curves (CRCs) were acquired using separate, in vivo adjacently positioned, segments. Endothelium-dependent relaxation to bradykinin (BK, 10^{-10}–10^{-6} mol/l) was recorded upon pre-constriction by the thromboxane analogue U46619 (10^{-6} mol/l) in a first set of segments. In order to determine nitric oxide (NO) dependent and NO-independent contributions, in a second set, the CRC for BK was constructed after 30 min of pre-incubation with the NO-synthase inhibitor *N*-nitro-L-arginine methyl ester (L-NAME, 10^{-4} mol/l) to block endogenous NO-production. From a third set, endothelium-independent but NO-mediated vasodilation to *S*-nitroso-*N*-acetylpenicillamine (SNAP, 10^{-9}–10^{-5} mol/l) was measured. Finally, CRCs for endothelin-1 (ET-1, 10^{-10}–10^{-7} mol/l) were constructed to study vasoconstriction in a fourth set of vessel segments.

In addition, small arteries were subjected to an extended protocol, due to availability of more vessel-segments and experimental set-ups, to study endothelial function in more detail. Additional sets of segments were incubated with the small conductance Ca^{2+}-activated K^+-channel inhibitor apamin (APA,10^{-7} mol/l), together with the intermediate conductance Ca^{2+}-activated K^+-channel inhibitor TRAM34 (10^{-5} mol/l) to block the endothelium-derived hyperpolarizing factor (EDHF) component of BK-induced relaxation [23] alone or in combination with L-NAME. This combination of blockers has previously been shown to almost completely abolish BK-induced vasodilation [19]. All reagents used were obtained from Sigma-Aldrich, The Netherlands.

1.5. Histology

Finally, conduit arterial segments were formaldehyde-fixed and stained en face with Oil-red-O (Sigma, The Netherlands) as a macroscopic stain of fat accumulation or stained with resorcin-fuchsin as a microscopic overview stain. Morphometry of the Oil-red-O staining was performed by measuring total area and stained area with an image analysis system (Clemex Technologies Inc., Canada) and data are presented as percentage lipid area.

1.6. Data analysis

Values are presented as mean ± SEM. Differences between outcome variables were analysed using paired *t*-testing, after normal distribution of data was confirmed with Komolgorov-Smirnov normality test. Vasodilator responses to BK and SNAP were expressed as percentage of pre-constriction to U46619. Vasoconstriction to ET-1 was normalized to the response to 0.1 mol/l KCl. Statistical analysis of CRCs was performed using two-way ANOVA, followed by Bonferroni's post hoc correction (StatView). $P < 0.05$ (two-tailed) was considered statistically significant.

2. Results

2.1. Model characteristics

Both DM + HFD and HFD swine showed elevated cholesterol levels, and only DM + HFD swine showed high glucose levels [19–21]. Plasma vWf-levels increased over time in both DM + HFD (0.28 ± 0.02 IU/ml at implantation; 0.34 ± 0.01 IU/ml at 6 months FU, $p < 0.05$) and HFD swine (0.30 ± 0.04 IU/ml at implantation, 0.37 ± 0.02 IU/ml at 6 months FU, $p < 0.05$), without a difference between the groups ($p > 0.1$).

2.2. QCA analysis

At 6 months FU, calculated mean lumen diameters both proximal and distal to the BVS were similar between BVS-treated coronaries and corresponding segments in non-scaffolded coronaries in DM + HFD and HFD animals (example shown in Fig. 1A). Mean lumen diameters of vessels used in the functional experiments were similar between groups (DM + HFD proximal to BVS: 4.06 ± 0.25 vs. Control proximal: 3.38 ± 0.46 mm; DM + HFD distal to BVS: 2.66 ± 0.26 vs. Control distal: 2.37 ± 0.34 mm; HFD proximal to BVS: 3.53 ± 0.42 vs. Control proximal 3.50 ± 0.04 mm; HFD distal to BVS: 2.09 ± 0.18 vs. Control distal 2.74 ± 0.41 mm; all, $p > 0.1$).

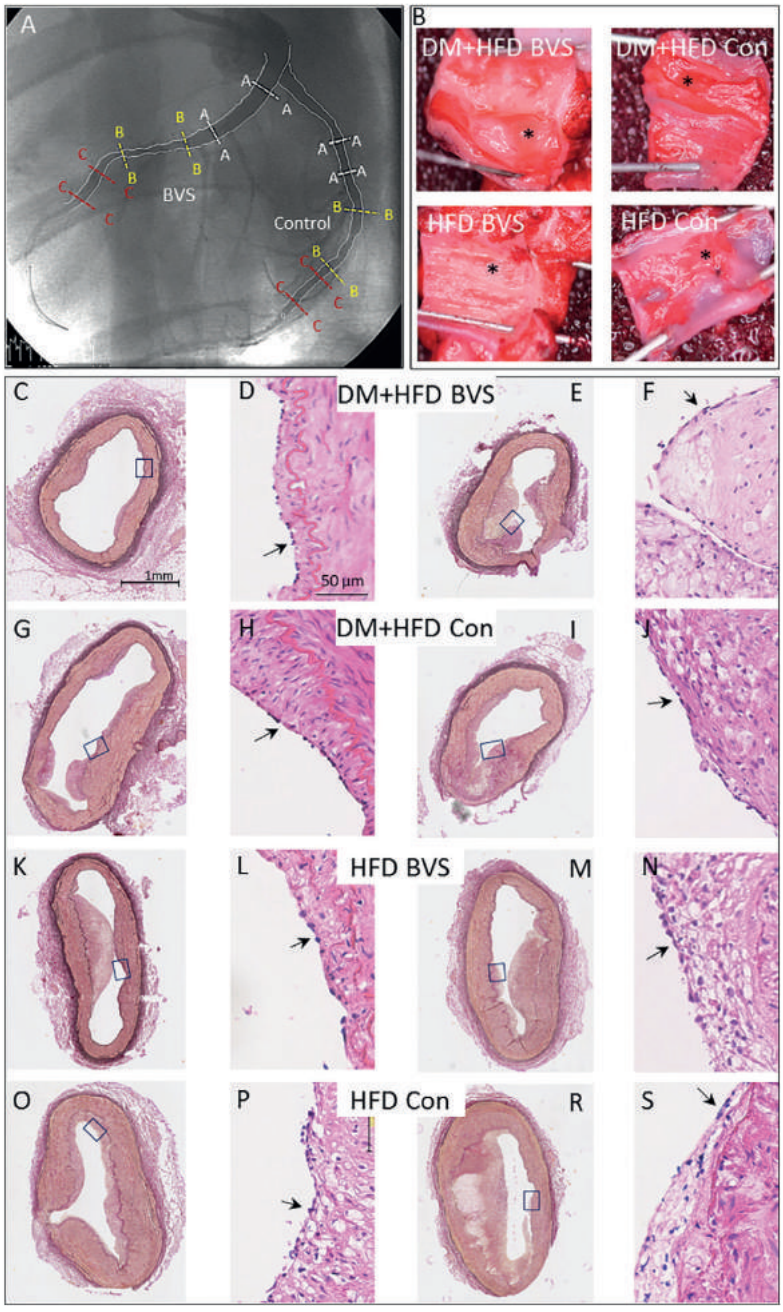

Fig. 1. Representative angiogram with depicted vessel segments located >5 mm proximal (delineated by the dashed white lines A–A) and distal (delineated by the dashed red lines C–C) to the BVS edges (delineated by the dashed yellow lines B–B), or corresponding segments of the reference (control) artery from which the mean lumen diameters were calculated (panel A). Representative segments (opened longitudinally), showing macroscopic fatty streaks, as visualized by en face Oil-red-O staining (panel B), and representative cross-sections (resorcin-fuchsin staining) showing plaques with different degrees of complexity from DM + HFD (panels C–J) and HFD (panels K–S) swine. *Indicates plaque. Arrows indicate endothelial lining.

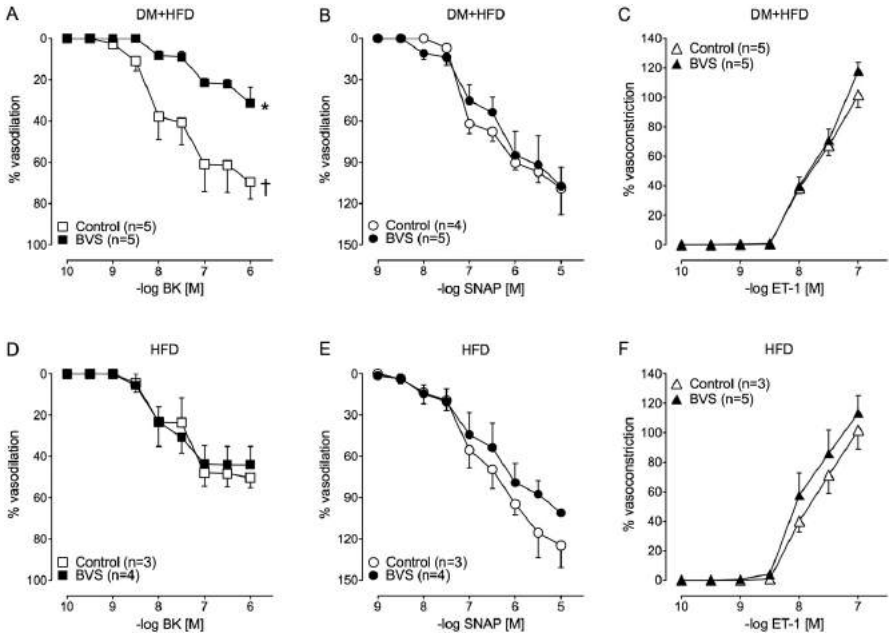

Fig. 2. Detailed coronary conduit artery function located >5 mm distal to the BVS and in control arteries, in dyslipidemic swine with or without DM. Figure highlighting the effects of six months of BVS implantation on BK-mediated vasodilation (A, D), SNAP-mediated vasodilation (B, E), and ET-1 mediated vasoconstriction (C, F) of distal conduit segments of DM + HFD (A-C) and HFD swine (D-F). Figure also highlighting the effect of DM + HFD on conduit arterial function of control segments (A–C) vs. HFD control segments (D–F). $^{*}p < 0.01$ DM + HFD BVS vs. DM + HFD Control; $^{\dagger}p = 0.051$ DM + HFD Control vs. HFD Control. BK = bradykinin, BVS = bioresorbable vascular scaffold, DM = diabetes mellitus, ET-1 = endothelin-1, HFD = high fat diet, n = number of animals, SNAP = *S*-nitroso-*N*-acetylpenicillamine.

2.3. In vitro vascular function

Contractile responses to KCl and U46619 were not significantly different between vessel segments of BVS-treated and control coronaries of DM + HFD and HFD swine, both for conduit and small arteries (data not shown).

2.3.1. Conduit arteries

DM on top of HFD slightly enhanced BK-induced dilation in control arteries (Fig. 2). BVS markedly blunted BK-induced vasodilation in DM + HFD swine, without altering the BK-response in HFD swine (Fig. 2). In accordance with previous studies from our laboratory [3], the BVS-induced attenuation of BK-mediated vasodilation was more pronounced in distal conduit artery segments as compared to proximal segments (Suppl. Fig. 1). Consequently, Fig. 2 only shows the responses in conduit artery segments located distal to the BVS, and vascular function was studied in more detail in these segments. Responses to SNAP and ET-1 were unaffected by either DM or BVS as compared to control vessels, indicating a BK-specific effect (Fig. 2).

L-NAME reduced BK-induced vasodilation under all conditions (Fig. 3). However, BVS significantly attenuated the surface area encompassed by the BK-response curves in the presence and absence of L-NAME in DM + HFD swine, so that the smallest NO-dependent area under the curve was observed in BVS treated vessels (25 ± 9), as compared to control vessels (101 ± 18) in DM + HFD swine and compared to BVS-treated vessels in HFD swine (56 ± 8; both $p < 0.05$). These observations indicate that loss of NO contributed to the blunted BK-induced vasodilation in conduit artery segments located >5 mm distal to the BVS in DM + HFD swine (Fig. 3).

2.3.2. Small arteries

In HFD swine, BVS did not alter the response to BK in small arteries of the microcirculation distal to the BVS (Fig. 4). However, in HFD + DM swine, BVS significantly enhanced the response to BK, both versus its own control and versus the BVS group of HFD swine (Fig. 4A, E). This difference remained apparent during L-NAME, TRAM34 and apamin, and the combination of these inhibitors. Inhibition of eNOS, with or without concomitant EDHF blockade, reduced the responses to BK, the largest reductions being observed in the presence of all inhibitors. However, this reduction appeared smaller in the BVS group of DM + HFD swine, indicating a remaining non-NO/non-EDHF mediated component of the BK-response, although this failed to reach statistical significance (Fig. 4A–H). Responses to SNAP (Fig. 4I, J) and ET-1 (Fig. 4K, L) were unaltered by either DM or BVS.

2.4. Histology

The Oil-red-O area was similar in conduit arterial segments located >5 mm distal to the BVS implant as compared to control coronary conduit arteries in both DM + HFD and HFD swine respectively

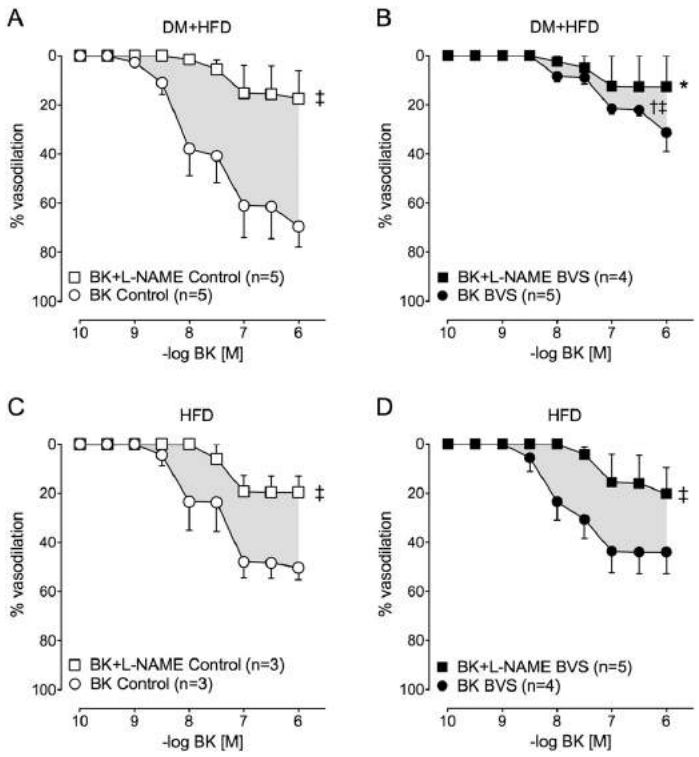

Fig. 3. NO- and non NO-mediated endothelial function located >5 mm distal to the BVS and in control arteries, in dyslipidemic swine with or without DM. Figure highlighting the effects of six months of BVS implantation on NO-mediated endothelium-dependent vasodilation of distal conduit segments of DM + HFD (A, B) and HFD swine (C, D). The grey area in between the BK and L-NAME curves depicts the specific contribution of the NO-mediated component of the BK-response. $^{*}p < 0.05$ area DM + HFD BVS vs. area DM + HFD Control; $^{\dagger}p < 0.05$ area DM + HFD BVS vs. area HFD BVS; $^{\ddagger}p < 0.05$ BK vs. BK + L-NAME. Abbreviations as in Fig. 2. In addition: L-NAME = *N*-nitro-L-arginine methyl ester, NO = nitric oxide.

(DM + HFD: BVS vs. Control: 30 ± 7% vs. 27 ± 8%, HFD: BVS vs. Control: 30 ± 6% vs. 26 ± 9%; all $p > 0.1$). Representative segments are shown in Fig. 1B.

As published previously [20], plaques with different degrees of complexity were observed to a similar extent in the coronary conduit arteries from DM + HFD and HFD swine, with presence of intact endothelium in both the lesion area as well as in the structurally unaltered vessel wall. Representative examples are shown in Fig. 1C–J, K–S. Also, as reported previously [19], coronary small arteries of both groups showed fatty streak lesions. The effect of BVS implantation on the atherosclerosis process distal to the BVS was not studied in detail in the present study.

3. Discussion

In the present study, we evaluated the effects of BVS implantation on endothelial function in vitro, of the vasculature located in the proximity (>5 mm from the edges) of the implanted BVS in a dyslipidemic swine model with or without DM. We hypothesized that the coronary circulation distal to the BVS would be at increased risk for endothelial dysfunction, especially in DM. The main findings were that: (i) only in the presence of DM, coronary conduit arteries showed decreased endothelium-dependent vasodilation, particularly distal to the BVS. This was principally due to loss of NO-mediated dilation; (ii) interestingly, the microcirculation within the distal perfusion territory showed slightly enhanced endothelium-dependent vasodilation that appeared to be independent of NO- or EDHF-mediated mechanisms.

In the present animal model, the high fat diet resulted in a similar degree of non-obstructive coronary atherosclerosis in DM + HFD compared to HFD swine [19,20], as well as increased plasma vWf-levels over time, indicating systemic endothelial dysfunction associated with CAD development [24]. In contrast, specific components of both systemic and coronary microvascular function were altered only in the presence of DM, similar to diabetic patients [19,25], making it a relevant model for the study of coronary interventions in the context of CAD and DM. BVS implantation within this model resulted in a similar vascular healing response with or without DM, with a heterogeneous coverage of the scaffold and a low polymer mass loss of the BVS at six months [21]. Therefore, the scaffold is likely to be immobile at this time-point according to prior results [8,18], although we did not perform vasomotion experiments to confirm this. For the present study, we focused on coronary vascular function in the segments located >5 mm from the scaffold's edges.

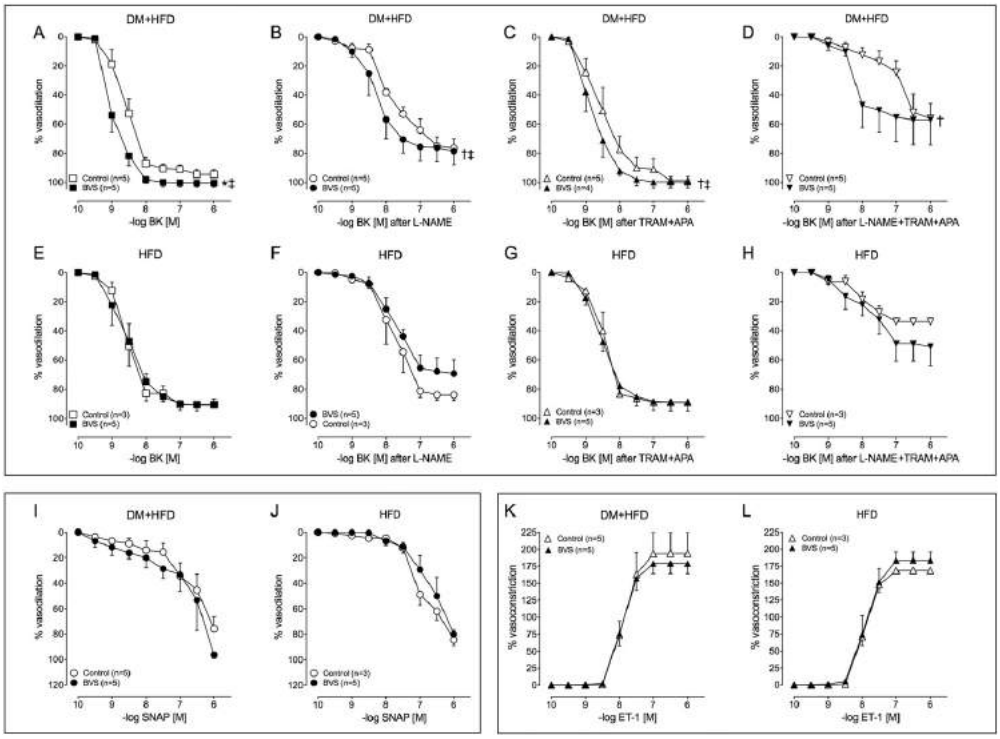

Fig. 4. Detailed coronary small arterial function in the distal perfusion area of the BVS and in control segments, in dyslipidemic swine with or without DM. Figure highlighting the effects of BVS on endothelium-dependent BK-induced vasodilation (A, E) after specific blockers (B, C, D, F, G, H), as well as endothelium-independent SNAP-induced vasodilation (I, J) and ET-1-induced vasoconstriction (K, L) of segments from the distal coronary microcirculation of DM + HFD (A, B, C, D, I, K) and HFD swine (E, F, G, H, J, L). Figure also highlighting the effect of DM + HFD on BK-mediated small arterial function distal to BVS (A) vs. BVS-treated vessels of HFD swine (E). L-NAME: blockage of endogenous NO (B, F). TRAM + APA: blockage of specific EDHFs (C, G). L-NAME + TRAM + APA: blockage of both endogenous NO and of specific EDHFs (D, H). $^{*}p < 0.01$ DM + HFD BVS vs. DM + HFD Control; $^{\dagger}p < 0.05$ DM + HFD BVS vs. DM + HFD Control; $^{\ddagger}p < 0.01$ DM + HFD BVS vs. HFD BVS. Abbreviations as in Fig. 2. In addition: EDHF = endothelium-derived hyperpolarizing factor, TRAM + APA = TRAM34 and apamin.

Only in swine with DM, we observed impaired coronary conduit endothelium-dependent vasodilation distal to the BVS. This impairment is in accordance with previous DES-studies, which also showed endothelial dysfunction in the peri-stent area, particularly in the distal segment, 6–16 months after implantation, in particular for first generation [2], and less extensively also for second generation [4–6] DES. In addition, endothelial dysfunction has also been demonstrated adjacent to the BVS, with signs of improvement up to five years after implantation [7–9,14]. Overall, these clinical studies demonstrated impaired adjacent vasomotion in small groups of both DM and non-DM patients, which were too limited to examine the subgroup of DM specifically. However, a relation between DM and early BVS failure has been observed [11]. In addition, none of these studies addressed vascular responsiveness of the untreated vessel as a control. This is relevant since atherosclerosis can also result in endothelial dysfunction, which makes it difficult to directly relate the observed vascular effects to the intervention per se. In the present study, six months of BVS implantation without DM did not affect adjacent endothelial function, which is in accordance with the results found by Gogas et al., one and two years after scaffold implantation in a healthy porcine model [17]. These observations suggest that our findings are specific to BVS combined with DM. Indeed, DM is known to complicate PCI success as shown by a reduced clinical outcome after two years in a large DES-study [26], as well as being an independent predictor of treatment failure up to one year after BVS implantation [11], highlighting again the interaction of DES, including BVS, with DM.

Specifically, in the present study, we showed that the endothelial impairment was caused by a reduced NO-mediated vasodilation. Impairment of NO bioavailability adjacent to DES has been described before [27]. Increased inflammation and oxidative stress due to vascular injury caused by the procedure, drug or other components of the BVS, have been proposed as possible mechanisms [27–29]. While everolimus has been shown to reduce NO-release [30], it is unlikely that the drug is responsible for this effect six months after implantation, as most of it has been released from the scaffold after three months [31]. Other scaffold related processes, including a change in regional wall shear stress and the consequent alterations in local gene expression [32], could also have contributed to the loss of NO synthase activity, although this does not readily explain why this was observed only in the DM + HFD-group. Recently, the AIDA trial was halted after two years due to safety concerns of the BVS with a higher incidence of scaffold thrombosis as compared to the metallic everolimus-coated DES [12]. A recent meta-analysis of all randomized BVS trials to date reported a similar concern for BVS as compared to its DES counterpart in clinical practice [13]. This further indicates

that not the drug everolimus, but the scaffold and its degradation products or the resulting pathology may be responsible for the observed endothelial dysfunction. These effects are thought to extend downstream through accumulation and diffusion within the vasa vasorum, explaining the more pronounced distal effects. Furthermore, DM is known to be strongly associated with NO-mediated endothelial dysfunction [16], although we did not find any evidence of DM-induced altered NO-mediated coronary function within the present model [19,20]. However, combined effects of both BVS and DM might explain the observed reduced NO-availability.

To study the extent of the endothelial dysfunction, we examined small arterial function in the distal perfusion area of the BVS. Previously, we and others have reported distal microvascular dysfunction after first generation DES implantation [3,27]. Therefore, the distal microcirculation is considered at increased risk of dysfunction. Surprisingly, we found an enhanced microvascular endothelium-dependent response, however only in the presence of reduced NO-mediated conduit endothelial function. This effect can be explained by the assumption that the distal microcirculation is reacting to the endothelial dysfunction occurring more proximally. Indeed, the coronary microcirculation is known to enable substantial variations in coronary flow due to several endothelium-dependent regulatory mechanisms including NO, EDHF, and prostacyclins [15]. This heterogeneity supports the concept of compensatory mechanisms that allow substitution of one dilator for another in the presence of disease [33], as shown in the coronary circulation of DM-patients [34]. Therefore, also within the present study, we propose a mechanism of local autoregulation of endothelial function between coronary conduit and small arteries in which a loss of NO-mediated component in the conduit artery is compensated for by NO-, EDHF-, and non-NO/non-EDHF-mediated components in the distal microcirculation.

3.1. Study limitations

Although the present large animal model with cardiovascular risk factors and early atherosclerosis does not completely mimic human obstructive CAD, it allows extensive functional analysis of early alterations in coronary vascular function. However, vascular function was only assessed in vitro. Although it is clear that in vitro several modulators of vascular tone are altered compared to the in vivo situation, including autonomic influences, myocardial metabolism, and blood flow, the in vitro approach allowed us to examine vascular function in parallel and in great detail. In an in vivo setting, such extensive vascular function studies would be hampered both by the potential systemic effects of the various compounds as well as by the long half-life of some of the substances and thus by the interaction of different substances within each animal. Nevertheless, the results from the present study warrant further studies to examine the alterations in endothelial function produced by the BVS in DM in vivo over an extended period of time, in order to assess the longitudinal pattern of coronary vascular impairment following BVS implantation.

A second limitation is that the functional measurements in isolated coronary vessels did not allow pressure fixation of the coronary vascular bed in situ, precluding detailed quantitative investigation of BVS-induced alterations in coronary microvascular structure.

3.2. Conclusions

This is the first study evaluating the effect of six months of BVS-implantation on coronary endothelial function in segments proximal and distal to the BVS. Specifically, in the presence of DM, coronary conduit artery segments located >5 mm distal to the BVS, showed decreased NO-mediated vasodilation. In contrast, the coronary microcirculation in the distal flow area of the BVS showed enhanced endothelium-dependent vasodilation, possibly acting as a compensatory mechanism.

3.3. Perspectives

The present study demonstrates that significant endothelial dysfunction is present in epicardial coronary artery segments located >5 mm proximal or distal to the BVS in diabetic swine on a high fat diet, as late as 6 months after BVS implantation. These observations may explain, at least in part, recent clinical studies reporting late scaffold thrombosis after BVS implantation as well as early treatment failure up to one year after BVS implantation, particularly in diabetic patients.

Conflict of interest

The authors report no relationships that could be construed as a conflict of interest.

Supplementary data to this article can be found online at https://doi.org/10.1016/j.ijcard.2017.11.037.

Acknowledgements

The article is dedicated to Professor W.J. van der Giessen, MD, PhD, who sadly passed away June 6, 2011.

Cindy Niles is kindly acknowledged for performing and analyzing the Oil-red-O staining of the coronary conduit segments.

References

[1] M. Roffi, D.J. Angiolillo, A.P. Kappetein, Current concepts on coronary revascularizа-tion in diabetic patients, Eur. Heart J. 32 (22) (2011) 2748–2757.
[2] M. van den Heuvel, O. Sorop, H.M. van Beusekom, W.J. van der Giessen, Endothelial dysfunction after drug-eluting stent implantation, Minerva Cardioangiol. 57 (5)(2009) 629–643.
[3] M. van den Heuvel, O. Sorop, W.W. Batenburg, C.L. Bakker, R. de Vries, S.J. Koopmans, et al., Specific coronary drug-eluting stents interfere with distal microvascular function after single stent implantation in pigs, JACC Cardiovasc. Interv. 3 (7) (2010) 723–730.
[4] E. Gutierrez, A.J. Flammer, L.O. Lerman, J. Elizaga, A. Lerman, F. Fernandez-Aviles, En-dothelial dysfunction over the course of coronary artery disease, Eur. Heart J. 34 (41)(2013) 3175–3181.
[5] S. Puricel, Z. Kallinikou, J. Espinola, D. Arroyo, J.J. Goy, J.C. Stauffer, et al., Comparison of endothelium-dependent and -independent vasomotor response after abluminal biodegradable polymer biolimus-eluting stent and persistent polymer everolimus-eluting stent implantation (COMPARE-IT), Int. J. Cardiol. 202 (2016) 525–531.
[6] A. Sumida, B.D. Gogas, H. Nagai, J. Li, S.B. King 3rd, N. Chronos, et al., A comparison of drug eluting stent biocompatibility between third generation NOBORI biolimus A9-eluting stent and second generation XIENCE V everolimus-eluting stent in a porcine coronary artery model, Cardiovasc. Revasc. Med. 16 (6) (2015) 351–357.
[7] P.W. Serruys, Y. Onuma, H.M. Garcia-Garcia, T. Muramatsu, R.J. van Geuns, B. de Bruyne, et al., Dynamics of vessel wall changes following the implantation of the ab-sorb everolimus-eluting bioresorbable vascular scaffold: a multi-imaging modality study at 6, 12, 24 and 36 months, EuroIntervention 9 (11) (2014) 1271–1284.
[8] S. Brugaletta, J.H. Heo, H.M. Garcia-Garcia, V. Farooq, R.J. van Geuns, B. de Bruyne, et al., Endothelial-dependent vasomotion in a coronary segment treated by ABSORB everolimus-eluting bioresorbable vascular scaffold system is related to plaque composition at the time of bioresorption of the polymer: indirect finding of vascular reparative therapy? Eur. Heart J. 33 (11) (2012) 1325–1333.
[9] D. Dudek, L. Rzeszutko, Y. Onuma, Y. Sotomi, R. Depukat, S. Veldhof, et al., Vasomo-tor response to nitroglycerine over 5 years follow-up after everolimus-eluting biore-sorbable scaffold implantation, JACC Cardiovasc. Interv. 10 (8) (2017) 786–795.
[10] P.W. Serruys, J. Ormiston, R.J. van Geuns, B. de Bruyne, D. Dudek, E. Christiansen, et al., A polylactide bioresorbable scaffold eluting everolimus for treatment of coro-nary stenosis: 5-year follow-up, J. Am. Coll. Cardiol. 67 (7) (2016) 766–776.
[11] D. Capodanno, T. Gori, H. Nef, A. Latib, J. Mehilli, M. Lesiak, et al., Percutaneous cor-onary intervention with everolimus-eluting bioresorbable vascular scaffolds in rou-tine clinical practice: early and midterm outcomes from the European multicentre GHOST-EU registry, EuroIntervention 10 (10) (2015) 1144–1153.
[12] J.J. Wykrzykowska, R.P. Kraak, S.H. Hofma, R.J. van der Schaaf, E.K. Arkenbout, A.J. IJsselmuiden, et al., Bioresorbable scaffolds versus metallic stents in routine PCI, N. Engl. J. Med. 376 (24) (2017) 2319–2328.
[13] Z.A. Ali, P.W. Serruys, T. Kimura, R. Gao, S.G. Ellis, D.J. Kereiakes, et al., 2-Year outcomes with the Absorb bioresorbable scaffold for treatment of coronary artery disease: a sys-tematic review and meta-analysis of seven randomised trials with an individual pa-tient data substudy, Lancet 390 (10096) (2017) 760–772.
[14] P.W. Serruys, B. Chevalier, Y. Sotomi, A. Cequier, D. Carrie, J.J. Piek, et al., Comparison of an everolimus-eluting bioresorbable scaffold with an everolimus-eluting metallic stent for the treatment of coronary artery stenosis (ABSORB II): a 3 year, randomised, controlled, single-blind, multicentre clinical trial, Lancet 388 (10059)(2016) 2479–2491.

[15] D.J. Duncker, A. Koller, D. Merkus, J.M. Canty Jr., Regulation of coronary blood flow in health and ischemic heart disease, Prog. Cardiovasc. Dis. 57 (5) (2015) 409–422.
[16] C.M. Sena, A.M. Pereira, R. Seica, Endothelial dysfunction - a major mediator of dia-betic vascular disease, Biochim. Biophys. Acta 1832 (12) (2013) 2216–2231.
[17] B.D. Gogas, J.J. Benham, S. Hsu, A. Sheehy, D.J. Lefer, T.T. Goodchild, et al., Vasomotor function comparative assessment at 1 and 2 years following implantation of the absorb everolimus-eluting bioresorbable vascular scaffold and the Xience V everolimus-eluting metallic stent in porcine coronary arteries: insights from in vivo angiography, ex vivo assessment, and gene analysis at the stented/scaffolded segments and the proximal and distal edges, JACC Cardiovasc. Interv. 9 (7) (2016) 728–741.
[18] J.P. Lane, L.E. Perkins, A.J. Sheehy, E.J. Pacheco, M.P. Frie, B.J. Lambert, et al., Lumen gain and restoration of pulsatility after implantation of a bioresorbable vascular scaffold in porcine coronary arteries, JACC Cardiovasc. Interv. 7 (6) (2014) 688–695.
[19] O. Sorop, M. van den Heuvel, N.S. van Ditzhuijzen, V.J. de Beer, I. Heinonen, R.W. van Duin, et al., Coronary microvascular dysfunction after long-term diabetes and hyper-cholesterolemia, Am. J. Physiol. Heart Circ. Physiol. 311 (6) (2016) H1339–H1351.
[20] N.S. van Ditzhuijzen, M. van den Heuvel, O. Sorop, A. Rossi, T. Veldhof, N. Bruining, et al., Serial coronary imaging of early atherosclerosis development in fast-food-fed diabetic and nondiabetic swine, JACC Basic Trans Science 1 (6) (2016) 449–460.
[21] N.S. van Ditzhuijzen, M. Kurata, M. van den Heuvel, O. Sorop, R.W.B. van Duin, I. Krabbendam-Peters, et al., Neoatherosclerosis development following bioresorbable vascular scaffold implantation in diabetic and non-diabetic swine, PLoS One 12 (9)(2017), e0183419.
[22] J.E. van Loon, M.A. Sonneveld, S.F. Praet, M.P. de Maat, F.W. Leebeek, Performance re-lated factors are the main determinants of the von Willebrand factor response to ex-haustive physical exercise, PLoS One 9 (3) (2014), e91687.
[23] W.W. Batenburg, R. Popp, I. Fleming, R. de Vries, I.M. Garrelds, P.R. Saxena, et al., Bradykinin-induced relaxation of coronary microarteries: S-nitrosothiols as EDHF?Br. J. Pharmacol. 142 (1) (2004) 125–135.
[24] M.C. van Schie, J.E. van Loon, M.P. de Maat, F.W. Leebeek, Genetic determinants of von Willebrand factor levels and activity in relation to the risk of cardiovascular disease: a review, J. Thromb. Haemost. 9 (5) (2011) 899–908.
[25] M. Khairoun, M. van den Heuvel, B.M. van den Berg, O. Sorop, R. de Boer, N.S. van Ditzhuijzen, et al., Early systemic microvascular damage in pigs with atherogenic di-abetes mellitus coincides with renal angiopoietin dysbalance, PLoS One 10 (4)(2015), e0121555.
[26] G.W. Stone, E. Kedhi, D.J. Kereiakes, H. Parise, M. Fahy, P.W. Serruys, et al., Differen-tial clinical responses to everolimus-eluting and Paclitaxel-eluting coronary stents in patients with and without diabetes mellitus, Circulation 124 (8) (2011) 893–900.
[27] L.K. Pendyala, J. Li, T. Shinke, S. Geva, X. Yin, J.P. Chen, et al., Endothelium-dependent vasomotor dysfunction in pig coronary arteries with Paclitaxel-eluting stents is as-sociated with inflammation and oxidative stress, JACC Cardiovasc. Interv. 2 (3)(2009) 253–262.
[28] R.P. Juni, H.J. Duckers, P.M. Vanhoutte, R. Virmani, A.L. Moens, Oxidative stress and pathological changes after coronary artery interventions, J. Am. Coll. Cardiol. 61 (14) (2013) 1471–1481.
[29] F. Otsuka, A.V. Finn, S.K. Yazdani, M. Nakano, F.D. Kolodgie, R. Virmani, The impor-tance of the endothelium in atherothrombosis and coronary stenting, Nat. Rev. Cardiol. 9 (8) (2012) 439–453.
[30] S. Banerjee, H. Xu, E. Fuh, K.T. Nguyen, J.A. Garcia, E.S. Brilakis, et al., Endothelial pro-genitor cell response to antiproliferative drug exposure, Atherosclerosis 225 (1)(2012) 91–98.
[31] J.A. Ormiston, M.W. Webster, G. Armstrong, First-in-human implantation of a fully bioabsorbable drug-eluting stent: the BVS poly-L-lactic acid everolimus-eluting cor-onary stent, Catheter. Cardiovasc. Interv. 69 (1) (2007) 128–131.
[32] C.V. Bourantas, H.M. Garcia-Garcia, C.A. Campos, Y.J. Zhang, T. Muramatsu, M.A. Morel, et al., Implications of a bioresorbable vascular scaffold implantation on vessel wall strain of the treated and the adjacent segments, Int. J. Card. Imaging 30 (3)(2014) 477–484.
[33] A.M. Beyer, D.D. Gutterman, Regulation of the human coronary microcirculation, J. Mol. Cell. Cardiol. 52 (4) (2012) 814–821.
[34] Z. Bagi, A. Feher, T. Beleznai, Preserved coronary arteriolar dilatation in patients with type 2 diabetes mellitus: implications for reactive oxygen species, Pharmacol. Rep. 61 (1) (2009) 99–104.

Part III

Endothelial dysfunction related to diabetes mellitus and the renin-angiotensin-aldosterone system

Diabetic complications: a role for the prorenin-(pro)renin receptor-TGF-beta1 axis?

van den Heuvel M., Batenburg W.W. and Danser A.H.

Mol Cell Endocrinol. 2009 Apr 29;302(2):213-8

14

Diabetic complications: A role for the prorenin–(pro)renin receptor–TGF-β_1 axis?

Mieke van den Heuvel, Wendy W. Batenburg, A.H. Jan Danser*

Division of Pharmacology, Vascular and Metabolic Diseases, Department of Internal Medicine, Erasmus MC, Dr. Molewaterplein 50, 3015 GE Rotterdam, The Netherlands

ARTICLE INFO

Article history:
Received 11 August 2008
Received in revised form 28 August 2008
Accepted 5 September 2008

Keywords:
Diabetes
Cardiovascular disease
Renin–angiotensin system
Prorenin
(Pro)renin receptor
TGF-β_1

ABSTRACT

Morbidity and mortality of diabetes mellitus are strongly associated with cardiovascular disease including nephropathy. A discordant tissue renin–angiotensin system (RAS) might be a mediator of the endothelial dysfunction leading to both micro- and macrovascular complications of diabetes. The elevated plasma levels of prorenin in diabetic subjects with microvascular complications might be part of this discordant RAS, especially since the plasma renin levels in diabetes are low. Prorenin, previously thought of as an inactive precursor of renin, is now known to bind to a (pro)renin receptor, thus activating locally angiotensin-dependent and -independent pathways. In particular, the stimulation of the transforming growth factor-β (TGF-β) system by prorenin could be an important contributor to diabetic disease complications. This review discusses the concept of the prorenin–(pro)renin receptor–TGF-β_1 axis, concluding that interference with this pathway might be a next logical step in the search for new therapeutic regimens to reduce diabetes-related morbidity and mortality.

1. Diabetes mellitus and the renin–angiotensin system

Cardiovascular disease, including nephropathy, accounts for most of the morbidity and mortality in patients with diabetes mellitus (Grundy et al., 1999). Both macrovascular and microvascular injury, with endothelial dysfunction as the main initiating event, are thought to underlie diabetic disease complications (de Jager et al., 2006; Ladeia et al., 2005). Prospective studies have demonstrated that endothelial dysfunction is highly predictive of future cardiovascular disease (Schachinger et al., 2000).

The renin–angiotensin system (RAS) is a major contributor to the cardiovascular and renal complications of diabetes mellitus (Gilbert et al., 2003; Hollenberg et al., 2004). While the systemic RAS is undoubtedly of importance in the regulation of blood pressure and volume homeostasis, a 'local' RAS has been linked to tissue damage (Danser, 2003). Inhibition of the RAS, by blocking the generation or action of its end-product angiotensin (Ang) II, with angiotensin-converting enzyme (ACE) inhibitors and Ang II type 1 (AT_1) receptor blockers, respectively, not only improves blood pressure control but also ameliorates endothelial function and cardiovascular/renal outcomes in patients with diabetes and nephropathy (Lewis et al.,

* Corresponding author at: Division of Pharmacology, Vascular and Metabolic Diseases, Room EE1418b, Department of Internal Medicine, Erasmus MC, Dr. Molewaterplein 50, 3015 GE Rotterdam, The Netherlands. Tel.: +31 10 7043540; fax: +31 10 7044733.
E-mail address: a.danser@erasmusmc.nl (A.H.J. Danser).

2001; Yusuf et al., 2000; Zuanetti et al., 1997). In addition, RAS inhibition is capable of reducing the incidence of new-onset diabetes (Perkins and Davis, 2008).

Remarkably, the circulating renin levels in diabetic subjects are low to normal (Danser et al., 1998; Stankovic et al., 2006). The additional, blood pressure-independent effect of RAS inhibition in diabetes may therefore point to increased tissue RAS activity in diabetic patients, e.g. in the vascular wall and kidney. This would imply that the systemic and tissue RAS are discordant in diabetes mellitus (Gilbert et al., 2003). The underlying mechanism of this phenomenon is unknown.

2. Prorenin–(pro)renin receptor–TGF-β_1 axis

2.1. Prorenin

The components required to synthesize Ang II in multiple tissues are generated at specific sites in the body: renin in the kidney, angiotensinogen in the liver, and ACE on the cell surface of endothelial and various other cells. With the cloning of the renin gene in 1984, prorenin was proven to be the precursor of renin (Hobart et al., 1984). A 43-amino acid N-terminal propeptide explains the absence of enzymatic activity of prorenin as compared to renin. This propeptide covers the enzymatic cleft and obstructs access of angiotensinogen to the active site of renin to generate Ang I. Circulating prorenin is mainly derived from the juxtaglomerular epithelioid cells of the kidney, although the reproductive organs, together with the adrenal, eye, and submandibular gland also generate and release prorenin (Krop and Danser, 2008; Krop et al., 2008). Prorenin release occurs constitutively, and the prorenin levels in human blood plasma are ≈10-fold higher than those of renin (Danser et al., 1998). Renin and prorenin levels are highly correlated but do not always alter in parallel (Danser et al., 1998). This is due, at least in part, to the fact that renin, unlike prorenin, is not synthesized extrarenally. Consequently, following a nephrectomy, only prorenin is detectable in blood plasma (Krop et al., 2008).

For unknown reasons, prorenin is elevated in patients with diabetes mellitus with microvascular complications (Luetscher et al., 1985). In fact, this elevation appears to precede the occurrence of these complications (Deinum et al., 1999). A recent study suggests that the source of the elevated prorenin in diabetes mellitus is the collecting duct. Unexpectedly, at this site Ang II stimulates the synthesis of prorenin (Kang et al., 2008), as opposed to its inhibiting effects in the juxtaglomerular apparatus. Furthermore, plasma prorenin in diabetic subjects was found to correlate with the renovascular response to captopril (Stankovic et al., 2006). This would imply a direct effect of prorenin in the renal vascular bed. Taken together, these findings suggest that circulating prorenin, in contrast to what was originally thought (i.e., that it has no function), may have some function after all.

An attractive postulate is that the elevated prorenin levels in diabetic subjects are responsible for the increased tissue RAS activity in this disease, thus causing the above-mentioned disease complications (Danser and Deinum, 2005). Supporting evidence for a local role of prorenin comes from studies in transgenic rodents with (inducible) prorenin expression in the liver. These animals display increased tissue angiotensin levels, and cardiac and renal pathology independently of hypertension (Prescott et al., 2002; Véniant et al., 1996). However, no clear evidence exists for local prorenin–renin conversion (Saris et al., 2001a), and infusing prorenin does not result in the appearance of renin (Lenz et al., 1991). In the absence of extrarenal renin generation, the question then remains how prorenin might exert a local effect. The recent discovery of a receptor for both renin and prorenin offers an explanation.

2.2. (Pro)renin receptor

The heart and vascular wall do not express the renin gene. Therefore, renal renin and/or prorenin need to be taken up from the circulation to allow Ang I generation in these organs. Simple diffusion cannot explain the renin levels at cardiac tissue sites (Danser et al., 1994; Katz et al., 1997; van Kesteren et al., 1999), and thus receptor-mediated uptake mechanisms might be involved (Danser et al., 1999). Indeed, endothelial cells, cardiomyocytes and cardiac fibroblasts are all capable of binding and internalizing renin and prorenin (Admiraal et al., 1999; van Kesteren et al., 1997). At least two candidate receptors have been proposed: the mannose 6-phosphate/insulin-like growth factor II receptor (M6P/IGF2R) (Saris et al., 2001a,b; van den Eijnden et al., 2001; van Kesteren et al., 1997) and the (pro)renin receptor (Nguyen et al., 2002). The M6P/IGF2R non-selectively binds M6P-containing proteins like prorenin and renin. However, such binding did not result in Ang II generation, and it is now believed that the M6P/IGF2R actually is a clearance receptor for prorenin and renin (Saris et al., 2002).

This leaves the (pro)renin receptor as the most promising candidate for specific tissue uptake of circulating prorenin and renin. This receptor binds prorenin with higher affinity than renin and, unlike the M6P/IGF2R, it does not internalize these proteins (Batenburg et al., 2007, 2008). Prorenin binding to the (pro)renin receptor allows the renin precursor to become catalytically active without proteolytic cleavage of the prosegment (Batenburg et al., 2007; Nguyen et al., 2002; Nurun et al., 2007) (Fig. 1). Such 'non-proteolytic activation' (involving a conformational change of the prorenin molecule) is also known to occur at low temperature ('cryo-activation') and low pH ('acid-activation') (Schalekamp et al., 2008). Apparently,

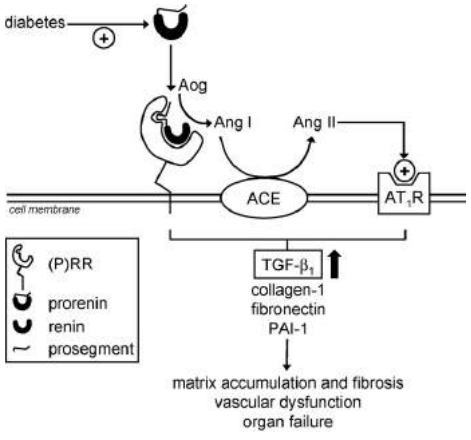

Fig. 1. Schematic overview of the prorenin–(pro)renin receptor–TGF-β_1 axis. A 43-amino acid N-terminal propeptide normally covers the enzymatic cleft of prorenin, thus obstructing access of angiotensinogen (Aog). (Pro)renin receptor-binding however induces a conformational change in the prorenin molecule, now allowing prorenin, like renin, to generate angiotensin (Ang) I from Aog, despite the fact that the prosegment is still present. In addition, prorenin binding per se (i.e., independently of angiotensin generation) activates intracellular signaling pathways. Theoretically, a (pro)renin receptor blocker will block both the (pro)renin receptor-mediated prorenin activation (resulting in angiotensin-dependent effects) and the direct (pro)renin receptor-induced intracellular signaling (resulting in angiotensin-independent effects), whereas a renin inhibitor will only block the angiotensin-mediated effects. ACE, Angiotensin-converting enzyme; AT_1R, Ang II type 1 receptor; (P)RR, (pro)renin receptor, PAI-1 plasminogen-activator inhibitor-1; TGF-β_1, transforming growth factor β_1.

binding to the receptor allows the prorenin molecule to undergo the same conformational change as exposure to low temperature or low pH. Receptor-mediated, non-proteolytic activation of prorenin solves the problem related to the absence of prorenin–renin converting enzymes at extrarenal tissue sites: binding of prorenin to its receptor is apparently sufficient to allow the inactive precursor to gain full enzymatic activity.

The (pro)renin receptor is a 350-amino acid protein with a single transmembrane domain. Although it was first described on cultured human mesangial cells (Nguyen et al., 2002), the C-terminal part of the receptor had been described earlier as an 8.9 kDa fragment being associated with a vacuolar H^+-ATPase (Ludwig et al., 1998). This part is highly homologous in both mammalian and non-mammalian species, suggesting that it has an important conserved function (Burcklé and Bader, 2006). Indeed, inactivation of the (pro)renin receptor gene before the end of embryogenesis is lethal in zebrafish (Amsterdam et al., 2004). The extracellular, prorenin- and renin-binding part of the receptor, retains high similarity between mammals only (Burcklé and Bader, 2006). This part of the (pro)renin receptor might therefore have developed later in evolution, for instance because there are advantages upon its binding with prorenin or renin (Bader, 2007). Interestingly, (pro)renin receptor expression appears to be upregulated under pathological conditions, e.g. at cardiac tissue sites of stroke-prone spontaneously hypertensive rats on a high salt diet (Ichihara et al., 2006a), and in the clipped kidneys of Goldblatt rats (Krebs et al., 2007).

After the discovery of the (pro)renin receptor, peptidic antagonists were designed based on the idea that the prosegment of prorenin contains a 'handle region' which binds to the receptor, allowing prorenin to become catalytically active (Ichihara et al., 2004; Nurun et al., 2007). These antagonists, known as 'handle region peptides' (HRPs), mimic the handle region and thus will bind competitively to the receptor, thereby preventing receptor-mediated prorenin activation and reducing tissue RAS activity. In support of this, HRP infusion normalized the elevated renal Ang II content in diabetic rats (Ichihara et al., 2004), as well as the cardiac Ang II content in stroke-prone spontaneously hypertensive rats, without affecting blood pressure (Ichihara et al., 2006a). Concomitantly, the development of diabetic nephropathy and cardiac fibrosis were prevented, suggesting that these phenomena depended on prorenin-induced tissue Ang II generation. Surprisingly however, identical renal effects of HRP occurred in diabetic AT_{1a} receptor deficient mice (Ichihara et al., 2006b), despite the fact that in these animals Ang II is no longer able to exert its normal effects (van Esch et al., 2006). This raises the possibility that (pro)renin receptor activation also results in Ang II-independent effects, in other words, that prorenin and renin act as agonists of the (pro)renin receptor, in addition to their capacity to generate Ang I when bound to the receptor.

2.3. Angiotensin-independent effects of (pro)renin receptor stimulation

Experiments with cells expressing the (pro)renin receptor have confirmed the concept of Ang II-independent effects mediated via this receptor. Both prorenin and renin were found to activate mitogen-activated protein kinases (MAPK) in the presence of RAS blockers (Huang et al., 2006, 2007b; Ichihara et al., 2006b; Nguyen et al., 2002; Saris et al., 2006). In neonatal rat cardiomyocytes, prorenin-induced MAPK p38 activation resulted in heat shock protein 27 phosphorylation and an alteration in actin filament dynamics, potentially affecting cardiac hypertrophy (Saris et al., 2006). In addition, in mesangial cells renin stimulated transforming growth factor β_1 (TGF-β_1) production via MAPK p42/p44, which subsequently resulted in an upregulation of profibrotic and prothrombotic molecules like fibronectin, collagen-1, and plasminogen-activator inhibitor-1 (PAI-1) (Huang et al., 2006, 2007b; Nguyen et al., 2002). Increased expression of TGF-β_1 is of particular interest in relation to the disease complications of diabetes mellitus (Fig. 1). The RAS and TGF-β system have been suggested to act together, providing an 'emergency response' to tissue injury (Border and Noble, 1998). However, when this response is inappropriate, as in diabetes, continued activation of the RAS and TGF-β system leads to progressive tissue injury with fibrosis and ultimately organ failure (Border and Noble, 1998; Gilbert et al., 2003). The TGF-β system regulates tissue remodeling by stimulation of matrix synthesis and inhibition of matrix degradation (Border and Noble, 1998). Indeed, overexpression of the TGF-β axis induces hyperplasia, apoptosis and fibrosis (Schulick et al., 1998), potentially leading to vascular and cardiac dysfunction (Chen et al., 2007). Furthermore, via upregulation of PAI-1 (Huang et al., 2007a), thrombotic cardiovascular events may occur, especially in the presence of a dysfunctional endothelium. TGF-β_1 also plays a pivotal role in the pathogenesis of diabetic nephropathy (Sharma et al., 1997; Yamamoto et al., 1993).

Results from in vivo studies in transgenic rats overexpressing the human (pro)renin receptor are in agreement with the concept of (pro)renin-induced, angiotensin-independent effects (Burcklé et al., 2006; Kaneshiro et al., 2007). The human (pro)renin receptor binds, but does not activate rat prorenin (Kaneshiro et al., 2007), and thus rat prorenin will only induce signaling via the human (pro)renin receptor. Indeed, the plasma and tissue angiotensin levels of transgenic rats overexpressing the human (pro)renin receptor were unaltered. Yet, these animals displayed increased levels of aldosterone in blood plasma and of cyclooxygenase-2 in the renal cortex. Moreover, from the age of 7 months, they developed hypertension, proteinuria and/or glomerulosclerosis. The latter was accompanied by increased MAPK p42/p44 phosphorylation and TGF-β_1 expression. HRP prevented the development of glomerulosclerosis in human (pro)renin transgenic rats (Kaneshiro et al., 2007). Moreover, it even reversed the glomerulosclerosis that had developed in diabetic rats (Takahashi et al., 2007).

In contrast with these observations, glomerulosclerosis did not occur in transgenic rats with inducible prorenin expression, despite the fact that such rats, following induction, displayed a 200-fold rise in plasma prorenin and were hypertensive (Peters et al., 2008). Moreover, HRP blocked neither prorenin binding to cells overexpressing the human (pro)renin receptor (Batenburg et al., 2007), nor prorenin-induced signaling in U937 monocytes (Feldt et al., 2008a). It was also ineffective in double transgenic rats expressing both human renin and human angiotensinogen (Feldt et al., 2008b), and in spontaneously hypertensive rats on a normal salt diet (Susic et al., 2008). Remarkably, in the latter model, it did decrease cardiac hypertrophy and fibrosis during high-salt conditions (Susic et al., 2008). Furthermore, HRP bound to cells which expressed a (pro)renin receptor variant lacking the transmembrane region, so that binding should actually not have occurred (Feldt et al., 2008a). Thus, at present it is uncertain to what degree the beneficial in vivo effects of HRP are solely due to prorenin blockade. Possibly, HRP has an alternative, as yet unknown mechanism of action, unrelated to the (pro)renin receptor, and/or its effectiveness is limited to animal models with a high prorenin/renin ratio (like in diabetes).

3. Prorenin inhibition

The beneficial effects of ACE inhibitors and AT_1 receptor antagonists involve interference with the generation or effects of Ang II at tissue sites (van Kats et al., 1998, 2000). Thus if, as discussed above, prorenin is a major determinant of tissue angiotensin production, prorenin is an obvious drug target. There are potentially two ways to

inhibit prorenin:renin inhibitors will block the enzymatic activity of prorenin (as present after 'unfolding' of the prosegment (Batenburg et al., 2008; Feldman et al., 2008)), and (pro)renin receptor blockers will block both the receptor-induced prorenin activation and any receptor-mediated, angiotensin-independent effects of prorenin (Fig. 1).

The current RAS blockers (i.e., the ACE inhibitors and AT_1 receptor blockers) act downstream of any prorenin-induced Ang I generation. Since Ang II, like prorenin, stimulates TGF-β_1, their beneficial effects in diabetes might involve, at least in part, a reduction of TGF-β_1. Indeed, the ACE inhibitor-induced reduction in the serum levels of TGF-β_1 correlated with long-term renoprotection in diabetic patients (Sharma et al., 1999). Recently renin inhibitors have been introduced into the clinical arena. These drugs act directly at the start of the angiotensin generation cascade, and the question is whether they will do better than the existing RAS blockers. The first clinical results with the only renin inhibitor that is currently available, aliskiren, suggest they do. Aliskiren reduced albuminuria on top of optimal antihypertensive therapy (including AT_1 receptor blockade) in type 2 diabetic subjects with nephropathy (Parving et al., 2008), and increased renal plasma flow far greater than any other RAS blocker (Fisher et al., 2008). To explain these beneficial findings, one has to assume that renin inhibitors either block the RAS more effectively or that they exert additional, unexpected effects, e.g. related to the (pro)renin receptor.

So far, in vitro studies do not reveal any blocking effects of aliskiren towards the direct effects of renin/prorenin via their receptor. Aliskiren neither affected the binding of renin/prorenin to the receptor, nor their signaling cascade following receptor activation (Batenburg et al., 2008; Feldman et al., 2008; Feldt et al., 2008a). Aliskiren however did block angiotensin generation by receptor-bound prorenin (Batenburg et al., 2008). In addition, renin inhibitors will suppress the consequences of the renin rise that occurs in response to every type of RAS blocker. During both ACE inhibition and AT_1 receptor blockade this renin rise will result in the generation of substantial amounts of Ang I, allowing an Ang II 'escape' during ACE inhibition and the stimulation of non-AT_1 receptors during AT_1 receptor blockade (Danser, 2007). During renin inhibition however, the continuous presence of the renin inhibitor prevents such Ang I generation (Danser et al., 2008), and thus the angiotensin levels will remain low (Fisher et al., 2008). Therefore, the most important reason for the effectiveness of aliskiren, particularly on top of maximum doses of other RAS blockers, appears to be that renin inhibitors offer superior RAS blockade.

RAS blockers not only cause a rise in renin, but also (although to a lesser degree) a rise in prorenin (Schalekamp et al., 2008). One might argue that this would result in increased (pro)renin receptor activation, thus potentially causing detrimental effects. However, no such detrimental effects have been observed during any of the many clinical trials with RAS blockers. A possible explanation for the lack of such effects comes from the work of Schefe et al. (2006, 2008), who showed that, on activation of the receptor, the transcription factor promyelocytic zinc finger is translocated to the nucleus and represses transcription of the (pro)renin receptor itself, thus creating a short negative feedback loop. In other words: high (pro)renin levels, as occurring during RAS blockade, will suppress (pro)renin receptor expression, thereby preventing excessive receptor activation. In fact, diabetic rats treated with aliskiren, displayed a decrease in (pro)renin receptor expression (Feldman et al., 2008), possibly due to the above described feedback mechanism. Such downregulation might also explain, at least in part, the absence of glomerulosclerosis in transgenic rats with inducible prorenin expression (Peters et al., 2008).

Given the lack of effect of aliskiren versus direct prorenin/renin-induced effects, (pro)renin receptor blockers would be expected to exert additional effects on top of renin inhibitors, e.g. they might induce a (further) reduction in TGF-β_1 levels. Although the first results with such blockers, particularly in diabetic animals, indeed look promising (Ichihara et al., 2004, 2006a; Kaneshiro et al., 2007), the lack of effect of HRP observed in animals with high-renin hypertension (Feldt et al., 2008a,b) suggests that more work and/or better blockers are needed. No clinical data are currently available with these drugs.

4. Conclusions

The prorenin–(pro)renin receptor–TGF-β_1 axis is an exciting new pathway that finally provides a role for the 'inactive' precursor of renin. This is of particular relevance in diabetes accompanied by microvascular complications given the high prorenin (and low renin) levels observed in this condition. Why prorenin is elevated in the first place and whether in humans, as in rats (Kang et al., 2008), it originates in the collecting duct remains to be determined. Prorenin might be the 'missing link' explaining the high tissue RAS activity and low plasma RAS activity in diabetes. Its local activation does not require a prorenin–renin converting enzyme (for which there is no evidence (Saris et al., 2001a)), but simple binding to a receptor. Renin inhibitors will efficiently block any Ang I generation by receptor-bound prorenin (Batenburg et al., 2008), thus potentially explaining why they exert effects on top of optimal therapy with 'classical' RAS blockers like the ACE inhibitors and AT_1 receptor antagonists. Renin inhibitors do not interfere with the direct, angiotensin-independent effects of prorenin mediated via the (pro)renin receptor. Since the latter involve, among others, TGF-β_1 production (Huang et al., 2007b), a (pro)renin receptor blocker might theoretically reduce TGF-β_1 on top of maximal RAS blockade. This is attractive since combined RAS blockade and TGF-β inhibition already resulted in enhanced antifibrotic effects (Yu et al., 2004).

Acknowledgement

The Dutch Kidney Foundation (NSN C08.2246) has supported this study.

References

Admiraal, P.J.J., van Kesteren, C.A.M., Danser, A.H.J., Derkx, F.H.M., Sluiter, W., Schalekamp, M.A.D.H., 1999. Uptake and proteolytic activation of prorenin by cultured human endothelial cells. J. Hypertens. 17, 621–629.

Amsterdam, A., Nissen, R.M., Sun, Z., Swindell, E.C., Farrington, S., Hopkins, N., 2004. Identification of 315 genes essential for early zebrafish development. Proc. Natl. Acad. Sci. U.S.A. 101, 12792–12797.

Bader, M., 2007. The second life of the (pro)renin receptor. J. Renin Angiotensin Aldosterone Syst. 8, 205–208.

Batenburg, W.W., Krop, M., Garrelds, I.M., de Vries, R., de Bruin, R.J.A., Burcklé, C., Müller, D.N., Bader, M., Nguyen, G., Danser, A.H.J., 2007. Prorenin is the endogenous agonist of the (pro)renin receptor. Binding kinetics of renin and prorenin in rat vascular smooth muscle cells overexpressing the human (pro)renin receptor. J. Hypertens. 25, 2441–2453.

Batenburg, W.W., de Bruin, R.J.A., van Gool, J.M.G., Müller, D.N., Bader, M., Nguyen, G., Danser, A.H.J., 2008. Aliskiren-binding increases the half life of renin and prorenin in rat aortic vascular smooth muscle cells. Arterioscler. Thromb. Vasc. Biol. 28, 1151–1157.

Border, W.A., Noble, N.A., 1998. Interactions of transforming growth factor-beta and angiotensin II in renal fibrosis. Hypertension 31, 181–188.

Burcklé, C., Bader, M., 2006. Prorenin and its ancient receptor. Hypertension 48, 549–551.

Burcklé, C.A., Danser, A.H.J., Müller, D.N., Garrelds, I.M., Gasc, J.M., Popova, E., Plehm, R., Peters, J., Bader, M., Nguyen, G., 2006. Elevated blood pressure and heart rate in human renin receptor transgenic rats. Hypertension 47, 552–556.

Chen, L.L., Yin, H., Huang, J., 2007. Inhibition of TGF-beta1 signaling by eNOS gene transfer improves ventricular remodeling after myocardial infarction through angiogenesis and reduction of apoptosis. Cardiovasc. Pathol. 16, 221–230.

Danser, A.H.J., 2003. Local renin–angiotensin systems: the unanswered questions. Int. J. Biochem. Cell. Biol. 35, 759–768.
Danser, A.H.J., 2007. Novel drugs targeting hypertension: renin inhibitors. J. Cardiovasc. Pharmacol. 50, 105–111.
Danser, A.H.J., Deinum, J., 2005. Renin, prorenin and the putative (pro)renin receptor. Hypertension 46, 1069–1076.
Danser, A.H.J., van Kats, J.P., Admiraal, P.J.J., Derkx, F.H.M., Lamers, J.M.J., Verdouw, P.D., Saxena, P.R., Schalekamp, M.A.D.H., 1994. Cardiac renin and angiotensins. Uptake from plasma versus in situ synthesis. Hypertension 24, 37–48.
Danser, A.H.J., Derkx, F.H.M., Schalekamp, M.A.D.H., Hense, H.W., Riegger, G.A.J., Schunkert, H., 1998. Determinants of interindividual variation of renin and prorenin concentrations: evidence for a sexual dimorphism of (pro)renin levels in humans. J. Hypertens. 16, 853–862.
Danser, A.H.J., Saris, J.J., Schuijt, M.P., van Kats, J.P., 1999. Is there a local renin–angiotensin system in the heart? Cardiovasc. Res. 44, 252–265.
Danser, A.H.J., Charney, A., Feldman, D.L., Nussberger, J., Fisher, N., Hollenberg, N., 2008. The renin rise with aliskiren: it's simply stoichiometry. Hypertension 51, e27–e28.
de Jager, J., Dekker, J.M., Kooy, A., Kostense, P.J., Nijpels, G., Heine, R.J., Bouter, L.M., Stehouwer, C.D., 2006. Endothelial dysfunction and low-grade inflammation explain much of the excess cardiovascular mortality in individuals with type 2 diabetes: the Hoorn Study. Arterioscler. Thromb. Vasc. Biol. 26, 1086–1093.
Deinum, J., Ronn, B., Mathiesen, E., Derkx, F.H.M., Hop, W.C., Schalekamp, M.A.D.H., 1999. Increase in serum prorenin precedes onset of microalbuminuria in patients with insulin-dependent diabetes mellitus. Diabetologia 42, 1006–1010.
Feldman, D., Jin, L., Xuan, H., Contrepas, A., Zhou, Y., Webb, R.L., Mueller, D.N., Feldt, S., Cumin, F., Maniara, W., Persohn, E., Schuetz, H., Danser, A.H.J., Nguyen, G., 2008. Effects of aliskiren on blood pressure, albuminuria, and (pro)renin receptor expression in diabetic TG(mREN-2)-27 rats. Hypertension 52, 130–136.
Feldt, S., Batenburg, W.W., Mazak, I., Maschke, U., Wellner, M., Kvakan, H., Dechend, R., Fiebeler, A., Burckle, C., Contrepas, A., Danser, A.H.J., Bader, M., Nguyen, G., Luft, F.C., Müller, D.N., 2008a. Prorenin and renin-induced extracellular signal-regulated kinase 1/2 activation in monocytes is not blocked by aliskiren or the handle-region peptide. Hypertension 51, 682–688.
Feldt, S., Maschke, U., Dechend, R., Luft, F.C., Müller, D.N., 2008b. The putative (pro)renin receptor blocker HRP fails to prevent (pro)renin signaling. J. Am. Soc. Nephrol. 19, 743–748.
Fisher, N.D.L., Danser, A.H.J., Nussberger, J., Dole, W.P., Hollenberg, N.K., 2008. Renal and hormonal responses to direct renin inhibition with aliskiren in healthy humans. Circulation 117, 3199–3205.
Gilbert, R.E., Krum, H., Wilkinson-Berka, J., Kelly, D.J., 2003. The renin–angiotensin system and the long-term complications of diabetes: pathophysiological and therapeutic considerations. Diabet. Med. 20, 607–621.
Grundy, S.M., Benjamin, I.J., Burke, G.L., Chait, A., Eckel, R.H., Howard, B.V., Mitch, W., Smith Jr., S.C., Sowers, J.R., 1999. Diabetes and cardiovascular disease: a statement for healthcare professionals from the American Heart Association. Circulation 100, 1134–1146.
Hobart, P.M., Fogliano, M., O'Connor, B.A., Schaefer, I.M., Chirgwin, J.M., 1984. Human renin gene: structure and sequence analysis. Proc. Natl. Acad. Sci. U.S.A. 81, 5026–5030.
Hollenberg, N.K., Stevanovic, R., Agarwal, A., Lansang, M.C., Price, D.A., Laffel, L.M., Williams, G.H., Fisher, N.D., 2004. Plasma aldosterone concentration in the patient with diabetes mellitus. Kidney Int. 65, 1435–1439.
Huang, Y., Wongamorntham, S., Kasting, J., McQuillan, D., Owens, R.T., Yu, L., Noble, N.A., Border, W., 2006. Renin increases mesangial cell transforming growth factor-beta1 and matrix proteins through receptor-mediated, angiotensin II-independent mechanisms. Kidney Int. 69, 105–113.
Huang, Y., Border, W.A., Noble, N.A., 2007a. Functional renin receptors in renal mesangial cells. Curr. Hypertens. Rep. 9, 133–139.
Huang, Y., Noble, N.A., Zhang, J., Xu, C., Border, W.A., 2007b. Renin-stimulated TGF-beta1 expression is regulated by a mitogen-activated protein kinase in mesangial cells. Kidney Int. 72, 45–52.
Ichihara, A., Hayashi, M., Kaneshiro, Y., Suzuki, F., Nakagawa, T., Tada, Y., Koura, Y., Nishiyama, A., Okada, H., Uddin, M.N., Nabi, A.H., Ishida, Y., Inagami, T., Saruta, T., 2004. Inhibition of diabetic nephropathy by a decoy peptide corresponding to the "handle" region for nonproteolytic activation of prorenin. J. Clin. Invest. 114, 1128–1135.
Ichihara, A., Kaneshiro, Y., Takemitsu, T., Sakoda, M., Suzuki, F., Nakagawa, T., Nishiyama, A., Inagami, T., Hayashi, M., 2006a. Nonproteolytic activation of prorenin contributes to development of cardiac fibrosis in genetic hypertension. Hypertension 47, 894–900.
Ichihara, A., Suzuki, F., Nakagawa, T., Kaneshiro, Y., Takemitsu, T., Sakoda, M., Nabi, A.H., Nishiyama, A., Sugaya, T., Hayashi, M., Inagami, T., 2006b. Prorenin receptor blockade inhibits development of glomerulosclerosis in diabetic angiotensin II type 1a receptor-deficient mice. J. Am. Soc. Nephrol. 17, 1950–1961.
Kaneshiro, Y., Ichihara, A., Sakoda, M., Takemitsu, T., Nabi, A.H., Uddin, M.N., Nakagawa, T., Nishiyama, A., Suzuki, F., Inagami, T., Itoh, H., 2007. Slowly progressive, angiotensin II-independent glomerulosclerosis in human (pro)renin receptor-transgenic rats. J. Am. Soc. Nephrol. 18, 1789–1795.
Kang, J.J., Toma, I., Sipos, A., Meer, E.J., Vargas, S.L., Peti-Peterdi, J., 2008. The collecting duct is the major source of prorenin in diabetes. Hypertension 51, 1597–1604.
Katz, S.A., Opsahl, J.A., Lunzer, M.M., Forbis, L.M., Hirsch, A.T., 1997. Effect of bilateral nephrectomy on active renin, angiotensinogen, and renin glycoforms in plasma and myocardium. Hypertension 30, 259–266.
Krebs, C., Hamming, I., Sadaghiani, S., Steinmetz, O.M., Meyer-Schwesinger, C., Fehr, S., Stahl, R.A., Garrelds, I.M., Danser, A.H.J., van Goor, H., Contrepas, A., Nguyen, G., Wenzel, U., 2007. Antihypertensive therapy upregulates renin and (pro)renin receptor in the clipped kidney of Goldblatt hypertensive rats. Kidney Int. 72, 725–730.
Krop, M., Danser, A.H.J., 2008. Circulating versus tissue renin–angiotensin system: on the origin of (pro)renin. Curr. Hyp. Rep. 10, 112–118.
Krop, M., de Bruyn, J.H.B., Derkx, F.H.M., Danser, A.H.J., 2008. Renin and prorenin disappearance in humans post-nephrectomy: evidence for binding? Front. Biosci. 13, 3931–3939.
Ladeia, A.M., Ladeia-Frota, C., Pinho, L., Stefanelli, E., Adan, L., 2005. Endothelial dysfunction is correlated with microalbuminuria in children with short-duration type 1 diabetes. Diabetes Care 28, 2048–2050.
Lenz, T., Sealey, J.E., Maack, T., James, G.D., Heinrikson, R.L., Marion, D., Laragh, J.H., 1991. Half-life, hemodynamic, renal, and hormonal effects of prorenin in cynomolgus monkeys. Am. J. Physiol. 260, R804–R810.
Lewis, E.J., Hunsicker, L.G., Clarke, W.R., Berl, T., Pohl, M.A., Lewis, J.B., Ritz, E., Atkins, R.C., Rohde, R., Raz, I., 2001. Renoprotective effect of the angiotensin-receptor antagonist irbesartan in patients with nephropathy due to type 2 diabetes. N. Engl. J. Med. 345, 851–860.
Ludwig, J., Kerscher, S., Brandt, U., Pfeiffer, K., Getlawi, F., Apps, D.K., Schägger, H., 1998. Identification and characterization of a novel 9.2-kDa membrane sector-associated protein of vacuolar proton-ATPase from chromaffin granules. J. Biol. Chem. 273, 10939–10947.
Luetscher, J.A., Kraemer, F.B., Wilson, D.M., Schwartz, H.C., Bryer-Ash, M., 1985. Increased plasma inactive renin in diabetes mellitus. A marker of microvascular complications. N. Engl. J. Med. 312, 1412–1417.
Nguyen, G., Delarue, F., Burcklé, C., Bouzhir, L., Giller, T., Sraer, J.-D., 2002. Pivotal role of the renin/prorenin receptor in angiotensin II production and cellular responses to renin. J. Clin. Invest. 109, 1417–1427.
Nurun, N.A., Uddin, N.M., Nakagawa, T., Iwata, H., Ichihara, A., Inagami, T., Suzuki, F., 2007. Role of "handle" region of prorenin prosegment in the non-proteolytic activation of prorenin by binding to membrane anchored (pro)renin receptor. Front. Biosci. 12, 4810–4817.
Parving, H.H., Persson, F., Lewis, J.B., Lewis, E.J., Hollenberg, N.K., 2008. Aliskiren combined with losartan in type 2 diabetes and nephropathy. N. Engl. J. Med. 358, 2433–2446.
Perkins, J.M., Davis, S.N., 2008. The renin–angiotensin–aldosterone system: a pivotal role in insulin sensitivity and glycemic control. Curr. Opin. Endocrinol. Diabetes Obes. 15, 147–152.
Peters, B., Grisk, O., Becher, B., Wanka, H., Kuttler, B., Ludemann, J., Lorenz, G., Rettig, R., Mullins, J.J., Peters, J., 2008. Dose-dependent titration of prorenin and blood pressure in Cyp1a1ren-2 transgenic rats: absence of prorenin-induced glomerulosclerosis. J. Hypertens. 26, 102–109.
Prescott, G., Silversides, D.W., Reudelhuber, T.L., 2002. Tissue activity of circulating prorenin. Am. J. Hypertens. 15, 280–285.
Saris, J.J., Derkx, F.H.M., de Bruin, R.J.A., Dekkers, D.H.W., Lamers, J.M.J., Saxena, P.R., Schalekamp, M.A.D.H., Danser, A.H.J., 2001a. High-affinity prorenin binding to cardiac man-6-P/IGF-II receptors precedes proteolytic activation to renin. Am. J. Physiol. 280, H1706–H1715.
Saris, J.J., Derkx, F.H.M., Lamers, J.M.J., Saxena, P.R., Schalekamp, M.A.D.H., Danser, A.H.J., 2001b. Cardiomyocytes bind and activate native human prorenin: role of soluble mannose 6-phosphate receptors. Hypertension 37, 710–715.
Saris, J.J., van den Eijnden, M.M.E.D., Lamers, J.M.J., Saxena, P.R., Schalekamp, M.A.D.H., Danser, A.H.J., 2002. Prorenin-induced myocyte proliferation: no role for intracellular angiotensin II. Hypertension 39, 573–577.
Saris, J.J., 't Hoen, P.A.C., Garrelds, I.M., Dekkers, D.H.W., den Dunnen, J.T., Lamers, J.M.J., Danser, A.H.J., 2006. Prorenin induces intracellular signalling in cardiomyocytes independently of angiotensin II. Hypertension 48, 564–571.
Schachinger, V., Britten, M.B., Zeiher, A.M., 2000. Prognostic impact of coronary vasodilator dysfunction on adverse long-term outcome of coronary heart disease. Circulation 101, 1899–1906.
Schalekamp, M.A.D.H., Derkx, F.H.M., Deinum, J., Danser, A.H.J., 2008. Newly developed renin and prorenin assays and the clinical evaluation of renin inhibitors. J. Hypertens. 26, 928–937.
Schefe, J.H., Menk, M., Reinemund, J., Effertz, K., Hobbs, R.M., Pandolfi, P.P., Ruiz, P., Unger, T., Funke-Kaiser, H., 2006. A novel signal transduction cascade involving direct physical interaction of the renin/prorenin receptor with the transcription factor promyelocytic zinc finger protein. Circ. Res. 99, 1355–1366.
Schefe, J.H., Neumann, C., Goebel, M., Danser, A.H.J., Kirsch, S., Gust, R., Kintscher, U., Unger, T., Funke-Kaiser, H., 2008. Prorenin engages the (pro)renin receptor like renin and both ligand activities are unopposed by aliskiren. J. Hypertens. 26, 1787–1794.
Schulick, A.H., Taylor, A.J., Zuo, W., Qiu, C.B., Dong, G., Woodward, R.N., Agah, R., Roberts, A.B., Virmani, R., Dichek, D.A., 1998. Overexpression of transforming growth factor beta1 in arterial endothelium causes hyperplasia, apoptosis, and cartilaginous metaplasia. Proc. Natl. Acad. Sci. U.S.A. 95, 6983–6988.
Sharma, K., Ziyadeh, F.N., Alzahabi, B., McGowan, T.A., Kapoor, S., Kurnik, B.R., Kurnik, P.B., Weisberg, L.S., 1997. Increased renal production of transforming growth factor-beta1 in patients with type II diabetes. Diabetes 46, 854–859.
Sharma, K., Eltayeb, B.O., McGowan, T.A., Dunn, S.R., Alzahabi, B., Rohde, R., Ziyadeh, F.N., Lewis, E.J., 1999. Captopril-induced reduction of serum levels of transforming growth factor-beta1 correlates with long-term renoprotection in insulin-dependent diabetic patients. Am. J. Kidney Dis. 34, 818–823.

Stankovic, A.R., Fisher, N.D.L., Hollenberg, N.K., 2006. Prorenin and angiotensin-dependent renal vasoconstriction in type 1 and type 2 diabetes. J. Am. Soc. Nephrol. 17, 3293–3299.

Susic, D., Zhou, X., Frohlich, E.D., Lippton, H.L., Knight, M., 2008. Cardiovascular effects of prorenin blockade in genetically hypertensive rats (SHR) on normal and high salt diet. Am. J. Physiol. Heart Circ. Physiol. 295, H1117–H1121.

Takahashi, H., Ichihara, A., Kaneshiro, Y., Inomata, K., Sakoda, M., Takemitsu, T., Nishiyama, A., Itoh, H., 2007. Regression of nephropathy developed in diabetes by (Pro)renin receptor blockade. J. Am. Soc. Nephrol. 18, 2054–2061.

van den Eijnden, M.M.E.D., Saris, J.J., de Bruin, R.J.A., de Wit, E., Sluiter, W., Reudelhuber, T.L., Schalekamp, M.A.D.H., Derkx, F.H.M., Danser, A.H.J., 2001. Prorenin accumulation and activation in human endothelial cells. Importance of mannose 6-phosphate receptors. Arterioscler. Thromb. Vasc. Biol. 21, 911–916.

van Esch, J.H.M., Schuijt, M.P., Sayed, J., Choudry, Y., Walther, T., Danser, A.H.J., 2006. AT2 receptor-mediated vasodilation in the mouse heart depends on AT1A receptor activation. Br. J. Pharmacol. 148, 452–458.

van Kats, J.P., Danser, A.H.J., van Meegen, J.R., Sassen, L.M., Verdouw, P.D., Schalekamp, M.A.D.H., 1998. Angiotensin production by the heart: a quantitative study in pigs with the use of radiolabeled angiotensin infusions. Circulation 98, 73–81.

van Kats, J.P., Duncker, D.J., Haitsma, D.B., Schuijt, M.P., Niebuur, R., Stubenitsky, R., Boomsma, F., Schalekamp, M.A.D.H., Verdouw, P.D., Danser, A.H.J., 2000. Angiotensin-converting enzyme inhibition and angiotensin II type 1 receptor blockade prevent cardiac remodeling in pigs after myocardial infarction: role of tissue angiotensin II. Circulation 102, 1556–1563.

van Kesteren, C.A.M., Danser, A.H.J., Derkx, F.H.M., Dekkers, D.H.W., Lamers, J.M.J., Saxena, P.R., Schalekamp, M.A.D.H., 1997. Mannose 6-phosphate receptor-mediated internalization and activation of prorenin by cardiac cells. Hypertension 30, 1389–1396.

van Kesteren, C.A.M., Saris, J.J., Dekkers, D.H.W., Lamers, J.M.J., Saxena, P.R., Schalekamp, M.A.D.H., Danser, A.H.J., 1999. Cultured neonatal rat cardiac myocytes and fibroblasts do not synthesize renin or angiotensinogen: evidence for stretch-induced cardiomyocyte hypertrophy independent of angiotensin II. Cardiovasc. Res. 43, 148–156.

Véniant, M., Ménard, J., Bruneval, P., Morley, S., Gonzales, M.F., Mullins, J.J., 1996. Vascular damage without hypertension in transgenic rats expressing prorenin exclusively in the liver. J. Clin. Invest. 98, 1966–1970.

Yamamoto, T., Nakamura, T., Noble, N.A., Ruoslahti, E., Border, W.A., 1993. Expression of transforming growth factor beta is elevated in human and experimental diabetic nephropathy. Proc. Natl. Acad. Sci. U.S.A. 90, 1814–1818.

Yu, L., Border, W.A., Anderson, I., McCourt, M., Huang, Y., Noble, N.A., 2004. Combining TGF-beta inhibition and angiotensin II blockade results in enhanced antifibrotic effect. Kidney Int. 66, 1774–1784.

Yusuf, S., Sleight, P., Pogue, J., Bosch, J., Davies, R., Dagenais, G., 2000. Effects of an angiotensin-converting-enzyme inhibitor, ramipril, on cardiovascular events in high-risk patients. The Heart Outcomes Prevention Evaluation Study Investigators. N. Engl. J. Med. 342, 145–153.

Zuanetti, G., Latini, R., Maggioni, A.P., Franzosi, M., Santoro, L., Tognoni, G., 1997. Effect of the ACE inhibitor lisinopril on mortality in diabetic patients with acute myocardial infarction: data from the GISSI-3 study. Circulation 96, 4239–4245.

Urinary renin, but not angiotensinogen or aldosterone, reflects the renal renin-angiotensin-aldosterone system activity and the efficacy of renin-angiotensin-aldosterone system blockade in the kidney

van den Heuvel M., Batenburg W.W., Jainandunsing S., Garrelds I.M., van Gool J.M., Feelders R.A., van den Meiracker A.H. and Danser A.H.

J. Hypertens. 2011 Nov;29(11):2147-55

15

Urinary renin, but not angiotensinogen or aldosterone, reflects the renal renin – angiotensin – aldosterone system activity and the efficacy of renin – angiotensin – aldosterone system blockade in the kidney

Mieke van den Heuvel[a,c], Wendy W. Batenburg[a], Sjaam Jainandunsing[a], Ingrid M. Garrelds[a], Jeanette M.G. van Gool[a], Richard A. Feelders[b], Anton H. van den Meiracker[a], A.H. Jan Danser[a]

Objective **To study which renin–angiotensin–aldosterone system (RAAS) component best reflects renal RAAS activity.**

Methods and results **We measured urinary and plasma renin, prorenin, angiotensinogen, aldosterone, albumin and creatinine in 101 diabetic and nondiabetic patients with or without hypertension. Plasma prorenin was elevated in diabetic patients. Urinary prorenin was undetectable. Urinary albumin and renin were higher in diabetic patients. Men had higher plasma renin/prorenin levels, and lower plasma angiotensinogen levels than women. Plasma creatinine and albumin were also higher in men. Urinary RAAS components showed no sexual dimorphism, whereas urinary creatinine and albumin were higher in men. Angiotensin-converting enzyme inhibitors and angiotensin II type 1 receptor blockers increased plasma renin and decreased plasma angiotensinogen, without altering plasma aldosterone. In contrast, in urine, these drugs decreased renin and aldosterone without affecting angiotensinogen. When analyzing all patients together, urinary angiotensinogen excretion closely mimicked that of albumin, whereas urinary angiotensinogen and albumin levels both were 0.05% or less of their concomitant plasma levels. This may reflect the identical glomerular filtration and tubular handling of both proteins, which have a comparable molecular weight. In contrast, urinary renin excretion did not correlate with urinary albumin excretion, and the urinary/plasma concentration ratio of renin was more than 200 times the ratio of albumin, despite its comparable molecular weight. Urinary aldosterone excretion closely followed urinary creatinine excretion.**

Conclusion **The increased urinary renin levels in diabetes and the decreased urinary renin levels following RAAS blockade, occurring independently of changes in plasma renin, reflect the activated renal RAAS in diabetes and the success of RAAS blockade in the kidney, respectively. Urinary renin, therefore, more closely reflects renal RAAS activity than urinary angiotensinogen or aldosterone.**
J Hypertens **29:2147–2155**

Journal of Hypertension 2011, **29**:2147–2155

Keywords: aldosterone, angiotensinogen, collecting duct, diabetes, glomerular filtration, prorenin, renin

Abbreviations: ACEi, angiotensin-converting enzyme inhibitor; Ang, angiotensin; ARB, Ang II type 1 receptor blocker; eGFR, estimated glomerular filtration rate; EKA, enzyme-kinetic assay; RAAS, renin–Ang–aldosterone system; RAS, renin–Ang system

[a]Division of Pharmacology and Vascular Medicine, [b]Division of Endocrinology, Department of Internal Medicine and [c]Department of Cardiology, Erasmus MC, Rotterdam, The Netherlands

Correspondence to Professor Dr A.H. Jan Danser, PhD, Division of Pharmacology and Vascular Medicine, Department of Internal Medicine, Room EE1418b, Erasmus MC, Dr Molewaterplein 50, 3015 GE Rotterdam, The Netherlands
Tel: +31 10 7043540; fax: +31 10 7044733; e-mail: a.danser@erasmusmc.nl

Received 19 May 2011 **Revised** 6 July 2011
Accepted 8 August 2011

Introduction

Urinary angiotensinogen has been suggested to reflect intrarenal angiotensin (Ang) production, that is, to provide an indication of the Ang generation at renal tissue sites [1–6]. A putative site of angiotensinogen synthesis in the kidney is the proximal tubulus [7]. Urinary angiotensinogen levels are elevated in patients with chronic kidney disease [1–4], and studies infusing 100 μg human angiotensinogen in rats followed by a 5-h collection of urine did not result in the appearance of human angiotensinogen in urine [4]. This implies that urinary angiotensinogen might originate at the proximal tubulus rather than the circulation. Indeed, given its molecular weight (65 kD), at most only very modest amounts of angiotensinogen will be filtered across the glomerular membrane. Yet, the same applies to albumin (molecular weight 67 kD), and urinary albumin and angiotensinogen levels correlated significantly according to several studies [3,8]. Thus, a careful analysis involving the simultaneous measurement of both proteins in urine and plasma, in order to allow a correction for the filtration of albumin, is warranted.

Alternative markers of intrarenal renin–Ang–aldosterone system (RAAS) activity might be renin, its precursor prorenin and/or aldosterone. Diabetic patients display low-to-normal plasma renin levels [9–10]. Yet their renal plasma flow response to Ang-converting enzyme

inhibitors (ACEi) or Ang II type 1 receptor blockers (ARBs) is greatly enhanced [11–13], so that it has been postulated that there is an activated RAAS in the diabetic kidney. Even more intriguing, diabetic patients suffering from the microvascular complications of this disease have elevated plasma prorenin levels and the higher these levels, the worse their retinopathy and/or nephropathy [9–10,14–15]. Prorenin might even serve as an early marker of these complications [16]. In rats, the collecting duct has been reported to be the source of this prorenin [17] and, unexpectedly, Ang II stimulates prorenin release in the collecting duct in contrast to its negative feedback effect on juxtaglomerular renin release. Finally, aldosterone synthesis is believed to occur in the kidney, independently of the adrenals, and this renal aldosterone synthesis is increased in diabetic animals [18].

In the present study, we set out to measure urinary renin, prorenin, angiotensinogen and aldosterone in non-diabetic and diabetic patients in order to determine which of these RAAS components best reflects intrarenal RAAS activity. We simultaneously measured these components in plasma, and we measured creatinine, albumin and total protein in plasma and urine, to allow a correction for filtration from blood. Finally, given the well known sexual dimorphism of renin, prorenin and angiotensinogen [19], as well as data indicating that ACEi and/or ARBs may affect the release of angiotensinogen in urine [1–2], we evaluated the role of sex and the consequences of RAAS blockade in our analysis.

Patients and methods

Patients

The experimental protocol of this study was approved by the Medical Ethical Review Board of the Erasmus MC. All patients willing to participate and visiting the outpatient hypertension clinic of the Department of Internal Medicine of the Erasmus MC between November 2008 and September 2010 were included. They were diagnosed with (type 1, $n=3$ and type 2, $n=40$) or without ($n=58$) diabetes mellitus, and of the type 2 diabetic patients, 19 were insulin-dependent. Most patients were hypertensive according to the European Society of Hypertension/European Society of Cardiology 2007 guidelines. After written informed consent had been obtained, body weight, height, BMI, present medication use, disease duration and disease complications were recorded. SBP and DBP were measured with an automatic oscillometric device (Datascope Accutorr Plus Inc., Montvale, New Jersey, USA) after at least a 5-min rest in the sitting position. A peripheral venous blood sample was taken in tubes containing EDTA (final concentration 6.25 mmol/l) and patients were asked to collect and to hand in a urine portion on the same day. Plasma was obtained after centrifugation at 3000*g* for 10 min, and both plasma and urine were stored at −20°C until analysis.

Biochemical measurements

Plasma and urine concentrations of sodium, total protein, albumin and creatinine were measured at the clinical chemical laboratory of the Erasmus MC using standard protocols.

Plasma renin was measured with a commercial immunoradiometric kit (Renin III; Cisbio, Gif-sur-Yvette, France). Total plasma renin was determined simultaneously with the same kit after the induction of a conformational change in the prorenin molecule with aliskiren (10 μmol/l for 48 h at 4°C), which enabled its recognition by the active site-directed radiolabeled antibodies applied in the Cisbio kit [20]. Subtraction of the renin concentration from the total renin concentration yielded the prorenin concentration. The detection limit of this assay is 1 pg/ml. The urinary renin concentrations were often below this detection limit. Therefore, urinary renin was measured with the more sensitive enzyme-kinetic assay (EKA), that is, by quantifying Ang I generation in the presence of excess sheep angiotensinogen [21]. Urinary total renin was determined after incubation with trypsin coupled to Sepharose [22]. The detection limit of the EKA is 0.05 ng Ang I/ml per hour, and the Ang I-generating activities were converted to renin concentrations based on the fact that 1 ng Ang I/ml per hour corresponds with 2.6 pg human renin/ml [23]. In a selected set of urine samples, prorenin was also measured with a direct prorenin assay (Molecular Innovations, Novi, Michigan, USA), making use of an antibody that recognizes an epitope near prorenin's cleavage site. Urine was concentrated five-fold with Amicon Ultra-10 centrifugal filter devices (Millipore, Cork, Ireland) before applying the samples in the assay. The detection limit of the direct prorenin assay under these conditions was 2 pg/ml.

Angiotensinogen in plasma and urine was measured as the maximum quantity of Ang I that was generated during incubation with excess recombinant renin [24]. The detection limit of this assay is 0.50 pmol/ml. Aldosterone was measured by solid-phase radioimmunoassay (Diagnostic Products Corporation, Los Angeles, California, USA), with detection limit of 25 pg/ml [25].

Statistical analysis

Datasets were complete for virtually all parameters. Only in a few cases, due to technical reasons, one or two measurements were missing. Data are expressed as mean ± SD or geometric mean and range. In case of nonnormal distribution, data were logarithmically transformed before analysis. Levels that were below the detection limit were taken to be equal to the detection limit to allow statistical evaluation. The estimated glomerular filtration rate (eGFR) was calculated using creatinine clearance according to the simplified Modification of Diet in Renal Disease formula [26]. Univariate linear associations between the urine/plasma

concentration ratios of the various parameters were assessed by calculating Pearson's coefficient of correlation. Differences between groups were evaluated by Student's *t*-test. A P value less than 0.05 was considered significant. Statistical analysis was performed with the SPSS 7.0 package (SPSS Inc., Chicago, Illinois, USA).

Results

Patient characteristics, markers of renal function and RAAS components in plasma and urine are presented in Tables 1 and 2. On average, patients were middle-aged, and approximately 60% had secondary cardiovascular complications such as nephropathy, retinopathy, neuropathy, coronary artery disease and peripheral vascular disease. Almost 90% of the patients used antihypertensive medication consisting of (combinations of) renin–Ang system (RAS) blockers (71%), diuretics (52%), calcium antagonists (51%), β-blockers (30%), mineralocorticoid receptor antagonists (13%), α-adrenoceptor blockers (11%) and other antihypertensives (centrally acting antihypertensives or direct vasodilators, 2%) (Table 3).

In urine, the EKA results before and after trypsin activation of prorenin were identical. This suggests that urine does not contain prorenin. Measurements with a direct prorenin assay in five-fold concentrated urine samples ($n = 10$) confirmed this view. To rule out the possibility that urinary prorenin had been converted to renin, either *in vivo* or during storage and handling of the samples, recombinant human prorenin was added to urine (approximately 50 pg/ml) and incubated at 4, 22 or 37°C for 22 h maximally ($n = 3$ for each condition). At 4 and 22°C, maximally approximately 5% of prorenin was found to become recognizable as renin (Fig. 1, left and middle panel), whereas at 37°C prorenin was found to disappear without becoming recognizable as renin (Fig. 1, right panel). Importantly, at 4 and 22°C, the sum of renin and prorenin (i.e. total renin) remained unaltered over the entire 22-h period, whereas at 37°C total renin decreased with a half-life of 102 ± 24 h. These data support the concept that at lower temperatures, the prorenin prosegment unfolds from the enzymatic cleft, allowing prorenin to become recognizable in a renin assay, although the prosegment is still present. This conformational change is reversible and, at higher temperatures, the equilibrium shifts into the direction of the closed conformation. Clearly, therefore, at 37°C, when there is no rise in renin, the prorenin disappearance is due to metabolism. Such metabolism also occurred when studying the fate of renin at 37°C ($n = 3$, data not shown). Taken together, these data suggest that the absence of prorenin in urine is not due to its rapid conversion to renin, either *in vivo* or *in vitro*. Consequently, Table 2 only shows urinary renin levels.

Table 1 Patient characteristics and markers of renal function and renin–angiotensin–aldosterone system components in plasma

	All ($n = 101$)	No diabetes ($n = 58$)	Diabetes ($n = 43$)	Men ($n = 55$)	Women ($n = 46$)	ACEi/ARB yes ($n = 72$)	ACEi/ARB no ($n = 29$)
Patient characteristics							
Age (years)	55 ± 11	51 ± 12	59 ± 8.0#	56 ± 12	53 ± 9.8	56 ± 10	52 ± 12
Sex (*n* males, *n* females)	55, 46	31, 27	24, 19	–	–	43, 29	12, 17
Diabetes (no, yes)	58, 43	–	–	31, 24	27, 19	44, 28	14, 15
Height (m)	1.72 ± 0.10	1.72 ± 0.09	1.71 ± 0.12	1.78 ± 0.07	1.64 ± 0.07#	1.72 ± 0.09	1.69 ± 0.11
Weight (kg)	86 ± 18	84 ± 19	90 ± 17	92 ± 15	80 ± 20#	89 ± 18	80 ± 18*
BMI (kg/m^2)	29 ± 6.0	28 ± 5.6	31 ± 6.4*	29 ± 4.4	30 ± 7.5	30 ± 6.3	28 ± 5.0
SBP (mmHg)	139 ± 21	138 ± 21	140 ± 22	139 ± 22	139 ± 20	142 ± 21	132 ± 21*
DBP (mmHg)	81 ± 12	84 ± 12	77 ± 11#	81 ± 13	82 ± 11	83 ± 13	76 ± 9.9#
Plasma data							
Sodium (mmol/l)	142 ± 2.4	142 ± 2.3	142 ± 2.6	142 ± 2.5	142 ± 2.4	142 ± 2.3	142 ± 2.7
Creatinine (μmol/l)	83 ± 34	78 ± 18	90 ± 47	93 ± 35	70 ± 28#	90 ± 37	66 ± 17#
Albumin (g/l)	44 ± 2.8	45 ± 3.1	44 ± 2.2	45 ± 2.5	44 ± 2.9	45 ± 2.6	44 ± 3.2
Total protein (g/l)	70 ± 5.4	70 ± 5.9	70 ± 4.6	70 ± 5.5	69 ± 5.3	70 ± 5.7	69 ± 4.5
Renin (pg/ml)	14.8 (1–1306)	14.1 (1–1306)	15.8 (1–185)	19.3 (1–352)	10.7* (1–1306)	16.9 (1–1306)	10.7** (1–131)
Prorenin (pg/ml)	83 (8.7–683)	66 (8.7–253)	111# (23–683)	99 (17–683)	67* (8.7–413)	89 (8.7–683)	71 (20–315)
Angiotensinogen (pmol/ml)	1530 (643–4469)	1598 (786–4469)	1445 (643–2621)	1441 (643–3509)	1644* (786–4469)	1466 (643–4469)	1705* (965–4186)
Aldosterone (pg/ml)	56 (25–1237)	52 (25–649)	62 (25–1237)	67 (25–1237)	45 (25–649)	53 (25–649)	65 (25–1237)

Subdivisions according to the presence or absence diabetes, sex and the use of angiotensin-converting enzyme inhibitors (ACEi) and/or angiotensin II type 1 receptor blockers (ARB). Values are mean ± SD or geometric mean with range. * $P < 0.05$ vs. comparator group. # $P < 0.01$ vs. comparator group. ** $P = 0.08$ vs. comparator group.

Table 2 Markers of renal function and renin–angiotensin–aldosterone system components in urine

	All ($n=101$)	No diabetes ($n=58$)	Diabetes ($n=43$)	Men ($n=55$)	Women ($n=46$)	ACEi/ARB yes ($n=72$)	ACEi/ARB no ($n=29$)
Urine data							
Sodium (mmol/l)	98 ± 43	102 ± 43	93 ± 44	97 ± 39	100 ± 49	100 ± 45	95 ± 40
Creatinine (mmol/l)	8.3 ± 4.3	8.2 ± 3.7	8.5 ± 5.0	9.3 ± 3.9	7.1 ± 4.5*	8.0 ± 3.8	9.1 ± 5.3
Albumin (g/l)	0.012 (0.002–1.120)	0.008 (0.002–0.708)	0.019# (0.002–1.120)	0.015 (0.002–1.120)	0.008* (0.002–0.708)	0.013 (0.002–1.120)	0.008 (0.002–0.055)
Total protein (g/l)	0.10 (0.02–1.52)	0.09 (0.02–0.95)	0.11 (0.02–1.52)	0.12 (0.02–1.52)	0.08* (0.02–0.95)	0.10 (0.02–1.52)	0.09 (0.02–0.23)
Renin (pg/ml)	0.91 (0.13–157)	0.64 (0.13–13)	1.46# (0.13–157)	0.83 (0.13–28)	1.02 (0.13–157)	0.73 (0.13–157)	1.59* (0.13–9.9)
Angiotensinogen (pmol/ml)	0.76 (0.50–11)	0.78 (0.50–11)	0.73 (0.50–3.0)	0.78 (0.50–3.0)	0.74 (0.50–11)	0.76 (0.5–11)	0.76 (0.5–4)
Aldosterone (pg/ml)	45 (25–1845)	40 (25–444)	52 (25–1845)	51 (25–1845)	38 (25–444)	38 (25–444)	66* (25–1845)
Kidney function							
eGFR (ml/min)	77 ± 17	80 ± 11	73 ± 22*	76 ± 17	79 ± 16	73 ± 18	86 ± 8.2*

Subdivisions according the presence or absence diabetes, sex and the use of angiotensin-converting enzyme inhibitors (ACEi) and/or angiotensin II type 1 receptor blockers (ARBs). Values are mean ± SD or geometric mean with range. eGFR, estimated glomerular filtration rate. * $P<0.05$ vs. comparator group. # $P<0.01$ vs. comparator group.

Diabetes mellitus

Diabetic patients were older ($P<0.01$), more obese ($P<0.05$) and displayed a lower DBP ($P<0.01$) and eGFR ($P<0.05$) than nondiabetic individuals (Tables 1 and 2). In addition, urinary albumin levels were higher in diabetic patients ($P<0.01$). Plasma RAAS components did not differ between diabetic and nondiabetic individuals, with the exception of prorenin that was almost doubled in diabetic patients ($P<0.01$). In urine, renin was twice as high in diabetic patients ($P<0.01$), whereas all other RAAS components were identical in the two groups. Importantly, the use of antihypertensive medication was identical in both groups (Table 3).

Sex

Men and women displayed the well known differences with regard to height, weight and creatinine ($P<0.01$ for all, Table 1). In agreement with previously published data [19], men had higher plasma renin and prorenin levels and lower plasma angiotensinogen levels ($P<0.05$ for all). Remarkably, despite these differences in plasma levels, urinary RAAS component levels in men and women were identical (Table 2). Men had higher urinary levels of total protein, albumin and creatinine ($P<0.05$ for all). They also used more antihypertensive medication ($P<0.05$, Table 3).

Use of angiotensin-converting enzyme inhibitors and/or angiotensin II type 1 receptor blockers

Weight ($P<0.05$), plasma creatinine ($P<0.01$), SBP ($P<0.05$) and DBP ($P<0.01$) were higher in patients using ACEi and/or ARBs, whereas eGFR was lower ($P<0.01$, Tables 1 and 2). On top of these two blockers, these patients used significantly more antihypertensive medication ($P<0.01$) than patients not using ACEi or ARBs (Table 3). As expected, the use of ACEi and/or ARBs was accompanied by higher plasma renin levels ($P=0.08$) and lower levels of plasma angiotensinogen and urinary aldosterone ($P<0.05$ for both). Plasma aldosterone levels tended to be decreased. Remarkably, urinary renin was lower during the application of ACEi and/or ARBs ($P<0.05$).

Correction for urinary creatinine levels

Previous studies expressed their urinary RAAS component, albumin and total protein levels as per gram creatinine. In the present cohort, this resulted in angiotensinogen [geometric mean (range) 0.9 nmol/g (0.2–10)]; albumin [14.2 mg/g (1.5–1586)]; total protein [118 mg/g (9–2170)] and aldosterone [55 ng/g (1–1256)] levels that were in the same range as those reported earlier [1,3,8]. Urinary renin levels ranged from 0.06 to 433 ng/g (geometric mean 1.12). The results of subdividing the creatinine-corrected data according to the presence or absence of diabetes mellitus, sex or RAS blocker treatment were identical to those of the subdivisions described above without the correction for creatinine (data not shown).

Table 3 Antihypertensive medication use in patient (sub)groups

Antihypertensive treatment	All ($n=101$)	No diabetes ($n=58$)	Diabetes ($n=43$)	Men ($n=55$)	Women ($n=46$)	ACEi/ARB yes ($n=72$)	ACEi/ARB no ($n=29$)
RAS-blocker	72	44	28	43	29	72	0
Diuretic	53	33	20	30	23	46	7
Calcium antagonist	52	34	18	32	20	31	11
β-Blocker	30	13	17	20	10	22	8
Mineralocorticoid receptor antagonist	13	9	4	10	3	12	1
α-Adrenoceptor blocker	11	8	3	7	4	8	3
Other	2	2	0	1	1	2	0
Number of different antihypertensive drugs (n)							
0	12	4	8	3	9	0	12
1	19	9	10	9	10	13	6
2	24	17	7	13	11	15	9
3	25	17	8	16	9	23	2
4	15	7	8	10	5	15	0
5	6	4	2	4	2	6	0
Mean ± SD	2.3 ± 1.4	2.4 ± 1.3	2.1 ± 1.5	2.6 ± 1.3	1.9 ± 1.4*	2.8 ± 1.2	1.0 ± 1.0#

ACEi, angiotensin-converting enzyme inhibitor; ARB, angiotensin II type 1 receptor blocker; RAS, renin–angiotensin system. * $P<0.05$ vs. comparator group. # $P<0.01$ vs. comparator group.

Origin of urinary renin–angiotensin–aldosterone system components

Given their comparable molecular weight, we first compared the urine/plasma concentration ratios (×100%) of albumin (geometric mean 0.026, range 0.004–2.6), angiotensinogen (geometric mean 0.050, range 0.014–0.246) and renin (geometric mean 6.2, range 0.13–4300), and second those of aldosterone (geometric mean 78, range 12–868) and creatinine (geometric mean 9.3, range 1.4–46). This was done based on the assumptions that, first, urinary albumin and creatinine are plasma-derived and, second, the urine/plasma concentration ratio provides an indication of urinary excretion. Figure 2 (panels a and c) and Table 4 show that the ratios of albumin and angiotensinogen were correlated ($r=0.28$, $P<0.01$) in contrast to those of albumin and renin ($r=-0.10$, $P=$NS). When replacing albumin by total protein (geometric mean urine/plasma concentration ratio × 100% 0.14, range 0.02–2), the findings were identical ($r=0.35$, $P<0.01$ for angiotensinogen; $r=-0.14$, $P=$NS for renin) (Table 4 and Fig. 2b and d).

Moreover, the urine/plasma concentration ratios of aldosterone and creatinine correlated highly significantly ($r=0.55$, $P<0.01$) (Fig. 3). The urine/plasma concentration ratio of aldosterone did not correlate with that of

Fig. 1

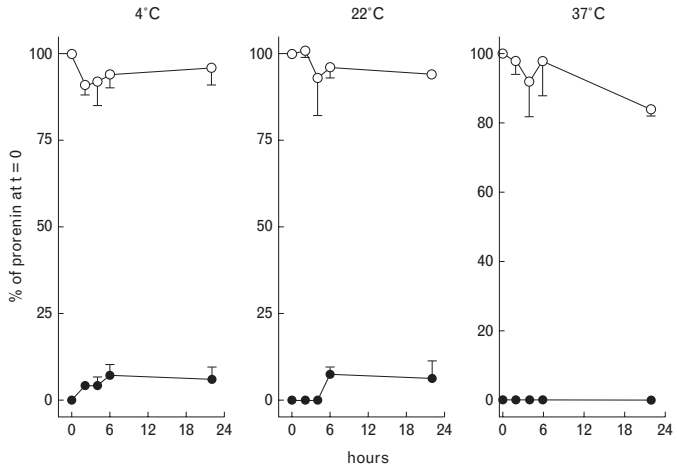

Prorenin decay (open circles) and the appearance of immunoreactive renin (closed symbols) in human urine at various temperatures. Data are mean ± SD ($n=3$).

Fig. 2

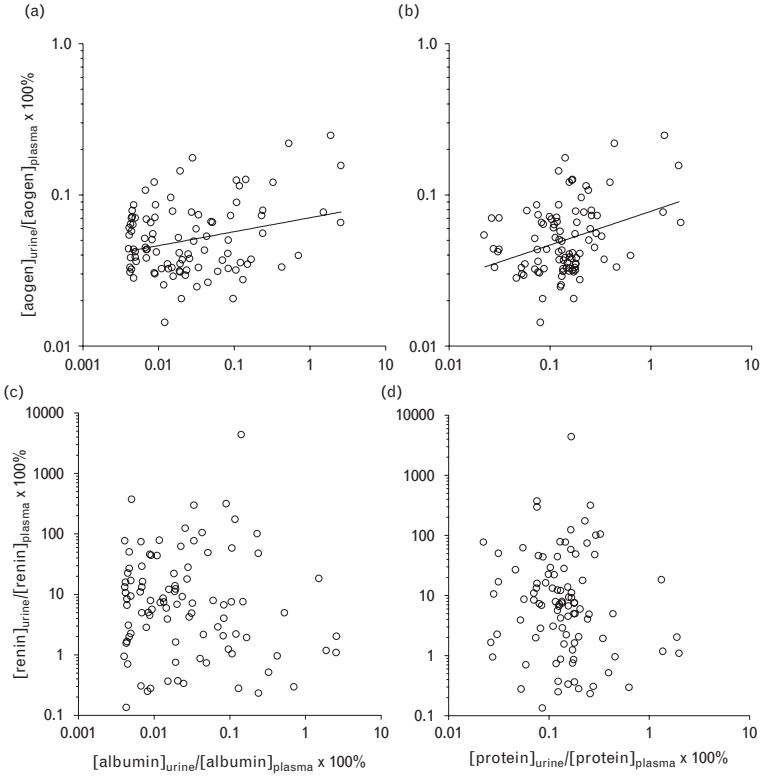

Correlations between the urine/plasma concentration ratios of albumin [a ($r=0.28$, $P<0.01$); c ($r=-0.10$, $P=$NS)] or total protein [b ($r=0.35$, $P<0.01$); d ($r=-0.14$, $P=$NS)] and that of angiotensinogen (aogen) (top panels) or renin (bottom panels).

albumin ($r=-0.08$, $P=$NS) or total protein ($r=0.09$, $P=$NS), whereas the urine/plasma concentration ratio of creatinine did not correlate with that of angiotensinogen ($r=0.01$, $P=$NS) or renin ($r=0.05$, $P=$NS). Finally, eGFR correlated negatively with the urine/plasma concentration ratios of both albumin ($r=-0.44$, $P<0.01$) and angiotensinogen ($r=-0.32$, $P<0.01$), but not that of renin ($r=0.13$, $P=$NS) (Fig. 4).

Table 4 Pearson's coefficient of correlation

Urine/plasma concentration ratios	Albumin		Total protein		Creatinine	
	r	*P*	*r*	*P*	*r*	*P*
Renin	−0.10	0.35	−0.14	0.17	0.05	0.65
Angiotensinogen	0.28	<0.01	0.35	<0.01	0.01	0.93
Aldosterone	−0.08	0.46	0.09	0.42	0.55	<0.01

Correlation describing the relationship between the urine/plasma concentration ratios of renin–angiotensin–aldosterone system components and those of albumin, total protein and creatinine.

Taken together, these data indicate that urinary angiotensinogen excretion closely mimics urinary albumin (and total protein) excretion, and that urinary aldosterone excretion mimics urinary creatinine excretion. Urinary renin excretion does not resemble the excretion of any of these components.

Discussion

This article is the first to show that urinary renin levels in humans do not parallel plasma renin levels nor follow the urinary albumin excretion pattern. Urinary renin levels are elevated in diabetic patients, in parallel with the putative activation of the renal RAAS in diabetes, and treatment with ACEi and/or ARBs decreased urinary renin levels, as opposed to the well known increase in plasma renin that occurs during such treatment. The latter is the consequence of interference with the negative feedback loop between Ang II and juxtaglomerular

Fig. 3

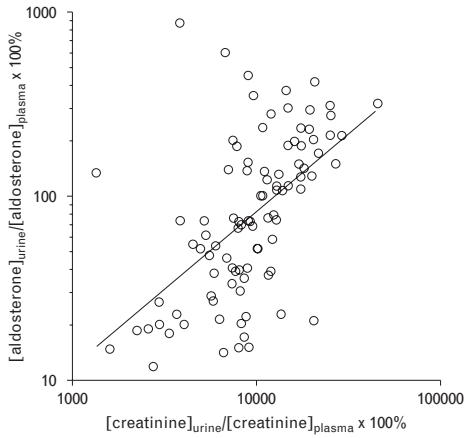

Correlation between the urine/plasma concentration ratios of creatinine and aldosterone ($r = 0.55$, $P < 0.01$).

renin release. As the opposite occurs at the site of the collecting duct [17,27], the decrease in urinary renin during treatment with ACEi and/or ARBs might reflect the consequence of Ang II blockade at the site of the collecting duct. Possibly, therefore, urinary renin originates at this location and as such reflects renal RAAS activity.

In agreement with previous studies [3,8], urinary angiotensinogen excretion paralleled urinary albumin excretion. Not only did their urine/plasma concentration ratios mimic each other but their levels in urine, expressed as a percentage of their levels in plasma, were also identical. Moreover, their fractional excretion (100% × urinary/plasma concentration ratio of albumin or angiotensinogen divided by the urine/plasma concentration ratio of creatinine) was identical: 0.0003% (0.00003–0.08) for albumin vs. 0.0005% (0.0001–0.007) for angiotensinogen. Our data, thus, support the concept that only very modest amounts of large molecular weight proteins such as angiotensinogen and albumin will be filtered across the glomerular membrane (or, more likely, that angiotensinogen and albumin, once filtered, are largely reabsorbed in the tubules [28]): the urinary angiotensinogen and albumin levels were more than 2000-fold lower than those in plasma. A previous study in rats, infusing human angiotensinogen, did not detect human angiotensinogen in urine [4]. However, the authors performed a western blot analysis with 0.1 μl plasma vs. 1.5 μl urine. Given the concentration difference of more than three orders of magnitude between plasma and urine, the application of a 15-fold larger urine sample will

Fig. 4

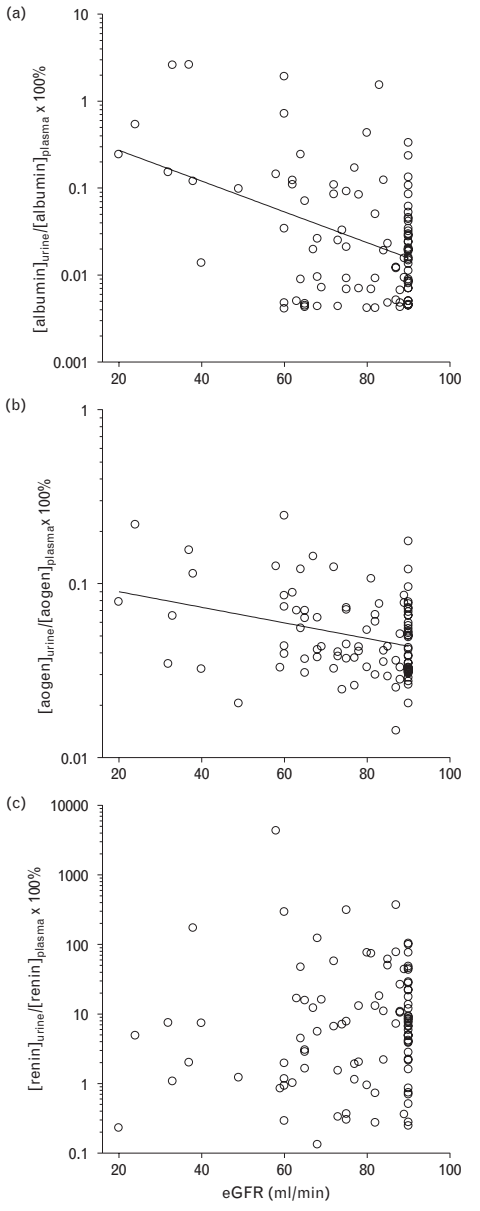

Correlations between estimated glomerular filtration rate (eGFR) and the urine/plasma concentration ratios of albumin [a ($r = -0.44$, $P < 0.01$)], angiotensinogen (aogen) [b ($r = -0.32$, $P < 0.01$)] or renin [c ($r = 0.13$, $P =$ NS)].

have been insufficient to accurately measure human angiotensinogen in urine. Consequently, the lack of human angiotensinogen in urine under those conditions cannot be taken as evidence that there is no filtration of circulating angiotensinogen. Obviously, given its close correlation with albumin, urinary angiotensinogen will reflect both renal dysfunction and the beneficial effects of RAS blockade – hence, also its negative correlation with eGFR in this and a previous study [1]. In other words, urinary angiotensinogen levels are likely to provide the same information as urinary albumin levels and, as such, are a valid biomarker of renal dysfunction. In our study, nondiabetic individuals, women and patients not using ACEi or ARBs had higher plasma angiotensinogen levels, which is in full agreement with previous reports [19,25]. However, these three groups also displayed the lowest urinary albumin levels and, as a consequence, their urinary angiotensinogen levels were not different from the levels in their comparator groups (diabetic patients, men and users of ACEi and/or ARBs).

Unexpectedly, urine did not contain detectable amounts of prorenin. This was not due to prorenin–renin conversion in urine, either *in vivo* (at 37°C) or *ex vivo* (at 4 or 22°C). As plasma prorenin levels are much higher than plasma renin levels, this finding, combined with the comparable molecular weights of renin (48 kD), prorenin (54 kD), angiotensinogen and albumin, strongly argues against the appearance of renin in urine as the mere consequence of glomerular filtration. Such filtration does occur, as has been previously reported in mice [29–30], but is accompanied by virtually complete tubular reabsorption, both for renin and prorenin. The same applies to albumin and angiotensinogen [28]. From this point of view, the urinary renin and prorenin levels (relative to plasma) should have been of the same magnitude as those of albumin and angiotensinogen, that is, more than 2000-fold below their plasma levels. Such low levels would have been beyond the detection limit of our assay. Consequently, it seems reasonable to assume that prorenin was in fact present in urine at such levels. Urinary renin levels were, however, more than 200-fold higher than expected, and the sexual dimorphism of renin in plasma did not apply to renin in urine. Moreover, urinary renin decreased during treatment with ACEi and/or ARBs, whereas the opposite occurred in plasma. Most likely, therefore, urinary renin does not originate in blood, but is rather released from renal tissue sites. Given the predominant release of prorenin from the collecting duct [17], at least in rats, it appears that either this prorenin is retained in the tubular cells (e.g. due to its binding to the (pro)renin receptor), allowing selective secretion of renin in urine, and/or that collecting duct prorenin is converted to renin before its release into urine.

Xue and Siragy [18] recently reported that in rats the renal aldosterone levels, as opposed to plasma aldosterone levels, did not disappear following adrenalectomy. Remarkably, in their study, renal aldosterone levels were approximately 15000 pg/g vs. aldosterone levels in blood plasma and renal interstitial fluid of approximately 700 and approximately 15 pg/ml, respectively. As renal tissue contains approximately 5% blood plasma, and approximately 10% interstitial fluid, this implies that more than 99% of renal aldosterone is located intracellularly. The half-life of such intracellular aldosterone is unknown and, thus, future studies should exclude that this represents internalized, adrenal-derived aldosterone. Indeed, the heart is another location where, despite initial reports on local aldosterone synthesis, eventually it was concluded that this does not occur [31–32]. Remarkably in this regard, Xue and Siragy localized aldosterone synthase in glomerular nucleoli, that is, outside its usual site of action, the mitochondria. Our data now reveal that urinary aldosterone levels are almost identical to plasma aldosterone levels, and that the urine/plasma concentration ratio of aldosterone (molecular weight 0.4 kD) mimics that of creatinine (molecular weight 0.1 kD). This strongly suggests that urinary aldosterone is entirely blood-derived. Had the kidney been an important site of aldosterone production, resulting in the overflow of renal aldosterone in urine, no correlation between the urine/plasma concentration ratios of aldosterone and creatinine should have been present. In fact, when analyzing urinary samples of four bilaterally adrenalectomized patients (two men and two women, age 60 ± 10 years, adrenalectomized because of Cushing's syndrome 1, 9, 17 and 32 years ago, respectively), aldosterone levels were found to be undetectable (R.A. Feelders, unpublished observations). Moreover, we are not aware of data showing release of aldosterone into blood from renal tissue sites.

In summary, the current study reveals that urinary renin, and not urinary prorenin, angiotensinogen or aldosterone, is an important marker of renal RAAS activity. Our data are the first to demonstrate directly renal RAAS activation in diabetic patients (and not indirectly by quantifying the renal effect of RAAS blockers). This might explain why such patients, despite low-to-normal plasma renin levels, respond strongly to RAAS blockers. The data also show that the consequences of RAAS blockade in plasma and kidney are not necessarily the same. A limitation of our study is the large diversity of the patients, particularly with regard to treatment. For instance, 30% received a β-blocker, 51% a calcium antagonist and 13% a mineralocorticoid receptor antagonist, that is, drugs that may also (modestly) affect RAAS component levels. Future studies should now carefully address the effect of such drugs on urinary renin in a prospective manner, as well as that of ACEi, ARBs and renin inhibitors. Renin inhibitors are of particular interest, given the large rise in plasma renin that occurs during renin inhibition [12,33–34].

Acknowledgements

This study was supported by the Dutch Kidney Foundation (grant number C08.2246). The authors thank Mrs E. van Beugen, Mrs M. Boeije and Mrs S. Mohkamsing for their excellent technical assistance.

Conflicts of interest

There are no conflicts of interest.

References

1 Yamamoto T, Nakagawa T, Suzuki H, Ohashi N, Fukasawa H, Fujigaki Y, *et al.* Urinary angiotensinogen as a marker of intrarenal angiotensin II activity associated with deterioration of renal function in patients with chronic kidney disease. *J Am Soc Nephrol* 2007; **18**:1558–1565.
2 Nishiyama A, Konishi Y, Ohashi N, Morikawa T, Urushihara M, Maeda I, *et al.* Urinary angiotensinogen reflects the activity of intrarenal renin-angiotensin system in patients with IgA nephropathy. *Nephrol Dial Transplant* 2011; **26**:170–177.
3 Kobori H, Alper AB Jr, Shenava R, Katsurada A, Saito T, Ohashi N, *et al.* Urinary angiotensinogen as a novel biomarker of the intrarenal renin-angiotensin system status in hypertensive patients. *Hypertension* 2009; **53**:344–350.
4 Kobori H, Nishiyama A, Harrison-Bernard LM, Navar LG. Urinary angiotensinogen as an indicator of intrarenal angiotensin status in hypertension. *Hypertension* 2003; **41**:42–49.
5 Jang HR, Kim SM, Lee YJ, Lee JE, Huh W, Kim DJ, *et al.* The origin and the clinical significance of urinary angiotensinogen in proteinuric IgA nephropathy patients. *Ann Med* 2011; (in press).
6 Lantelme P, Rohrwasser A, Vincent M, Cheng T, Gardier S, Legedz L, *et al.* Significance of urinary angiotensinogen in essential hypertension as a function of plasma renin and aldosterone status. *J Hypertens* 2005; **23**:785–792.
7 Kobori H, Harrison-Bernard LM, Navar LG. Expression of angiotensinogen mRNA and protein in angiotensin II-dependent hypertension. *J Am Soc Nephrol* 2001; **12**:431–439.
8 Kobori H, Urushihara M, Xu JH, Berenson GS, Navar LG. Urinary angiotensinogen is correlated with blood pressure in men (Bogalusa Heart Study). *J Hypertens* 2010; **28**:1422–1428.
9 Danser AHJ, van den Dorpel MA, Deinum J, Derkx FHM, Franken AAM, Peperkamp E, *et al.* Renin, prorenin, and immunoreactive renin in vitreous fluid from eyes with and without diabetic retinopathy. *J Clin Endocrinol Metab* 1989; **68**:160–167.
10 Franken AAM, Derkx FHM, Man in 't Veld AJ, Hop WC, van Rens GH, Peperkamp E, *et al.* High plasma prorenin in diabetes mellitus and its correlation with some complications. *J Clin Endocrinol Metab* 1990; **71**:1008–1015.
11 Lansang MC, Price DA, Laffel LM, Osei SY, Fisher ND, Erani D, Hollenberg NK. Renal vascular responses to captopril and to candesartan in patients with type 1 diabetes mellitus. *Kidney Int* 2001; **59**:1432–1438.
12 Persson F, Rossing P, Reinhard H, Juhl T, Stehouwer CD, Schalkwijk C, *et al.* Renal effects of aliskiren compared with and in combination with irbesartan in patients with type 2 diabetes, hypertension, and albuminuria. *Diabetes Care* 2009; **32**:1873–1879.
13 Hollenberg NK, Price DA, Fisher ND, Lansang MC, Perkins B, Gordon MS, *et al.* Glomerular hemodynamics and the renin-angiotensin system in patients with type 1 diabetes mellitus. *Kidney Int* 2003; **63**:172–178.
14 Luetscher JA, Kraemer FB, Wilson DM, Schwartz HC, Bryer-Ash M. Increased plasma inactive renin in diabetes mellitus. A marker of microvascular complications. *N Engl J Med* 1985; **312**:1412–1417.
15 van den Heuvel M, Batenburg WW, Danser AHJ. Diabetic complications: a role for the prorenin-(pro)renin receptor-TGF-beta1 axis? *Mol Cell Endocrinol* 2009; **302**:213–218.
16 Danser AHJ, Deinum J. Renin, prorenin and the putative (pro)renin receptor. *Hypertension* 2005; **46**:1069–1076.
17 Kang JJ, Toma I, Sipos A, Meer EJ, Vargas SL, Peti-Peterdi J. The collecting duct is the major source of prorenin in diabetes. *Hypertension* 2008; **51**:1597–1604.
18 Xue C, Siragy HM. Local renal aldosterone system and its regulation by salt, diabetes, and angiotensin II type 1 receptor. *Hypertension* 2005; **46**:584–590.
19 Danser AHJ, Derkx FHM, Schalekamp MADH, Hense HW, Riegger GAJ, Schunkert H. Determinants of interindividual variation of renin and prorenin concentrations: evidence for a sexual dimorphism of (pro)renin levels in humans. *J Hypertens* 1998; **16**:853–862.
20 Batenburg WW, de Bruin RJA, van Gool JMG, Müller DN, Bader M, Nguyen G, Danser AHJ. Aliskiren-binding increases the half life of renin and prorenin in rat aortic vascular smooth muscle cells. *Arterioscler Thromb Vasc Biol* 2008; **28**:1151–1157.
21 de Lannoy LM, Danser AHJ, van Kats JP, Schoemaker RG, Saxena PR, Schalekamp MADH. Renin-angiotensin system components in the interstitial fluid of the isolated perfused rat heart. Local production of angiotensin I. *Hypertension* 1997; **29**:1240–1251.
22 Danser AHJ, van Kats JP, Admiraal PJJ, Derkx FHM, Lamers JMJ, Verdouw PD, *et al.* Cardiac renin and angiotensins. Uptake from plasma versus in situ synthesis. *Hypertension* 1994; **24**:37–48.
23 Krop M, Garrelds IM, de Bruin RJA, van Gool JMG, Fisher NDL, Hollenberg NK, Danser AHJ. Aliskiren accumulates in renin secretory granules and binds plasma prorenin. *Hypertension* 2008; **52**:1076–1083.
24 Danser AHJ, van Kesteren CAM, Bax WA, Tavenier M, Derkx FHM, Saxena PR, Schalekamp MADH. Prorenin, renin, angiotensinogen, and angiotensin-converting enzyme in normal and failing human hearts. Evidence for renin binding. *Circulation* 1997; **96**:220–226.
25 Klotz S, Burkhoff D, Garrelds IM, Boomsma F, Danser AHJ. The impact of left ventricular assist device-induced left ventricular unloading on the myocardial renin-angiotensin-aldosterone system: therapeutic consequences? *Eur Heart J* 2009; **30**:805–812.
26 Manjunath G, Sarnak MJ, Levey AS. Prediction equations to estimate glomerular filtration rate: an update. *Curr Opin Nephrol Hypertens* 2001; **10**:785–792.
27 Prieto-Carrasquero MC, Harrison-Bernard LM, Kobori H, Ozawa Y, Hering-Smith KS, Hamm LL, Navar LG. Enhancement of collecting duct renin in angiotensin II-dependent hypertensive rats. *Hypertension* 2004; **44**:223–229.
28 Birn H, Christensen EI. Renal albumin absorption in physiology and pathology. *Kidney Int* 2006; **69**:440–449.
29 Mazanti I, Hermann KL, Nielsen AH, Poulsen K. Ultrafiltration of renin in the mouse kidney studied by inhibition of tubular protein reabsorption with lysine. *Clin Sci (Lond)* 1988; **75**:331–336.
30 Nielsen AH, Hermann KL, Mazanti I, Poulsen K. Urinary excretion of inactive renin during blockade of the renal tubular protein reabsorption with lysine. *J Hypertens* 1989; **7**:77–82.
31 Chai W, Hofland J, Jansen PM, Garrelds IM, de Vries R, van den Bogaerdt AJ, *et al.* Steroidogenesis vs. steroid uptake in the heart: do corticosteroids mediate effects via cardiac mineralocorticoid receptors? *J Hypertens* 2010; **28**:1044–1053.
32 Chai W, Danser AHJ. Why are mineralocorticoid receptor antagonists cardioprotective? *Naunyn Schmiedebergs Arch Pharmacol* 2006; **374**:153–162.
33 Fisher NDL, Danser AHJ, Nussberger J, Dole WP, Hollenberg NK. Renal and hormonal responses to direct renin inhibition with aliskiren in healthy humans. *Circulation* 2008; **117**:3199–3205.
34 Persson F, Rossing P, Reinhard H, Juhl T, Stehouwer CD, Schalkwijk C, *et al.* Optimal antiproteinuric dose of aliskiren in type 2 diabetes mellitus: a randomised crossover trial. *Diabetologia* 2010; **53**:1576–1580.

The (pro)renin receptor blocker handle region peptide upregulates endothelium-derived contractile factors in aliskiren-treated diabetic transgenic (mREN2)27 rats

Batenburg W.W.*, van den Heuvel M.*, van Esch J.H., van Veghel R.,
Garrelds I.M., Leijten F. and Danser A.H.
*Shared first authorship

J. Hypertens. 2013 Feb;31(2):292-302

16

The (pro)renin receptor blocker handle region peptide upregulates endothelium-derived contractile factors in aliskiren-treated diabetic transgenic (mREN2)27 rats

Wendy W. Batenburg*, Mieke van den Heuvel*, Joep H.M. van Esch, Richard van Veghel, Ingrid M. Garrelds, Frank Leijten, Alexander H.J. Danser

Background: Elevated prorenin levels associate with microvascular complications in patients with diabetes mellitus, possibly because prorenin affects vascular function in diabetes mellitus, for example by generating angiotensins following its binding to the (pro)renin receptor [(P)RR]. Here we evaluated whether the renin inhibitor aliskiren, with or without the putative (P)RR antagonist handle region peptide (HRP) improved the disturbed vascular function in diabetic TGR(mREN2)27 rats, a high-prorenin, high-(P)RR hypertensive model.

Methods: Telemetry transmitters were implanted to monitor blood pressure. After 3 weeks of treatment, rats were sacrificed, and iliac and mesenteric arteries were removed to evaluate vascular reactivity.

Results: Diabetes mellitus enhanced the contractile response to nitric oxide synthase (NOS) blockade, potentiated the response to phenylephrine, diminished the effectiveness of endothelin type A (ET_A) receptor blockade and allowed acetylcholine to display constrictor, cyclo-oxygenase-2 mediated, endothelium-dependent responses in the presence of NOS inhibition and blockers of endothelium-derived hyperpolarizing factors. Aliskiren normalized blood pressure, suppressed renin activity, and reversed the above vascular effects, with the exception of the altered effectiveness of ET_A receptor blockade. Remarkably, when adding HRP on top of aliskiren, its beneficial vascular effects either disappeared or were greatly diminished, although HRP did not alter the effect of aliskiren on blood pressure and renin activity.

Conclusions: Renin inhibition improves vascular dysfunction in diabetic hypertensive rats, and HRP counteracts this effect independently of blood pressure and angiotensin. (P)RR blockade therefore is unlikely to be a new tool to further suppress the renin–angiotensin system (RAS) on top of existing RAS blockers.

Keywords: (pro)renin receptor blockade, diabetes, endothelium-derived contracting factor, nitric oxide, prorenin, renin inhibition

Abbreviations: (P)RR, (pro)renin receptor; ACh, acetylcholine; Ang, angiotensin; COX, cyclo-oxygenase; CRC, concentration–response curve; EDCF, endothelium-derived contractile factor; EDHF, endothelium-derived hyperpolarizing factor; EKA, enzyme-kinetic assay; ET_A/ET_B receptor, endothelin receptor type A or B; HPRT1, hypoxanthine phosphoribosyl transferase-1; HRP, handle region peptide; MAP, mean arterial pressure; MAPK, mitogen-activated protein kinases; NOS, NO synthase; PRA, plasma renin activity; RAS, renin–angiotensin system; Ren2, TGR(mREN2)27; SK_{Ca}/IK_{Ca} channels, small/intermediate conductance Ca^{2+}-activated K^+-channel; SNAP, S-nitroso-N-penicillamine; STZ, streptozotocin; U46619, 9,11-dideoxy-11α,9α-epoxy-methano-prostaglandin $F_{2\alpha}$

INTRODUCTION

The renin–angiotensin (Ang) system (RAS) contributes to the pathogenesis of diabetic nephropathy, since RAS blockers prevent the deterioration of renal function in patients with diabetes mellitus [1,2]. Remarkably however, diabetic patients tend to have low renin levels, whereas their levels of prorenin, the inactive precursor of renin, are greatly elevated [3]. In fact, these high prorenin levels are an early predictor of the microvascular complications of diabetes, including retinopathy and nephropathy [4,5]. The protective effect of RAS blockade, particularly in the diabetic kidney, has therefore been attributed to interference with prorenin-dependent RAS activation. This may occur through binding of prorenin to the so-called (pro)renin receptor [(P)RR]. This receptor binds both renin and prorenin, and binding of the latter induces a conformational change in the prorenin molecule, allowing it to display full enzymatic activity

Journal of Hypertension 2013, 31:292–302

Division of Pharmacology and Vascular Medicine, Department of Internal Medicine, Erasmus MC, Rotterdam, The Netherlands

Correspondence to Professor Dr. A.H.J. Danser, PhD, Division of Pharmacology and Vascular Medicine, Department of Internal Medicine, Erasmus MC, Room EE1418b, Dr Molewaterplein 50, 3015 GE, Rotterdam, The Netherlands. Tel: +31 10 7043540; fax: +31 10 7044733; e-mail: a.danser@erasmusmc.nl

*Wendy W. Batenburg and Mieke van den Heuvel contributed equally to the writing of this article.

Received 8 June 2012 **Revised** 27 August 2012 **Accepted** 30 October 2012

J Hypertens 31:292–302

without cleavage of the prosegment (i.e. without being converted to renin).

In support of a role for the (P)RR in the diabetic kidney and eye, the (P)RR inhibitor handle region peptide (HRP) exerted renoprotective and oculoprotective effects in diabetic rodents [6–9]. HRP represents the part of the prosegment that determines prorenin binding to its receptor. Unexpectedly, (P)RR-bound prorenin not only displayed Ang I-generating activity [10,11], but also stimulated cellular signal transduction in an angiotensin-independent manner [10,12]. This signaling resulted in the upregulation of fibrotic pathways, involving mitogen-activated protein kinases (MAPK p42/44, p38) activation, transforming growth factor-β1 synthesis and plasminogen activator-inhibitor 1 release [10,12,13]. In addition, a positive feedback loop exists between the (P)RR and cyclo-oxygenase 2 (COX-2), which is regulated by the level of glucose [14–17]. It is therefore feasible that (P)RR blockade with HRP also exerts effects beyond RAS suppression.

However, not all studies with HRP were positive, and its capacity to block the (P)RR is not uniformly accepted [12,18–21]. Moreover, there is some doubt whether prorenin truly interacts with the (P)RR *in vivo*, given its picomolar levels and the nanomolar affinity of the receptor [10,11,22].

A suitable animal model to study prorenin–(P)RR interaction is the TGR(mREN2)27 rat (Ren2 rat). These rats, which overexpress the mouse Ren2 gene, not only have greatly elevated prorenin and Ang II levels, but also display increased (P)RR expression and are severely hypertensive [23–26]. After streptozotocin injection, they develop a diabetic phenotype that closely mimics that in human diabetic patients, characterized by high prorenin levels, retinal pathology, vascular dysfunction and nephropathy [27–30]. We and others have already demonstrated that the renin inhibitor aliskiren lowers blood pressure and improves albuminuria in this model [24,31]. In the present study, we focused on the effects of aliskiren on vascular dysfunction in diabetic Ren2 rats, evaluating in particular the altered endothelium-dependent and endothelin-1 (ET-1)-mediated responses that have been noted before in diabetic animals [32]. We also determined to what degree HRP exerts vascular effects on top of renin inhibition. We reasoned that, if anywhere, the beneficial effects of this putative (P)RR blocker should be observed in this high-prorenin, high-(P)RR model.

METHODS

Animal studies

Homozygous Ren2 rats (400–500 g; a kind gift of Dr M. Bader, Berlin, Germany), were crossed with Sprague–Dawley rats (Harlan, Boxmeer, The Netherlands) to generate heterozygous Ren2 rats. Heterozygous rats were subsequently used in all studies, as these rats, in contrast to homozygous Ren2 rats, did not require lisinopril treatment (10 μg/ml in drinking water) to decrease mortality. All studies were performed under the regulation and permission of the Animal Care Committee of the Erasmus MC. Rats were housed in individual cages and maintained on a 12-h light/dark cycle, having access to standard laboratory rat chow and water *ad libitum*. Radiotelemetry transmitters were implanted as described before [33] for continuous measurement of heart rate, blood pressure, and activity. Two weeks later, to induce diabetes mellitus, rats were fasted overnight and administered streptozotocin (STZ; 55 mg/kg i.p.; Sigma–Aldrich, Zwijndrecht, The Netherlands). Rats were checked regularly for blood glucose and β-ketone levels by tail incision (Precision Xceed; Abbott, Zwolle, The Netherlands). Only rats with a glucose level more than 15 mmol/l were considered diabetic, and they subsequently received 2–4 U insulin per day (Levemir; Novo Nordisk, Denmark). After 2 weeks of diabetic status osmotic minipumps (2ML4; ALZET, Cupertino, California, USA) were implanted subcutaneously under isoflurane anesthesia to infuse vehicle (saline; $n=8$) or aliskiren (a gift of Novartis, 10 mg/kg per day) with ($n=8$) or without ($n=7$) rat HRP (NH_2-RILLKKMPSV-COOH, 1 mg/kg per day; Biosynthan, Berlin, Germany). In the animals receiving two drugs, two separate minipumps were implanted at both sides of the body. Three weeks later, animals were anaesthetized by pentobarbital injection i.p., and the hepatic portal vein was cannulated to collect blood for the measurement of renin, prorenin and plasma renin activity (PRA). Mesenteric arteries and iliac arteries were isolated and transported to ice-cold oxygenated Krebs bicarbonate solution (in mmol/l: NaCl 118, KCl 4.7, $CaCl_2$ 2.5, $MgSO_4$ 1.2, KH_2PO_4 1.2, $NaHCO_3$ 25 and glucose 8.3; pH 7.4) until the start of the experiment the same day. Blood and vessels were also obtained from six diabetic Ren2 rats treated with saline for 3 weeks, eight untreated nondiabetic Ren2 rats, and eight age-matched untreated Sprague–Dawley rats. None of these rats underwent haemodynamic measurements.

Myograph studies

Following isolation, mesenteric arteries and iliac arteries were cut into segments of approximately 2 mm length and mounted in a Mulvany myograph (Danish Myo Technology, Aarhus, Denmark) with separated 6-ml organ baths containing Krebs bicarbonate solution, aerated with 95% O_2 and 5% CO_2, and maintained at 37°C. Tissue responses were measured as changes in isometric force, using Powerlab with Labchart software. To remove the endothelium, a human hair was gently rubbed through the lumen of the mesenteric artery. Following a 30-min stabilization period, the optimal internal diameter was set to a tension equivalent to 0.9 times the estimated diameter at 100 mmHg effective transmural pressure as described by Mulvany and Halpern [34]. Endothelial removal was verified by observing no relaxation to 1 μmol/l acetylcholine (ACh) after preconstriction with 100 nmol/l of the thromboxane A_2 analogue U46619 (9,11-dideoxy-11α,9α-epoxy-methano-prostaglandin $F_{2\alpha}$). Subsequently, to determine the maximum contractile response, the tissue was exposed to 100 mmol/l KCl. The segments were then allowed to equilibrate in fresh organ bath fluid for 30 min. Next, segments were preincubated for 30 min with the NO synthase (NOS) inhibitor L-NAME (100 μmol/l), the small conductance Ca^{2+}-activated K^+-channel (SK_{Ca}) inhibitor apamin (100 nmol/l), the intermediate conductance Ca^{2+}-activated K^+-channel (IK_{Ca}) inhibitor TRAM34 (10 μmol/l),

the endothelin type A (ET_A) receptor antagonist BQ123 (1 and 10 μmol/l), the endothelin type B (ET_B) receptor antagonist BQ788 (10 nmol/l), the nonselective cyclo-oxygenase (COX) inhibitor indomethacin (10 μmol/l), the COX-2-selective inhibitor NS398 (10 μmol/l), the thromboxane/endoperoxide receptor antagonist GR32191B (1 μmol/l) and/or the superoxide scavenger tempol (1 mmol/l). Thereafter, concentration–response curves (CRCs) were constructed to Ang II and phenylephrine (iliac arteries) or ET-1 (mesenteric arteries). To construct CRCs to ACh or S-nitroso-N-penicillamine (SNAP), mesenteric arteries were preconstricted with U46619 (0.1–0.3 μmol/l) or phenylephrine (in the studies with GR32191B; 1 μmol/l). All drugs were from Sigma–Aldrich. To mimic the diabetic in-vivo conditions in the organ bath, parallel experiments in six mesenteric arteries of diabetic rats were performed with 25 instead of 8.3 mmol/l glucose. ACh-induced relaxations (pEC_{50} 7.7 ± 0.1 vs. 7.5 ± 0.1 and E_{max} 97 ± 2 vs. $97 \pm 2\%$) were identical under both conditions, and all studies were therefore performed in regular Krebs buffer.

Biochemical measurements

PRA was measured by quantifying Ang I generation during incubation of plasma for 60 min at pH 7.4 and 37°C in the presence of a mixture of inhibitors to block Ang I degradation, Ang I–II conversion, and prorenin–renin conversion, and to prevent bacterial growth [33]. Plasma renin and prorenin concentration were measured by enzyme-kinetic assay (EKA) in the presence of excess sheep angiotensinogen. Total renin was measured after prorenin had been converted to renin by incubation of the sample for 48 h at 4°C with trypsin coupled to Sepharose [35]. Subtraction of the renin concentration from the total renin concentration yielded the prorenin concentration. In all assays, the generated Ang I was measured by radioimmunoassay.

Cyclo-oxygenase-2 and endothelin type A receptor expression

Total RNA was isolated from snap-frozen rat aortas using Trizol (Life Technologies, Grand Island, Nebraska, USA) and reverse transcribed into cDNA using the QuantiTect Reverse Transcription Kit (Qiagen, Venlo, The Netherlands). The resulting cDNA was amplified in 40 cycles (denaturation at 95°C for 10 min; thermal cycling at 95°C for 15 s, annealing/extension at 60°C for 1 min) with a Step-One cycler (NYSE, Life Technologies) using the SYBR Green PCR Master Mix (Life Technologies). The intron-spanning oligonucleotide primers for qPCR were designed with NCBI (Primer-BLAST). The comparative cycle time method (ΔΔCT) was used for relative quantification of gene expression, using the geometric mean of the housekeeping genes hypoxanthine phosphoribosyl transferase-1 (HPRT1) and β-actin for normalization. The following primers were used: rat HPRT1 forward 5′-GGACAGGACTGAAAGACTTGCTCG-3′, reverse 5′-TTCAGCACACAGAGGGCCACA-3′; rat β-actin forward 5′-GGGAAATCGTGCGTGACATT-3′, reverse 5′-GCGGCAGTGGCCATCTC-3′; rat ET_A receptor forward 5′-CGTCCGAGGAGCTCTAAGGGGAA-3′, reverse 5′-ACG CCAGAAAGCAAAGGACACCC-3′; rat COX-2 forward 5′-ATTGCTGGCCGGGTTGCTGG-3′, reverse 5′-TCAATGGA GGCCTTTGCCACTGC-3′.

Statistical analysis

Data are given as mean ± SEM. Relaxant responses to either acetylcholine or SNAP are expressed as a percentage of the contraction to U46619 or phenylephrine where appropriate. Contractile responses to Ang II, phenylephrine or ET-1 are expressed as a percentage of the contraction to 100 mmol/l KCl. CRCs were analyzed as described [36] to obtain pEC_{50} ($-^{10}\log EC_{50}$) values. In experiments wherein no clear maximum effect (E_{max}) was reached, E_{max} was defined as the effect obtained at the highest concentration tested. pEC_{50} values were not calculated when E_{max} was less than 20%, and in such cases statistical analysis was performed under the assumption that pEC_{50} equalled the highest concentration tested. Haemodynamic parameters were compared by two-way ANOVA. All other data were analyzed by Student's *t*-test or one-way ANOVA, followed by posthoc evaluation according to Dunnet or Tukey (for comparisons within and between groups, respectively). $P < 0.05$ was considered significant.

RESULTS

Induction of diabetes mellitus and hemodynamic parameters

Diabetes mellitus induction increased blood glucose from 5.8 ± 0.2 before STZ injection to maximally 25.8 ± 0.9 mmol/l at 2 weeks after STZ injection ($n = 11$; $P < 0.001$), and the 3-week treatment period did not alter this further in any of the three groups (data not shown). Plasma β-ketone levels remained unaltered after STZ injection (0.3 ± 0.1 mmol/l before STZ vs. 0.5 ± 0.1 mmol/l at 2 weeks after STZ), and were also not affected by treatment. The levels of blood glucose (4.7 ± 0.6 mmol/l) and plasma β-ketone (0.3 ± 0.1 mmol/l) in Sprague–Dawley rats were identical to those in nondiabetic Ren2 rats.

The renin inhibitor aliskiren, either alone or combined with the (P)RR blocker HRP lowered mean arterial pressure (MAP) versus saline, with no effect on heart rate or activity (Fig. 1). Significance for the effect on MAP vs. saline was reached by day 7 ($P < 0.05$), and on day 21 MAP in the rats treated with aliskiren or aliskiren+HRP was 104 ± 5 and 103 ± 3 mmHg, respectively (vs. 123 ± 4 mmHg in saline-treated diabetic Ren2 rats; $P < 0.05$ for both). MAP in the presence of aliskiren+HRP did not differ from MAP with aliskiren alone.

Prorenin, renin and plasma renin activity

Nondiabetic Ren2 rats ($n = 12$) displayed higher prorenin and lower renin levels than Sprague–Dawley rats ($n = 6$; Fig. 2, $P < 0.05$ for both). PRA was also lower in nondiabetic Ren2 rats. Diabetes increased prorenin two-fold to three-fold ($P < 0.05$ vs. nondiabetic Ren2 rats), without affecting renin or PRA. Renin and prorenin could not be measured in the aliskiren-treated animals, due to the interference of aliskiren with the enzyme-kinetic assay [33]. Aliskiren

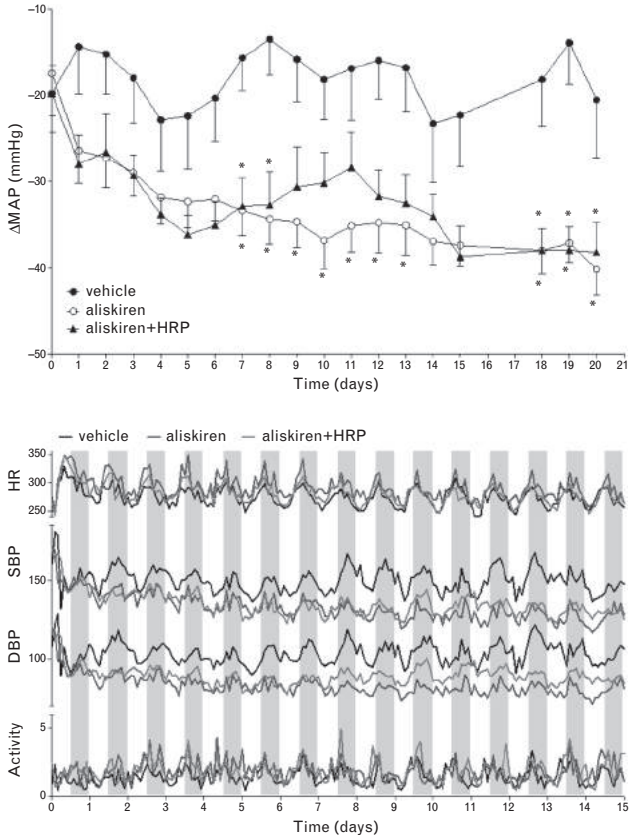

FIGURE 1 Top, mean arterial pressure (MAP) during a 3-week infusion of vehicle, aliskiren or aliskiren + HRP in diabetic Ren2 rats. Data are mean ± SEM of 7–8 rats. * $P < 0.05$ vs. vehicle. Bottom, heart rate (HR), SBP DBP and activity level in the above rats. Data are means of 7–8 rats.

reduced PRA by more than 60%, both with and without HRP ($P < 0.05$ for both).

Vascular reactivity

To determine the diabetes mellitus-induced changes in vascular function, as well as the possible reversal of these changes by treatment, iliac arteries of Sprague–Dawley rats, nondiabetic Ren2 rats and diabetic Ren2 rats treated with vehicle, aliskiren, or aliskiren + HRP, were exposed to the vasoconstrictors Ang II and phenylephrine, and mesenteric arteries of these animals were exposed to the vasoconstrictor ET-1 and the vasodilators SNAP and ACh. Experiments were repeated in the presence of endothelin receptor blockers (BQ123, BQ788) and inhibitors of the NO (L-NAME) and endothelium-derived hyperpolarizing factor (TRAM34 + apamin) pathways [32], to determine potential causes of the changes in vascular function.

Iliac artery

Ang II constricted iliac arteries of Sprague–Dawley rats to maximally 47 ± 14% of the response to K^+ (Fig. 3, Table 1). The NOS inhibitor L-NAME greatly increased the response to Ang II ($P < 0.05$), without altering its potency. L-NAME did not affect baseline contractility in Sprague–Dawley rats. In contrast, in nondiabetic Ren2 rats, L-NAME marginally increased baseline contractility ($P = 0.06$ vs. Sprague–Dawley), whereas in vehicle-treated diabetic Ren2 rats it increased baseline contractility to ≈65% of the response to K^+ ($P < 0.01$ vs. Sprague–Dawley and nondiabetic Ren2). Aliskiren reduced the effect of L-NAME in diabetic Ren2 rats to the levels in nondiabetic Ren2 rats ($P < 0.05$ vs. vehicle-treated diabetic Ren2 rats), and HRP reversed this effect of aliskiren. The Ang II E_{max} doubled in nondiabetic and diabetic-vehicle Ren2 rats compared with Sprague–Dawley rats, and aliskiren alone, but not aliskiren + HRP,

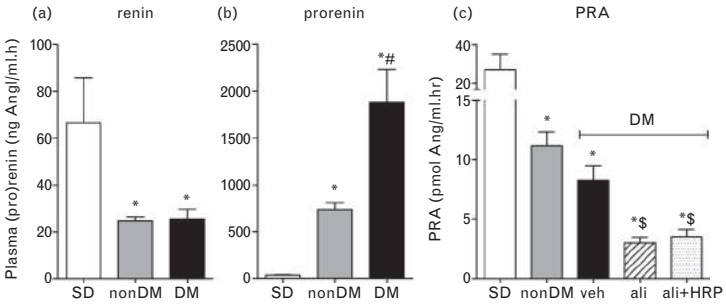

FIGURE 2 Plasma renin (a) and prorenin (b) concentration, and plasma renin activity (c) in Sprague–Dawley rats, nondiabetic Ren2 rats, and diabetic Ren2 rats after a 3-week infusion of vehicle (veh), aliskiren (ali) or aliskiren + HRP. Data are mean ± SEM of 6–8 rats. * $P < 0.05$ vs. Sprague–Dawley, # $P < 0.05$ vs. nondiabetic Ren2, $ $P < 0.05$ vs. vehicle-treated diabetic Ren2. DM, diabetes mellitus.

tended to normalize this response. However, none of the changes in E_{max} were significant, and no changes in pEC_{50} were observed. The Ang II E_{max} in the presence of L-NAME was identical in all groups, and its pEC_{50} with L-NAME was also not affected by treatment.

Phenylephrine constricted iliac arteries in Sprague–Dawley rats to maximally 348 ± 62% (Fig. 3, Table 1). L-NAME shifted the phenylephrine CRC in Sprague–Dawley rats ≈10-fold to the left ($P < 0.01$), without altering its E_{max}. Results in nondiabetic Ren2 rats were identical to those in Sprague–Dawley rats. Diabetes mellitus potentiated the effect of phenylephrine in Ren2 rats, and reduced its E_{max} ($P < 0.05$ for both), while eliminating the leftward shift induced by L-NAME. Aliskiren normalized phenylephrine's potency, increased its E_{max}, and re-introduced the leftward shift by L-NAME (Table 1). HRP, when given on top of aliskiren, counteracted the effect of aliskiren alone on the phenylephrine E_{max}.

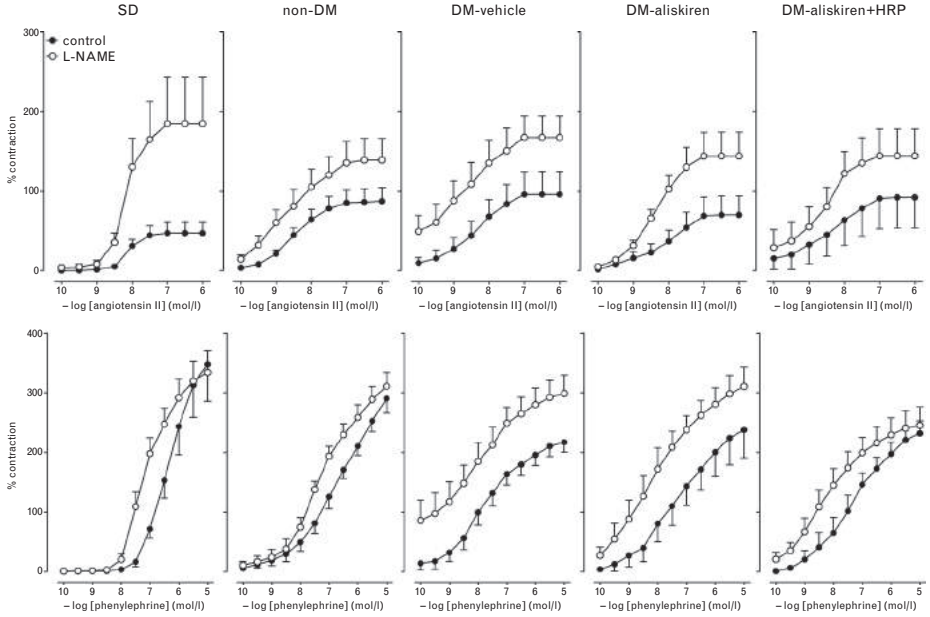

FIGURE 3 Contractions of iliac arteries, obtained from Sprague–Dawley rats, nondiabetic Ren2 rats, and diabetic Ren2 rats treated for 3 weeks with vehicle, aliskiren or aliskiren + HRP, to angiotensin II or phenylephrine in the absence or presence of 100 μmol/l L-NAME. Contractions (mean ± SEM of $n = 5–8$) have been expressed as a percentage of the response to 100 mmol/l K^+. See Table for statistical information. DM, diabetes mellitus.

TABLE 1. pEC_{50} and E_{max} values (mean ± SEM of $n = 5–8$) for angiotensin (Ang) II, phenylephrine (PE), endothelin-1 (ET-1), SNAP, acetylcholine (ACh) and L-NAME in iliac (Ang II, PE, L-NAME) or mesenteric (ET-1, SNAP, ACh) arteries of Sprague–Dawley rats, nondiabetic Ren2 rats, and diabetic Ren2 rats treated for 3 weeks with vehicle, aliskiren (10 mg/kg per day) or aliskiren + HRP (10 and 1 mg/kg per day, respectively), in the absence or presence of L-NAME (100 μmol/l), BQ123 (1 μmol/l), BQ788 (10 nmol/l), TRAM34 (T; 10 μmol/l) and/or apamin (A; 100 nmol/l)

pEC_{50}	Sprague–Dawley	Non-DM	DM-vehicle	DM-aliskiren	DM-aliskiren+HRP
Ang II	7.7 ± 0.4	8.3 ± 0.3	7.9 ± 0.4	7.2 ± 0.4	7.5 ± 0.5
Ang II+L-NAME	7.8 ± 0.4	8.5 ± 0.2	8.7 ± 0.2	8.6 ± 0.2	8.3 ± 0.4
PE	6.3 ± 0.1	6.6 ± 0.1	7.8 ± 0.2$^{*\#}$	7.0 ± 0.4	7.4 ± 0.2
PE+L-NAME	7.2 ± 0.1‡	7.4 ± 0.2$^{\$}$	8.0 ± 0.3	8.3 ± 0.3^{+}	8.2 ± 0.2$^{\$}$
ET_1	8.2 ± 0.2	8.3 ± 0.1	7.8 ± 0.1$^{\#}$	7.5 ± 0.1$^{\#}$	7.8 ± 0.1$^{\#}$
ET_1+BQ123	7.6 ± 0.2$^{\$}$	7.7 ± 0.1$^{\$}$	7.5 ± 0.1	7.4 ± 0.1	7.4 ± 0.1‡
ET_1+BQ788	8.3 ± 0.2	8.4 ± 0.1	7.8 ± 0.2	7.5 ± 0.1	8.0 ± 0.2
SNAP	8.0 ± 0.3	8.0 ± 0.3	7.4 ± 0.2$^{\#}$	6.9 ± 0.1$^{\#}$	6.9 ± 0.1$^{\#}$
ACh	7.3 ± 0.2	8.0 ± 0.1*	8.1 ± 0.1*	7.9 ± 0.1	7.9 ± 0.1
ACh+L-NAME	7.3 ± 0.3	7.5 ± 0.3	7.3 ± 0.3$^{\$}$	7.4 ± 0.1$^{\$}$	7.3 ± 0.2$^{\$}$
ACh+T+A	7.4 ± 0.2	8.0 ± 0.1*	8.1 ± 0.1*	7.9 ± 0.1	8.0 ± 0.1
ACh+L-NAME+T+A	6.7 ± 0.2	7.0 ± 0.4	–	–	–
E_{max}	Sprague–Dawley	Non-DM	DM-vehicle	DM-aliskiren	DM-aliskiren+HRP
Ang II	47 ± 14	87 ± 17	96 ± 29	70 ± 24	92 ± 38
Ang II+L-NAME	185 ± 59$^{\$}$	139 ± 27$^{\$}$	168 ± 30$^{\$}$	144 ± 30$^{\$}$	145 ± 34$^{\$}$
PE	348 ± 62	291 ± 24	217 ± 17*	245 ± 40†	232 ± 21
PE+L-NAME	334 ± 37	311 ± 23	299 ± 31	311 ± 32	245 ± 31
ET_1	244 ± 37	156 ± 18*	153 ± 14*	181 ± 13	152 ± 5
ET_1+BQ123	199 ± 18	185 ± 18	168 ± 8	171 ± 9	140 ± 16
ET_1+BQ788	274 ± 52	166 ± 14	165 ± 6	177 ± 7	141 ± 16
SNAP	103 ± 4	103 ± 6	77 ± 5$^{*\#}$	71 ± 5$^{\#}$	75 ± 5$^{\#}$
ACh	88 ± 7	90 ± 3	87 ± 2	89 ± 1	91 ± 2
ACh+L-NAME	76 ± 13	67 ± 8$^{\$}$	65 ± 9$^{\$}$	76 ± 7	75 ± 5$^{\$}$
ACh+T+A	84 ± 8	84 ± 6	76 ± 5	79 ± 5	81 ± 5
ACh+L-NAME+T+A	47 ± 16$^{\$}$	34 ± 8$^{\$}$	−29 ± 17$^{\$\Delta}$	11 ± 9$^{\$†}$	−6.7 ± 9$^{\$\#}$
L-NAME	3 ± 2	13 ± 4	66 ± 19$^{*\#}$	15 ± 7†	25 ± 12

ACh, acetylcholine; Ang, angiotensin; DM, diabetes mellitus; ET-1, endothelin type 1; HRP, handle region peptide; PE, phenylephrine; SNAP, S-nitroso-N-penicillamine.
$^{*}P < 0.05$ *vs.* SD.
$^{\Delta}P < 0.01$ vs. non-DM.
$^{\#}P < 0.05$ vs. non-DM.
$^{†}P < 0.05$ vs. vehicle.
$^{‡}P < 0.01$ vs. no inhibitor.
$^{\$}P < 0.05$ *vs.* no inhibitor.
$^{+}P = 0.06$ vs. no inhibitor.

Mesenteric artery

ET-1 constricted mesenteric arteries in Sprague–Dawley rats to maximally 244 ± 37% (Fig. 4, Table 1). The ET-1 E_{max} was greatly diminished in nondiabetic Ren2 rats ($P < 0.05$), although its potency was unchanged. The induction of diabetes mellitus diminished the potency of ET-1 in Ren2 rats, without affecting its E_{max}. Aliskiren increased the latter to Sprague–Dawley values, and HRP prevented this. The ET_A receptor antagonist BQ123 (1 μmol/l), but not the ET_B receptor antagonist BQ788, shifted the ET-1 CRC in Sprague–Dawley rats and nondiabetic Ren2 rats four-fold to five-fold to the right ($P < 0.05$), and the effect of BQ123 (1 μmol/l) + BQ788 was identical to that of BQ123 alone (data not shown). Remarkably, following the induction of diabetes mellitus, the effect of 1 μmol/l BQ123 disappeared, and returned only by increasing its concentration 10-fold. Aliskiren alone did not alter the effect of diabetes mellitus, whereas the addition of HRP allowed the return of the blocking effect of 1 μmol/l BQ123 ($P < 0.01$ vs. no BQ123). With HRP, 10 μmol/l BQ123 fully blocked the effect of ET-1. These data indicate a diminished sensitivity of ET_A receptors to BQ123 in diabetes mellitus, which is restored to normal by HRP but not aliskiren.

SNAP relaxed preconstricted mesenteric arteries of Sprague–Dawley and nondiabetic Ren2 rats to the same degree (Fig. 5 and Table 1). Diabetes mellitus induction shifted the SNAP CRC ≈10-fold to the right ($P < 0.05$) and reduced E_{max} ($P < 0.05$). Treatment did not alter this.

ACh fully relaxed preconstricted mesenteric arteries of Sprague–Dawley rats, and L-NAME combined with TRAM34 (IK_{Ca} inhibitor) + apamin (SK_{Ca} inhibitor), but not L-NAME alone or TRAM34 + apamin alone, blocked this effect (Fig. 5, Table 1). ACh also fully relaxed mesenteric arteries of nondiabetic Ren2 rats. L-NAME, with or without TRAM34 + apamin (but not TRAM34 + apamin alone), partially prevented this effect ($P < 0.05$). ACh identically relaxed mesenteric arteries of diabetic Ren2 rats. However, L-NAME now not only reduced its E_{max}, but also diminished its potency ($P < 0.05$ for both). Moreover, the combined application of L-NAME and TRAM34 + apamin uncovered a constrictor action of ACh ($P < 0.01$ vs. nondiabetic Ren2 rat). Aliskiren annihilated these diabetes mellitus-induced alterations, whereas HRP reversed this effect of aliskiren.

To further investigate the contractile effect induced by ACh in the presence of L-NAME and TRAM34 + apamin, CRCs to ACh were constructed in preconstricted mesenteric arteries of a second set of untreated diabetic Ren2 rats. COX

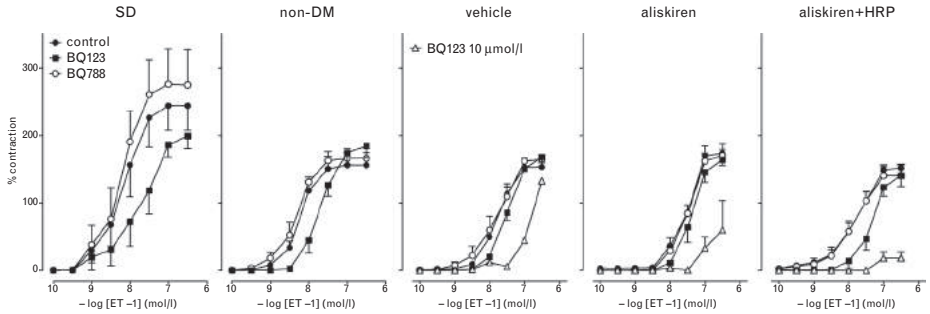

FIGURE 4 Contractions of mesenteric arteries, obtained from Sprague–Dawley rats, nondiabetic Ren2 rats, and diabetic Ren2 rats treated for 3 weeks with vehicle, aliskiren or aliskiren+HRP, to endothelin-1 in the absence or presence of BQ123 (1 μmol/l, closed squares, or 10 μmol/l, open triangles) or 10 nmol/l BQ788. Contractions (mean ± SEM, $n = 5–8$) have been expressed as a percentage of the response to 100 mmol/l K^+. Please note that the 10 μmol/l BQ123 data in the middle panel represent 1 experiment. See Table for statistical information. DM, diabetes mellitus.

inhibition with the nonselective COX inhibitor indomethacin or the COX-2-selective inhibitor NS398, as well as endothelium removal, but not the thromboxane/endoperoxide receptor antagonist GR32191B or the superoxide scavenger tempol, prevented this effect (Fig. 6).

Vascular cyclo-oxygenase 2 and endothelin type A receptor expression

Since the vascular reactivity studies revealed potential changes in COX-2 and ET_A receptor reactivity, we quantified the vascular COX-2 and ET_A receptor expression. These studies were performed in aortic tissue since

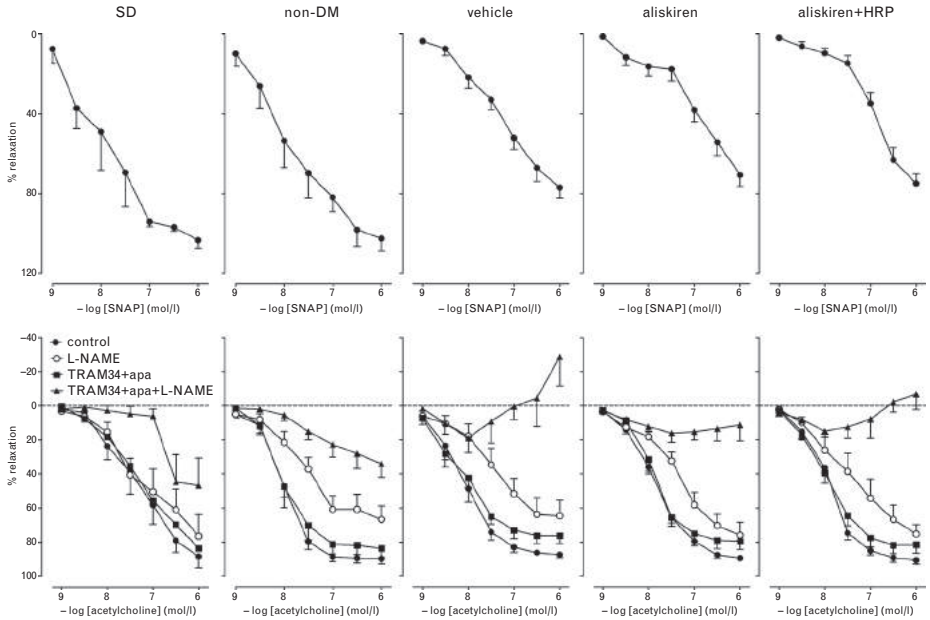

FIGURE 5 Relaxations/constrictions of mesenteric arteries, obtained from Sprague–Dawley rats, nondiabetic Ren2 rats, and diabetic Ren2 rats treated for 3 weeks with vehicle, aliskiren or aliskiren+HRP, to S-nitroso-N-penicillamine (SNAP) or acetylcholine in the absence or presence of 100 μmol/l L-NAME, 10 μmol/l TRAM34 + 100 nmol/l apamin, or L-NAME + TRAM34 + apamin. Effects (mean ± SEM, $n = 4–8$) have been expressed as a percentage of the response to U46619 (0.1–0.3 μmol/l). See Table for statistical information. DM, diabetes mellitus.

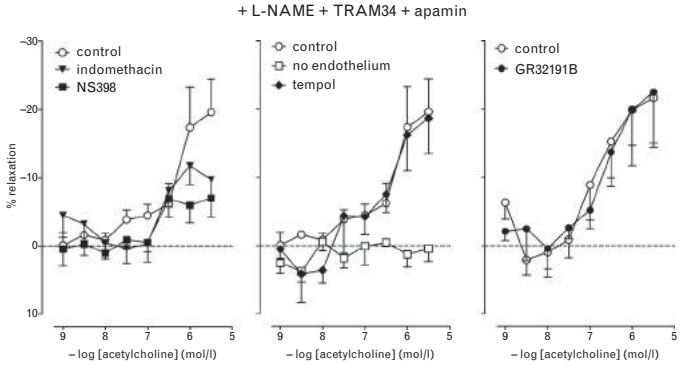

FIGURE 6 Constrictions of mesenteric arteries, obtained from diabetic Ren2 rats, to acetylcholine in the presence of 100 μmol/l L-NAME + 10 μmol/l TRAM34 + 100 nmol/l apamin with or without 10 μmol/l indomethacin, 10 μmol/l NS398, 1 mmol/l tempol, 1 μmol/l GR32191B or after removal of the endothelium (no endothelium). Effects (mean ± SEM, $n = 6$) have been expressed as a percentage of the response to U46619 (0.1–0.3 μmol/l) or phenylephrine (1 μmol/l in the case of GR32191B). See Table for statistical information.

insufficient mesenteric arterial material was left for such measurements after performing the above organ bath studies. Aortic ET_A receptor mRNA expression was decreased in nondiabetic Ren2 rats compared with Sprague–Dawley rats. Induction of diabetes mellitus increased ET_A receptor mRNA expression, and this was prevented ($P < 0.05$) by aliskiren + HRP only (Fig. 7). Aortic COX-2 mRNA expression was unaltered in nondiabetic rats vs. Sprague–Dawley rats, and was also unaffected by the induction of diabetes mellitus. Neither aliskiren nor aliskiren + HRP altered the aortic COX-2 mRNA expression.

DISCUSSION

This study shows that HRP unexpectedly counteracted the beneficial vascular effects of aliskiren in diabetic Ren2 rats in a blood pressure-independent manner. Ren2 rats did not display a greatly altered vascular responsiveness vs. Sprague–Dawley rats, in full agreement with previous studies [37,38]: Ang II and phenylephrine responses were identical in both strains, and ET-1 displayed a reduced efficacy in Ren2 rats. Furthermore, ACh-induced, endothelium-dependent responses, as well as the direct vascular smooth muscle cell responsiveness to NO were fully intact in Ren2 rats. Yet, their sensitivity to NOS inhibition was increased, as evidenced by the large rightward shift of the ACh CRC in the presence of L-NAME. This rightward shift was also present in diabetic animals. Moreover, following the induction of diabetes, L-NAME increased contractility per se, suggesting an enhanced baseline NO exposure in diabetic animals, for example, due to eNOS upregulation [39]. Indeed, in accordance with such NO upregulation, the potency of the NO donor SNAP diminished ≈10-fold in diabetic animals, confirming that the continuous exposure to elevated NO levels had decreased the sensitivity of the soluble guanylyl cyclase-cGMP pathway to NO [40,41]. Moreover, the phenylephrine response decreased by one third, returning to its prediabetic E_{max} only in the presence

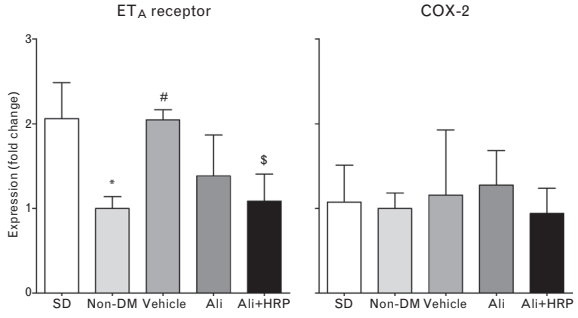

FIGURE 7 ET_A receptor and COX-2 mRNA expression in aortic segments obtained from Sprague–Dawley rats, nondiabetic Ren2 rats, and diabetic Ren2 rats treated for 3 weeks with vehicle, aliskiren or aliskiren+HRP. Data (mean ± SEM, $n = 4–8$) are expressed as fold change compared to nondiabetic rats (geometric mean = 1). $* P < 0.05$ vs. Sprague–Dawley, $\# P < 0.05$ vs. nondiabetic Ren2 rat, $^{\$}P < 0.05$ vs. vehicle. DM, diabetes mellitus.

of L-NAME. The latter emphasizes the possibility that high endogenous NO levels in diabetic rats counteracted the constrictor effects of phenylephrine.

In addition to NO, diabetes also upregulated endothelium-derived contractile factor(s) (EDCFs) and vascular ET_A receptor expression in Ren2 rats. As a consequence, ACh induced vasoconstriction during combined blockade of the NO and endothelium-derived hyperpolarizing factor pathways, and 10-fold higher BQ123 concentrations were required to block ET-1-induced constriction. To what degree the upregulation of the constrictor pathways are the consequence of the NO upregulation, or vice versa, cannot be concluded from our data. COX-2 inhibition, as well as nonselective COX inhibition, prevented the ACh-induced vasoconstriction. Yet, we did not observe a significant increase in vascular COX-2 mRNA expression following the induction of diabetes when studying the aorta. This does not exclude that increased COX-2 protein levels contributed to EDCF production in mesenteric arteries, but rather suggests that the increased EDCF synthesis may also involve the upregulation of one or more of the enzymes that metabolise the COX-2 product prostaglandin H_2 (PGH_2), for example thromboxane synthase, prostacyclin synthase, prostaglandin D synthase, prostaglandin E_2 synthase or prostaglandin F_2 synthase. Our data with the thromboxane/endoperoxide receptor antagonist GR32191B exclude a role for thromboxane A_2, and raise the possibility that either PGH_2 itself, and/or its metabolites PGI_2, PGD_2, PGE_2 and $PGF_{2\alpha}$ acted as COX-derived EDCF(s) [42]. Altered COX metabolism has been noted before in diabetes [43], as have ET-1 and ET_A receptor abundance [44,45]. The latter are believed to be the consequence of increased reactive oxygen species (ROS) generation and protein kinase C activation in diabetes [46,47]. Increased ROS were not responsible for the acute ACh-induced vasoconstrictor effects in the present study, as these effects could not be prevented by the ROS scavenger tempol.

Aliskiren normalized most diabetes-induced vascular alterations: it annihilated the upregulated effect of L-NAME on baseline contractility, and normalized the phenylephrine and ACh responses. After aliskiren, ACh no longer caused constriction. Aliskiren did not alter the diminished SNAP responsiveness, possibly because a 3-week treatment period is not long enough to reverse the consequences of increased NO exposure. It also did not affect the absent ET_A receptor blocker response, and at most showed a tendency to downregulate the increased vascular ET_A receptor expression.

Remarkably, and contrary to our expectation, HRP on top of renin inhibition, reversed the above effects of aliskiren. In addition, it fully normalized the ET-1 responsiveness, that is, it allowed the return of the BQ123-dependent rightward shift, which was observed only in the nondiabetic state (Fig. 4). Since HRP did not significantly affect the blood pressure-lowering effects of aliskiren, it can be concluded that the vascular reactivity alterations in the present study were not the consequence of changes in blood pressure. Rather, they represent the interference of aliskiren with local, vascular Ang II generation. Similar observations have been made before in the coronary vascular bed of the spontaneously hypertensive rat [21,33], and in the forearm vascular bed of hypertensive patients [48].

The lack of effect of HRP on blood pressure is in agreement with previous studies [6,18,21,49], and seems to suggest that the (P)RR does not contribute to the generation of Ang II that determines blood pressure, but at most to the generation of Ang II that determines blood pressure-independent effects, for example at tissue sites. Indeed, HRP counteracted retinopathy and nephropathy in diabetic rodents [6,9,50], and suppressed fibrosis in the hypertensive rat heart [51]. As its beneficial effects in diabetes were also observed in animals lacking the most important angiotensin receptor (i.e., the AT_{1a} receptor) [7], they may even represent blockade of the direct (angiotensin-independent) effects of prorenin–(P)RR interaction. In support of an angiotensin-independent effect of HRP, our current data show no interference of HRP with the aliskiren-induced suppression of PRA. Similarly, in a previous study in spontaneously hypertensive rats, HRP did not affect the aliskiren-induced changes in angiotensin levels [21].

Yet, whether prorenin–(P)RR interaction truly occurs *in vivo*, given the nanomolar affinity of the receptor for prorenin (which occurs in blood at picomolar levels) [11,22], is still a matter of debate. We have chosen the Ren2 rat because of its high endogenous prorenin levels, which are further elevated (up to 55-fold vs. Sprague–Dawley rats) following the induction of diabetes (Fig. 2). Nevertheless, even under those conditions, no beneficial add-on effect of HRP was observed. Importantly, recent studies in (P)RR knockout animals point to the possibility that the (P)RR may exert functions that are entirely unrelated to the RAS. For instance, cardiomyocyte-specific (P)RR knockout in mice results in the development of heart failure due to defective autophagy and ultimately cell death [52]. Moreover, the (P)RR functions as an adaptor between vacuolar H^+-ATPase and receptors for members of the Wnt family of signaling molecules [53]. In addition, (P)RR overexpressing rats display increased COX-2 levels, and COX-2 overexpression in podocytes exacerbates diabetic nephropathy by increasing (P)RR expression [15]. Thus, a positive feedback loop appears to exist between the (P)RR and COX-2 [16]. Interference of HRP with this feedback loop (instead of blocking direct prorenin–(P)RR interaction) may underlie its upregulation of the EDCF pathway. In fact, its role as a (P)RR antagonist in general might be sufficient to explain some of the controversial, RAS-independent observations made on this drug [12,18–21]. To address this possibility, additional studies are required investigating the effects of HRP alone.

In conclusion, renin inhibition normalizes vascular dysfunction in diabetic hypertensive rats, and (P)RR blockade counteracts this effect independently of blood pressure and angiotensin. Although (P)RR blockade did reduce vascular ET_A receptor expression, its antagonizing effects towards renin inhibition do not warrant its application as add-on drug on top of RAS blockade.

ACKNOWLEDGEMENTS

This study was supported by the Dutch Kidney Foundation (grant nr. C08.2246).

Conflicts of interest

There are no conflicts of interest.

REFERENCES

1. Parving HH, Lehnert H, Brochner-Mortensen J, Gomis R, Andersen S, Arner P. The effect of irbesartan on the development of diabetic nephropathy in patients with type 2 diabetes. *N Engl J Med* 2001; 345:870–878.
2. Parving HH, Persson F, Lewis JB, Lewis EJ, Hollenberg NK. Aliskiren combined with losartan in type 2 diabetes and nephropathy. *N Engl J Med* 2008; 358:2433–2446.
3. Hollenberg NK, Fisher NDL, Nussberger J, Moukarbel GV, Barkoudah E, Danser AHJ. Renal responses to three types of renin-angiotensin system blockers in patients with diabetes mellitus on a high-salt diet: a need for higher doses in diabetic patients? *J Hypertens* 2011; 29:2454–2461.
4. Deinum J, Ronn B, Mathiesen E, Derkx FHM, Hop WC, Schalekamp MADH. Increase in serum prorenin precedes onset of microalbuminuria in patients with insulin-dependent diabetes mellitus. *Diabetologia* 1999; 42:1006–1010.
5. Luetscher JA, Kraemer FB, Wilson DM, Schwartz HC, Bryer-Ash M. Increased plasma inactive renin in diabetes mellitus. A marker of microvascular complications. *N Engl J Med* 1985; 312:1412–1417.
6. Ichihara A, Hayashi M, Kaneshiro Y, Suzuki F, Nakagawa T, Tada Y, *et al*. Inhibition of diabetic nephropathy by a decoy peptide corresponding to the 'handle' region for nonproteolytic activation of prorenin. *J Clin Invest* 2004; 114:1128–1135.
7. Ichihara A, Suzuki F, Nakagawa T, Kaneshiro Y, Takemitsu T, Sakoda M, *et al*. Prorenin receptor blockade inhibits development of glomerulosclerosis in diabetic angiotensin II type 1a receptor-deficient mice. *J Am Soc Nephrol* 2006; 17:1950–1961.
8. Wilkinson-Berka JL, Heine R, Tan G, Cooper ME, Hatzopoulos KM, Fletcher EL, *et al*. RILLKKMPSV influences the vasculature, neurons and glia, and (pro)renin receptor expression in the retina. *Hypertension* 2010; 55:1454–1460.
9. Satofuka S, Ichihara A, Nagai N, Noda K, Ozawa Y, Fukamizu A, *et al*. (Pro)renin receptor-mediated signal transduction and tissue renin-angiotensin system contribute to diabetes-induced retinal inflammation. *Diabetes* 2009; 58:1625–1633.
10. Nguyen G, Delarue F, Burcklé C, Bouzhir L, Giller T, Sraer JD. Pivotal role of the renin/prorenin receptor in angiotensin II production and cellular responses to renin. *J Clin Invest* 2002; 109:1417–1427.
11. Batenburg WW, Krop M, Garrelds IM, de Vries R, de Bruin RJA, Burcklé CA, *et al*. Prorenin is the endogenous agonist of the (pro)renin receptor. Binding kinetics of renin and prorenin in rat vascular smooth muscle cells overexpressing the human (pro)renin receptor. *J Hypertens* 2007; 25:2441–2453.
12. Batenburg WW, Lu X, Leijten F, Maschke U, Müller DN, Danser AHJ. Renin- and prorenin-induced effects in rat vascular smooth muscle cells overexpressing the human (pro)renin receptor: does (pro)renin-(pro)renin receptor interaction actually occur? *Hypertension* 2011; 58:1111–1119.
13. Huang Y, Noble NA, Zhang J, Xu C, Border WA. Renin-stimulated TGF-beta1 expression is regulated by a mitogen-activated protein kinase in mesangial cells. *Kidney Int* 2007; 72:45–52.
14. Kaneshiro Y, Ichihara A, Takemitsu T, Sakoda M, Suzuki F, Nakagawa T, *et al*. Increased expression of cyclooxygenase-2 in the renal cortex of human prorenin receptor gene-transgenic rats. *Kidney Int* 2006; 70:641–646.
15. Cheng H, Fan X, Moeckel GW, Harris RC. Podocyte COX-2 exacerbates diabetic nephropathy by increasing podocyte (pro)renin receptor expression. *J Am Soc Nephrol* 2011; 22:1240–1251.
16. Huang J, Siragy HM. Glucose promotes the production of interleukine-1beta and cyclooxygenase-2 in mesangial cells via enhanced (pro)renin receptor expression. *Endocrinology* 2009; 150:5557–5565.
17. Batenburg WW, Danser AHJ. (Pro)renin and its receptors: pathophysiological implications. *Clin Sci (Lond)* 2012; 123:121–133.
18. Müller DN, Klanke B, Feldt S, Cordasic N, Hartner A, Schmieder RE, *et al*. (Pro)renin receptor peptide inhibitor 'handle-region' peptide does not affect hypertensive nephrosclerosis in Goldblatt rats. *Hypertension* 2008; 51:676–681.
19. Krebs C, Hamming I, Sadaghiani S, Steinmetz OM, Meyer-Schwesinger C, Fehr S, *et al*. Antihypertensive therapy upregulates renin and (pro)renin receptor in the clipped kidney of Goldblatt hypertensive rats. *Kidney Int* 2007; 72:725–730.
20. Feldt S, Batenburg WW, Mazak I, Maschke U, Wellner M, Kvakan H, *et al*. Prorenin and renin-induced extracellular signal-regulated kinase 1/2 activation in monocytes is not blocked by aliskiren or the handle-region peptide. *Hypertension* 2008; 51:682–688.
21. van Esch JHM, van Veghel R, Garrelds IM, Leijten F, Bouhuizen AM, Danser AHJ. Handle region peptide counteracts the beneficial effects of the renin inhibitor aliskiren in spontaneously hypertensive rats. *Hypertension* 2011; 57:852–858.
22. Nabi AH, Kageshima A, Uddin MN, Nakagawa T, Park EY, Suzuki F. Binding properties of rat prorenin and renin to the recombinant rat renin/prorenin receptor prepared by a baculovirus expression system. *Int J Mol Med* 2006; 18:483–488.
23. Campbell DJ, Rong P, Kladis A, Rees B, Ganten D, Skinner SL. Angiotensin and bradykinin peptides in the TGR(mRen-2)27 rat. *Hypertension* 1995; 25:1014–1020.
24. Feldman DL, Jin L, Xuan H, Contrepas A, Zhou Y, Webb RL, *et al*. Effects of aliskiren on blood pressure, albuminuria, and (pro)renin receptor expression in diabetic TG(mRen-2)27 rats. *Hypertension* 2008; 52:130–136.
25. Connelly KA, Advani A, Kim S, Advani SL, Zhang M, White KE, *et al*. The cardiac (pro)renin receptor is primarily expressed in myocyte transverse tubules and is increased in experimental diabetic cardiomyopathy. *J Hypertens* 2011; 29:1175–1184.
26. Lee MA, Bohm M, Paul M, Bader M, Ganten U, Ganten D. Physiological characterization of the hypertensive transgenic rat TGR(mREN2)27. *Am J Physiol* 1996; 270:E919–E929.
27. Moravski CJ, Skinner SL, Stubbs AJ, Sarlos S, Kelly DJ, Cooper ME, *et al*. The renin-angiotensin system influences ocular endothelial cell proliferation in diabetes: transgenic and interventional studies. *Am J Pathol* 2003; 162:151–160.
28. Kelly DJ, Wilkinson-Berka JL, Allen TJ, Cooper ME, Skinner SL. A new model of diabetic nephropathy with progressive renal impairment in the transgenic (mRen-2)27 rat (TGR). *Kidney Int* 1998; 54:343–352.
29. Makino A, Ohuchi K, Kamata K. Mechanisms underlying the attenuation of endothelium-dependent vasodilatation in the mesenteric arterial bed of the streptozotocin-induced diabetic rat. *Br J Pharmacol* 2000; 130:549–556.
30. Dunn WR, Gardiner SM. Differential alteration in vascular structure of resistance arteries isolated from the cerebral and mesenteric vascular beds of transgenic [(mRen-2)27], hypertensive rats. *Hypertension* 1997; 29:1140–1147.
31. Kelly DJ, Zhang Y, Moe G, Naik G, Gilbert RE. Aliskiren, a novel renin inhibitor, is renoprotective in a model of advanced diabetic nephropathy in rats. *Diabetologia* 2007; 50:2398–2404.
32. van den Heuvel M, Sorop O, Koopmans SJ, Dekker R, de Vries R, van Beusekom HMM, *et al*. Coronary microvascular dysfunction in a porcine model of early atherosclerosis and diabetes. *Am J Physiol Heart Circ Physiol* 2012; 302:H85–H99.
33. van Esch JHM, Moltzer E, van Veghel R, Garrelds IM, Leijten F, Bouhuizen AM, *et al*. Beneficial cardiac effects of the renin inhibitor aliskiren in spontaneously hypertensive rats. *J Hypertens* 2010; 28:2145–2155.
34. Mulvany MJ, Halpern W. Contractile properties of small arterial resistance vessels in spontaneously hypertensive and normotensive rats. *Circ Res* 1977; 41:19–26.
35. de Lannoy LM, Danser AHJ, van Kats JP, Schoemaker RG, Saxena PR, Schalekamp MADH. Renin-angiotensin system components in the interstitial fluid of the isolated perfused rat heart. Local production of angiotensin I. *Hypertension* 1997; 29:1240–1251.
36. MaassenVanDenBrink A, de Vries R, Saxena PR, Schalekamp MADH, Danser AHJ. Vasoconstriction by in situ formed angiotensin II: role of ACE and chymase. *Cardiovasc Res* 1999; 44:407–415.
37. Randall MD, March JE. Characterization of endothelium-dependent relaxations in mesenteries from transgenic hypertensive rats. *Eur J Pharmacol* 1998; 358:31–40.
38. Tschudi MR, Noll G, Arnet U, Novosel D, Ganten D, Lüscher TF. Alterations in coronary artery vascular reactivity of hypertensive Ren-2 transgenic rats. *Circulation* 1994; 89:2780–2786.
39. Taguchi K, Matsumoto T, Kamata K, Kobayashi T. Angiotensin II type 2 receptor-dependent increase in nitric oxide synthase activity in the endothelium of db/db mice is mediated via a MEK pathway. *Pharmacol Res* 2012; 66:41–50.

40. Botden IP, Langendonk JG, Meima ME, Boomsma F, Seynhaeve ALB, ten Hagen TLM, *et al*. Daily red wine consumption improves vascular function by a soluble guanylyl cyclase-dependent pathway. *Am J Hypertens* 2011; 24:162–168.
41. Davis JP, Vo XT, Sulakhe PV. Altered responsiveness of guanylyl cyclase to nitric oxide following treatment of cardiomyocytes with S-nitroso-D,L-acetylpenicillamine and sodium nitroprusside. *Biochem Biophys Res Commun* 1997; 238:351–356.
42. Félétou M, Huang Y, Vanhoutte PM. Endothelium-mediated control of vascular tone: COX-1 and COX-2 products. *Br J Pharmacol* 2011; 164:894–912.
43. Vennemann A, Gerstner A, Kern N, Ferreiros Bouzas N, Narumiya S, Maruyama T, *et al*. PTGS-2-PTGER2/4 signaling pathway partially protects from diabetogenic toxicity of streptozotocin in mice. *Diabetes* 2012; 61:1879–1887.
44. Zanatta CM, Veronese FV, Loreto Mda S, Sortica DA, Carpio VN, Eldeweiss MI, *et al*. Endothelin-1 and endothelin a receptor immunoreactivity is increased in patients with diabetic nephropathy. *Ren Fail* 2012; 34:308–315.
45. Minchenko AG, Stevens MJ, White L, Abatan OI, Komjati K, Pacher P, *et al*. Diabetes-induced overexpression of endothelin-1 and endothelin receptors in the rat renal cortex is mediated via poly(ADP-ribose) polymerase activation. *FASEB J* 2003; 17:1514–1516.
46. Chen HC, Guh JY, Shin SJ, Tsai JH, Lai YH. Reactive oxygen species enhances endothelin-1 production of diabetic rat glomeruli in vitro and in vivo. *J Lab Clin Med* 2000; 135:309–315.
47. Park JY, Takahara N, Gabriele A, Chou E, Naruse K, Suzuma K, *et al*. Induction of endothelin-1 expression by glucose: an effect of protein kinase C activation. *Diabetes* 2000; 49:1239–1248.
48. Virdis A, Ghiadoni L, Qasem AA, Lorenzini G, Duranti E, Cartoni G, *et al*. Effect of aliskiren treatment on endothelium-dependent vasodilation and aortic stiffness in essential hypertensive patients. *Eur Heart J* 2012; 33:1530–1538.
49. Seki Y, Ichihara A, Mizuguchi Y, Sakoda M, Kurauchi-Mito A, Narita T, *et al*. Add-on blockade of (pro)renin receptor in imidapril-treated diabetic SHRsp. *Front Biosci (Elite Ed)* 2010; 2:972–979.
50. Kaneshiro Y, Ichihara A, Sakoda M, Takemitsu T, Nabi AH, Uddin MN, *et al*. Slowly progressive, angiotensin II-independent glomerulosclerosis in human (Pro)renin receptor-transgenic rats. *J Am Soc Nephrol* 2007; 18:1789–1795.
51. Ichihara A, Kaneshiro Y, Takemitsu T, Sakoda M, Suzuki F, Nakagawa T, *et al*. Nonproteolytic activation of prorenin contributes to development of cardiac fibrosis in genetic hypertension. *Hypertension* 2006; 47:894–900.
52. Kinouchi K, Ichihara A, Sano M, Sun-Wada GH, Wada Y, Kurauchi-Mito A, *et al*. The (pro)renin receptor/ATP6AP2 is essential for vacuolar H+-ATPase assembly in murine cardiomyocytes. *Circ Res* 2010; 107:30–34.
53. Cruciat CM, Ohkawara B, Acebron SP, Karaulanov E, Reinhard C, Ingelfinger D, *et al*. Requirement of prorenin receptor and vacuolar H+-ATPase-mediated acidification for Wnt signaling. *Science* 2010; 327:459–463.

Deterioration of kidney function by the (pro) renin receptor blocker handle region peptide in aliskiren-treated diabetic transgenic (mRen2)27 rats

te Riet L., van den Heuvel M., Peutz-Kootstra C.J., van Esch J.H., van Veghel R., Garrelds I.M., Musterd-Bhaggoe U., Bouhuizen A.M., Leijten F.P., Danser A.H. and Batenburg W.W.

Am J. Physiol Renal Physiol. 2014 May 15;306(10)

17

Deterioration of kidney function by the (pro)renin receptor blocker handle region peptide in aliskiren-treated diabetic transgenic (mRen2)27 rats

Luuk te Riet[1], Mieke van den Heuvel[1], Carine J. Peutz-Kootstra[2], Joep H.M. van Esch[1], Richard van Veghel[1], Ingrid M. Garrelds[1], Usha Musterd-Bhaggoe[1], Angelique M. Bouhuizen[1], Frank P.J. Leijten[1], A.H. Jan Danser[1], Wendy W. Batenburg[1]

[1] Division of Pharmacology and Vascular Medicine, Department of Internal Medicine, Erasmus MC, Rotterdam, The Netherlands; [2] Department of Pathology, Maastricht University Medical Center, Maastricht, The Netherlands

Submitted 7 January 2014; accepted in final form 25 March 2014

te Riet L, van den Heuvel M, Peutz-Kootstra CJ, van Esch JH, van Veghel R, Garrelds IM, Musterd-Bhaggoe U, Bouhuizen AM, Leijten FP, Danser AH, Batenburg WW. Deterioration of kidney function by the (pro)renin receptor blocker handle region peptide in aliskiren-treated diabetic transgenic (mRen2)27 rats. *Am J Physiol Renal Physiol* 306: F1179–F1189, 2014. First published April 2, 2014; doi:10.1152/ajprenal.00010.2014.—Dual renin-angiotensin system (RAS) blockade in diabetic nephropathy is no longer feasible because of the profit/side effect imbalance. (Pro)renin receptor [(P)RR] blockade with handle region peptide (HRP) has been reported to exert beneficial effects in various diabetic models in a RAS-independent manner. To what degree (P)RR blockade adds benefits on top of RAS blockade is still unknown. In the present study, we treated diabetic TGR(mREN2)27 rats, a well-established nephropathy model with high prorenin levels [allowing continuous (P)RR stimulation in vivo], with HRP on top of renin inhibition with aliskiren. Aliskiren alone lowered blood pressure and exerted renoprotective effects, as evidenced by reduced glomerulosclerosis, diuresis, proteinuria, albuminuria, and urinary aldosterone levels as well as diminished renal (P)RR and ANG II type 1 receptor expression. It also suppressed plasma and tissue RAS activity and suppressed cardiac atrial natriuretic peptide and brain natriuretic peptide expression. HRP, when given on top of aliskiren, did not alter the effects of renin inhibition on blood pressure, RAS activity, or aldosterone. However, it counteracted the beneficial effects of aliskiren in the kidney, induced hyperkalemia, and increased plasma plasminogen activator-inhibitor 1, renal cyclooxygenase-2, and cardiac collagen content. All these effects have been linked to (P)RR stimulation, suggesting that HRP might, in fact, act as a partial agonist. Therefore, the use of HRP on top of RAS blockade in diabetic nephropathy is not advisable.

prorenin; diabetes; renin inhibition; (pro)renin receptor blockade; kidney

HYPERTENSIVE PATIENTS WITH DIABETES exhibit an increased risk for cardiovascular complications such as nephropathy, stroke, and heart failure. The renin-angiotensin system (RAS) is believed to modulate the underlying structural and functional changes in the kidney and heart (29, 33), thereby explaining the beneficial effects of RAS blockers in this condition. Elevated levels of prorenin, the precursor of renin, are an early indicator of nephropathy in diabetes (9, 32). Prorenin has been speculated to contribute to ANG generation in the kidney via binding to the so-called (pro)renin receptor [(P)RR]. Indeed, (P)RR-bound prorenin displays ANG I-generating activity (1, 37). However, it also stimulates (P)RR-mediated signal transduction in an ANG-independent manner, resulting in the activation of ERK1/2, cyclooxygenase (COX)-2, and fibrotic pathways (2, 37). The latter includes enhanced transforming growth factor (TGF)-β_1 synthesis, plasminogen activator inhibitor (PAI)-1 release, and the upregulation of fibronectin and collagens (2, 18, 19, 37). In agreement with this concept, ubiquitous expression of the human (P)RR in rats leads to proteinuria, glomerulosclerosis, and nephropathy, which could be reversed by the putative (P)RR blocker handle region peptide (HRP) (25). Beneficial renal effects of HRP were also observed in ANG II type 1a receptor ($AT_{1a}R$)-deficient mice, suggesting that they are not solely due to interference with the RAS. However, the capacity of HRP to block (P)RR is controversial (34), and recent studies (28, 38, 40) in knockout animals have suggested that (P)RR deletion in cardiomyocytes or podocytes is actually lethal. Thus, a relevant question is to what degree HRP should still be used, e.g., on top of RAS blockade in diabetic patients with nephropathy and heart failure. This is of particular importance now that the combination of two or more RAS blockers is no longer advocated in diabetic patients, since the side effect profile (hypotension and hyperkalemia) of this approach outweighs the beneficial effects (7, 39).

In the present study, we therefore set out to study the effects of HRP on top of renin inhibition (with aliskiren) in a well-established high-prorenin model, the TGR(mRen2)27 (Ren2) rat, which overexpresses the mouse Ren2 gene (36) and also displays elevated (P)RR levels (5). Aliskiren is renoprotective in this model, and its effects are comparable with those observed during AT_1R blockade or ANG-converting enzyme inhibition, despite the nonequivalent blood pressure-lowering effects of these three types of RAS blockers (27, 45). Cardioprotective effects of aliskiren have also been observed in diabetic rodents (10, 47).

Rats were made diabetic with streptozotocin (STZ) and treated for 3 wk with aliskiren and/or HRP. We used a dose of HRP that has been applied before in several rodent studies (12, 22, 23, 25). We reasoned that, if anywhere, the beneficial effects of this putative (P)RR blocker on the kidney and heart should be observed in this high-prorenin, high-(P)RR model.

METHODS

Animal Experiments

Homozygous Ren2 rats (400–500 g, a kind gift from Dr. M. Bader, Berlin, Germany) were crossed with Sprague-Dawley rats (Harlan, Boxmeer, The Netherlands) to generate heterozygous Ren2 rats. Heterozygous rats were subsequently used in all experiments, since

Address for reprint requests and other correspondence: W. W. Batenburg, Div. of Pharmacology and Vascular Medicine, Dept. of Internal Medicine, Erasmus MC, Rm. EE1402b, Dr. Molewaterplein 50, Rotterdam 3015 GE, The Netherlands (e-mail: w.batenburg@erasmusmc.nl).

Table 1. *Real-time RT-PCR primers*

Gene	Forward Primer	Reverse Primer
HPRT-1	5′-TGGACAGGACTGAAAGACTTGCTCG-3′	5′-CTTCAGCACACAGAGGGCCACA-3′
β-Actin	5′-AGCCATGTACGTAGCCATCCA-3′	5′-TCTCCGGAGTCCATCACAATG-3′
β_2-Microglobulin	5′-ATGGCTCGCTCGGTGACCG-3′	5′-TGGGGAGTTTTCTGAATGGCAAGCA-3′
Rat renin	5′-CGGGAGGAGGATGCCTCTCTGG-3′	5′-CAAGATTCGTCCAAAGCTGGCTGT-3′
Collagen-1	5′-TCTGGCGCAAGAGGCGAGAGA-3′	5′-GTTGCCGGGGGCACCATTGT-3′
TGF-β_1	5′-AGTGGCTGAACCAAGGAGACGGA-3′	5′-TGCCCAGGTCACCTCGACGT-3′
(P)RR	5′-TGAAGGAAGACCTGTCTTGGCCAGG-3′	5′-ATAATGGTAGCCCGGGGCCGG-3′
AT_1R	5′-ACTGCCTGAACCCTCTGTTC-3′	5′-TCGTAGACAGGCTTGAGTGG-3′
COX-2	5′-ATTGCTGGCCGGGTTGCTGG-3′	5′-TCAATGGAGGCCTTTGCCACTGC-3′
TNF-α	5′-GACCCTCACACTCAGATCATCTTCT-3′	5′-TGCTACGACGTGGGCTACG-3′
NF-κB	5′-TCTGATTGGCCAGAGGCTCCC-3′	5′-GGGCGTGGCCATAGTTCAAGGG-3′
ANP	5′-ATGGGCTCCTTCTCCATCAC-3′	5′-TCTACCGGCATCTTCTCCTC-3′
BNP	5′-ACAATCCACGATGCAGAAGCT-3′	5′-GGGCCTTGGTCCTTTGAGA-3′
β-MHC	5′-ATGGACCTGGAGCGAGCAAA-3′	5′-GTCCTTCTTTTTGAGTCGCTCATCC-3′
Ngal	5′-GGGCTGTCCGATGAACTGAA-3′	5′-CATTGGTCGGTGGGAACAGA-3′

HPRT-1, hypoxanthine phosphoribosyltransferase 1; TGF-β_1, transforming growth factor-β_1; (P)RR, (pro)renin receptor; AT_1R, angiotensin II type 1 receptor; COX-2, cyclooxygenase 2; ANP, atrial natriuretic peptide; BNP, brain natriuretic peptide; β-MHC, β-myosin heavy chain; Ngal, neutrophil gelatinase-associated lipocalin.

these rats, in contrast to homozygous Ren2 rats, did not require lisinopril treatment (10 μg/ml in drinking water) to decrease mortality. All experiments were performed under the regulation and permission of the Animal Care Committee of the Erasmus MC. Rats were housed in individual cages and maintained on a 12:12-h light-dark cycle with access to standard laboratory rat chow and water ad libitum. Radiotelemetry transmitters were implanted as previously described (42) for continuous measurements of heart rate, blood pressure, and activity. Two weeks later, to induce diabetes mellitus (DM), rats were fasted overnight and administered STZ (1 injection of 55 mg/kg STZ ip, Sigma-Aldrich, Zwijndrecht, The Netherlands). Rats were checked for nonfasting blood glucose and β-ketone levels by tail incision daily during the first 3 days after STZ injection and once weekly thereafter (Precision Xceed, Abbott, Zwolle, The Netherlands). Only rats with glucose levels of >15 mM were considered diabetic, and they subsequently received 2–4 U insulin/day (Levemir, Novo Nordisk, Denmark). Diabetic Ren2 rats had an average blood glucose level of 25.8 ± 0.9 mmol/l. After 2 wk of DM status, osmotic minipumps (2ML4, Alzet) were implanted subcutaneously under isoflurane anesthesia to infuse vehicle (saline, $n = 8$), aliskiren (a gift from Novartis, 10 $mg \cdot kg^{-1} \cdot day^{-1}$, $n = 8$), or aliskiren + rat HRP (NH_2-RILLKKMPSV-COOH, 1 $mg \cdot kg^{-1} \cdot day^{-1}$, Biosynthan, Berlin, Germany, $n = 7$). In animals that received aliskiren + HRP, two separate minipumps were implanted in both sides of the body. During the study, rats were placed in metabolic cages on *day −14* (non-DM), *day 0* (DM), and *day 21* (DM + treatment) to collect 24-h urine. Each rat served as its own control for the non-DM state. Urine was frozen and stored until analysis of total protein, albumin, creatinine, Na^+, endothelin (ET)-1, and aldosterone. After three weeks of treatment, animals were anesthetized by an intraperitoneal pentobarbital injection, and the hepatic portal vein was cannulated to collect blood for measurements of ANG I, ANG II, aldosterone, ET-1, TGF-β_1, PAI-1, K^+, cystatin C (a marker of glomerular filtration that is less dependent on muscle mass compared with creatinine), and creatinine (*day 21*). The kidney and heart were excised, weighed, divided into transverse segments, and fixed in 4% paraformaldhyde for histological analysis or frozen in liquid nitrogen for gene expression analysis. Blood and organs were also obtained from six DM Ren2 rats treated with saline for 3 wk and eight untreated non-DM Ren2 rats, which did not undergo hemodynamic measurements.

Table 2. *Main characteristics as well as urine and plasma analysis in non-DM Ren2 rats and DM rats treated with vehicle, aliskiren, or aliskiren + HRP*

		DM Rats		
	Non-DM Rats	Vehicle	Aliskiren	Aliskiren + HRP
Mean arterial pressure on *day 21*, mmHg‡	ND	123 ± 7	104 ± 9†	103 ± 4†
Body weight, kg	0.562 ± 0.02	0.409 ± 0.01*	0.419 ± 0.01*	0.422 ± 0.01*
Heart weight, g	2.15 ± 0.06	1.55 ± 0.07*	1.51 ± 0.04*	1.60 ± 0.05*
Heart weight/body weight, g/kg	3.9 ± 0.10	3.7 ± 0.11	3.6 ± 0.12	3.7 ± 0.09
Kidney weight, g	1.48 ± 0.06	1.58 ± 0.07	1.69 ± 0.04*	1.63 ± 0.05
Kidney weight/body weight, g/kg	2.7 ± 0.12	4.1 ± 0.15*	4.0 ± 0.10*	3.9 ± 0.12*
Blood glucose, mM‡	6.0 ± 0.5	24.5 ± 0.8*	26.1 ± 1.0*	24.8 ± 1.0*
Urine				
Creatinine, μmol/day	128 ± 4	114 ± 9	116 ± 13	109 ± 5
Endothelin-1, pg/day	3.6 ± 0.7	7 ± 3	0.5 ± 0.5	3.8 ± 2
Creatinine clearance, ml/min	ND	3.4 ± 0.3	3.3 ± 0.3	2.8 ± 0.2
Plasma				
Creatinine, nmol/ml	32.6 ± 1.6	23.9 ± 0.9*	23.9 ± 0.7*	27.8 ± 1.8
Endothelin-1, pg/ml	9.1 ± 4	12.4 ± 9	19.6 ± 8	18.4 ± 14
Plasminogen activator inhibitor-1, ng/ml	3.2 ± 0.5	7.7 ± 1.2	7.6 ± 1.9	11.8 ± 3.9*
TGF-β_1, pg/ml	423 ± 99	266 ± 78	408 ± 124	268 ± 80

Data are means ± SE; n 7–8 rats/group. Non-DM, nondiabetic; DM, diabetic; HRP, handle region peptide; ND, not determined. Creatinine clearance in non-DM rats could not be calculated since plasma and urine creatinine levels in this group were determined on *day 21* and *day −14*, respectively, i.e., not on the same day. *$P < 0.05$ vs. non-DM rats; †$P < 0.05$ vs. vehicle. ‡Data are from Batenburg et al. (3).

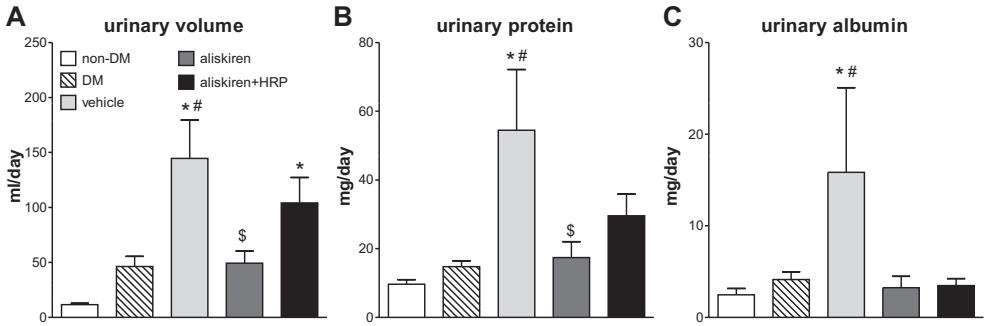

Fig. 1. Urinary volume (*A*), urinary protein (*B*), and urinary albumin (*C*) in nondiabetic (non-DM) and DM Ren2 rats treated with vehicle, aliskiren (ali), or aliskiren + handle region peptide (HRP). Urine was collected on *day −14* (non-DM), *day 0* (2-wk DM), and *day 21* (after 3-wk treatment, 5-wk DM, with vehicle, aliskiren, and aliskiren + HRP). Please note that the *day 0* data (DM) reflect measurements taken immediately before the start of treatment. Data are means ± SE; $n = 7–8$. *$P < 0.05$ vs. non-DM; #$P < 0.05$ vs. 2-wk DM; \$$P < 0.05$ vs. vehicle.

Biochemical Measurements

ET-1 was assessed by chemiluminescent ELISA (QuantiGlo, R&D Systems), albumin by enzyme immunoassay (Spi-Bio, Montigny-Le-Bretonneux, France), and aldosterone by radioimmunoassay (Coat-a-Count, Siemens Medical Solutions Diagnostics, Los Angeles, CA). TGF-β_1, cystatin C (Quantikine, R&D systems), and PAI-1 (Zymutest, Tebu-Bio, Le Perray-en-Yvelines, France) were measured by ELISA. Creatinine, K^+, Na^+, and total protein were measured at the clinical chemical laboratory of the Erasmus MC. ANG I and ANG II were measured by radioimmunoassay, after SepPak extraction and reverse-phase HPLC separation as previously described (6, 8).

Histology

After fixation, kidney and heart sections were dehydrated and paraffin embedded. Gomori silver staining was applied to sections (5 μm) of the left ventricle of the heart to visualize individual cardiomyocytes. Sirius red staining was applied to visualize collagen as a measure of cardiac fibrosis. Cardiomyocyte size and the amount of collagen were measured using Qwin (Leica).

Transversely sliced kidney sections (deparaffinized, 2 μm) were stained with periodic acid-Schiff to localize kidney damage and α-smooth muscle actin to identify interlobar arteries. The glomerular volume, arterial wall thickness, and lumen diameter of interlobar arteries were blindly assessed in the sections. To measure glomerular volume, 50 individual glomeruli from each kidney section were traced along Bowman's capsule to measure glomerular circumference using the system of NanoZoomer Digital Pathology. Glomerular volume was calculated from the glomerular circumference and radius according the method of van Damme et al. (41) using the following formula: $4/3\pi r^2$, where r is the radius. To measure the arterial wall thickness-to-lumen diameter ratio, the arterial and lumen circumference of 6 interlobar arteries/kidney section was measured using the system of NanoZoomer Digital Pathology. Arterial wall thickness was calculated by deduction of the lumen radius from the arterial outer radius. Data were also expressed as arterial wall thickness divided by the lumen diameter ratio to correct for the size of the arteries measured.

The presence of focal segmental glomerulosclerosis was assessed in all glomeruli of one kidney section per animal with a mean of 181 ± 4 glomeruli per section. All sections were semiquantitatively scored by a renal pathologist in a blinded manner. Renal scarring of all glomeruli was scored on an arbitrary scale from *0* to *4*, where *grade 0* (n_0) indicates no glomerulosclerosis, *grade 1* (n_1) indicates <25% of sclerosis, *grade 2* (n_2) indicates 25–50% of sclerosis, *grade*

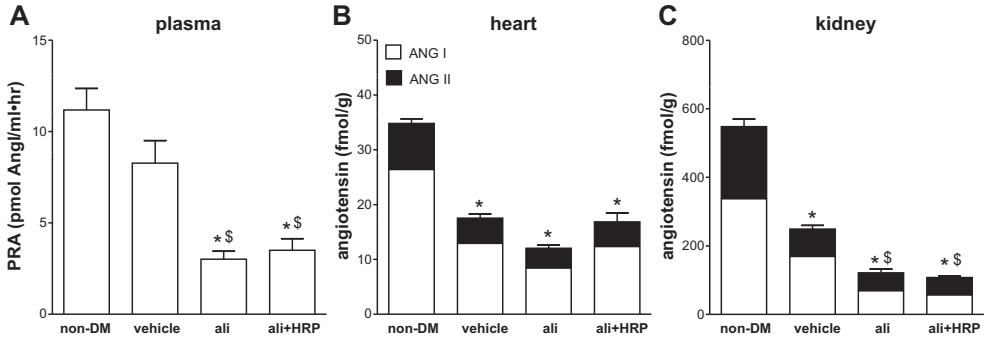

Fig. 2. Plasma renin activity (PRA; *A*) and ANG levels in the heart (*B*) and kidneys (*C*) from non-DM and DM Ren2 rats, with the latter treated for 3 wk with vehicle, aliskiren, or aliskiren + HRP. Data are means ± SE; $n = 7–12$. *$P < 0.05$ vs. non-DM; \$$P < 0.05$ vs. vehicle.

3 (n_3) indicates 50–75% of sclerosis, and *grade 4* (n_4) indicates >75% of sclerosis per glomerulus. Hereafter, the individual glomerulosclerosis index (GSI) was calculated for each rat with the following formula: $[(1\times n_1) + (2\times n_2) + (3\times n_3) + (4\times n_4)]/(n_0 + n_1 + n_2 + n_3 + n_4)$. Furthermore, 10 images of each kidney section (×100 magnification) were analyzed for arterial hyalinosis, intima fibrosis, and mediahypertrophy as well as tubular atrophy, interstitial fibrosis, and renal inflammation according to the Banff classification (35). Each parameter was graded in 10 fields with a score of *0–3*, in which *0* indicates no changes in pathology, *grade 1* indicates <25% of change, *grade 2* indicates 25–50% of change, and *grade 3* indicates >50% of change in affected tissue. From these data, the tubulointerstitial score was calculated by dividing the combined score of tubular atrophy, interstitial fibrosis, and renal inflammation with the number of parameters.

Quantitative Real-Time RT-PCR

Total RNA was isolated from snap-frozen rat kidneys and hearts using TRIzol (Life Technologies) and reverse transcribed into cDNA using the QuantiTect Reverse Transcription Kit (Qiagen, Venlo, The Netherlands). The resulting cDNA was amplified for 40 cycles (denaturation at 95°C for 10 min, thermal cycling at 95°C for 15 s, and annealing/extension at 60°C for 1 min) with a Step-One cycler (NYSE, Life Technologies) using SYBR Green PCR Master Mix (Life Technologies). The intron-spanning oligonucleotide primers for quantitative PCR were designed with Primer-BLAST (National Center for Biotechnology Information; Table 1). The comparative cycle time method ($\Delta\Delta C_T$, where C_T is threshold cycle) was used for the relative quantification of gene expression using the geometric mean of the housekeeping genes hypoxanthine phosphoribosyl transferase-1,

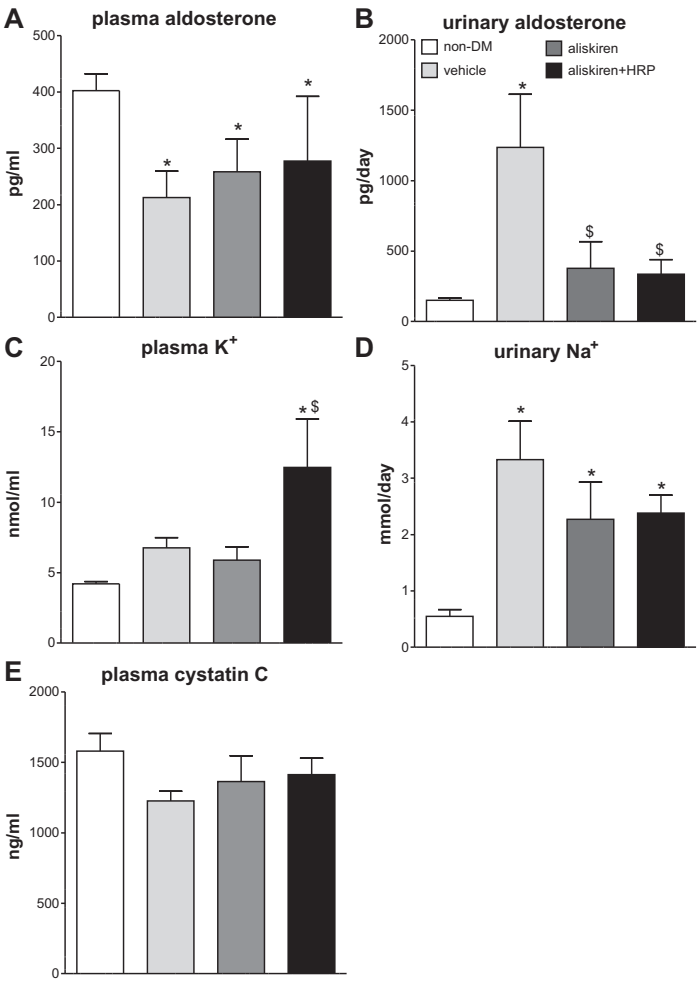

Fig. 3. Levels of plasma aldosterone (*A*), urinary aldosterone (*B*), plasma K^+ (*C*), urinary Na^+ (*D*), and plasma cystatin C (*E*) in non-DM and DM Ren2 rats, with the latter treated for 3 wk with vehicle, aliskiren, or aliskiren + HRP. Data are means ± SE; $n = 7–13$. *$P < 0.05$ vs. non-DM; \$$P < 0.05$ vs. vehicle.

β_2-microglobulin, and β-actin for normalization. In cardiac left ventricular tissue, gene expression of atrial natriuretic peptide (ANP), brain natriuretic peptide (BNP), β-myosin heavy chain (β-MHC), (P)RR, and AT_1R was determined. Gene expression of rat renin, (P)RR, AT_1R, collagen-1, TGF-β_1, TNF-α, NF-κB, COX-2, and neutrophil gelatinase-associated lipocalin (Ngal; a marker of tubular damage) was measured in the kidney medulla and cortex.

Statistical Analysis

Statistical analysis was performed using an unpaired *t*-test after one-way ANOVA with a Bonferroni posttest confirmed differences between groups. Data are given as means ± SE. *P* values of <0.05 were considered significant.

RESULTS

Animal Characteristics

Hemodynamic data have been previously reported (3). In brief, diabetic Ren2 rats were severely hypertensive, and a 3-wk treatment with aliskiren (but not vehicle) lowered blood pressure (Table 2). The effect on blood pressure was unaltered by HRP. Diabetic Ren2 rats displayed reduced body weight and heart weight and an increased kidney weight; as a result, the heart weight-to-body weight ratio was unaltered in diabetic animals, whereas their kidney weight-to-body weight ratio was increased (Table 2). Treatment with aliskiren with or without HRP did not affect these parameters.

Biochemical Measurements

STZ-induced DM increased blood glucose in Ren2 rats approximately fourfold, and this was unaffected by treatment (Table 2). DM increased urinary volume time dependently. It was up ≈4-fold after 2 wk and after an additional 3 wk (during treatment with vehicle) ≈13-fold (Fig. 1). Aliskiren prevented this rise in diuresis, most likely due to its effects on blood pressure, whereas HRP negated the protective effects of aliskiren. Changes in urinary protein and albumin ran in parallel with the changes in urinary volume, although HRP did not prevent the effect of aliskiren on albumin (Fig. 1).

DM decreased plasma creatinine, and this was unaffected by aliskiren treatment. HRP, when given on top of aliskiren, normalized plasma creatinine. No significant changes in urinary creatinine or creatinine clearance were observed after DM induction with or without treatment (Table 2). Likewise, there was no change in plasma cystatin C, indicating no change in the glomerular filtration rate due to 5 wk of DM with or without treatment (Fig. 3).

DM marginally decreased plasma renin activity [*P* = not significant (NS)], and this was accompanied by a significant decrease in ANG levels in the heart and kidney (Fig. 2). Aliskiren further reduced these levels in the kidney, both with and without HRP. Plasma aldosterone levels were also decreased in diabetic Ren2 rats, and this resulted in increased natriuresis and a (nonsignificant) increase in plasma K^+ levels (Fig. 3). Remarkably, despite the reduction in plasma aldosterone, urinary aldosterone excretion rose eightfold. Aliskiren

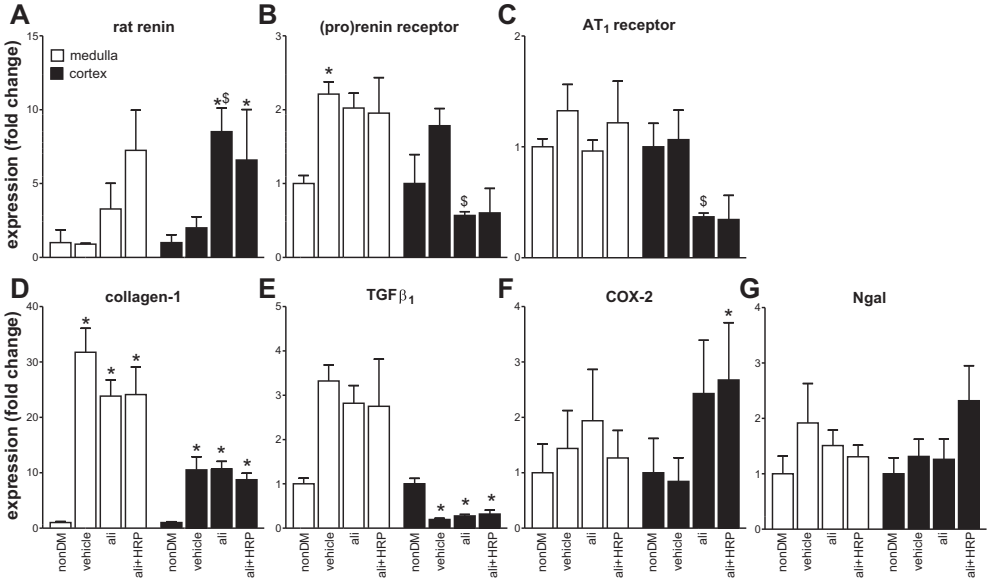

Fig. 4. Gene expression analysis of rat renin (*A*), (pro)renin receptor [(P)RR; *B*], ANG II type 1 (AT_1) receptor (*C*), collagen-1 (*D*), transforming growth factor (TGF)-β_1 (*E*), cyclooxygenase (COX)-2 (*F*), and neutrophil gelatinase-associated lipocalin (Ngal; *G*) in the kidney medulla and cortex from non-DM and DM Ren2 rats, with the latter treated for 3 wk with vehicle, aliskiren, or aliskiren + HRP. Data are means ± SE; $n = 5–9$. Values are expressed as fold changes versus non-DM. $*P < 0.05$ vs. non-DM; $\$P < 0.05$ vs. vehicle.

with or without HRP greatly reduced the latter and yet non-significantly increased plasma aldosterone. As a result, natriuresis tended to diminish (P = NS). Of interest, HRP on top of aliskiren further increased plasma K^+.

Plasma levels of TGF-β_1 and PAI-1 were not affected by diabetes or treatment with aliskiren. However, HRP on top of aliskiren increased plasma PAI-1 by 50% compared with vehicle- or aliskiren-treated rats without affecting TGF-β_1

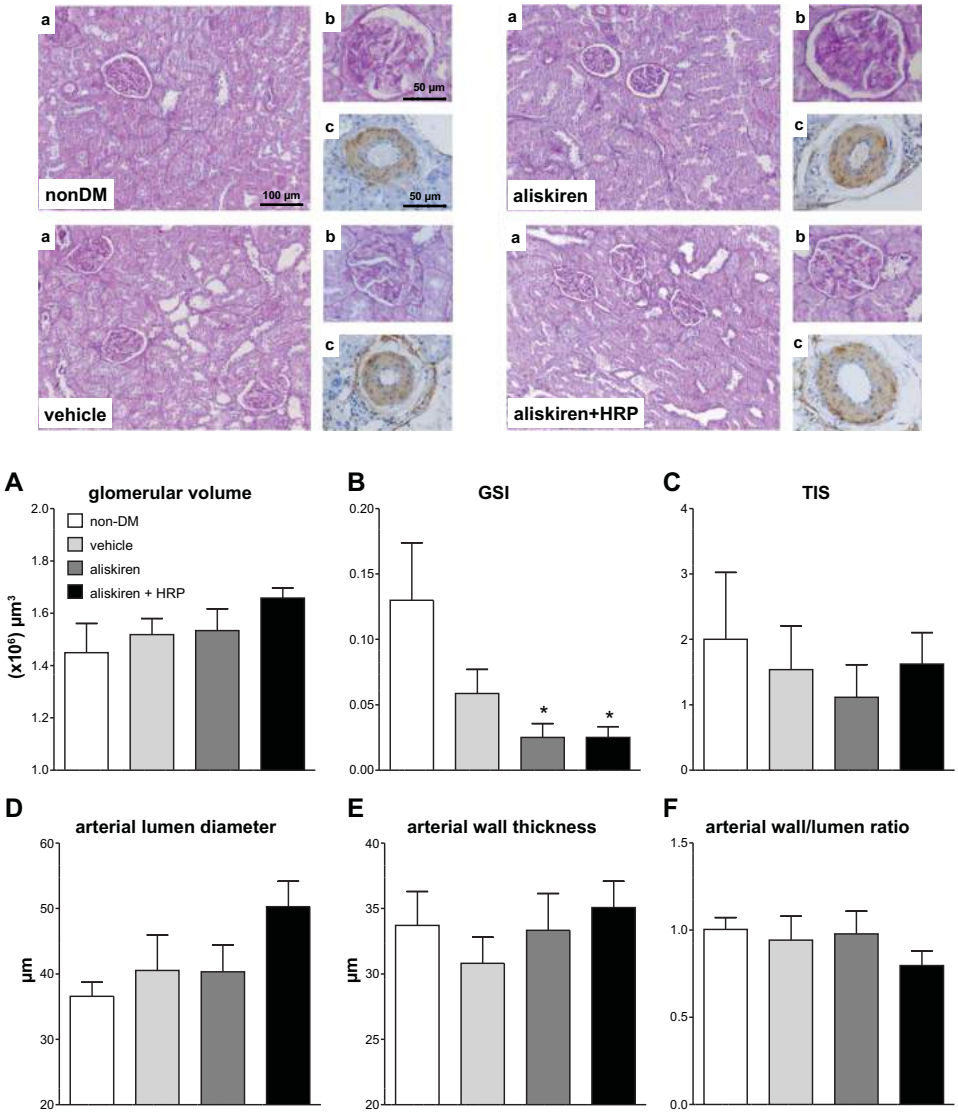

Fig. 5. *Top*: representative images of periodic acid-Schiff-stained kidney sections (*a* and *b*) and α-smooth muscle actin-stained interlobar arteries (*c*). *Bottom*: glomerular volume (*A*), glomerulosclerosis index (GSI; *B*), tubulointerstitial score (TIS; *C*), interlobar arterial lumen diameter (*D*), wall thickness (*E*), and wall-to-lumen ratio (*F*) in kidney sections from non-DM and DM Ren2 rats, with the latter treated for 3 wk with vehicle, aliskiren, or aliskiren + HRP. Data are means ± SE; n = 7–8. *P < 0.05 vs. non-DM.

(Table 2). Plasma and urinary ET-1 levels were unaffected by DM or treatment (Table 2).

The Kidney

Gene expression. DM did not alter rat renin, AT_1R, COX-2, or Ngal expression in the medulla or cortex (Fig. 4). It increased (P)RR and collagen-1 expression in the medulla and, to a lesser degree (P = NS), in the cortex. DM decreased TGF-β_1 expression in the cortex, whereas it induced a nonsignificant increase in TGF-β_1 expression in the medulla. Similar changes were observed for TNF-α and NF-κB, but these were not significant (data not shown). Aliskiren did not alter DM-induced changes in TGF-β_1 and collagen-1 and increased cortical rat renin expression. A similar increase in renin expression, albeit nonsignificant, was observed in the medulla. Aliskiren diminished cortical (P)RR and AT_1R expression without affecting these parameters in the medulla. Aliskiren tended to increase cortical COX-2 expression (P = NS). Changes by aliskiren were unaltered in the presence of HRP except for the increase in COX-2, which became significant after the addition of HRP.

Histology. DM did not alter tubulointerstitial score, glomerular volume, interlobar arterial lumen diameter, and wall thickness (nor the ratio of the latter two) and nonsignificantly decreased GSI (Fig. 5). Arterial hyalinose, intima fibrosis, and media hypertrophy were not observed. Aliskiren reduced GSI without affecting any of the other parameters. HRP, when given on top of aliskiren, did not alter its effects on GSI but tended to increase glomerular volume and lumen diameter, with the latter resulting in a decrease in the lumen diameter-to-wall thickness ratio. However, none of these changes were significant.

The Heart

Gene expression. DM did not affect cardiac ANP, BNP, and (P)RR expression and increased β-MHC and AT_1R expression (Fig. 6). Aliskiren with HRP, but not aliskiren alone, normalized the latter. Drug treatment did not affect (P)RR or β-MHC expression. Aliskiren, with or without HRP, reduced cardiac BNP expression, and similar trends were observed for cardiac ANP expression, although the changes were significant only during combination treatment.

Histology. DM increased cardiac collagen content without altering myocyte size. Aliskiren did not affect these changes, whereas aliskiren with HRP further increased collagen content and marginally diminished myocyte size (Fig. 7).

DISCUSSION

This study shows that HRP counteracts the favorable effects of aliskiren on early renal damage in diabetic Ren2 rats. In

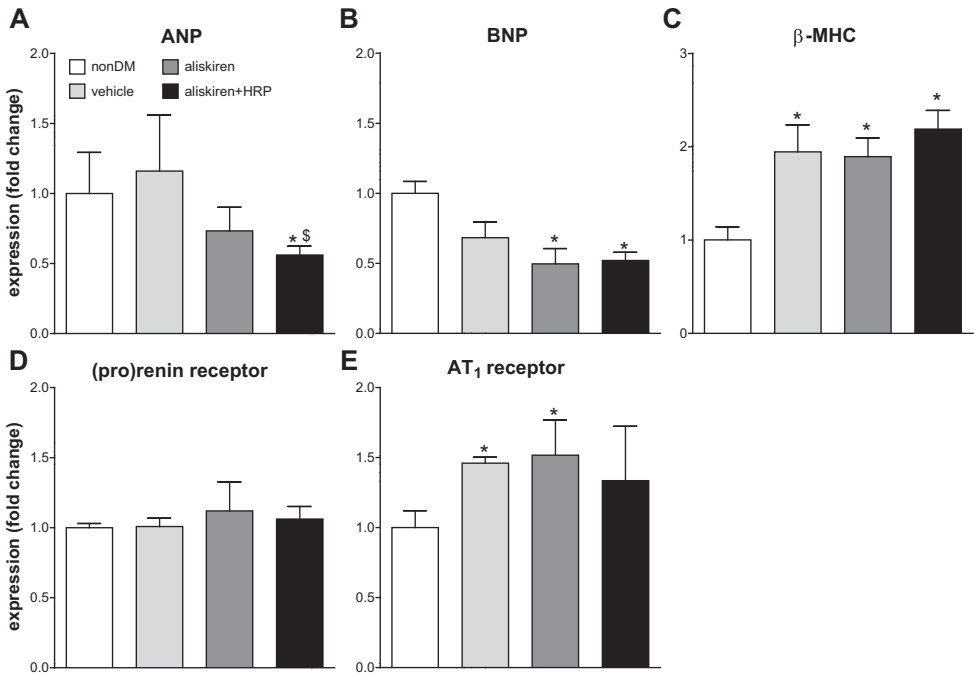

Fig. 6. Gene expression analysis of atrial natriuretic peptide (ANP; *A*), brain natriuretic peptide (BNP; *B*), β-myosin heavy chain (β-MHC; *C*), (P)RR (*D*), and AT_1 receptor (*E*) in hearts from non-DM and DM Ren2 rats, with the latter treated for 3 wk with vehicle, aliskiren, or aliskiren + HRP. Data are means ± SE; n = 7–10. Values are expressed as fold changes versus non-DM. *$P < 0.05$ vs. non-DM; \$$P < 0.05$ vs. vehicle.

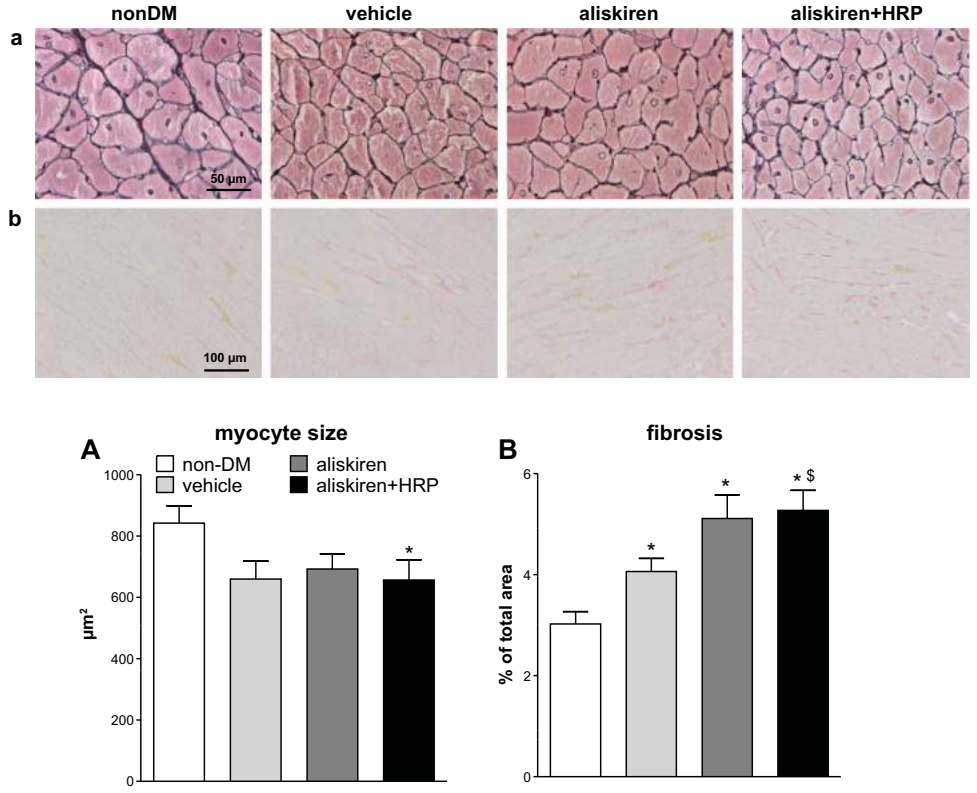

Fig. 7. Top: representative images of Gomori-stained cardiomyocytes (*a*) and of Sirius red-stained left ventricular tissue. *Bottom*: cardiomyocyte size (*A*) and fibrotic area (*B*) in left ventricular tissue of hearts from non-DM and DM Ren2 rats, with the latter treated for 3 wk with vehicle, aliskiren, or aliskiren + HRP. Data are means ± SE; $n = 7–8$. *$P < 0.05$ vs non-DM, $$P < 0.05$ vs vehicle.

agreement with previous studies (3, 26), the hypertensive Ren2 rat, when made diabetic with STZ, displayed mild glomerulosclerosis, accompanied by albuminuria, proteinuria, and diuresis. A 3-wk treatment with aliskiren improved these parameters, whereas the addition of HRP on top of aliskiren negated the protective effects of aliskiren on the latter two. HRP also induced hyperkalemia and increased plasma PAI-1, renal COX-2, and cardiac collagen content. This argues against the application of HRP in combination with aliskiren in diabetic patients.

Plasma creatinine decreased after the induction of DM, most likely reflecting the weight (and muscle) loss occurring in these animals. There were no changes in cystatin C or renal Ngal expression, suggesting that indeed the renal damage in our DM animals was at an early stage, not yet resulting in alterations in glomerular filtration or tubular damage. Of interest, aliskiren alone did not alter these parameters, whereas HRP on top of aliskiren increased plasma creatinine and tended to increase (P = NS) cortical Ngal expression, again suggesting that HRP, if anything, worsened renal function when combined with aliskiren.

DM reduced plasma, cardiac, and renal RAS activity in the Ren2 rat, although only the reduction in tissue was significant. The reduction in plasma renin activity was modest, in full agreement with the consequence of diabetes in humans (15). Along with this RAS suppression, plasma aldosterone decreased by almost 50%. Not surprisingly, this resulted in natriuresis and a (nonsignificant) rise in plasma K^+. Yet, urinary aldosterone excretion increased eightfold. This is suggestive for a net rise in adrenal aldosterone production, most likely to compensate the loss of aldosterone via urine (≈1.5 ng/day). Of interest, aliskiren greatly diminished the urinary aldosterone loss, reflecting a reduction in aldosterone production, although plasma aldosterone, if anything, tended to go up, thereby counteracting the above effects on natriuresis and hyperkalemia. The effects of aliskiren on aldosterone and natriuresis were unaltered by HRP. However, it greatly elevated plasma K^+. Since this occurred independently of

changes in aldosterone, it might be the consequence of direct effects of HRP, e.g., via (P)RR (31).

The aliskiren-induced reduction in renal ANG content, together with the reduction of cortical AT_1R expression, probably underlies the beneficial effect of renin inhibition in the kidney. Aliskiren-induced AT_1R suppression has been previously reported, both in the kidney and other organs (11, 30, 43). At 5 wk after STZ injection, we observed modest regional changes in renal TGF-β_1, TNF-α, NF-κB, and collagen-1 expression, although no fibrosis or inflammation could be detected. It is therefore not surprising that aliskiren did not significantly affect these parameters in the kidney. Such effects have been observed before, but this required a longer duration of DM (10 wk) and aliskiren treatment starting at the moment of STZ injection (11). HRP did not alter the effect of aliskiren on TGF-β_1 but unexpectedly increased the levels of PAI-1. These observations contrast with the idea that HRP prevents (pro)renin-(P)RR interactions, thereby blocking the rise in PAI-1 that result from such (P)RR stimulation, at least in vitro (19, 48). Possibly, the increase in renal (rat) renin expression after aliskiren was too modest to increase PAI-1. In addition, aliskiren suppressed (P)RR expression. Recently, HRP has been reported to act as a partial agonist of (P)RR (31, 46). Thus, its stimulatory effects on PAI-1 on top of aliskiren might also be the consequence of direct (P)RR stimulation.

Hyperglycemia elevates (P)RR expression in rat mesangial cells via PKC, ERK1/2, and JNK (17), and this has been suggested to facilitate ANG II generation and AT_1R-dependent COX-2 induction (13). Ubiquitous overexpression of human (P)RR in the rat also resulted in COX-2 upregulation (25). Simultaneously, COX-2 inhibition reduced the glucose-induced (P)RR upregulation, suggesting that COX-2 itself upregulates (P)RR (16). Our study confirms renal (P)RR upregulation in diabetic Ren2 rats. However, significant COX-2 upregulation was only seen after concomitant HRP administration, even in the face of aliskiren-induced (P)RR suppression. This suggest that (P)RR upregulation per se is insufficient to increase COX-2 and requires additional (P)RR stimulation, either by renin, HRP, or their combination. COX-2 elevation has been previously reported in the macula densa after renin upregulation due to salt restriction (14). Such COX-2 upregulation has detrimental effects, for instance, COX-2 generated endothelium-derived contractile factors in diabetic Ren2 rats, thereby inducing vascular dysfunction (3), and the COX-2 upregulation in human (P)RR-overexpressing rats was accompanied by proteinuria and glomerulosclerosis (25).

Natriuretic peptides are released by the hypertrophied heart, and their levels are elevated in patients with heart failure (4) and in homozygous Ren2 rats (44). Aliskiren reduced cardiac ANP and BNP expression in the diabetic, heterozygous Ren2 rats of the present study, most likely due to its blood pressure-lowering effect. Yet, aliskiren did not affect cardiac hypertrophy, β-MHC expression, or myocyte size. These effects were unaltered by HRP. Moreover, no changes occurred in cardiac (P)RR expression, suggesting that (P)RR upregulation by hyperglycemia is not a uniform phenomenon. Although aliskiren with or without HRP did not significantly reduce cardiac ANG content, HRP combined with aliskiren did suppress cardiac AT_1R expression, suggesting that this combination may have reduced the consequences of ANG II-AT_1R interactions. However, this did not result in a reduction of cardiac fibrosis, possibly because the degree of fibrosis in our model was still modest. Remarkably, however, cardiac fibrosis increased significantly after cotreatment of aliskiren with HRP. This contrasts with a previous study (21) showing antifibrotic effects of HRP in stroke-prone spontaneously hypertensive rats and once again illustrates the partial agonistic capacities of HRP.

In conclusion, renin inhibition improves renal function in diabetic Ren2 rats with early kidney damage, and (P)RR blockade with HRP not only counteracted this effect in a RAS-independent manner but also increased K^+, PAI-1, renal COX-2, and cardiac fibrosis. This contrasts with the beneficial cardiac and renal effects of HRP observed in various models (20, 22, 24) but agrees with the deleterious effects of (P)RR knockout in the heart and kidney (28, 40). A uniform explanation might be that HRP acts as a partial agonist (43, 46). Nevertheless, given these controversial findings, it seems that, at this stage, HRP should not be considered as add-on drug in diabetics treated with a RAS inhibitor. Furthermore, given the uncertainty whether HRP is a (P)RR blocker or not, future studies should carefully examine the exact function of (P)RR in diabetes, e.g., making use of (inducible) renal cell-specific knockout models, to define its role as a treatment target.

DISCLOSURES

No conflicts of interest, financial or otherwise, are declared by the author(s).

AUTHOR CONTRIBUTIONS

Author contributions: L.t.R., M.v.d.H., J.H.v.E., R.v.V., I.M.G., U.M.-B., A.M.B., F.P.L., and W.W.B. performed experiments; L.t.R., C.J.P.-K., and W.W.B. analyzed data; L.t.R., A.H.J.D., and W.W.B. edited and revised manuscript; L.t.R., M.v.d.H., C.J.P.-K., J.H.v.E., R.v.V., I.M.G., U.M.-B., A.M.B., F.P.L., A.H.J.D., and W.W.B. approved final version of manuscript; J.H.v.E., A.H.J.D., and W.W.B. interpreted results of experiments; A.H.J.D. and W.W.B. conception and design of research; A.H.J.D. and W.W.B. drafted manuscript; W.W.B. prepared figures.

REFERENCES

1. **Batenburg WW, Krop M, Garrelds IM, de Vries R, de Bruin RJA, Burcklé CA, Müller DN, Bader M, Nguyen G, Danser AHJ.** Prorenin is the endogenous agonist of the (pro)renin receptor. Binding kinetics of renin and prorenin in rat vascular smooth muscle cells overexpressing the human (pro)renin receptor. *J Hypertens* 25: 2441–2453, 2007.
2. **Batenburg WW, Lu X, Leijten F, Maschke U, Müller DN, Danser AHJ.** Renin- and prorenin-induced effects in rat vascular smooth muscle cells overexpressing the human (pro)renin receptor: does (pro)renin-(pro)renin receptor interaction actually occur? *Hypertension* 58: 1111–1119, 2011.
3. **Batenburg WW, van den Heuvel M, van Esch JH, van Veghel R, Garrelds IM, Leijten F, Danser AH.** The (pro)renin receptor blocker handle region peptide upregulates endothelium-derived contractile factors in aliskiren-treated diabetic transgenic (mREN2)27 rats. *J Hypertens* 31: 292–302, 2013.
4. **Burnett JC Jr, Kao PC, Hu DC, Heser DW, Heublein D, Granger JP, Opgenorth TJ, Reeder GS.** Atrial natriuretic peptide elevation in congestive heart failure in the human. *Science* 231: 1145–1147, 1986.
5. **Connelly KA, Advani A, Kim S, Advani SL, Zhang M, White KE, Kim YM, Parker C, Thai K, Krum H, Kelly DJ, Gilbert RE.** The cardiac (pro)renin receptor is primarily expressed in myocyte transverse tubules and is increased in experimental diabetic cardiomyopathy. *J Hypertens* 29: 1175–1184, 2011.
6. **Danser AHJ, van Kats JP, Admiraal PJJ, Derkx FHM, Lamers JMJ, Verdouw PD, Saxena PR, Schalekamp MADH.** Cardiac renin and angiotensins. Uptake from plasma versus in situ synthesis. *Hypertension* 24: 37–48, 1994.
7. **de Boer RA, Azizi M, Danser AH, Nguyen G, Nussberger J, Ruilope LM, Schmieder RE, Volpe M.** Dual RAAS suppression: recent devel-

opments and implications in light of the ALTITUDE study. *J Renin Angiotensin Aldosterone Syst* 13: 409–412, 2012.
8. **de Lannoy LM, Danser AHJ, van Kats JP, Schoemaker RG, Saxena PR, Schalekamp MADH.** Renin-angiotensin system components in the interstitial fluid of the isolated perfused rat heart. Local production of angiotensin I. *Hypertension* 29: 1240–1251, 1997.
9. **Deinum J, Ronn B, Mathiesen E, Derkx FHM, Hop WC, Schalekamp MADH.** Increase in serum prorenin precedes onset of microalbuminuria in patients with insulin-dependent diabetes mellitus. *Diabetologia* 42: 1006–1010, 1999.
10. **Dong YF, Liu L, Kataoka K, Nakamura T, Fukuda M, Tokutomi Y, Nako H, Ogawa H, Kim-Mitsuyama S.** Aliskiren prevents cardiovascular complications and pancreatic injury in a mouse model of obesity and type 2 diabetes. *Diabetologia* 53: 180–191, 2010.
11. **Feldman DL, Jin L, Xuan H, Contrepas A, Zhou Y, Webb RL, Mueller DN, Feldt S, Cumin F, Maniara W, Persohn E, Schuetz H, Jan Danser AH, Nguyen G.** Effects of aliskiren on blood pressure, albuminuria, and (pro)renin receptor expression in diabetic TG(mRen-2)27 rats. *Hypertension* 52: 130–136, 2008.
12. **Feldt S, Maschke U, Dechend R, Luft FC, Müller DN.** Role of the (pro)renin receptor in transgenic rats with human renin hypertension. *J Am Soc Nephrol*. In press.
13. **Gonzalez AA, Luffman C, Bourgeois CR, Vio CP, Prieto MC.** Angiotensin II-independent upregulation of cyclooxygenase-2 by activation of the (pro)renin receptor in rat renal inner medullary cells. *Hypertension* 61: 443–449, 2013.
14. **Harris RC, McKanna JA, Akai Y, Jacobson HR, Dubois RN, Breyer MD.** Cyclooxygenase-2 is associated with the macula densa of rat kidney and increases with salt restriction. *J Clin Invest* 94: 2504–2510, 1994.
15. **Hollenberg NK, Fisher NDL, Nussberger J, Moukarbel GV, Barkoudah E, Danser AHJ.** Renal responses to three types of renin-angiotensin system blockers in patients with diabetes mellitus on a high-salt diet: a need for higher doses in diabetic patients? *J Hypertens* 29: 2454–2461, 2011.
16. **Huang J, Siragy HM.** Glucose promotes the production of interleukine-1beta and cyclooxygenase-2 in mesangial cells via enhanced (pro)renin receptor expression. *Endocrinology* 150: 5557–5565, 2009.
17. **Huang J, Siragy HM.** Regulation of (pro)renin receptor expression by glucose-induced mitogen-activated protein kinase, nuclear factor-κB, and activator protein-1 signaling pathways. *Endocrinology* 151: 3317–3325, 2010.
18. **Huang Y, Noble NA, Zhang J, Xu C, Border WA.** Renin-stimulated TGF-β1 expression is regulated by a mitogen-activated protein kinase in mesangial cells. *Kidney Int* 72: 45–52, 2007.
19. **Huang Y, Wongamorntham S, Kasting J, McQuillan D, Owens RT, Yu L, Noble NA, Border W.** Renin increases mesangial cell transforming growth factor-beta1 and matrix proteins through receptor-mediated, angiotensin II-independent mechanisms. *Kidney Int* 69: 105–113, 2006.
20. **Ichihara A, Hayashi M, Kaneshiro Y, Suzuki F, Nakagawa T, Tada Y, Koura Y, Nishiyama A, Okada H, Uddin MN, Nabi AH, Ishida Y, Inagami T, Saruta T.** Inhibition of diabetic nephropathy by a decoy peptide corresponding to the "handle" region for nonproteolytic activation of prorenin. *J Clin Invest* 114: 1128–1135, 2004.
21. **Ichihara A, Kaneshiro Y.** Response to cardiovascular effects of nonproteolytic activation of prorenin. *Hypertension*. In press.
22. **Ichihara A, Kaneshiro Y, Takemitsu T, Sakoda M, Nakagawa T, Nishiyama A, Kawachi H, Shimizu F, Inagami T.** Contribution of nonproteolytically activated prorenin in glomeruli to hypertensive renal damage. *J Am Soc Nephrol* 17: 2495–2503, 2006.
23. **Ichihara A, Kaneshiro Y, Takemitsu T, Sakoda M, Suzuki F, Nakagawa T, Nishiyama A, Inagami T, Hayashi M.** Nonproteolytic activation of prorenin contributes to development of cardiac fibrosis in genetic hypertension. *Hypertension* 47: 894–900, 2006.
24. **Ichihara A, Suzuki F, Nakagawa T, Kaneshiro Y, Takemitsu T, Sakoda M, Nabi AH, Nishiyama A, Sugaya T, Hayashi M, Inagami T.** Prorenin receptor blockade inhibits development of glomerulosclerosis in diabetic angiotensin II type 1a receptor-deficient mice. *J Am Soc Nephrol* 17: 1950–1961, 2006.
25. **Kaneshiro Y, Ichihara A, Sakoda M, Takemitsu T, Nabi AH, Uddin MN, Nakagawa T, Nishiyama A, Suzuki F, Inagami T, Itoh H.** Slowly progressive, angiotensin ii-independent glomerulosclerosis in human (pro)renin receptor-transgenic rats. *J Am Soc Nephrol* 18: 1789–1795, 2007.
26. **Kelly DJ, Wilkinson-Berka JL, Allen TJ, Cooper ME, Skinner SL.** A new model of diabetic nephropathy with progressive renal impairment in the transgenic (mRen-2)27 rat (TGR). *Kidney Int* 54: 343–352, 1998.
27. **Kelly DJ, Zhang Y, Moe G, Naik G, Gilbert RE.** Aliskiren, a novel renin inhibitor, is renoprotective in a model of advanced diabetic nephropathy in rats. *Diabetologia* 50: 2398–2404, 2007.
28. **Kinouchi K, Ichihara A, Sano M, Sun-Wada GH, Wada Y, Kurauchi-Mito A, Bokuda K, Narita T, Oshima Y, Sakoda M, Tamai Y, Sato H, Fukuda K, Itoh H.** The (pro)renin receptor/ATP6AP2 is essential for vacuolar H^+-ATPase assembly in murine cardiomyocytes. *Circ Res* 107: 30–34, 2010.
29. **Kobori H, Kamiyama M, Harrison-Bernard LM, Navar LG.** Cardinal role of the intrarenal renin-angiotensin system in the pathogenesis of diabetic nephropathy. *J Investig Med* 61: 256–264, 2013.
30. **Lastra G, Habibi J, Whaley-Connell AT, Manrique C, Hayden MR, Rehmer J, Patel K, Ferrario C, Sowers JR.** Direct renin inhibition improves systemic insulin resistance and skeletal muscle glucose transport in a transgenic rodent model of tissue renin overexpression. *Endocrinology* 150: 2561–2568, 2009.
31. **Lu X, Garrelds IM, Wagner CA, Danser AH, Meima ME.** (Pro)renin receptor is required for prorenin-dependent and -independent regulation of vacuolar H^+-ATPase activity in MDCK.C11 collecting duct cells. *Am J Physiol Renal Physiol* 305: F417–F425, 2013.
32. **Luetscher JA, Kraemer FB, Wilson DM, Schwartz HC, Bryer-Ash M.** Increased plasma inactive renin in diabetes mellitus. A marker of microvascular complications. *N Engl J Med* 312: 1412–1417, 1985.
33. **Mandavia CH, Aroor AR, Demarco VG, Sowers JR.** Molecular and metabolic mechanisms of cardiac dysfunction in diabetes. *Life Sci* 92: 601–608, 2013.
34. **Maschke U, Muller DN.** The (pro)renin receptor and the mystic HRP–is there a role in cardiovascular disease? *Front Biosci (Elite Ed)* 2: 1250–1253, 2010.
35. **Mengel M, Reeve J, Bunnag S, Einecke G, Jhangri GS, Sis B, Famulski K, Guembes-Hidalgo L, Halloran PF.** Scoring total inflammation is superior to the current Banff inflammation score in predicting outcome and the degree of molecular disturbance in renal allografts. *Am J Transplant* 9: 1859–1867, 2009.
36. **Mullins JJ, Peters J, Ganten D.** Fulminant hypertension in transgenic rats harbouring the mouse Ren-2 gene. *Nature* 344: 541–544, 1990.
37. **Nguyen G, Delarue F, Burcklé C, Bouzhir L, Giller T, Sraer JD.** Pivotal role of the renin/prorenin receptor in angiotensin II production and cellular responses to renin. *J Clin Invest* 109: 1417–1427, 2002.
38. **Oshima Y, Kinouchi K, Ichihara A, Sakoda M, Kurauchi-Mito A, Bokuda K, Narita T, Kurosawa H, Sun-Wada GH, Wada Y, Yamada T, Takemoto M, Saleem MA, Quaggin SE, Itoh H.** Prorenin receptor is essential for normal podocyte structure and function. *J Am Soc Nephrol* 22: 2203–2212, 2011.
39. **Parving HH, Brenner BM, McMurray JJ, de Zeeuw D, Haffner SM, Solomon SD, Chaturvedi N, Persson F, Desai AS, Nicolaides M, Richard A, Xiang Z, Brunel P, Pfeffer MA, Investigators A.** Cardiorenal end points in a trial of aliskiren for type 2 diabetes. *N Engl J Med* 367: 2204–2213, 2012.
40. **Riediger F, Quack I, Qadri F, Hartleben B, Park JK, Potthoff SA, Sohn D, Sihn G, Rousselle A, Fokuhl V, Maschke U, Purfurst B, Schneider W, Rump LC, Luft FC, Dechend R, Bader M, Huber TB, Nguyen G, Muller DN.** Prorenin receptor is essential for podocyte autophagy and survival. *J Am Soc Nephrol* 22: 2193–2202, 2011.
41. **van Damme B, Koudstaal J.** Measuring glomerular diameters in tissue sections. *Virchows Arch A Pathol Anat Histol* 369: 283–291, 1976.
42. **van Esch JHM, Moltzer E, van Veghel R, Garrelds IM, Leijten F, Bouhuizen AM, Danser AHJ.** Beneficial cardiac effects of the renin inhibitor aliskiren in spontaneously hypertensive rats. *J Hypertens* 28: 2145–2155, 2010.
43. **van Esch JHM, van Veghel R, Garrelds IM, Leijten F, Bouhuizen AM, Danser AHJ.** Handle region peptide counteracts the beneficial effects of the Renin inhibitor aliskiren in spontaneously hypertensive rats. *Hypertension* 57: 852–858, 2011.
44. **Wegner M, Ganten D, Stasch JP.** Neutral endopeptidase inhibition potentiates the effects of natriuretic peptides in renin transgenic rats. *Hypertens Res* 19: 229–238, 1996.
45. **Whaley-Connell A, Nistala R, Habibi J, Hayden MR, Schneider RI, Johnson MS, Tilmon R, Rehmer N, Ferrario CM, Sowers JR.** Comparative effect of direct renin inhibition and AT_1R blockade on glomerular

filtration barrier injury in the transgenic Ren2 rat. *Am J Physiol Renal Physiol* 298: F655–F661, 2010.

46. **Wilkinson-Berka JL, Heine R, Tan G, Cooper ME, Hatzopoulos KM, Fletcher EL, Binger KJ, Campbell DJ, Miller AG.** RILLK-KMPSV influences the vasculature, neurons and glia, and (pro)renin receptor expression in the retina. *Hypertension* 55: 1454–1460, 2010.
47. **Ye Y, Qian J, Castillo AC, Perez-Polo JR, Birnbaum Y.** Aliskiren and Valsartan reduce myocardial AT_1 receptor expression and limit myocardial infarct size in diabetic mice. *Cardiovasc Drugs Ther* 25: 505–515, 2011.
48. **Zhang J, Noble NA, Border WA, Owens RT, Huang Y.** Receptor-dependent prorenin activation and induction of PAI-1 expression in vascular smooth muscle cells. *Am J Physiol Endocrinol Metab* 295: E810–E819, 2008.

Combined renin inhibition/(pro)renin receptor blockade in diabetic retinopathy- a study in transgenic (mREN2)27 rats

Batenburg W.W., Verma A., Wang Y., Zhu P., van den Heuvel M., van Veghel R., Danser A.H. and Li Q.

PLoS One. 2014 Jun 26;9(6)

18

Combined Renin Inhibition/(Pro)Renin Receptor Blockade in Diabetic Retinopathy- A Study in Transgenic (mREN2)27 Rats

Wendy W. Batenburg[1], Amrisha Verma[2], Yunyang Wang[2], Ping Zhu[2], Mieke van den Heuvel[1], Richard van Veghel[1], A.H. Jan Danser[1], Qiuhong Li[2]*

[1] Division of Pharmacology, Vascular and Metabolic Diseases, Department of Internal Medicine, rasmus MC, GE Rotterdam, The Netherlands, [2] Department of Ophthalmology, College of Medicine, University of Florida, Gainesville, Florida, United States of America

Abstract

Dysfunction of renin-angiotensin system (RAS) contributes to the pathogenesis of diabetic retinopathy (DR). Prorenin, the precursor of renin is highly elevated in ocular fluid of diabetic patients with proliferative retinopathy. Prorenin may exert local effects in the eye by binding to the so-called (pro)renin receptor ((P)RR). Here we investigated the combined effects of the renin inhibitor aliskiren and the putative (P)RR blocker handle-region peptide (HRP) on diabetic retinopathy in streptozotocin (STZ)-induced diabetic transgenic (mRen2)27 rats (a model with high plasma prorenin levels) as well as prorenin stimulated cytokine expression in cultured Müller cells. Adult (mRen2)27 rats were randomly divided into the following groups: (1) non-diabetic; (2) diabetic treated with vehicle; (3) diabetic treated with aliskiren (10 mg/kg per day); and (4) diabetic treated with aliskiren+HRP (1 mg/kg per day). Age-matched non-diabetic wildtype Sprague-Dawley rats were used as control. Drugs were administered by osmotic minipumps for three weeks. Transgenic (mRen2)27 rat retinas showed increased apoptotic cell death of both inner retinal neurons and photoreceptors, increased loss of capillaries, as well as increased expression of inflammatory cytokines. These pathological changes were further exacerbated by diabetes. Aliskiren treatment of diabetic (mRen2)27 rats prevented retinal gliosis, and reduced retinal apoptotic cell death, acellular capillaries and the expression of inflammatory cytokines. HRP on top of aliskiren did not provide additional protection. In cultured Müller cells, prorenin significantly increased the expression levels of IL-1α and TNF-α, and this was completely blocked by aliskiren or HRP, their combination, (P)RR siRNA and the AT1R blocker losartan, suggesting that these effects entirely depended on Ang II generation by (P)RR-bound prorenin. In conclusion, the lack of effect of HRP on top of aliskiren, and the Ang II-dependency of the ocular effects of prorenin in vitro, argue against the combined application of (P)RR blockade and renin inhibition in diabetic retinopathy.

Citation: Batenburg WW, Verma A, Wang Y, Zhu P, van den Heuvel M, et al. (2014) Combined Renin Inhibition/(Pro)Renin Receptor Blockade in Diabetic Retinopathy- A Study in Transgenic (mREN2)27 Rats. PLoS ONE 9(6): e100954. doi:10.1371/journal.pone.0100954

Editor: Knut Stieger, Justus-Liebig-University Giessen, Germany

Received February 18, 2014; **Accepted** May 31, 2014; **Published** June 26, 2014

Funding: Supported in part by grants from American Diabetes Association, American Heart Association, Research to Prevent Blindness, NIH grants EY021752 and EY021721 Dr. Q. Li, and the Dutch Kidney Foundation to Dr. A. H.J. Danser (grant nr. C08.2246). The funders had no role in study design, data collection and analysis, decision to publish, or preparation of the manuscript.

Competing Interests: The authors have declared that no competing interests exist.

* Email: qli@ufl.edu

Introduction

Diabetic retinopathy (DR) is the most common diabetic microvascular complication and the leading cause of severe vision loss in people under the age of sixty [1]. The prevalence of DR increases with the duration of diabetes, and nearly all individuals with type 1 diabetes and more than 60% of those with type 2 diabetes have some form of retinopathy after 20 years [2,3].

Several molecular, biochemical and hemodynamic pathways have been identified to contribute to the pathogenesis of DR [4]. Hyperactivity of the renin-angiotensin system (RAS), resulting in elevated concentrations of its principal effector peptide, angiotensin (Ang) II, plays a key role in activating pathways leading to increased vascular inflammation, oxidative stress, endothelial dysfunction and tissue remodeling in variety of conditions, including diabetes and its associated complications [5,6]. As a result, RAS inhibitors are first-line therapeutic agents for treating patients with cardiovascular diseases, cardiometabolic syndrome and diabetes. Although the RAS was classically considered a circulating system having general systemic effects, it is now recognized that there are also local tissue RASs, for instance in the retina [7]. Activation of such local RASs may contribute to end-organ damage in diabetes and associated complications [7,8].

It has long been recognized that diabetes with microvascular complications is associated with increased plasma prorenin [9,10]. Relative to albumin, ocular fluids contain higher concentrations of prorenin than plasma, and ocular prorenin increases even further in diabetic patients with proliferative retinopathy [10–12]. This has led to the suggestion that prorenin may be a marker of diabetic complications [10]. Elevated prorenin may contribute to diabetic complications by binding to its putative receptor, the so-called (pro)renin receptor ((P)RR). Such binding activates prorenin, leading to increased angiotensin generation in target tissue and subsequent signaling by the classic RAS pathway [13]. In addition, binding of (pro)renin to the (P)RR also directly initiates a cascade

of signaling events involving mitogen-activated protein kinases such as ERK1/2 and p38, that are known to be associated with profibrotic and proliferative actions independent of Ang II [13,14]. The role of (P)RR in end-organ damage and diabetic complications is supported by several studies demonstrating that an inhibitor of (P)RR, a peptide derived from the prosegment of prorenin, the so-called handle-region peptide (HRP), afforded renal and cardiovascular protection [15,16], presumably by inhibiting the binding of prorenin to the (P)RR [17]. HRP has also been shown to be beneficial in ocular pathologies [18–21].

Aliskiren is the first renin inhibitor that blocks the activity of renin, a key rate-limiting enzyme in the first step of the RAS cascade [22]. It has shown high efficacy not only in controlling blood pressure [23], but also in renal and cardiovascular protection [24,25]. It is also effective in patients with metabolic syndrome, obesity and diabetes [26,27], as well as in experimental atherosclerosis [28,29]. Although aliskiren is able to bind to (P)RR-bound renin and prorenin [30–32], its role in (P)RR-mediated Ang II-independent signaling remains controversial with conflicting reports [33,34]. We have previously shown that HRP unexpectedly counteracted some of the beneficial effects of aliskiren [35,36]. In the present study, we investigated the effects of aliskiren on diabetes-induced retinopathy in a transgenic rat model overexpressing the mouse renin gene, i.e., the (mRen2)27 rat (Ren2 rat). This rat exhibits significantly elevated prorenin and Ang II levels, and displays increased PRR expression and severe hypertension [37–40]. After streptozotocin injection, these animals develop a diabetic phenotype that closely mimics that in diabetic patients, characterized by high prorenin levels, retinal pathology, vascular dysfunction and nephropathy [41,42]. We also examined the effects of HRP on top of renin inhibition with aliskiren. Our data show that renin inhibition with aliskiren reduced both neuronal and vascular pathologies in the diabetic Ren2 rat retina, and that HRP on top of aliskiren did not provide additional protection, nor counteracted the beneficial effects of aliskiren.

Materials and Methods

Animals and treatment groups

Adult heterozygous Ren2 rats (400–500 g) with a Sprague–Dawley (SD) background [36] were used in this study. Rats were housed in individual cages and maintained on a 12-h light/dark cycle, having access to standard laboratory rat chow and water ad libitum. All procedures were performed under the regulation and approval of the Animal Care Committee of the Erasmus MC. Blood pressure was measured by radiotelemetry transmitters that were implanted as described before [43] two weeks prior to diabetes induction. To induce diabetes, rats were fasted overnight and administered streptozotocin (STZ; 55 mg/kg i.p., Sigma–Aldrich, Zwijndrecht, The Netherlands). Blood glucose levels were checked by tail incision (Precision Xceed, Abbott, Zwolle, The Netherlands). Only rats with a glucose level >15 mmol/L were considered diabetic, and they subsequently received 2–4 U insulin per day (Levemir, Novo Nordisk, Denmark). Aliskiren (a gift of Novartis, 10 mg/kg per day) with (n = 8) or without (n = 7) rat HRP (NH_2- RILLKKMPSV-COOH, 1 mg/kg per day, Biosynthan, Berlin, Germany), or vehicle (saline, n = 8) were administered for 3 weeks by osmotic minipumps (2ML4 ALZET, Cupertino, USA) implanted subcutaneously two weeks after diabetes induction. In the animals receiving two drugs, two separate minipumps were implanted at both sides of the body. Eyes were collected at the end of the treatment period. For comparison, eyes were also collected from 9 untreated nondiabetic Ren2 rats, and 5 age-matched untreated SD rats.

Retinal histology and immunofluorescence

Eyes were fixed in 4% paraformaldehyde freshly made in phosphate-buffered saline (PBS) at 4°C overnight. Eyecups were cryoprotected in 30% sucrose/PBS for several hours or overnight prior to quick freezing in optical cutting temperature (OCT) compound. Then 12 μm thick sections were cut at –20 to –22°C. A rabbit polyclonal antibody against glial fibrillary acidic protein (GFAP, 1:1000, Sigma, St. Louis, MO), was used. The secondary antibody (conjugated with Alexa594) was from Molecular Probes (Invitrogen, Carlsbad, CA) and used according to the manufacturer's instruction. Sections were coverslipped using VECTASHIELD (Vector Laboratories, Burlingame, CA), and examined with a Zeiss (AxionVision, Carl Zeiss MicroImaging, Inc, NY) microscope equipped with epifluorescence illumination and a high resolution digital camera. For morphological analysis, eyes were fixed in 10% formalin solution, processed for paraffin embedding, sectioned at a thickness of 4 μm, and stained with hematoxylin and eosin (H&E). For quantitative measurement of retinal ganglion cell (RGC) density, the number of nuclei in the RGC layer was counted from at least 10 sections from each eye, 4 eyes from each group.

In situ cell death detection

To detect apoptotic cells, an In Situ Cell Death Detection Kit based on TUNEL technology (In Situ Cell Death Detection Kit, TMR red, Roche Applied Science, Indianapolis, IN, USA) was used according to the instructions supplied by the manufacturer.

Retinal vascular preparation and H&E staining

Retinal vasculature was prepared using method as described previously [44]. Briefly, eyes were fixed in 4% paraformaldehyde freshly made in PBS overnight. Retinas were dissected out from the eyecups and digested in 3% trypsin (GIBCO-BRL) for 2–3 hours at 37°C. Retinal vessels were separated from other retinal neuronal cells by gentle shaking and manipulation under a dissection microscope. The vessels were then mounted on a clean slide, allowed to dry, and stained with PAS-H&E (Periodic Acid Solution- Hematoxylin, Gill No.3, Sigma, St. Louis, MO) according to the instruction manual. After staining and washing in water, the tissue was dehydrated and mounted in permount mounting media. The prepared retinal vessels were photographed using a Zeiss microscope equipped with a high resolution digital camera (AxioCam MRC5, Zeiss Axionvert 200). Six to eight representative, non-overlapping fields from each quadrant of the retina were imaged. Acellular capillaries were counted from images for each retina, and expressed as number of acellular vessels per mm^2.

RT-PCR of inflammatory cytokines

Total RNA was isolated from freshly dissected retinas using Trizol Reagent (Invitrogen, Carlsbad, CA) according to the manufacturer's instruction. Reverse transcription was performed using Enhanced Avian HS RT-PCR kit (Sigma, St. Louis, MO) following the manufacturer's instructions. Real time PCR was carried out on a real time thermal cycler (iCycler, Bio-Rad Life Sciences) using iQTM Syber Green Supermix (Bio-Rad Life Sciences). The threshold cycle number (Ct) for real-time PCR was set by the cycler software. Optimal primer concentration for PCR was determined separately for each primer pair. The primer sequences used in this study are shown in Table 1. Each reaction was run in duplicate or in triplicate, and reaction tubes with target primers and those with GAPDH/actin primers were always included in the same PCR run. To test the primer efficiencies, the

one-step RT-PCR was run with each target primer. Relative quantification was achieved by the comparative 2-ΔΔCt method1. The relative increase/decrease (fold-induction/repression) of mRNA of target X in the experimental group (EG) was calculated using the control group as the calibrator: 2-ΔΔCt, where ΔΔ Ct is {Ct.x [EG] -Ct. GAPDH [EG]} - {Ct.x [control] - Ct. GAPDH [control]}.

Cell culture and treatment

Müller cells (a kind gift of Dr. G. Astrid Limb, UCL Institute of Ophthalmology, London, United Kingdom) [45] were cultured in 24-well plates with Dulbecco's Modified Eagle Medium (DMEM) (Thermo Fisher Scientific, Waltham, MA) containing 10% fetal bovine serum (FBS) (Thermo Fisher Scientific, Waltham, MA). The ON-Target plus (P)RR siRNA and scrambled control siRNA were from (Thermo Fisher Scientific, Waltham, MA). Different concentrations and incubation times of (P)RR-siRNA were pre-tested to determine the optimal concentration and incubation time according to the manufacturer's recommendation. Cells grown to 70% confluence in the serum medium were replaced by Opti-MEM I-reduced serum medium (Life Technologies, Carlsbad, CA), and the ON-Target plus (P)RR siRNA or control siRNA, or vehicle only was added into the medium at a final concentration of 30 nmol/L. After 24-hour incubation with the siRNA, the cells were replaced with serum-free DMEM medium (Thermo Fisher Scientific, Waltham, MA) for 2 hours. Following the serum starvation, the cells were either untreated (control) or treated with prorenin (100 nmol/L) alone, prorenin (100 nmol/L) + HRP (10 μmol/L, GenScript), prorenin + aliskiren (10 μmol/L), prorenin + HRP (10 μmol/L) + aliskiren (10 μmol/L), and prorenin (100 nmol/L) + losartan (10 μmol/L, according to previous studies [46]). After the 6 hour incubation, cells were harvested and total RNA was extracted, real time RT-PCR was performed and analyzed using the methods described previously.

Statistics

All values are presented as mean ± SD. Paired Student's t-test was used to assess significance between two groups. One-way ANOVA followed by the post hoc Tukey (Fisher's protected least significant difference) test was used to assess statistical significance between multiple groups. Differences were considered significant at $p<0.05$.

Results

Induction of diabetes mellitus and blood pressure

Blood glucose levels and mean arterial pressure (MAP) have been reported before [36] . In short, Ren2 rats had a normal blood glucose level, identical to that in Sprague–Dawley (SD) rats. STZ-induced diabetes mellitus increased blood glucose levels ~5-fold, and treatment with aliskiren or aliskiren+HRP did not alter this. Aliskiren lowered MAP in Ren2 rats from 123±4 mmHg to 104±5 mm Hg, and this effect was unaltered by simultaneous administration of HRP [47].

Retinal gliosis

Retinal gliosis, a salient feature of the retina under stress or injury including diabetic retinopathy, is characterized by elevated expression of the intermediate filament, glial fibrillary acidic protein (GFAP) in Müller cells and astrocytes. GFAP is normally predominantly expressed in astrocytes in the inner retinal fiber layer (Figure 1a, b). A slight increase of GFAP expression was observed in astrocytes of the retina of non-diabetic Ren2 rats, but this was not different from the wildtype SD rat retina (Figure 1c, d). GFAP expression was elevated in the diabetic Ren2 rat retina (Figure 1e, f), and aliskiren prevented this elevation, both without (Figure 1g, h) and with HRP (Figure 1i, j).

Apoptosis and RGC loss

In the SD rat retina, very few apoptotic cells could be detected (data not shown). The Ren2 rat retina showed a significant increase of TUNEL positive apoptotic cells in both inner retina

Table 1. Primers used for Real-Time RT-PCR analysis.

Gene name	Accession #	Sequences
Rat VEGF	NM_031836	Forward: 5′ -TGCACCCACGACAGAAGGGGA-3′
		Reverse: 5′-TCACCGCCTTGGCTTGTCACAT-3′
Rat MCP1	NM_031530	Forward: 5′ -GCAGCAGGTGTCCCAAAGAAGCT-3′
		Reverse: 5′-AGAAGTGCTTGAGGTGGTTGTGGAA-3′
Rat ICAM1	NM_012967	Forward: 5′ -CCCCACCTACATACATTCCTAC-3′
		Reverse: 5′-ACATTTTCTCCCAGGCATTC-3′
Rat TNFα	NM_012675	Forward: 5′ -CCTTATCTACTCCCAGGTTCTC-3′
		Reverse: 5′-TTTCTCCTGGTATGAAATGGC-3′
Rat GAPDH	AF106860	Forward: 5′ -TGCTGGGGCTGGCATTGCTC-3′
		Reverse: 5′- CCCCAGGCCCCTCCTGTTGT-3′
Human IL-1α	NM_000575	Forward: 5′-ATCAGTACCTCACGGCTGCT-3′
		Reverse: 5′-TGGGTATCTCAGGCATCTCC-3′
Human TNFα	NM_000594	Forward: 5′-ATCTACTCCCAGGTCCTCTTCAA-3′
		Reverse: 5′-GCAATGATCCCAAAGTAGACCT-3′
Human β actin	NM_001101	Forward: 5′-GCAGGAGTATGACGAGTCCG-3′
		Reverse: 5′-AGGGACTTCCTGTAACAATGC-3′

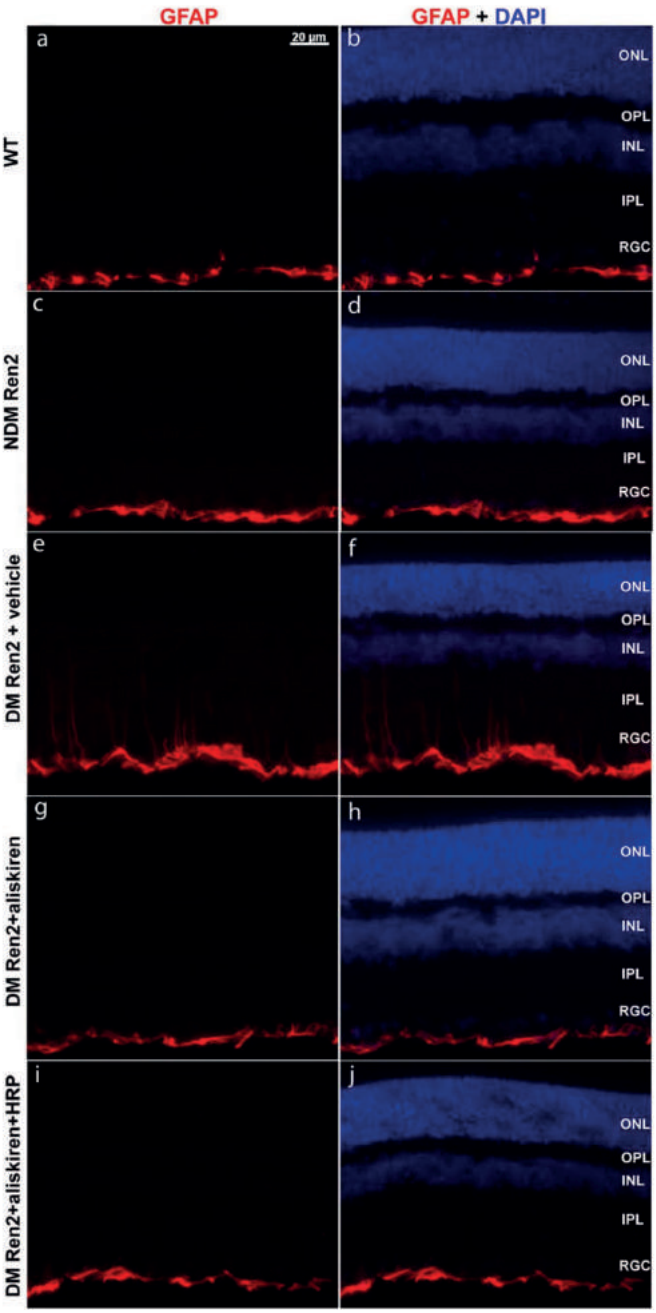

Figure 1. Immunofluorescence detection of GFAP expression in the retinas of wildtype (WT) Sprague–Dawley rats, non-diabetic (NDM) Ren2, diabetic (DM) Ren2 rats treated with vehicle, aliskiren or aliskiren+HRP. ONL: outer nuclear layer; OPL: outer plexiform layer; INL: inner nuclear layer; IPL: inner plexiform layer; RGC: retinal ganglion cell layer.

and photoreceptor layer (Figure 2a, b), and this increase was more prominent in the peripheral retina (Figure 2b) compared with the central retina (Figure 2a). This increase in apoptotic cells was dramatically further exacerbated in the diabetic Ren2 rat retina (Figure 2c, d). Treatment with either aliskiren alone or aliskiren+HRP significantly reduced apoptotic cell death to levels in the SD rat retina (Figure 2e, f, g). Morphologically the central retina of non-diabetic Ren2 rat is indistinguishable from wild type rat retina, however there is significant cell loss in the retinal ganglion cell (RGC) layer in peripheral retina (Figure 3). The diabetic Ren2 rat retina showed significantly increased cell loss in the RGC layer, which was more profound in the peripheral retina. The cell loss was normalized by either aliskiren or aliskiren+HRP treatment (Figure 3).

Retinal capillaries

The Ren2 rat retina showed an increased loss of capillaries compared to age-matched SD rat retinas (Figure 4A and B), and this loss was further exacerbated in diabetic Ren2 rat retinas (Figure 4C). Aliskiren reduced the acellular capillaries to the level seen in non-diabetic Ren2 rat retina (Figure 4D), but the number of acellular capillaries was still significantly higher compared to that of the SD retina. HRP treatment in combination with aliskiren did not add additional protection against capillary loss (Figure 4E). Figure 4F displays these results in a quantitative manner.

Retinal inflammatory cytokines

Inflammatory cytokine expression in the retina was evaluated by real-time RT-PCT. VEGF expression was increased >2-fold in the Ren2 rat retina compared to age-matched SD rat retinas, and this increase was even larger in diabetic Ren2 rat retinas. Treatment with either aliskiren alone or combined with HRP reduced VEGF to non-diabetic Ren2 rat levels (Figure 5). MCP-1 expression was also significantly increased in Ren2 rat retinas with or without diabetes mellitus and aliskiren alone or in combination with HRP normalized this (Figure 5). A significant increase of ICAM1 was only seen in diabetic Ren2 rat retinas, and both aliskiren and aliskiren+HRP normalized this (Figure 5). TNFα expression was also highly increased in the Ren2 rat retina, and diabetes mellitus further upregulated this. Aliskiren significantly reduced TNFα to non-diabetic Ren2 rat levels. Aliskiren+HRP tended to reduce this even further, but the difference versus aliskiren was not statistically significant.

Increased cytokine expression stimulated by recombinant prorenin in cultured human Müller glial cells and blockade by HRP and aliskiren

Müller cells, which span the entire neural retina, are the primary glial cell of the retina. They not only provide architectural support of the neural layers, but also have multiple functions such as providing metabolic support to energy-demanding retinal neurons, regulation of retinal synaptic activity by neurotransmitter recycling, and regulation of retinal water and ion homeostasis [48,49]. Müller cells are intimately connected with retinal endothelial cells, pericytes, and astrocytes and play a crucial role to establish and maintain the blood–retinal barrier (BRB) [48,49]. In addition, Müller cells modulate retinal immunity [50]. Moreover, Müller cells express several RAS components [7,51], including (pro)renin [52] and its receptor (P)RR, so that Müller cell dysfunction might contribute to ocular dysregulation in diabetes [18,21,53,54]. In fact, ocular prorenin upregulation is known to occur in patients with proliferative [10–12]. Prorenin was previously shown to increase proinflammatory cytokine expression in cultured neurons [55], To determine whether prorenin is also able to increase the expression of proinflammatory cytokines in Müller cells, cultured Müller cells were treated with prorenin, with and without HRP, aliskiren and/or the AT1R blocker losartan. The expression levels of IL-1α and TNF-α at 6 hours after the prorenin treatment were examined. Our results showed that the prorenin treatment significantly increased the expression of IL-1α (by ~12-fold) TNF-α (by ~3-fold) (Figure 6). Both aliskiren and HRP when given separately completely blocked these increases, and the results were identical when given in combination. Losartan treatment also completely blocked prorenin stimulated increased expression of IL-1α and TNF-α (Figure 6), suggesting that the increased expression of these cytokines is Ang II- dependent. (P)RR-siRNA completely blocked the prorenin stimulated increase of these cytokines, whereas the control scrambled siRNA had no effect (Figure 6), suggesting that the prorenin stimulated, Ang II-dependent increase in cytokine expression in Müller cells involves (P)RR binding.

Discussion

The present study demonstrates that the Ren2 rat retina exhibited increased capillary loss and inflammatory cytokine expressions, and neuronal apoptotic cells. Diabetes mellitus further exacerbated these changes and enhanced gliosis. Renin inhibition counterbalanced these phenomena, whereas (P)RR blockade on top of renin inhibition did not offer additional advantages. The protective effect of aliskiren on retinal vasculopathy and inflammation in diabetic Ren2 rats is consistent with a previous report [56]. Diabetic retinopathy is not only associated with vascular dysfunction, but also with a loss of retinal neurons [57]. Our study further showed that aliskiren treatment normalized both photoreceptor and RGC loss in Ren2 rats to wildtype (SD rat) level.

Elevated plasma prorenin levels associate with microvascular complications in patients with diabetes mellitus. Prorenin is also highly elevated in ocular fluid in patients with diabetic retinopathy and its level correlates with the severity of DR in diabetic patients [10,11]. Prorenin may contribute to diabetic complication and end-organ damage by binding to the (P)RR, resulting in increased generation of Ang II by the classic RAS pathway at the cell/tissue level [13]. Alternatively, such binding may initiate a cascade of signaling events that are associated with profibrotic and proliferative actions, independent of Ang II [13]. To what degree prorenin-(P)RR interaction is physiologically relevant, given the nanomolar prorenin levels (i.e., several orders above its normal plasma levels) that are required for such interaction, is still a matter of debate [58]. Nevertheless, since the eye is a prorenin-producing organ, with Müller cells releasing prorenin in the retina [52], if anywhere, such interaction might occur at ocular sites.

The importance of the (P)RR in the pathogenesis of end-stage organ damage in diabetes and hypertension has been demonstrated by in vitro and in vivo animal studies using HRP, the only (P)RR blocker that is currently available [15]. The possible

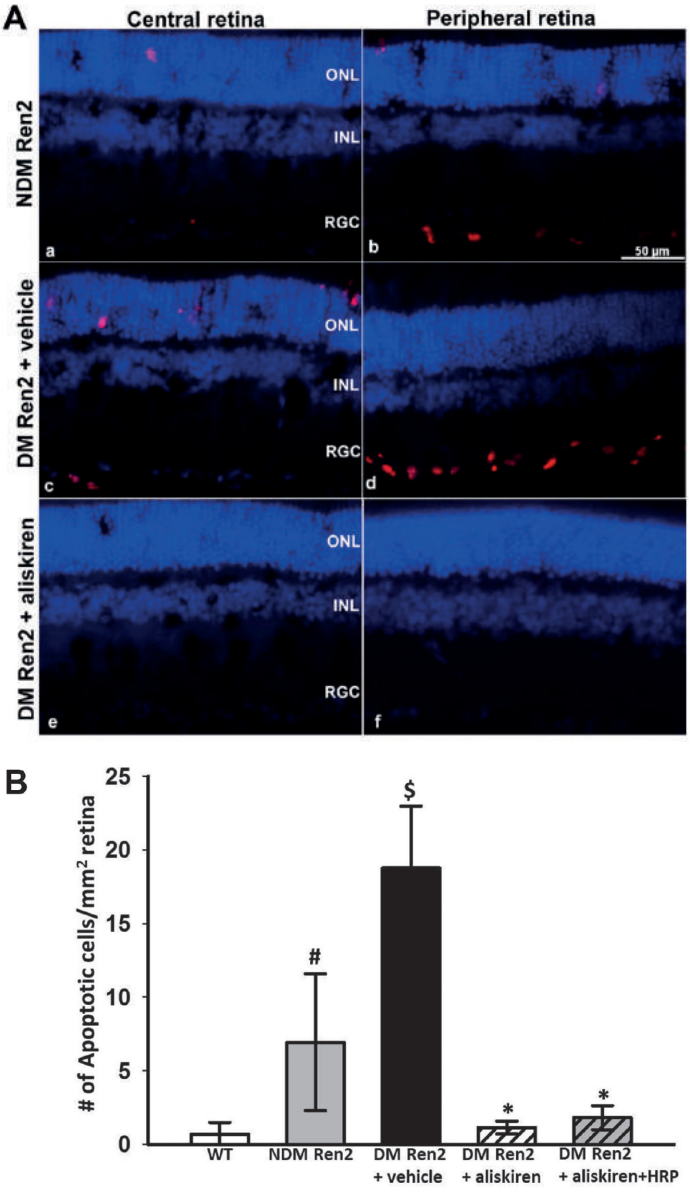

Figure 2. In situ cell death detection in the retina. A, Apoptotic cells were detected in situ by TUNEL assay in the retinas from non-diabetic (NDM) Ren2 rats (a & b), diabetic (DM) Ren2 rats treated with vehicle (c & d), and aliskiren (e & f). ONL: outer nuclear layer; INL: inner nuclear layer; RGC: retinal ganglion cell layer. B, Quantitative measurement of apoptotic cells detected by TUNEL assay. #p<0.01 (vs. wildtype (WT) Sprague–Dawley rats); $p<0.01 (vs. NDM Ren2 and WT); *p<0.01 (vs. NDM Ren2 and DM Ren2+ vehicle).

pathological role of the PRR in the retina has been established by several reports in which HRP was shown to prevent pathological angiogenesis [18,21], and ocular inflammation induced by endotoxin [20] and diabetes [19]. It was thus expected that blockade of both the Ang II-dependent pathway (by aliskiren) and the (P)RR-mediated, Ang II-independent pathway (by HRP) would provide better protection against diabetes-induced retinal pathophysiology. However, the present study showed that HPR

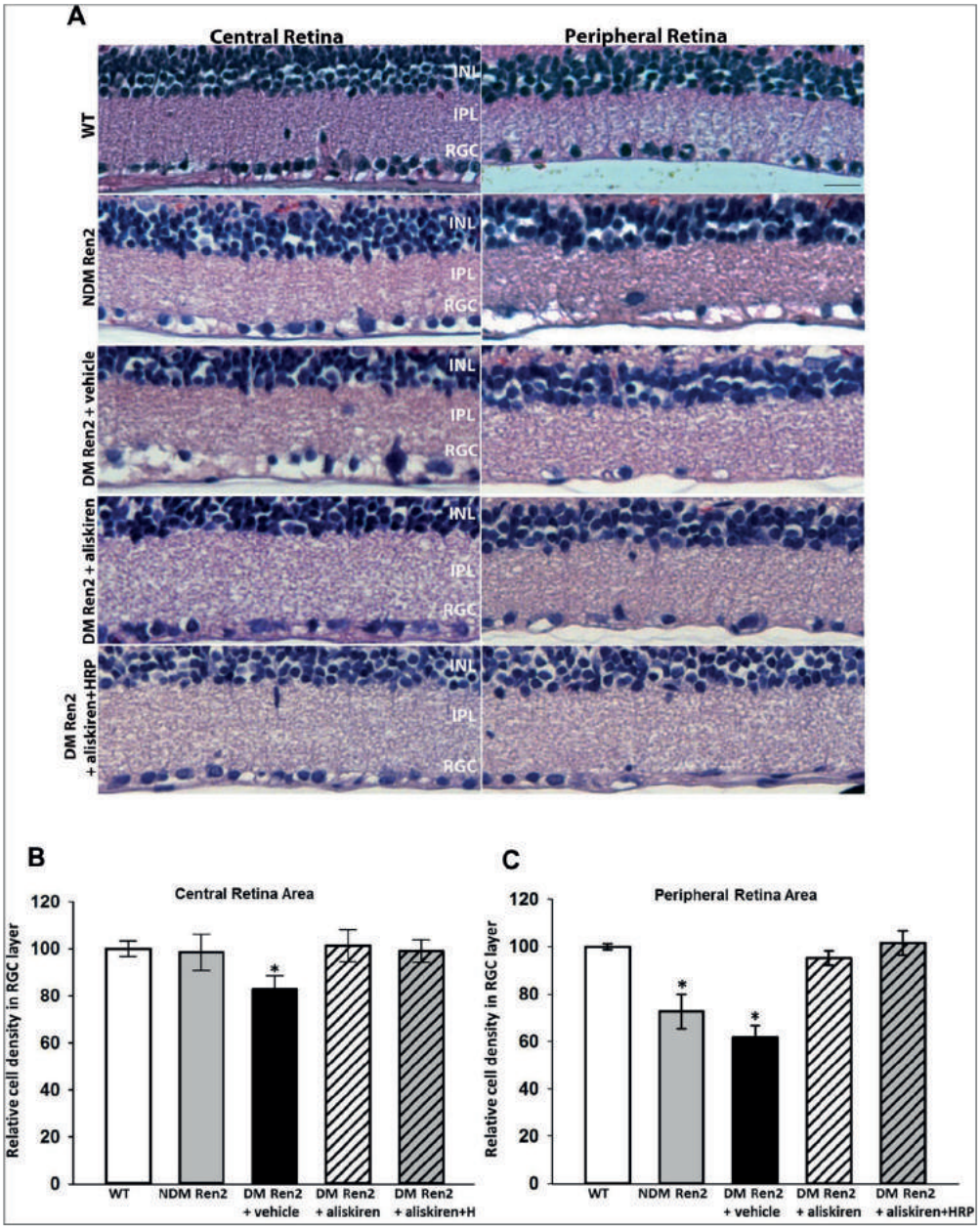

Figure 3. Representative retinal micrographs of wildtype (WT) Sprague–Dawley rats, non-diabetic (NDM) Ren2 rats, and diabetic (DM) Ren2 rats treated with vehicle, aliskiren or aliskiren+HRP (A). INL: inner nuclear layer; IPL: inner plexiform layer; RGC: retinal ganglion cell layer. Quantitative measurement of cell density in RGC layer in the central (B) and peripheral (C) retinas of wildtype (WT) Sprague–Dawley rats, non-diabetic (NDM) Ren2 rats, and diabetic (DM) Ren2 rats treated with vehicle, aliskiren or aliskiren+HRP. N = 4. *$p<0.01$ (vs. WT).

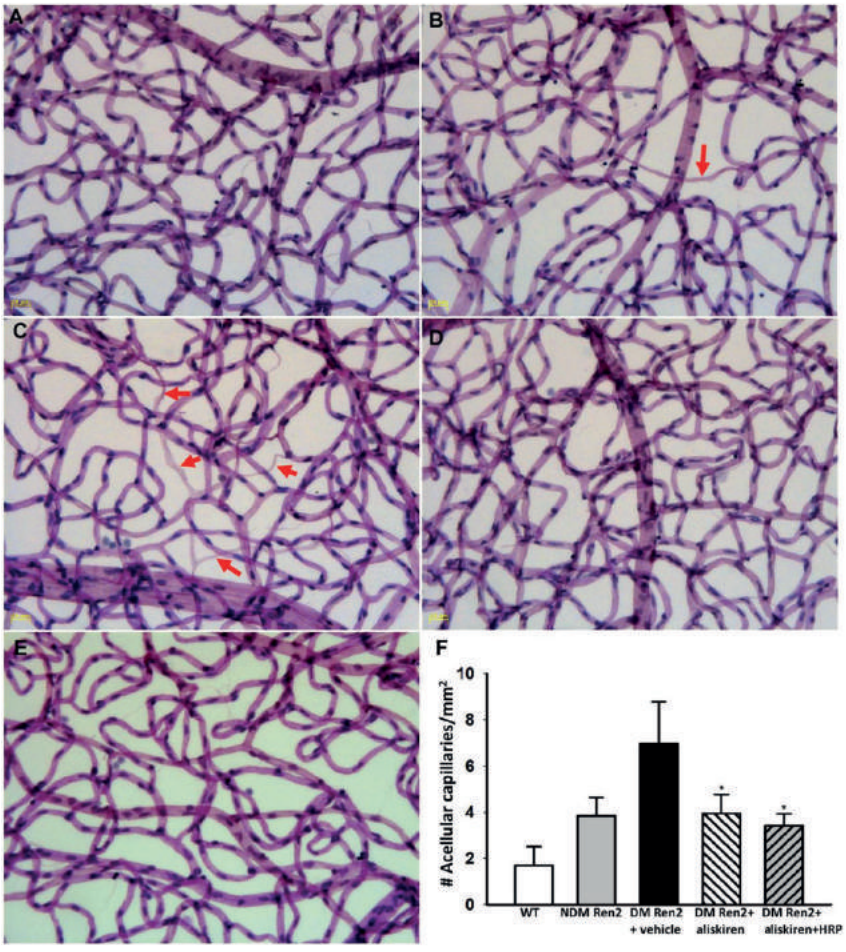

Figure 4. Representative capillary images of wildtype (WT) Sprague–Dawley rats (A), non-diabetic (NDM) Ren2 rats (B), and diabetic (DM) Ren2 rats treated with vehicle (C), aliskiren (D) or aliskiren+HRP (E). Diabetic Ren2 rat retinas showed further increased acellular capillaries (arrow) and both aliskiren and aliskiren+HRP reduced this. F: Quantitative measurements of acellular capillaries. *P<0.01 (vs. DM Ren2+ vehicle group).

did not provide additional beneficial effects on top of aliskiren. In part, this is due to the fact that, with regard to at least some parameters, aliskiren already provided maximal benefit. This would suggest that prorenin-dependent effects, if present, might be largely due to activation of the Ang II-AT_1 receptor axis. Obviously, aliskiren will block angiotensin generation by receptor-bound prorenin (or renin) [31,32]. In addition, renin inhibition may lower (P)RR expression [33], thus potentially diminishing the capacity of HRP to exert an effect at all. It is unlikely that aliskiren blocked renin/prorenin-(P)RR interaction, since renin/prorenin binding to the (P)RR was unaltered in the presence of aliskiren, while aliskiren also did not affect (pro)renin-induced signaling [58,59].

We previously reported that aliskiren normalized vascular dysfunction in diabetic hypertensive rats, while HRP unexpectedly counteracted these beneficial vascular effects in a blood pressure- and angiotensin-independent manner [35,36]. This may be explained on the basis of partial agonism of HRP towards the (P)RR [21,60]. Intriguingly, although HRP did not exert beneficial effects on top of aliskiren in the diabetic Ren2 rat retina, it also did not counteract the protective ocular effects of aliskiren. Thus, possibly the retinal levels of HRP (when administered systemically) were not sufficiently high to generate similar counteracting effects. Yet, when infused at similar doses alone, HRP did exert beneficial effects in the diabetic eye [21]. It cannot be excluded that such effects are (P)RR-independent, but if so, they can apparently no longer be seen on top of RAS blockade.

Hypertension plays an important role in retinal pathophysiology and is one of the major risk factors that exacerbates the initiation and progression of DR [1]. As shown in our previous report [36], diabetic Ren2 rats displayed severely elevated blood pressure; aliskiren normalized blood pressure, suppressed renin activity, and

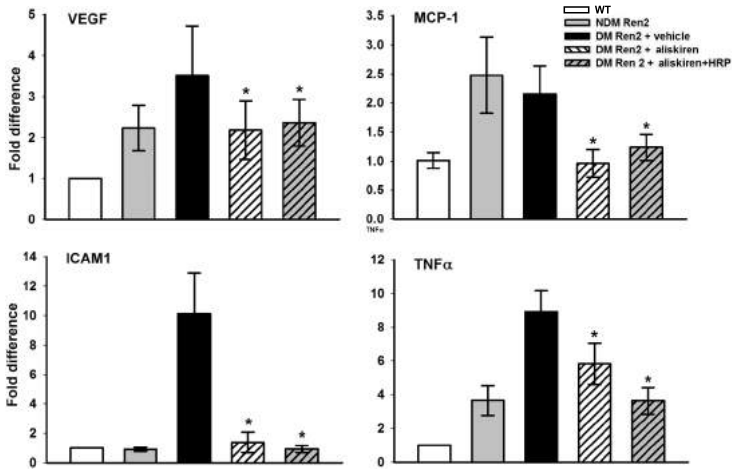

Figure 5. Real-time RT-PCR analysis of retinal expression of inflammatory cytokines: VEGF, MCP1, ICAM1 and TNFα. Values on y-axis represent fold change in mRNA levels compared to WT (normalized as 1). *P<0.01 (vs. DM Ren2+vehicle group). WT, wildtype, DM/NDM, diabetic/nondiabetic. N = 5.

reversed vascular dysfunction, whereas HRP did not affect the blood pressure-lowering effects of aliskiren [15,35,61]. The beneficial effects of aliskiren in the diabetic Ren2 rat retina may be due to its blood pressure-lowering effect and associated improvement of renal and other systemic cardiovascular function. However, in a previous study in the same model, ACE inhibition resulted in better blood pressure control, while aliskiren provided greater retinal protection [56]. This strongly suggests that the beneficial effects of renin inhibition extend beyond the blood pressure-lowering effects of aliskiren. Clearly, this needs to be tested in normotensive animal models of diabetic retinopathy in future studies.

In cultured Müller cells, prorenin significantly increased the expression levels of IL-1α and TNF-α, consistent with previous observations [55]. Both aliskiren and HRP completely blocked these effects as did treatment with (P)RR siRNA and the AT1R blocker losartan. This suggests that these prorenin-induced effects are entirely (P)RR- and Ang II-dependent, i.e., involve Ang II generation by (P)RR-bound prorenin, identical to the prorenin-dependent Ang II generation described earlier in vascular smooth muscle cells [58]. Possibly, such generation also contributes to the elevated ocular Ang II levels under many pathological conditions [10–12,51,62–64].

Recent evidence clearly indicates the (P)RR as multi-functional receptor, affecting a wide range of signaling pathways, many of which are not necessarily related to prorenin and Ang II/AT1R signaling. In fact, a truncated form of (P)RR at the C-terminal region was previously described as a vacuolar H^+ -ATPase (V-

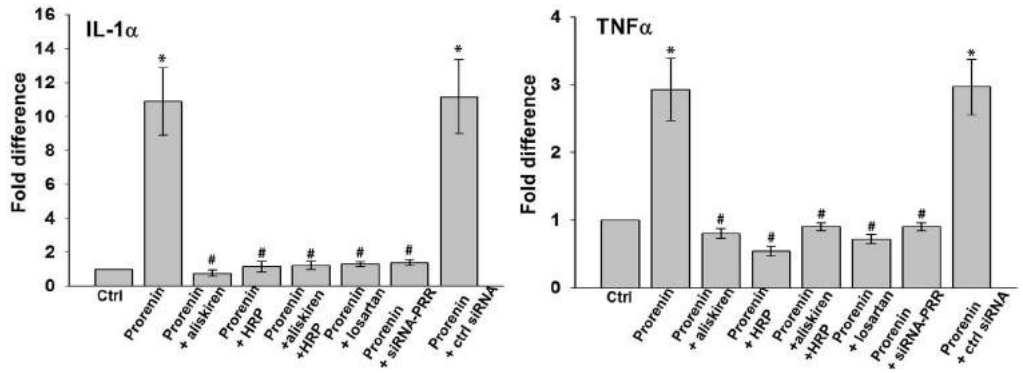

Figure 6. Real-time RT-PCR analysis of the expression of inflammatory cytokines IL-1α and TNF-α in cultured Müller cells. Values on y-axis represent fold change in mRNA levels compared to control (non-treated, normalized as 1). *P<0.01 (vs. control); # P<0.01 (vs. prorenin treated group). N = 4.

ATPase) associated protein (Atp6ap2), and the (P)RR may thus also affect V-ATPase activity [65]. Such activity determines the intracellular pH homeostasis that is critical in diverse physiological cellular functions including endocytosis, processing of proteins and signaling molecules, membrane sorting and trafficking, activation of lysosomal and autophagosomal enzymes, and patterning during development [66,67]. Consequently, it is conceivable that the (P)RR contributes not only to tissue RAS activation but also to multiple molecular and cellular processes via its V-ATPase connection. Further studies are required to further elucidate whether prorenin affects these functions.

In conclusion, the renin inhibitor aliskiren reduced both neuronal and vascular pathologies, including retinal gliosis, apoptotic cell death of retinal neurons, acellular capillaries and expression of inflammatory cytokines in diabetic mRen2 rats. The putative (P)RR blocker HRP did not provide add-on beneficial effects when combined with aliskiren, nor counteracted the effects of aliskiren in the retina of diabetic mRen2 rats. The latter contrasts with earlier observations in the kidney of diabetic mRen2 rats, where HRP counteracted the beneficial effects of aliskiren [47]. The former agrees with our in-vitro studies in Müller cells, showing prorenin-induced effects that are entirely Ang II-dependent. Taken together, these results suggest that aliskiren is a promising treatment option for patients with diabetic retinopathy, and that its combination with HRP in this condition is not advisable.

Author Contributions

Conceived and designed the experiments: AHJD QL. Performed the experiments: WWB MVH RV AV YW PZ. Analyzed the data: AHJD QL AV. Wrote the paper: AHJD QL.

References

1. Yau JW, Rogers SL, Kawasaki R, Lamoureux EL, Kowalski JW, et al. (2012) Global prevalence and major risk factors of diabetic retinopathy. Diabetes Care 35: 556–564.
2. Fong DS, Aiello L, Gardner TW, King GL, Blankenship G, et al. (2004) Retinopathy in diabetes. Diabetes Care 27 Suppl 1: S84–87.
3. Williams R, Airey M, Baxter H, Forrester J, Kennedy-Martin T, et al. (2004) Epidemiology of diabetic retinopathy and macular oedema: a systematic review. Eye 18: 963–983.
4. Ola MS, Nawaz MI, Siddiquei MM, Al-Amro S, Abu El-Asrar AM (2012) Recent advances in understanding the biochemical and molecular mechanism of diabetic retinopathy. J Diabetes Complications 26: 56–64.
5. Cohn JN (2010) Role of the renin-angiotensin system in cardiovascular disease. Cardiovasc Drugs Ther 24: 341–344.
6. Ghattas A, Lip PL, Lip GY (2011) Renin-angiotensin blockade in diabetic retinopathy. Int J Clin Pract 65: 113–116.
7. Fletcher EL, Phipps JA, Ward MM, Vessey KA, Wilkinson-Berka JL (2010) The renin-angiotensin system in retinal health and disease: Its influence on neurons, glia and the vasculature. Prog Retin Eye Res: 1–28.
8. Hanes DS, Nahar A, Weir MR (2004) The tissue renin-angiotensin-aldosterone system in diabetes mellitus. Curr Hypertens Rep 6: 98–105.
9. Luetscher JA, Kraemer FB, Wilson DM (1989) Prorenin and vascular complications of diabetes. Am J Hypertens 2: 382–386.
10. Luetscher JA, Kraemer FB, Wilson DM, Schwartz HC, Bryer-Ash M (1985) Increased plasma inactive renin in diabetes mellitus. A marker of microvascular complications. N Engl J Med 312: 1412–1417.
11. Danser AH, van den Dorpel MA, Deinum J, Derkx FH, Franken AA, et al. (1989) Renin, prorenin, and immunoreactive renin in vitreous fluid from eyes with and without diabetic retinopathy. J Clin Endocrinol Metab 68: 160–167.
12. Franken AA, Derkx FH, Schalekamp MA, Man in t'Veld AJ, Hop WC, et al. (1988) Association of high plasma prorenin with diabetic retinopathy. J Hypertens Suppl 6: S461–463.
13. Nguyen G, Delarue F, Burckle C, Bouzhir L, Giller T, et al. (2002) Pivotal role of the renin/prorenin receptor in angiotensin II production and cellular responses to renin. J Clin Invest 109: 1417–1427.
14. Huang Y, Wongamorntham S, Kasting J, McQuillan D, Owens RT, et al. (2006) Renin increases mesangial cell transforming growth factor-beta1 and matrix proteins through receptor-mediated, angiotensin II-independent mechanisms. Kidney Int 69: 105–113.
15. Ichihara A, Hayashi M, Kaneshiro Y, Suzuki F, Nakagawa T, et al. (2004) Inhibition of diabetic nephropathy by a decoy peptide corresponding to the "handle" region for nonproteolytic activation of prorenin. J Clin Invest 114: 1128–1135.
16. Ichihara A, Suzuki F, Nakagawa T, Kaneshiro Y, Takemitsu T, et al. (2006) Prorenin receptor blockade inhibits development of glomerulosclerosis in diabetic angiotensin II type 1a receptor-deficient mice. J Am Soc Nephrol 17: 1950–1961.
17. Suzuki F, Hayakawa M, Nakagawa T, Nasir UM, Ebihara A, et al. (2003) Human prorenin has "gate and handle" regions for its non-proteolytic activation. J Biol Chem 278: 22217–22222.
18. Satofuka S, Ichihara A, Nagai N, Koto T, Shinoda H, et al. (2007) Role of nonproteolytically activated prorenin in pathologic, but not physiologic, retinal neovascularization. Invest Ophthalmol Vis Sci 48: 422–429.
19. Satofuka S, Ichihara A, Nagai N, Noda K, Ozawa Y, et al. (2009) (Pro)renin receptor-mediated signal transduction and tissue renin-angiotensin system contribute to diabetes-induced retinal inflammation. Diabetes 58: 1625–1633.
20. Satofuka S, Ichihara A, Nagai N, Yamashiro K, Koto T, et al. (2006) Suppression of ocular inflammation in endotoxin-induced uveitis by inhibiting nonproteolytic activation of prorenin. Invest Ophthalmol Vis Sci 47: 2686–2692.
21. Wilkinson-Berka JL, Heine R, Tan G, Cooper ME, Hatzopoulos KM, et al. (2010) RILLKKMPSV influences the vasculature, neurons and glia, and (pro)renin receptor expression in the retina. Hypertension 55: 1454–1460.
22. Jadhav M, Yeola C, Zope G, Nabar A (2012) Aliskiren, the first direct renin inhibitor for treatment of hypertension: the path of its development. J Postgrad Med 58: 32–38.
23. Gradman AH, Kad R (2008) Renin inhibition in hypertension. J Am Coll Cardiol 51: 519–528.
24. Pilz B, Shagdarsuren E, Wellner M, Fiebeler A, Dechend R, et al. (2005) Aliskiren, a human renin inhibitor, ameliorates cardiac and renal damage in double-transgenic rats. Hypertension 46: 569–576.
25. Kelly DJ, Zhang Y, Moe G, Naik G, Gilbert RE (2007) Aliskiren, a novel renin inhibitor, is renoprotective in a model of advanced diabetic nephropathy in rats. Diabetologia 50: 2398–2404.
26. Whaley-Connell A, Habibi J, Rehmer N, Ardhanari S, Hayden MR, et al. (2013) Renin Inhibition and ATR blockade improve metabolic signaling, oxidant stress and myocardial tissue remodeling. Metabolism 62: 861–872.
27. Chou CL, Pang CY, Lee TJ, Fang TC (2013) Direct renin inhibitor prevents and ameliorates insulin resistance, aortic endothelial dysfunction and vascular remodeling in fructose-fed hypertensive rats. Hypertens Res 36: 123–128.
28. Nussberger J, Aubert JF, Bouzourene K, Pellegrin M, Hayoz D, et al. (2008) Renin inhibition by aliskiren prevents atherosclerosis progression: comparison with irbesartan, atenolol, and amlodipine. Hypertension 51: 1306–1311.
29. Lu H, Rateri DL, Feldman DL, Jr RJ, Fukamizu A, et al. (2008) Renin inhibition reduces hypercholesterolemia-induced atherosclerosis in mice. J Clin Invest 118: 984–993.
30. Biswas KB, Nabi AH, Arai Y, Nakagawa T, Ebihara A, et al. (2010) Aliskiren binds to renin and prorenin bound to (pro)renin receptor in vitro. Hypertens Res 33: 1053–1059.
31. Batenburg WW, Danser AJ (2008) Prorenin and the (pro)renin receptor: binding kinetics, signalling and interaction with aliskiren. J Renin Angiotensin Aldosterone Syst 9: 181–184.
32. Batenburg WW, de Bruin RJ, van Gool JM, Muller DN, Bader M, et al. (2008) Aliskiren-binding increases the half life of renin and prorenin in rat aortic vascular smooth muscle cells. Arterioscler Thromb Vasc Biol 28: 1151–1157.
33. Ferri N, Greco CM, Maiocchi G, Corsini A (2011) Aliskiren reduces prorenin receptor expression and activity in cultured human aortic smooth muscle cells. J Renin Angiotensin Aldosterone Syst 12: 469–474.
34. Sakoda M, Ichihara A, Kurauchi-Mito A, Narita T, Kinouchi K, et al. (2010) Aliskiren inhibits intracellular angiotensin II levels without affecting (pro)renin receptor signals in human podocytes. Am J Hypertens 23: 575–580.
35. van Esch JH, van Veghel R, Garrelds IM, Leijten F, Bouhuizen AM, et al. (2011) Handle region peptide counteracts the beneficial effects of the Renin inhibitor aliskiren in spontaneously hypertensive rats. Hypertension 57: 852–858.
36. Batenburg WW, van den Heuvel M, van Esch JH, van Veghel R, Garrelds IM, et al. (2013) The (pro)renin receptor blocker handle region peptide upregulates endothelium-derived contractile factors in aliskiren-treated diabetic transgenic (mREN2)27 rats. J Hypertens 31: 292–302.
37. Lee MA, Bohm M, Paul M, Bader M, Ganten U, et al. (1996) Physiological characterization of the hypertensive transgenic rat TGR(mREN2)27. Am J Physiol 270: E919–929.
38. Campbell DJ, Rong P, Kladis A, Rees B, Ganten D, et al. (1995) Angiotensin and bradykinin peptides in the TGR(mRen-2)27 rat. Hypertension 25: 1014–1020.
39. Feldman DL, Jin L, Xuan H, Contrepas A, Zhou Y, et al. (2008) Effects of aliskiren on blood pressure, albuminuria, and (pro)renin receptor expression in diabetic TG(mRen-2)27 rats. Hypertension 52: 130–136.
40. Mullins JJ, Peters J, Ganten D (1990) Fulminant hypertension in transgenic rats harbouring the mouse Ren-2 gene. Nature 344: 541–544.

41. Moravski CJ, Skinner SL, Stubbs AJ, Sarlos S, Kelly DJ, et al. (2003) The renin-angiotensin system influences ocular endothelial cell proliferation in diabetes: transgenic and interventional studies. Am J Pathol 162: 151–160.
42. Kelly DJ, Wilkinson-Berka JL, Allen TJ, Cooper ME, Skinner SL (1998) A new model of diabetic nephropathy with progressive renal impairment in the transgenic (mRen-2)27 rat (TGR). Kidney Int 54: 343–352.
43. van Esch JH, Moltzer E, van Veghel R, Garrelds IM, Leijten F, et al. (2010) Beneficial cardiac effects of the renin inhibitor aliskiren in spontaneously hypertensive rats. J Hypertens 28: 2145–2155.
44. Li Q, Verma A, Han PY, Nakagawa T, Johnson RJ, et al. (2010) Diabetic eNOS-knockout mice develop accelerated retinopathy. Invest Ophthalmol Vis Sci 51: 5240–5246.
45. Limb GA, Salt TE, Munro PM, Moss SE, Khaw PT (2002) In vitro characterization of a spontaneously immortalized human Muller cell line (MIO-M1). Invest Ophthalmol Vis Sci 43: 864–869.
46. Lanz TV, Ding ZQ, Ho PP, Luo JA, Agrawal AN, et al. (2010) Angiotensin II sustains brain inflammation in mice via TGF-beta. Journal of Clinical Investigation 120: 2782–2794.
47. Te Riet L, van den Heuvel M, Peutz-Kootstra CJ, van Esch JH, van Veghel R, et al. (2014) Deterioration of kidney function by the (pro)renin receptor blocker handle region peptide in aliskiren-treated diabetic transgenic (mRen2)27 rats. Am J Physiol Renal Physiol 306: F1179–1189.
48. Bringmann A, Wiedemann P (2012) Muller glial cells in retinal disease. Ophthalmologica 227: 1–19.
49. Reichenbach A, Bringmann A (2013) New functions of Muller cells. Glia 61: 651–678.
50. Kumar A, Pandey RK, Miller LJ, Singh PK, Kanwar M (2013) Muller glia in retinal innate immunity: a perspective on their roles in endophthalmitis. Crit Rev Immunol 33: 119–135.
51. Wilkinson-Berka JL, Agrotis A, Deliyanti D (2012) The retinal renin-angiotensin system: roles of angiotensin II and aldosterone. Peptides 36: 142–150.
52. Berka JL, Stubbs AJ, Wang DZ, DiNicolantonio R, Alcorn D, et al. (1995) Renin-containing Muller cells of the retina display endocrine features. Invest Ophthalmol Vis Sci 36: 1450–1458.
53. Wilkinson-Berka JL, Miller AG, Fletcher EL (2010) Prorenin and the (pro)renin receptor: do they have a pathogenic role in the retina? Front Biosci (Elite Ed) 2: 1054–1064.
54. Yokota H, Takamiya A, Nagaoka T, Hikichi T, Ishida Y, et al. (2008) Role of prorenin in the pathogenesis of retinal neovascularization. Hokkaido Igaku Zasshi 83: 159–165.
55. Zubcevic J, Jun JY, Lamont G, Murca TM, Shi P, et al. (2013) Nucleus of the solitary tract (pro)renin receptor-mediated antihypertensive effect involves nuclear factor-kappaB-cytokine signaling in the spontaneously hypertensive rat. Hypertension 61: 622–627.
56. Wilkinson-Berka JL, Tan G, Binger KJ, Sutton L, McMaster K, et al. (2011) Aliskiren reduces vascular pathology in diabetic retinopathy and oxygen-induced retinopathy in the transgenic (mRen-2)27 rat. Diabetologia 54: 2724–2735.
57. Barber AJ, Lieth E, Khin SA, Antonetti DA, Buchanan AG, et al. (1998) Neural apoptosis in the retina during experimental and human diabetes. Early onset and effect of insulin. J Clin Invest 102: 783–791.
58. Batenburg WW, Lu X, Leijten F, Maschke U, Muller DN, et al. (2011) Renin- and prorenin-induced effects in rat vascular smooth muscle cells overexpressing the human (pro)renin receptor: does (pro)renin-(pro)renin receptor interaction actually occur? Hypertension 58: 1111–1119.
59. Batenburg WW, Krop M, Garrelds IM, de Vries R, de Bruin RJ, et al. (2007) Prorenin is the endogenous agonist of the (pro)renin receptor. Binding kinetics of renin and prorenin in rat vascular smooth muscle cells overexpressing the human (pro)renin receptor. J Hypertens 25: 2441–2453.
60. Lu X, Garrelds IM, Wagner CA, Danser AH, Meima ME (2013) (Pro)renin Receptor is Required for Prorenin-Dependent and -Independent Regulation of Vacuolar H+-ATPase Activity in MDCK.C11 Collecting Duct Cells. Am J Physiol Renal Physiol.
61. Muller DN, Klanke B, Feldt S, Cordasic N, Hartner A, et al. (2008) (Pro)renin receptor peptide inhibitor "handle-region" peptide does not affect hypertensive nephrosclerosis in Goldblatt rats. Hypertension 51: 676–681.
62. Danser AH, Derkx FH, Admiraal PJ, Deinum J, de Jong PT, et al. (1994) Angiotensin levels in the eye. Invest Ophthalmol Vis Sci 35: 1008–1018.
63. Deinum J, Derkx FH, Danser AH, Schalekamp MA (1990) Identification and quantification of renin and prorenin in the bovine eye. Endocrinology 126: 1673–1682.
64. Franken AA, Derkx FH, Blankestijn PJ, Janssen JA, Mannesse CK, et al. (1992) Plasma prorenin as an early marker of microvascular disease in patients with diabetes mellitus. Diabete Metab 18: 137–143.
65. Ludwig J, Kerscher S, Brandt U, Pfeiffer K, Getlawi F, et al. (1998) Identification and characterization of a novel 9.2-kDa membrane sector-associated protein of vacuolar proton-ATPase from chromaffin granules. J Biol Chem 273: 10939–10947.
66. Nishi T, Forgac M (2002) The vacuolar (H+)-ATPases–nature's most versatile proton pumps. Nat Rev Mol Cell Biol 3: 94–103.
67. Adams DS, Robinson KR, Fukumoto T, Yuan S, Albertson RC, et al. (2006) Early, H+-V-ATPase-dependent proton flux is necessary for consistent left-right patterning of non-mammalian vertebrates. Development 133: 1657–1671.

Summary
Samenvatting

19

Summary

Part I Endothelial dysfunction in the development of coronary artery disease

It is clear that endothelial dysfunction precedes and propagates the atherosclerotic disease process and subsequently the development of CAD.[1] Therefore, the measurement of endothelial function might predict the presence of CAD in patients.[2] In **chapter 2**, we tested the applicability of peripheral endothelial dysfunction as a measurement for the presence of CAD in symptomatic patients in a hospital outpatient setting. We showed that endothelial function measurement with peripheral arterial tonometry (PAT) at the fingertip is a heterogeneous measurement with poor correlation with traditional noninvasive CAD diagnostic measurements. Moreover, the PAT measurement failed to predict revascularization within one year. Therefore, in spite of the pathophysiological basis of endothelial dysfunction in CAD, no evidence was found for peripheral endothelial function measurement as a diagnostic tool to detect clinically relevant CAD.

Since patient studies to unravel underlying disease processes are usually hampered by limited measurements because of ethical concerns; experimental disease models in animals can enhance our understanding of the pathogenesis of CAD. In **chapter 3**, an overview of relevant animal models for atherosclerosis research was presented. We concluded that for the study of CAD and related diagnostic and therapeutic interventions, a porcine disease model is the most suitable since it has almost the same anatomy and physiology of the cardiovascular system as humans.[3] Pig models, with DM induction and with use of specific diets, have been proposed for the study of atherosclerosis.[4] The study presented in **chapter 4** demonstrated that in a diabetic porcine model, a diet high of saturated fats and cholesterol rich can induce a systemic inflammatory response related to aortic atherosclerosis development. This corresponds to how human atherosclerosis is thought to develop,[5] making it likely to be a relevant model for the study of human CAD. In the study presented in **chapter 5**, we demonstrated that only small coronary arteries (as a reflection of the coronary microcirculation), and not coronary conduit arteries, showed functional alterations ***in vitro*** with regard to NO and ET-1 systems in the process of early systemic atherosclerosis in diabetic pigs on a saturated fat and cholesterol rich diet. Specifically, in coronary conduit arteries, both endothelium-dependent as well as endothelium-independent vasodilation and vasoconstriction were unaltered. In contrast, coronary small arteries showed decreased endothelium-dependent vasodilation due to loss of endogenous NO, and reduced vasoconstriction to exogenous ET-1, possibly because of decreased endothelin type A (ET_A) receptor dominance. The changes in NO and ET-1 systems were associated. This could reflect an altered coronary microvascular balance.[6]

The diabetic, atherosclerotic pig model was also used to study more advanced CAD development. We showed in the study of **chapter 6,** that both diabetic and non-diabetic pigs on a high saturated fat and cholesterol rich diet gradually developed CAD after 12 to

15 months of study duration. This coronary atherosclerosis was too small to visualize with coronary computed tomography angiography, but could be demonstrated by intracoronary optical coherence tomography (OCT) and near-infrared spectroscopy (NIRS). Therefore, this study showed very elegantly, with clinically used coronary imaging techniques, that this animal model develops spontaneous coronary atherosclerosis over time, highly resembling the human disease process. We examined in the study of **chapter 7**, whether the CAD progress resulted in further impairment of coronary microvascular balance of NO and ET-1. CAD progress was demonstrated by the presence of early atherosclerotic plaques, also in the small coronary arteries of both diabetic and non-diabetic atherosclerotic pigs. Surprisingly, endothelium-dependent vasodilation was maintained due to an increase in endogenous NO availability relative to EDHF. However, exogenous ET-1 mediated vasoconstriction was increased in both diabetic and non-diabetic atherosclerotic animals, resulting mainly from endothelin type B (ET_B) receptor mediated vasoconstriction. In addition, the coronary small arteries of both groups of pigs showed characteristics of increased vascular stiffness. Taken together, this study clearly showed that *in vitro* the balance of vasodilator and vasoconstrictor mechanisms of the coronary microcirculation changed markedly during the CAD progress. This altered endothelial balance is a systemic process contributing to cardiovascular disease, which we demonstrated in the study of **chapter 8**. Again, in the diabetic, atherosclerotic pig model with presence of CAD, we showed that systemic microvascular damage is present in the form of augmented mucosal capillary tortuosity, as well as a dysbalance of renal angiopoietins which correlated to diabetic nephropathy.

Part II Endothelial dysfunction after percutaneous coronary interventions

In **chapter 9,** we presented an overview of the available literature on endothelial dysfunction after DES implantation. Stenting in general impairs several aspects of endothelial function. First generation DES even further impair endothelium-dependent vascular function of the peri-stent area up to one year after implantation. As an explanation, it has been postulated that DES imposes oxidative stress on the vascular wall, causing impaired endothelial NO-bioavailability and perhaps also EDHF-availability under certain circumstances. In addition, even the microcirculation in the distal perfusion area of specific DES might be at risk for endothelium-dependent vasodilatory alterations. We described in the study of **chapter 10**, coronary endothelial dysfunction early after certain types of DES implantation and compared it to BMS implantation in a healthy porcine model. DES did not impair endothelial coverage of the stent struts five days after implantation, nor neointimal formation 28 days after implantation. However, each drug type of DES demonstrated a specific cellular appearance within this neointima. PES specifically, showed the least endothelial nitric oxide synthase (eNOS) expression within the stent 28 days after implantation. However, this did not affect endothelial function of the

microcirculation distal to the stent, although a reduced NO-contribution was observed five days after implantation. This suggested that PES induces at least a temporary abnormal functioning of eNOS and therefore shows evidence of endothelial dysfunction. In addition, microvascular dysfunction distal to the DES did not correlate with in-stent delayed endothelialisation. We studied in **chapter 11,** also in a healthy porcine model, coronary conduit and microvascular endothelial function distal to the stent in relation to different DES as well as to BMS, both ***in vivo*** and ***in vitro***. No differences in endothelial vasodilatory response distal to the stent were noted ***in vivo*** five weeks after implantation. In addition, distal coronary conduit function was unaffected ***in vitro***. However, distal small artery function ***in vitro*** was affected by PES implantation, showing a reduced endothelium dependent vasodilation mediated by a NO-independent component, possibly EDHF. This study clearly demonstrated that the effect of PES can extend into the distal microcirculation.

In response to the possible disadvantages of DES, the BVS has been developed in an attempt to overcome these disadvantages by providing only a temporary scaffold. In **chapter 12**, the BVS was implanted in a porcine model with CAD with or without DM, and the coronary response to BVS implantation was examined by ***in vivo*** coronary imaging (OCT and NIRS), as well as with ***ex vivo*** histology. The coronary response of the scaffold showed a high percentage of lumen loss at three months after implantation with complete BVS strut coverage, which remained stable at six months after implantation. This late lumen loss consisted of a heterogeneous neointimal burden in both diabetic and non-diabetic pigs, with focal lipid accumulation, irregular collagen distribution and calcification. The absolute percentages of these neointimal substances changed over time, indicative for the formation of neoatherosclerosis. In addition, the number of discernible struts of the BVS decreased only slightly over time and also the polymer of the scaffold was shown to be preserved at six months after implantation. DM or the presence of inflammation did not influence the coronary response or the process of scaffold degradation. The response of neoatherosclerosis formation within the BVS might be caused by a dysfunctional barrier function of the endothelium, indicating the presence of endothelial dysfunction. We continued to study coronary endothelial function adjacent to the BVS and of the distal microcirculation in **chapter 13**. Again, in the porcine model of CAD with or without DM, the effect six months after BVS implantation on distal coronary endothelial function was studied ***in vitro***. Only in DM pigs, coronary conduit segments proximal and distal to the BVS edges showed reduced endothelium-dependent vasodilation, with the distal segments being most prominently affected. This endothelial dysfunction was principally due to a loss of NO. Surprisingly, segments from the microcirculation distal to the BVS showed slightly enhanced endothelium-dependent vasodilation. This enhanced vasodilation was again only observed in DM pigs and did not appear to be either NO- or EDHF-mediated. It was striking that specifically the DM animals showed an altered endothelial response.

Part III Endothelial dysfunction related to diabetes mellitus and the renin-angiotensin-aldosterone system

In **chapter 14**, we gave an overview of the role of an overactive RAAS in cardiovascular complications of DM. It was postulated that a discordant tissue RAAS might be a mediator of endothelial dysfunction leading to both micro- and macrovascular complications of DM resulting in cardiovascular disease. The elevated plasma levels of prorenin in DM might be part of this overactive RAAS. Prorenin is thought to bind to a (pro)renin receptor, thus activating locally Ang II-dependent and -independent pathways. Inducing inflammation and fibrosis by (pro)renin receptor stimulation could be an important contributor to the cardiovascular disease complications of DM. Therefore, blocking this receptor would be a next logical step in the search for new therapeutics to reduce DM-related cardiovascular disease. To examine which RAAS components are activated in DM, we studied in **chapter 15** these components in both plasma and urine samples of both diabetic and non-diabetic patients with hypertension. We demonstrated that diabetic patients show besides elevated plasma prorenin levels, also elevated urinary renin levels. In addition, we proved that urinary renin more closely reflects renal RAAS activity than urinary angiotensinogen or aldosterone.

The relation between an overactive RAAS, DM and endothelial dysfunction was further studied in **chapter 16** with use of diabetic, hypertensive, transgenic rats with high prorenin, renin and (pro)renin receptor levels, resulting in continuous (pro)renin receptor activation ***in vivo***. We evaluated whether the renin inhibitor aliskiren, with or without the putative (pro)renin receptor antagonist HRP, improved the disturbed vascular function of diabetic transgenic rats. Both diabetic and non-diabetic animals showed slightly enhanced Ang II mediated contractile responses of peripheral conduit arteries; only DM animals showed a marked increase after eNOS blockade, suggesting an NO upregulation in DM. The DM rats showed reduced responsiveness to phenylephrine, possibly because of this NO-upregulation. Again, both diabetic and non-diabetic rats showed a reduced response to exogenous ET-1, however only DM animals showed a diminished effectiveness of ET_A receptor blockade besides increased ET_A receptor expression. Moreover, peripheral small arteries of DM rats showed ***in vitro*** a COX-2 dependent vasoconstrictive response to acetylcholine, only when eNOS and EDHF were inhibited. This indicates an upregulation of EDCF. Therefore endothelial dysfunction with an altered vasomotor balance seems to be present within this animal model, involving upregulation of NO and EDCF, possibly resulting in reduced responsiveness to exogenous phenylephrine and ET-1. In this study we also demonstrated that treatment of the diabetic, transgenic rats with the renin inhibitor aliskiren reversed the above mentioned vascular effects, with the exception of the altered effectiveness of ET_A receptor blockade and the diminished endothelium independent vasodilation. This indicates that renin inhibition can at least partially reverse the altered endothelial balance of DM and an overactive RAAS, possibly via affecting NO, ET-1 and EDCF

mechanisms. Remarkably, when blocking the (pro)renin receptor on top of renin inhibition, the beneficial vascular effects either disappeared or were greatly diminished, although ET_A receptor responsiveness normalized and also the effects on blood pressure and plasma renin activity were maintained.

We also studied the effect of (pro)renin receptor blockade on cardiovascular end organ disease. In **chapter 17**, we tested whether (pro)renin receptor blockade adds benefits on top of renin inhibition with regard to DM nephropathy. Within the same animals, it was demonstrated that aliskiren treatment lowered blood pressure and exerted reno-protective effects. It also suppressed plasma and tissue RAAS activity. (Pro)renin receptor blockade with HRP, when given on top of renin blockade, did not alter the effects on blood pressure or RAAS activity. However, it counteracted the beneficial effects of aliskiren in the kidney. In **chapter 18**, we tested whether (pro)renin receptor blockade adds benefits on top of renin blockade with regard to DM retinopathy. The same DM animals as used in **chapters 16** and **17**, showed increased loss of capillaries, as well as increased expression of inflammatory cytokines within the retina. Aliskiren treatment reduced these effects, and HRP on top of aliskiren treatment did not provide additional protection.

References

1. Verma S, Anderson TJ. Fundamentals of endothelial function for the clinical cardiologist. Circulation 2002;105:546-9.
2. Celermajer DS. Reliable endothelial function testing: at our fingertips? Circulation 2008;117:2428-30.
3. Duncker DJ, Bache RJ. Regulation of coronary blood flow during exercise. Physiol Rev 2008;88:1009-86.
4. Gerrity RG, Natarajan R, Nadler JL, Kimsey T. Diabetes-induced accelerated atherosclerosis in swine. Diabetes 2001;50:1654-65.
5. Ross R. The pathogenesis of atherosclerosis: a perspective for the 1990s. Nature 1993;362:801-9.
6. McAuley DF, McGurk C, Nugent AG, Hanratty C, Hayes JR, Johnston GD. Vasoconstriction to endothelin-1 is blunted in non-insulin-dependent diabetes: a dose-response study. J Cardiovasc Pharmacol 2000;36:203-8.

Nederlandse samenvatting

Hart- en vaatziekten zijn een van de hoofdoorzaken van morbiditeit en mortaliteit in Nederland. Het begrijpen van de onderliggende pathofysiologie is belangrijk om de morbiditeit en mortaliteit te verminderen en ook om de meest optimale behandeling te vinden. Endotheel disfunctie is betrokken in het gehele pathologische proces van atherosclerose: vroeg in het proces van atherogenese, later in de beheersing van dynamische plaques, in de klinische manifestaties van hart- en vaatziekten zoals coronairlijden, en het beïnvloedt zelfs het behandelresultaat van PCI. Diabetes is een onafhankelijke en sterke voorspeller van hart- en vaatziekten, gekenmerkt door atherosclerose van de slagaders en disfunctie van de microcirculatie. Endotheel disfunctie speelt een belangrijke rol bij het ontstaan van diabetes gerelateerde macro- en microvasculaire complicaties. Een overactief renine-angiotensine-aldosteron systeem is geïdentificeerd als een belangrijke bijdragend systeem aan de cardiovasculaire complicaties van diabetes. Echter, de exacte onderliggende mechanismen en de relatie met endotheel disfunctie zijn op dit moment nog onbekend. Voorafgaande studies hebben al laten zien dat endotheel disfunctie zeer voorspellend is voor toekomstige cardiovasculaire aandoeningen. Daarom is gedetailleerde studie van endotheel disfunctie van het grootste belang.

Het doel van dit proefschrift was om veranderingen in endotheel functie in verschillende stadia van het cardiovasculaire ziekteproces te bestuderen, met speciale aandacht voor de microcirculatie. Dit proefschrift richtte zich specifiek op endotheel disfunctie in de ontwikkeling van coronairlijden in **deel I**; op endotheel disfunctie na percutane coronaire interventies in **deel II**; en op endotheel disfunctie in relatie tot diabetes en het renine-angiotensine-aldosteron systeem in **deel III**.

Deel I Endotheel disfunctie in de ontwikkeling van coronairlijden

Het is duidelijk dat endotheel disfunctie voorafgaat en bijdraagt aan het atherosclerotische ziekteproces en vervolgens aan de ontwikkeling van coronairlijden. Daarom kan de meting van endotheel functie mogelijk de aanwezigheid van coronairlijden bij patiënten voorspellen. In **hoofdstuk 2** hebben we de toepasbaarheid van perifere endotheel disfunctie getest als een maat voor de aanwezigheid van coronairlijden bij symptomatische patiënten op de polikliniek. We hebben aangetoond dat de meting van endotheel functie met perifere arteriële tonometrie (PAT) aan de vingertop een heterogene meting is, met een slechte correlatie met traditionele niet-invasieve diagnostische metingen van coronairlijden. Bovendien kon de PAT-meting revascularisatie, wegens obstructief coronairlijden, binnen een jaar niet voorspellen. Daarom werd er, ondanks de pathofysiologische basis van endotheel disfunctie in coronairlijden, geen bewijs gevonden voor de perifere meting van endotheel functie als een diagnostisch hulpmiddel om klinisch relevant coronairlijden te detecteren.

Omdat patiënten-studies, om onderliggende ziekteprocessen te kunnen ontrafelen, meestal worden belemmerd door beperkte metingen vanwege ethische bezwaren, kunnen experimentele ziektemodellen met gebruik van dieren ons begrip van de pathogenese van coronairlijden vergroten. In **hoofdstuk 3** werd een overzicht gegeven van relevante diermodellen voor onderzoek naar coronairlijden en gerelateerde diagnostische en therapeutische interventies. Wij concludeerden dat voor de studie van coronairlijden en gerelateerde diagnostische en therapeutische interventies, een varkensmodel met ziekte het meest geschikt is omdat een varken bijna dezelfde anatomie en fysiologie van het cardiovasculaire systeem heeft als de mens. Varkensmodellen, met diabetes-inductie en met gebruik van specifieke diëten, zijn voorgesteld voor de studie van atherosclerose. De studie gepresenteerd in **hoofdstuk 4** toonde aan dat binnen een diabetisch varkensmodel, een dieet met veel verzadigde vetten en cholesterolrijk, een systemische inflammatoire respons kan veroorzaken die gerelateerd is aan de ontwikkeling van atherosclerose in de aorta. Dit komt overeen met hoe atherosclerose zich in de mens ontwikkelt, waardoor dit waarschijnlijk een relevant model is voor de studie van coronairlijden in mensen. In de studie van **hoofdstuk 5** hebben we aangetoond dat alleen de kleine kransslagadertjes (als een reflectie van de coronaire microcirculatie) en niet de grote kransslagaders, functionele veranderingen toonden *in vitro* met betrekking tot de vasoactieve stikstof monoxide en endotheline systemen in het proces van vroege atherosclerose vorming in diabetische varkens op een verzadigd vet- en cholesterolrijk dieet. Specifiek in de grote kransslagaders waren zowel endotheel-afhankelijke als endotheel-onafhankelijke vasodilatatie en vasoconstrictie onveranderd. Terwijl de kleine kransslagadertjes verminderde endotheel-afhankelijke vasodilatatie lieten zien, wat te wijten was aan verlies van endogeen stikstof monoxide, als ook aan verminderde vasoconstrictie door exogeen endotheline, mogelijk als gevolg van verminderde endotheline type A-receptor dominantie. De veranderingen in stikstof monoxide en endotheline systemen waren geassocieerd. Dit zou een gewijzigde coronaire microvasculaire balans kunnen weerspiegelen.

Het diabetische, atherosclerotische varkensmodel werd ook gebruikt om de ontwikkeling van meer gevorderd coronairlijden te bestuderen. We hebben in de studie van **hoofdstuk 6** aangetoond dat zowel diabetische als niet-diabetische varkens op een verzadigd vet en cholesterolrijk dieet geleidelijk coronairlijden ontwikkelden na 12 tot 15 maanden studieduur. Deze atherosclerose was te weinig om met coronaire computer tomografie-angiografie in beeld te brengen, maar kon wel worden aangetoond door intra-coronaire optische coherentie tomografie (OCT) en door nabij-infrarood spectroscopie (NIRS). Deze studie toonde daarom zeer elegant aan dat met klinisch toegepaste coronaire beeldvormingstechnieken dit diermodel na verloop van tijd spontane coronaire atherosclerose ontwikkelt, die zeer sterk lijkt op het menselijke ziekteproces. We onderzochten in de studie van **hoofdstuk 7** of de ontwikkeling van coronairlijden in het diermodel resulteerde in verdere verslechtering van de coronaire microvasculaire balans van stikstof monoxide en endotheline. De ontwikkeling van coronairlijden

werd aangetoond door de aanwezigheid van vroege atherosclerotische plaques, ook in de kleine kransslagadertjes van zowel diabetische als niet-diabetische varkens. Verrassend genoeg, bleef de endotheel-afhankelijke vasodilatatie gehandhaafd als gevolg van een toename in endogene stikstof monoxide beschikbaarheid ten opzichte van endotheel afkomstige hyperpolariserende factoren (EDHF). Echter, exogene endotheline gemedieerde vasoconstrictie was versterkt bij zowel diabetische als niet-diabetische atherosclerotische dieren, voornamelijk als gevolg van endotheline type B receptor gemedieerde vasoconstrictie. Bovendien vertoonden de kleine kransslagadertjes van beide groepen varkens kenmerken van toegenomen vaatstijfheid. Daarom toonde deze studie duidelijk aan dat ***in vitro*** de balans van vaatverwijdende en vaatvernauwende mechanismes van de coronaire microcirculatie aanzienlijk veranderde tijdens de progressie van coronairlijden. Deze veranderde endotheel balans is een systemisch proces dat bijdraagt aan cardiovasculaire ziekte vorming, zoals aangetoond in de studie van **hoofdstuk 8**. In het diabetische, atherosclerotische varkensmodel met coronairlijden, hebben we aangetoond dat er systemische microvasculaire schade aanwezig is in de vorm van verhoogde mucosale capillaire tortuositeit, evenals een disbalans van renale angioproteïnen die gecorreleerd zijn aan diabetische nefropathie.

Deel II Endotheel disfunctie na percutane coronaire interventies

In **hoofdstuk 9** gaven we een overzicht van de beschikbare literatuur over endotheel disfunctie na drug eluting stent (DES) implantatie. Stent implantatie in het algemeen, beschadigt verschillende aspecten van endotheel functie. Eerste generatie DES beschadigen echter de endotheel-afhankelijke vaatfunctie van het peri-stent gebied nog meer, tot één jaar na DES-implantatie. Als een verklaring wordt er verondersteld dat DES oxidatieve stress induceerde op de vaatwand, dat de stikstof monoxide beschikbaarheid van het endotheel verminderde en dat mogelijk ook de EDHF-beschikbaarheid onder bepaalde omstandigheden verminderde. Bovendien kan zelfs de microcirculatie in het distale perfusiegebied van specifieke DES bedreigd worden door veranderingen in endotheel-afhankelijke vaatverwijding. We beschreven in de studie van **hoofdstuk 10**, coronaire endotheel disfunctie vroeg na de implantatie van specifieke DES en vergeleken deze met bare metal stent (BMS) implantatie in een gezond varkensmodel. DES had geen nadelige invloed op de endotheel bedekking van de stent vijf dagen na implantatie, en ook niet op neo-intima vorming 28 dagen na implantatie. Echter, ieder medicijn van de verschillende DES liet een specifieke samenstelling van cellen zien in deze neo-intima. Specifiek vertoonde paclitaxel eluting stent (PES) de minste endotheliale stikstofmonoxide synthase (eNOS) expressie binnen in de stent, 28 dagen na implantatie. Dit had echter geen invloed op de endotheel functie van de microcirculatie distaal van de stent, hoewel er wel een verminderde stikstof monoxide bijdrage vijf dagen na implantatie werd waargenomen. Dit suggereert dat PES op zijn minst een tijdelijk abnormaal functioneren van eNOS en daarmee van de endotheel

disfunctie induceert. Bovendien correleerde microvasculaire disfunctie distaal van de DES niet met vertraagde endothelialisatie binnen in de stent. We bestudeerden in **hoofdstuk 11**, ook in een gezond varkensmodel, kransslagader functie en microvasculaire functie distaal van de stent van verschillende DES en van BMS, zowel ***in vivo*** als ***in vitro***. Er werden geen verschillen in de endotheel afhankelijke vaatverwijdende respons distaal van de stent opgemerkt ***in vivo***, vijf weken na implantatie. Bovendien werd de kransslagaderfunctie distaal van de stent niet beïnvloed ***in vitro***. De functie van kleine kransslagadertjes werd echter wel beïnvloed door PES-implantatie ***in vitro***, die een verminderde endotheel-afhankelijke vaatverwijding vertoonden, die werd gemedieerd door een component die niet van stikstof monoxide afhankelijk is, mogelijk is dit EDHF. Deze studie toonde duidelijk aan dat het effect van specifieke DES zich kan uitstrekken tot in de distale microcirculatie van de stent.

Als reactie op de mogelijke nadelen van DES, is de bioresorbeerbare vasculaire scaffold (BVS) ontwikkeld in een poging om deze nadelen te overwinnen door slechts een tijdelijke ondersteuning te bieden. In de studie van **hoofdstuk 12** werd de BVS geïmplanteerd in een varkensmodel met coronairlijden met of zonder de aanwezigheid van diabetes, en werd de coronaire respons op de BVS implantatie onderzocht door coronaire beeldvorming ***in vivo*** met OCT en NIRS en ***ex vivo*** met histologie. De coronaire respons van de scaffold vertoonde een hoog percentage lumen verlies op drie maanden na de implantatie met volledige bedekking van de BVS, een proces wat stabiel bleef tot zes maanden na de implantatie. Dit late lumen verlies bestond uit een heterogene neo-intima bij zowel de diabetische als de niet-diabetische varkens, met lokale lipiden accumulatie, onregelmatige collageenverdeling en verkalking. De absolute percentages van deze neo-intima substanties veranderden in de tijd, wat indicatief is voor de vorming van neo-atherosclerose. Bovendien nam het aantal waarneembare stutten van de BVS slechts weinig af in de loop van de tijd en bleek ook dat het polymeer van de scaffold zes maanden na implantatie nog niet was verdwenen. Diabetes of de aanwezigheid van ontsteking had geen invloed op de coronaire respons of op het afbraakproces van de scaffold. De reactie van neo-atherosclerose-vorming binnenin de BVS kan worden veroorzaakt door een disfunctionele barrière functie van het endotheel, wat wijst op de aanwezigheid van endotheel disfunctie. Vervolgens onderzochten we de coronaire endotheel functie direct naast de BVS en van de distale microcirculatie in **hoofdstuk 13**. Wederom in het varkensmodel met coronairlijden met of zonder diabetes, werd het effect van zes maanden BVS-implantatie op de distale coronaire endotheel functie ***in vitro*** bestudeerd. Alleen in DM-varkens vertoonden de kransslagader segmenten proximaal en distaal ten opzichte van de BVS-randen, een verminderde endotheel-afhankelijk vaatverwijding, waarbij het effect op de distale segmenten het grootst was. Deze endotheel disfunctie was voornamelijk te wijten aan een verlies van stikstof monoxide. Verrassend genoeg, vertoonden segmenten van de microcirculatie distaal van de BVS een iets verbeterde endotheel-afhankelijke vaatverwijding. Deze verhoogde vasodilatatie werd opnieuw alleen waargenomen bij diabetische varkens en leek niet stikstof monoxide- of EDHF-

gemedieerd te zijn. Het is opvallend dat alleen de diabetische dieren een veranderde endotheel respons vertoonden.

Deel III Endotheel disfunctie gerelateerd aan diabetes mellitus en het renine-angiotensine-aldosteron systeem

In **hoofdstuk 14** gaven we een overzicht van de rol van het overactieve renine-angiotensine-aldosteron systeem in de cardiovasculaire complicaties van diabetes. Er werd verondersteld dat een disharmonisch weefsel specifiek renine-angiotensine-aldosteron systeem een mediator zou kunnen zijn voor endotheel disfunctie wat zou kunnen leiden tot zowel de micro- als de macrovasculaire complicaties van diabetes, wat uiteindelijk resulteert in cardiovasculaire ziekte. De verhoogde plasmaspiegels van prorenine, de voorloper van renine, bij diabetische patiënten met microvasculaire complicaties kunnen deel uitmaken van dit disharmonische renine-angiotensine-aldosteron systeem. Prorenine wordt verondersteld te binden aan de (pro) renine receptor, waardoor lokale angiotensine-afhankelijke en angiotensine-onafhankelijke processen worden geactiveerd. Door (pro)renine receptor stimulatie zouden ontsteking en fibrose geïnduceerd kunnen worden, wat daarmee zou bijdragen aan de cardiovasculaire complicaties van diabetes. Daarom is blokkering van deze receptor de volgende logische stap in de zoektocht naar nieuwe therapeutische regimes om diabetes gerelateerde cardiovasculaire aandoeningen te verminderen. Om te onderzoeken welke specifieke componenten van het renine-angiotensine-aldosteron systeem in diabetes worden geactiveerd, bestudeerden we in **hoofdstuk 15** deze componenten in zowel plasma- als urinemonsters van zowel diabetische als niet-diabetische patiënten met hypertensie. We toonden aan dat diabetici naast verhoogde plasma prorenine, ook verhoogde urine renine spiegels hebben. Bovendien hebben we aangetoond dat urine renine beter de activiteit van het renine-angiotensine-aldosteron systeem in de nieren weerspiegelt dan urine angiotensinogeen of aldosteron.

De relatie tussen het over geactiveerde renine-angiotensine-aldosteron systeem van diabetes met endotheel disfunctie werd verder bestudeerd in **hoofdstuk 16** door gebruik te maken van diabetische, hypertensieve transgene ratten met hoge prorenine, renine en (pro) renine-receptor concentraties, wat zou kunnen resulteren in continue (pro)renine receptor activatie *in vivo*. We evalueerden of de renine remmer aliskiren, met of zonder de vermeende (pro)renine receptor antagonist HRP, de gestoorde vaatfunctie van de diabetische transgene ratten verbeterde. Zowel diabetische als niet-diabetische dieren vertoonden enigszins versterkte contractiele responsen van perifere slagaders, wat angiotensine gemedieerd was, met een duidelijke toename na eNOS blokkade bij alleen de diabetische dieren, hetgeen een opregulering van stikstof monoxide in diabetes suggereert. De diabetische ratten vertoonden een verminderde respons op fenylefrine, mogelijk vanwege deze stikstof monoxide opregulatie. Opnieuw vertoonden zowel niet-diabetische als diabetische ratten een verminderde respons

op exogeen endotheline, maar alleen de diabetische dieren vertoonden een verminderde effectiviteit van endotheline receptor type A blokkade naast verhoogde endotheline receptor type A expressie. Bovendien vertoonden de perifere kleine slagadertjes van alleen de diabetische ratten een acetylcholine geïnduceerde endotheel afhankelijke constrictie, die COX-2 gemedieerd bleek, in de aanwezigheid van eNOS-remming en blokkers van EDHF ***in vitro***. Dit duidt op een opregulatie vanuit het endotheel afkomstige contractiele factoren. Daarom lijkt er endotheel disfunctie met een veranderde vasomotorische balans aanwezig te zijn ook in dit diabetische diermodel, met opregulatie van stikstof monoxide en uit het endotheel afkomstige contractiele factoren, wat mogelijk resulteerde in een verminderde respons op exogeen fenylefrine en endotheline. In deze studie hebben we ook aangetoond dat behandeling van de diabetische, transgene ratten met de renine-remmer aliskiren de bovengenoemde vasculaire effecten omkeerde, met uitzondering van de veranderde effectiviteit van endotheline type A receptor blokkade en de verminderde endotheel-onafhankelijke vasodilatatie. Dit geeft aan dat renine inhibitie de veranderde endotheel balans van diabetes en van een overactief renine-angiotensine-aldosteron systeem ten minste gedeeltelijk kan omkeren, mogelijk door mechanismen van stikstof monoxide, endotheline en uit het endotheel afkomstige contractiele factoren te beïnvloeden. Opmerkelijk genoeg verdwenen de gunstige vasculaire effecten na het blokkeren van de (pro)renine receptor bovenop renine blokkade of waren deze sterk verminderd, hoewel de responsiviteit van de endotheline type A receptor normaliseerde en de effecten op de bloeddruk en de plasma renine activiteit gehandhaafd bleven. Het effect van (pro)renine receptor blokkade op eind orgaan schade werd verder bestudeerd in de **hoofdstukken 17** en **18**. In **hoofdstuk 17** testten we of (pro)renine receptor blokkade extra voordelen geeft bovenop renine blokkade met betrekking tot diabetes gerelateerde nefropathie. Door gebruik te maken van dezelfde dieren, werd aangetoond dat renine blokkade met aliskiren bloeddruk verlagende en nier beschermende effecten uitoefende. Het onderdrukte ook plasma- en weefsel renine-angiotensine-aldosteron systeem activiteit. (Pro)renine-receptor blokkering met HRP, indien toegediend bovenop de renine blokkade, had geen invloed op de bloeddruk of op renine-angiotensine-aldosteron systeem activiteit. Het ging echter ten koste van de gunstige effecten van aliskiren op de nier. In **hoofdstuk 18** testten we of (pro)renine receptor blokkade extra voordelen geeft bovenop renine blokkade ten aanzien van diabetische retinopathie. Wederom in dezelfde dieren, werd aangetoond dat de diabetische dieren een verhoogd verlies van retinale capillairen vertoonden, evenals een verhoogde expressie van ontstekingscytokinen in het netvlies. Renine remming met aliskiren verminderde deze effecten en HRP bovenop aliskiren gaf geen extra bescherming.

General discussion and clinical perspectives

20

General discussion and clinical perspectives

The experiments described in **this thesis** were performed both in patients and in animal models and their results can be translated into clinical practice and provide a basis for future research. However, the intriguing question is: which results obtained in which model are useful? This was already answered in 1983 by Prof. W.J. van der Giessen and still remains valuable today: "The apparent discrepancies in results obtained from different models tend to be confusing. However, one often forgets that these models may have different features, and that these differences are responsible for the spread in results. With this in mind, one might be able to select data from relevant models to direct a human validation study, finally resulting in therapy which is of benefit to patients, as no single animal model can provide a situation which completely mimics the derangements of the human".[1] An animal model mimicking the human disease process as close as possible, which can be followed over time and is accessible for human diagnostics and therapeutics, is probably the most ideal,[2-4] but that should be verified in future experiments.

Part I clinical considerations of coronary artery disease development

In **part I of this thesis**, we demonstrated a nonlinear relationship between obstructive CAD and microvascular endothelial dysfunction. This can partially be explained by the fact that clinically relevant CAD results from an underlying complex disease process that is likely to be present for many years and is influenced by multiple factors over time, which cannot be expressed in a single measurement of endothelial function at one vascular location and at one time point. We showed that coronary microvascular endothelial dysfunction alters in the process of CAD, highlighting the importance of assessment of endothelial dysfunction over time and to separate the evaluation of coronary conduit arteries from the evaluation of the microcirculation. Indeed, in clinical practice, the relation between symptoms, the presence of obstructive CAD and microvascular dysfunction is not always straightforward, as has been demonstrated with patients with microvascular angina.[5] These patients, who previously all belonged to cardiac syndrome X, are now considered to represent a spectrum of diseases: (i) coronary microvascular dysfunction in the absence of myocardial disease and obstructive CAD; (ii) coronary microvascular dysfunction in the presence of myocardial diseases; (iii) coronary microvascular dysfunction in the presence of obstructive CAD; and (iv) iatrogenic coronary microvascular dysfunction (e.g. related to PCI). In all of them microvascular endothelial dysfunction is thought to play a role.[6] Therefore, endothelial function studies in these subgroups of patients will be of particular interest to assess the relation between peripheral and coronary microvascular dysfunction, as well as the relation between microvascular dysfunction and obstructive CAD. In addition, future studies have to resolve whether the assessment of microvascular dysfunction will result in a specific treatment strategy and whether this strategy will improve microvascular function, and finally if it will yield

an improved clinical outcome. Finally, the development of direct and quantitative methods to detect coronary microvascular disease is essential to diagnose patients with non-obstructive CAD, as well as to guide therapy.[7-9]

We also aimed to unravel the mechanisms of endothelial dysfunction related to cardiovascular disease. Traditionally, NO has been considered to be the key endothelium-derived vasodilating factor that plays a prominent role in the maintenance of vascular tone.[10] Indeed, many studies have reported endothelial dysfunction as a loss of NO-mediated vasodilator capacity. However, endothelial function not only depends on NO. For example, vessel size influences the relative contribution of NO: with a large role in conduit arteries but a small role in resistance arteries, where EDHF has a dominant role.[11-13] As the studies of **chapters 5, 7** and **16** showed, the term endothelial dysfunction should rather describe a defect in the homeostatic mechanism of endothelial function. These studies clearly indicate that disturbances in the balance between vasodilation and vasoconstriction are modulated during the progression of cardiovascular disease, rather than pathology of a single molecule. Indeed, striking functional interactions seem to exist between NO and ET-1 in the regulation of coronary tone via not completely understood mechanisms influenced by cardiovascular risk factors.[14] The clinical relevance of a dysfunctional endothelial balance has already been demonstrated in the pathology of vasospastic angina.[5] Over time this dysbalance will probably become more irreversible and will finally result in pathological sequelae. Future studies are necessary to unravel this irreversibility and the following pathological events. We also demonstrated an altered endothelial balance of NO and ET-1 in the mesenteric circulation with a role for EDCF. Indeed, in the presence of hypertension, the endothelium can become a source of EDCF, contributing to endothelial dysbalance.[15] However, the mechanisms regulating the balance between NO, EDCF and ET-1 need to be elucidated further. Finally, one has to realize that endothelial control mechanisms can vary between organs and that the impact of cardiovascular risk factors on the microcirculation can also differ between organs hampering the translation of the findings in one organ to another.[16]

Besides an altered endothelial balance over time, we also demonstrated structural remodeling of the coronary microcirculation, in combination with coronary atherosclerosis formation (see **chapters 5, 6** and **7)**. Therefore, this model is a representative model for a subgroup of patients with microvascular angina, in whom the presence of both coronary microvascular dysfunction and obstructive CAD plays a role.[6] In addition, coronary endothelial dysbalance and structural remodeling have an impact on the surrounding cardiomyocytes, which could finally result in the development of heart failure.[16] However, more studies are necessary to unravel the underlying processes and the development of myocardial dysfunction over time, but animal models with cardiovascular disease hold great promise for the study of heart failure[3,4]. The studies of **chapters 8**, **17** and **18** already demonstrated that the vascular alterations at least coincide with specific organ pathology**,** making these animal models interesting candidates also because of the presence of comorbidity, e.g. renal dysfunction. However, translation to

the clinical situation with more heterogeneous disease is still needed. Finally, measurement of endothelial dysfunction over time, for example with use of a multimarker strategy that would include a broad set of endothelial biomarkers could help in the assessment of patients at risk of cardiovascular disease or to guide therapy.[17-19]

Part II clinical considerations of percutaneous coronary interventions

In clinical practice, more stent thrombosis has been observed after first generation DES.[20] Indeed, clinical studies have demonstrated coronary endothelial dysfunction in the peri-stent area after coronary intervention with PES, a first generation of DES.[21] The studies of **chapters 10** and **11** also clearly demonstrated different endothelial alterations after PES implantation. Our results suggest including delayed restoration of endothelial function rather than only endothelial absence, thereby extending the concept of delayed healing after PES, as a possible explanation for unwanted clinical sequelae. In diabetic patients, a worse clinical outcome one year after implantation has been reported for first generation DES as compared to second generation DES.[22] This observation can partly be explained by our results that the adverse effects of PES can extend into the distal microcirculation. The loss of microvascular EDHF-mediated vasodilation might be of particular importance in diabetic patients given their already reduced microvascular NO-availability,[23] which could result in a clinically relevant endothelial dysbalance. Therefore, further studies are necessary focusing on subpopulations at risk of endothelial dysfunction after DES implantation.

With the development of the fourth generation of DES, a first generation of BVS has appeared aiming at restoration of vascular function. However, **chapters 12** and **13** demonstrated convincingly the presence of endothelial dysfunction after BVS implantation, although distal microvascular function was preserved in DM because of a non-NO or non-EDHF mediated upregulation. Again, this demonstrates the intricate balance of different vascular mechanisms interacting and determining overall coronary microvascular endothelial function. Clinical studies confirm the presence of endothelial dysfunction after BVS implantation,[24] and clinical practice has demonstrated an increased risk of scaffold thrombosis.[25] In addition, the BVS has been associated with the formation of neoatherosclerosis.[26] Also, our study demonstrated the presence of this process. Finally, BVS failure has been reported more often in DM patients,[27] again in accordance with our study results. These observations confirm the consistency between our experimental results and clinical observations with the BVS. Endothelial dysfunction might predispose to a pro-coagulant and pro-inflammatory state within the scaffold, and to paradoxical vasoconstriction outside the scaffold. This may result in clinically relevant symptoms of thrombosis and restenosis. However, future studies are still warranted to prove this causality.

These findings indicate that with the BVS, the optimal balance in endothelial function has not been reached. Therefore, it is clear that the BVS needs to be optimized further and

future studies should focus on the degradation process, endothelial dysfunction over time and neoatherosclerosis formation, with special attention for the increased risk in DM. For now, the BVS has been removed from routine clinical practice and second or third generation DES remain the first choice of treatment. As stated by prof. W.J. van der Giessen, already in 1989: "The intracoronary stent, (in this case the BVS), seems to be following the well-worn path of initially elated euphoria where enthusiasm holds sway over scientific evidence, followed by critical skepticism with little optimism for the future." "A period of critical scientific evaluation is now needed, in which the lessons learned from the past are implemented".[28] Indeed, next generations of new PCI devices should be tested extensively in experimental settings, preferably with use of human-like disease models, as well as in clinical settings before being adopted in daily clinical practice. Polymer-free DES and second generation bioresorbable scaffolds, e.g. with a magnesium backbone, hold promise with regard to stent or scaffold thrombosis.[29]

Part III clinical considerations of diabetes and the renin-angiotensin-aldosterone system

We demonstrated in the study of **chapter 15** that diabetic patients showed elevated urinary renin levels, indicating an overactive renal RAAS in DM, thereby possibly reflecting a discordant tissue RAAS in these patients. Whether elevated urinary renin levels correlate with endothelial dysfunction and future cardiovascular disease is a topic of further studies. If such a relation would exist, this could reinforce the need of RAAS blockade treatment in these patients. However, more studies are needed to detect the exact source of the elevated urinary renin: probably a part will originate from the plasma filtration, a part will originate from the collecting duct of the kidney and a part will originate from the intrarenal conversion of prorenin to renin.[30] It is well known that as a consequence of RAAS blockade, plasma renin levels increase. In addition to this increase, we demonstrated that treatment with RAAS blockers decreased urinary renin levels. An explanation for this decrease could be the inhibition of a discordant tissue RAAS. Therefore, measurement of urinary renin might also be a useful marker to assess the success of RAAS blockade. Future studies are needed to address the effects of specific RAAS blockers on urinary renin amount, as well as the correlation with clinical outcome.

In **chapters 16, 17** and **18** we studied the concept of an overactive RAAS in DM further and demonstrated that it resulted in systemic endothelial dysfunction, nephropathy and retinopathy, since renin inhibition reversed these effects. However, blockade of the (pro)renin receptor with HRP on top of traditional RAAS blockade did not result in additional disease modifying effects. On the contrary, when administered in a high dose, it resulted in a reversal of the beneficial effects of traditional RAAS blockade apart from the blood pressure lowering effect. This suggests that HRP interferes with traditional RAAS blockade in a manner that does not affect blood pressure, possibly via activation of tissue RAAS. Indeed, HRP has now been reported to act as a partial agonist of the (pro)renin receptor instead of an antagonist.[31] Importantly, recent studies

have pointed to the possibility that the (pro)renin receptor may also exert functions that are entirely unrelated to the RAAS.[32] The (pro)renin receptor is now thought to be a multi-functional receptor, which has been linked to generalized cellular processes related to vacuolar H^+-ATPase integrity.[33] In addition, it may have a role in the regulation of lipid and glucose metabolism and thereby possibly influencing cardiovascular disease indirectly.[34] Given the uncertainty whether HRP acts as a (pro)renin receptor blocker or not, future studies should examine the exact function of the (pro)renin receptor in DM to define its role. In addition, to what degree prorenin – (pro)renin receptor interaction is physiologically relevant, given the nanomolar affinity of the receptor for prorenin and the picomolar levels of prorenin in blood,[32] is still a matter of debate and requires further research. Therefore, the concept of prorenin – (pro)renin receptor interaction and subsequent sequelae in DM still remain unclear and are possibly unrelated to the RAAS.[35] Blockade of the (pro)renin receptor does not hold great therapeutic promise, since (pro)renin receptor knockout mice die at an early age.[36]

Also, in **chapters 16, 17** and **18** we demonstrated promising effects of the renin inhibitor aliskiren on the reduction of diabetic cardiovascular pathology, at least within the animal model. In clinical practice, adequate blood pressure lowering effects of aliskiren have been demonstrated.[37] Two weeks after ending aliskiren treatment beneficial effects on blood pressure were still present as well as reduced plasma renin activity.[38] This cannot solely be explained because of the long half-life of aliskiren in plasma, but could also point to the accumulation of aliskiren in the kidney with subsequent suppression of tissue RAAS.[39] Suppression of discordant tissue RAAS was thought to result in better long-term cardiovascular outcomes. However, large randomized controlled trials showed disappointing results with no additional benefits and even adverse effects like renal dysfunction and hypotension especially when dual RAAS blockade was present, as demonstrated for diabetic patients with cardiovascular disease,[40] as well as for patients with acute obstructive CAD,[41] and heart failure patients.[42,43] These findings suggest that maximal RAAS blockade in high risk patients is deleterious because of renal failure.[44] This is called the "nephrocentric" reaction to almost complete RAAS blockade.[45] Possibly, aliskiren has more beneficial effects early on in cardiovascular disease development. Indeed in a small pilot study, aliskiren demonstrated favorable effects on endothelial function as well as on myocardial function after three months of treatment in DM patients under stable glycemic control and with mild essential hypertension, independent from the blood pressure lowering effect,[46] possibly because of increased NO availability.[47] This would point again to differences in disease state: early versus advanced cardiovascular disease, as **this thesis** also clearly demonstrates.

The exact mechanism of an overactive RAAS on cardiovascular disease development is still incompletely understood.[48] Although double RAAS blockade with an ACE inhibitor or an Ang II type 1 receptor blocker in combination with a mineralocorticoid receptor antagonist has proven to be very beneficial for the treatment of heart failure; double RAAS blockade with both a renin inhibitor and an ACE inhibitor or an Ang II type 1 receptor blocker has proven to

be detrimental. However, the ten-year results of renin inhibition need to be awaited and the treatment in specific patient populations might be beneficial. Especially the disease spectrum of hypertension, diastolic dysfunction and heart failure with preserved ejection fraction is of interest, in which endothelial dysfunction is thought to play a crucial role. Indeed, plasma angiotensinogen might be a useful biomarker of this disease spectrum, as well as a potential therapeutic target.[49] The combination of RAAS blockade therapy with measurement of both intrarenal and extrarenal RAAS activity[50] and subsequent tailoring of optimal RAAS blockade therapy seems to be the next logical step in future studies. Finally, the role of (pro)renin receptor stimulation in the development of cardiovascular disease is ambiguous. Via indirect pathways related to cardiovascular risk factors it might have effects, which future studies need to resolve. Only selective blockade of this receptor may hold promise, because of its now known multifunctional connections to vital processes.

Main conclusions and implications

Main conclusions and implications derived from Part I:

Peripheral arterial tonometry cannot predict patients at low risk of CAD in a clinical setting, most likely because of the presence of heterogeneous disease within the patients and because of the presence of uncontrollable variables in a clinical setting.

A porcine model of CAD is a suitable model for the study of coronary conduit and microvascular dysfunction, for diagnostic and therapeutic interventions of CAD, as well as for the study of end-organ pathology in cardiovascular disease. Therefore, this model could help to unravel disease processes involved in microvascular angina and heart failure.

Coronary microvascular dysfunction shows a dysbalance of vasodilating and vasoconstricting mechanisms that changes over time in CAD development. Therefore, measurement of endothelial dysfunction at a single moment in time is not likely to predict dysfunction during later stages of the disease process.

Main conclusions and implications derived from Part II:

Endothelial function has several properties including a permeable barrier function, an anti-thrombotic and anti-inflammatory defense, as well as the regulation of vascular tone. All of these properties can be impaired to some extent by coronary stenting in general.

Specifically PES, a first generation DES, can impair distal microvascular function under conditions of reduced NO bioavailability. This could be, at least partly, an explanation for the worse clinical outcomes for DM patients after first generation DES.

With the development of the BVS, endothelial dysfunction within the scaffold, resulting in neoatherosclerosis as well as dysfunction adjacent to the scaffold, still remains an issue, in particular in the presence of DM. This could be an explanation for the observations of increased scaffold thrombosis and restenosis in clinical practice, with DM patients having the greatest risk.

Main conclusions and implications derived from Part III:

DM patients are at increased risk of cardiovascular disease development, with an important role for an overactive RAAS. A discordant tissue RAAS is likely to play a role in specific end-organ disease of DM. However, a role for prorenin – (pro)renin receptor interaction within this pathology has become questionable.

Urinary renin may represent renal RAAS activity in DM patients and its measurement can be used not only to reflect this activation but also to measure the success of RAAS blockade. Therefore, it could possibly guide therapy in selected patients to improve clinical outcome.

Renin inhibition can improve endothelial dysfunction and end-organ pathology related to diabetic cardiovascular disease, at least in an animal model with a highly activated RAAS. The clinical effects of renin inhibition in clinical practice are hampered by the “nephrocentric” reaction to almost complete RAAS blockade, but may show long-term benefit in selected patients.

References

1. Verdouw PD, Wolffenbuttel BH, van der Giessen WJ. Domestic pigs in the study of myocardial ischemia. Eur Heart J 1983;4 Suppl C:61-7.
2. Valero-Munoz M, Backman W, Sam F. Murine Models of Heart Failure with Preserved Ejection Fraction: a "Fishing Expedition". JACC Basic Transl Sci 2017;2:770-89.
3. van den Dorpel MMP, Heinonen I, Snelder SM, et al. Early detection of left ventricular diastolic dysfunction using conventional and speckle tracking echocardiography in a large animal model of metabolic dysfunction. Int J Cardiovasc Imaging 2017. DOI: 10.1007/s10554-017-1287-8.
4. van Dijk CG, Oosterhuis NR, Xu YJ, et al. Distinct Endothelial Cell Responses in the Heart and Kidney Microvasculature Characterize the Progression of Heart Failure With Preserved Ejection Fraction in the Obese ZSF1 Rat With Cardiorenal Metabolic Syndrome. Circ Heart Fail 2016;9:e002760.
5. Shimokawa H. 2014 Williams Harvey Lecture: importance of coronary vasomotion abnormalities-from bench to bedside. Eur Heart J 2014;35:3180-93.
6. Crea F, Camici PG, Bairey Merz CN. Coronary microvascular dysfunction: an update. Eur Heart J 2014;35:1101-11.
7. Camici PG, Crea F. Coronary microvascular dysfunction. N Engl J Med 2007;356:830-40.
8. de Waard GA, Nijjer SS, van Lavieren MA, et al. Invasive minimal Microvascular Resistance Is a New Index to Assess Microcirculatory Function Independent of Obstructive Coronary Artery Disease. J Am Heart Assoc 2016;5. DOI: 10.1161/JAHA.116.004482.
9. Labazi H, Trask AJ. Coronary microvascular disease as an early culprit in the pathophysiology of diabetes and metabolic syndrome. Pharmacol Res 2017;123:114-21.
10. Moncada S, Higgs A. The L-arginine-nitric oxide pathway. N Engl J Med 1993;329:2002-12.
11. Batenburg WW, Garrelds IM, van Kats JP, Saxena PR, Danser AH. Mediators of bradykinin-induced vasorelaxation in human coronary microarteries. Hypertension 2004;43:488-92.
12. Batenburg WW, Popp R, Fleming I, et al. Bradykinin-induced relaxation of coronary microarteries: S-nitrosothiols as EDHF? Br J Pharmacol 2004;142:125-35.
13. Kato M, Shiode N, Yamagata T, Matsuura H, Kajiyama G. Bradykinin induced dilatation of human epicardial and resistance coronary arteries in vivo: effect of inhibition of nitric oxide synthesis. Heart 1997;78:493-8.
14. Nguyen A, Thorin-Trescases N, Thorin E. Working under pressure: coronary arteries and the endothelin system. Am J Physiol Regul Integr Comp Physiol 2010;298:R1188-94.
15. Versari D, Daghini E, Virdis A, Ghiadoni L, Taddei S. Endothelium-dependent contractions and endothelial dysfunction in human hypertension. Br J Pharmacol 2009;157:527-36.
16. Sorop O, Olver TD, van de Wouw J, et al. The microcirculation: a key player in obesity-associated cardiovascular disease. Cardiovasc Res 2017;113:1035-45.
17. Robson R, Kundur AR, Singh I. Oxidative stress biomarkers in type 2 diabetes mellitus for assessment of cardiovascular disease risk. Diabetes Metab Syndr 2017. DOI: 10.1016/j.dsx.2017.12.029.
18. Mayyas F, Baydoun D, Ibdah R, Ibrahim K. Atorvastatin Reduces Plasma Inflammatory and Oxidant Biomarkers in Patients With Risk of Atherosclerotic Cardiovascular Disease. J Cardiovasc Pharmacol Ther 2018. DOI: 10.1177/1074248417753677.
19. de Boer RA, Nayor M, deFilippi CR, et al. Association of Cardiovascular Biomarkers With Incident Heart Failure With Preserved and Reduced Ejection Fraction. JAMA Cardiol 2018. DOI: 10.1001/jamacardio.2017.4987.
20. Camenzind E, Steg PG, Wijns W. Stent thrombosis late after implantation of first-generation drug-eluting stents: a cause for concern. Circulation 2007;115:1440-55.
21. Togni M, Raber L, Cocchia R, et al. Local vascular dysfunction after coronary paclitaxel-eluting stent implantation. Int J Cardiol 2007;120:212-20.

22. Bundhun PK, Soogund MZ, Pursun M, Chen MH. Stent thrombosis and adverse cardiovascular outcomes observed between six months and five years with sirolimus-eluting stents and other drug-eluting stents in patients with Type 2 diabetes mellitus complicated by coronary artery disease: A systematic review and meta-analysis. Medicine (Baltimore) 2016;95:e4130.
23. Beckman JA, Creager MA, Libby P. Diabetes and atherosclerosis: epidemiology, pathophysiology, and management. JAMA 2002;287:2570-81.
24. Dudek D, Rzeszutko L, Onuma Y, et al. Vasomotor Response to Nitroglycerine Over 5 Years Follow-Up After Everolimus-Eluting Bioresorbable Scaffold Implantation. JACC Cardiovasc Interv 2017;10:786-95.
25. Ali ZA, Serruys PW, Kimura T, et al. 2-year outcomes with the Absorb bioresorbable scaffold for treatment of coronary artery disease: a systematic review and meta-analysis of seven randomised trials with an individual patient data substudy. Lancet 2017;390:760-72.
26. Alfonso F, Cuesta J. Bioresorbable Vascular Scaffolds Restenosis: Pathophysiology and Predictors. JACC Cardiovasc Interv 2017;10:1828-31.
27. Capodanno D, Gori T, Nef H, et al. Percutaneous coronary intervention with everolimus-eluting bioresorbable vascular scaffolds in routine clinical practice: early and midterm outcomes from the European multicentre GHOST-EU registry. EuroIntervention 2015;10:1144-53.
28. Serruys PW, Beatt KJ, van der Giessen WJ. Stenting of coronary arteries. Are we the sorcerer's apprentice? Eur Heart J 1989;10:774-82.
29. Kristensen SD, Maeng M, Capodanno D, Wijns W. The year in cardiology 2017: coronary interventions. Eur Heart J 2018. DOI: 10.1093/eurheartj/ehx798.
30. Roksnoer LC, Verdonk K, van den Meiracker AH, Hoorn EJ, Zietse R, Danser AH. Urinary markers of intrarenal renin-angiotensin system activity in vivo. Curr Hypertens Rep 2013;15:81-8.
31. Lu X, Garrelds IM, Wagner CA, Danser AH, Meima ME. (Pro)renin receptor is required for prorenin-dependent and -independent regulation of vacuolar H(+)-ATPase activity in MDCK.C11 collecting duct cells. Am J Physiol Renal Physiol 2013;305:F417-25.
32. Batenburg WW, Lu X, Leijten F, Maschke U, Muller DN, Danser AH. Renin- and prorenin-induced effects in rat vascular smooth muscle cells overexpressing the human (pro)renin receptor: does (pro)renin-(pro)renin receptor interaction actually occur? Hypertension 2011;58:1111-9.
33. Kinouchi K, Ichihara A, Sano M, et al. The (pro) renin receptor/ATP6AP2 is essential for vacuolar H+-ATPase assembly in murine cardiomyocytes. Circ Res 2010;107:30-4.
34. Sun Y, Danser AHJ, Lu X. (Pro)renin receptor as a therapeutic target for the treatment of cardiovascular diseases? Pharmacol Res 2017;125:48-56.
35. Danser AH. The Role of the (Pro)renin Receptor in Hypertensive Disease. Am J Hypertens 2015;28:1187-96.
36. Sihn G, Rousselle A, Vilianovitch L, Burckle C, Bader M. Physiology of the (pro)renin receptor: Wnt of change? Kidney Int 2010;78:246-56.
37. Zeymer U, Dechend R, Riemer T, et al. 1-Year outcomes of hypertension management in 13,000 outpatients under practice conditions: prospective 3A registry. Int J Cardiol 2014;176:589-94.
38. Oh BH, Mitchell J, Herron JR, Chung J, Khan M, Keefe DL. Aliskiren, an oral renin inhibitor, provides dose-dependent efficacy and sustained 24-hour blood pressure control in patients with hypertension. J Am Coll Cardiol 2007;49:1157-63.
39. Feldman DL, Jin L, Xuan H, et al. Effects of aliskiren on blood pressure, albuminuria, and (pro)renin receptor expression in diabetic TG(mRen-2)27 rats. Hypertension 2008;52:130-6.
40. Parving HH, Brenner BM, McMurray JJ, et al. Cardiorenal end points in a trial of aliskiren for type 2 diabetes. N Engl J Med 2012;367:2204-13.
41. Scirica BM, Morrow DA, Bode C, et al. Patients with acute coronary syndromes and elevated levels of natriuretic peptides: the results of the AVANT GARDE-TIMI 43 Trial. Eur Heart J 2010;31:1993-2005.
42. Gheorghiade M, Bohm M, Greene SJ, et al. Effect of aliskiren on postdischarge mortality and heart failure readmissions among patients hospitalized for heart failure: the ASTRONAUT randomized trial. JAMA 2013;309:1125-35.

43. McMurray JJ, Krum H, Abraham WT, et al. Aliskiren, Enalapril, or Aliskiren and Enalapril in Heart Failure. N Engl J Med 2016;374:1521-32.
44. Pantzaris ND, Karanikolas E, Tsiotsios K, Velissaris D. Renin Inhibition with Aliskiren: A Decade of Clinical Experience. J Clin Med 2017. DOI: 10.3390/jcm6060061.
45. Balcarek J, Seva Pessoa B, Bryson C, et al. Multiple ascending dose study with the new renin inhibitor VTP-27999: nephrocentric consequences of too much renin inhibition. Hypertension 2014;63:942-50.
46. Raptis AE, Markakis KP, Mazioti MC, et al. Effect of aliskiren on circulating endothelial progenitor cells and vascular function in patients with type 2 diabetes and essential hypertension. Am J Hypertens 2015;28:22-9.
47. Virdis A, Ghiadoni L, Qasem AA, et al. Effect of aliskiren treatment on endothelium-dependent vasodilation and aortic stiffness in essential hypertensive patients. Eur Heart J 2012;33:1530-8.
48. Mirabito Colafella KM, Danser AHJ. Recent Advances in Angiotensin Research. Hypertension 2017;69:994-9.
49. Uijl E, Danser AHJ. Renin-Angiotensin-Aldosterone System Parameters as Biomarker in Heart Failure Patients With Preserved Ejection Fraction: Focus on Angiotensinogen. Am J Hypertens 2018;31:175-7.
50. Kwakernaak AJ, Roksnoer LC, Lambers Heerspink HJ, et al. Effects of Direct Renin Blockade on Renal & Systemic Hemodynamics and on RAAS Activity, in Weight Excess and Hypertension: A Randomized Clinical Trial. PLoS One 2017;12:e0169258.

Abbreviations
Curriculum vitae
PhD portfolio
Publicatielijst
Dankwoord
Addendum

Abbreviations and acronyms

ACE	angiotensin-converting enzyme
Ang II	angiotensin II
AT_1	Ang II type 1 receptor
BMS	bare metal stents
BVS	bioresorbable vascular scaffold
CAD	coronary artery disease
cGMP	cyclic guanoside monophosphate
COX-2	cyclooxygenase 2
DES	drug-eluting stents
DM	diabetes mellitus
EDCF	endothelium derived contracting factor
EDHF	endothelium derived hyperpolarizing factor
eNOS	endothelial nitric oxide synthase
ET_A	endothelin type A
ET_B	endothelin type B
ET-1	endothelin-1
HRP	handle region peptide
NIRS	near-infrared spectroscopy
NO	nitric monoxide
OCT	optical coherence tomography
PAT	peripheral arterial tonometry
PCI	percutaneous coronary intervention
PES	paclitaxel eluting stent
RAAS	renin angiotensin aldosterone system
TGF-β	transforming growth factor-β

Curriculum vitae

De auteur van dit proefschrift, Mieke van den Heuvel, werd geboren op 29 december 1976 te Oss. In 1995 behaalde zij aldaar haar VWO diploma aan het Titus Brandsma Lyceum. In hetzelfde jaar begon zij aan de studie Medische Biologie aan de universiteit van Utrecht. In 2000 begon zij aldaar ook aan de studie Geneeskunde. In 2002 maakte zij voor het eerst kennis met de experimentele cardiologie in het laboratorium van Prof.dr. G. Pasterkamp tijdens een onderzoeksstage onder supervisie van Dr. J.I. Rotmans waarbij zij startte met onderzoek doen naar de pathologie van bloedvaten. Vanuit deze afdeling, deed zij in 2003 een extra onderzoeksstage te Stanford University in de VS, in het Cardiovascular Core Analysis Laboratory van Dr. A. Yeung. Hier maakte zij voor het eerst kennis met pathologie verbonden aan drug eluting stents. In 2004 ronde zij haar studie Medische Biologie af en in 2005 de studie Geneeskunde. In 2006 was zij werkzaam als ANIOS interne geneeskunde / cardiologie eerst in het Sint Franciscus Gasthuis te Rotterdam, later in het Albert Schweitzer ziekenhuis te Dordrecht. In 2007 begon zij met haar promotieonderzoek op de afdelingen experimentele cardiologie en farmacologie van het Erasmus MC te Rotterdam met als promotoren Prof.dr. W.J. van der Giessen, na zijn overlijden Prof.dr. D.J. Duncker en Prof.dr. A.H.J. Danser. De resultaten van dit onderzoek zijn in dit proefschrift beschreven. Eind 2012 is zij begonnen met de opleiding cardiologie in het Erasmus MC na een korte periode als ANIOS cardiologie in het Sint Elisabeth Hospitaal te Willemstad in Curaçao en in het Erasmus MC te hebben gewerkt. Zij heeft de twee jaar vooropleiding interne geneeskunde in het Albert Schweitzer ziekenhuis gedaan onder supervisie van Dr. E.F.H. van Bommel en in 2015 de B-opleiding cardiologie, onder supervisie van Dr. E.J. van den Bos en Dr. M.J.M. Kofflard. Vanaf eind 2015 is zij bezig met de A-opleiding cardiologie in het Erasmus MC, onder supervisie van Dr. T.W. Galema en Dr. E.A. Dubois. Zij woont samen met Alexander Cupido te Rotterdam.

PhD Portfolio

Name PhD student:	Mieke van den Heuvel
Erasmus MC Department:	Cardiology
Research School:	COEUR
PhD Period:	2007 – 2017
Promotors:	Prof.dr. D.J. Duncker
	Prof.dr. A.H.J. Danser

1. PhD training	**Year**	**Workload (ECTS)**
General academic skills		
-Integrity in Research	2007	0.5
-Laboratory animal science	2007	4.5
-English biomedical writing and communication	2008	4
Research skills		
-Statistics (NIHESS course)	2007, 2008	6
In-depth courses		
-COEUR courses	2007 – 2011	6
-NHS Papendal PhD training course	2007	4
-Methodologie voor patientgebonden onderzoek	2007	2
Presentations		
-Oral presentation, EASD	2007	
-Oral presentation COEUR Research seminars	2007, 2011, 2012	
-Oral presentation, TCT	2008	
-Poster presentations, European Society of Cardiology	2008, 2009, 2010	
-Poster presentation, American Heart Association	2009	
-Poster presentation, European Society of Hypertension	2009	
-Oral presentation, EuroPCR	2009	
-Poster presentation, High Blood Pressure Counsil	2010	
-Oral presentation, European Society of Hypertension	2011	

(International) conferences

-EAS meeting	2007	1
-EASD, 43rd annual meeting	2007	1
-NHS Molecular Cardiology	2007	1
-NVVC-Voorjaarscongres	2007	1
-Pfizer HDL symposium	2007	0.5
-Vasculair Spreekuur	2007	0.5
-Cardiology and Vascular Medicine Update and Perspective	2007 – 2009	2
-COEUR research seminars	2007 – 2011	2
-TCT conference	2008	1
-FIGON Dutch medicines days	2008	0.5
-ESC conference	2008 – 2010	3
-MIVAB	2008 – 2011	4
-DAS symposium	2009	1
-19th ESH meeting	2009	1
-AHA conference	2009	1
-EuroPCR conference	2009	1
-High Blood Pressure Counsil	2010	1
-9th Dutch German Joint meeting	2011	1
-NCCV conference	2011	0.5
-21st ESH meeting	2011	1

Seminars and workshops

-MolMed Writing successful grant proposals	2008	0.5
-Shear stress symposium	2008	0.5
-Geavanceerde beeldvormende technieken voor doctors	2009	0.5
-Pigs: “The missing link?”	2010	0.5
-Farewell symposium of Prof. J.A.E. Spaan	2010	0.5
-Diabetes Platform Erasmus MC	2010	0.5
-The first Bioresorbable Vascular Scaffold summit	2011	0.5
-Symposium Microcirculation in Health and Disease	2011	0.5

2. Teaching and organisation activities

-2nd year medical students: review writing	2009	2
-Organisation COEUR PhD day	2010	4

3. Awards and grants

-Erasmus MC-grant: Pilot project	2007
Microvascular dysfunction in diabetes mellitus type 2 and its relation to metabolic control	
-Travelgrant ESC counsil on Basic Cardiovascular Science	2008
-Prize for best poster, 19th ESH meeting, Milan	2009
-Travelgrant EuroPCR, Barcelona, Erasmus Trustfonds	2009
-Prize for best poster, 13th DAS Symposium	2010
-Travelgrant High Blood Pressure Counsil, Washington	
Nederlandse Vereniging voor Farmacologie	2010
-Dirk Durrer prize	2011
-Van Noordwijk stipendium, Kolff conference	2011
-3th prize Young Investigators Award, ACS platform	2011
-Travelgrant AHA, Orlando, Erasmus Trustfonds	2011
-Prize for best oral presentation,	2011
Nederlands Hypertensie Genootschap,	
CardioVasculaire Conferentie	

Total	62

Publicatielijst

The effect of bioresorbable vascular scaffold implantation on distal coronary endothelial function in dyslipidemic swine with and without diabetes.

van den Heuvel M, Sorop O, van Ditzhuijzen NS, de Vries R, van Duin RWB, Krabbendam-Peters I, van Loon JE, de Maat MP, van Beusekom HM, van der Giessen WJ, Danser AHJ, Duncker DJ.

Int J Cardiol. 2018 Feb 1;252:44-51.

Neoatherosclerosis development following bioresorbable vascular scaffold implantation in diabetic and non-diabetic swine.

van Ditzhuijzen NS, Kurata M, **van den Heuvel M**, Sorop O, van Duin RWB, Krabbendam-Peters I, Ligthart J, Witberg K, Murawska M, Bouma B, Villiger M, Garcia-Garcia HM, Serruys PW, Zijlstra F, van Soest G, Duncker DJ, Regar E, van Beusekom HMM.

PLoS One. 2017 Sep 12;12(9):e0183419.

Serial Coronary Imaging of Early Atherosclerosis Development in Fast-Food-Fed Diabetic and Nondiabetic Swine.

Nienke S. van Ditzhuijzen, MSC, **Mieke van den Heuvel, MD**, Oana Sorop, PHD, Alexia Rossi, MD, PHD, Timothy Veldhof, MSC, Nico Bruining, PHD, Stefan Roest, BSC, Jurgen M.R. Ligthart, RT, Karen Th. Witberg, CCRN, Marcel L. Dijkshoorn, BSC, Koen Nieman, MD, PHD, Monique T. Mulder, PHD, Felix Zijlstra, MD, PHD, Dirk J. Duncker, MD, PHD, Heleen M.M. van Beusekom, PHD, Evelyn Regar, MD, PHD.

JACC Basic to Translational Science. 2016 Oct;449-6.

Coronary microvascular dysfunction after long-term diabetes and hypercholesterolemia.

Sorop O*, **van den Heuvel M***, van Ditzhuijzen NS, de Beer VJ, Heinonen I, van Duin RW, Zhou Z, Koopmans SJ, Merkus D, van der Giessen WJ, Danser AH & Duncker DJ.

*Shared first authorship

Am J Physiol Heart Circ Physiol. 2016 Dec 1;311(6).

Peripheral arterial tonometry cannot detect patients at low risk of coronary artery disease.

van den Heuvel M, Sorop O, Musters PJ, van Domburg RT, Galema TW, Duncker DJ, van der Giessen WJ & Nieman K.

Neth Heart J. 2015 Sep;23(10):468-74.

Early systemic microvascular damage in pigs with atherogenic diabetes mellitus coincides with renal angiopoietin dysbalance.

Khairoun M, **van den Heuvel M**, van den Berg BM, Sorop O, de Boer R, van Ditzhuijzen NS, Bajema IM, Baelde HJ, Zandbergen M, Duncker DJ, Rabelink TJ, Reinders ME, van der Giessen WJ & Rotmans JI.

PLoS One. 2015 Apr 24;10(4).

The impact of Fourier-Domain optical coherence tomography catheter induced motion artefacts on quantitative measurements of a PLLA-based bioresorbable scaffold.

van Ditzhuijzen NS, Karanasos A, Bruining N, **van den Heuvel M**, Sorop O, Ligthart J, Witberg K, Garcia-Garcia HM, Zijlstra F, Duncker DJ, van Beusekom HM & Regar E.

Int J Cardiovasc Imaging. 2014 Aug;30(6):1013-26.

Combined renin inhibition/(pro)renin receptor blockade in diabetic retinopathy--a study in transgenic (mREN2)27 rats.

Batenburg WW, Verma A, Wang Y, Zhu P, **van den Heuvel M**, van Veghel R, Danser AH & Li Q.

PLoS One. 2014 Jun 26;9(6).

Deterioration of kidney function by the (pro)renin receptor blocker handle region peptide in aliskiren-treated diabetic transgenic (mRen2)27 rats.

te Riet L, **van den Heuvel M**, Peutz-Kootstra CJ, van Esch JH, van Veghel R, Garrelds IM, Musterd-Bhaggoe U, Bouhuizen AM, Leijten FP, Danser AH & Batenburg WW.

Am J Physiol Renal Physiol. 2014 May 15;306(10).

The (pro)renin receptor blocker handle region peptide upregulates endothelium-derived contractile factors in aliskiren-treated diabetic transgenic (mREN2)27 rats.

Batenburg WW*, **van den Heuvel M***, van Esch JH, van Veghel R, Garrelds IM, Leijten F & Danser AH.

*Shared first authorship

J Hypertens. 2013 Feb;31(2):292-302.

Coronary microvascular dysfunction in a porcine model of early atherosclerosis and diabetes.

van den Heuvel M*, Sorop O*, Koopmans SJ, Dekker R, de Vries R, van Beusekom HM, Eringa EC, Duncker DJ, Danser AH & van der Giessen WJ.

*Shared first authorship

Am J Physiol Heart Circ Physiol. 2012 Jan 1;302(1).

Urinary renin, but not angiotensinogen or aldosterone, reflects the renal renin-angiotensin-aldosterone system activity and the efficacy of renin-angiotensin-aldosterone system blockade in the kidney.

van den Heuvel M, Batenburg WW, Jainandunsing S, Garrelds IM, van Gool JM, Feelders RA, van den Meiracker AH & Danser AH.

J Hypertens. 2011 Nov;29(11):2147-55.

Invasive coronary imaging in animal models of atherosclerosis.

van Ditzhuijzen NS*, **van den Heuvel M***, Sorop O, van Duin RW, Krabbendam-Peters I, van Haeren R, Ligthart JM, Witberg KT, Duncker DJ, Regar E, van Beusekom HM & van der Giessen WJ.

*Shared first authorship

Neth Heart J. 2011 Oct;19(10):442-6.

Dietary saturated fat/cholesterol, but not unsaturated fat or starch, induces C-reactive protein associated early atherosclerosis and ectopic fat deposition in diabetic pigs.

Koopmans SJ, Dekker R, Ackermans MT, Sauerwein HP, Serlie MJ, van Beusekom HM, **van den Heuvel M** & van der Giessen WJ.

Cardiovasc Diabetol. 2011 Jul 14;10:64.

The Authors Reply.
Response to 'Angiotensin II-induced phosphorylation of the sodium chloride cotransporter'.
Nils van der Lubbe, **Mieke van den Heuvel**, Robert Zietse, Ewout J. Hoorn, Alexander H.J. Danser.
Kidney International. 2011 June 79(12):1382.

On the origin of urinary angiotensin II.
van den Heuvel M, van Esch JH & Danser AH.
Hypertension. 2010 Oct;56(4).

Specific coronary drug-eluting stents interfere with distal microvascular function after single stent implantation in pigs.
van den Heuvel M, Sorop O, Batenburg WW, Bakker CL, de Vries R, Koopmans SJ, van Beusekom HM, Duncker DJ, Danser AH & van der Giessen WJ.
JACC Cardiovasc Interv. 2010 Jul;3(7):723-30.

Endothelial function rather than endothelial restoration is altered in paclitaxel- as compared to bare metal-, sirolimus- and tacrolimus-eluting stents.
van Beusekom HM, Sorop O, **van den Heuvel M**, Onuma Y, Duncker DJ, Danser AH & van der Giessen WJ.
EuroIntervention. 2010 May;6(1):117-25.

Endothelial dysfunction after drug eluting stent implantation.
van den Heuvel M, Sorop O, van Beusekom HM & van der Giessen WJ.
Minerva Cardioangiol. 2009 Oct;57(5):629-43.

Diabetic complications: a role for the prorenin-(pro)renin receptor-TGF-beta1 axis?
van den Heuvel M, Batenburg WW & Danser AH.
Mol Cell Endocrinol. 2009 Apr 29;302(2):213-8.

Local overexpression of C-type natriuretic peptide ameliorates vascular adaptation of porcine hemodialysis grafts.
Rotmans JI, Verhagen HJ, Velema E, de Kleijn DP, **van den Heuvel M**, Kastelein JJ, Pasterkamp G, & Stroes ES.
Kidney Int. 2004 May;65(5):1897-905.

Dankwoord

Promoveren doe je nooit alleen, maar met de steun van collega's, vrienden en familie. Hierbij wil ik iedereen bedanken die bijgedragen heeft aan het tot stand komen van dit proefschrift. Zonder volledig te kunnen zijn, wil ik een aantal mensen in het bijzonder benoemen.

Nadat ik uit de klinische praktijk wist cardioloog te willen worden, ben ik op de afdeling experimentele cardiologie in het EMC gaan praten over promotieonderzoek. In een aangenaam gesprek met Wim, Dirk en Heleen werd mij duidelijk dat de afdeling meerdere projecten te bieden had en dat ik daar ook een eigen weg in kon bewandelen. Het laatste, in combinatie met het opzetten van een diabetes varkensmodel als een ziektemodel voor stent-studies, sprak me aan en sloot goed aan bij eerder onderzoek wat ik had gedaan.

In de maanden die volgden, bleek het opzetten van het model nog niet zo snel te gaan als ik zou willen, maar gelukkig kon ik uit eerder materiaal van pilots van Sietse Jan, Heleen en Oana putten. De vaatfunctie studies van Oana vond ik het meest interessant, die me dan ook in het "badjeslab" op de 14e verdieping binnen de afdeling farmacologie introduceerde. De sfeer daar en het zelf "prutsen" met vaatjes onder de microscoop verkregen uit slachthuisharten die ruimschoots voorhanden waren bevielen en hiermee was de samenwerking tussen de afdelingen experimentele cardiologie en farmacologie geboren. De loop der jaren kenmerkten zich doordat inmiddels meerdere projectjes gingen lopen en doordat ook het diabetes varkensmodel echt in Rotterdam zou gaan starten. Wat me altijd is bijgebleven is dat Wim eigenlijk in alles aanmoedigde en niet te veel stuurde zowel in experimenten, analyses, subsidie aanvragen, abstracts voor congressen als in manuscripten zodat ik het gevoel kreeg en altijd heb gehad mijn eigen promotie traject te bewandelen, wat misschien wel iets langer heeft geduurd dan gepland maar waarin ik alles heb afgerond waaraan ik ooit begonnen was. Ik kan me achteraf geen betere promotor voorstellen en ik hoop dat je tevreden geweest zou zijn met het resultaat. Wim bedankt!

Beste Jan, door de experimenten op het "badjeslab" kwam ik gedurende mijn onderzoeksjaren met veel plezier op jouw afdeling en ik ben ook erg blij dat al snel duidelijk werd dat mijn promotieonderzoek door twee promotoren zou worden ondersteund zodat de vaatfunctie experimenten een belangrijk onderdeel zouden vormen binnen mijn promotie traject. Het meedenken over de uitkomsten van de vaatfunctie stent-experimenten, maar ook het helpen met toekomst-ideeën zoals het isoleren van vaatjes uit bilbiopten, maar geeft wel aan dat er op de 14e altijd goed en breed mee werd gedacht. Uiteindelijk bleken de bilbiopten niet succesvol en heb ik samen met Wendy o.b.v. haar Nierstichting subsidie een aantal mooie experimenten kunnen doen die tot goede publicaties hebben geleid. Vanaf het moment van schrijven van het

review behorend bij dit project, het verrichten van de experimenten en tot aan het schrijven van de manuscripten o.b.v. de resultaten, stond alles in het teken van hoge efficiëntie en snelheid waarmee het voor elkaar kwam. Ik ken niemand die sneller uit geanalyseerde gegevens een manuscript kan destilleren, dan jij. De samenwerking en de sfeer op de afdeling was altijd prettig. Het discussiëren over resultaten was altijd leerzaam, hoewel ik wat betreft de RAAS experimenten vaak pas achteraf als jij het manuscript al zo'n beetje klaar had, door had wat ze nu eigenlijk betekenden. Ook het lab-uitje naar New York was memorabel. Uiteindelijk is de lange nasleep van dit promotie-traject niet helemaal wat jij wilde, maar ik denk dat het werk op zowel van de afdelingen farmacologie als experimentele cardiologie uiteindelijk wel zijn vruchten heeft afgeworpen. Jan, ik wil je graag bedanken voor de samenwerking en ik vind het een eer gewerkt te mogen hebben met een wereldwijde expert op het gebied van het RAAS en ik ben blij daar nu ook iets meer vanaf te weten.

Beste Dirk, na het overlijden van Wim werd jij mijn tweede promotor. Maar zoals gezegd was je al vanaf dag 1 van mijn promotieonderzoek betrokken en ook tussentijds was je altijd al bereid om mee te denken. Ik denk dat door je vriendelijke enthousiasme iedereen wel met je wil samenwerken, en ik dus ook. Ik ben blij en trots dat het diabetes varkensmodel nog altijd gebruikt wordt op de afdeling experimentele cardiologie en ik wil je hartelijk bedanken voor de steun en begeleiding tijdens het promotie-traject en met name voor je geduld in de afronding van het laatste deel. De discussies rondom de analyses van de resultaten en het schrijven van de manuscripten waren altijd leerzaam en ik heb het altijd kunnen waarderen dat je ruimte voor mij liet voor klinische uitstapjes zowel in de discussies van de manuscripten als voor het vaatfunctie onderzoek in de kliniek, als in het aangaan van samenwerkingen wat betreft het diabetes varkensmodel.

Geachte Prof. van Bavel, Prof. de Boer en Prof. Zijlstra, graag wil ik u allen bedanken voor de bereidheid om deel te nemen in de leescommissie voor de beoordeling van mijn proefschrift.

Beste Oana, zonder jouw hulp en steun was mijn promotieonderzoek waarschijnlijk niet tot stand gekomen. Je bent bij ieder van mijn projecten, die vanaf de 23ste gestart zijn, betrokken geweest inclusief de endotheel functie metingen in de kliniek. Hartelijk dank voor alle ondersteuning en prettige samenwerking en ook voor hulp in de afgelopen jaren voor de afronding van de laatste artikelen van dit boekje. Jouw voorliefde voor microvaatfunctie heb je op mij overgedragen en ik hoop dat je hier nog veel mensen in de toekomst voor kunt enthousiasmeren. Ik ben blij dat na al het harde werken om het diabetes varkensmodel in Rotterdam gestart te krijgen gelukt is en dat je daar met een groepje "sterke mannen" nog altijd verder aan werkt.

Beste Wendy, naast Oana was ook jij een belangrijke steun en toeverlaat gedurende mijn promotie onderzoek. Als "koningin" van het "badjeslab" wist je alles over de ***in vitro*** vaatfunctie experimenten en het uitwerken daarvan. Het diabetes ratten project was een heel leuk project om samen aan te werken waarbij we de dieren maximaal efficiënt hebben gebruikt.

Beste Siete Jan, in de begin jaren heb ik geworsteld met jouw pilotdata van varkensmodellen met enige mate van cardiovasculaire ziekte. Uiteindelijk hebben we een bepaalde strategie overgenomen voor het model in Rotterdam maar ik begrijp nu beter dat ieder model zijn voors en tegens heeft. Hartelijk dank voor de altijd fijne samenwerking en je bereidheid om materiaal van je studies met ons te delen!

Op de 23ste heb ik tijdens de projecten met vele mensen samengewerkt: Heleen: bedankt voor je expertise in de histologie; Ilona: bedankt voor de kleuringen en metingen die je hebt gedaan; Richard: bedankt voor de hulp tijdens de dierexperimenten en succes met de afronding van je eigen promotie. Mensen die inmiddels vertrokken zijn: Charlotte: dank voor je hulp tijdens de dier experimenten en met de histologie; Rorry: bedankt voor je hulp bij de histologie; Nienke: bedankt voor de samenwerking tijdens het diabetes varkens project en het schrijven van de bijbehorende manuscripten; Zhichao: bedankt voor je interesse in microvaatfunctie op het "badjeslab". Daphne: bedankt voor het meedenken tijdens subsidie aanvragen, de analyses van data en tips voor presentaties. Rob: hartelijk dank voor je gezelligheid en ICT ondersteuning; Liesbeth: ook hartelijk dank voor je ICT ondersteuning en het veelvuldig activeren van mijn toegang tot de harde schijf van de 23ste; Monique: hartelijk dank voor de secretariële en administratieve ondersteuning. Elles: ook hartelijk dank voor de secretariële en administratieve ondersteuning in de tijd dat Wim er nog was. Mensen die bijdroegen aan de prettige werksfeer: Marc: hartelijk dank voor je gezelschap en steun tijdens de laatste onderzoeks-jaren; Elza: bedankt voor de gezelligheid inclusief road-trip door de Everglades en de Florida Keys; Maaike: hartelijk dank voor al je advies en ondersteuning; Martine: dank voor je gezelligheid; Andre: bedankt voor het zijn van de beste buurman die een promovenda zich kan wensen: altijd vrolijk, behendig in krav maga en altijd in voor een meloen cocktail! Bianca: bedankt als luisterend oor en gezellige buurvrouw; Tuncay: altijd rustig aanwezig en inmiddels allang gepromoveerd! Vincent: allang vertrokken maar hij blijft maar terugkeren naar de 23ste… In het begin waren we kamergenoten: bedankt daarvoor! Last but not least: de mensen van mijn laatste werkplek: Ruben, Jens en Maarten: er is weer meer plaats in de kamer!

Ook op de 14e heb ik met vele mensen samengewerkt: René: hartelijk dank voor alle "grote" vaatexperimenten en je rustige aanwezigheid; Richard: hartelijk dank voor alle hulp met de ratten experimenten en voor je gezellige praatjes. Ingrid: hartelijk dank voor je snelle analyses van de urine en bloed monsters. Anton: bedankt voor het meedenken met experimenten en

fameuze farmacologie filmavonden en sinterklaasfeesten. Antoinette: hartelijk dank voor het meedenken met uitkomstresultaten. Birgitte: heel erg bedankt voor de secretariële en administratieve ondersteuning en de gezellige relaxte sfeer van de 14e. Mensen die inmiddels vertrokken zijn: Jeanette: ook hartelijk dank voor de hulp bij de analyses van de urine en plasma monsters. Joep: bedankt voor je hulp tijdens de ratten experimenten en voor de gezellige sfeer op het "badjeslab", Ka Yi: bedankt voor de gezelligheid inclusief mijn eerste Chinese bruiloft.

Tijdens mijn onderzoekstijd had ik het geluk te kunnen samenwerken met meerdere mensen van ook andere afdelingen. Ton van den Meiracker: hartelijk dank voor je interesse in humane vaatfunctie experimenten, hoewel het afnemen van bilbiopten niet zo gemakkelijk bleek. Jurgen Lighthart en Karen Witberg: bedankt voor de in vivo vaatfunctie metingen. Etto Eringa: bedankt voor je hulp bij de Western Blot analyses. Joris Rotmans en Meriem Khairoun: hartelijk dank voor de glycocalyx metingen en de nier analyses. Janine Elshout en Moniek de Maat: hartelijk dank voor de plasma vWf metingen. Paul Musters en Tjebbe Galema voor het mogelijk maken van de endotheel functie metingen in de kliniek. Ron van Domburg en Magdalena Murawska: bedankt voor de statistische ondersteuning. Koen Nieman: bedankt voor je hulp en ondersteuning in de afronding van het perifere endotheel functie artikel.
Mijn opleiders, Tjebbe Galema en Eric Dubois, en mijn collega arts-assistenten wil ik bedanken voor de mogelijkheid die zij mij hebben gegeven tot de afronding van dit proefschrift tijdens de opleiding tot cardioloog.

Mijn paranimfen Karin en Diana wil ik bedanken voor hun ondersteuning tijdens de promotie plechtigheid, maar vooral voor hun vriendschap van afgelopen jaren en de garantie dat daarmee 15 mei een feest gaat worden!

Natuurlijk kan ik ook de andere "In Viva" ladies niet vergeten: Evelyn, Maja, Michelle en Yvonne, bedankt voor de steun door jarenlange gezellige borrels, etentjes en uitjes!

Als laatste wil ik uiteraard ook mijn ouders en Alexander bedanken. Zonder jullie was het zeker niet gelukt!

Addendum

De auteur wil Myrrhe van Spronsen, de artistieke vormgever van de illustraties van de kaft en in het proefschrift bedanken voor haar bijdrage.

De auteur erkent dankbaar de financiële ondersteuning voor het drukken van dit proefschrift door:

- Erasmus University Rotterdam
- Abbott Vascular Netherlands B.V.
- Boehringer Ingelheim B.V.
- Chipsoft B.V.
- Sanofi Nederland B.V.
- Servier Nederland Farma B.V.